

THIS FILE IS MADE AVAILABLE THROUGH THE DECLASSIFICATION EFFORTS AND RESEARCH OF:

# THE BLACK VAULT

THE BLACK VAULT IS THE LARGEST ONLINE FREEDOM OF INFORMATION ACT / GOVERNMENT RECORD CLEARING HOUSE IN THE WORLD. THE RESEARCH EFFORTS HERE ARE RESPONSIBLE FOR THE DECLASSIFICATION OF THOUSANDS OF DOCUMENTS THROUGHOUT THE U.S. GOVERNMENT, AND ALL CAN BE DOWNLOADED BY VISITING:

[HTTP://WWW.BLACKVAULT.COM](http://www.blackvault.com)

YOU ARE ENCOURAGED TO FORWARD THIS DOCUMENT TO YOUR FRIENDS, BUT PLEASE KEEP THIS IDENTIFYING IMAGE AT THE TOP OF THE .PDF SO OTHERS CAN DOWNLOAD MORE!



**UNCLASSIFIED**

---

**AD 271 500**

---

*Reproduced  
by the*

**ARMED SERVICES TECHNICAL INFORMATION AGENCY  
ARLINGTON HALL STATION  
ARLINGTON 12, VIRGINIA**

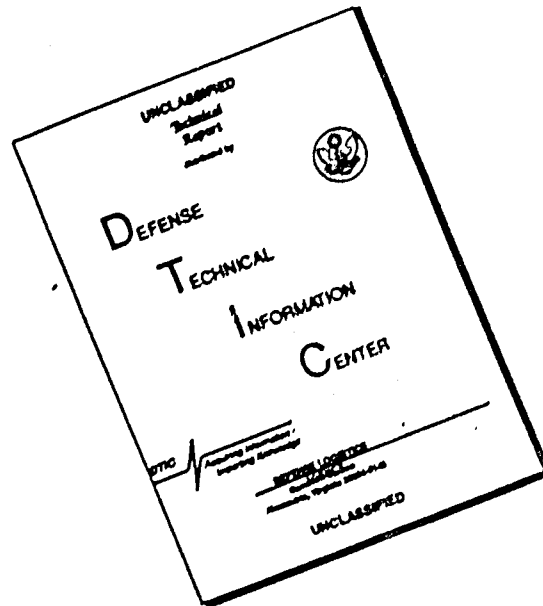


---

**UNCLASSIFIED**

NOTICE: When government or other drawings, specifications or other data are used for any purpose other than in connection with a definitely related government procurement operation, the U. S. Government thereby incurs no responsibility, nor any obligation whatsoever; and the fact that the Government may have formulated, furnished, or in any way supplied the said drawings, specifications, or other data is not to be regarded by implication or otherwise as in any manner licensing the holder or any other person or corporation, or conveying any rights or permission to manufacture, use or sell any patented invention that may in any way be related thereto.

# DISCLAIMER NOTICE



THIS DOCUMENT IS BEST QUALITY AVAILABLE. THE COPY FURNISHED TO DTIC CONTAINED A SIGNIFICANT NUMBER OF PAGES WHICH DO NOT REPRODUCE LEGIBLY.



271 500

271 500

AD NO.

ASTIA FILE COPY

ANALYSIS OF TESTS OF THE AVROCAR

IN THE N.A.S.A. 40 X 80 FT. WIND TUNNEL

AMES RESEARCH CENTER

500/AERO TEST

FILE COPY

Return to  
ASTIA

ARLINGTON HALL STATION  
ARLINGTON 12, VIRGINIA

Attn: TIRS

XEROX

# 18-00



AVRO AIRCRAFT LIMITED

ANALYSIS OF TESTS OF THE AVROCAR IN THE  
N. A. S. A. 40 x 80 FT. WIND TUNNEL,  
AMES RESEARCH CENTER

500/AERO TEST/407

February 1961

Issued by:

Avro Aircraft Limited  
Malton, Ontario, Canada

Under

USAF Contract No. AF33(600)42163  
U.S. Army Designation VZ-9AV  
(S. o. W. 1)

Written by:

*D. C. Whittley*  
D. C. Whittley

*D. B. Garland*  
D. B. Garland

Approved by:

T. D. Earl  
Chief Aerodynamicist

*T. D. Earl*

The number of pages in this report including the Title Page and Table of Contents is 288.

To:

Date:

Copy No: 4



## TABLE OF CONTENTS

Section	Title	Page
	SUMMARY	1
1	INTRODUCTION	2
2	NOTATION	3
3	THEORETICAL BASIS OF DATA ANALYSIS	7
4	DISCUSSION OF RESULTS	10
5	MODIFICATIONS TO AIRCRAFT FOR PHASE II TESTS	38
6	CONCLUSIONS	40
7	REFERENCES	42
TABLE 1	SUMMARY OF CONFIGURATIONS	44
TABLE 2	PRESSURE FORCE COEFFICIENT DERIVATIVES	47
	LIST OF ILLUSTRATIONS	48

SUMMARY

This report presents an analysis of some aspects of the full scale wind tunnel tests of the Avrocar vehicle, which were conducted in the 40 x 80 foot tunnel at Ames Research Center, Moffett Field, in March - April 1960. *is presented*

Methods used to analyze the force and pressure data are formulated and results are compared with theory and small scale model tests.

Aerodynamically, the performance demonstrated by the first Avrocar vehicle in its initial configuration was disappointing in that a low lift curve slope, a large nose-up pitching moment and insufficient jet vectoring capability precluded flight in free air and in the ground cushion above about 35 mph.

Modifications to the aircraft based on these and other test results have been made, the major change being in the redesign of the trailing edge region where a rearward-facing nozzle, containing a pitch control vane to provide adequate jet vectoring control, has been incorporated. The jet flap effect thus obtained is expected to allow flight in free-air as well as at higher speeds in the ground cushion.

A second series of tests at Ames is scheduled for February-March 1961.

1. INTRODUCTION

The first Avrocar vehicle was tested in the 40 x 80 ft. wind tunnel at NASA Ames Research Center, Moffett Field, California (Fig. 1) during March and April 1960, the main objective (detailed in Ref. 1, 2) being to establish a transition trajectory from hovering flight to forward flight and vice versa.

Two reports covering these tests have been issued so far. The first (Ref. 3) summarizes and highlights the major problems encountered and the second (Ref. 4) is a data report, presenting details of test equipment, procedures, data reduction, vehicle configurations and test schedules as well as graphs of lift, drag and pitching moment for each test run. The present analysis report is meant to be read in conjunction with the data report.

Early in this series of tests it became obvious that the aircraft in its basic configuration had certain shortcomings which would prevent the realization of the main test objective. Some modification to the aircraft was therefore attempted in the tunnel but with limited success as far as rectifying the aerodynamic defects was concerned. As a result of analysis of the test data from the 40 x 80 ft. tunnel and also from small scale tests in the Company's wind tunnel (Ref. 5) further modifications have been proposed and a second series of wind tunnel tests at Ames is now scheduled for early 1961.

2. NOTATION

$A$	Aspect ratio
$a$	Sectional lift slope coefficient
$a_o$	Two-dimensional lift curve slope
$c$	Wing root chord (i.e. wing diameter for circular wing)
$\bar{c}$	Mean aerodynamic chord
$C_{DB}$	Basic drag coefficient, jet-off
$C_{Di}$	Induced drag coefficient
$C_{Dm}$	Momentum drag coefficient
$C_{D_o}$	Drag coefficient at zero lift
$C_{D-F}$	Coefficient of (drag-thrust)
$C_F$	Component of jet reaction coefficient in direction of flight
$C_j$	Jet reaction coefficient
$C_L$	Lift coefficient
$C_{LB}$	Basic lift coefficient, jet-off
$C_{Lc}$	Lift coefficient due to camber
$C_{LF}$	Component of jet reaction coefficient normal to direction of flight
$C_{Li}$	Induced lift coefficient
$C_{LJ}$	Increase in lift coefficient due to a jet flap for a finite aspect ratio wing at zero incidence
$C_{LJ\infty}$	Increase in lift coefficient due to a jet flap for infinite aspect ratio wing at zero incidence
$C_{L_o}$	Theoretical total lift coefficient for jet-flapped wing at angle of attack for zero lift, jet-off

$C_M$	Pitching moment coefficient
$C_{MB}$	Basic pitching moment coefficient, jet-off
$C_{Mc}$	Pitching moment coefficient due to camber
$C_{Mi}$	Induced pitching moment coefficient
$C_{MJ}$	Increase in pitching moment coefficient due to a jet flap for a wing of finite aspect ratio at zero incidence
$C_{Mo}$	Pitching moment coefficient at zero lift
$C_{MS}$	$M_s / qSc$
$D$	Drag force or diameter
$D-F$	(Drag-thrust)
$e$	Oswald lift efficiency factor
$F_s$	Static propulsive thrust
$h/D$	Non-dimensional height parameter
$h/c$	Aerodynamic center position of pressure lift, $C_{L_{B+i}}$
$\{h/c\}$	Aerodynamic center position for "saddle-back" loading
$J$	Jet momentum
$Je$	Non-dimensional control position ( $\pm 1.0$ is full travel)
$Je'$	Non-dimensional control position. the rear $120^\circ$ of the focussing control ring being removed
$K$	Free-air thrust efficiency, $R_s / X_{Gs}$
$k$	(i) Factor applied to $a_0$ to account for flow viscosity effects; (ii) Factor used to express profile drag; (iii) Factor used to express pitching moment coefficient; (iv) Equal to $\left( \frac{V_i}{V_o} \right) \left( \frac{S}{c} \right)$



L	Lift force
$L_o$	Theoretical total lift of jet flapped wing at angle of attack for zero lift, jet-off
$L_s$	Static lift
M	Pitching moment
$M_R$	Pitching moment due to jet reaction
$M_R'$	Effective pitching moment due to jet reaction
$M_S$	Static pitching moment due to jet reaction
m	Sink strength in potential flow solution of intake problem
M or $M_{jc}$	Corrected jet mass flow; includes fan and engine intake flows
n	See Ref. 7
q	Tunnel dynamic head
$R_s$	Static, measured jet reaction $= \sqrt{L_s^2 + F_s^2}$
S or $S_W$	Wing area
$S_F$	Fan area
t/c	Thickness chord ratio
$U_o$	Free stream velocity
$\bar{U}$	Free stream velocity in potential flow field
UTIA	University of Toronto, Institute of Aerophysics
V or $V_o$	Forward or tunnel speed
$V_i$	Intake velocity
$V_j$	Jet velocity
$V_i/V_o$	Intake velocity ratio

$X_G$	Potential gross thrust determined at nozzle exit (assumes expansion to ambient pressure)
$X_{GS}$	Static potential gross thrust
$\alpha$	Angle of attack
$\alpha_c$	Angle of attack corrected for tunnel flow misalignment
$\alpha_i$	Downwash angle
$\alpha_o$	Angle of attack for zero lift
$\alpha_{min}$	Angle of attack for minimum drag
$\beta$	Jet deflection angle for fan-in-wing tests of Ref. 13
$\epsilon$	Factor applied to $a_o$ to account for airfoil thickness
$\gamma$	Ratio of analogous mechanical flap chord to wing chord
$\theta$	Deflection angle of analogous mechanical flap
$\theta_s$	Angle between static jet vector and vertical
$\rho$	Air density (slugs/ft <sup>3</sup> )
$\omega$	Downwash factor ( $\omega = 2\eta$ )

### 3. THEORETICAL BASIS OF DATA ANALYSIS

A major part of the analysis of the force and moment data consists of separating the various components which comprise the total forces and moments.

In coefficient form the total lift is assumed to be

$$C_L = C_{LB} + C_{Li} + C_{LF}$$

where  $C_{LB}$  = basic lift coefficient (measured jet off with intake sealed at max  $h/D$ )

$C_{Li}$  = pressure lift coefficient induced by the jet and by ground effect, if any.

$C_{LF}$  = jet reaction lift coefficient

$$= \frac{(R_S)}{qS} \frac{X_G}{X_{GS}} \cos (\theta_S - \alpha_C)$$

$$= \frac{R_S}{X_{GS}} \frac{X_G}{qS} \cos (\theta_S - \alpha_C)$$

$$= K_j C_j \cos (\theta_S - \alpha_C)$$

The method of defining the jet reaction contribution is recognized to be less than perfect on several counts, the most important being the possibility of a change in flow pattern as wind speed is increased. In fact, for several configurations tested it is possible to show that a distinct change in flow pattern occurred in the region up to about  $q = 5 \text{ lb/ft}^2$ . In these cases an "effective" jet reaction is assumed to apply for all non-static points. It is determined by inspection and is taken to be that value of the lift force at a certain angle of attack, which does not change with variation of forward speed in the range, generally, above  $q = 5 \text{ lb/ft}^2$ .

Since the basic lift coefficient,  $C_{LB}$ , loses its significance to some extent when the jet is on, it has been customary in this analysis to use the combination  $C_{LB} + C_{Li}$  (sometimes referred to as  $C_{LB+i}$ ). Additionally, we desire to evaluate the total pressure forces since a study of these quantities will tell us how the wing is operating as a lifting surface in the presence of the complicated jet flow pattern.

The total drag coefficient is expressed as

$$C_{D-F} = C_{DB} + C_{Di} + C_{DM} - C_F$$

where

$C_{DB}$  = basic drag coefficient (measured jet-off, intake sealed at max.  $h/D$ )

$C_{Di}$  = induced drag coefficient due to pressure lift

$$C_{DB+i} = \frac{(C_{LB} + C_{Li})^2}{\pi A e}$$

$e$  = lift efficiency factor for the wing/jet combination (Ref. 6)

$$C_{DM} = \text{momentum drag coefficient} = \frac{mV}{qS}$$

$C_F$  = thrust component of the static jet reaction

The jet-off value of the drag coefficient,  $C_{DB}$ , is very large compared with the theoretical prediction and is no doubt due to flow break-away in the trailing edge region, aggravated by the presence of the control ring. The jet-on value, though impossible to measure directly, would likely be considerably smaller and hence no attempt is made to separate out  $C_{Di}$  in the analysis but to combine it with  $C_{DB}$ .

The momentum drag coefficient,  $\frac{mV}{qS}$ , includes the variation of mass flow through the fan and engines with forward speed, angle of attack, height above ground and engine RPM. Ref. 4 details the method of mass flow determination; a summary of the method is given here in Section 4.2.1.

The jet reaction contribution to propulsive thrust, given by

$$C_F = KC_j \sin(\theta_S - \alpha_C)$$

is subject to the same effect of flow pattern change as the lift component. In addition, some measure of thrust recovery would be expected considering the blunt leading and trailing edges on the Avrocar. The theoretical maximum thrust recovery increment is  $X_G [1 - \sin(\theta_S - \alpha_C)]$ . As for  $C_{LF}$ , the variation of  $X_G$  with forward speed, etc. is included.

The total pitching moment coefficient is written as

$$C_M = C_{MB} + C_{Mi} + C_{MS}$$

with notation as for  $C_L$  and  $C_{D-F}$  except that the jet reaction moment is assumed to be unaffected by forward speed, etc.



#### 4. DISCUSSION OF RESULTS

##### 4.1 Aerodynamic Characteristics - Power Off

Initial tests of the Avrocar in its basic configuration with power off and fan intake open showed that a large volume of air actually passed through the machine, especially at negative angles of attack, and the test results were therefore of little or no value. Sealing the fan intake with a plywood cover enabled consistent data to be obtained (Figs. 2 to 12).

Jet-off tests with a rounded trailing edge are of limited interest for two reasons. Firstly, the rounded trailing edge permits the rear stagnation point to wander, resulting in a low lift curve slope. Secondly, the rounded trailing edge will thicken the wake giving high profile drag - particularly so on an already thick aerofoil ( $t/c = 0.20$ ). With most jet flap schemes the presence of the jet rectifies both these faults.

First consider the lift curve slope, jet-off, for Runs 30, 33, 45 and 49 (Figs. 2 to 5). Measured values of  $\frac{dC_L}{d\alpha}$  range from 1.3 to 1.4

per radian compared with an expected theoretical value of approximately 1.8 derived from simple lifting line theory (Ref. 7) with the introduction of two factors  $n$  and  $\omega$ , where  $\omega = 2n$ .

For the circular wing with an aspect ratio of  $4/\pi$

$n = .6221$  and the sectional lift curve slope

$a = .672 a_0$  where  $a_0 = 2\pi$ , the theoretical two dimensional lift curve slope for this wing.

We then have

$$C_L = a (\alpha - \alpha_i) \text{ where } \alpha_i = \frac{\omega C_L}{\pi A}, \text{ the induced angle}$$

of incidence

$$\therefore C_L = \frac{a \alpha}{1 + \frac{\omega a}{\pi A}}$$

$$\therefore \frac{dC_L}{d\alpha} = a / (1 + \frac{\omega a}{\pi A})$$

$$\text{Putting } a = .672 a_0 = 4.221$$

$$\omega = 2\pi = 1.267$$

$$\text{and } A = 4/\pi$$

$$\text{then } \frac{dC_L}{d\alpha} = 1.80 \text{ per radian.}$$

Taking into account aerofoil thickness and flow viscosity effects, Ref. 7 suggests that

$$a_0 = 2\pi k (1 + \epsilon)$$

where

$$k = .92 \text{ and accounts for lift reduction due to the boundary layer}$$

$$\text{and } \epsilon = 0.8 (t/c)$$

$$\text{Therefore } a_0 = 2\pi \times 1.06 \text{ and hence } \frac{dC_L}{d\alpha} = 1.85 \text{ for the Avrocar wing.}$$

If we assume that the measured value of lift curve slope is below the theoretical prediction solely because of degradation in  $a_0$  due to wandering of the stagnation point then we may estimate the extent of this degradation as follows:

$$\text{The measured value of } \frac{dC_L}{d\alpha} = 1.4 = \frac{a}{1 + \frac{\omega a}{\pi A}}$$

so that  $a = 2.51$ . But by theory,  $a = 4.221 \times 1.06$ . Hence the reduction in lift curve slope due to wandering of the rear stagnation point is 44% or, in other words, the sectional lift curve slope is only 56% of its theoretical value with a sharp trailing edge.

Next consider the drag coefficient. With jet off the span loading should be elliptic with the induced drag given by  $\frac{C_L^2}{\pi A}$ . The fact

that the trailing edge is rounded and the lift curve slope lower than expected should not affect this. However, profile drag is large and will vary approximately with  $\alpha^2$ . At a given lift coefficient the wing angle of attack is much greater than it would normally be (due to the low lift curve slope) and the profile drag will be correspondingly higher.

A plot of  $C_D$  vs  $C_L^2$  (Fig. 6) reveals a low value of the wing lift efficiency,  $e$ , of about 0.5,

$$\text{where } C_D = C_{D_0} + \frac{C_L^2}{\pi A e},$$

and it seems probable that this is largely due to the high profile drag.

The presence of camber will modify the drag curve such that the minimum drag no longer occurs at  $C_L = 0$  and the  $C_D$  vs  $C_L^2$  curve is not necessarily linear. We therefore write

$$C_D = C_{D_0} + k(\alpha - \alpha_{\min})^2 + \frac{C_L^2}{\pi A}$$

where  $k(\alpha - \alpha_{\min})^2$  represents the variation of profile drag with angle of attack,  $\alpha_{\min}$  being the angle for minimum drag.

$$\text{Now } C_L = a(\alpha - \alpha_o)$$

where  $a$  = measured lift curve slope

and  $\alpha_o$  = angle for zero lift

$$\therefore C_{L_{\min}} = a(\alpha_{\min} - \alpha_o)$$

$$\therefore (C_L - C_{L_{\min}}) = a(\alpha - \alpha_{\min})$$

$$\text{Hence } C_D = C_{D_0} + \frac{k}{a^2} (C_L - C_{L_{\min}})^2 + \frac{C_L^2}{\pi A}$$

Plots of  $(C_D - \frac{C_L^2}{\pi A})$  versus  $(C_L - C_{L_{\min}})^2$  (Figs. 7 and 8) show

a linear relationship with the value of  $\frac{k}{a^2} = 0.2$  approximately, for positive angles of attack, and about 1.0 for negative angles, although here there was no consistency between the four tests.

$C_{L_{\min}}$  appears to be about 0.1 for all cases and the minimum drag coefficient, power-off, is in the range .05 to .07.

Finally, in considering the power-off tests, the  $C_m$  vs  $C_L$  curve is plotted (Figs. 9 to 12). It is fairly linear over the  $C_L$  range -0.2 to 0.3 with  $d C_m / d C_L = .328$  as compared with the theoretical value of .269 from Ref. 7.

#### 4.2 Basic Aircraft Configuration, Power-On, Static Tests

##### 4.2.1 Effect of Power on Lift and Nozzle Thrust

Static lift values with neutral control were comparable to those measured in the static test rig at Malton when corrected on the assumption that the engine inlet temperature was the same as the fan inlet, an assumption necessary because of the failure of the engine inlet temperature instrumentation. (Figs. 13 and 14).

In the tunnel, instrumentation for determining the total jet momentum at exit, or nozzle thrust, consisted of six gangs of total pressure tubes and six gangs of static pressure tubes in the annular nozzle (Ref. 2 and 4). The effect of ganging was to introduce errors in the average values recorded, particularly true in the case of static pressure, and instead of basing nozzle thrust and mass flow entirely on the nozzle rakes it became necessary first of all to use the intake static pressures for mass flow determination at zero forward speed. Engine mass flow was added from known engine characteristics and the ganged nozzle total/static pressure ratio was used to correct the static mass flow values for variation of angle of attack, height above ground and forward speed.

Secondly, the nozzle gross thrust was calculated using the expression

$$X_G = M_{jc} V_j$$

where  $M_{jc}$  = corrected intake flow

and  $V_j$  = potential jet velocity based on the ratio of the ganged total pressure at the nozzle to tunnel static pressure.

The level of nozzle thrust obtained in this manner was then somewhat higher than that indicated by the static test rig, despite the fact that the nozzle rakes were further upstream for the static rig tests. A not insignificant loss of thrust is caused by the presence of the undercarriage legs and fairings in three of the radial ducts. Because of the possibility of unduly low total pressure readings in the wake of these obstructions, the three ducts involved were avoided when installing the peripheral nozzle rakes. The magnitude of the nozzle thrust for the Ames tests is therefore to be accepted with caution.

#### 4.2.2 Effect of Extended Lip on Static Lift and Thrust

Also shown on Figs. 13 and 14 are the curves for the aircraft with a one inch extension on the control ring trailing edge (Fig. 15). It is seen that, although the reduction in nozzle exit area caused a corresponding reduction in nozzle thrust, the measured lift actually increased. It is concluded that the extended lip more effectively focussed the peripheral jet (Fig. 16) and thereby reduced the external mixing losses. In fact, the free-air thrust efficiency (K) with the extended lip was improved 22% compared with the aircraft with the standard control ring.

#### 4.2.3 Pitch Control Power, Static Tests

The object of the focussing ring control is to produce a maximum shift in centre of pressure position and a maximum longitudinal force for a minimum loss in lift. The performance achieved is shown in Figs. 17, 18 and 19, and is compared with the 1/20th scale model test data. The disappointing aircraft results prompted the modification to the control ring whereby it was first moved 3-1/2 inches aft of neutral, denoted by  $J_e = 1.75$  (the normal travel being  $J_e = \pm 1.0$  i.e.  $\pm 2$  inches), and then the rear  $120^\circ$  of the control ring was removed, the position of the remaining  $240^\circ$  being denoted by  $J_e = 1.75$ . With this configuration a resultant force vector inclination of  $32^\circ$  to the vertical was obtained with almost no loss of resultant force.

With the extended lip configuration control power was reduced considerably e.g. cp shift at  $J_e = 1.0$  was 4.7% as compared with 7.6% approximately for the normal focussing control ring (c.f. Figs. 18 and 21).

#### 4.2.4 Rudder Power, Static Tests

For all configurations, collective operation of the rudder vanes produced a static thrust of 100 lbs. and a static lift loss of about 100 lbs. The maximum available yawing moment would be approximately 800 lb. ft.

#### 4.3 Lift, Drag and Pitching Moment (Power-on, Wind-on, without ground board)

At the beginning of the program each control configuration was tested at tunnel speeds corresponding approximately to dynamic head values of 5, 10 and 15 lb/sq.ft. Later, this range was extended to  $q = 20$  and 25 lb/sq.ft. and finally a few tests were



conducted at  $q = 35$ . In addition, for each configuration, static values of lift, drag and pitching moment were obtained. Most tests were conducted at 90% max. engine r.p.m.

With a jet lift system, the jet coefficient becomes one of the similarity parameters in addition to Reynolds number and Mach Number. Full scale testing permits close approximation to Reynolds number, and the low velocity precludes serious consideration of Mach Number. It is the jet coefficient which then becomes the most important similarity parameter implying as it does that the ratio of jet velocity to flight velocity remains constant.

Tests at various tunnel speeds and fixed engine speed can then be interpreted in terms of variation in  $C_j$ . If jet effects on the aerodynamic characteristics were small then plots of coefficients would show little variation with tunnel speed (i.e. with  $q$ ). Any spread will then indicate the magnitude of influence of the jet. Influence of the jet must necessarily include the effects of fan inlet flow.

#### 4.3.1 The Measured Forces

As already explained, the basis of analysis used here is to separate the pressure or aerodynamic force from the total measured force by subtracting the jet reaction and then to study these pressure forces to find the way in which the wing is operating in the presence of the complicated jet flow pattern. To do this it is necessary to obtain reliable estimates of the jet reaction in terms of lift, drag and moment. Normally, when the nozzle and jet is well defined it is satisfactory to use the measured forces and moments at zero tunnel velocity - that is, the static values. However, in the case of the Avrocar, inspection of the measured forces and their variation with  $q$  showed that this procedure was not always reliable. In fact it was shown that distinct changes in the reactive forces and moments often took place between  $q = 0$  and  $q = 5$  and that further increase in speed apparently had little effect.

Plots of the variation of measured forces and moments versus  $q$  and versus  $\alpha$  are given for all runs in Ref. 4. These take a certain form which may be derived from simple considerations. Consider, for example, a conventional moment characteristic given by

$$C_m = C_{m_0} + k, C_L$$

If  $C_L$  varies linearly with  $\alpha$  then

$$\begin{aligned} C_m &= C_{m_0} + k_2 (\alpha - \alpha_0) \\ &= C_{m_0} + k_2 \alpha \end{aligned}$$

$$\text{Hence } M = (C_{m_0} S \bar{c} + k_2 S \bar{c} \alpha) q$$

and the variation of  $M$  versus  $q$  with  $\alpha$  as parameter would form a series of straight lines which intersect at the origin defined by  $M = 0, q = 0$ . (See Fig. 22, diagram 1).

When jet flow is added a constant reactive moment will exist which, for the present, we shall assume to be independent of both  $\alpha$  and  $q$ . The aerodynamic constants may be different but they seem to obey the same laws as given above and pitching moment is then given by

$$M = M_R' + (C_{m_0} S \bar{c} + k_2 S \bar{c} \alpha) q$$

where  $M_R'$  is the effective reactive moment due to jet.

The variation of moment with  $q$  and  $\alpha$  again takes the same general form except that the point of intersection is no longer at the origin. (See Fig. 22 diagram 2).

Now in many cases the Avrocar results for values of  $q = 5$  and above exhibited this simple form and experimental points formed a fan of lines intersecting at  $q = 0$ . However, the static measured value of moment ( $M_R$ ) and the value of the  $M_R$  given by this intersection did not coincide. This is illustrated in diagram 3 of Fig. 22. An example of Avrocar results is given in Figs. 23 and 24 for control position  $Je = 1.75$ . The measured value of  $M_R$  in this case was -2900 lb.ft; the effective value for  $q > 5$  was zero. The point at which the  $M$  vs  $\alpha$  curves intersect also indicates the effective value of  $M_R$  (see Fig. 24). In some cases the variations are not quite linear and this may be due to jet effects.

This method of obtaining the effective value of  $M_R$  is open to a certain amount of variation due to differences in the interpretation of experimental points (especially where few test points are available) but results given in Fig. 25 indicate very definite trends. This graph shows variation of measured static moment ( $M_R$ ) with control position and these are compared with the effective values ( $M_R'$ ). The measured static values of  $M_R$  show an almost linear variation with  $Je$  and for full aft position ( $Je = 1.75$ ) the control generated 2900 lb.ft. of nose down moment. However, the effective

values for  $J_e = 0.5$ ,  $1.0$  and  $1.75$  are all zero and therefore, as a reactive control with wind on, the system was completely ineffective. However, for negative control positions, large effective nose-up moments existed.

With these ideas in mind, the whole series of graphs in Ref. 4 showing measured forces vs  $q$  and vs  $\alpha$  may be inspected and further conclusions drawn.

For example, we may examine the variation of lift with  $\alpha$  for Run 17 (Fig. 26). Once again curves for various values of  $q$  intersect in a point. At this point  $C_{LB+i}$  is evidently zero and there is therefore no variation of lift with  $q$ . It should be noted that the variation with  $\alpha$  of the static values of lift, i.e. the  $q = 0$  values, have been computed from a single test point at  $\alpha = 0$ . (This simply takes care of the change in direction of the force vector as  $\alpha$  changes. In contrast, the static moment  $M_R$  has no variation with  $\alpha$ ).

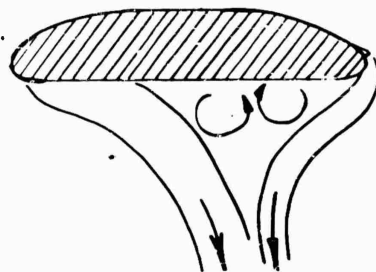
Another point of interest is this, that for all early tests (up to run 20), both with and without the rear part of the control ring removed, the  $q = 0$  values of lift intersected at the focal point formed by the curves at other  $q$  values. However, for tests in which the rear  $80^\circ$  formed a 'jet flap' over the wing tip (run 31 onward), this no longer remained so. Run 38, which has been reproduced in Fig. 27, is an excellent example of this.

This means that, whereas for the early test runs, only the static moment showed this peculiar shift between  $q = 0$  and  $q = 5$ , the latter tests with trailing edge jet flap, lift, drag and moment all exhibited a shift in the low speed range. The remaining graphs for Run 38 are given in Figs. 28 and 29. Effective static values have been shown as dotted lines and when these are used to compute new static variations of lift and drag it can be seen that they conform more nearly to a consistent pattern with the curves at other values of  $q$ .

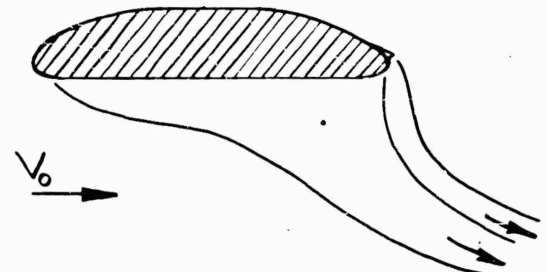
It has been shown that, for all the early tests (up to run 20) the nose down static moment generated at aft control positions disappeared at values of  $q$  greater than five. For runs 38/39 and for run 43 this trend was reversed and the in-flight values of effective static moment were more nose down.

In view of the above considerations, values of pressure force coefficients such as  $C_{mb+i}$  and  $C_{Lb+i}$  have been evaluated in two ways, first using the measured static values of lift, drag and moment and secondly using the 'effective' values. (See Section 4.4).

The reason for this apparent change in the reactive forces is not altogether clear but we do know that conventional jet flap schemes with the jet at the trailing edge do not show this change. It is quite likely therefore that the phenomenon is associated in some way with areas or pockets of separated flow which exist in the static case but disappear at moderate wind speeds. For example, we can consider runs 38/39 and refer to the sketch below:



Sketch 1 A

Suggested Flow Pattern  $q = 0$ 

Sketch 1 B

Suggested Flow Pattern  $q = 5$ 

In the static case it has been suggested that the thin jet from the rear  $80^\circ$  of the periphery will coalesce with the remaining jet forming a separated region of flow on the rear underside. (see sketch 1 A). The low pressure due to the region of separation results in a nose-up pitching moment. The effect of forward speed is then to sweep away the pocket of separation and restore the apparent reactive moment to its true value (see sketch 1 B) which, in this case, was more nose down. (See Fig. 29).

In the case of a clearly defined nozzle it is not likely that the reactive force itself can change with forward speed. In some configurations however, the Avrocar nozzle is not too well defined and the possibility of change in the reactive force with speed cannot be ruled out as an alternative explanation of this phenomenon.

Another insight into the pattern of the measured lift forces is obtained by the application of the theory of Ref. 8, Stratford's straight mechanical flap analogy of the jet flapped wing. It is shown that the total lift coefficient for a jet flapped wing at its angle of

attack for zero lift, jet-off, is given by

$$\begin{aligned} C_{L_o} &= C_{L_i} + C_{L_F} \quad (C_{L_B} = 0) \\ &= 2 (2\pi C_j \gamma \sin \theta)^{1/2} \left( 1 + \frac{\pi}{48} C_j \frac{\sin \theta}{\gamma} + \dots \right) \end{aligned}$$

$$\begin{aligned} \therefore L_o &= C_{L_o} qS = C_{L_o} \frac{1}{2} \rho U_o^2 S \\ &= 2U_o \left( \pi \rho J S \gamma \sin \theta \right)^{1/2} \left( 1 + \frac{\pi}{48} C_j \frac{\sin \theta}{\gamma} + \dots \right) \end{aligned}$$

Section 4.6.2 shows that there was little change of either mass flow or gross thrust with forward speed and therefore little change of jet momentum  $J$ . Hence the total lift force,

$$\begin{aligned} L_o &= K_1 U_o (1 + K_2 C_j) \\ &= K_1 U_o + \frac{K_3}{U_o} \end{aligned}$$

For the higher values of  $U_o$  therefore the second term becomes small compared with the first and the lift is proportional approximately to forward speed. At zero forward speed, however, the lift becomes infinite theoretically.

Referring to Figs. 2 to 5 the angle of attack for zero lift, jet-off, is seen to be in the region  $-2^\circ$  to  $-4^\circ$ . Plots of lift versus forward speed are given in Figs. 30 to 33 where it can be seen that for angles of attack in the neighborhood of  $-3.2^\circ$  a linear relationship holds good except for Configuration D-1 which, of course, can hardly be considered to be a jet-flapped wing.

The fact that the lift curves appear to emanate from the measured value of the static lift reaction (rather than the effective value) is not thought to be necessarily significant since there is no known theoretical reason why the curves should be straight lines in this low speed region.

A further examination of possible flow patterns for configurations with the rear  $120^\circ$  "jet flap" (e.g. Runs 38, 39) has produced the sketch, Fig. 34. Two pockets of separated flow, one on each side of the longitudinal plane of symmetry, are suggested, perhaps containing vortices trailing aft under the jet flap sheets above a certain forward speed.

#### 4.3.2 Drag - Wind-on and Jet-on

The breakdown of measured values of thrust-drag into components yields "basic plus induced" values which are small in comparison with the intake momentum drag and the jet reaction force. And since neither of these is easily determined with accuracy in forward flight, the computed magnitude of  $C_{DB+i}$  is not accepted with much confidence.

A method was evolved to provide a check on mass flow calculated from the intake static pressures. A plot of D-F versus free-stream velocity is made at constant  $\alpha$  corresponding to zero  $C_{Lb+i}$  (Fig. 35) and the tangent to the curve at  $V = 0$  is drawn. The slope of the tangent is then equal, approximately, to the total intake mass flow (i.e. fan and engine intake flow). Certain assumptions have to be made, of course. These are:

- (i) that the mass flow is constant with speed. This is believed to be a close approximation for most of the configurations tested. For reasons unknown, however, configuration A-1 showed a much greater variation of mass flow with both forward speed and angle of attack as determined from the peripheral nozzle instrumentation.
- (ii) that the horizontal component of jet reaction force remains constant with speed. In some cases this may not be so, but it is usually possible (see Section 4.3.1) to determine an effective wind-on value.
- (iii) when drawing the tangent to the D-F versus V curve, a certain amount of intuition is called for on occasions. Some guidance is obtained by assuming that the difference in drag between the "mass flow tangent" and the D-F curve (a relatively small quantity) varies as the velocity squared. This implies the assumption that  $C_{DB+i}$  is constant with speed, whereas it almost certainly varies slightly with the change of  $C_j$ .

However, within the limits of these assumptions, fairly close agreement was obtained between mass flow estimates based on this method and on the intake static probes.

#### 4.3.3 Aerodynamic Characteristics - Power On (No ground board)

##### General Remarks

Problems encountered by the Avrocar in the Ames Tunnel may be summarized as follows:

- (i) Presence of large nose up moments
- (ii) Low control power of the focussing ring control
- (iii) Absence of jet vectoring control

There were three sources of nose-up moment. First, large effective nose-up reactive moments (greater than the static measured values) occurred for all control positions. This has already been discussed in Section 4.3.1 and is illustrated in Figs. 23 to 25. Secondly, there existed an aerodynamic nose-up moment which is independent of control position and due to the intake flow. Also, the results showed a position of aerodynamic centre far forward on the wing and this provided a greater penalty for generating aerodynamic lift in terms of nose up moment than normally would have been expected.

Low control power of the focussing ring control was due to its inability to generate large induced values of lift coefficient; in other words, it was a rather poor jet flap. Low control power was also partly due to the virtual disappearance of the reactive moment (see Section 4.3.1 and Fig. 25).

With regard to jet vectoring, it was expected that the focussing ring control would deflect the jet through greater angles than it did (Fig. 19) and that such angles of deflection would provide the necessary trim power. As a result of the tests it is now apparent that means for jet vectoring must be separated from the pitch control and schemes which do this will be incorporated for the second series of Ames Tunnel tests.

A few general comments may be in order concerning the low value of lift curve slope and forward position of the aerodynamic centre which were measured in the tunnel. We refer here to the characteristics of the total pressure forces and moments, that is to  $C_{L_{b+i}}$  and  $C_{M_{b+i}}$ . The centre of aerodynamic lift, as angle of attack changes, should theoretically occur at about 26% of the centerline chord ahead of the center of aircraft. In fact, in the Ames tunnel, we find values at 47% of the centerline chord. We also note that the lift curve slope is about 1.0 per radian, see Table 1, instead of an expected theoretical value of about 1.85 or more.

Together, these two facts suggest that the effective aspect ratio is lower than the geometric value. Wing lift curve slope is known to fall as aspect ratio becomes smaller. Also, the theory for low

aspect wings suggested by D. Kuchemann (Ref. 7) is based on a corresponding forward movement of the aerodynamic center. The question arises, why should the Avrocar exhibit characteristics corresponding to an aspect ratio less than its geometric value? It has been suggested that the focussed jet flow is the cause of the trouble and that the pair of trailing vortices which normally stream from the wing tip are sucked under and toward the center by the inward flow of the jet. The pair of trailing vortices are then much closer together than they otherwise would be and the effective aspect ratio of the wing is thereby reduced. It has been proposed for future tests that the jet at the sides (or wing tip) be allowed to stream outward and backward (see Section 5) and it is expected that this will not only rectify the problem but possibly even reverse the trend and provide an effective aspect ratio greater than the geometric value.

Finally, it is pointed out that results of the tests fall into two distinct groups. Group one (Runs 1 to 27 and Runs 45 and 46) which contains all tests on the focussing ring control as originally designed or with modifications. Group two (Runs 28 to 44) which contains all runs with simulated jet flap over an  $80^\circ$  arc at the rear, albeit with the remaining  $240^\circ$  focussed. In addition, three tests were conducted (Runs 47 to 49) with the rear  $80^\circ$  of wing tip removed and the jet deflected by means of a spoiler in the nozzle.

Analysis of results is then concentrated on comparison between the two types of control schemes represented by group one and group two. Results are also compared to model tests of Project 1794 and of the Avrocar.

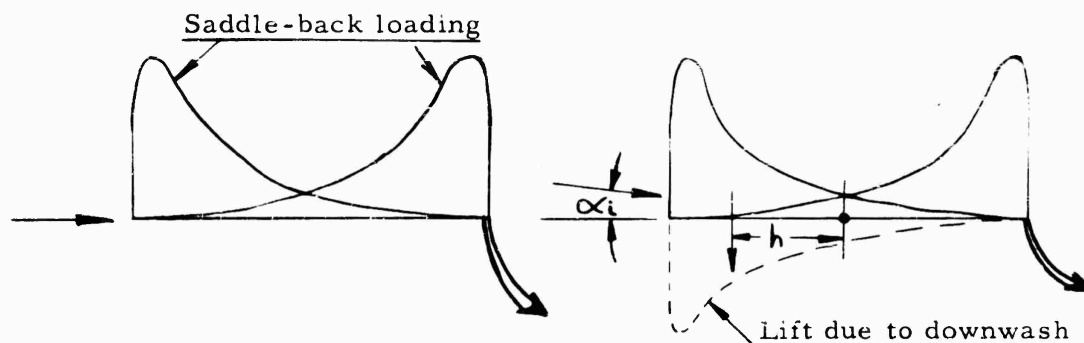
#### Control power of the jet-flapped wing

The jet flap is a device for generating aerodynamic lift at zero angle of attack and it does so by providing an approximately symmetric or "saddle-back" chordwise aerodynamic load distribution with centre of lift approximately at the half chord point. In addition, there is a lift component of jet reaction which acts at the nozzle.

In order to assess the control effectiveness of the two Avrocar control schemes tested in the tunnel an approximate theory has been developed which relates the change in nose down aerodynamic control moment at zero incidence to the increment in lift. Experimental values of lift at  $\alpha = 0^\circ$  are then used to predict the expected value of nose down control moment and this is compared to the experimental value.



An expression for control moment may be derived as follows:



Infinite aspect ratio

Finite aspect ratio

Lift due to jet flap

Consider a symmetrical wing section of infinite aspect ratio at zero incidence.

Let the increase in lift due to the jet flap be  $C_{LJ\infty}$

Now consider an elliptic wing of aspect ratio  $A$  and with the same jet strength (defined in terms of  $C_j$ , the jet coefficient)

Then using the wing theory of Ref. 7 we have downwash  $\alpha_i = \frac{\omega C_{LJ}}{\pi A}$

where  $C_{LJ}$  is the resulting lift coefficient defined by

$$C_{LJ} = C_{LJ\infty} - a \alpha_i$$

where 'a' is the sectional value of lift curve slope. We then have

$$C_{LJ} = C_{LJ\infty} - \frac{\omega a}{\pi A} \cdot C_{LJ}$$

$$\text{or } C_{LJ} \left[ 1 + \frac{\omega a}{\pi A} \right] = C_{LJ\infty}$$

$$\text{and } \frac{C_{LJ}}{C_{LJ\infty}} = \left[ \frac{1}{1 + \frac{\omega a}{\pi A}} \right]$$

where once again, for the circular planform of aspect ratio  $4/\pi$  and  $t/c = .20$   $\omega = 1.267$  and  $a = 4.221 \times 1.06$  (see para. 4.1)

Hence 
$$\frac{C_{LJ}}{C_{LJ\infty}} = .414$$

If we now assume that the chordwise loading due to jet flap is exactly symmetrical then the nose down aerodynamic moment about the half chord point is zero for the wing of infinite aspect ratio. There is then no "aerodynamic" control power and the reactive force provides the only moment.

For the wing of finite aspect ratio the aerodynamic pitching moment coefficient is entirely due to the induced angle of attack  $\alpha_i$  (with the above assumption of symmetry) and is given by:

$$-\left[ C_{LJ\infty} - C_{LJ} \right] \left( \frac{h}{c} \right) = C_{mJ}$$

$$\therefore \frac{C_{mJ}}{C_{LJ}} = - \left[ \frac{C_{LJ\infty}}{C_{LJ}} - 1 \right] \left( \frac{h}{c} \right)$$

and 
$$C_{mJ} = - \left( \frac{\omega a}{\pi A} \right) \left( \frac{h}{c} \right) C_{LJ}$$

where the value of  $\frac{h}{c}$  may be found from the slope of the  $C_{mb+i}$  vs  $C_{Lb+i}$  curve for the case under consideration.

In general it can be expected that this simple expression will overestimate the control moment of the jet flap since the saddle-back loading is not truly symmetrical and the forward peak is usually higher than the rear one. This fact comes about because the bound vortex elements are no longer confined to the wing as in classical aerofoil theory but now exist in the trailing jet sheet also.

According to the theory of Ref. 7 the values of ' $\omega$ ' and ' $a$ ' vary with aspect ratio and with the value of two dimensional lift curve slope of the section. In the case of the Avrocar, power off, the two dimensional lift curve slope has already been shown to be only about half the theoretical value of  $2\pi$  on account of the rounded trailing edge. Also, we have already referred to the low effective aspect ratio of the Avrocar with jet on.

We then have three cases of interest.

- 1) The circular planform in theory, with sharp trailing edge.
- 2) The circular planform with rounded trailing edge.
- 3) The circular planform with focussed jet and low effective aspect ratio of  $2/\pi$  (compared to geometric value of  $4/\pi$ )

Values of  $\frac{\omega a}{\pi A}$  and other pertinent factors have been evaluated and are given in the table below:

Case Number	A	$\eta = \omega / 2$	a	$\frac{dC_L}{d\alpha}$	$\frac{C_{LJ}}{C_{LJ\infty}}$	$\frac{\omega a}{\pi A}$
1	$4/\pi$	.634	4.22	1.805	.427	1.335
2	$4/\pi$	.634	2.51	1.40	.557	.795
3	$2/\pi$	.719	3.19	.966	.304	2.29

We are now in a position to apply the theory to some experimental results.

Consider first, the Avrocar in the Ames tunnel, power off (case 2 applies)

The theory has been derived for a saddle-back loading but will apply equally to the symmetrical chordwise load distribution which should result from symmetrical camber on the Avrocar.

Experimental values give  $C_L \alpha = 0 = .075$ ;  $\frac{dC_m}{dC_L} = \frac{h}{c} = .348$

(Figs. 2 and 11)

Using suffix C for camber in place of suffix J we have

$$C_{mC} = - \frac{\omega a}{\pi A} \cdot \frac{h}{c} \cdot C_{LC} = C_m \alpha = 0$$

$$= - .795 \times .348 \times .075 = - .021$$

The experimental value of  $C_m \alpha = 0$  is  $-.025$ , which represents tolerable agreement.

Consider next, results obtained from the model of Project 1794 in the twenty foot tunnel at WADC (Ref. 9). For these tests the values of lift curve slope and position of aerodynamic centre were found to be close to theoretical predictions for the circular planform. Factors given in the table for case I will then apply.

$$\text{Then } C_{mJ} = -1.335 \times .265 \times C_{LJ}$$

$$\frac{C_{mj}}{C_{LJ}} = -.354$$

Comparison of theory with experiment is given in Fig. 36 and we find that the simple theory greatly overestimates the control power. In fact the predicted control power is approximately three times the experimental value. This means that the a.c. of the saddle-back loading is not at the centre as was assumed but is further forward and provides a nose-up moment which detracts from the control power of the configuration. The reason for this has already been mentioned and some idea of the forward shift in a.c. of the saddle back loading may be found as follows:

The moment due to the jet flap control scheme of the circular planform wing may now be written

$$C_{mJ} = -\left(\frac{\omega a}{\pi A}\right) \left(\frac{h}{c}\right) C_{LJ} + C_{LJ} \omega \left(\frac{h}{c}\right)'$$

where  $\frac{h}{c}$  is the aerodynamic centre position for the saddle-back

$$\begin{aligned} \text{loading} &= -\left(\frac{\omega a}{\pi A}\right) \left(\frac{h}{c}\right) C_{LJ} + C_{LJ} \left(1 + \frac{\omega a}{\pi A}\right) \left(\frac{h}{c}\right)' \\ &= C_{LJ} \left[ \left(\frac{\omega a}{\pi A}\right) \frac{h}{c} - \left(1 + \frac{\omega a}{\pi A}\right) \left(\frac{h}{c}\right)' \right] \end{aligned}$$

Project 1794 results indicated that the simple theory overestimated the control power by a factor of three

$$\text{that is } \frac{\left(\frac{\omega a}{\pi A}\right) \frac{h}{c}}{\left(\frac{\omega a}{\pi A}\right) \left(\frac{h}{c}\right) - \left(1 + \frac{\omega a}{\pi A}\right) \left(\frac{h}{c}\right)'} \approx 3$$

$$\left[ \frac{1}{1 - \frac{\left(1 + \frac{\omega a}{\pi A}\right) \left(\frac{h}{c}\right)'}{\left(\frac{\omega a}{\pi A}\right) \left(\frac{h}{c}\right)}} \right] \approx 3$$

$$\left[ 1 - \frac{(1 + \frac{\omega_a}{\pi A}) (\frac{h}{c})'}{\frac{\omega_a}{\pi A} (\frac{h}{c})} \right] \approx 0.333$$

$$\frac{(\frac{h}{c})'}{(\frac{h}{c})} \cdot \left( \frac{1 + \frac{\omega_a}{\pi A}}{\frac{\omega_a}{\pi A}} \right) \approx .666$$

$$\text{so that } (\frac{h}{c})' \approx 0.666 \times .265 \times \frac{1.335}{2.335} = .101$$

that is, the centre of lift of the saddle-back or induced loading due to 'jet flap' was, in this case, approximately 10.1% of the centre line chord ahead of the centre of wing.

This then provides some background to the control power which may be expected from a jet flap scheme on a circular planform wing and with this in mind we now consider some Avrocar results. Ames results and 1/20 scale Avrocar model results are shown in Fig. 37 and, although the slope of the curves are of the same sense, there exists, in the case of the Ames test a large nose up moment corresponding approximately to  $\Delta C_m = +0.16$ . The 1/20th scale model tests, Ref. 5, shown here correspond to the new configuration which will be evaluated during the second series of Avrocar tests in the Ames tunnel (Ref. 10).

The existence of the nose-up moment means that high control power must be available from the Avrocar control scheme. The main advantage of the new Avrocar configuration seems to be that, by spreading the side jets outward and rearward (instead of inward toward the centre), much greater values of lift increment are obtained from the jet flap scheme. These higher values of lift increment can be expected to induce stronger nose down moments as already shown. (See Section 4.7 following).

The large nose-up moment is apparently due to intake flow. In the case of Project 1794 it did not exist since  $C_{m\alpha=0}$  tended to zero as  $C_{L\alpha=0}$  tended to zero (see Fig. 36). This was no doubt partly due to the fact that there were intakes on both top and bottom surfaces on this model and any intake effects would be self compensating. It is worth noting, however, that the nose-up moment is not necessarily altogether a bad thing for this reason. The low aspect ratio of the circular wing means low lift curve slope; this in turn means that a high angle of attack is required to provide lift which probably results in high profile drag of the thick wing section.

We therefore wish to provide some lift by means of 'jet-flap' and hold the angle of attack at cruise close to zero. It is then necessary to have just the right amount of nose-up moment to balance the nose-down moment from the jet flap. The moment due to intake is discussed further in the next section.

#### 4.3.4 Effect of Intake Flow

A considerable amount of research work has been undertaken to establish the fundamental characteristics of the jet flap (Ref. 11) but there is not much information available on the effect of intake flow which can be applied to fan-in-wing designs. In particular, a theoretical analysis would be very useful, and we are studying a potential flow solution which may be of some help in this regard (Ref. 12). In the meantime, we must rely largely on experimental results and the main difficulty here is that it is seldom possible to isolate the effects of the intake; for example, in the case of the Avrocar itself, and for most fan-in-wing models, intake flow cannot be provided without a corresponding jet flow. Induced values of lift and moment must therefore contain effects of both jet and intake flows. This difficulty has been overcome, in the case of the Avrocar, because the induced lift due to intake has been shown to be small.

Fig. 37 shows values of pitching moment obtained from the 1/20th scale model and from the Ames tests. It has been shown in Section 4.3.3 how the slope of these lines provides a measure of the moment correction due to jet lift and how the upward shift of the lines provides a measure of the nose-up intake moment. Note how the Ames "jet off" point lies close to the line through the origin - the lift in this case being due to wing camber - for which there is no corresponding intake flow or nose-up moment. This graph, however, provides a measure of the nose-up moment for only two specific cases, namely, the Avrocar in the Ames tunnel at 90% max. rpm and  $q = 15$  and for the 1/20th scale Avrocar model with jet supply pressure of 50 psig and  $q = 17$ .

A special series of tests was therefore carried out on the 1/20th scale model to extend our knowledge of this problem.

All test work so far suggests that, in the case of the Avrocar, the induced lift due to intake flow is very small and this means that, if we study the moment characteristics at zero  $\alpha$ , then any change in lift can be attributed to the exit jet flow and the pitching moment due to this jet lift computed according to the method given in Section 4.3.3. The measured change in moment can then be corrected

for jet lift effect and the moment due to intake found. If the jet deflection angle is kept small (or set at zero) then the nose-up moment due to intake flow is large compared to the jet flow correction and in this way an accurate assessment of the intake moment may be obtained.

Tests were therefore carried out on the 1/20th scale model set at zero  $\alpha$  and with zero jet deflection angle. Tests were made at  $q = 5.2$  and  $q = 18 \text{ lb/ft}^2$  for a range of supply pressures of 10, 20, 30, 40 and 50 psig. Results are given in Fig. 38 in the form of  $C_{m_i}$  vs  $C_{L_i}$  where these coefficients represent the difference between jet-on and jet-off for each case. Even though the jet deflection angle at the rear was set at zero there still remained some jet induced lift - this is so because the zero setting is only nominal and, also, the side jets are directed downward at  $30^\circ$ . Changes in lift have therefore been attributed solely to jet effects and corrections applied accordingly. Resulting values of moment due to intake are plotted vs. supply pressure in Fig. 39.

Variation of supply pressure from 10 to 50 at  $q$  of 18 is shown in Fig. 38 to change the lift coefficient from .065 to .125, that is, a change of only .06 and some of this, we believe, is due to downward deflection of the side jets and not due to the intake itself. It is for this reason that we state that effect of inlet on lift is small. Again, if we consider the Ames tests results and compare Run 38/39 with Run 47 we come to the same conclusion. Run 38/39 had a jet flap over the rear  $120^\circ$  arc whereas in Run 47 the wing tip was removed and the jet was permitted to issue backward without deflection. At  $q$  of 15 the values of  $C_{L_{b+i}}$  for  $\alpha = 0$  were 0.27 and 0.16 respectively whereas the jet-off value is .075. With jet deflection of zero (Run 47) the induced lift was only  $(0.16 - .075) = .085$  and once again we believe that most of this can be accounted for by the presence of the remaining  $240^\circ$  of focussed jet which then leaves little, if any, lift to charge to the inlet itself.

Theoretical considerations suggest that moment coefficient would depend upon the inlet velocity ratio ( $V_i/V_0$ ) and that all results should collapse on this basis. Measurements were made of the surface static pressures just inside the inlet lip at 10, 20, 30, 40 and 50 psi supply pressure with tunnel speed zero (see Fig. 40) and the corresponding local velocity,  $V_i$ , calculated. These local velocities were assumed to provide a measure of the mean intake velocity  $\bar{V}_i$  and from previous test work, these velocities were shown to be related by  $\bar{V}_i = 0.411 V_i$ . Fig. 40 shows pitching moment due to intake plotted against inlet velocity ratio and results at  $q = 5.2$  and  $q = 18$  are seen to form a single curve on this basis.

Further we can predict the value of nose-up moment expected from the Ames tunnel tests at 90% rpm and  $q = 15$  to be 0.16 and this value agrees closely with the value shown on Fig. 37. (90% rpm at  $q = 15$  corresponds to inlet mass flow of approximately 360 lb/sec and inlet velocity ratio  $V_i/V_o = 2.13$ ).

By way of comparison, a brief analysis along similar lines has been made using results contained in NAE LR-243 and NASA TN D-88 (Refs. 13 and 14). Also, a very simplified theory is discussed which provides some background to the problem.

NAE LR-243 provides results of tests on a wing which spanned a wind tunnel and in which was located a single fan at 30 percent chord position. Ratio of fan area to wing area  $S_f/S_w$  was .027. Values of lift ( $\Delta L$ ) and moment ( $\Delta M$ ) quoted in the report have had the clean wing values subtracted from them. Data is given for a range of jet deflection angles and inspection of moment and lift for  $\alpha = -5^\circ$  (Figs. 12a and 14a of Ref. 13) and for  $\alpha = 0$  (Figs. 12b and 14b) shows directly that large changes in lift result in a negligible change in moment. This means that the moments of Figs. 12b and 14b contain no spurious jet induced moments. We may then proceed to obtain fan intake moment coefficient directly from these data. This was done for  $\beta = 60^\circ$ ,  $\alpha = 0^\circ$  and values of fan inlet flow velocity were obtained from Fig. 20. The values of intake moment derived in this way are shown in Fig. 43 of this report.

NASA TN D-88 contains results on a fan-in-wing model of aspect ratio four. Fan area to wing area is .176 compared to .077 for the Avrocar.

We again wish to separate out the nose-up couple due to intake and must therefore decide upon a value for the position of the aerodynamic centre of the induced lift whether it be due to intake or jet. The moment theory at  $\alpha = 0^\circ$  given in Section 4.3.3 applies to generation of lift of any kind and includes for example, lift due to camber, intake flow or jet flow. For an aspect ratio of four the value of  $(h/c)$  can be taken as 0.25 but the value of  $(h/c)^{1/2}$  remains unknown. Once again it is not possible to vary inlet flow and hold jet flow constant. However, tests at various jet deflection angles are given on page 35 of the report and are shown in Fig. 41 for  $\theta = 0^\circ, 10^\circ, 20^\circ$  and  $30^\circ$  for a constant value of  $C_F = 1.6$  (where  $C_F$  is the propeller force coefficient which we assume to be proportional to the jet coefficient - in fact, with wind speed equal to zero,  $C_j = C_F/0.6$ , see page 7 of D-88). Theoretical variations of  $C_{m_i}$  vs  $C_{L_i}$  for  $\alpha = 0^\circ$  are given and we note that the AR = 4 wing has less variation of moment with lift than the AR = 1 wing.



However the TN D-88 results show no significant trend of moment with lift coefficient as jet angle is changed (Fig. 41) and therefore, for want of better guidance, we have assumed that the centre of induced lift is at the 30 percent chord point as in the case of the LR-243 tests. Using the simplified moment equation shown on Fig. 41 with  $(h/c) = .25$  and  $(h/c)^{1/2} = 0.2$  we then have  $C_{mi}$  (at  $\alpha = 0$ )  $= .175 C_{Li}$ . Values of  $C_{mb+i}$  and  $C_{Lb+i}$  at  $\alpha = 0^\circ$  have been extracted from Fig. 9 of TN-D88 at 4, 5, 6 and 7000 rpm for  $q = 4.3$  and 9.5. Results are given in the upper graph of Fig. 42; the lower graph shows variation of  $C_{mi}$  and  $C_{Li}$  with inlet velocity ratio  $V_i/V_o$ . The value of  $(V_i/V_o)$  was calculated from a knowledge of the static thrust of the complete model and the fan area.

The values of  $C_{mi}$  of Fig. 42 have been corrected for induced jet effects ( $\Delta C_m = .175 C_{Li}$ ) and the resulting values of nose-up moment due to fan are given in Fig. 43.

The Avrocar Ames test result for  $q = 16$  is taken from Fig. 37 and also shown in Fig. 43. Note that all results given on Fig. 43 have been corrected to correspond to  $S_f/S_w = .176$ , (that is to the TN-D88 values) simply by increasing moments in the proportion of the  $S_f/S_w$  value.

Finally, a very simplified theory is discussed. Consider a sink of strength  $m$  in a uniform stream of velocity  $\bar{U}$ . Replace the line of symmetry by a solid boundary and we then have the flow characteristics of a line sink in an infinite plate. When flow velocity is zero, the surface pressure force is considered to be part of the thrust of the lifting device. Superposition of flow velocity  $\bar{U}$  introduces an additional asymmetric loading which provides no lift but generates a nose-up couple. The infinite flow velocity at the sink is avoided by considering a finite slot width through which the flow passes at constant velocity  $V_i$ . We assume the lower surface of the airfoil to be unaffected by the sink on the upper surface and integrate the pressure forces over a chord of finite length.

This very crude approach yields the following expression for nose-up moment due to intake

$$C_m = \left( \frac{V_i}{V_o} \right)^k \left( \frac{S}{C} (1 - S/C) \right) \div \left( \frac{S}{C} \right) \left( \frac{V_i}{V_o} \right) \text{ for } S/C \text{ small.}$$

where  $(V_i/V_o)$  is the inlet velocity ratio and  $(S/C)$  is the ratio of

fan slot width to wing chord. A more accurate formulation of the problem which represents the flow past a flat plate of infinite span has just been completed. This is an exact potential solution with sink in upper surface of airfoil located at the half chord point. This gives, for  $S/C$  small,

$$C_m \doteq \frac{\pi}{4} k \left( 1 + \frac{3k}{4} \right)$$

$$\text{where } k = \left( \frac{V_i}{V_o} \right) \left( \frac{S}{\bar{C}} \right)$$

#### 4.4 Pressure Force Coefficients

Figures 45 to 138 comprise what might be called the pressure force coefficients, i.e. the jet reaction forces have been subtracted from the total measured forces after the manner detailed in Section 3. Coefficients based on both measured static forces and 'effective' jet reaction forces have been plotted wherever effective values were sufficiently well defined.

Table 2 lists values of lift curve slope  $\frac{\partial C_{LB+i}}{\partial \alpha}$ , moment curve slope  $\frac{\partial C_{mB+i}}{\partial \alpha}$  and aerodynamic centre position  $\frac{\partial C_{mB+i}}{\partial C_{LB+i}}$

Due to the non-linear nature of many of the graphs, these tabulated values are approximate only. It appears that a lift curve slope of about 1.0 was obtained for the earlier runs with a slight increase to possibly 1.2 in the later tests. Very little change in moment curve slope was shown, a value of about 0.5 being obtained for all runs. The aerodynamic centre position of the pressure lift, initially at or near the root chord leading edge, showed some signs of a rearward shift in the later tests, reflecting the increase in lift curve slope.

Some "C<sub>j</sub> effect" is apparent on the lift and moment curve slopes, i.e. there is in general a reduction in slope as forward speed is increased.

#### 4.5 Effect of Ground Proximity

The aircraft in its initial configuration (A-1) was tested at three heights, viz. 143 ins, 60 ins and 32 ins (measured from the ground plane to the centre of the lower surface of the aircraft at  $\alpha = 0^\circ$ ). Speeds up to  $q = 15 \text{ lb/ft}^2$  were used.

Extensive tests in ground effect were prevented (especially at zero and low forward speeds) by overheating of the load cells and aircraft instrumentation tubing. Test results were, presumably, affected to some extent by the presence of the aircraft support struts, especially at the lowest  $h/D$ .

It was found impossible, in practice, to vary angle of attack at constant  $h/D$  (Fig. 139) and, although this was not a serious problem at maximum  $h/D$ , it was most undesirable at low heights where the same change in height causes appreciable effects on lift, drag and pitching moment.

Carpets of force data, drawn imaginatively from the sparse test results, are shown in Figs. 140 to 166.

#### 4.6 Intake Performance

##### 4.6.1 Intake Flow Asymmetry

The effect of aircraft forward speed (tunnel speed) on the fan blade velocity vectors is illustrated in Fig. 167. It can be seen that, if we suppose a non-axial intake flow, both the relative wind and angle of attack of the forward moving blade are increased and vice versa for the retreating blade. The result is a higher pressure rise and nozzle peripheral velocity on the port side. Typical distributions are given in Fig. 168. Asymmetric forces are set up giving rise to side force, yawing and rolling moments as shown in Fig. 169. Generally speaking, these undesirable forces and moments were not much affected by the various modifications made to the aircraft in the latter part of the test series. The rolling moment capability of the focussing control ring (Fig. 170) is ample to compensate for the degree of asymmetry discovered but addition of intake guide vanes is expected to provide a much more uniform velocity distribution at the fan and at the peripheral nozzle.

Although the fore and aft total head rake under the fan is not sufficient by itself to give an indication of the intake total pressure recovery, it did show the presence of flow breakaway behind the forward intake lip and behind the centre body, (Fig. 171). Here also the addition of intake guide vanes is expected to radically improve the situation. The mean total head is also seen to decrease slightly with forward speed, whilst the larger nozzle exit area at the rear of the configuration shown ( $Je' = 1.75$ ) caused the appreciable lowering of the fan pressure rise indicated by the aft rake.

#### 4.6.2 Mass Flow and Gross Thrust

There was little change of either mass flow or gross thrust with forward speed and angle of attack except for configuration A-1 where, unaccountably, some appreciable variation was observed. (See Figs. 172 to 176 for configuration A-1 and Figs. 177 to 182 for other configurations). Fig. 183 compares the measured variation of gross thrust with the theoretically predicted variations. The apparently rapid increase in measured gross thrust in the range 0 to  $5q$  is thought to be associated with the change of flow pattern and effective jet reaction which also occurs in this range. Apart from this effect, it is seen that the predicted increase in gross thrust is not realized. Some improvement is expected with the new intake guide vanes.

#### 4.6.3 Effect of Forward Speed on Fan R. P. M.

Due to flow breakaway in the intake at forward speed, the fan partially stalls and blade drag increases resulting in a reduction of fan RPM (at constant engine RPM) (see Fig. 184). This results in a loss of mass flow and fan pressure ratio and approximately nullifies the beneficial ram effects.

#### 4.7 Pitching Control Power in Forward Flight

The variation with control position of total pitching moment and lift coefficients is plotted in Figs. 185 to 190. The approximate slopes of these non-linear curves are shown in Figs. 191 and 192. It will be seen that the degree of control power, i.e.  $\frac{\partial C_M}{\partial J_e}$ ,

achieved at the higher speeds (low values of  $K_{C_j}$ ) was of the same order as that measured on previous model tests. However, the lift increment,  $\frac{\partial C_L}{\partial J_e}$ , associated with the pitching control power

was negative, much worse than measured, for example, on the model of Project 1794 which employed deflected jets issuing from the wing surface at the rear of the wing.

#### 4.8 Avrocar Thrust - Drag Margin

An estimate of the propulsive thrust deficiency of the Avrocar in configuration Q-1 (Runs 41, 44) was obtained by plotting (D-F) and Moment versus Engine RPM at constant lift (Figs. 193 to 202) and combining them to give the thrust - drag margin (or strictly, the drag - thrust margin, D-F) in trim for various constant values of lift over the speed range up to  $q = 25 \text{ lb/ft}^2$ . It is seen (Fig. 203)

that no region for steady, level flight in free-air exists with the presently available thrust level and configuration. However, the modifications being incorporated into the Avrocar (see Section 5) are confidently expected to provide considerably greater propulsive thrust and a useful flight envelope.

#### 4.9 Comparison of 1/20th Scale Model and Avrocar Ames Tests

##### 4.9.1 Power-off, Intake Sealed

Fair agreement between model and aircraft is evident. The lift curve slopes at zero angle of attack are identical, although a  $2^\circ$  difference in zero lift angle was recorded (Fig. 204). The model shows an 8 percent larger moment curve slope (Fig. 205) and a  $3^\circ$  decrease in angle for zero pitching moment. The aerodynamic centre position for the model was at 38 percent forward of centre; the aircraft a.c. position was  $34\frac{1}{2}$  percent forward of centre. A difference of .04 in  $C_{m_0}$  was noted (Fig. 206). Comparison of lift efficiency (Fig. 207) was not feasible since the model was tested up to  $\pm 12^\circ$  angle of attack only, but a similar value of  $C_{D_0}$  was indicated, viz. .05. The discrepancies that do exist between model and aircraft can possibly be attributed to errors in strut corrections and differences in Reynolds number.

##### 4.9.2 Static Case; Power-on, Wind-off

For the first configuration tested at Ames (A-1) the static lift was approximately 1850 lb at a nominal 90 percent maximum engine RPM at the maximum height above ground with control neutral. The corresponding 1/20th scale model figure at 50 psig supply pressure was 4.5 lb which, scaled up to full size, is 1800 lb.

However, the intake mass flow for the model is considerably smaller since about 0.38 lb/sec (model scale) is supplied as primary air through the ejector gap. This amount entrains approximately 0.52 lb/sec (210 lb/sec full scale) of secondary air through the model intake. Hence the total mass flow in the model jet is 0.90 lb/sec (or 360 lb/sec full scale) which is just about the amount measured on the aircraft at Ames. It is concluded therefore that model and aircraft operate at about the same value of  $C_j$  and therefore similar configurations should be comparable (except for the difference in inlet flow).

#### 4.9.3 In-flight Case (Power-on; Wind-on)

Figs. 208 to 213 show the comparison of both total and pressure lift coefficients. The most obvious discrepancy between model and aircraft is the much higher lift curve slope of the model, e.g. the slopes of the pressure lift curves of Fig. 213 ( $J_e = 1.0$ , Config.A-1) are 1.26 for the aircraft at Ames and 1.96 for the 1/20th scale model. Model tests have shown that the degree of jet focussing has a very strong influence on both lift and lift curve slope. Fig. 214 shows how the pressure lift coefficient varies with the inside diameter of the outer nozzle, effectively a variation with jet focussing. Fig. 215 compares the test results from Ames of configuration A-1 with configuration E-1, the latter having a one inch extension on the focussing control ring. Here the large increase in lift due to a reduction in jet focussing, (at  $q = 10$ ), is apparent. The discrepancy in lift curve slope shown in Fig. 213 is believed due to a significant difference in degree of jet focussing between aircraft and model. However, the usual change in lift itself does not appear and therefore, to check the validity of the model test results obtained in the Company's wind tunnel, a series of comparative tunnel tests were carried out in the 4 foot tunnel of the University of Toronto (Ref. 15). These indicated that results obtained in the Avro tunnel were in fair agreement with those obtained at U.T.I.A. especially at the higher speeds for model configurations similar to the aircraft as tested at Ames. For example, the total lift curve slope at  $q = 15$  was found to be 1.42 at Avro, 1.26 at U.T.I.A. and 0.97 at Ames, even though a larger (scaled) mass flow was used. Larger differences were found for a configuration with wing tip blowing but these do not concern us at the moment. Since the model span/tunnel breadth ratio at U.T.I.A. was sufficiently small to expect good results, it can only be concluded that some difference in jet flow pattern is causing the discrepancy between model and full-scale aircraft results.

Figs. 216 to 218 show quite good correlation between pitching moment curve slopes, the displacement of the curves (about  $\Delta C_m = .075$ ) being due to the 150 lb/sec extra intake mass flow at Ames.

The aerodynamic centre of pressure lift (see Fig. 219) is much further forward on the aircraft than on the model (35% forward of centre as opposed to 25% for the model, with aft position of the focussing control ring) due to the lower lift curve slope measured at Ames.

A comparison of drag is given in Fig. 220.

The results of an attempt to simulate one of the 'jet-flap' configurations tested at Ames (Configuration N-1A, Runs 38, 39) by suitably modifying the 1/20th scale model are shown in Fig. 221. Fair agreement with pitching moment is apparent but the optimistic lift curve slope measured with the model precludes any close agreement as far as lift is concerned.

5. MODIFICATIONS TO THE AIRCRAFT FOR PHASE 2 TESTS

The first Avrocar vehicle will be modified to incorporate the following changes in order to achieve the control and performance improvements required:

5.1 Wing Tip Structure and Cascades (Fig. 222)

A large increase in forward thrust will be obtained by modifying the rear half (approximately) of the wing tip structure to incorporate a new radial duct and peripheral nozzle, extending from the existing radial ducts. This will provide an alternative flow path for the jet efflux. Fixed cascades will be situated at the radial extremities of the lateral quadrants of the new ducts to direct the jet flow in a rearwards and slightly outwards direction.

5.2 Transition Doors (Fig. 223)

Flow splitters will be introduced to direct the jet flow through either the peripheral or the annular nozzle and will be operable in such a manner as to provide a gradual transition from hovering to forward flight. The splitters will take the form of twelve doors hinged at their lower outboard edge and controlled by three electric motors connected by flexible drives to the door jacks. The doors may be operated simultaneously or in three separate groups, i.e. two sets of lateral doors and the rear doors, the final mode of operation being determined by test.

5.3 Forward Flight Control Vanes (Fig. 224)

In addition to the existing ring control, used in hovering and transition, it will be necessary to provide control in forward flight. This will be achieved by using the rear jet as a jet flap controlled by six vanes, occupying twenty degree segments at the rear one hundred and twenty degrees of the peripheral nozzle. These vanes will be hinged and coupled to the control system in such a manner as to operate in conjunction with the focussing ring control so that there will be no control hiatus during transition.

5.4 Yaw and Transition Vanes (Fig. 225)

To achieve the required deflection of the forward lateral jet sectors, the existing yaw control vanes will be relocated forward of the lateral centerline of the vehicle (Fig. 226) and deflected rearwards collectively in forward flight.



### 5.5 Increased Travel of Focussing Ring Control

The simplest way of increasing the pitch and roll control in the hovering state is to increase the travel of the focussing ring control. The hanger rods, supporting the focussing ring, will be relocated outboard of the ring, and the ratio of cable movement to bellows jack movement will be increased at the phasing levers, (situated beneath the turborotor near the center of the vehicle) giving  $\pm 3''$  travel of the focussing control ring.

### 5.6 Fin and Tailplane (Fig. 227)

Supplementary trim control and increased longitudinal stability may be obtained by the addition of a tailplane, and a tailplane will be designed and made available for tests. It will have a ten foot span and a chord of three feet and will be mounted on a single fin guyed in place with suitable struts and wires. The tailplane will initially be set at twenty degrees to the wing chord but provision is made for changing the incidence through  $\pm 12$  degrees with removable blocks.

The fin is expected to provide sufficient directional stability and to overcome the small adverse effects of the canopies. The fin is mandatory for forward flight but the tailplane is an insurance feature.

### 5.7 Rotor Inlet Cascades (Fig. 228)

It is intended to improve the flow distributions in forward flight by the addition of intake guide vanes, the design of which has been based on tests recently undertaken at NASA (Ames).

### 5.8 Instrumentation

There has been a complete re-appraisal of all pressure instrumentation on the first Avrocar vehicle to eliminate unnecessary piping and replace instrumentation damaged by the first series of wind tunnel tests at NASA. Furthermore, due to changes described in paras 5.1 to 5.7 inclusive, it has been necessary to re-evaluate the instrumentation requirements which are now detailed in Ref. 16.

### 5.9 First Avrocar Vehicle Repairs

Due to prolonged running at high engine rpm during the first series of wind tunnel tests at NASA, the first Avrocar vehicle rib structure has suffered from thermal and acoustic fatigue. Experience with the second Avrocar vehicle at the Avro Malton plant, has led to methods of repair to combat this deficiency, and these methods will be applied to the first Avrocar vehicle at NASA to establish a minimum life of thirty-five hours for further testing.

6. CONCLUSIONS

Insofar as these tests covered the performance of the Avrocar in free flight with a novel method of control which had proved satisfactory in hovering, the results can only be described as disappointing. From small scale model tests the control power shown to be available with the focussing ring control was much increased over that developed by the spoiler control system used previously on the Avrocar. The full scale tests confirm theory in that the chordwise position of the additional lift due to jet control is at approximately 75% from the leading edge. However, the present control scheme is not capable of providing the necessary lift increment at this chordwise position. In addition, it has reduced the effective aspect ratio and lift slope excessively. Furthermore, the tests show that the focussing ring control on the aircraft did not produce the same degree of jet vectoring as did the model and neither produced sufficient to equal aircraft minimum drag at any but the very lowest aircraft speeds. An additional loss of control at forward speeds greater than about  $q = 5 \text{ lb/ft}^2$  appears to be due to a change in the apparent or effective jet reaction thrust moment. No completely satisfactory explanation for this phenomenon is available but the existence of separated flow regions, pockets and/or vortices under the aircraft at low speeds, probably gives rise to this peculiarity. In a few isolated cases the effective reactive moment appeared to increase (i.e. became more nose-down) at speeds above  $q = 5 \text{ lb/ft}^2$ .

A generally large nose-up pitching moment was measured for the initial configurations tested, i.e. the aircraft with focussing ring control. Two main reasons are put forward to explain this: first, the jet pattern under the aircraft did not sufficiently simulate a jet flap; and secondly, the increased intake mass flow (being approximately twice as large for the Avrocar as for the scaled-up model) added a nose-up moment of considerable magnitude. This was a field in which knowledge had been particularly scant and the questions raised and knowledge accumulated as a result of the Avrocar tests have been of considerable value and of wide application.

Undoubtedly, one of the most surprising results to emerge from the Avrocar tests, was the very low value of the lift curve slope, jet-on. (The jet-off value, 1.4 per radians, agreed very closely with that predicted by the 1/20th scale model). Tests of the model arranged in a configuration to simulate the later 'jet flap' configurations (e.g. runs 38, 39, and 41, 44) gave a lift curve slope about 50% greater than that measured at Ames, which was generally in the region 1.0 to 1.2. In an attempt to determine whether the

small scale model in an admittedly small tunnel (model span/tunnel breadth = 0.6) was giving erroneous results, a comparative test of the identical model was carried out in the four foot tunnel of the Institute of Aerophysics, University of Toronto. At a  $q$  of 15, the lift curve slope was about 11% less than that measured in the eighteen inch square tunnel at Avro. The disparity between model and aircraft is therefore not entirely due to tunnel effects, and the only explanation possible appears to be that the jet flow pattern, for example, as regards the degree of focussing, is not reproduced on the model.

As a result of non-vertical flow into the fan intake at forward speeds the forward-moving fan blades generate more lift than the retreating fan blades and a biased peripheral nozzle velocity distribution is obtained, causing a side force and associated rolling and yawing moments on the aircraft. This, of course, is a problem which all fan-in-wing aircraft have to face and the remedy appears to lie in intake guide vanes whose development has been studied by NASA for similar applications.

One of the persistent difficulties in all work concerned with jet flows is the accurate determination of the jet momentum at the nozzle exit. The Avrocar tests proved to be no exception. The free air thrust efficiency measured at Ames (0.5 with the standard focussing ring control and 0.6 with the extended lip focussing ring) is therefore not regarded as the last word on the subject. Agreement with the lift measured at Malton in the Static Test Rig was good and the additional height above ground obtainable for static tests at Ames showed a slight ground cushion effect to exist at 60 inches.

Summing up, then, it appears that the solution to the major aerodynamic problems of the Avrocar revolves around the provision of adequate jet vectoring control. To this end modifications have been made to the aircraft principally to provide an effective jet flap at the rear of the aircraft and adequate, rearward facing nozzle area to obtain a large increase in propulsive thrust. With these modifications installed the second series of wind tunnel tests at the Ames Research Center are planned for February-March, 1961.

7. REFERENCES

1. RAND, M.I.  
EARL, T.D. "Specification for tests of an Avrocar in the 40' x 80' wind tunnel at N.A.S.A. Ames Aeronautical Laboratory." AVRO/SPG/TR 197 June 1959 I.D. No. 59RDZ-2873
2. Addendum No. 1 to AVRO/SPG/TR 197 February 1960
3. MARTIN, P. "General Review of the Tests of the Avrocar in the Ames Research Center 40' x 80' Wind Tunnel" 500/AERO TEST/403 March 1960
4. MARTIN, P. "Tests of the Avrocar in the Ames Research Center 40' x 80' Wind Tunnel (N.A.S.A.). Data Report" 500/AERO TEST/401 June 1960 I.D. No. 60DRZ-2263
5. McGEE, P.J. "Data Report for the 1/20th Scale Avrocar Model (Avrocar Continuation Program)" 500/AERO TEST/410 December 1960
6. PERKINS, C.D.  
HAGE, R.E. "Airplane Performance, Stability and Control" p. 93.
7. KUCHEMANN, D. "Span and Chordwise Loading on Straight and Swept Wings" RAE Report Aero 2476 August 1952
8. STRATFORD, B.S. "Early Thoughts on the Jet Flap" Aeronautical Quarterly Vol. VII February 1956-November 1956. p. 58.
9. WHITTLEY, D.C. Review of Lift and Drag Data from the First Series of Tests on the Sixth Scale Model, Project 1794 AVRO/SPG/TR 185 August 1958

10. GARLAND, D.B. "Specifications for Phase 2 Tests of an Avrocar in the 40' x 80' Wind Tunnel at N.A.S.A., Ames Research Center" 500/AERO TEST/405 July 1960
11. KORBACHER, G.K.  
SRIDHAR, K. "A Review of the Jet Flap" U.T.I.A. Review No. 14 May 1960
12. HAGUE, D.S. Unpublished work on potential flow solution of flow through a wing November 1960
13. WARDLAW, R.L.  
McEACHERN, N.V. A wing-submerged lifting fan: wind tunnel investigations and analysis of transition performance. N.R.C. Aeronautical Report LR-243 (Ottawa) April 1959
14. HICKEY, D.H.  
ELLIS, D.R. "Wind Tunnel Tests of a Semi Span Wing with a Fan Rotating in the Plane of the Wing" N.A.S.A. TN D-88 October 1959
15. McGEE, P.J. 1/20th scale Avrocar model - Comparison tests at U.T.I.A. and Avro Aircraft Ltd. 500/AERO TEST/418 January 1961
16. WATSON, M.B.P. "Avrocar Continuation Program - Instrumentation Specification for Ames Tunnel Tests - 1st Avrocar Vehicle" 500/AERO TEST/415 September 1960

TABLE 1SUMMARY OF CONFIGURATIONS

Each configuration tested has been given a coding, for example "G.S.-1"; the first letter specifies the aircraft condition as listed below; the second letter, if present, signifies a "power off" run, 'O' denoting the fan intake was not sealed and 'S' that the fan intake was sealed. The number denotes the height above the ground plane, '1' the maximum height tested of 12 feet 8 inches, '2' a height of 60 inches and '3' a height of 32 inches. Note that  $J_e'$  signifies the cases where the rear 120 degrees of focussing ring and skirt were removed. The suffix 'A' indicates all rudder vanes turned aft.

Configuration Code	Applicable Run No.	Configuration Details
A-1	1, 3, 8, 9, 10, 11, ) 12, 14, 15, 27 ) )	Basic Test Configuration (Focussing Ring Travel $\pm$ 2.0 inches)
AO-1	2 ) )	
AS-1	45 ) )	
A-2	21, 22, 23, 24 ) )	
AS-2	46 ) )	
A-3	26 ) )	
AS-3	25 )	
B-1	16	
C-1	18 ) )	
CO-1	19 ) )	
C-2	20 )	Rear 120 degrees of focussing ring and skirt removed, $J_e' = + .25$
D-1	17	
		Rear 120 degrees of focussing ring removed and skirt deleted, $J_e' + 1.75$ and lowered at front end

Configuration Code	Applicable Run No.	Configuration Details
E-1	13	Basic configuration with 1 inch lip extension on focussing ring trailing edge
F-1	28	Rear 120 degrees of focussing ring removed and skirt deleted in this area; top skins between wing tip and body raised to give a 3.0 inch deep upper slot over an 80 degrees arc at the rear; spoilers fitted over this 80 degrees arc with the top spoiler flush and the bottom spoiler up into nozzle 0.55 inches
G-1	29	The same as F-1 except that the bottom spoiler was flush and the top spoiler down into the nozzle 0.55 inches
GS-1	30	
H-1	31	The same as G-1 except that the slot between the top skin and the wing tip was reduced from 3.0 inches to 1.875 inches
J-1	32	The same as H-1 except that a curved extension was added to the trailing edge of the upper slot
K-1	34	The same as J-1 except that the bottom nozzle between the wing tip and body was blanked off over the rear 80 degrees arc
L-1	35	The same as K-1 but with the top slot increased to 3 inches from 1.875 inches
M-1	36, 37	The same as L-1 with the addition of a 2.75 inch extension on the trailing edge of the focussing ring over the front 120 degrees arc
N-1	38, 39	The same as M-1 with the top rear nozzle flap extended and the slot reduced to 2.5 inches
P-1	40	The same as N-1 with cascades having a turning angle of 90 degrees fitted at port and starboard sides

Configuration Code	Applicable Run No.	Configuration Details
Q-1	41, 44	The same as P-1 but with the cascade turning angle reduced to 60 degrees
R-1	42	The same as Q-1 but with end plates fitted to the cascades
T-1	43	The same as R-1 but with a central jet introduced
U-1	47	Basic configuration with rear 80 degrees of wing tip removed. $J_e^i + .25$ and 80 degrees arc nozzle spoilers fitted; set at top into the nozzle 0.4375 inches and bottom 0.25 inches
V-1	48	The same as U-1 but the bottom spoiler flush and the top down into the nozzle 0.55 inches
VS-1	49	



TABLE 2

Listed below are values of the principal derivatives of the pressure force coefficients. Gaps in the table indicate either that the data were not available or that the curves were non-linear to the extent that no meaningful slope could be obtained.

Config	$J_e$	$\partial C_{L_{B+i}}/\partial \alpha$				$\partial C_{M_{B+i}}/\partial \alpha$				$\partial C_{M_{B+i}}/\partial C_{L_{B+i}}$			
		$\alpha = 5$	10	15	25	5	10	15	25	5	10	15	25
A-1	0	.48	.38	1.34	-	.48	.41	.19	-	.47	-	-	-
	.5	.48	1.40	1.32	-	.52	.44	.44	-	.71	-	-	-
	1.0	1.10	1.14	1.27	-	.45	.45	.42	-	.42	-	.32	-
A-2	0	-	-	1.80	-	-	-	.20	-	-	-	-	-
	.5	-	2.12	1.72	-	-	.30	.21	-	-	-	-	-
	1.0	3.18	2.02	1.61	-	.10	.40	.40	-	.03	-	.23	-
A-3	0	6.40	3.21	2.32	-	-	.32	.32	-	-	.12	.14	-
	.5	4.47	2.98	2.52	-	-	.26	.29	-	-	-	-	-
	1.0	4.41	2.75	2.58	-	.23	.42	.33	-	-	-	-	-
B-1	1.75	-	1.20	1.20	-	.41	.43	.39	-	.28	.33	.35	-
C-1	.25 <sup>1</sup>	-	.93	.93	-	.54	.50	.46	-	.52	.53	.45	-
C-2	.25 <sup>1</sup>	-	1.34	1.48	-	.46	.50	.50	-	-	.39	.33	-
D-1	1.75 <sup>1</sup>	1.11	1.09	1.11	-	.52	.45	.41	-	.42	.42	.42	-
E-1	0	-	.65	-	-	-	.37	-	-	-	.62	-	-
	.5	-	.77	-	-	-	.46	-	-	-	.61	-	-
	1.0	-	.98	-	-	-	.31	-	-	-	.24	-	-
H-1A		1.10	.85	.88	-	.49	.49	.46	.43	.49	.52	.39	-
J-1A		.84	-	1.03	1.03	.54	-	.50	.46	.51	-	.44	.39
K-1A		.90	-	.85	.99	.57	-	.48	.46	.52	-	.52	.41
L-1A		1.29	-	1.00	.93	.54	-	.51	.54	.45	-	.42	.47
M-1A		1.18	-	.99	.87	.57	-	.47	.45	.43	-	.48	.54
N-1A		1.18	-	1.02	.81	.61	-	.48	.44	.51	-	.51	.51
P-1		1.58	-	-	-	.55	-	-	-	.30	-	-	-
Q-1		1.12	.96	1.42	1.25	.55	.50	.42	.43	.43	.54	.37	.37
T-1		1.26	-	1.22	1.13	.49	-	.45	.39	.28	-	-	.36
U-1		1.19	-	-	1.27	.46	-	.46	.46	.38	-	-	.31
V-1		.98	-	-	-	.45	-	.49	.39	.46	-	.45	-

LIST OF ILLUSTRATIONS

Section Ref.	Fig. No.	Title
1.0	1	Avrocar in the 40 x 80 foot tunnel, Ames Research Center
4.1	2	$C_L$ vs $\alpha$ , Power-off Run 30
	3	" " " 33
	4	" " " 45
	5	" " " 49
	6	$C_D$ vs $C_L^2$ " " 45
	7	$(C_D - \frac{C_L^2}{\pi A})$ vs $(C_L - C_{L_{min}})^2$ Power-off Run 30, 33
	8	" " " " 45, 49
	9	$C_M$ vs $C_L$ Power-off Run 30
	10	" " " 33
	11	" " " 45
	12	" " " 49
4.2.1	13	Lift vs corrected Engine rpm
	14	Nozzle thrust vs corrected engine rpm
4.2.2	15	Extended lip on Focussing Control Ring
	16	Effect of extended lip on Jet Focussing
4.2.3	17	Static lift and drag vs control position
	18	Static pitching moment and cp position vs control position
	19	Static resultant force and inclination vs control position
	20	Static lift and drag vs control position; extended lip
	21	Static pitching moment and cp position vs control position; extended lip

Section Ref.	Fig. No.	Title
4.3.1	22	Diagram illustrating effective static moment
	23	Pitching moment vs $q$ ; config. B-1; Run 16
	24	Pitching moment vs $\alpha$ ; config. B-1; Run 16
	25	Measured and effective static moment vs control position, Config. A-1
	26	Lift and drag vs $\alpha$ ; Run 17, Config. D-1
	27	Lift and drag vs $\alpha$ ; Run 38, Config. N-1A
	28	Lift and drag vs $\alpha$ ; Run 38, Config. N-1 with effective static values
	29	Pitching moment vs $\alpha$ ; Run 38, Config. N-1A
	30	Lift vs forward speed; Run 17, Config. D-1
	31	Lift vs forward speed, Run 34, Config. K-1A
	32	Lift vs forward speed; Run 38, Config. N-1A
	33	Lift vs forward speed; Run 41, 44, Config. Q-1
	34	Suggested flow pattern for 'jet flap' configurations
4.3.2	35	(D-F) vs forward speed, V
4.3.3	36	Pitching moment due to jet induced lift Project 1794
	37	Pitching moment due to jet induced lift - Avrocar
	38	$C_{M_i}$ vs $C_{L_i}$ at $\alpha = 0^\circ$ - 1/20th Scale Model
	39	Pitching moment due to intake flow - 1/20th scale model
	40	Intake characteristics - 1/20th scale model
	41	Intake analysis from NASA TN D-88
	42	$C_{M_{B+i}}$ vs $C_{L_{B+i}}$ ; $\alpha = 0^\circ$ ; NASA TN D-88

Section Ref.	Fig. No.	Title
4.3.3	43	Nose-up moment due to intake - theory and experiment
	44	Aircraft centerline pressure distribution
4.4	45	$C_{L_{B+i}}$ vs $\alpha_c$ ; $q = 5$ ; measured static; A-1
	46	" " $q = 10$ ; " " "
	47	" " $q = 15$ ; " " "
	48	$C_{M_{B+i}}$ vs $\alpha_c$ ; $J_e = 0, 0.5$ measured static; A-1
	49	" " $J_e = 1.0$ ; " " "
	50	" " $J_e = 0, 0.5$ ; effective static; A-1
	51	" " $J_e = 1.0$ ; " " "
	52	$C_{M_{B+i}}$ vs $C_{L_{B+i}}$ ; $q = 5$ ; " " "
	53	" " $q = 10$ ; " " "
	54	" " $q = 15$ ; " " "
	55	$C_{L_{B+i}}$ vs $\alpha_c$ ; $J_e = 0$ ; measured static A-2; Run 21
	56	" " $J_e = 0.5$ ; " " " "
	57	" " $J_e = 1.0$ ; " " " "
	58	$C_{M_{B+i}}$ vs $\alpha_c$ ; $J_e = 0, 0.5, 1.0$ ; measured static A-2; Run 21
	59	" " $J_e = 0, 0.5$ ; effective static A-2; Run 21
	60	" " $J_e = 1.0$ ; " " " "
	61	$C_{M_{B+i}}$ vs $C_{L_{B+i}}$ ; $J_e = 0, 0.5$ ; " " " "
	62	" " $J_e = 1.0$ ; " " " "
	63	$C_{L_{B+i}}$ vs $\alpha_c$ ; $J_e = 0$ ; measured static A-3; Run 26
	64	" " $J_e = 0.5$ ; " " " "

Section Ref.	Fig. No.	Title
4.4	65	$C_{LB+i}$ vs $\alpha_c$ ; $J_e = 1.0$ ; measured static A-3; Run 26
	66	$C_{MB+i}$ vs $\alpha_c$ ; $J_e = 0, 0.5, 1.0$ ; " " " "
	67	" " $J_e = 0, 0.5$ ; effective static " "
	68	" " $J_e = 1.0$ ; " " " "
	69	$C_{MB+i}$ vs $C_{LB+i}$ ; $J_e = 0, 0.5$ ; " " " "
	70	" " $J_e = 1.0$ ; " " " "
	71	$C_{LB+i}$ vs $\alpha_c$ ; $J_e = 1.75$ ; measured static B-1; Run 16
	72	$C_{MB+i}$ vs $\alpha_c$ ; $J_e = 1.75$ ; " " " "
	73	" " " effective static " "
	74	$C_{MB+i}$ vs $C_{LB+i}$ ; $J_e = 1.75$ ; " " " "
	75	$C_{LB+i}$ vs $\alpha_c$ ; $J_e' = .25$ ; measured static C-1; Run 18
	76	$C_{MB+i}$ vs $\alpha_c$ ; " " " "
	77	" " " effective static " "
	78	$C_{MB+i}$ vs $C_{LB+i}$ ; " " " "
	79	$C_{LB+i}$ vs $\alpha_c$ ; " measured static, C-2; Run 20
	80	$C_{MB+i}$ vs $\alpha_c$ ; " " " "
	81	" " " effective static " "
	82	$C_{MB+i}$ vs $C_{LB+i}$ ; " " " "
	83	$C_{LB+i}$ vs $\alpha_c$ ; $J_e' = 1.75$ ; measured static D-1; Run 17
	84	$C_{MB+i}$ vs $\alpha_c$ ; " " " "
	85	" " " effective static " "
	86	$C_{MB+i}$ vs $C_{LB+i}$ ; " " " "

Section Ref.	Fig. No.	Title			
4.4	87	$C_{LB+i}$ vs $\alpha_c$ ; $q = 10$ ; measured static	E-1; Run 13		
	88	$C_{MB+i}$ vs $\alpha_c$ ; "	" " " "		
	89	$C_{MB+i}$ vs $C_{LB+i}$ ; "	" " " "		
	90	$C_{LB+i}$ vs $\alpha_c$ ; $q = 5, 10, 15, 25$ ; "	" " H-1A; Run 31		
	91	" " "	effective static " "		
	92	$C_{MB+i}$ vs $\alpha_c$ ; "	measured static " "		
	93	" " "	effective static " "		
	94	$C_{MB+i}$ vs $C_{LB+i}$ ; "	" " " "		
	95	$C_{LB+i}$ vs $\alpha_c$ ; $q = 5, 15, 25$ ; measured static;	J-1A; Run 32		
	96	" " "	effective static " "		
	97	$C_{MB+i}$ vs $\alpha_c$ ; "	measured static " "		
	98	" " "	effective static " "		
	99	$C_{MB+i}$ vs $C_{LB+i}$ ; "	" " " "		
	100	$C_{LB+i}$ vs $\alpha_c$ ; "	measured static; K-1A; Run 34		
	101	" " "	effective static " "		
	102	$C_{MB+i}$ vs $\alpha_c$ ; "	measured static " "		
	103	" " "	effective static " "		
	104	$C_{MB+i}$ vs $C_{LB+i}$ ; "	" " " "		
	105	$C_{LB+i}$ vs $\alpha_c$ ; "	measured static; L-1A; Run 35		
	106	" " "	effective static " "		
	107	$C_{MB+i}$ vs $\alpha_c$ ; "	measured static; " "		
	108	" " "	effective static " "		

Section Ref.	Fig. No.	Title			
4.4	109	$C_{M_{B+i}}$ vs $C_{L_{B+i}}$ ; $q = 5, 15, 25$ ; effective static; L-1A; Run 35			
	110	$C_{L_{B+i}}$ vs $\alpha_c$ ; " measured static; M-1A; Runs 36, 37			
	111	" " " effective static " "			
	112	$C_{M_{B+i}}$ vs $\alpha_c$ ; " measured static; " "			
	113	" " " effective static " "			
	114	$C_{M_{B+i}}$ vs $C_{L_{B+i}}$ ; " " " " "			
	115	$C_{L_{B+i}}$ vs $\alpha_c$ ; " measured static; N-1A; Runs 38, 39			
	116	" " " effective static " "			
	117	$C_{M_{B+i}}$ vs $\alpha_c$ ; " measured static " "			
	118	" " " effective static " "			
	119	$C_{M_{B+i}}$ vs $C_{L_{B+i}}$ ; " " " " "			
	120	$C_{L_{B+i}}$ vs $\alpha_c$ ; $q = 5$ measured static; P-1; Run 40			
	121	$C_{M_{B+i}}$ vs $\alpha_c$ ; " " " " "			
	122	$C_{M_{B+i}}$ vs $C_{L_{B+i}}$ ; " " " " "			
	123	$C_{L_{B+i}}$ vs $\alpha_c$ ; $q = 5, 10, 15, 25$ " " Q-1; Runs 41, 44			
	124	" " " effective static " "			
	125	$C_{M_{B+i}}$ vs $\alpha_c$ ; " measured static " "			
	126	" " " effective static " "			
	127	$C_{M_{B+i}}$ vs $C_{L_{B+i}}$ ; " " " " "			
	128	$C_{L_{B+i}}$ vs $\alpha_c$ ; $q = 5, 15, 25$ ; measured static; T-1; Run 43			
	129	" " " effective static " "			
	130	$C_{M_{B+i}}$ vs $\alpha_c$ ; " measured static " "			

Section Ref.	Fig. No.	Title
4.4	131	$C_{M_{B+i}}$ vs $\alpha_c$ ; $q = 5, 15, 25$ ; effective static; T-1; Run 43
	132	$C_{M_{B+i}}$ vs $C_{L_{B+i}}$ ; " " " " "
	133	$C_{L_{B+i}}$ vs $\alpha_c$ ; " measured static; U-1; Run 47
	134	$C_{M_{B+i}}$ vs $\alpha_c$ ; " " " " "
	135	$C_{M_{B+i}}$ vs $C_{L_{B+i}}$ ; " " " " "
	136	$C_{L_{B+i}}$ vs $\alpha_c$ ; " " " V-1, Run 48
	137	$C_{M_{B+i}}$ vs $\alpha_c$ ; " " " " "
	138	$C_{M_{B+i}}$ vs $C_{L_{B+i}}$ ; " " " " "
4.5	139	Variation of $h/D$ with angle of attack
	140	Lift vs $\alpha$ and $h/D$ ; $J_e = 0$ ; $q = 5$ ; Config. A
	141	Lift vs $\alpha$ and $h/D$ ; $J_e = 0$ ; $q = 10$ ; Config. A
	142	" " " " $q = 15$ ; " "
	143	" " " $J_e = 0.5$ ; $q = 5$ ; " "
	144	" " " " $q = 10$ ; " "
	145	" " " " $q = 15$ ; " "
	146	" " " $J_e = 1.0$ ; $q = 5$ ; " "
	147	" " " " $q = 10$ ; " "
	148	" " " " $q = 15$ ; " "
	149	Drag vs $\alpha$ and $h/D$ ; $J_e = 0$ ; $q = 5$ ; " "
	150	" " " " $q = 10$ ; " "
	151	" " " " $q = 15$ ; " "
	152	" " " $J_e = 0.5$ ; $q = 5$ ; " "



Section Ref.	Fig. No.	Title
4.5	153	Drag vs $\alpha$ and h/D ; $J_e = 0.5$ ; $q = 10$ ; Config. A
	154	" " " " $q = 15$ ; " "
	155	" " " $J_e = 1.0$ ; $q = 5$ ; " "
	156	" " " " $q = 10$ ; " "
	157	" " " " $q = 15$ ; " "
	158	Pitching moment vs $\alpha$ and h/D; $J_e = 0$ ; $q = 5$ ; Config. A
	159	" " " " " $q = 10$ ; " "
	160	" " " " " $q = 15$ ; " "
	161	" " " " $J_e = 0.5$ ; $q = 5$ ; " "
	162	" " " " " $q = 10$ ; " "
	163	" " " " " $q = 15$ ; " "
	164	" " " " $J_e = 1.0$ ; $q = 5$ ; " "
	165	" " " " " $q = 10$ ; " "
	166	" " " " " $q = 15$ ; " "
4.6	167	Fan blade velocity vectors
	168	Peripheral nozzle dynamic head distribution
	169	Side force, yawing moment & rolling moment vs forward speed
	170	Rolling moment vs control position (aileron sense)
	171	Total pressure distribution under the fan
	172	Variation of mass flow with forward speed; Config.A-1; $J_e = 0$
	173	" " " " " " " " $J_e = 0.5$
	174	" " " " " " " " $J_e = 1.0$

Section Ref.	Fig. No.	Title	
4.6	175	Variation of mass flow with angle of attack, Config.A-1; $J_e = 1.0$	
	176	Variation of gross thrust with forward speed; " " "	
	177	Variation of mass flow with forward speed; Config. B-1	
	178	" " " " " " " Config. C-1	
	179	" " " " " " " Config. D-1	
	180	" " " " " " " Config. J-1	
	181	" " " " " " " Config. K-1A	
	182	" " " " " " " Config. N-1	
	183	Variation of gross thrust with forward speed;Config.K-1A, T-1, N-1A	
	184	Fan rpm vs engine % max. rpm	
4.7	185	$C_M$ vs $J_e$ $q = 5$ Config. A-1	
	186	" $q = 10$ " "	
	187	" $q = 15$ " "	
	188	$C_L$ vs $J_e$ $q = 5$ " "	
	189	" $q = 10$ " "	
	190	" $q = 15$ " "	
	191	$\left[ \begin{matrix} C_M \\ J_e \end{matrix} \right]_{\alpha}$ vs $KC_j$ Config. A-1	
	192	$\left[ \begin{matrix} C_L \\ J_e \end{matrix} \right]_{\alpha}$ vs $KC_j$ Config. A-1	
	4.8	193	$\left[ \begin{matrix} D - F \end{matrix} \right]_L$ vs $N\%$ $q = 5$ Config. Q-1 Runs 41,44
		194	" " $q = 10$ " " "
195		" " $q = 15$ " " "	
196		" " $q = 20$ " " "	

Section Ref.	Fig. No.	Title			
4.8	197	$[D - F]_L$ vs $N\%$	$q = 25$	Config. Q-1	Runs 41, 44
	198	$[M_C]_L$ vs $N\%$	$q = 5$	"	" "
	199	" "	$q = 10$	"	" "
	200	" "	$q = 15$	"	" "
	201	" "	$q = 20$	"	" "
	202	" "	$q = 25$	"	" "
	203	Trimmed (D-F) at constant lift vs $q$			
4.9	204	$C_L$ vs $\alpha_c$ ; Jet-off, Avrocar and 1/20th scale model			
	205	$C_M$ vs $\alpha_c$ ; Jet-off, Avrocar and 1/20th scale model			
	206	$C_M$ vs $C_L$ ; Jet-off, Avrocar and 1/20th scale model			
	207	$C_D$ vs $C_L^2$ ; Jet-off, Avrocar and 1/20th scale model			
	208	$C_L$ vs $\alpha_c$ ; Jet on, $J_e = 0$ ; $q = 15$ ; Avrocar and 1/20th scale model			
	209	" "	$J_e = 0.5$ ; $q = 15$ ;	"	"
	210	" "	$J_e = 1.0$ ;	"	"
	211	$C_{L_{B+i}}$ vs $\alpha_c$ ; Jet on, $J_e = 0$ ; $q = 15$ ;			
	212	" "	$J_e = 0.5$ ;	"	"
	213	" "	$J_e = 1.0$ ;	"	"
	214	Effect of jet focussing on lift - 1/20th scale model			
	215	Effect of jet focussing on lift - Avrocar at Ames			
	216	$C_M$ vs $\alpha_c$ Jet-on, $J_e = 0$ ; $q = 15$ ; Avrocar and 1/20th scale model			
	217	" "	$J_e = 0.5$ ;	"	"

Section Ref.	Fig. No.	Title
4.9	218	$C_M$ vs $\alpha_c$ ; Jet on; $J_e = 1.0$ ; $q = 15$ ; Avrocar & 1/20th scale model
	219	$C_{M_{B+i}}$ vs $C_{L_{B+i}}$ ; $J_e = 1.0$ and $1.75$ ; $q = 15$ ; Avrocar & 1/20th scale model
	220	$C_D$ components vs $\alpha_c$ ; $J_e = 1.0$ ; $q = 15$ ; Avrocar & 1/20th scale model
	221	$C_{L_{B+i}}$ vs $\alpha_c$ ; Run 38, Config. N-1A; $q = 15$ ; Avrocar & 1/20th scale model
5.1	222	Wing Tip Structure and Cascades
5.2	223	Transition Doors
5.3	224	Pitch and Roll Control Vanes
5.4	225	Yaw and Transition Vanes
	226	Arrangement of Controls
5.6	227	Fin and Tailplane
5.7	228	Fan Intake Guide Vanes

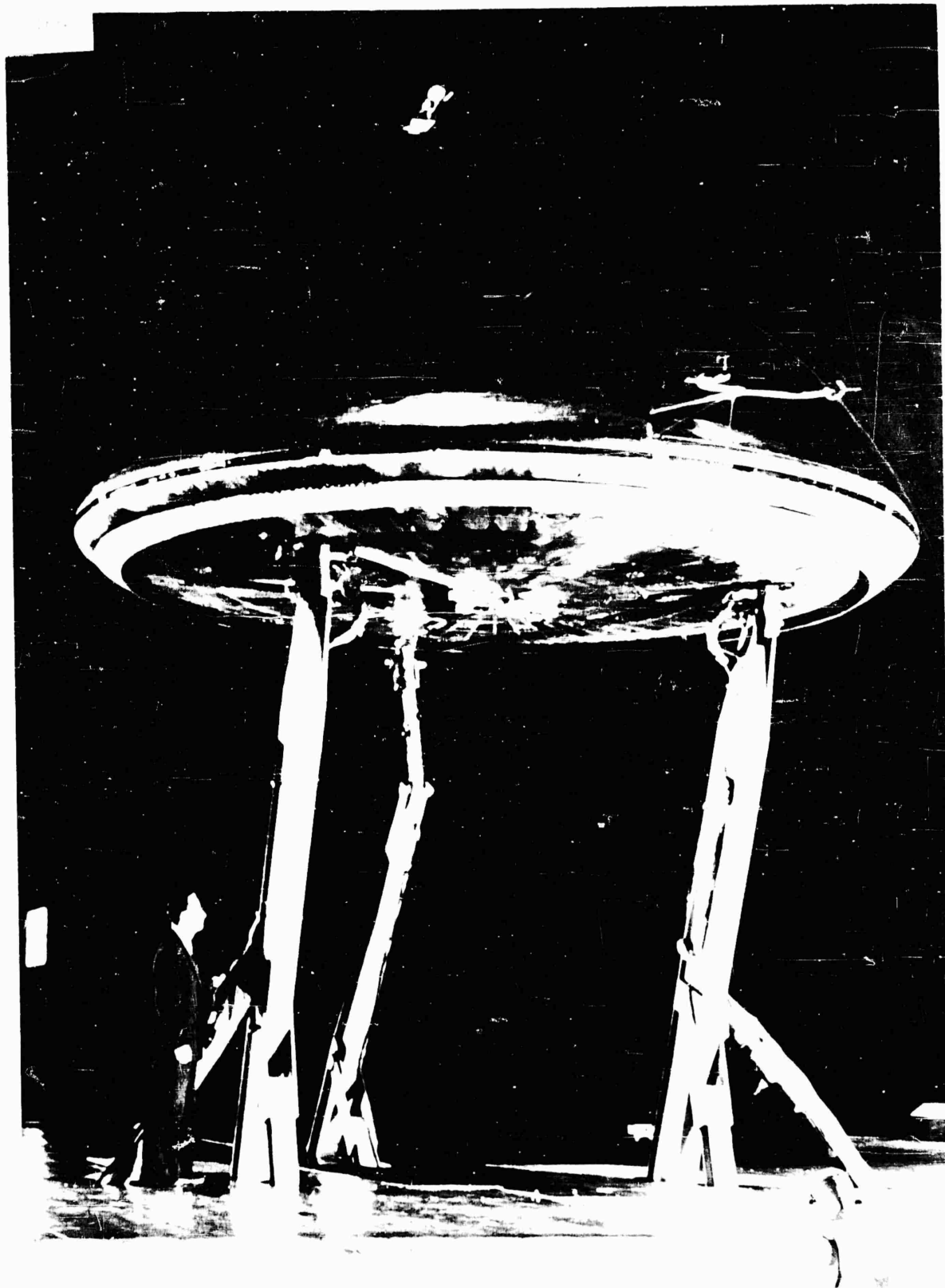
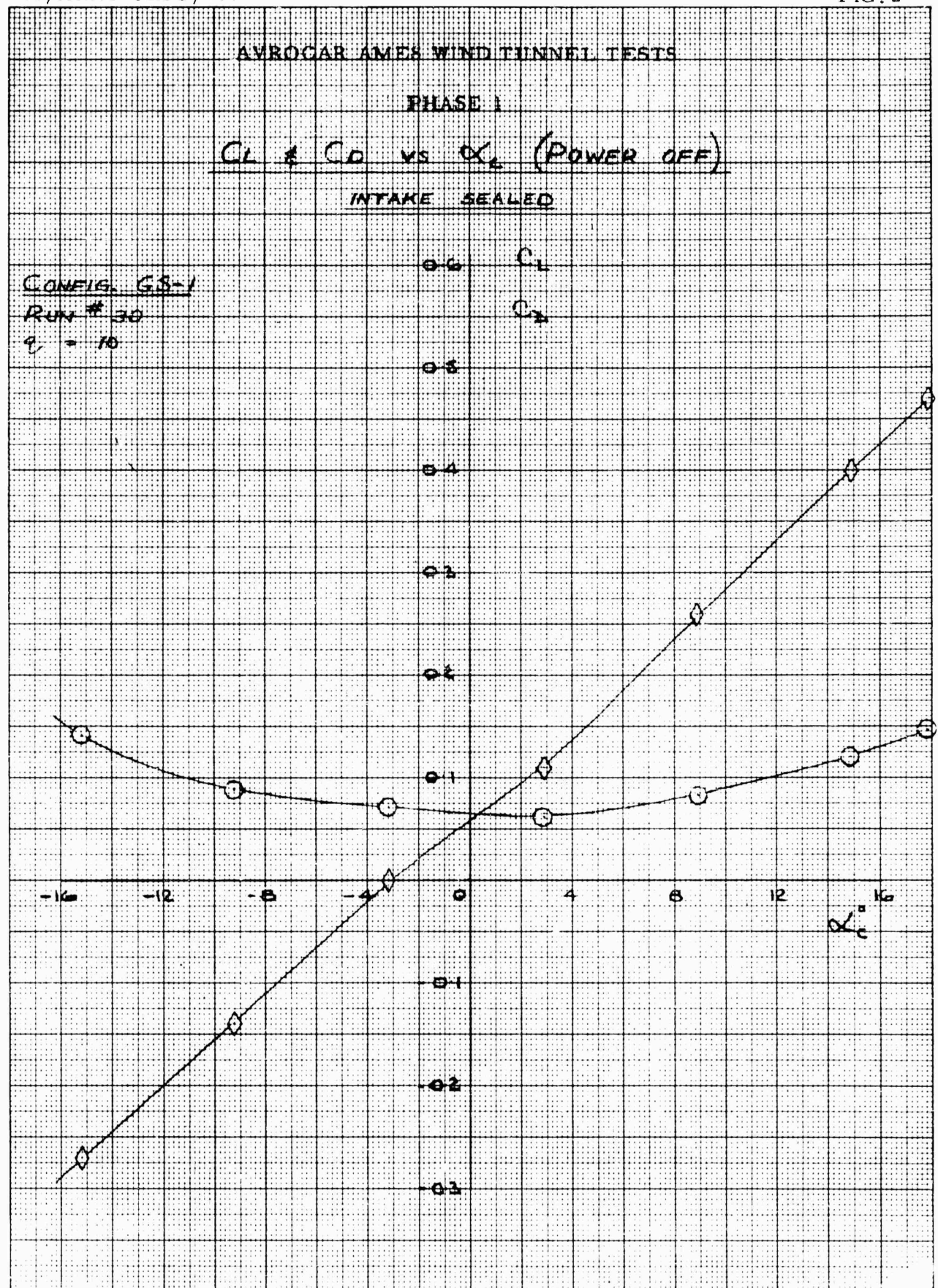
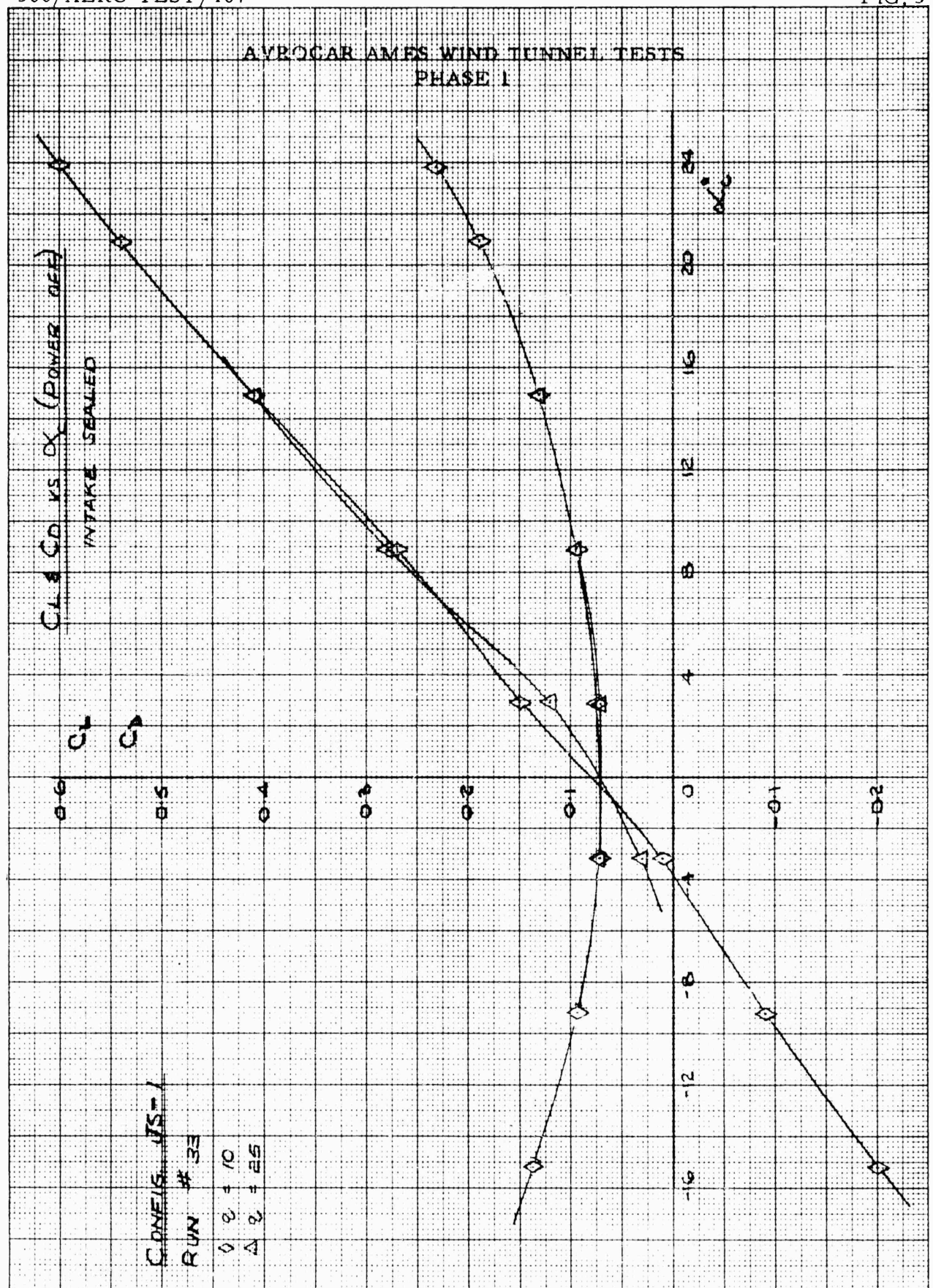
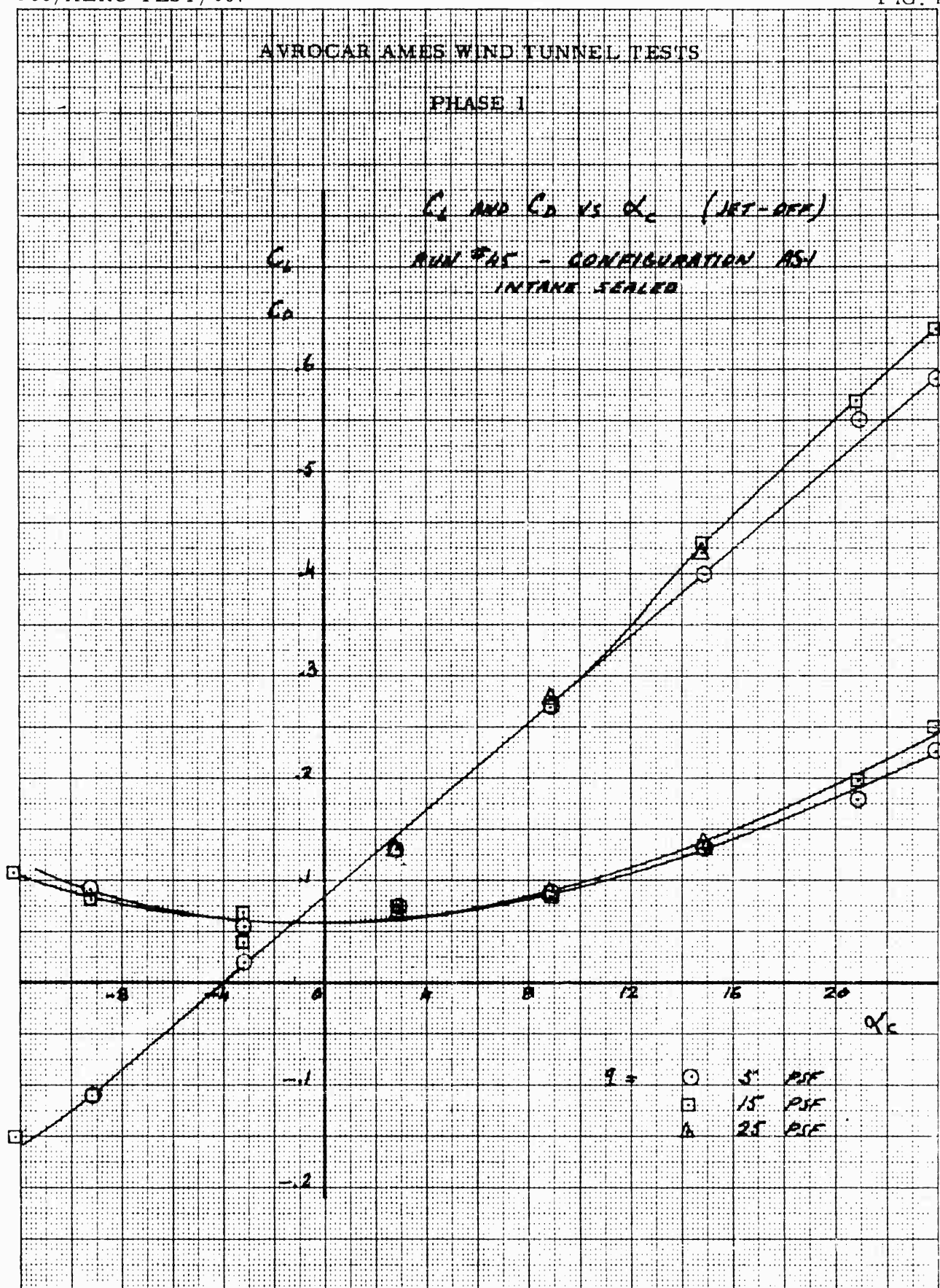


FIG. 1 AVROCAR IN THE 40 X 80 FOOT TUNNEL,  
AMES RESEARCH CENTER

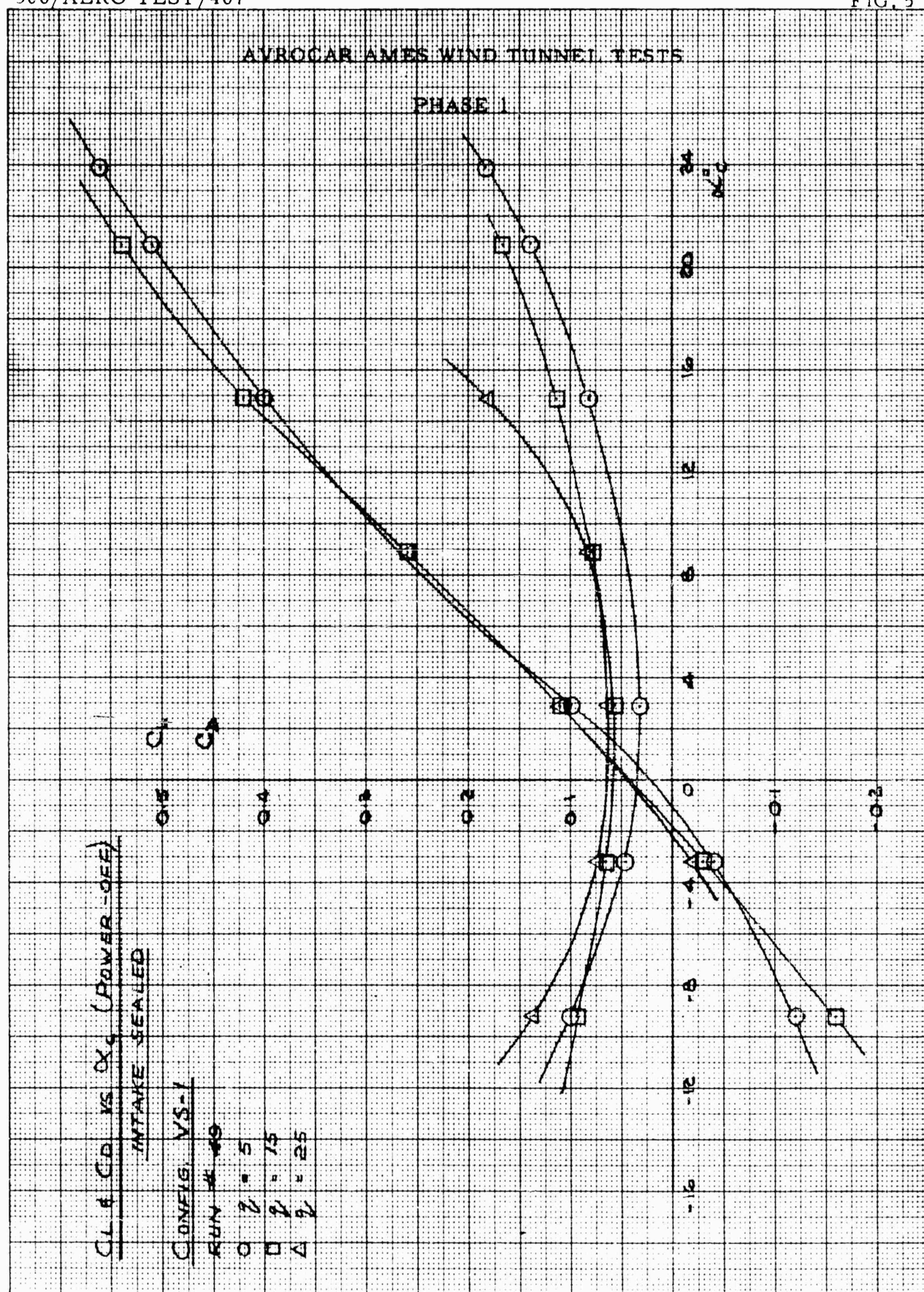


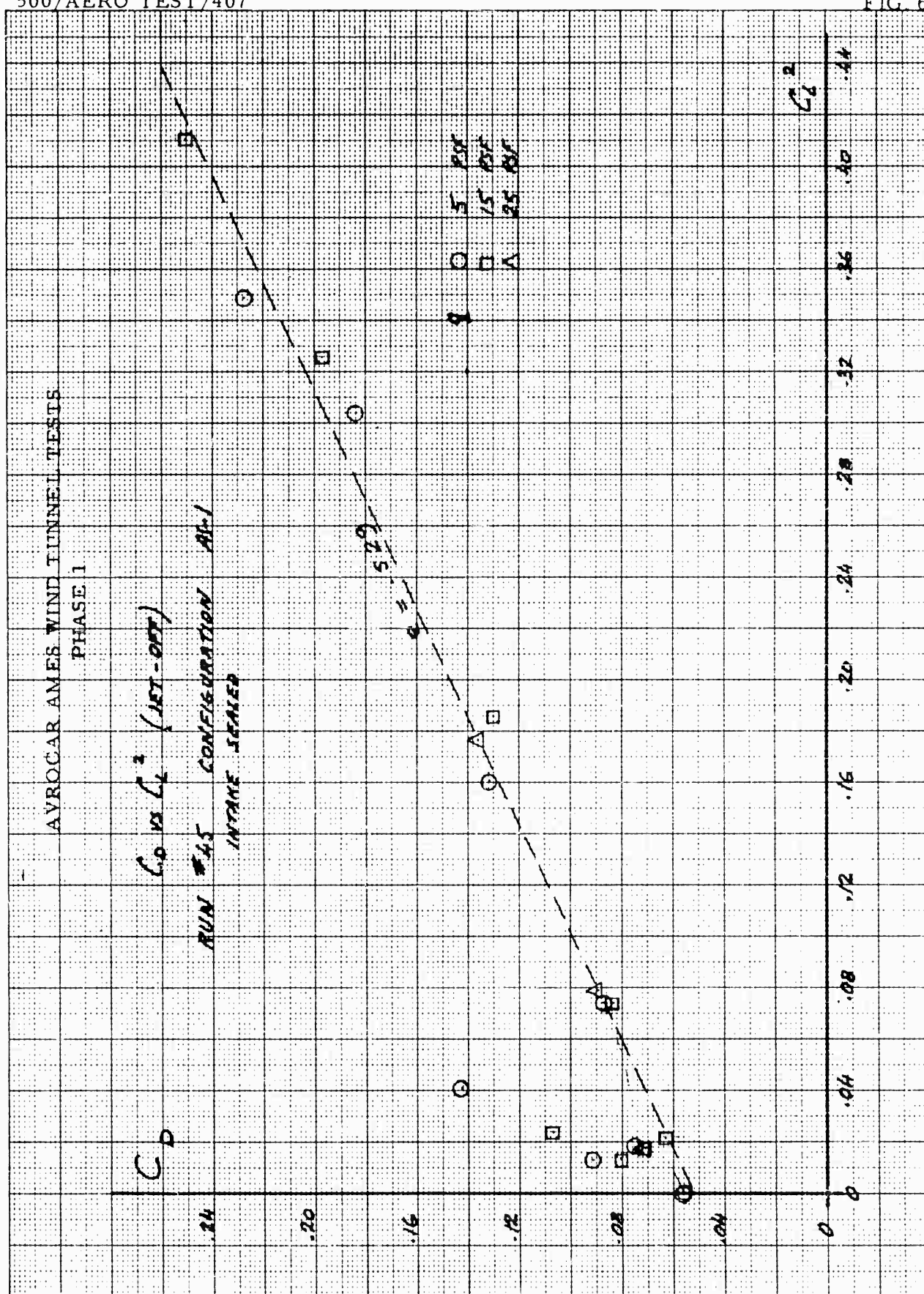














# AVROCAR AMES WIND TUNNEL TESTS PHASE I

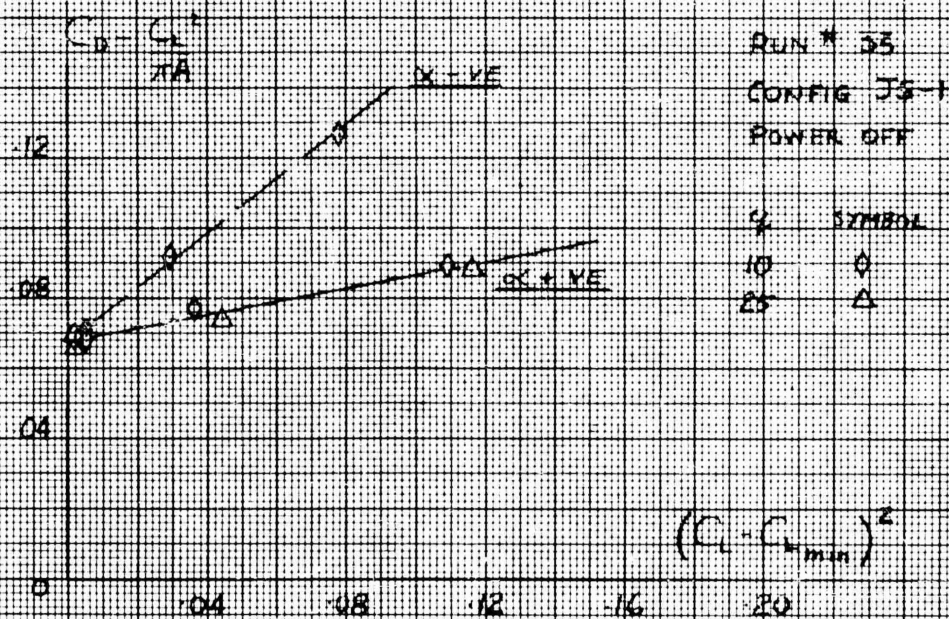
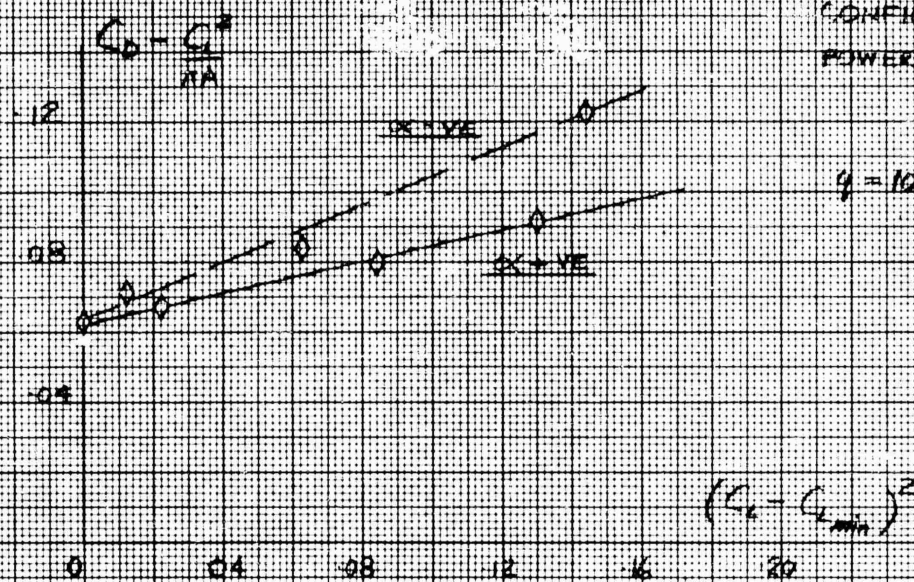
$$\frac{C_D - C_{D^*}}{RA} \text{ vs } (C_L - C_{L_{min}})^2$$

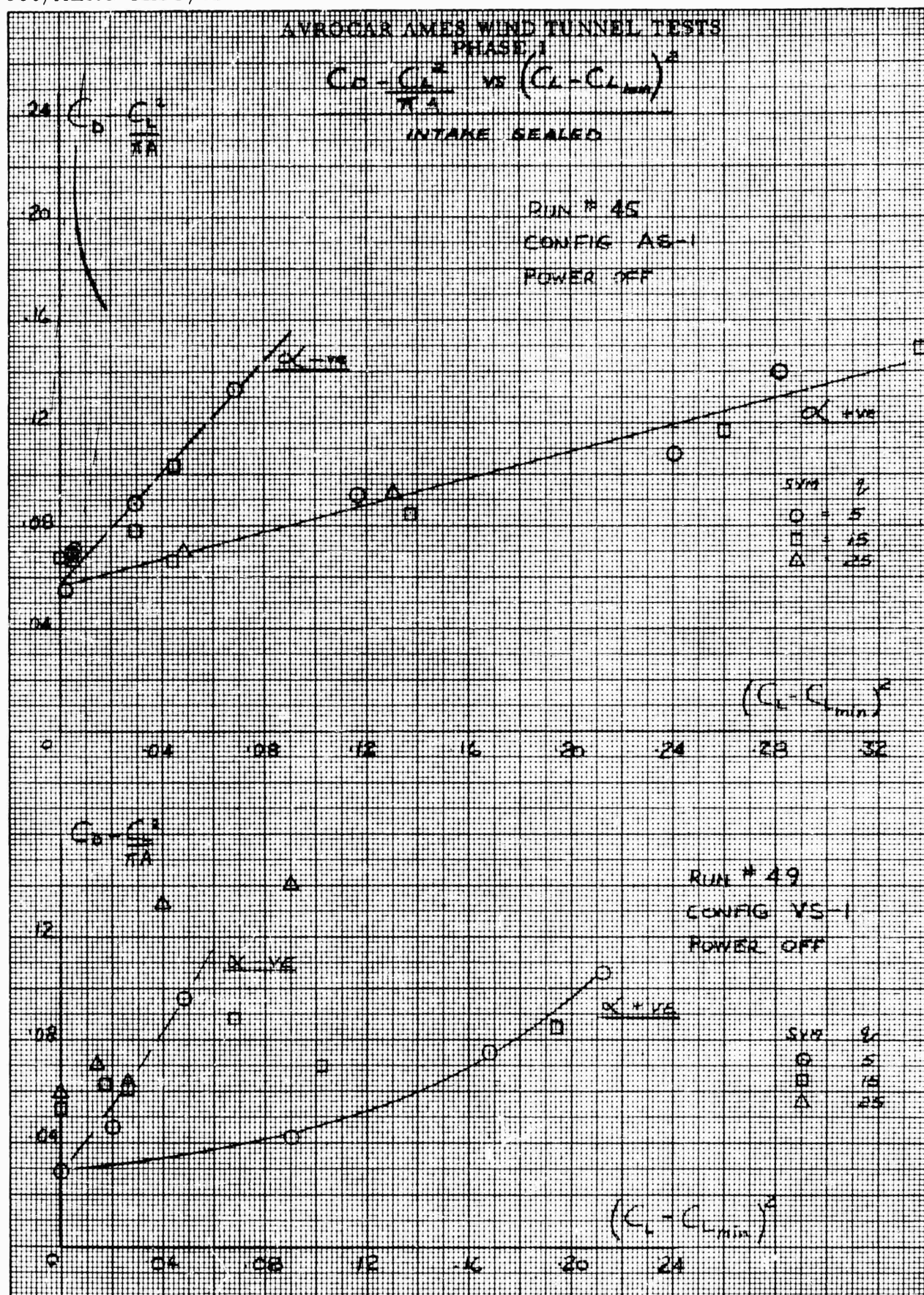
INTAKE SEALED

RUN # 30

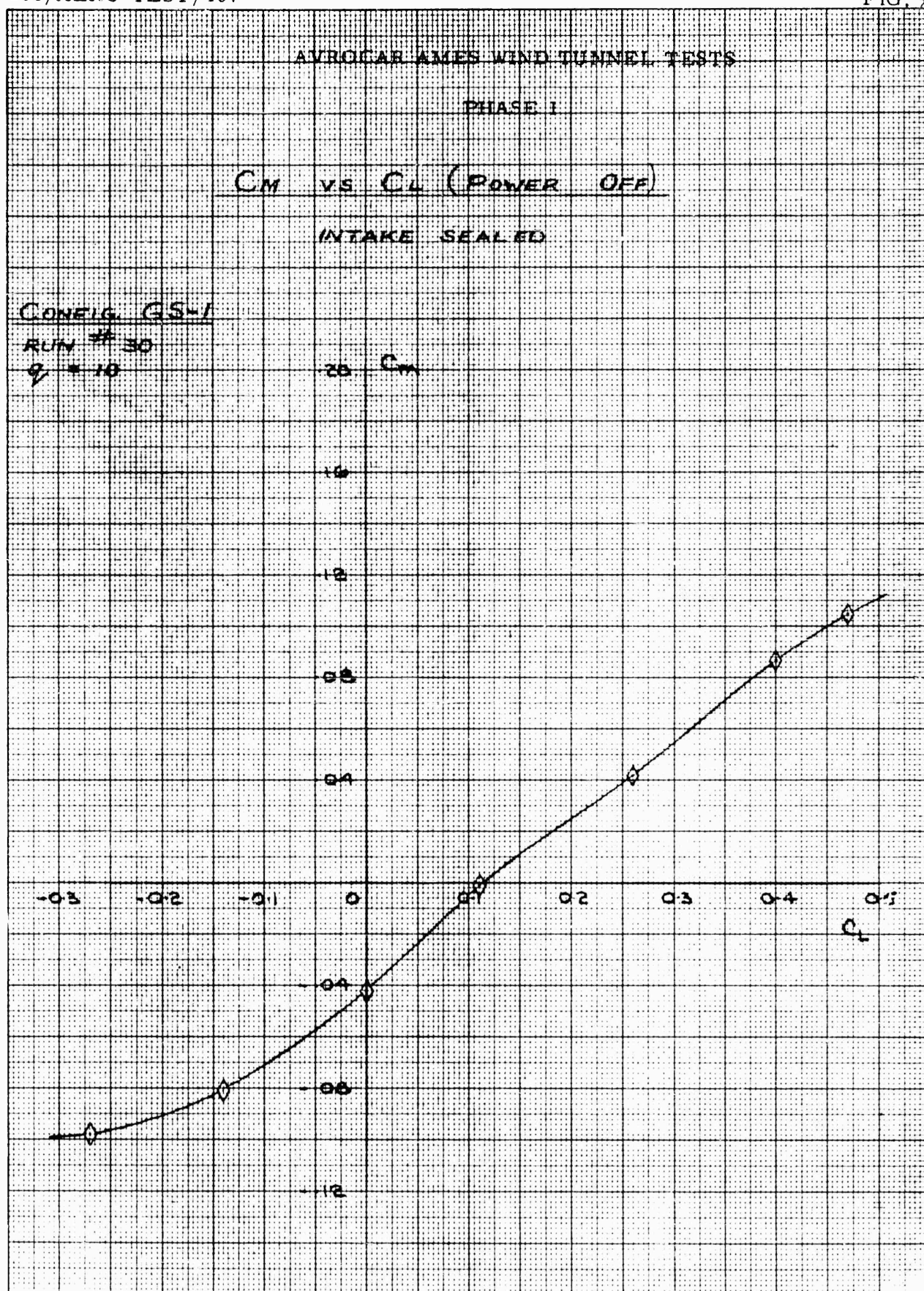
CONFIG GS-1

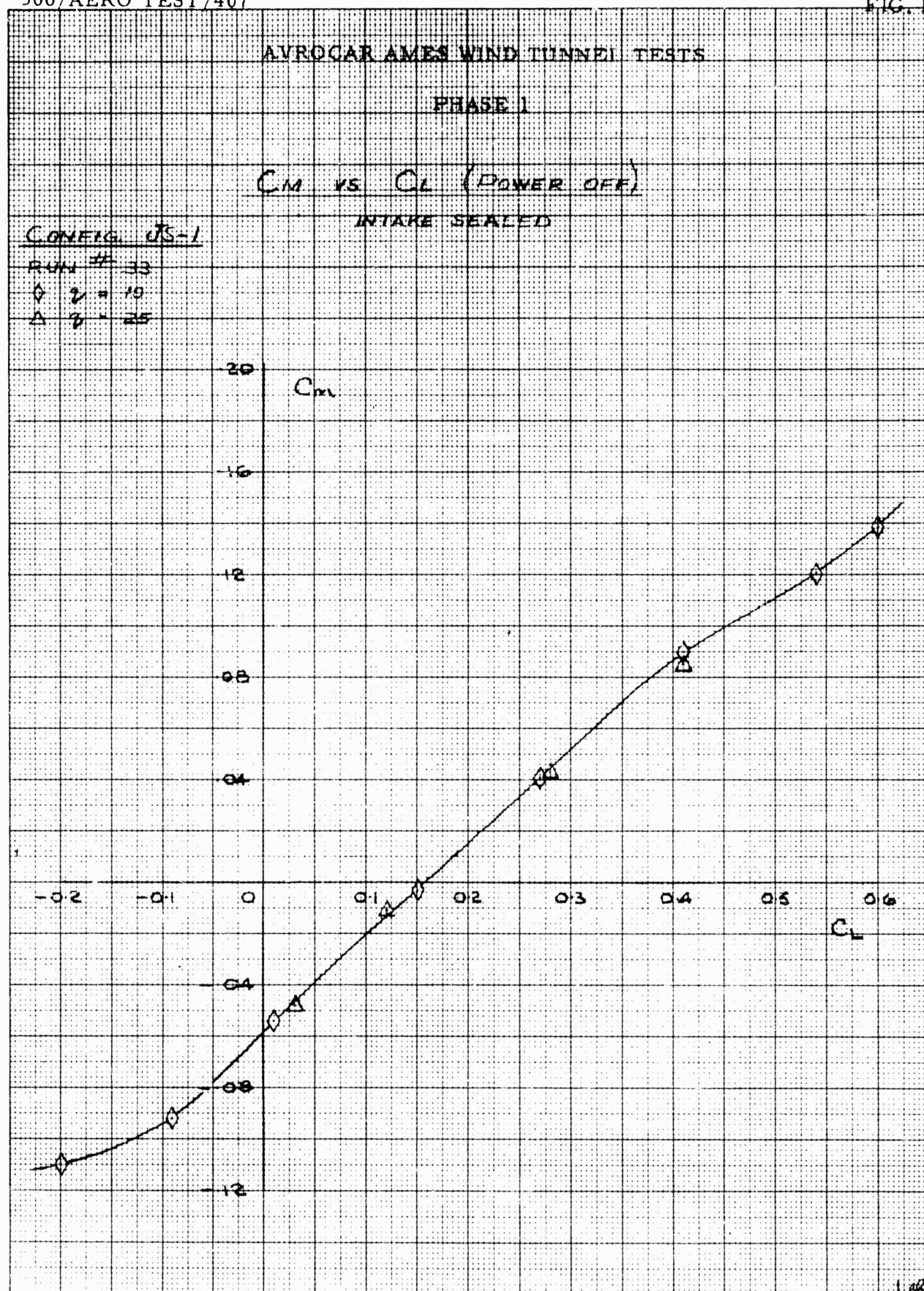
POWER OFF



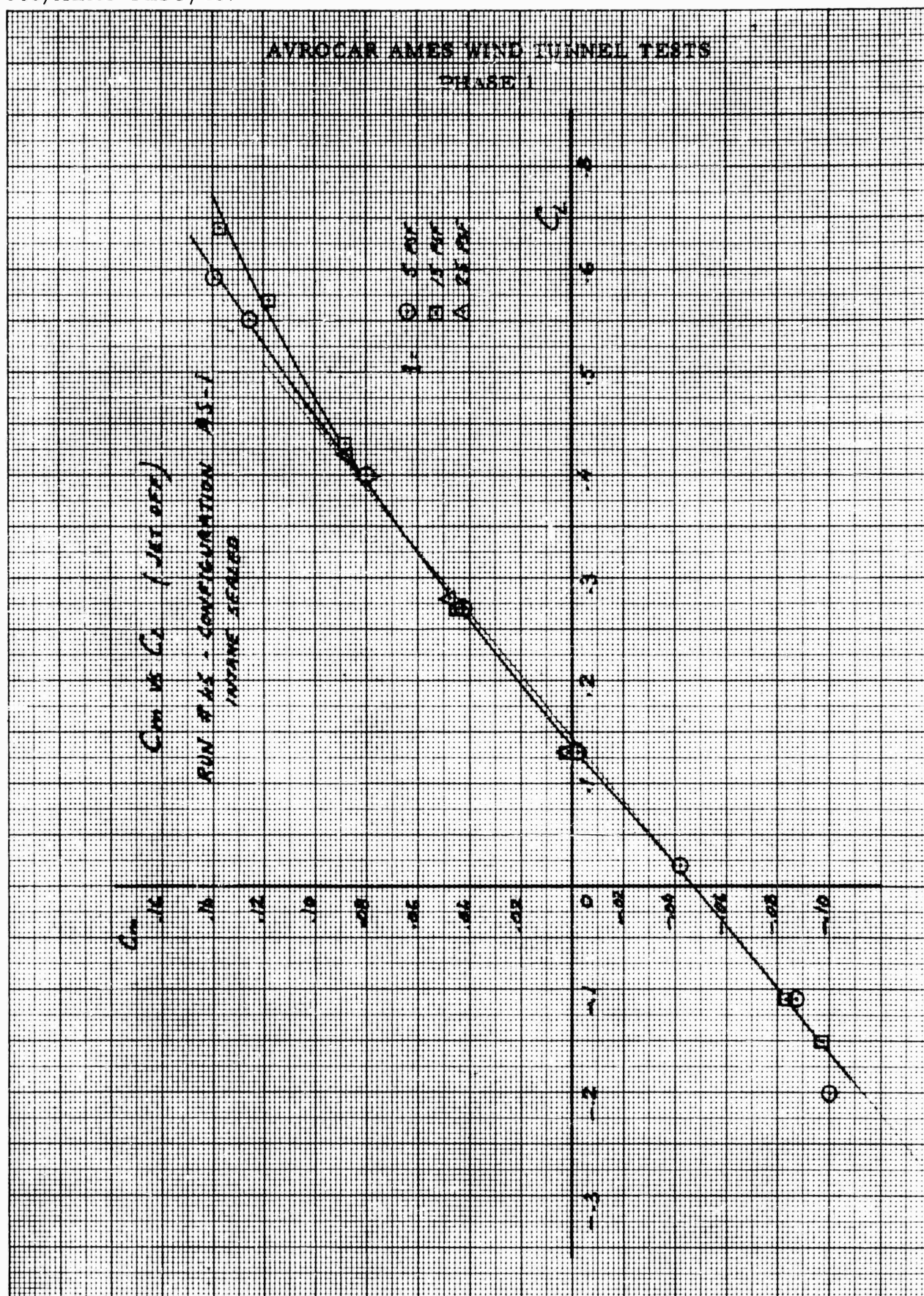


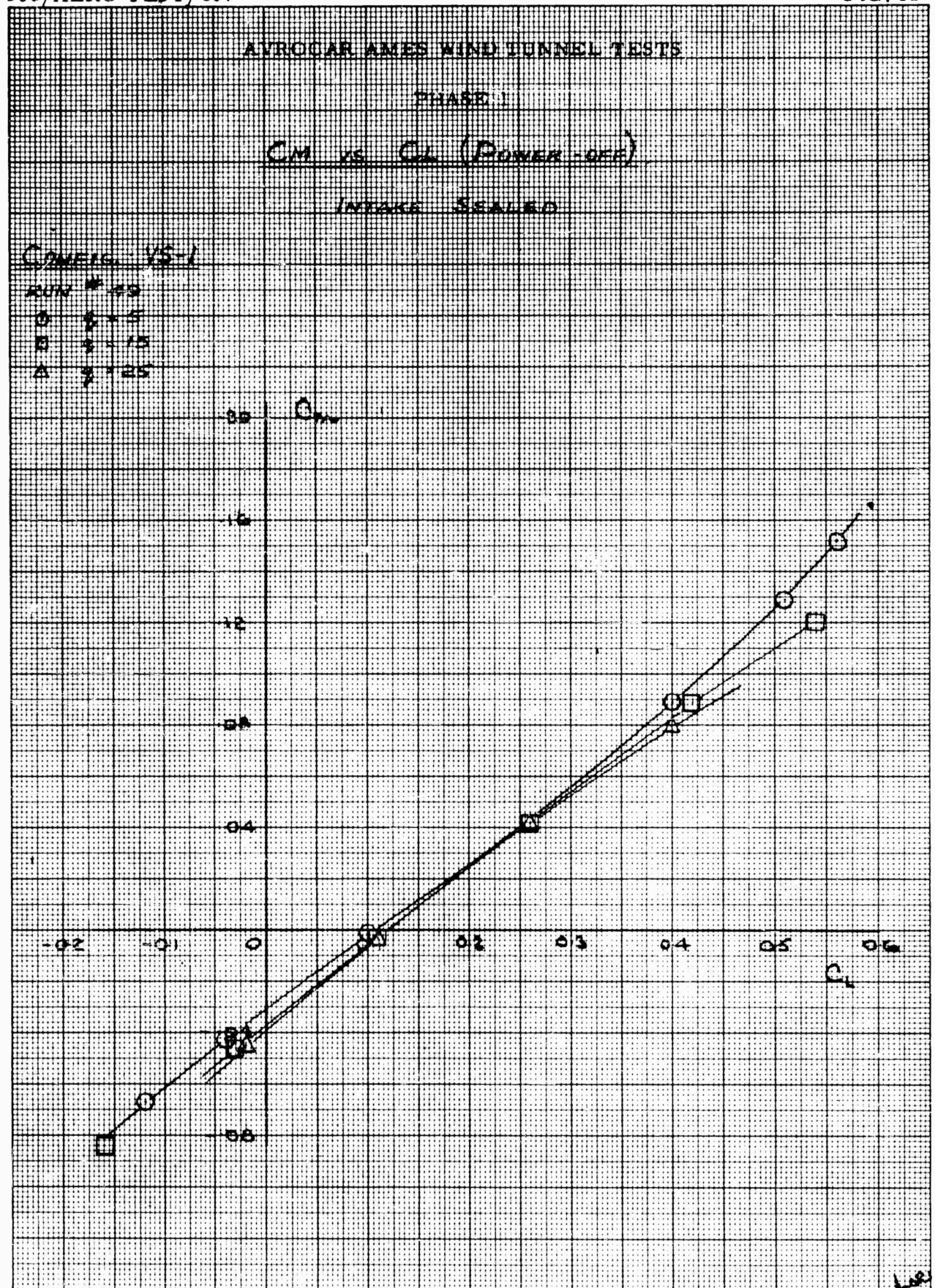










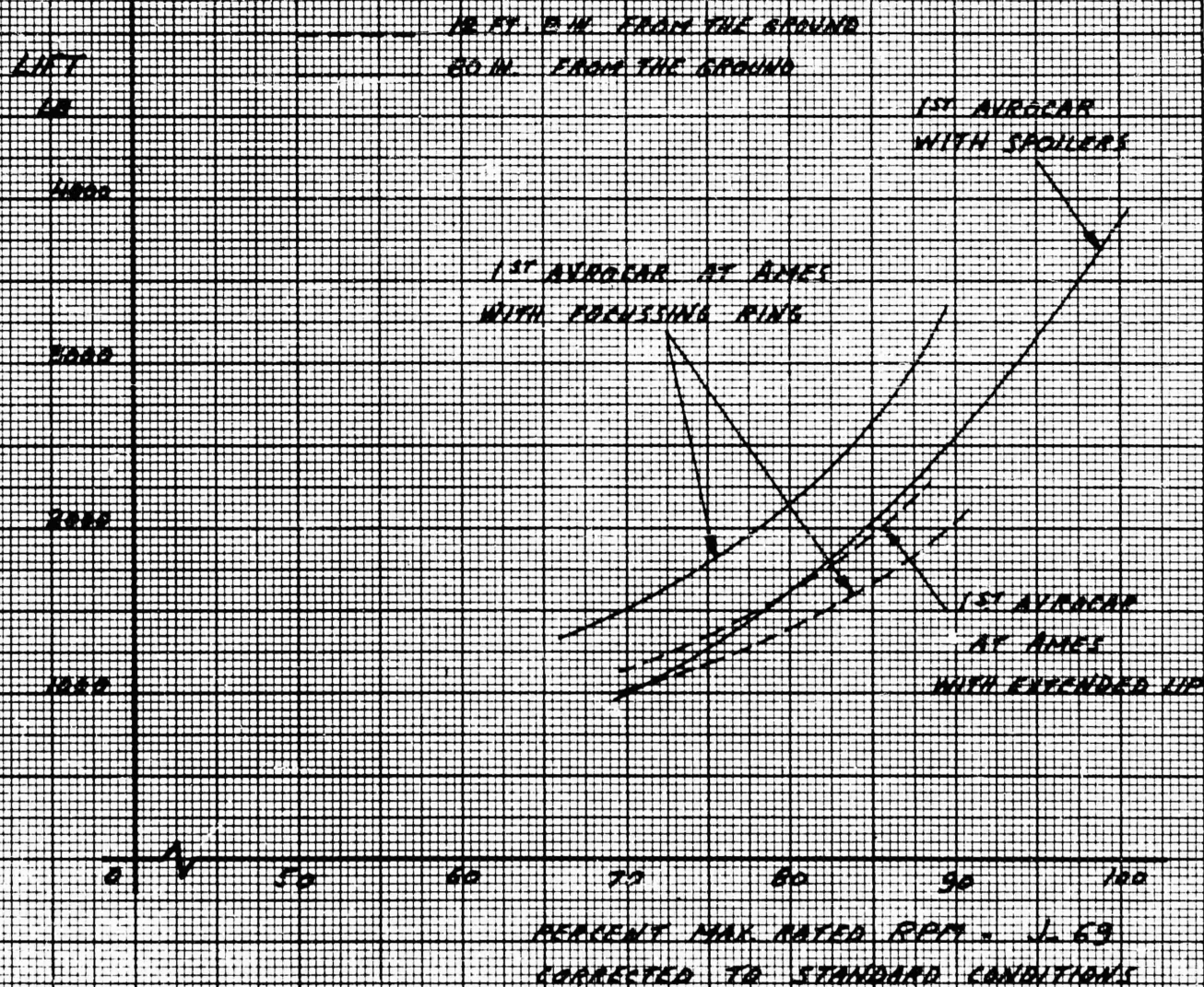


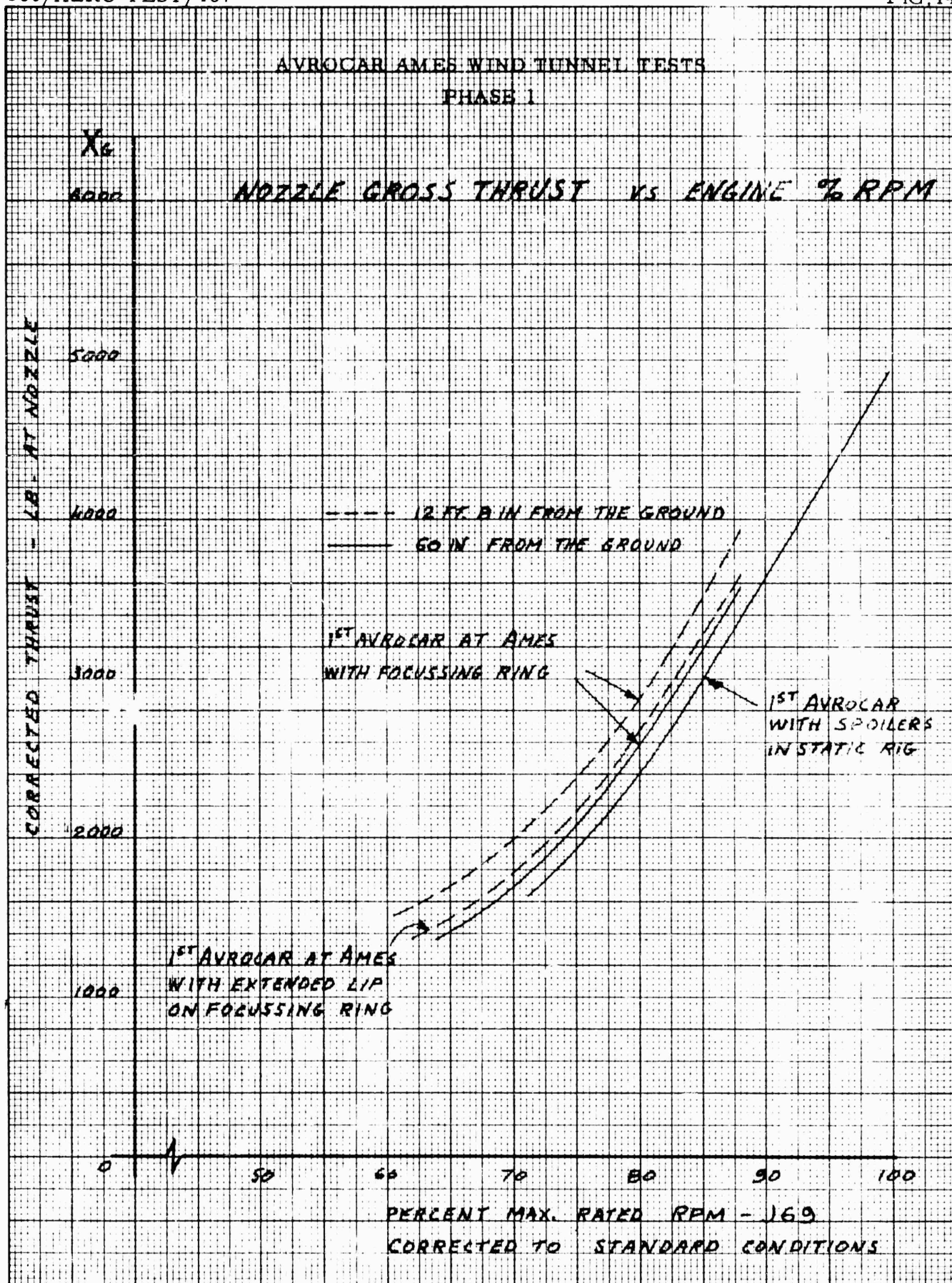


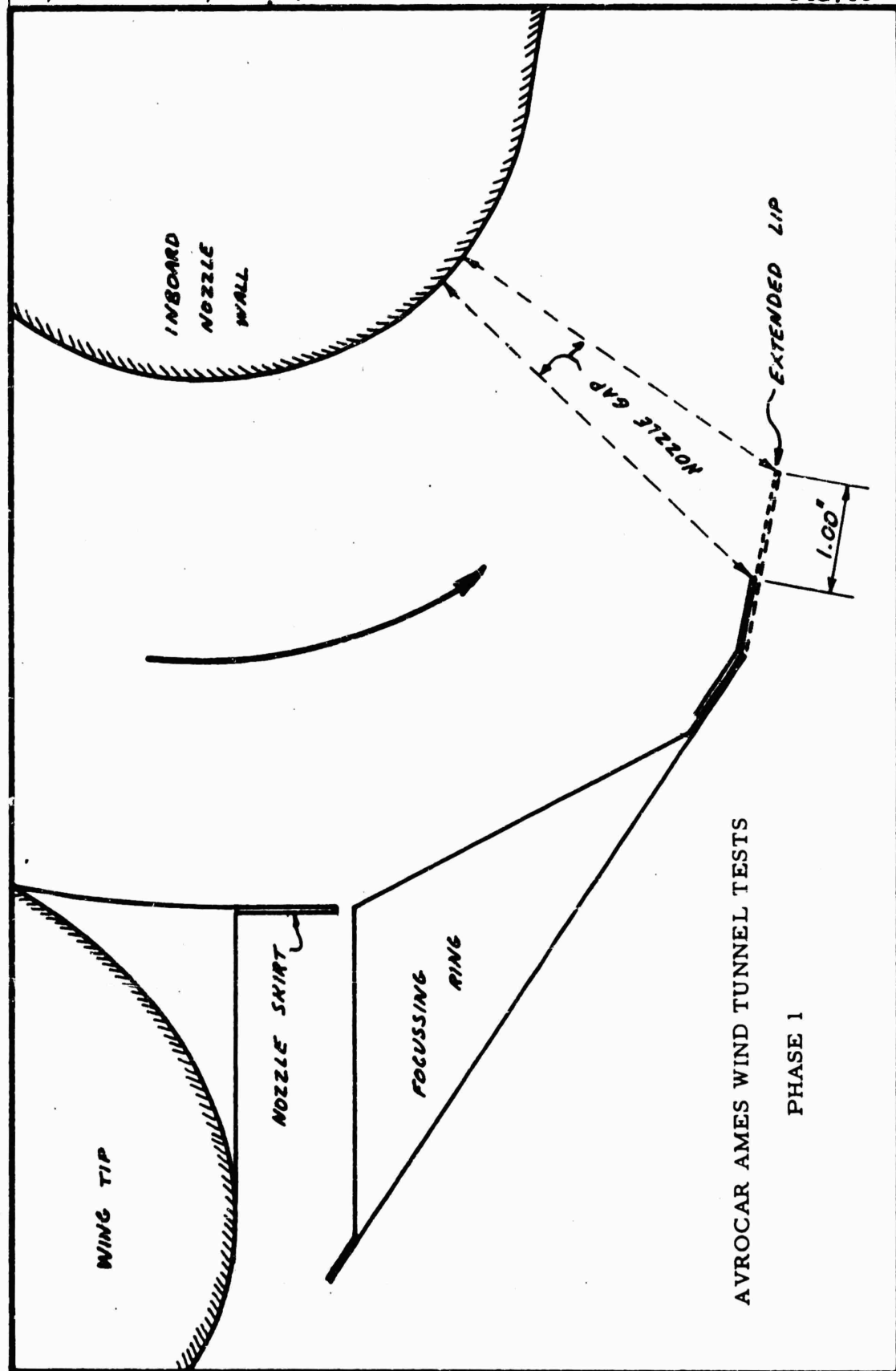
## AVROCAR AMES WIND TUNNEL TESTS

## PHASE I

## AVROCAR LIFT VS ENGINE % RPM.





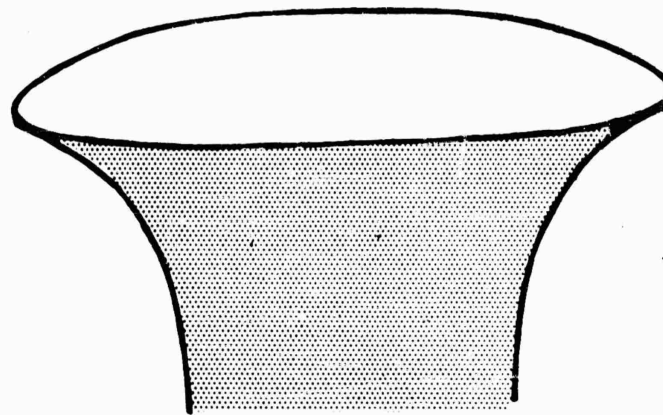


EXTENDED LIP ON FOCUSING CONTROL RING

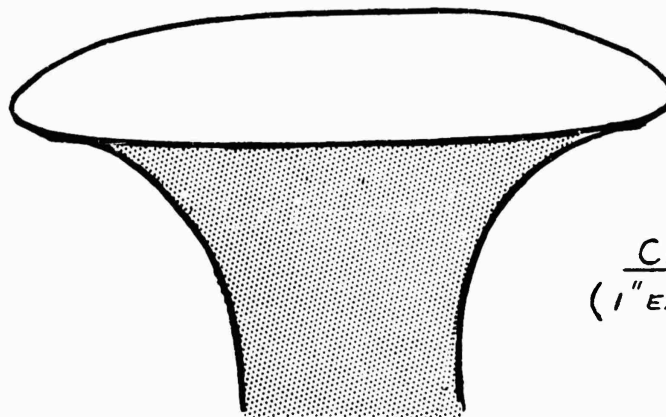
PHASE 1

AVROCAR AMES WIND TUNNEL TESTS

PHASE 1



CONFIG. A-1



CONFIG. E-1  
(1" EXTENDED LIP)

EFFECT OF EXTENSION TO FOCUSING CONTROL RING

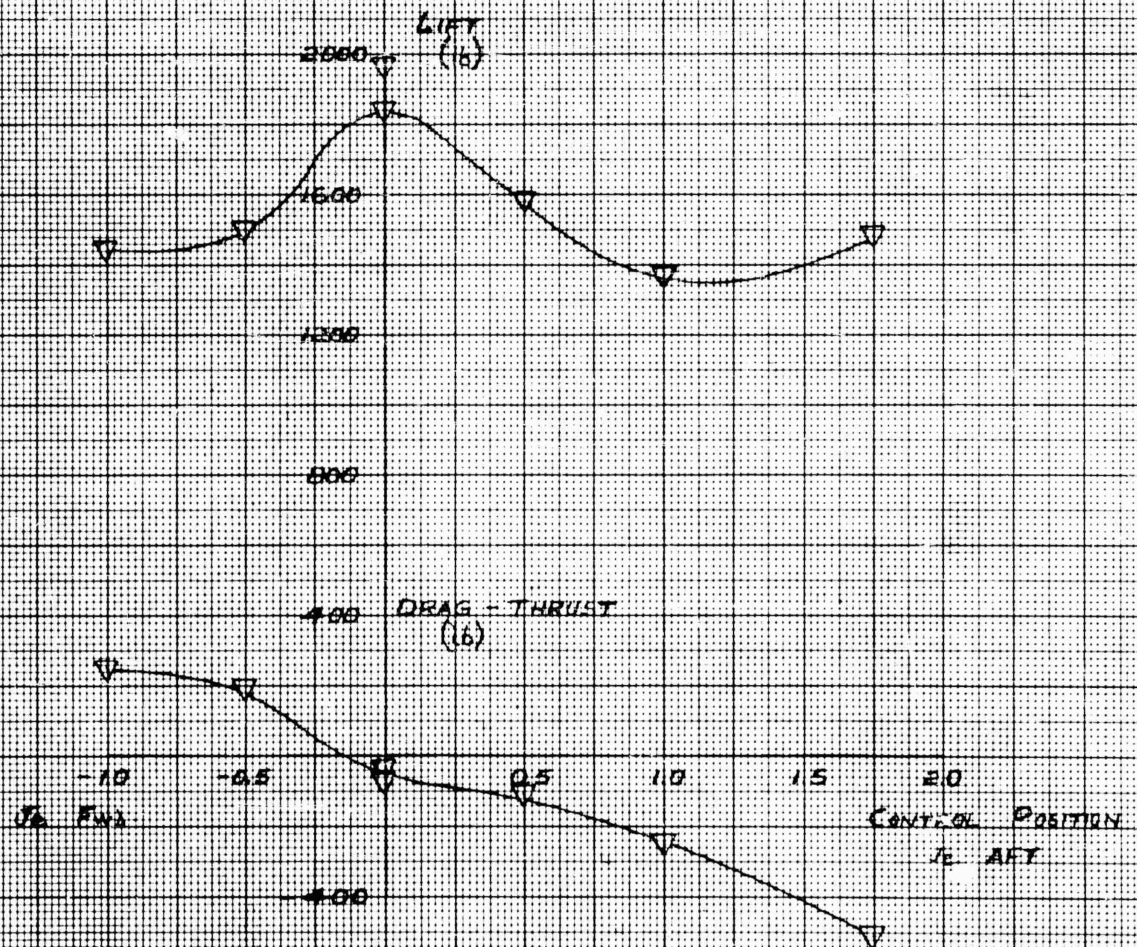


## AVROCAR AMES WIND TUNNEL TESTS

## PHASE 1

LIFT AND DRAG VS CONTROL POSITION

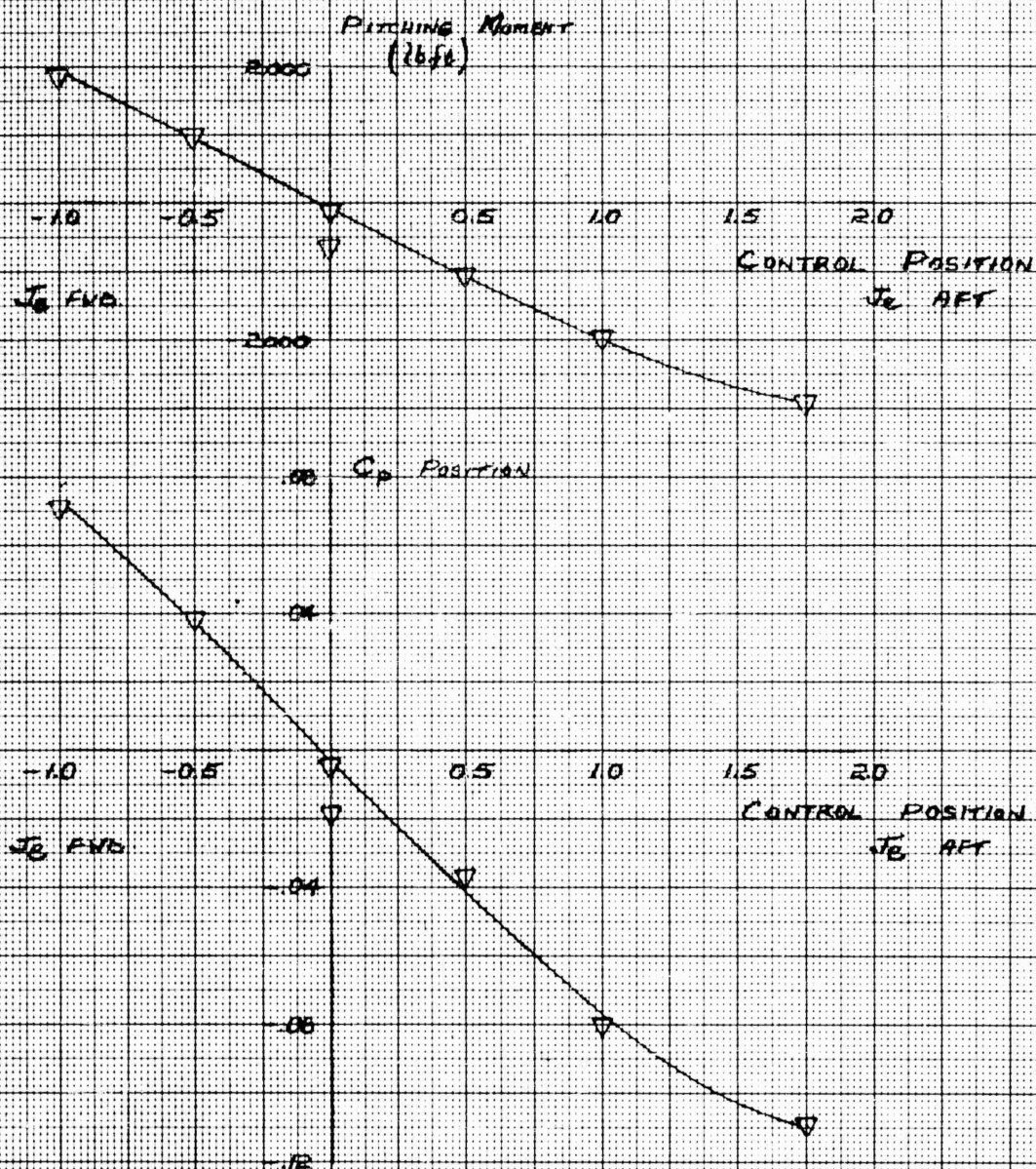
CONFIG. A-1 &amp; B-1

MAX  $\alpha/\delta$  $M = 90\%$  $\alpha_c = 0^\circ$  $\beta = 0$ 

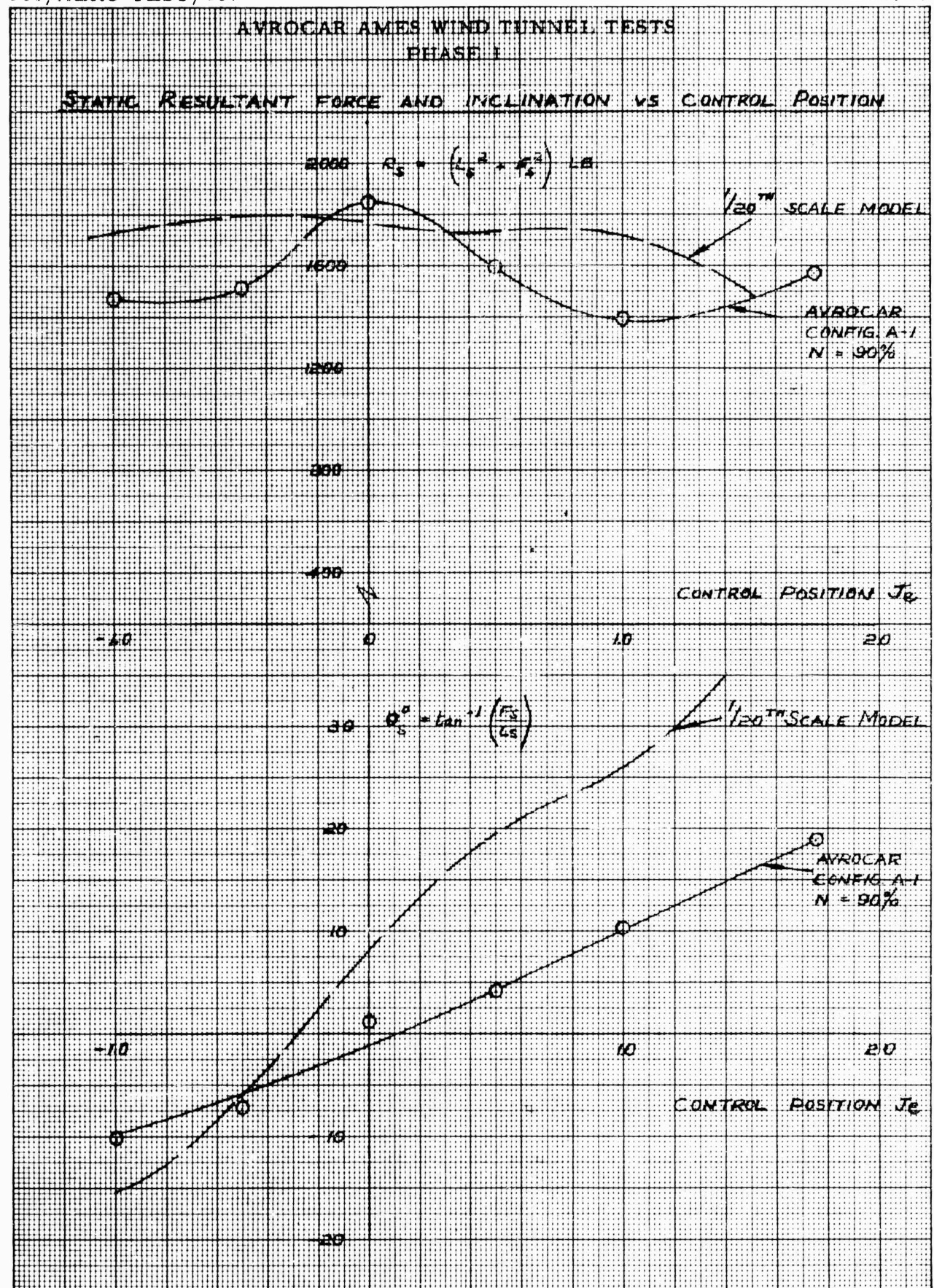
# AVROCAR AMES WIND TUNNEL TESTS PHASE I

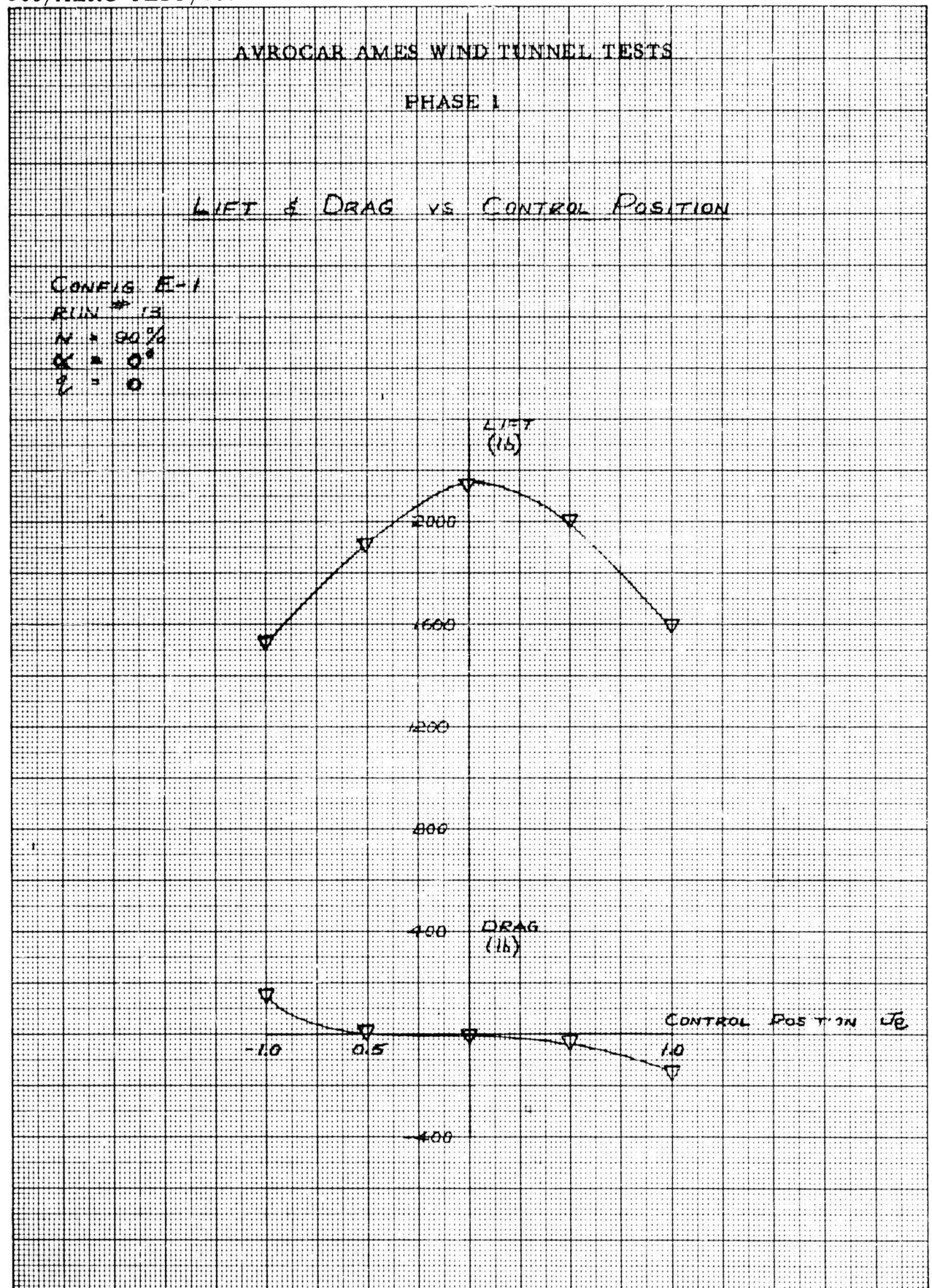
## PITCHING MOMENT & CENTRE OF PRESSURE VS CONTROL POSITION

CONFIG. A-1 & B-1  
MAX.  $h/D$   
 $\alpha_6 = 0^\circ$   
 $N = 90\%$   
 $q = 0$











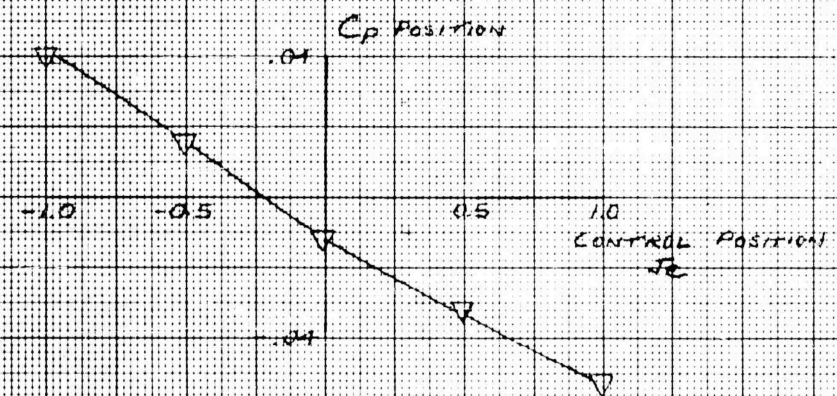
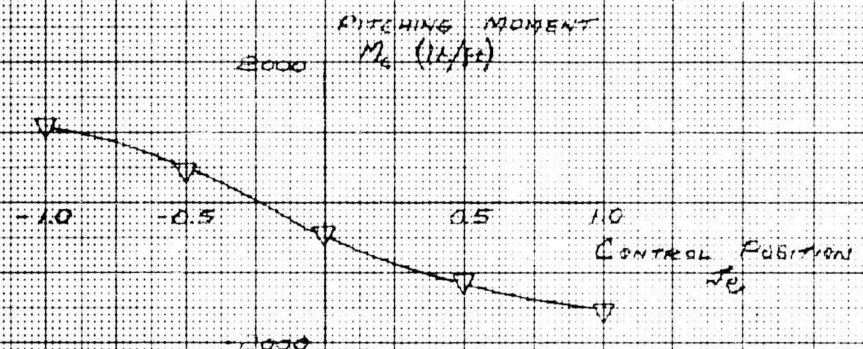
## AVROCAR AMES WIND TUNNEL TESTS

## PHASE I

## PITCHING MOMENT &amp; CENTRE OF PRESSURE VS. CONTROL POSITION

CONFIG. E-1

RUN # 13

 $M = 30\%$  $\alpha = 0^\circ$  $q = 0$ 

## AVROCAR AMES WIND TUNNEL TESTS

## PHASE 1

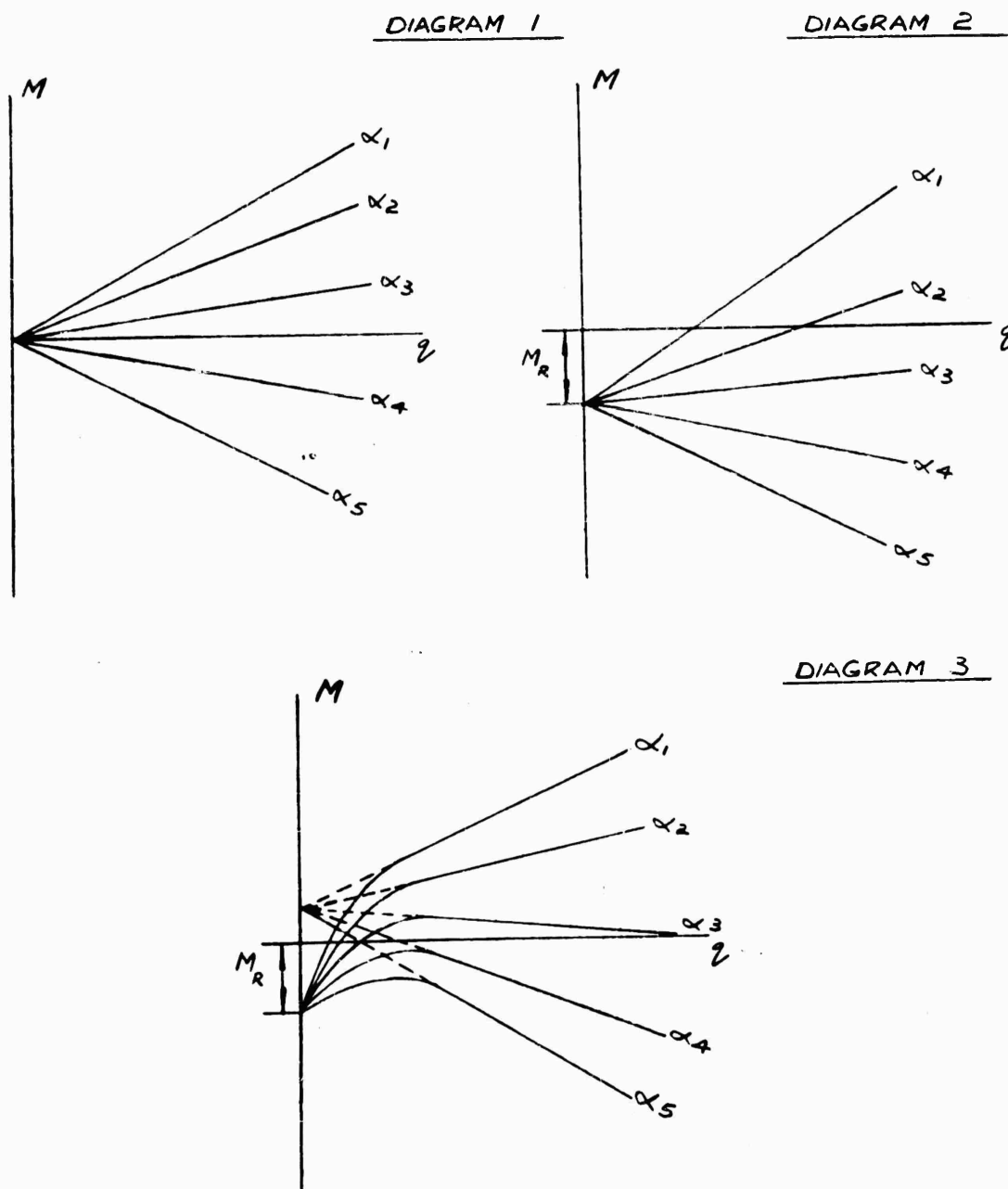
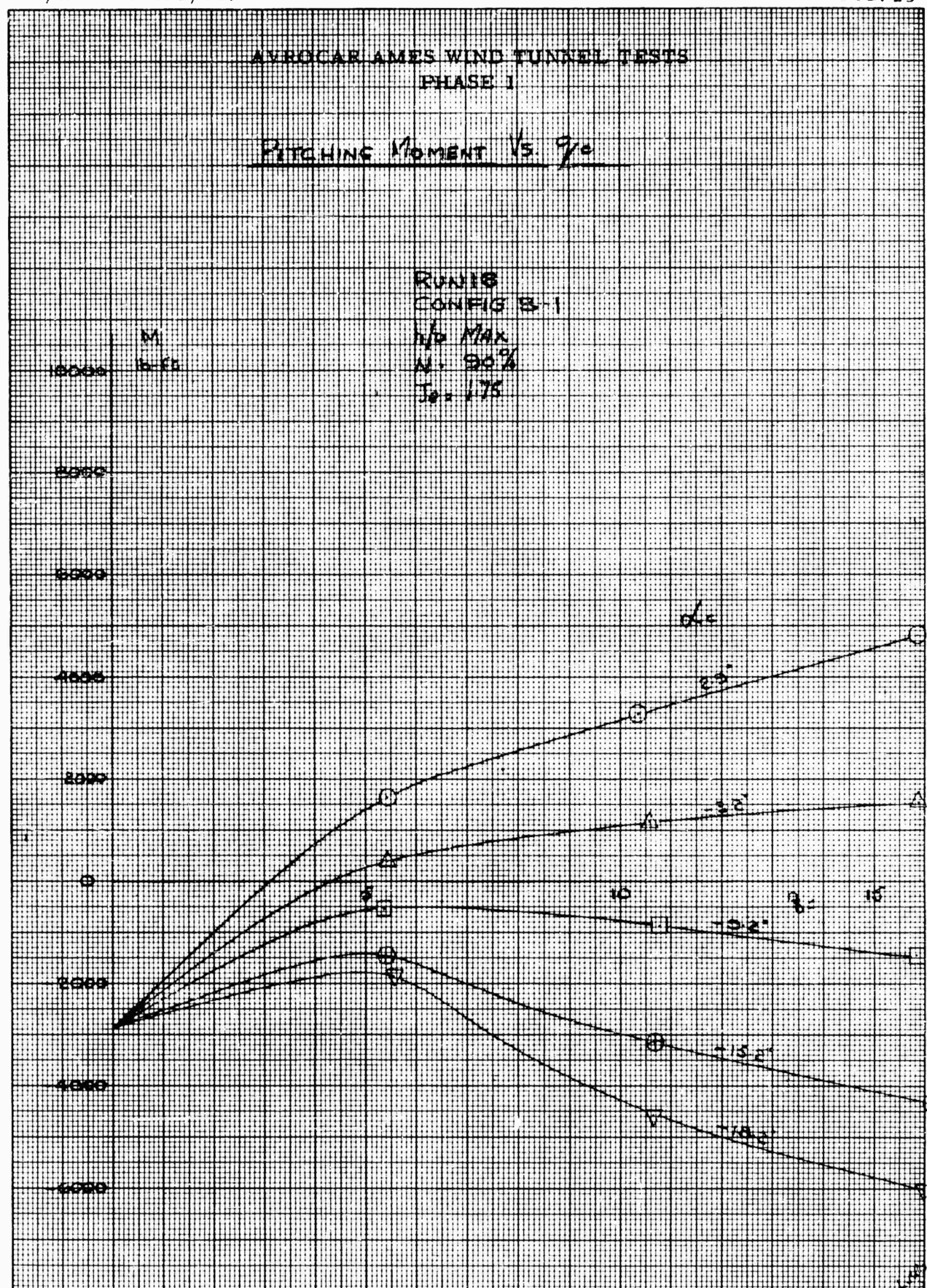


DIAGRAM ILLUSTRATING EFFECTIVE STATIC MOMENT



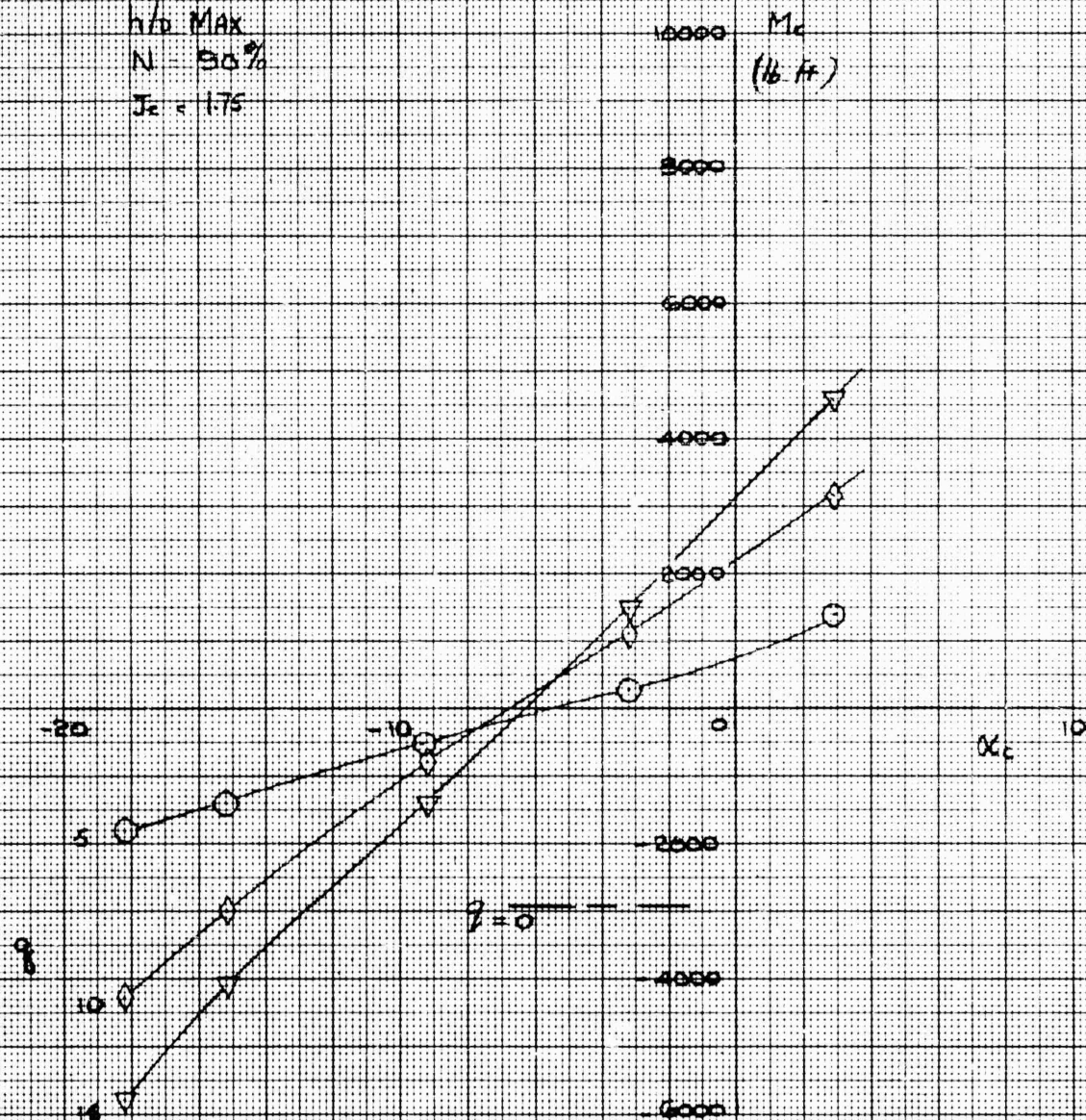


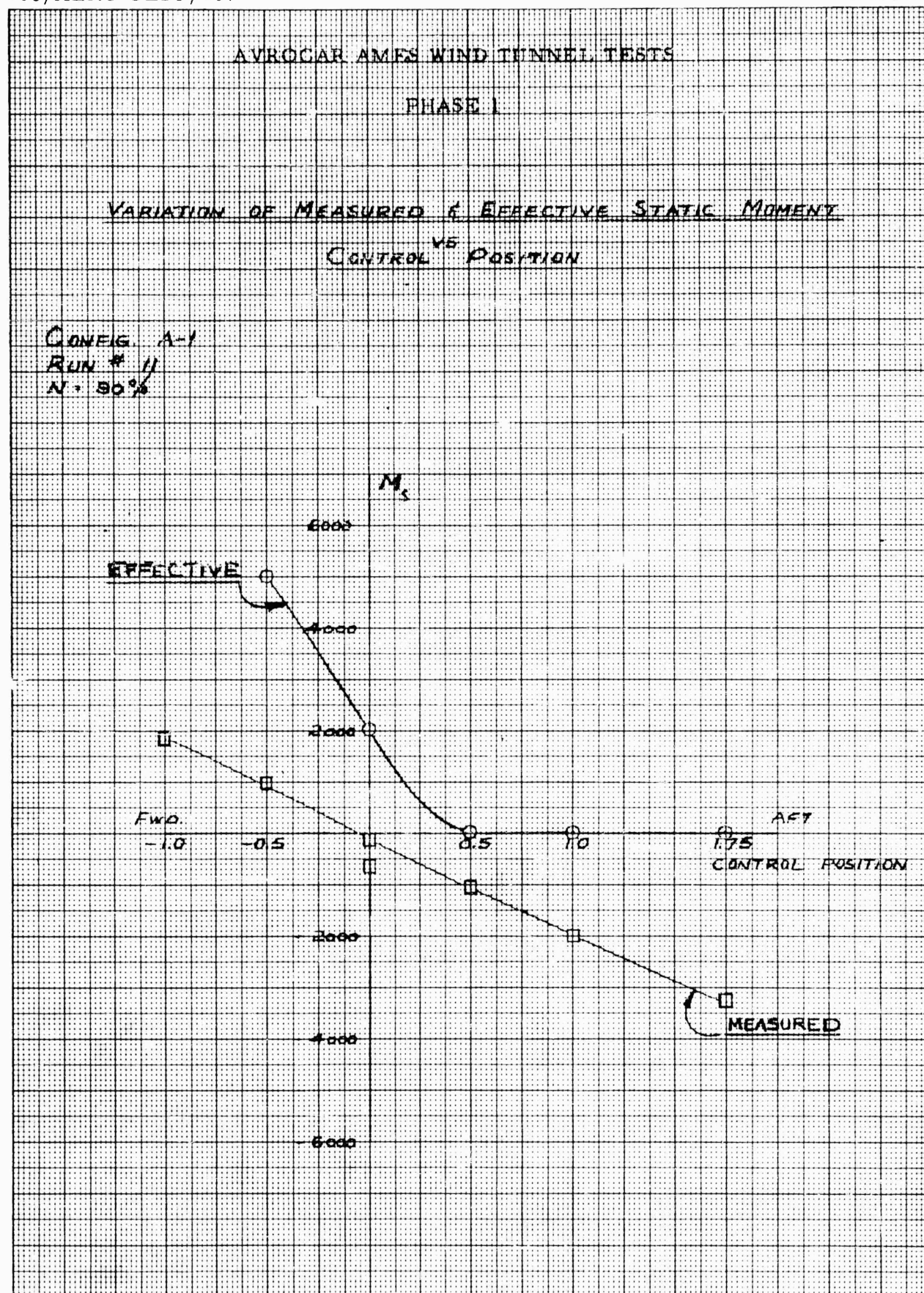
AVROCAR AMES WIND TUNNEL TESTS  
PHASE 1

PITCHING MOMENT  $\% \alpha_c$

RUN 16  
CONFIG B-1

h/d MAX  
N = 50%  
 $J_c = 1.75$





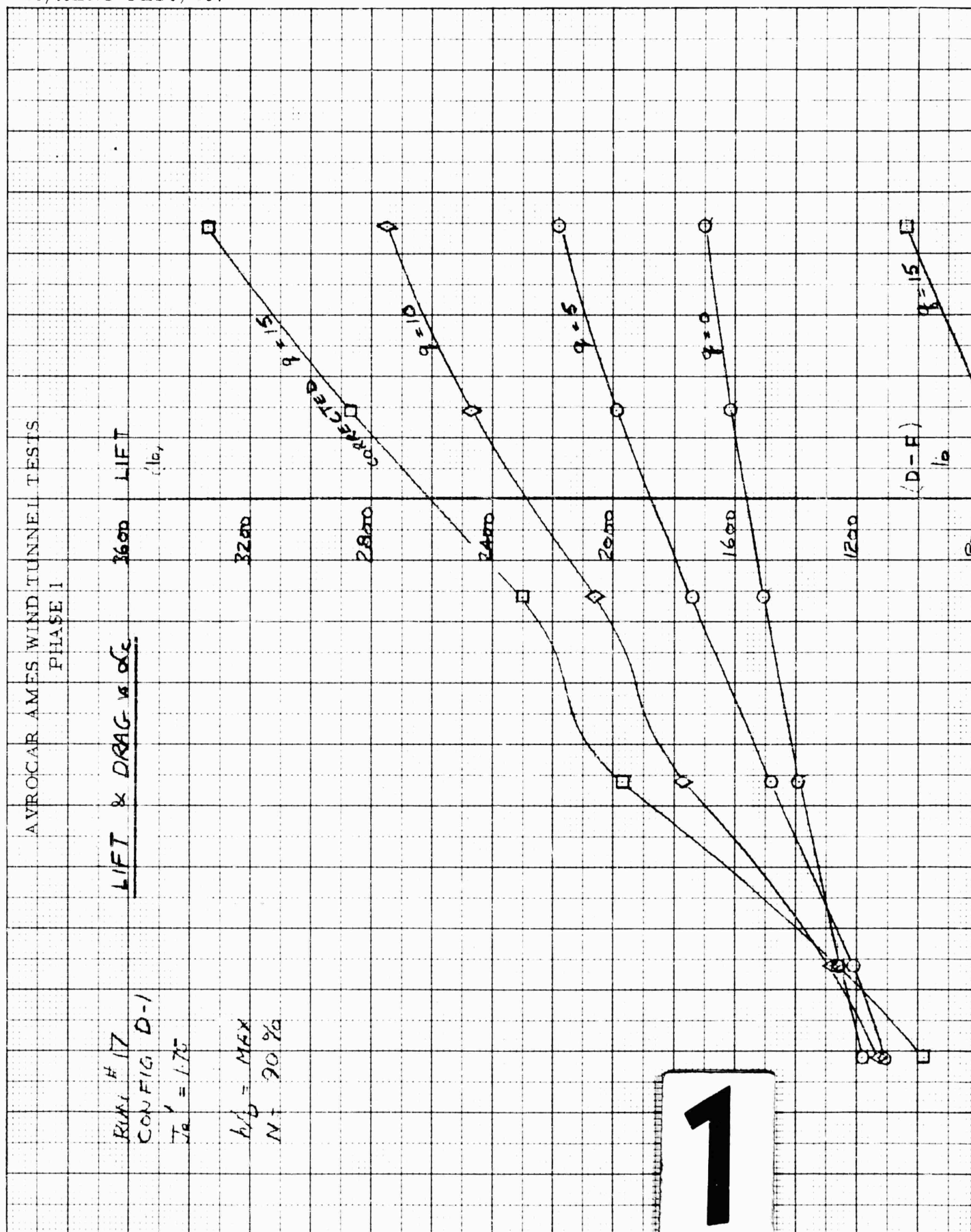
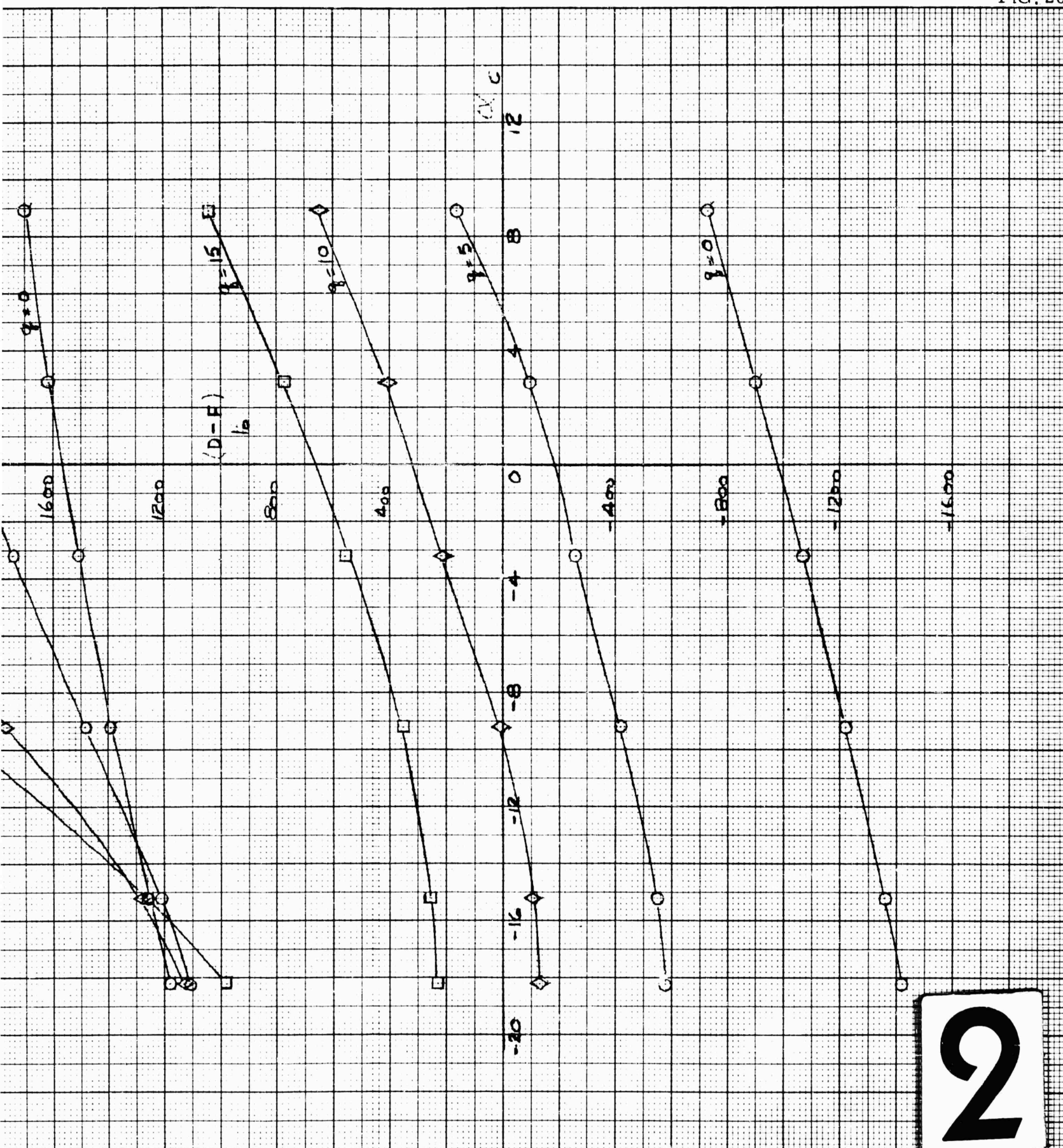




FIG. 26



2



AVROCAR AMES WIND TUNNEL TESTS  
PHASE I

LIFT & DRAG vs  $\alpha$

RUN 38

CONF 4 N-1A

$M = 90\%$

RUDDER: AFT

LIFT vs  $\alpha$

5200

4800

4400

4000

3600

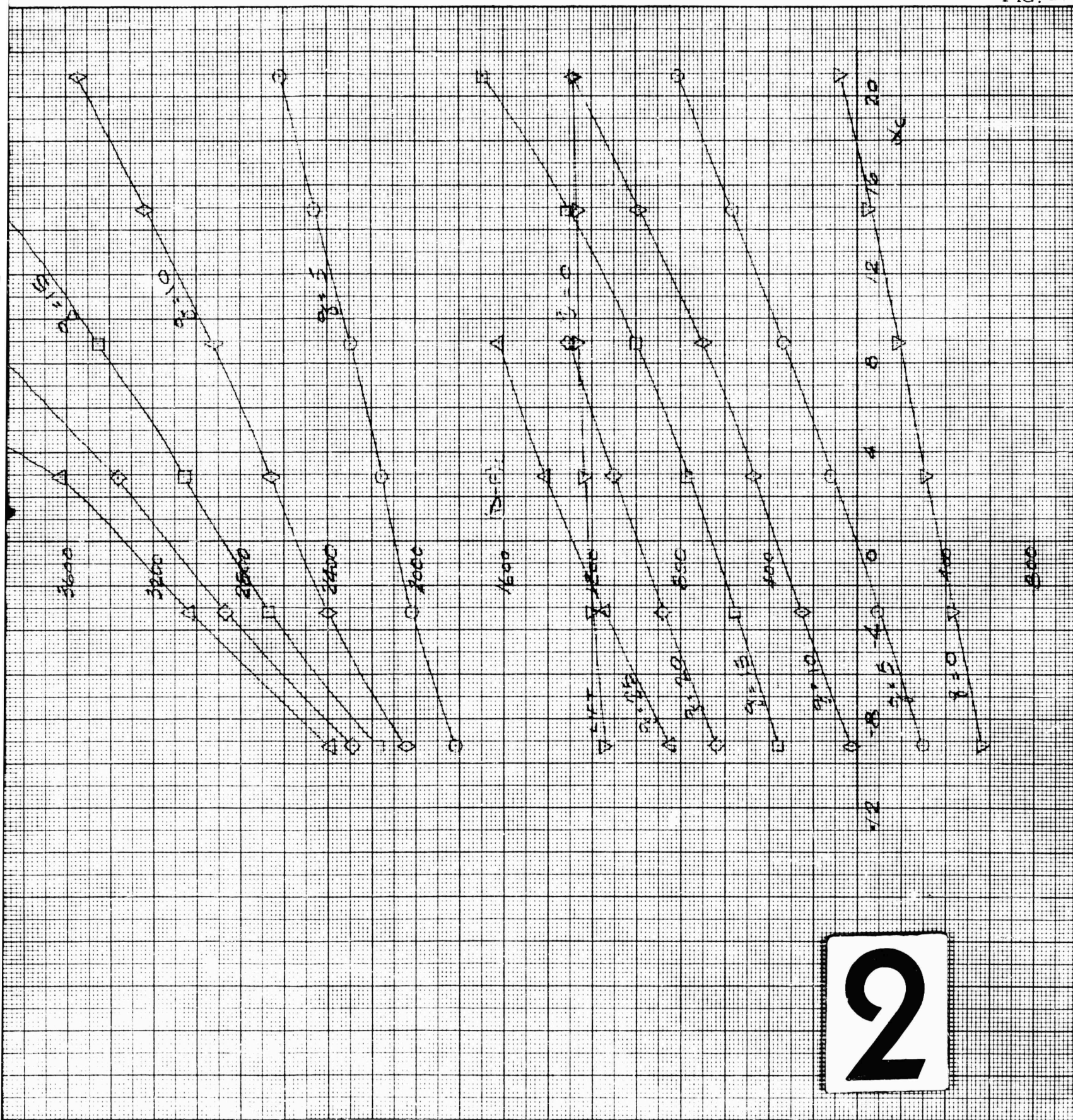
3200

2800

2400

1

FIG. 27





AVROCAR AMES WIND TUNNEL TESTS  
PHASE I

LIFT & DRAG vs  $\alpha_c$

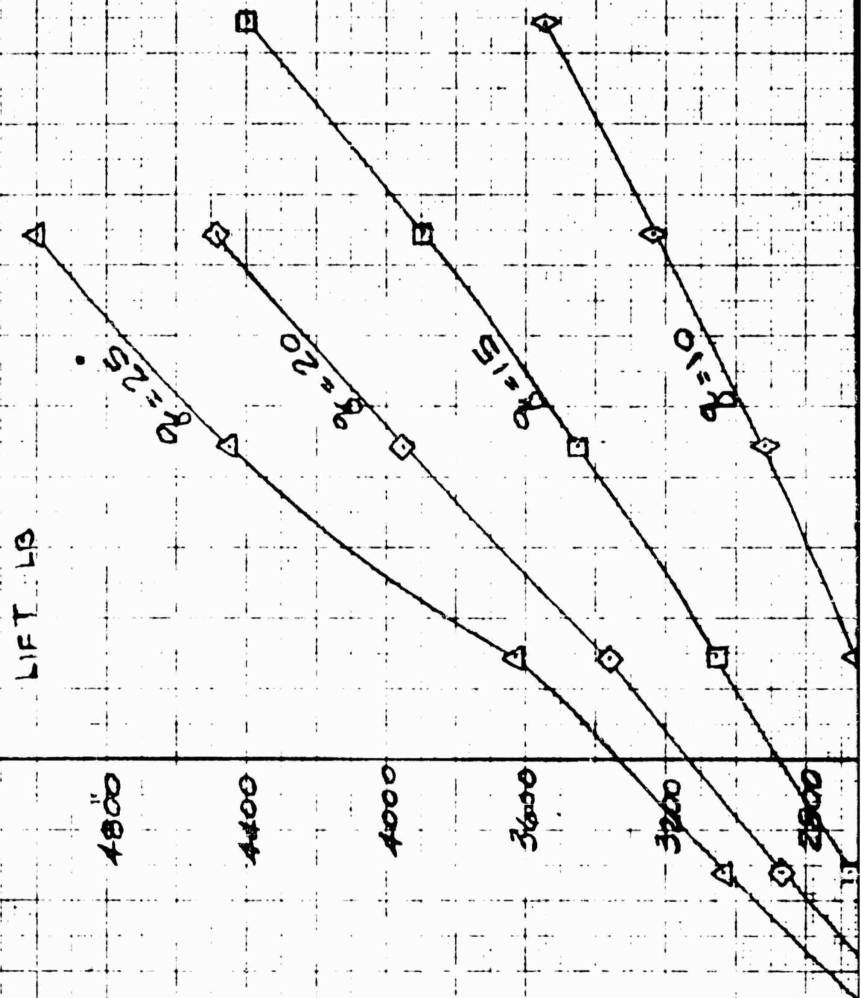
RUN 38

CONFIG N-1A

N = 90%

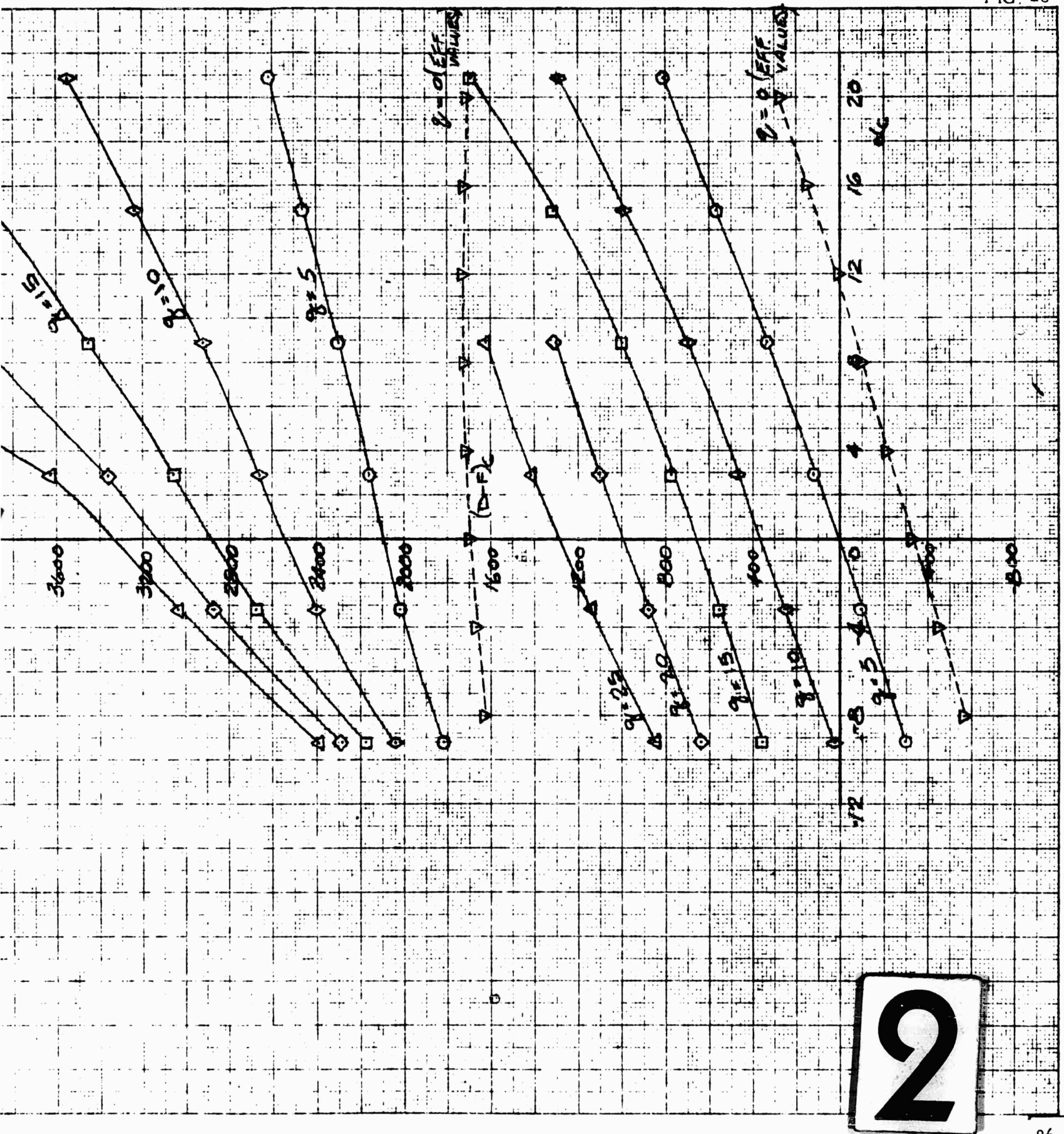
RUDDERS AFT

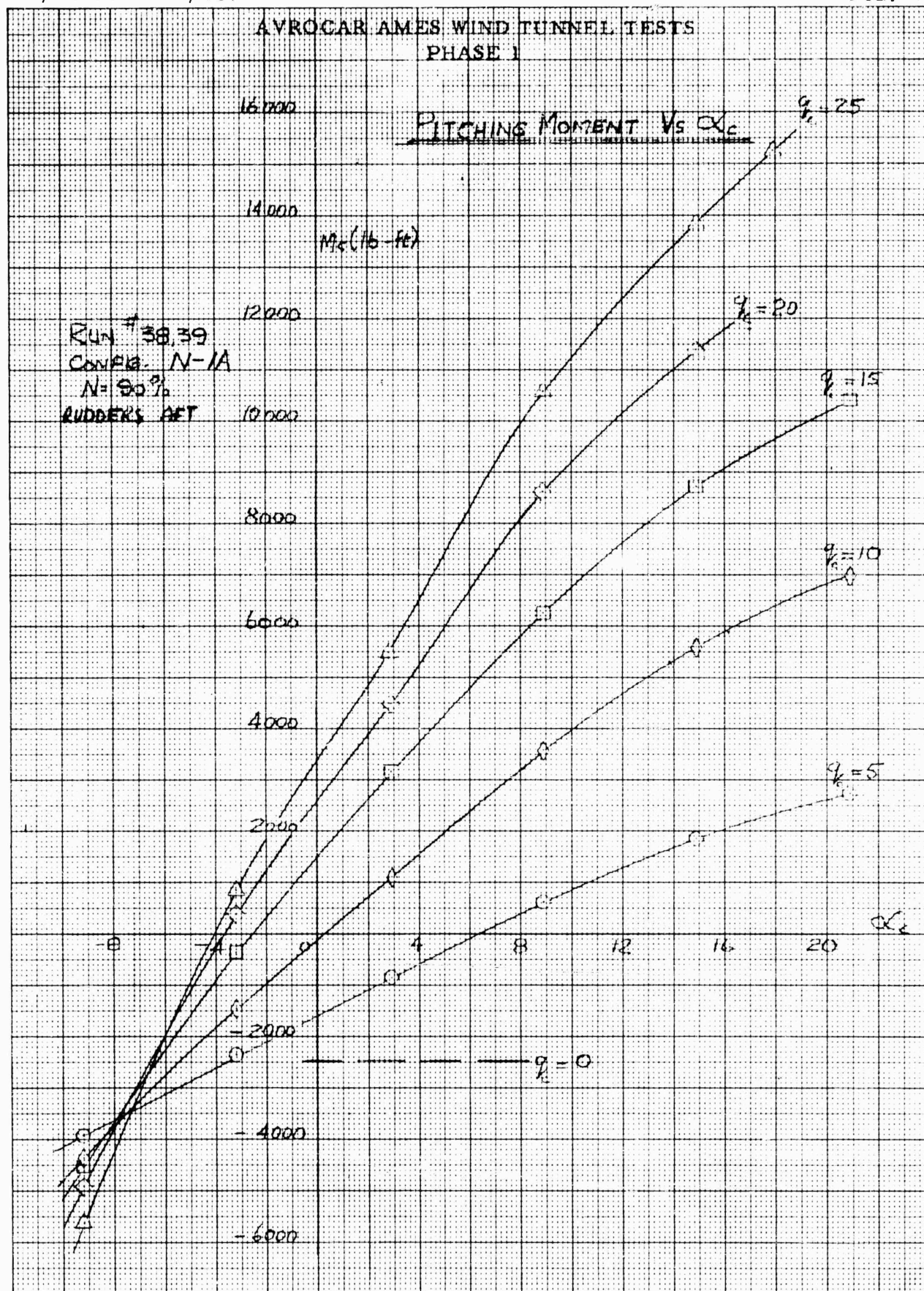
LIFT LB



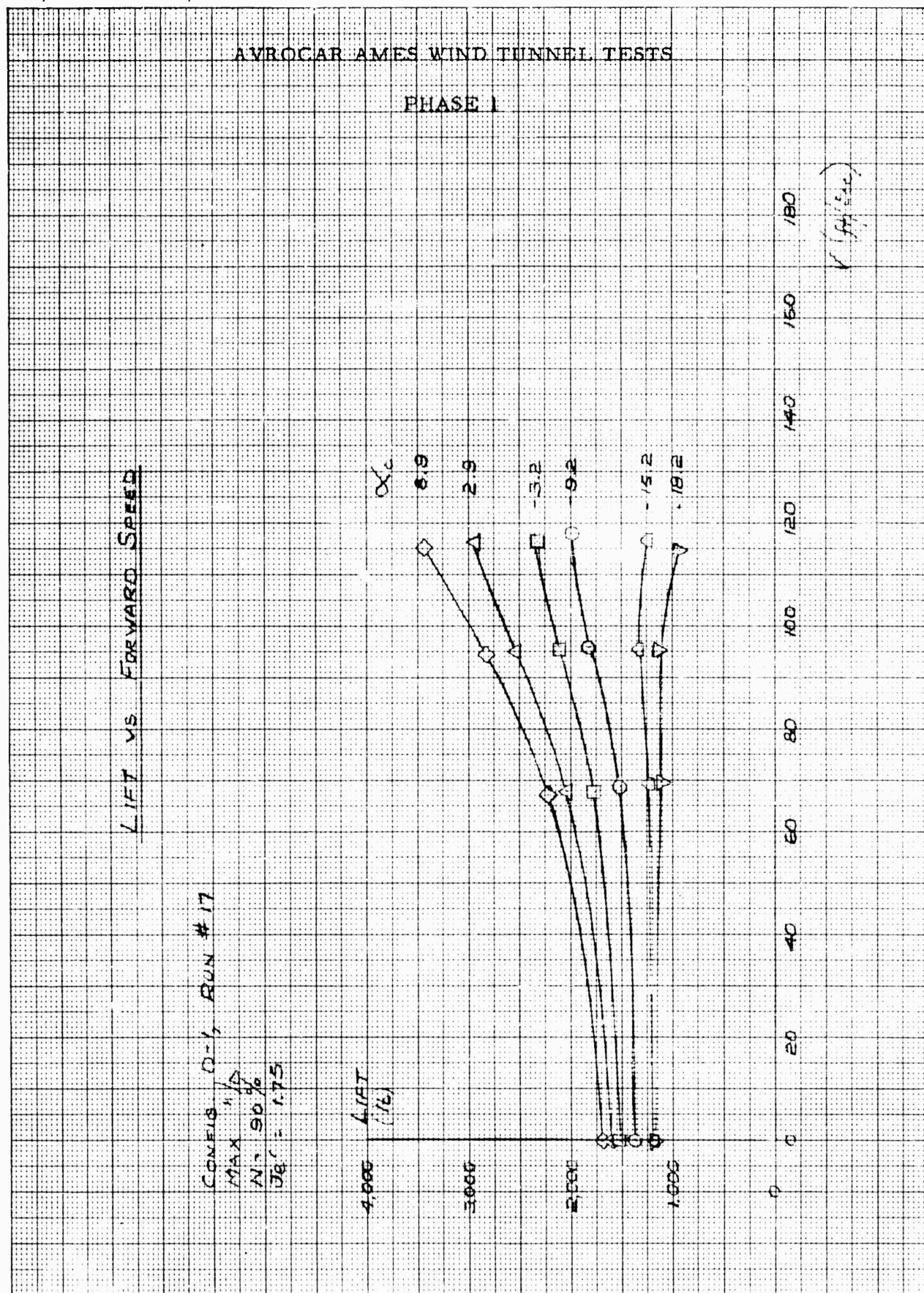
1

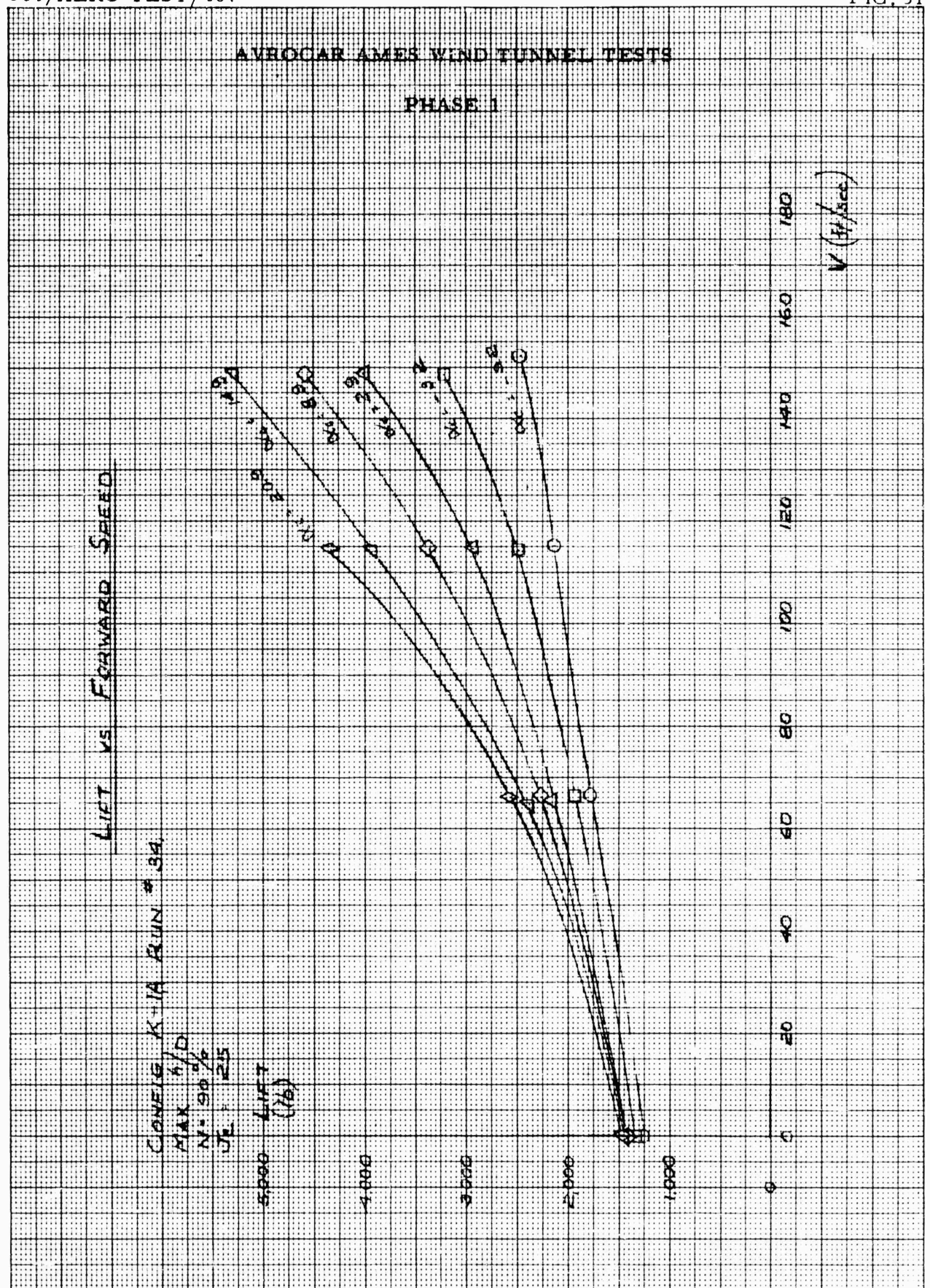
FIG. 28



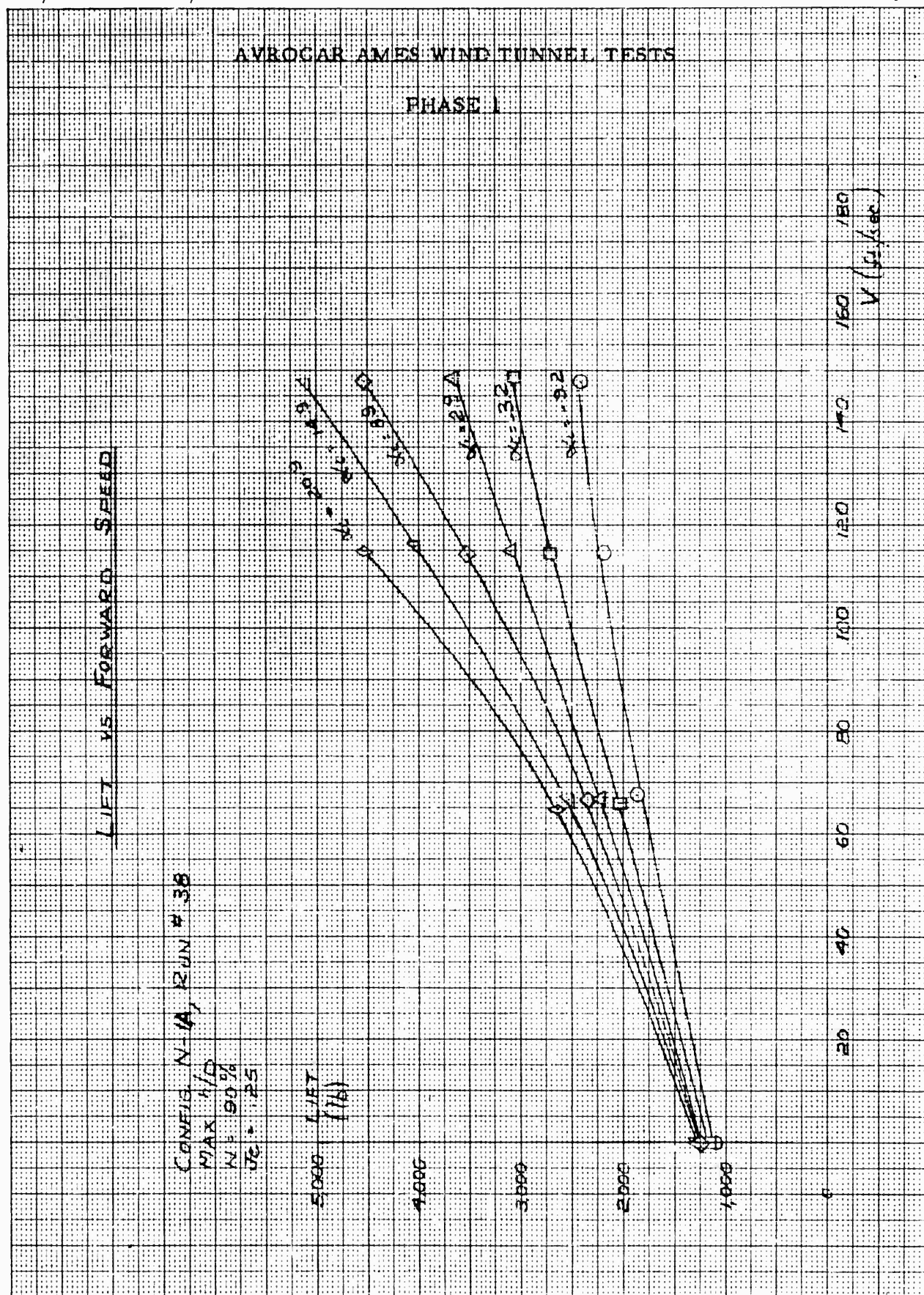


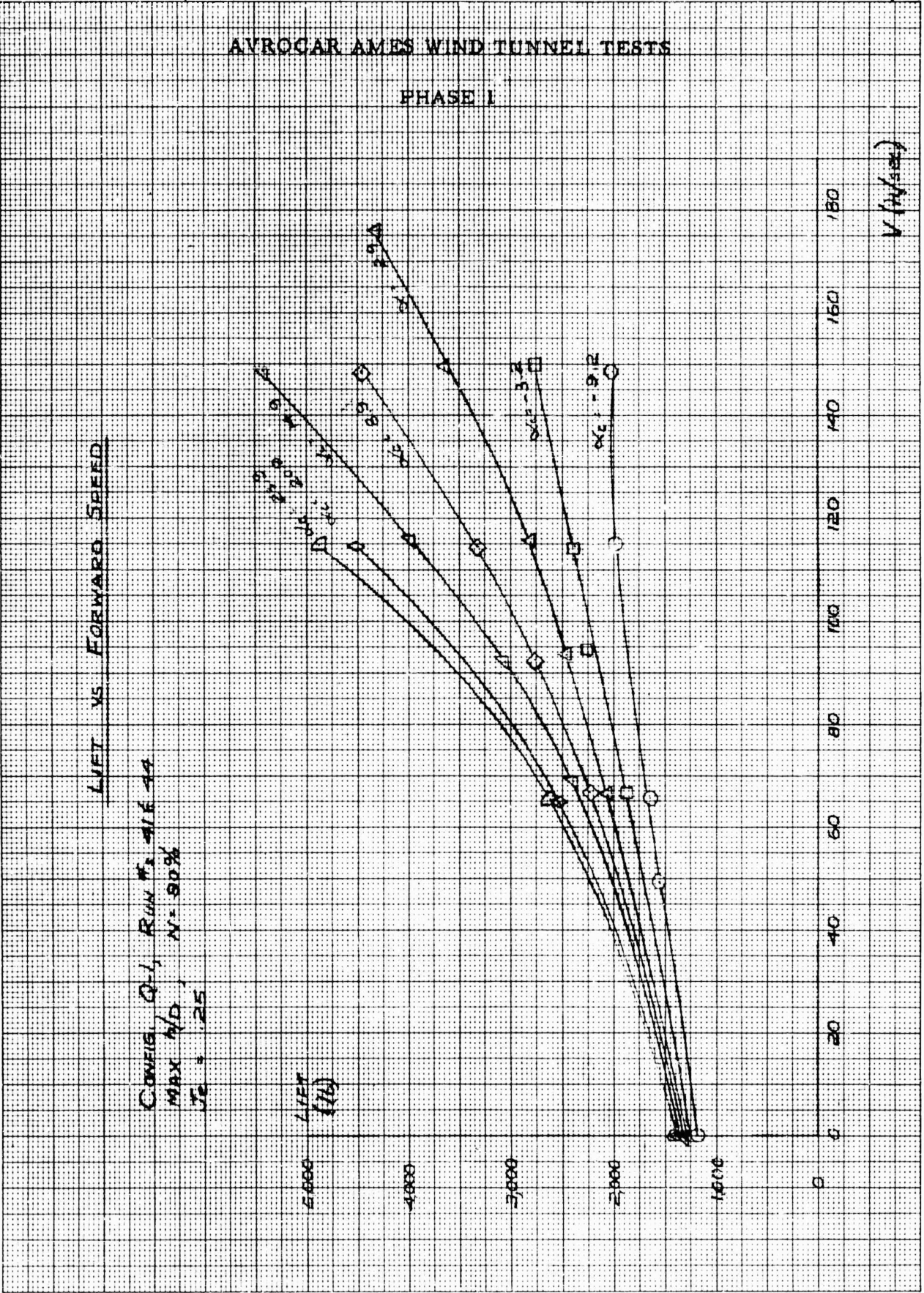







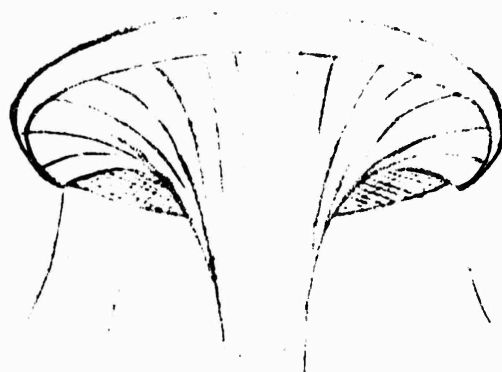




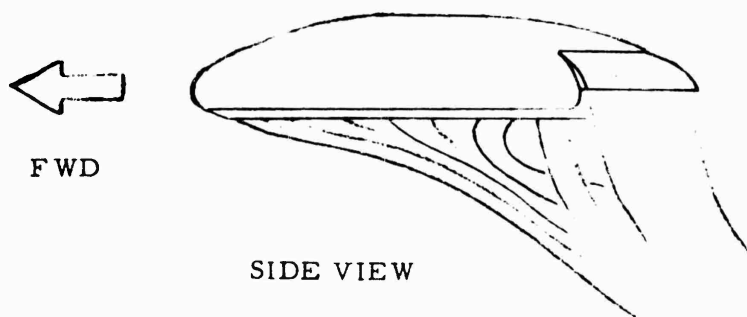


## AVROCAR AMES WIND TUNNEL TESTS

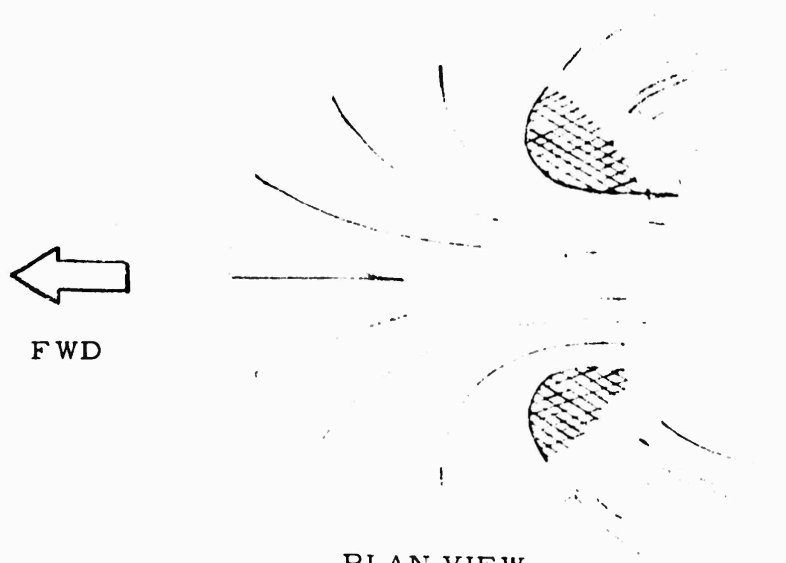
PHASE 1

 FWD

UNDERSIDE FRONT VIEW



SIDE VIEW



PLAN VIEW

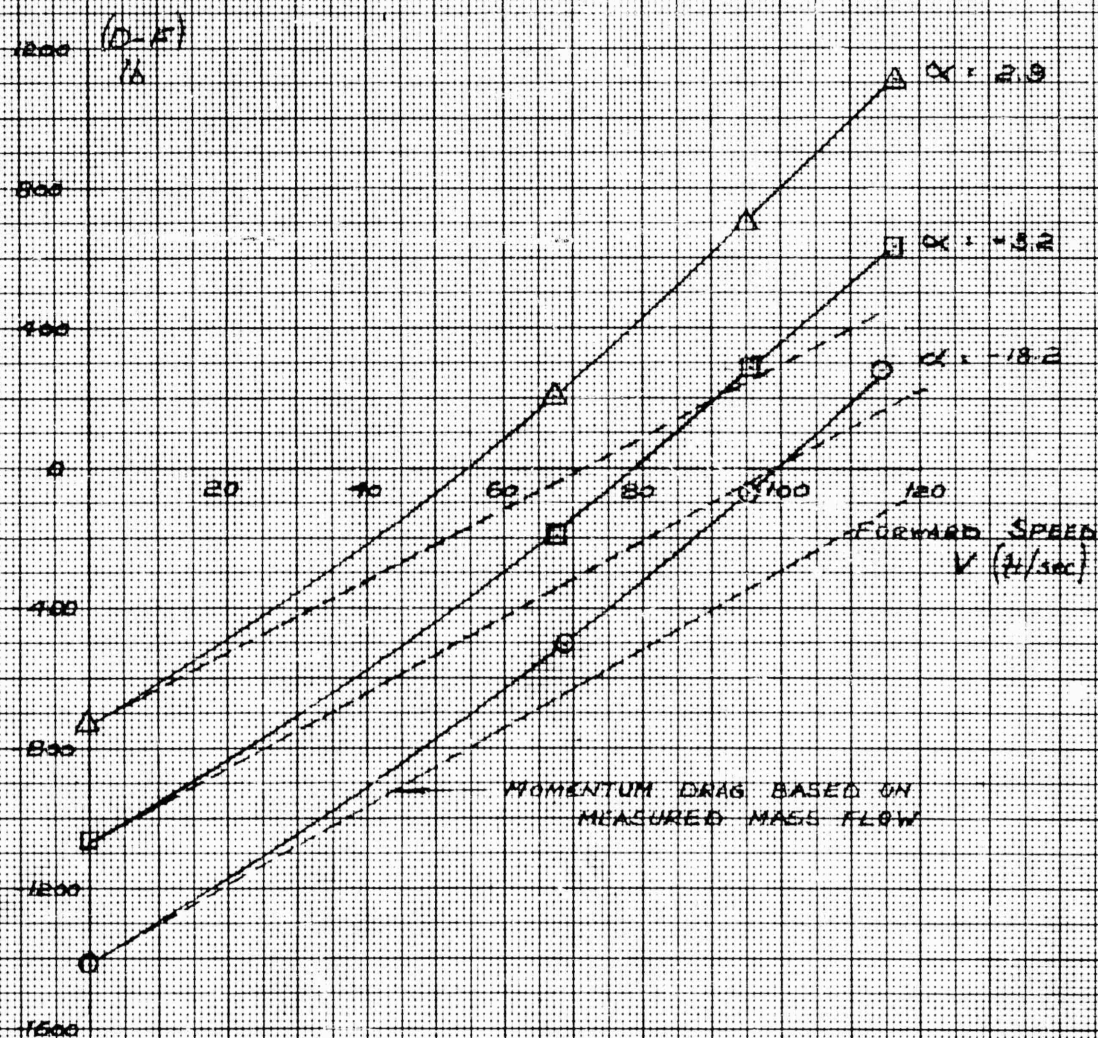
SUGGESTED FLOW PATTERN FOR 'JET-FLAP' CONFIGURATION



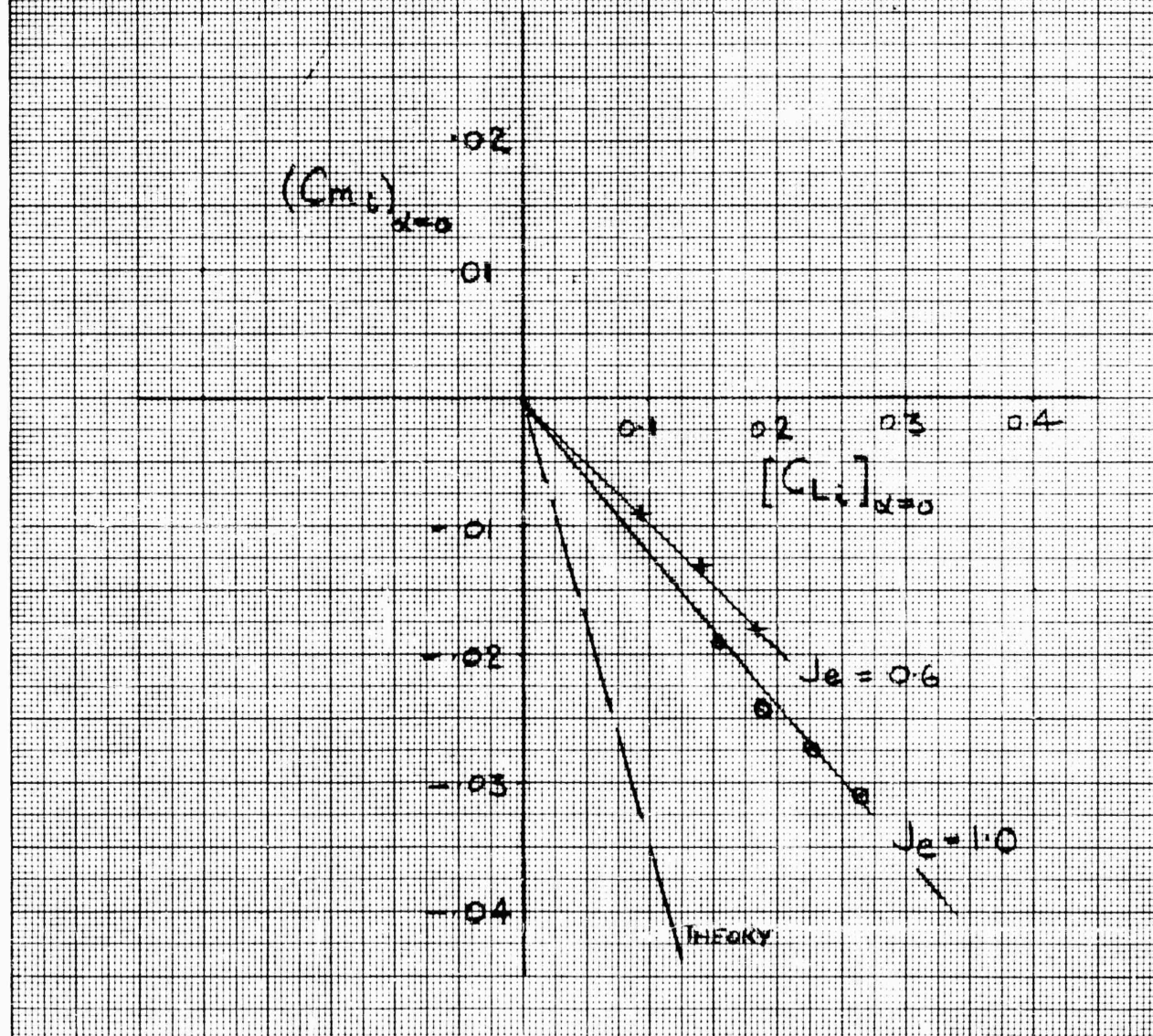
# AVROCAR AMES WIND TUNNEL TESTS PHASE I

## DRAG - THRUST vs FORWARD SPEED

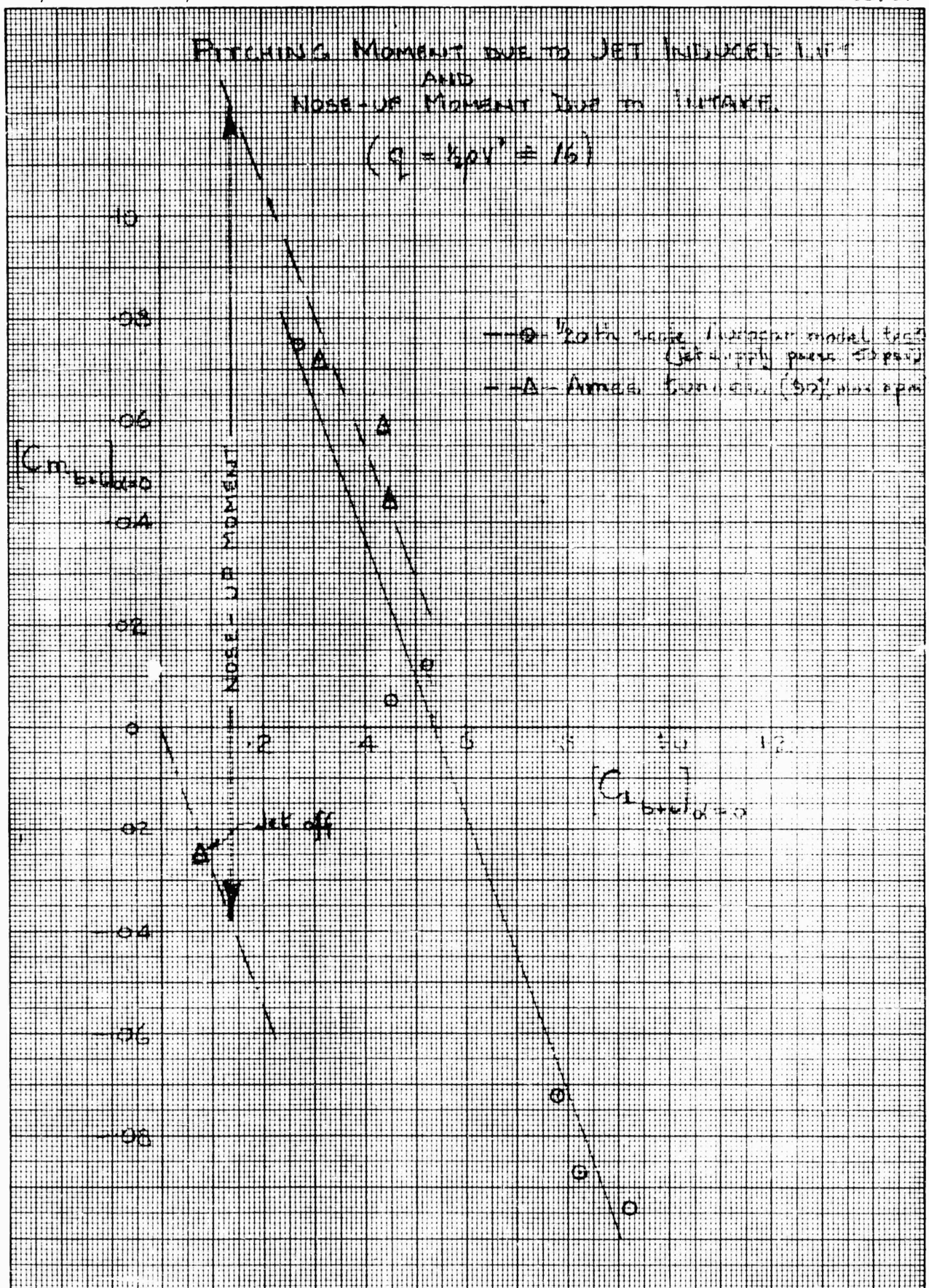
CONFIG D-1  
RUN # 17  
 $V_0' = 1.75$   
 $N = 80\%$



MOMENT DUE TO INDUCED LIFT  
PROJECT 1794

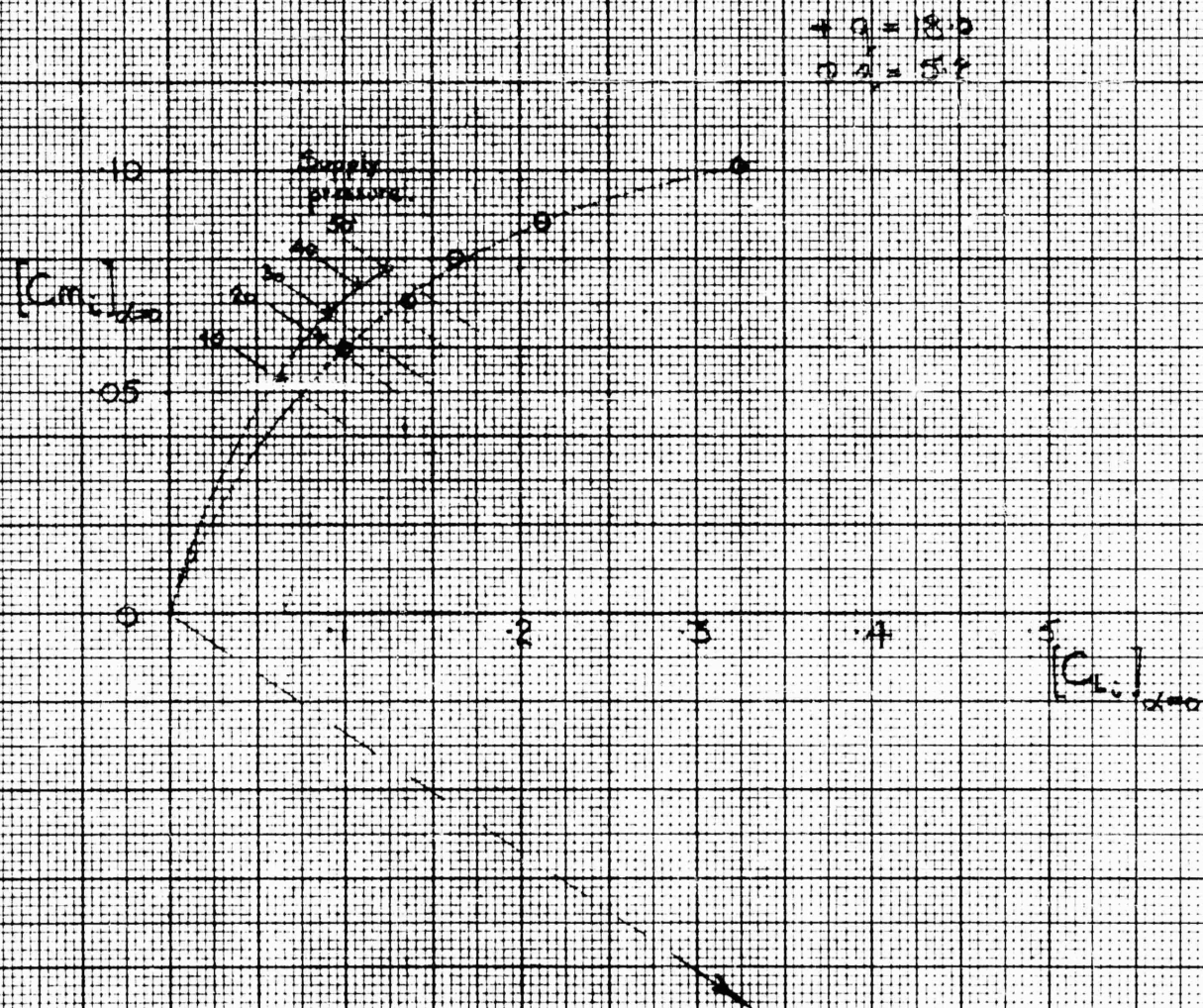




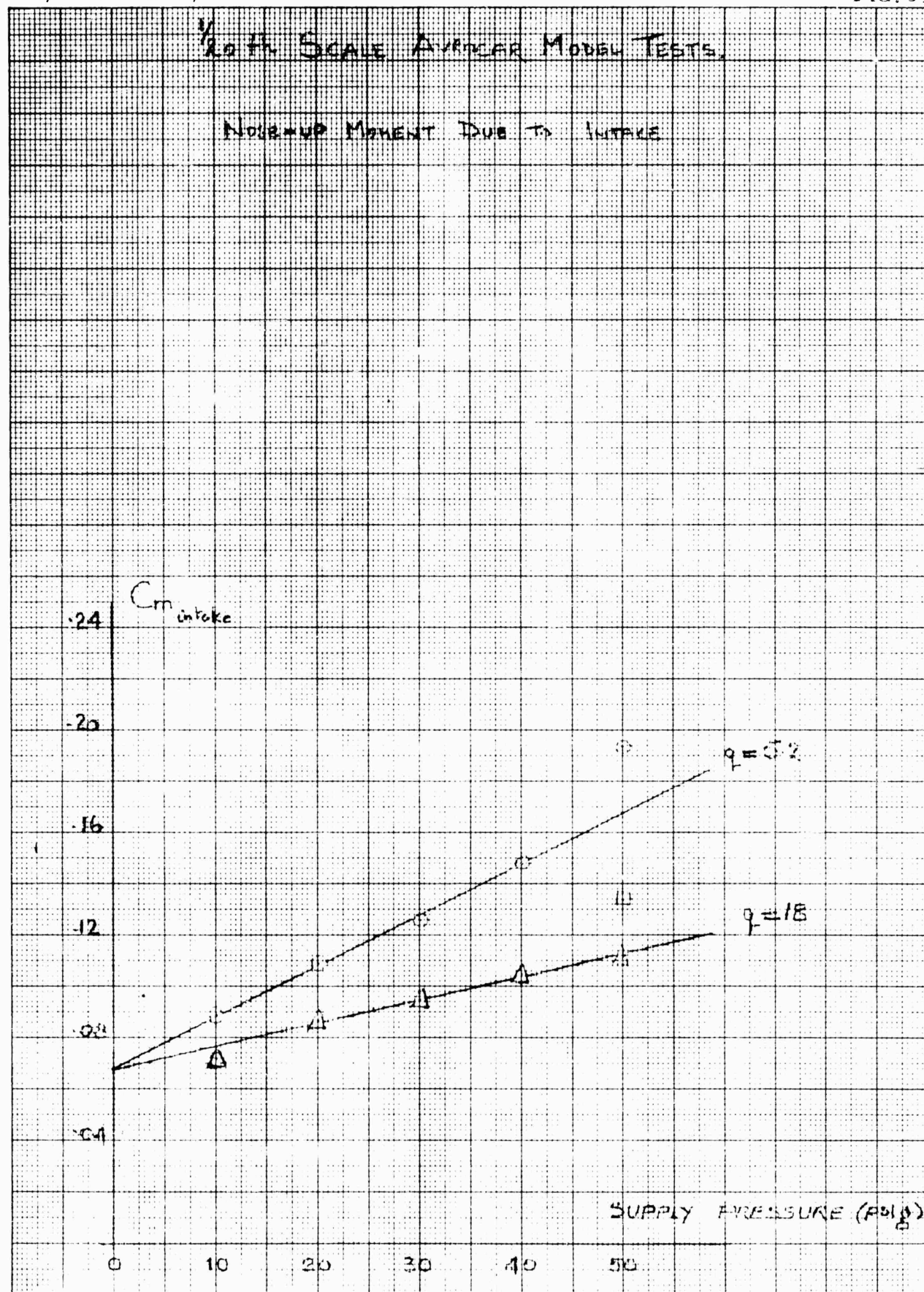


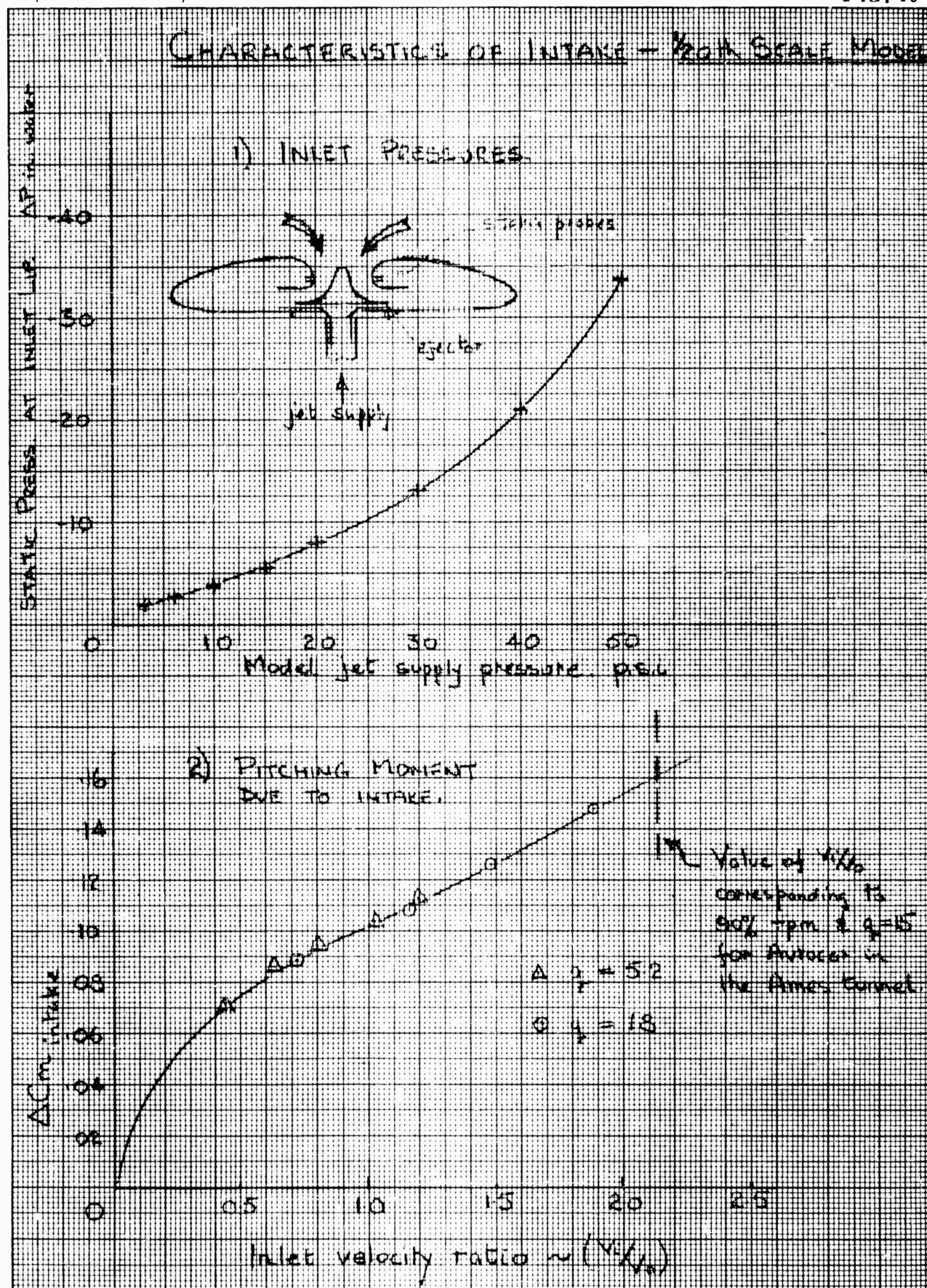
# 1/20th SCALE AEROEAL MODEL TESTS

VARIATION OF MOMENT AT ZERO  $\alpha$  WITH JET  
SUPPLY PRESSURE & TUNNEL SPEED.



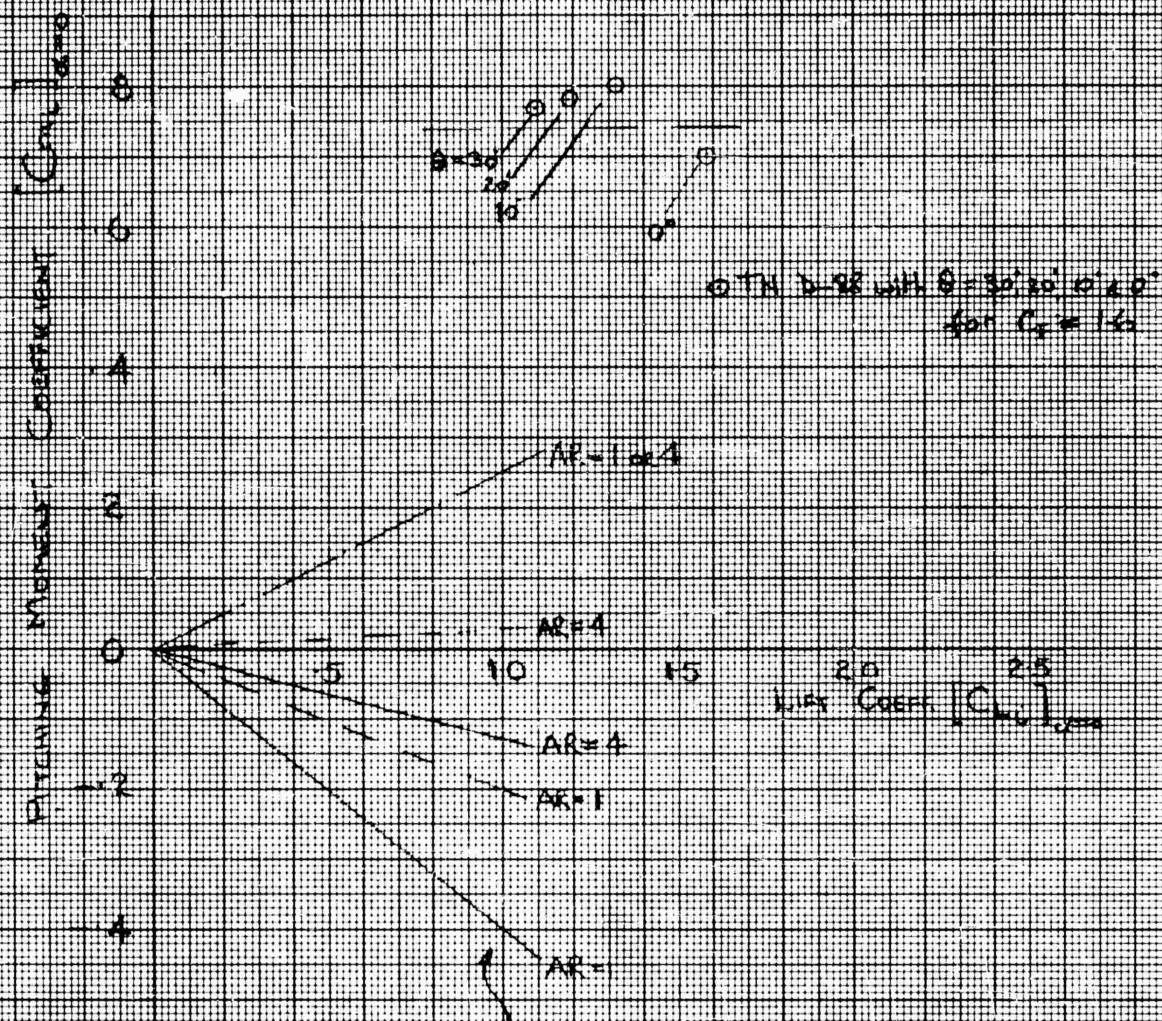








## ANALYSIS OF NASA TN D-28

Simplified Moment Theory for  $\alpha=0$ 

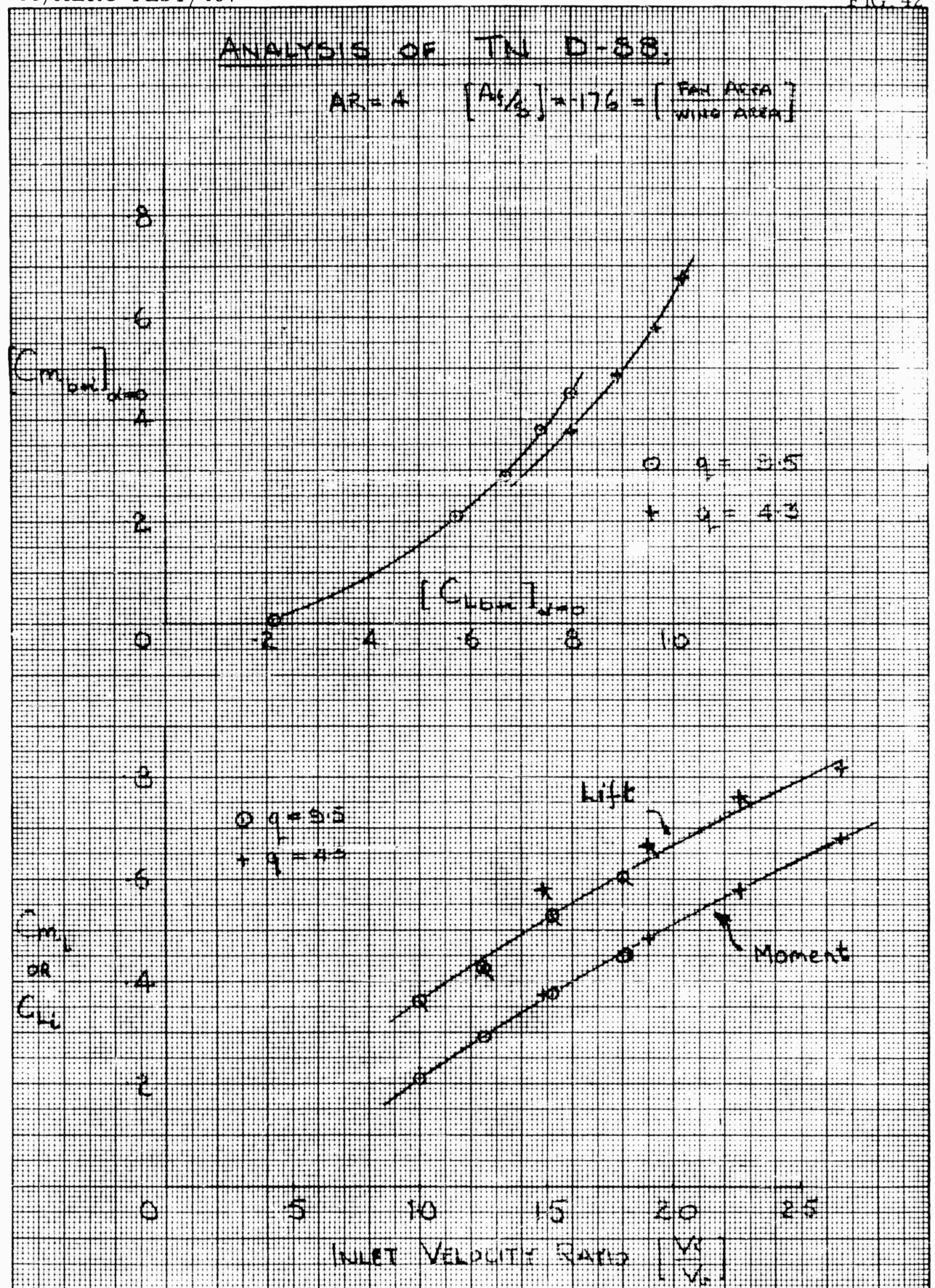
$$C_{m, \alpha=0} = -C_L \left[ \left( \frac{3}{AR} \right) \frac{h}{c} - \left( 1 + \frac{3}{AR} \right) \frac{b}{c} \right]$$

$$\text{---} \quad h/c = 0.25 \quad b/c = 0$$

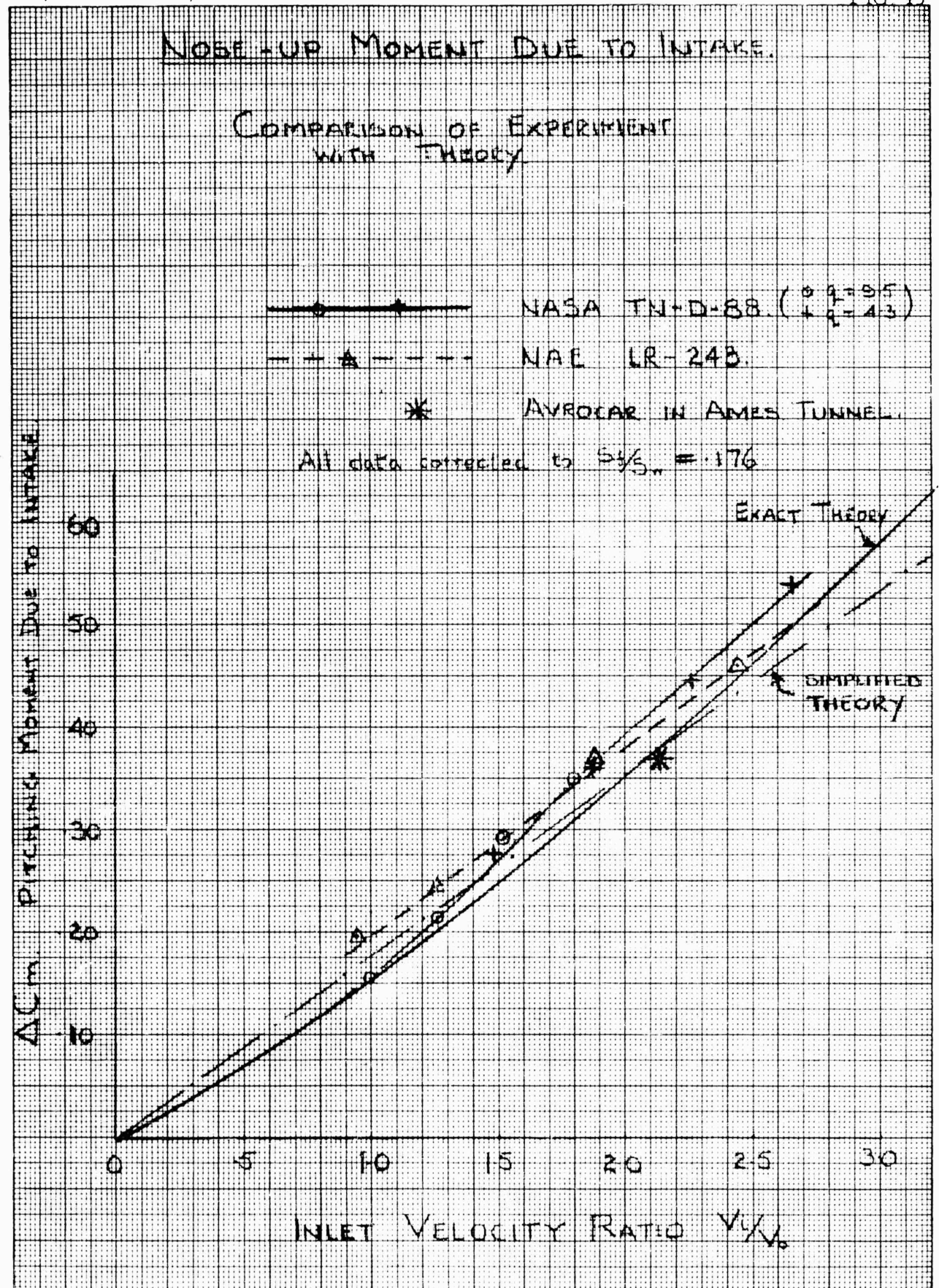
$$\text{---} \quad h/c = 0.25 \quad b/c = 0.1$$

$$\text{---} \quad h/c = b/c = 0.25$$

where  $h/c$  is position of  
lift centre measured from  
half chord point







CASE=17 DELT=20 OC= 18.0R ALPH= -3.20  
 V= 245.51 PM= 3162.72 DM= 132.46 FN= 235.88 FM= 139.35  
 CENTER LINE SECTION - PRESSURES IN PSF  
 P 01= -4.47 P 02= -4.00 P 03= -14.42 P 04= -17.02 P 05= -23.87 P 06= -46.43 P 07= -114.71 P 08= -160.46 P 09= -153.28  
 P 10= -138.25 P 11= -12.33 P 12= -116.73 P 13= -113.63 P 14= -117.46 P 15= -25.60 P 16= -29.34 P 17= -69.22 P 18= -17.76  
 P 19= -7.40 P 20= 10.53 P 21= 14.49 P 22= -8.29 P 23= -12.11 P 24= -11.18 P 25= -7.93 P 26= -13.03  
 MIDSPAN SECTION - PRESSURES IN PSF  
 P 27= -13.05 P 28= -7.07 P 29= -11.01 P 30= -4.54 P 31= -12.04 P 32= -6.71 P 33= -8.51 P 34= -24.96 P 35= -6.13  
 P 36= -7.21 P 37= -8.00 P 38= -8.80 P 39= -8.15 P 40= -7.93 P 41= -12.98  
 CL= 0.3577 CM= 0.0410 CDM= 0.0324  
 CENTER LINE SECTION - PRESSURE COEFFICIENTS  
 CP01= -0.26 CP02= -0.55 CP03= -0.90 CP04= -1.06 CP05= -1.48 CP06= -2.89 CP07= -7.13 CP08= -10.00 CP09= -9.53  
 CP10= -8.40 CP11= -0.77 CP12= -7.26 CP13= -7.07 CP14= -7.34 CP15= -1.59 CP16= -1.82 CP17= -4.30 CP18= -0.75  
 CP19= -0.63 CP20= 0.65 CP21= 0.90 CP22= -0.52 CP23= -0.75 CP24= -0.69 CP25= -0.49 CP26= -0.81  
 MIDSPAN SECTION - PRESSURE COEFFICIENTS  
 CP27= -0.81 CP28= -0.64 CP29= -0.89 CP30= -0.28 CP31= -0.75 CP32= -0.42 CP33= -0.53 CP34= -0.18 CP35= -0.38  
 CP36= -0.45 CP37= -0.50 CP38= -0.55 CP39= -0.51 CP40= -0.49 CP41= -0.81  
 \*\*\*\*\* CENTER LINE CP \*\*\*\*\*  
 -14.00 -14.00 -12.00 -10.00 -8.00 -6.00 -4.00 -2.00 -0.00 2.00  
 \*\*\*\*\* MIDSPAN CP \*\*\*\*\*  
 -14.00 -14.00 -12.00 -10.00 -8.00 -6.00 -4.00 -2.00 -0.00 2.00

## AVROCAR AMES WIND TUNNEL TESTS

## PHASE I

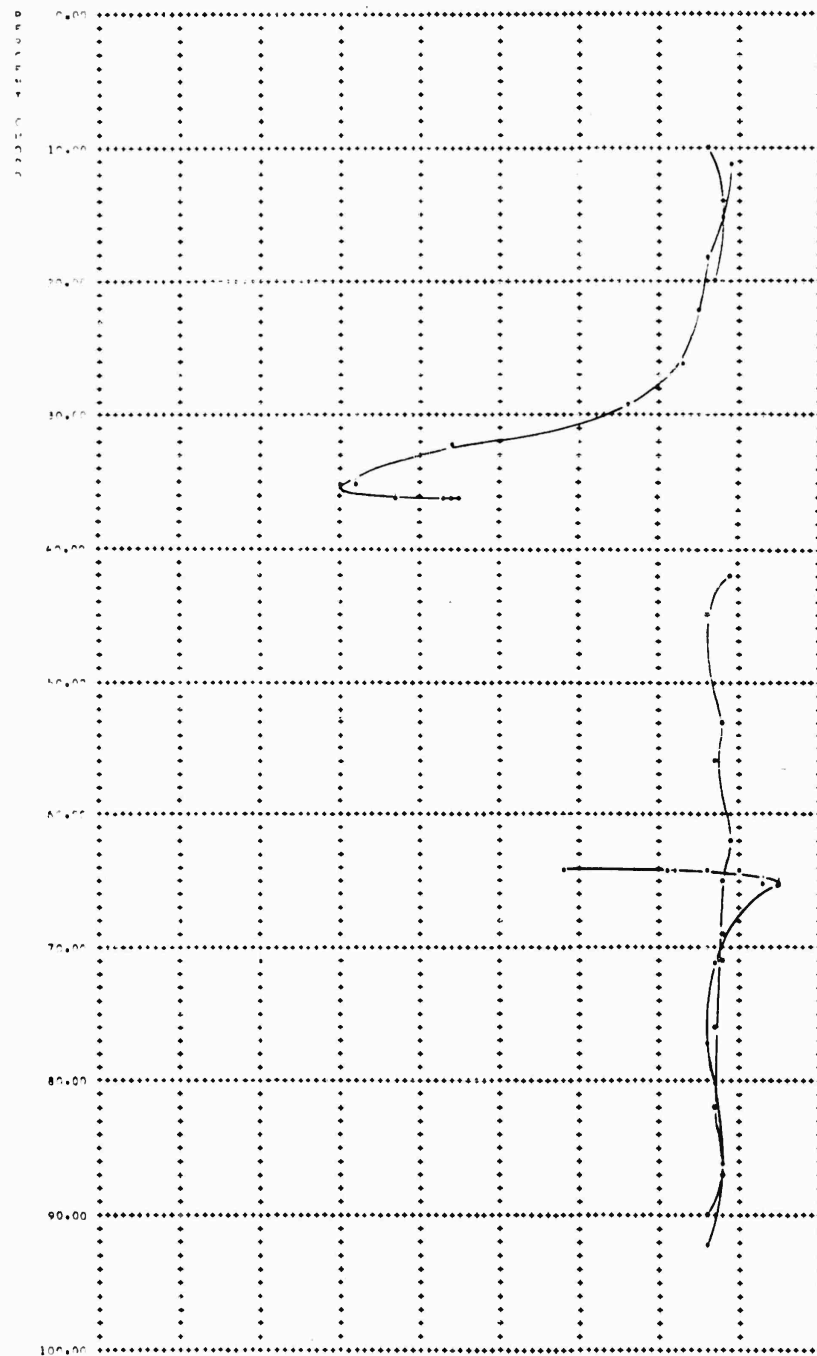
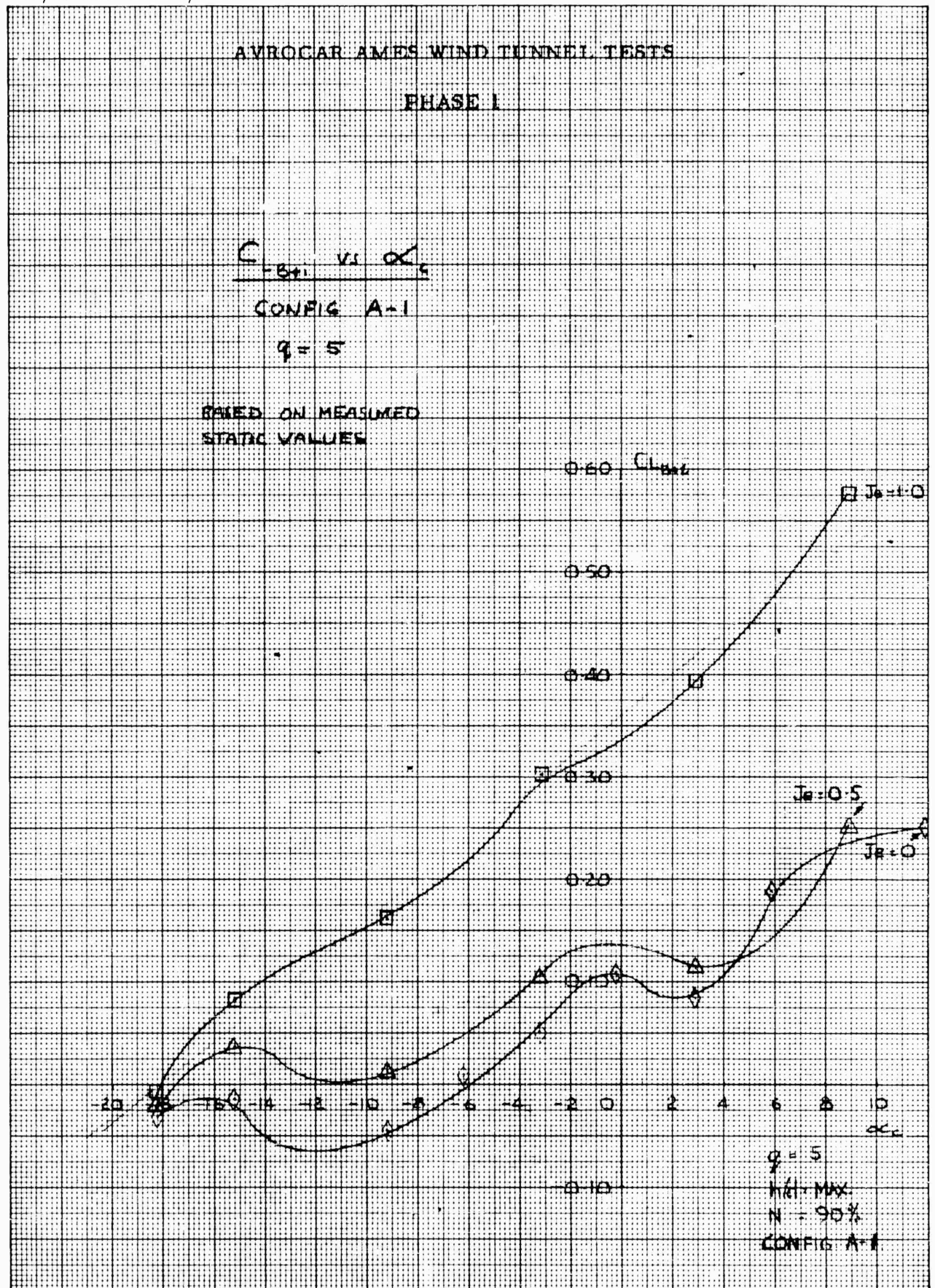
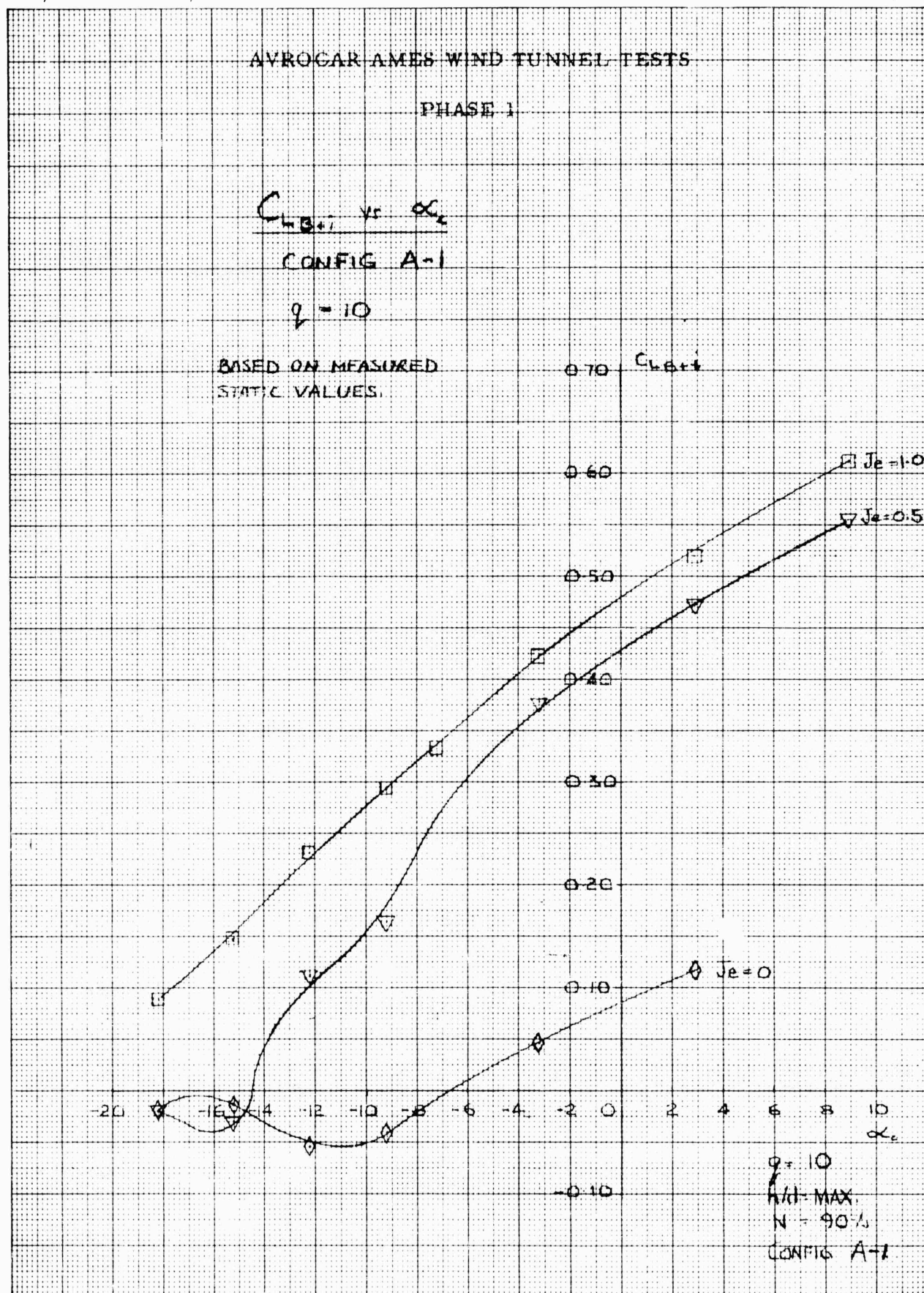


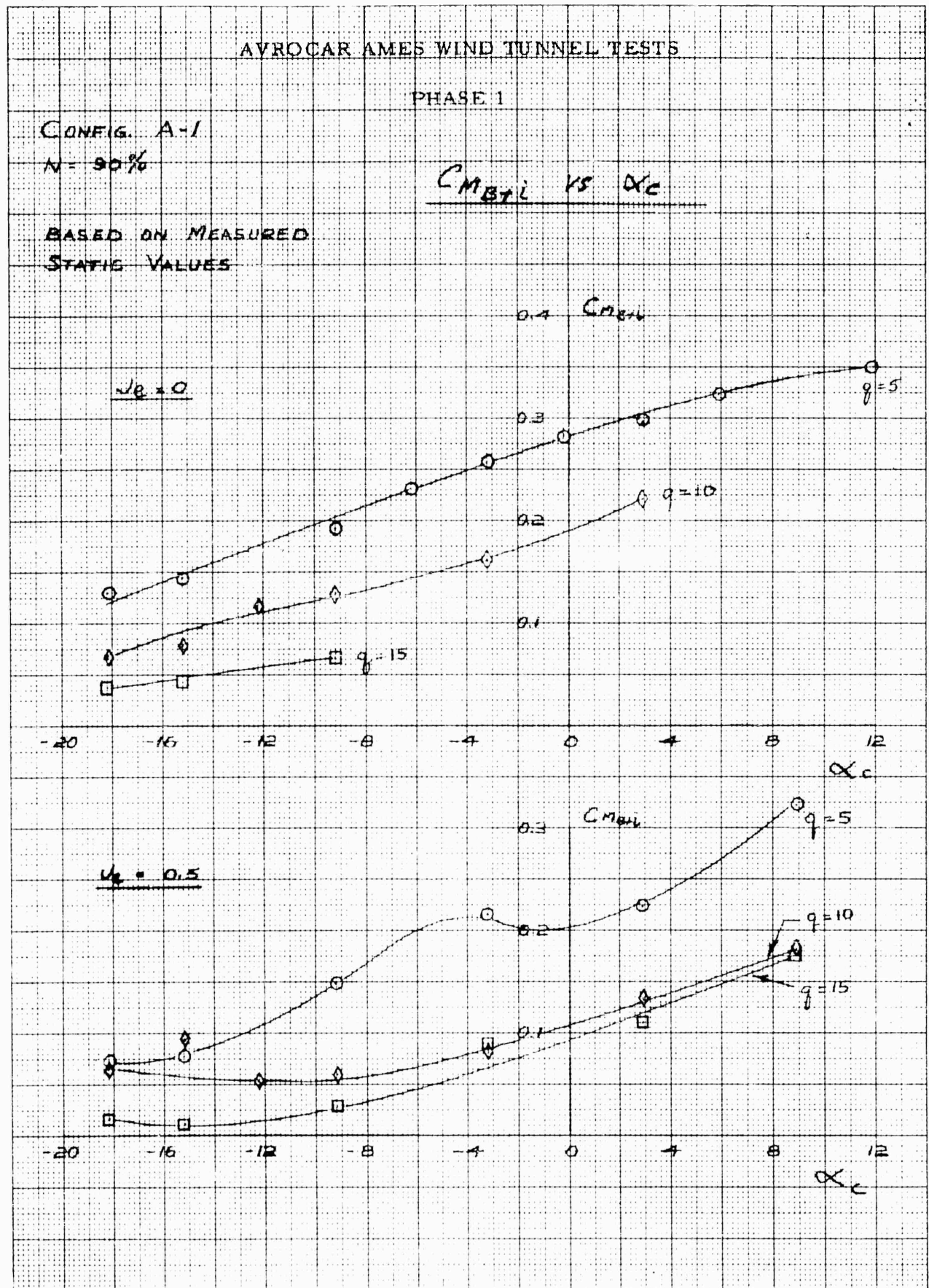
FIG. 44 AIRCRAFT CENTERLINE PRESSURE DISTRIBUTION













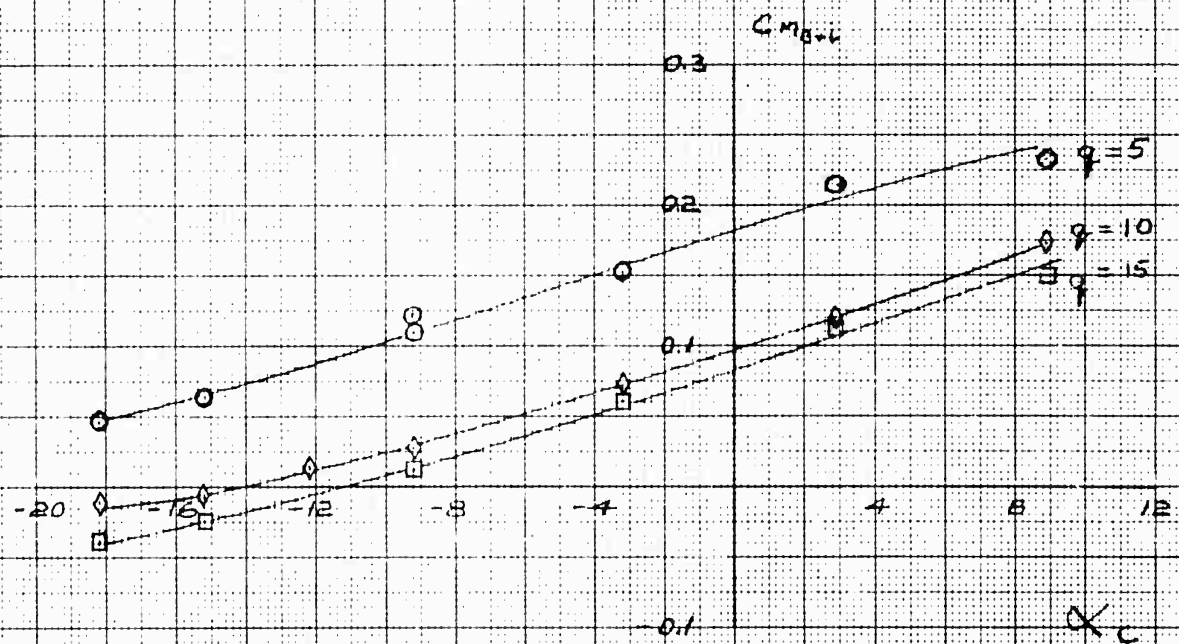
## AVROCAR AMES WIND TUNNEL TESTS

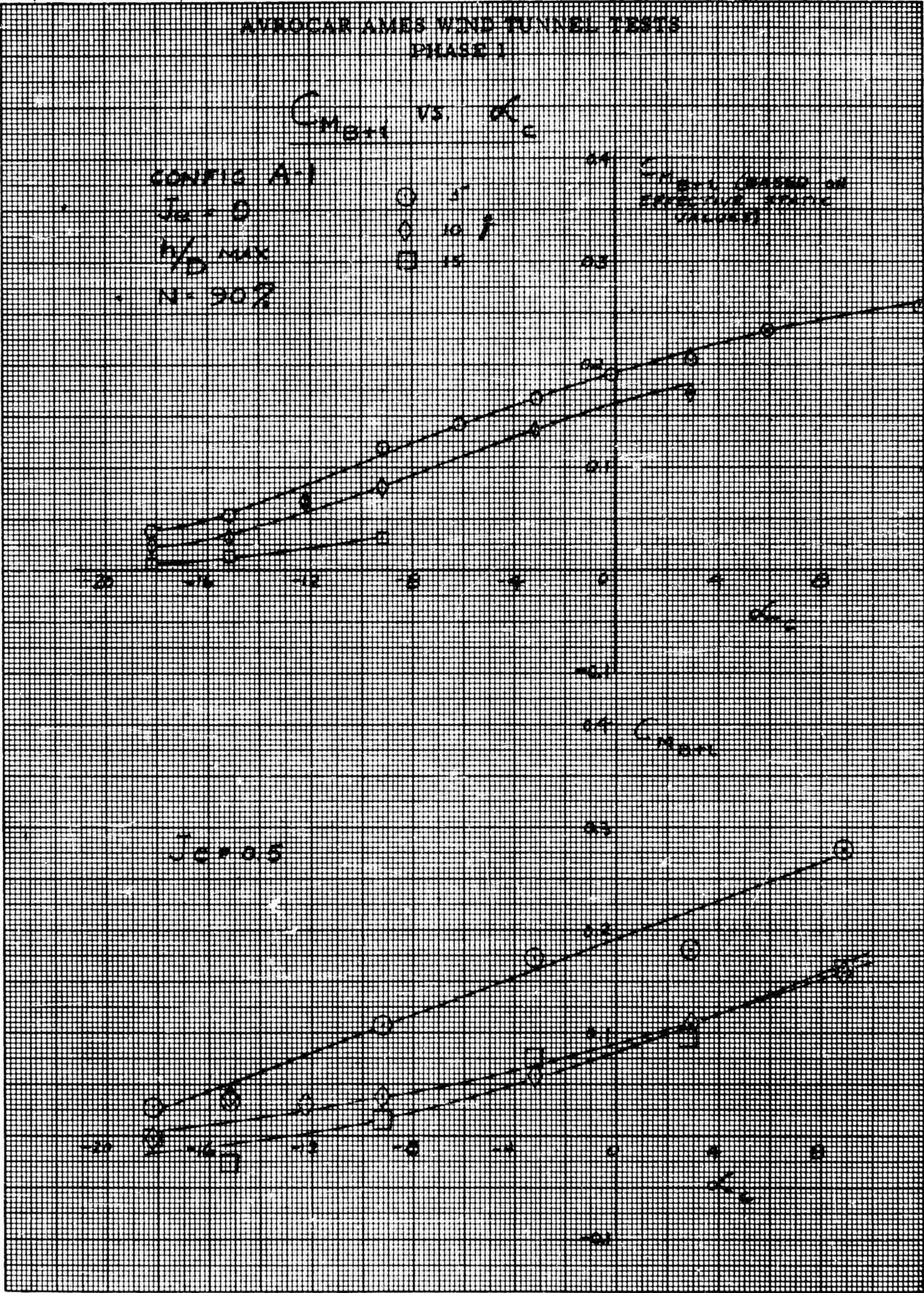
PHASE I

 $C_{M_{B+L}}$  vs  $\alpha_c$ 

CONFIG A-1  
 $N = 90\%$   
 $\mu_e = 10$

BASED ON MEASURED  
 STATIC VALUES







## AVROCAR AMES WIND TUNNEL TESTS

## PHASE I

$C_{MB+i}$  vs.  $\alpha_c$

CONFIG A-1

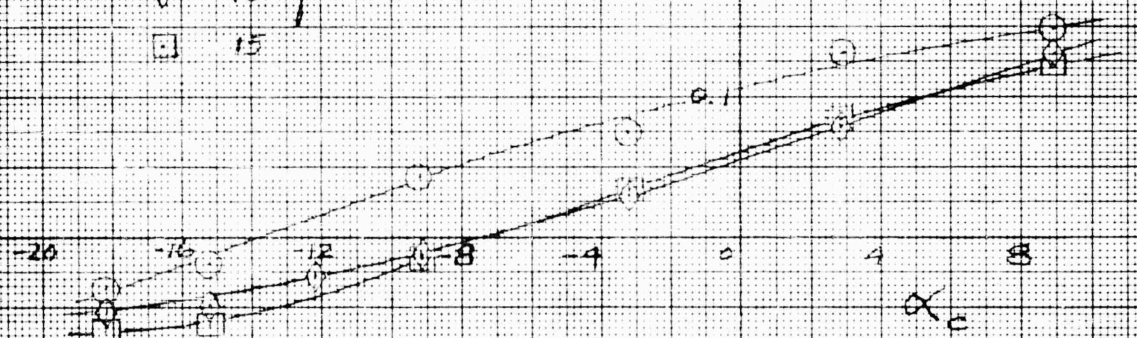
$Je = 10$

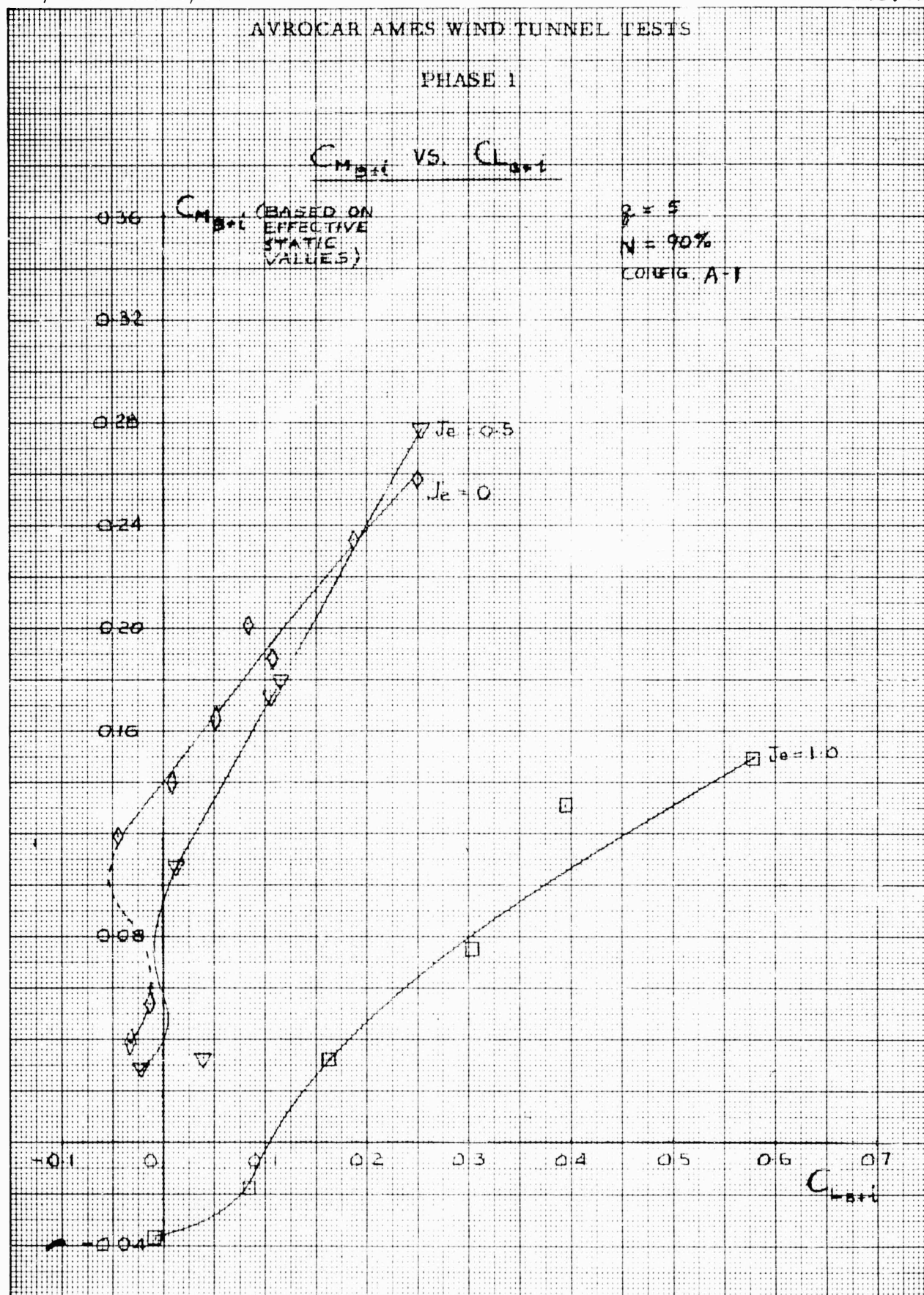
$h/D = \text{MAX}$

$N = 90\%$

○ 5  
◇ 10  
□ 15

$C_{MB+i}$   
(BASED ON  
EFFECTIVE  
STATIC VALUES)

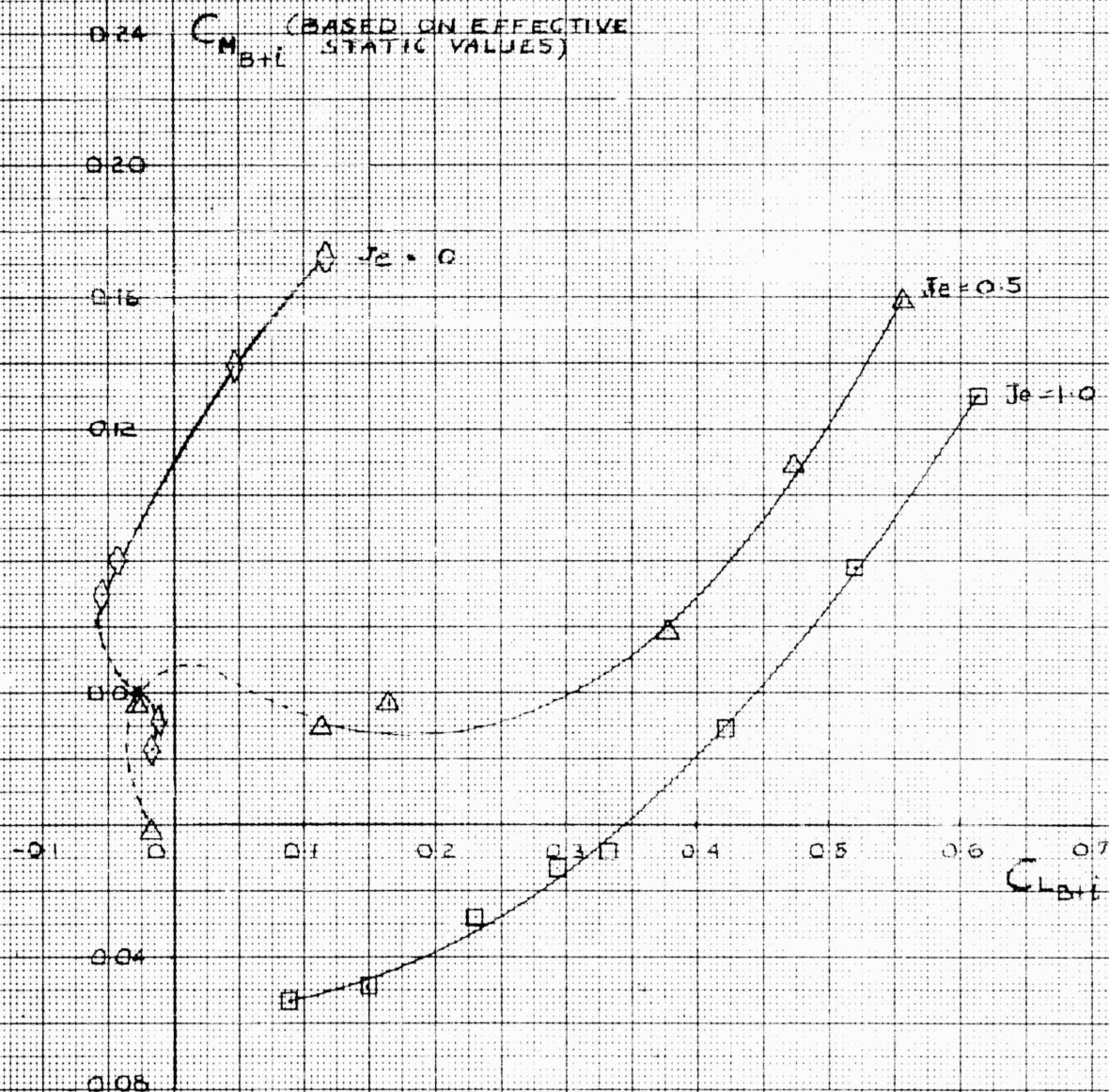




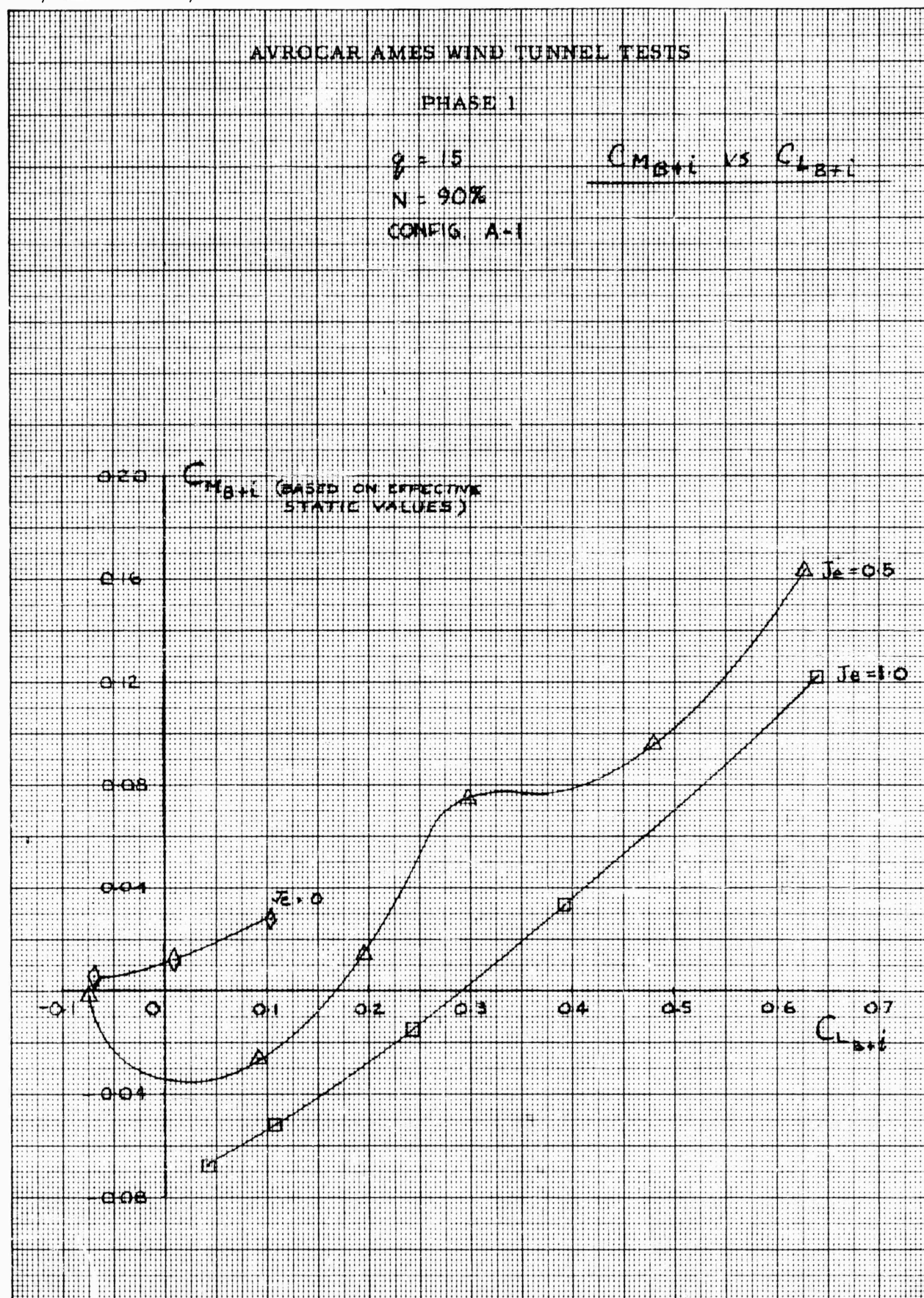
## AVROCAR AMES WIND TUNNEL TESTS

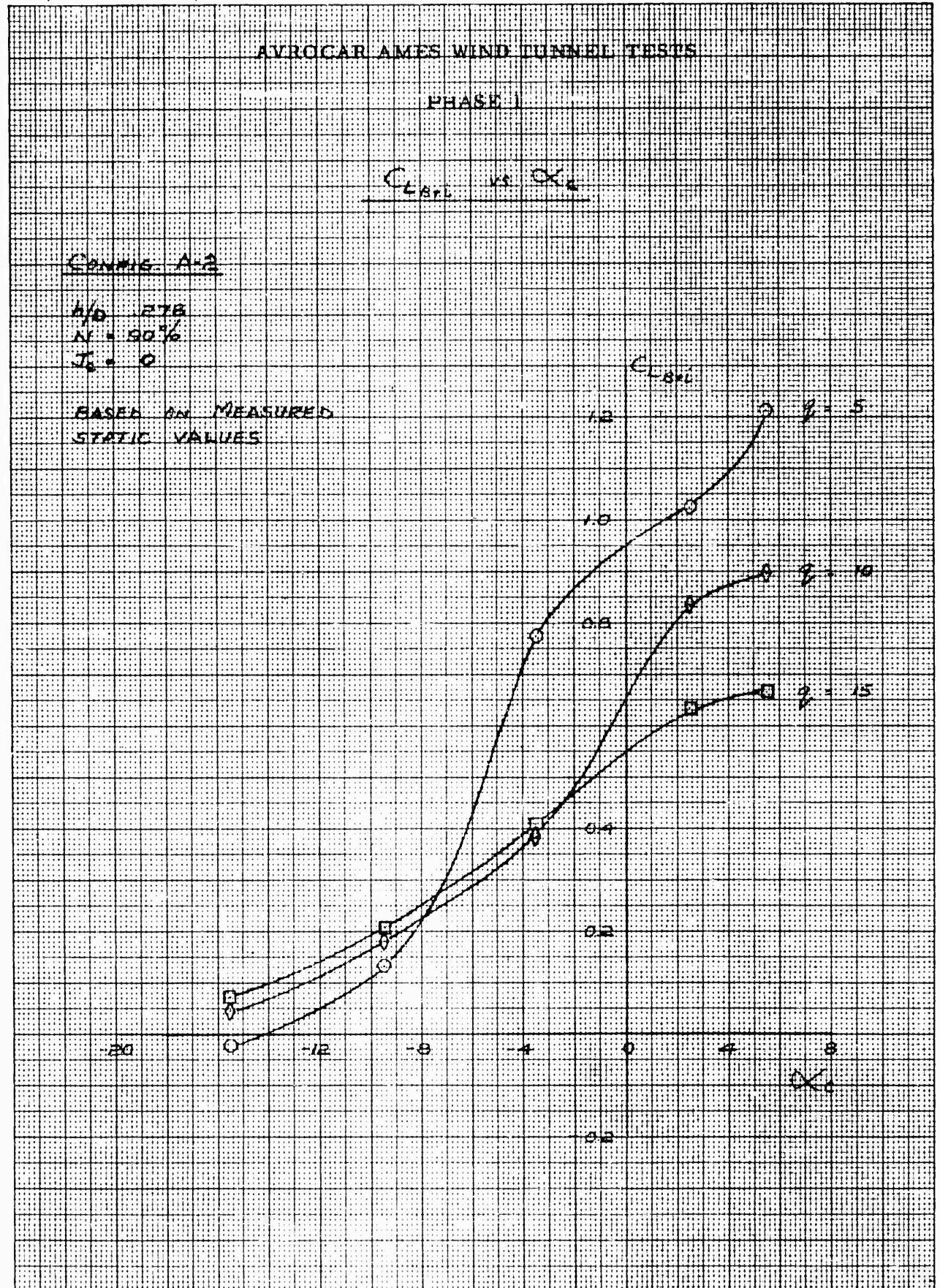
PHASE 1

$q = 10$   
 $N = 90\%$   
 CONFIG A-1

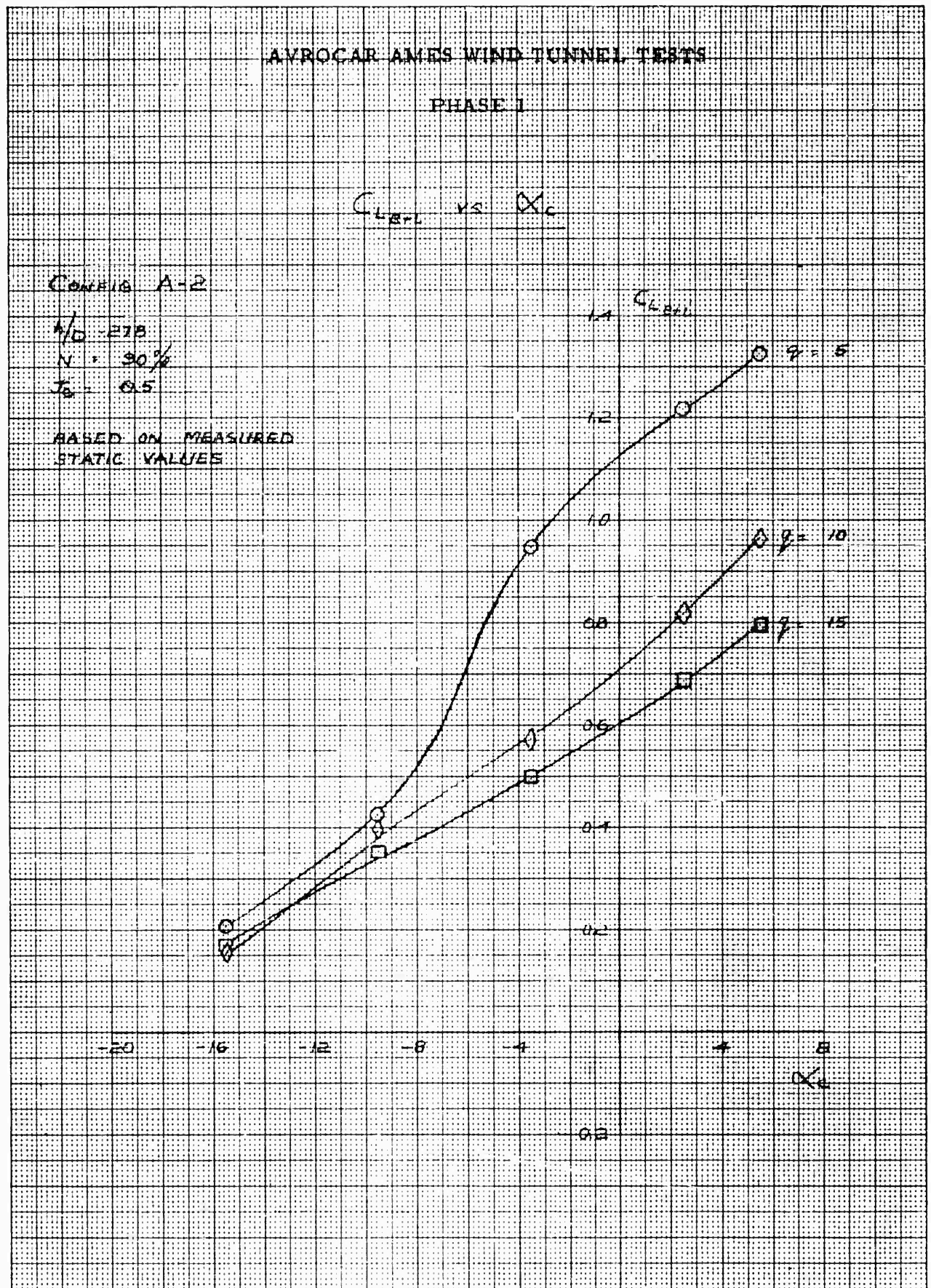
 $C_{MB+L}$  VS  $C_{LB+L}$ 

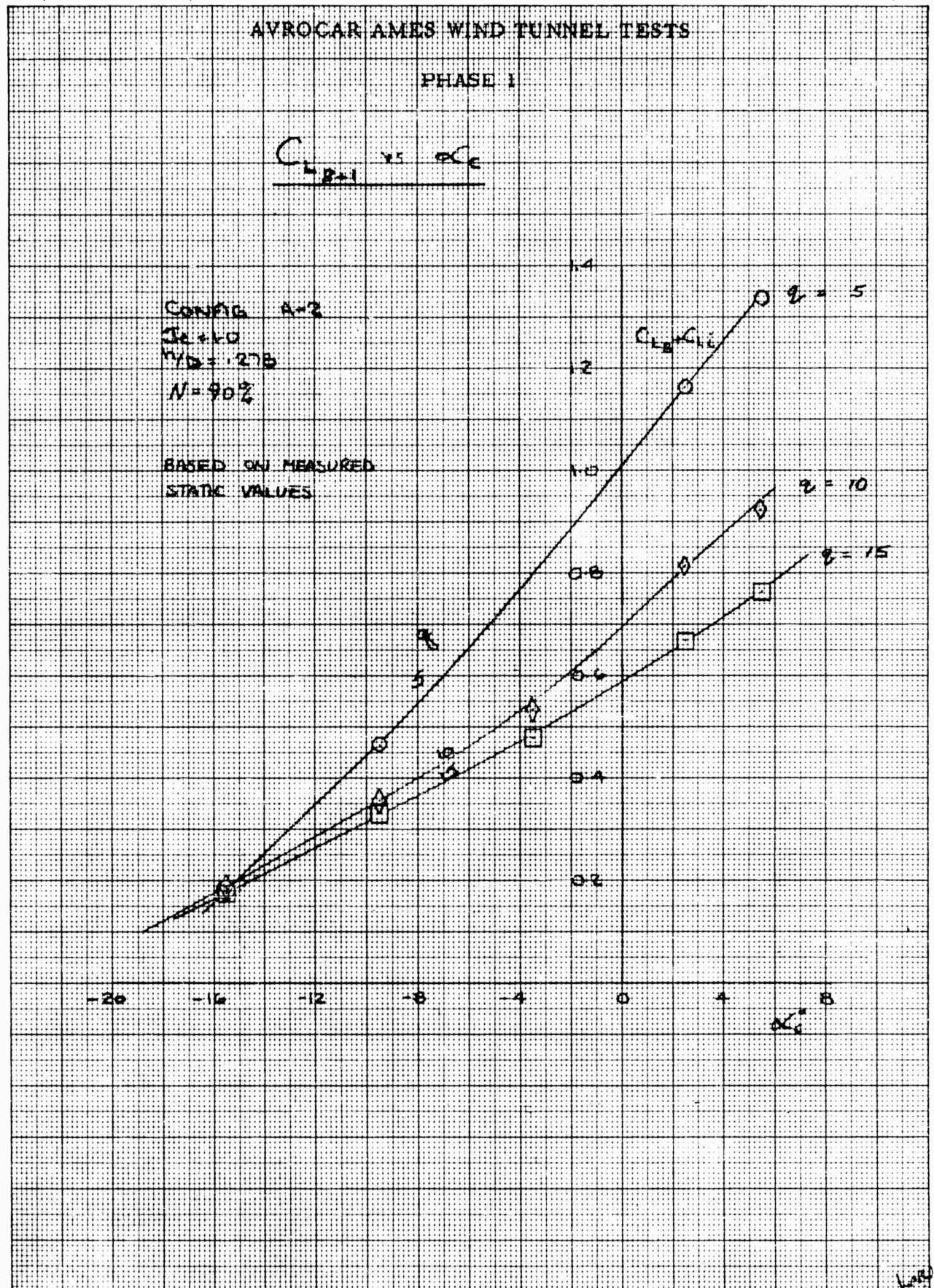




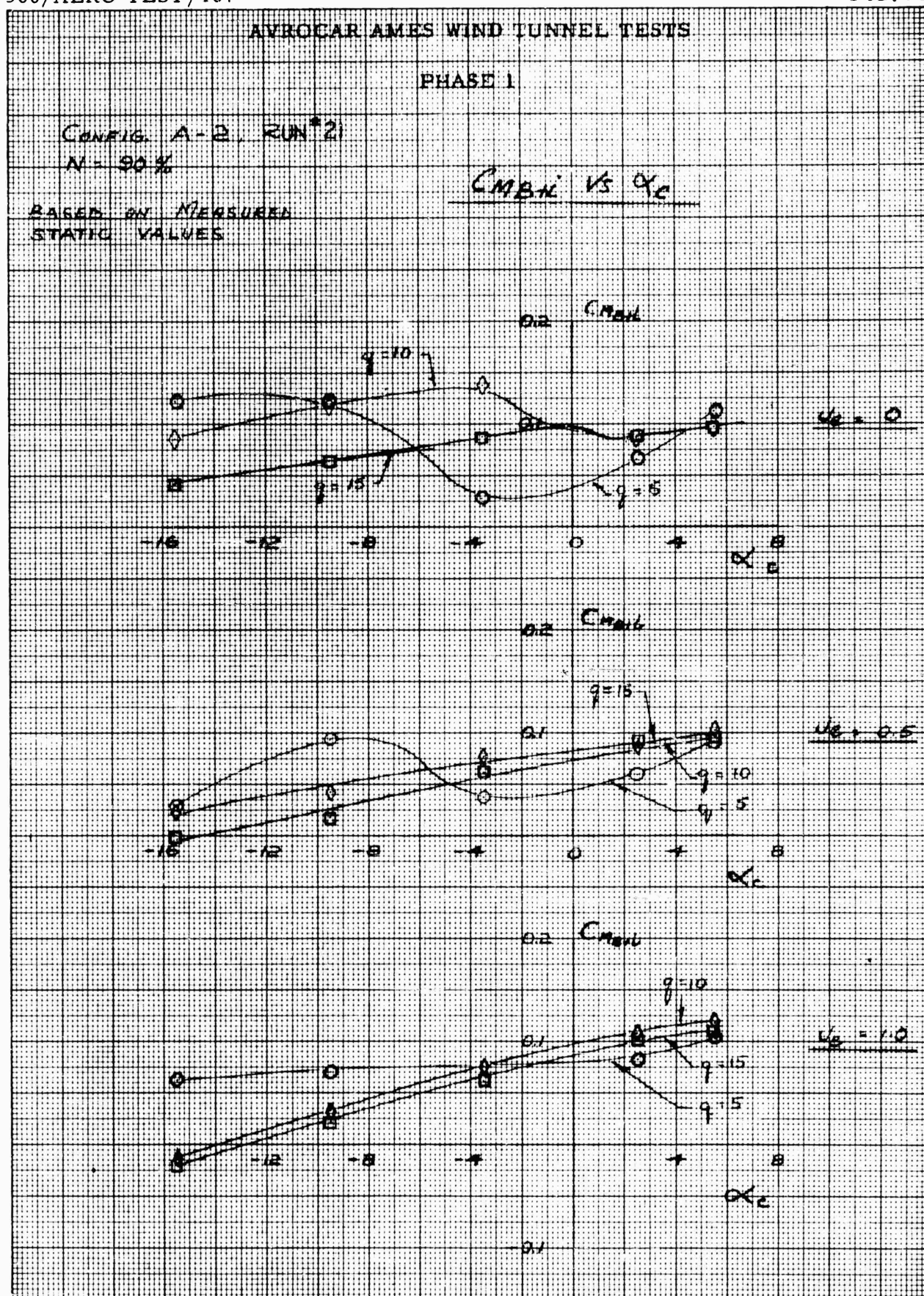


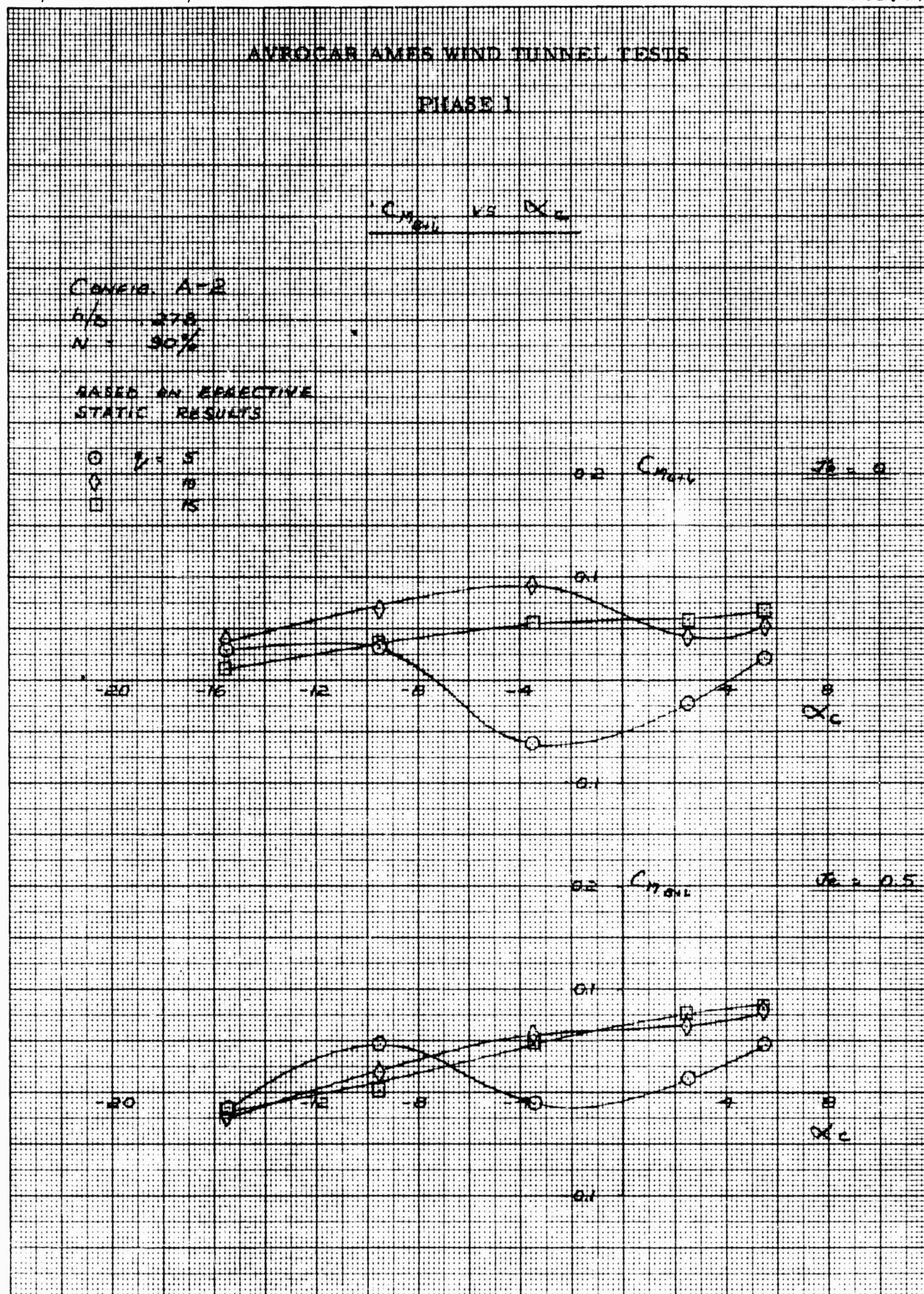














## AVROCAR AMES WIND TUNNEL TESTS

## PHASE I

 $C_{M_{B+L}}$  vs  $\alpha_c$ 

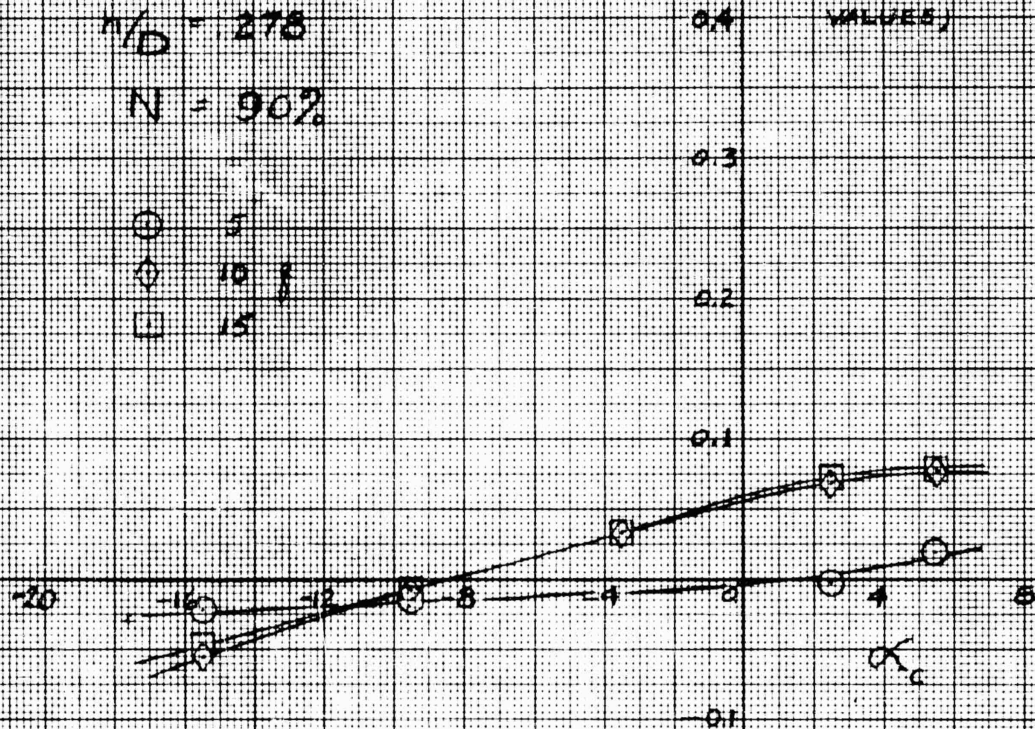
CONFIG A-2

 $Je = 1.0$  $n/D = 278$  $N = 90\%$ 

○ 5

◇ 10

□ 15

 $C_{M_{B+L}}$  (BASED ON  
EFFECTIVE STATIC  
VALUES)



## AVROCAR AMES WIND TUNNEL TESTS

## PHASE 1

 $C_{M_{0.25}}$  vs  $C_{L_{0.25}}$ 

CONFIG A2

1/8 B7B  
N = 95%BASED ON EFFECTIVE  
STATIC RESULTS0.2  $C_{M_{0.25}}$  $\alpha_0 = 0$ 

0.1

 $\beta = 15$  $\beta = 10$  $\beta = 5$ 1.4  
 $C_{L_{0.25}}$ 

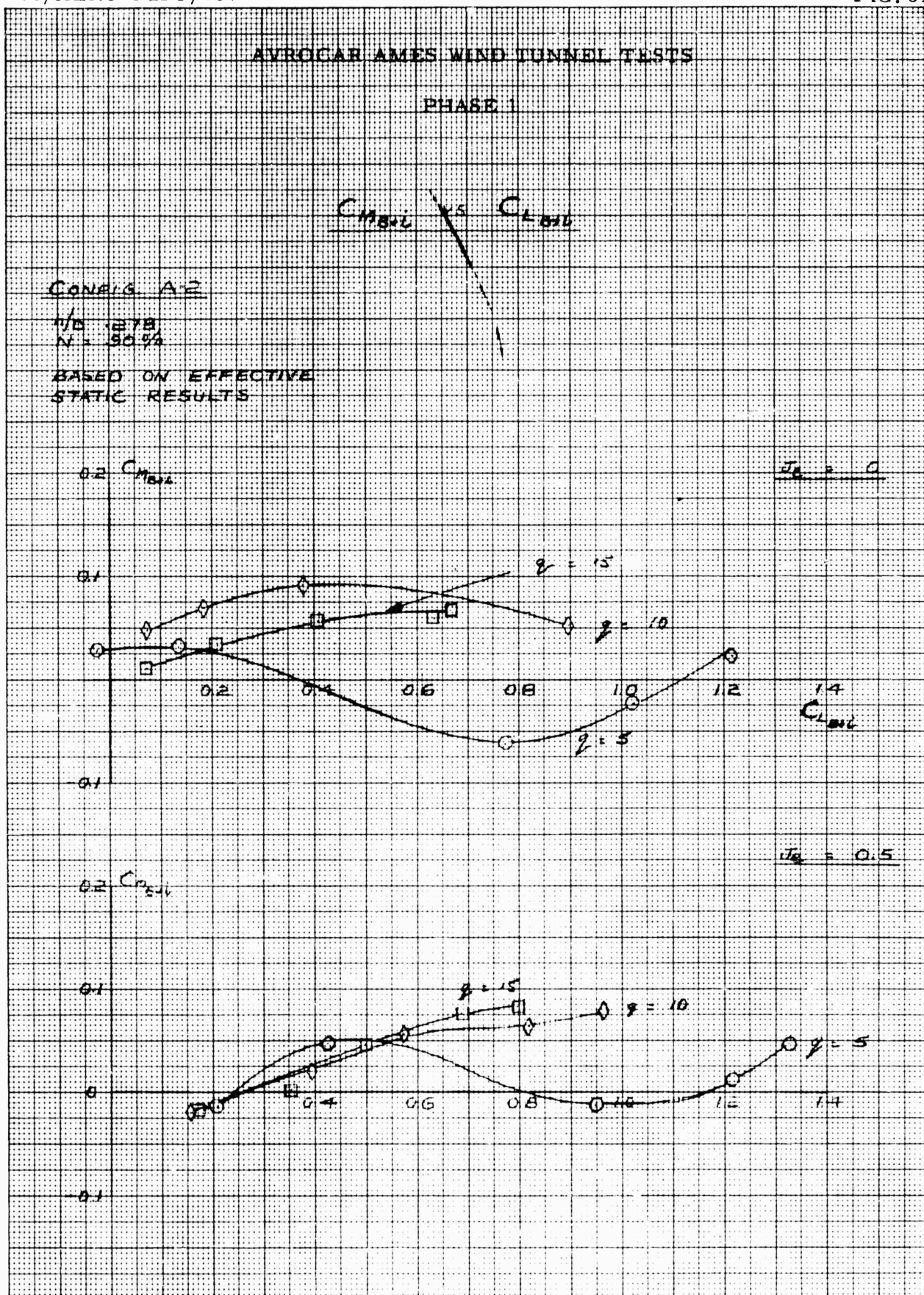
0.1

 $\alpha_0 = 0.5$ 0.2  $C_{M_{0.25}}$ 

0.1

 $\beta = 15$  $\beta = 10$  $\beta = 5$ 

0.1



## AVROCAR AMES WIND TUNNEL TESTS

## PHASE I

 $C_{MAG}$  vs  $C_{LAB}$ 

CONFIG A-2

M/D 210

N = 90%

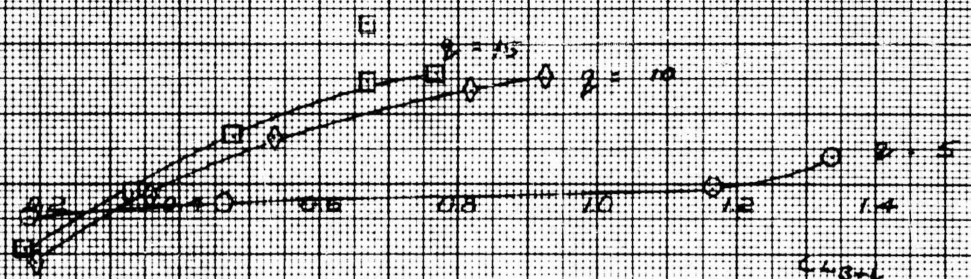
 $T_0 = 1.0$  $C_{MAG}$ (BASED ON EFFECTIVE  
STATIC VALUES)

0.3

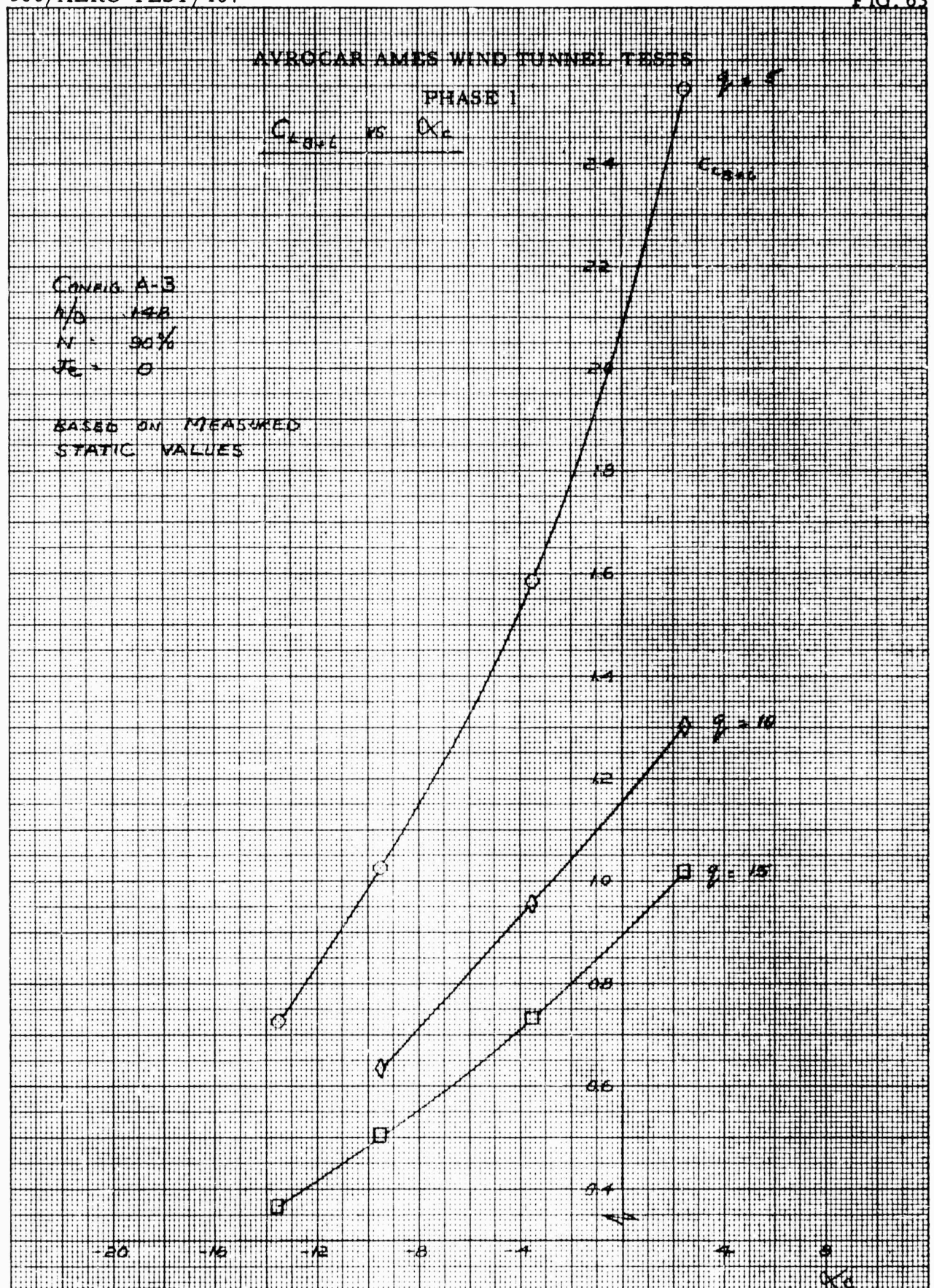
0.1

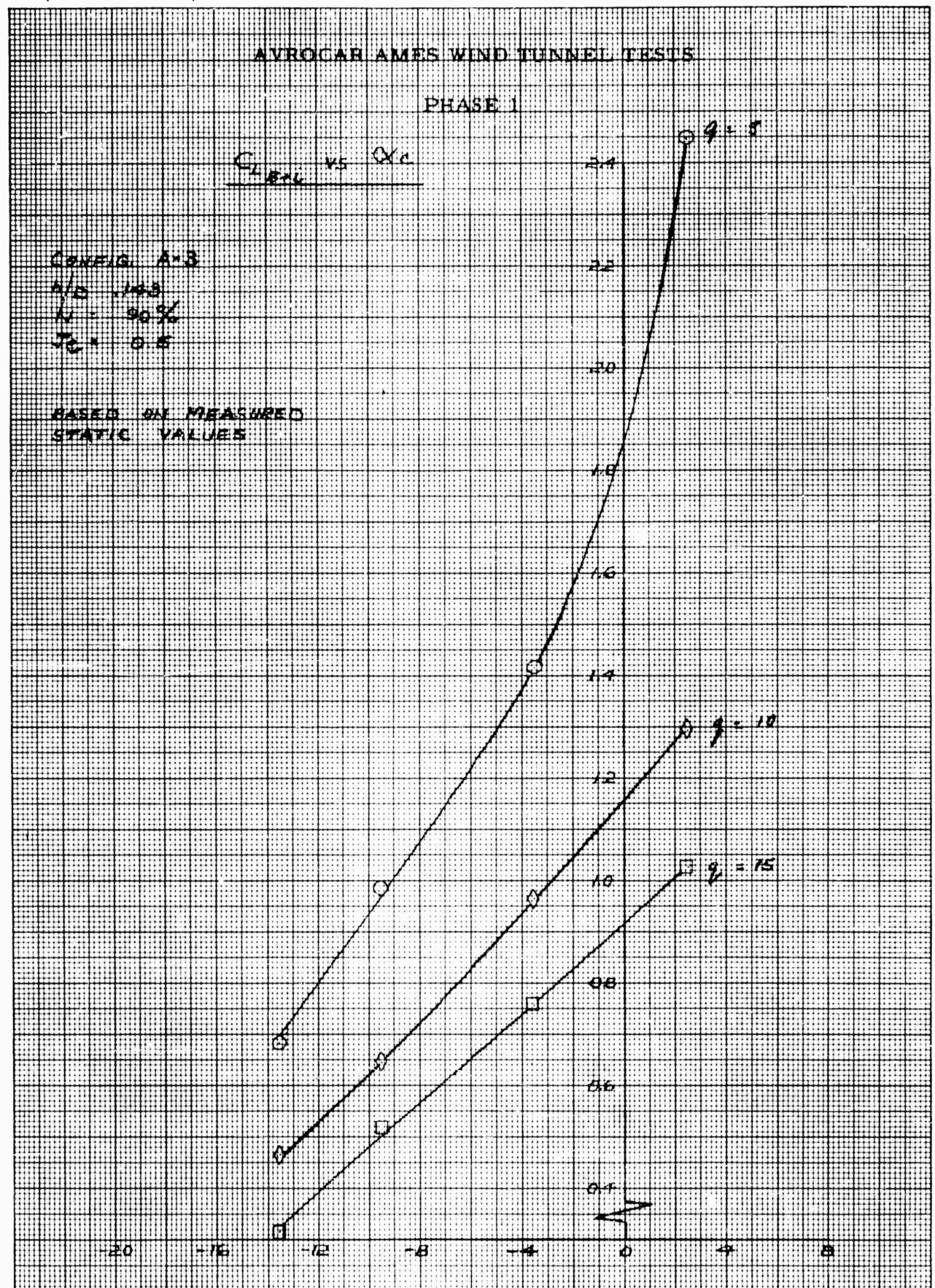
0

-0.1











# AVROCAR AMES WIND TUNNEL TESTS PHASE I

$C_{L_{B+i}}$  vs  $\alpha_c$

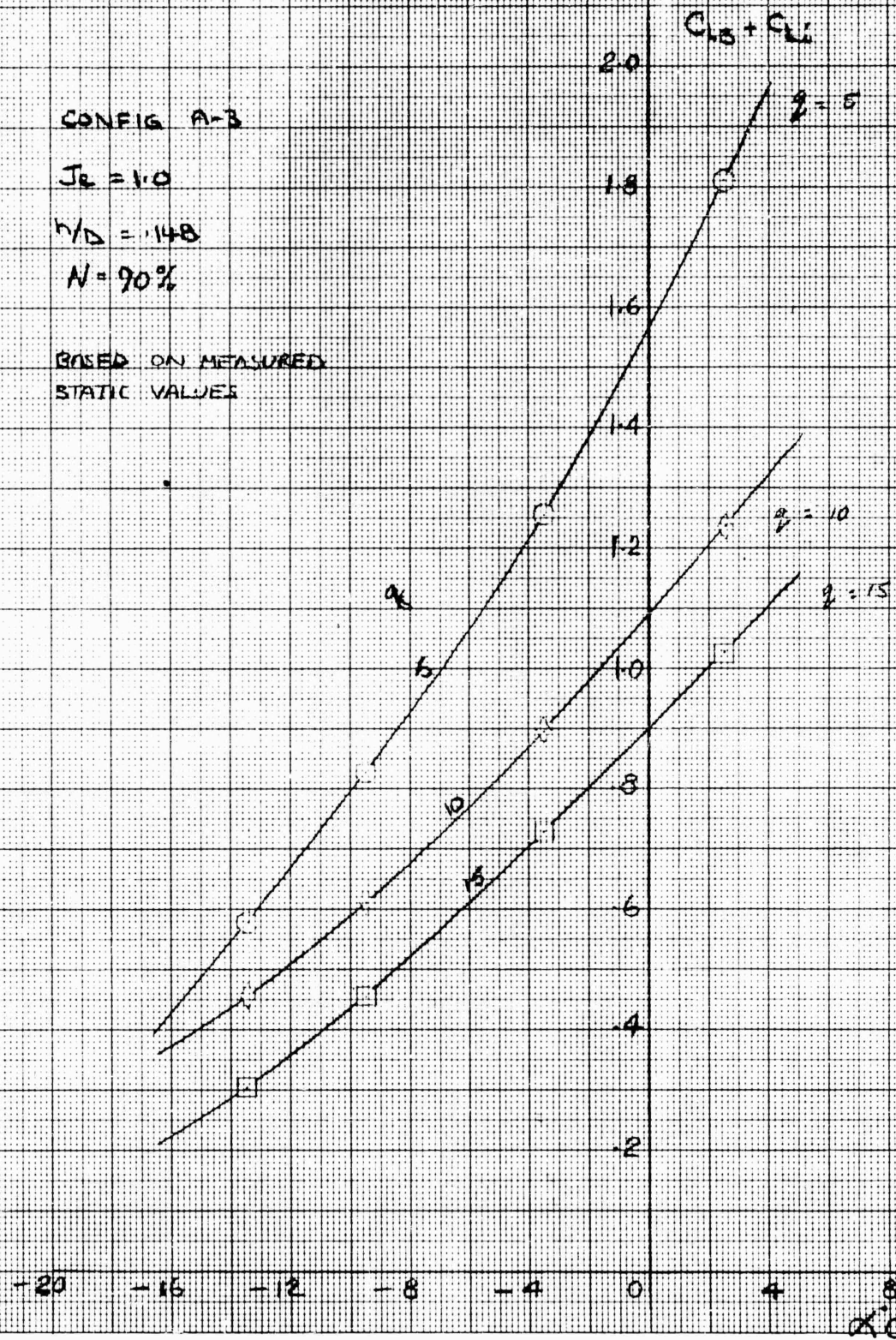
CONFIG A-B

$J_R = 1.0$

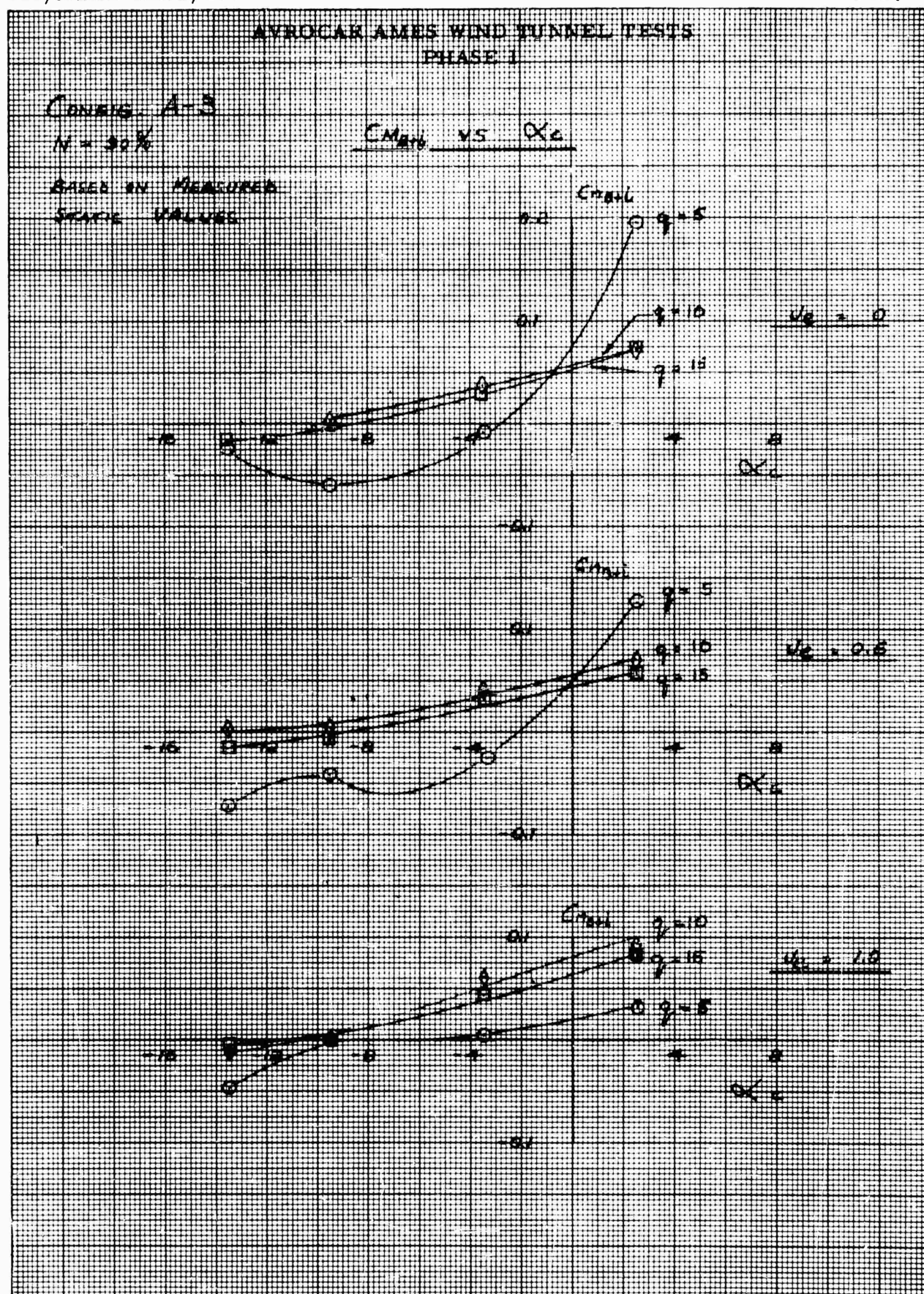
$h/D = .148$

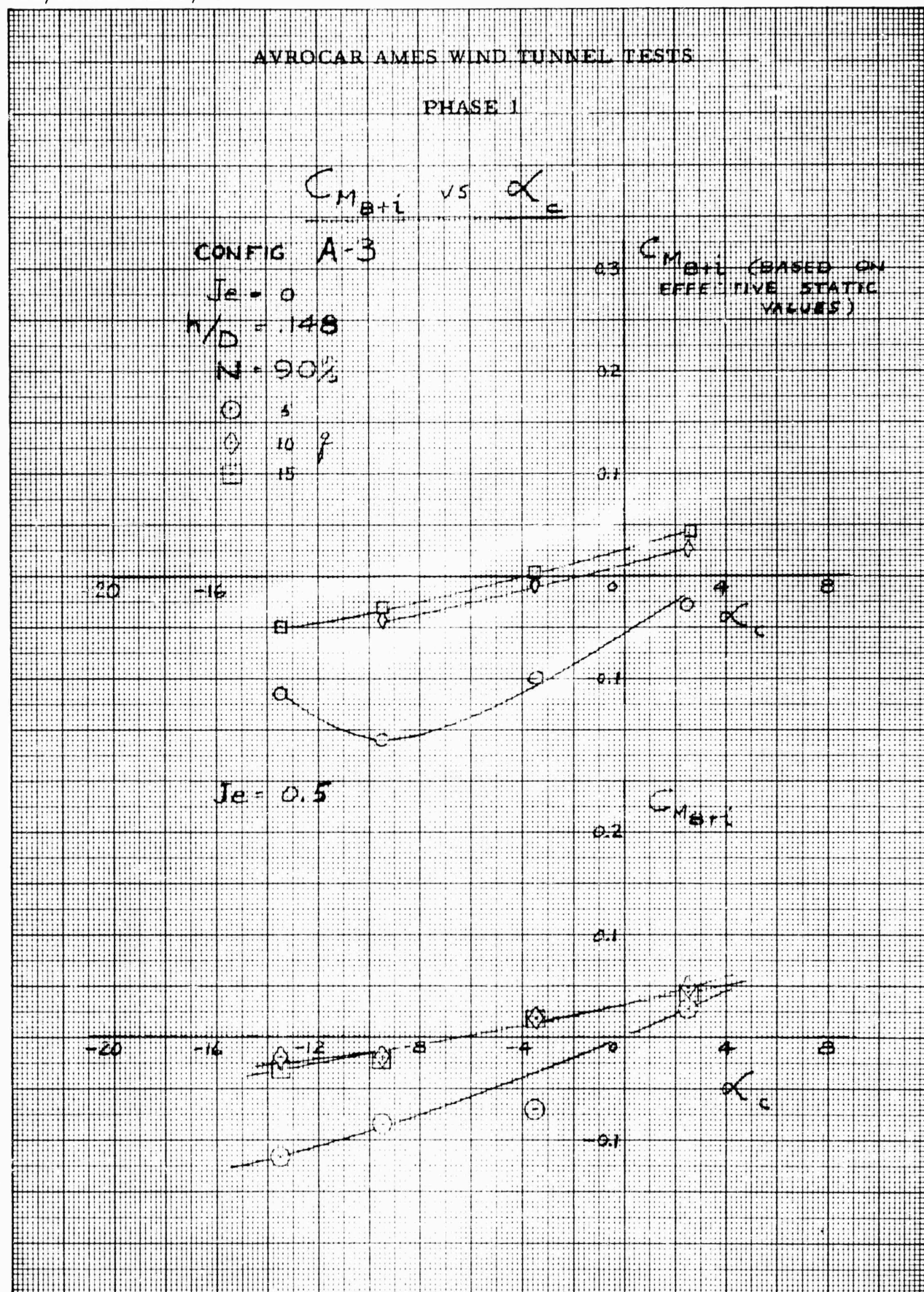
$N = 90\%$

BASED ON MEASURED  
STATIC VALUES











## AVROCAR AMES WIND TUNNEL TESTS

## PHASE I

 $C_{MB+L}$  vs  $\alpha_c$ 

CONFIG A-3

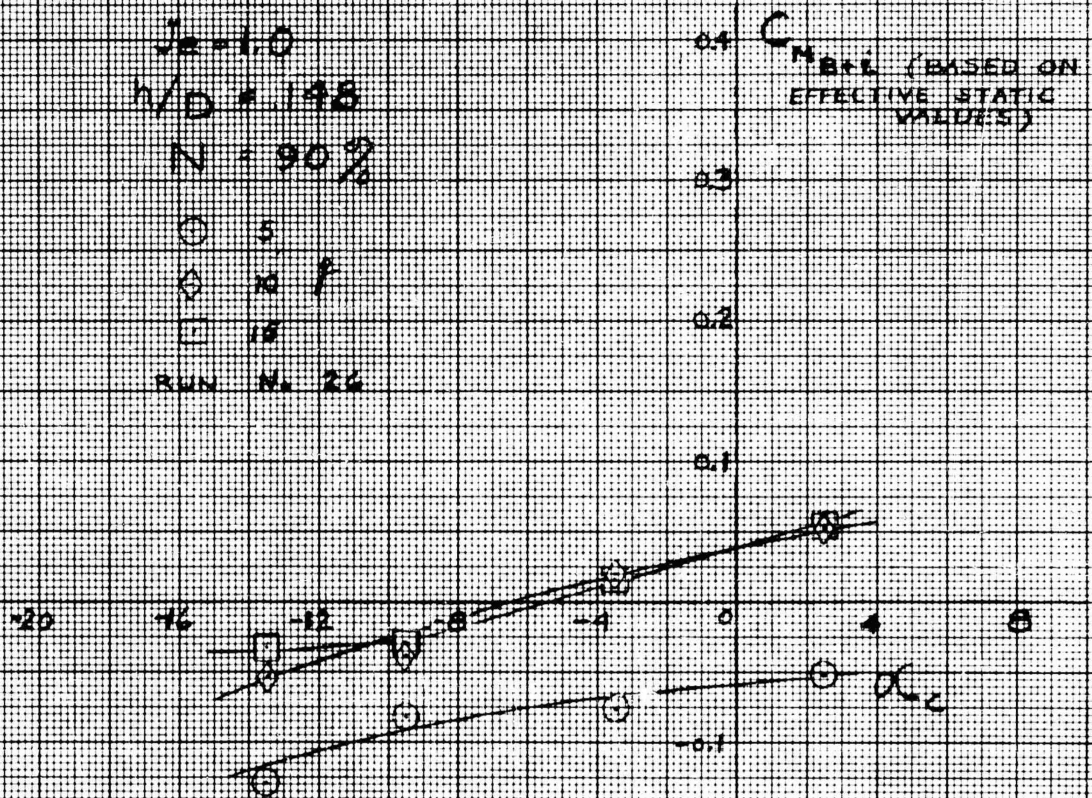
 $J_z = 1.0$  $h/D = 1.48$  $N = 90\%$ 

○ 5

◇ 10

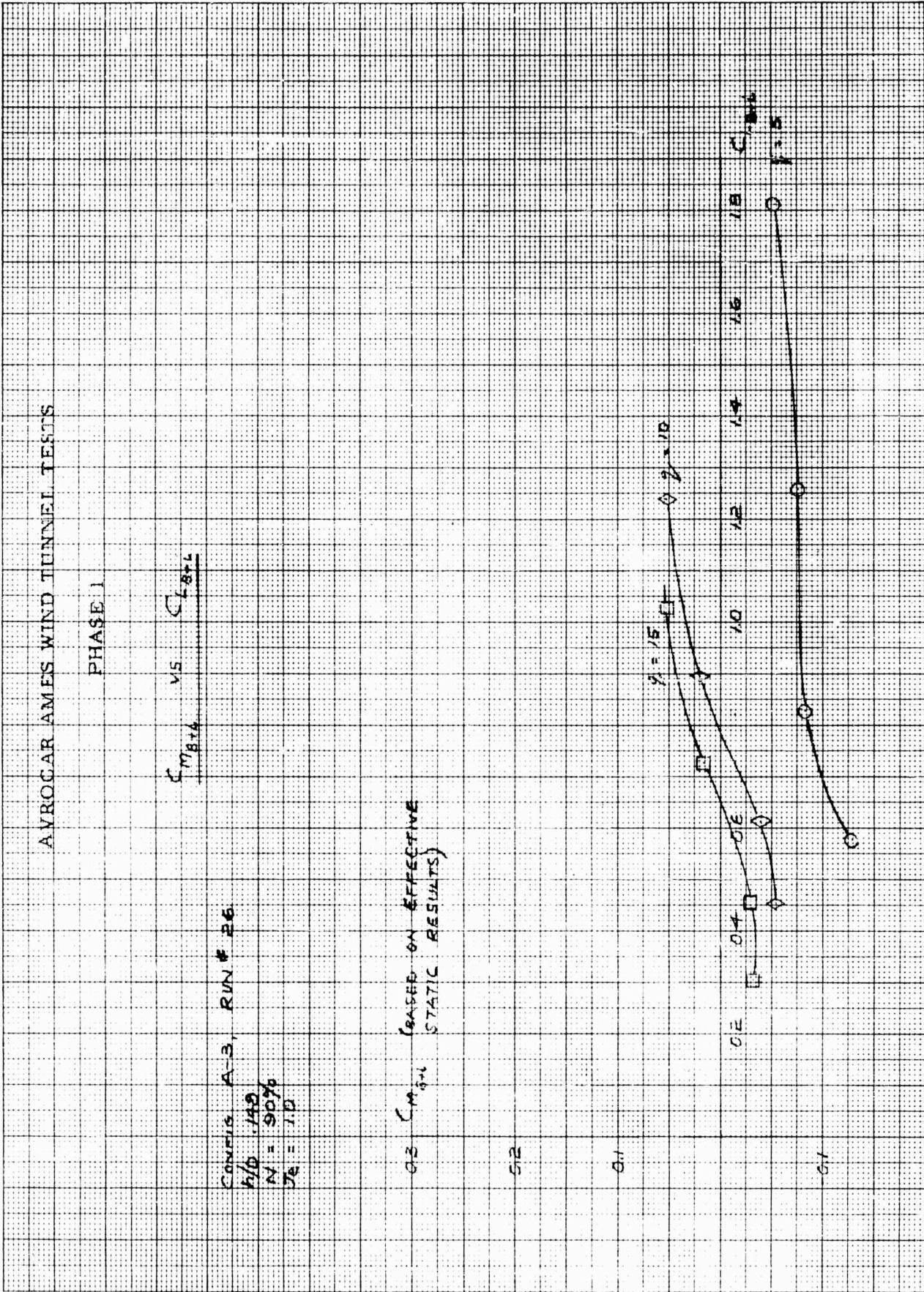
□ 15

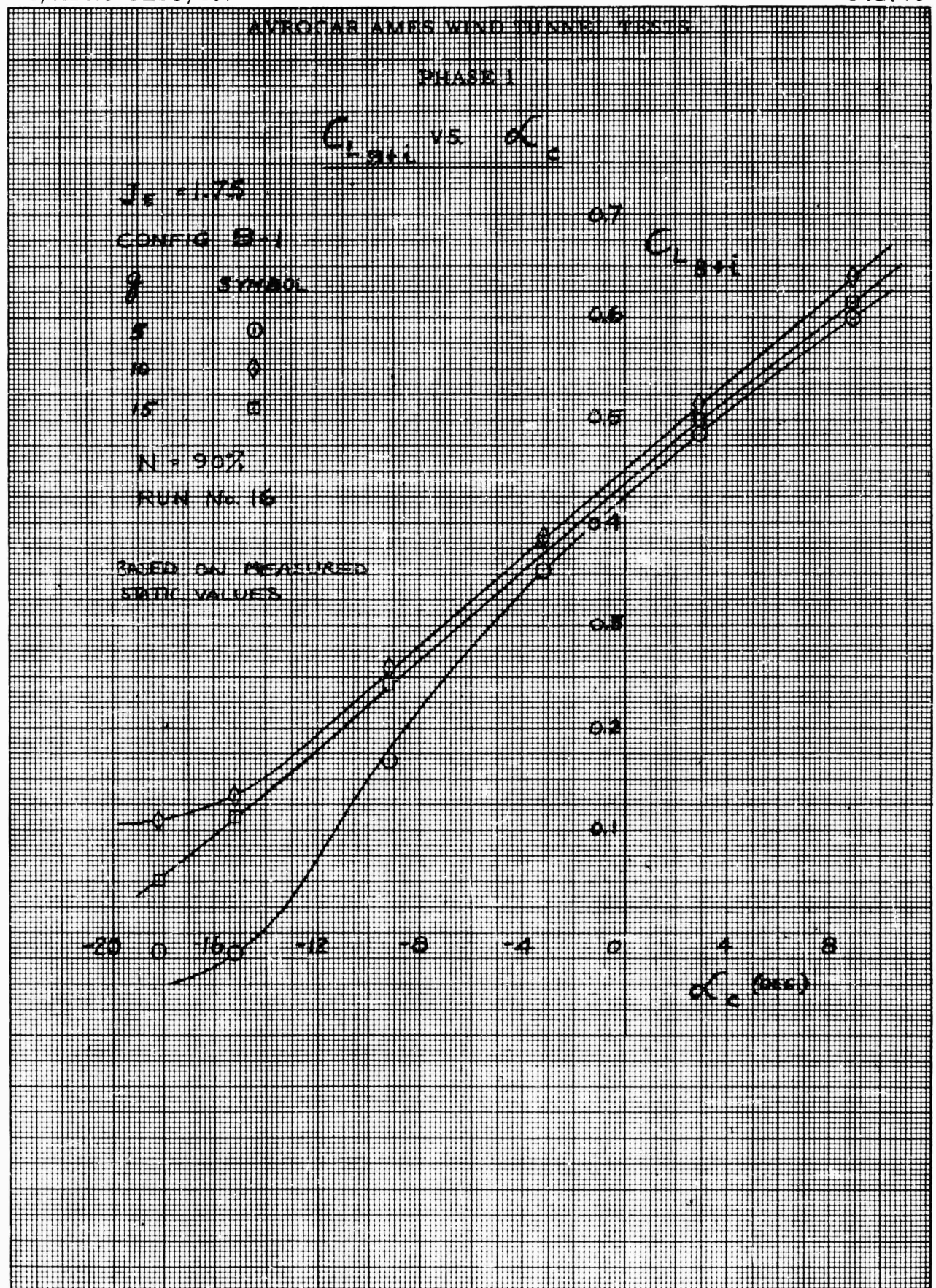
RUN No. 26

 $C_{MB+L}$  (BASED ON  
EFFECTIVE STATIC  
VALUES)











## AVROCAR AMES WIND TUNNEL TESTS

## PHASE I

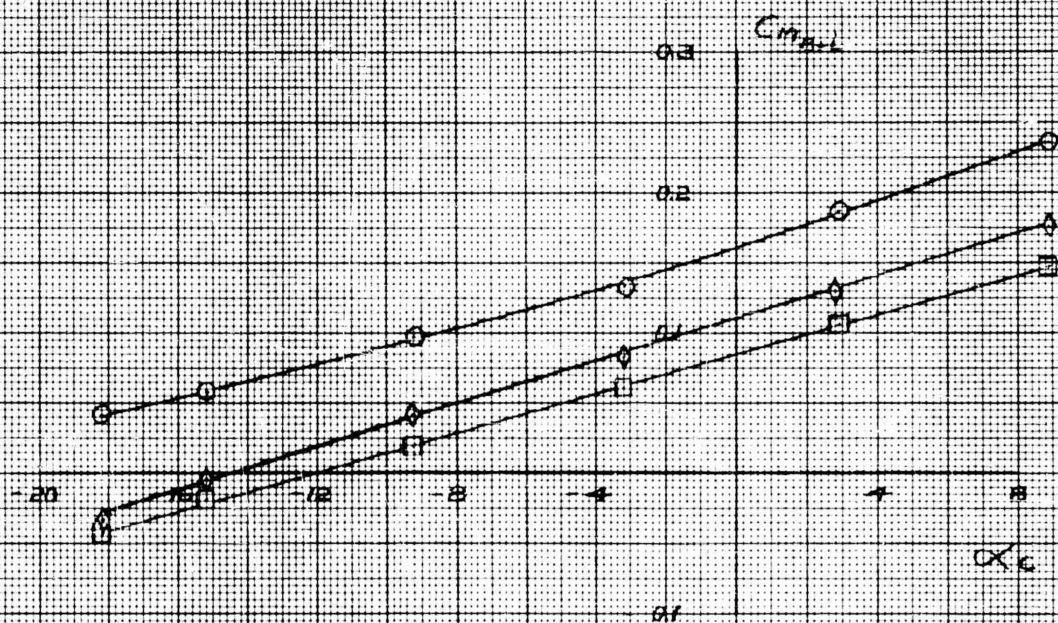
 $C_{M_{B+L}}$  VS  $\alpha_c$ 

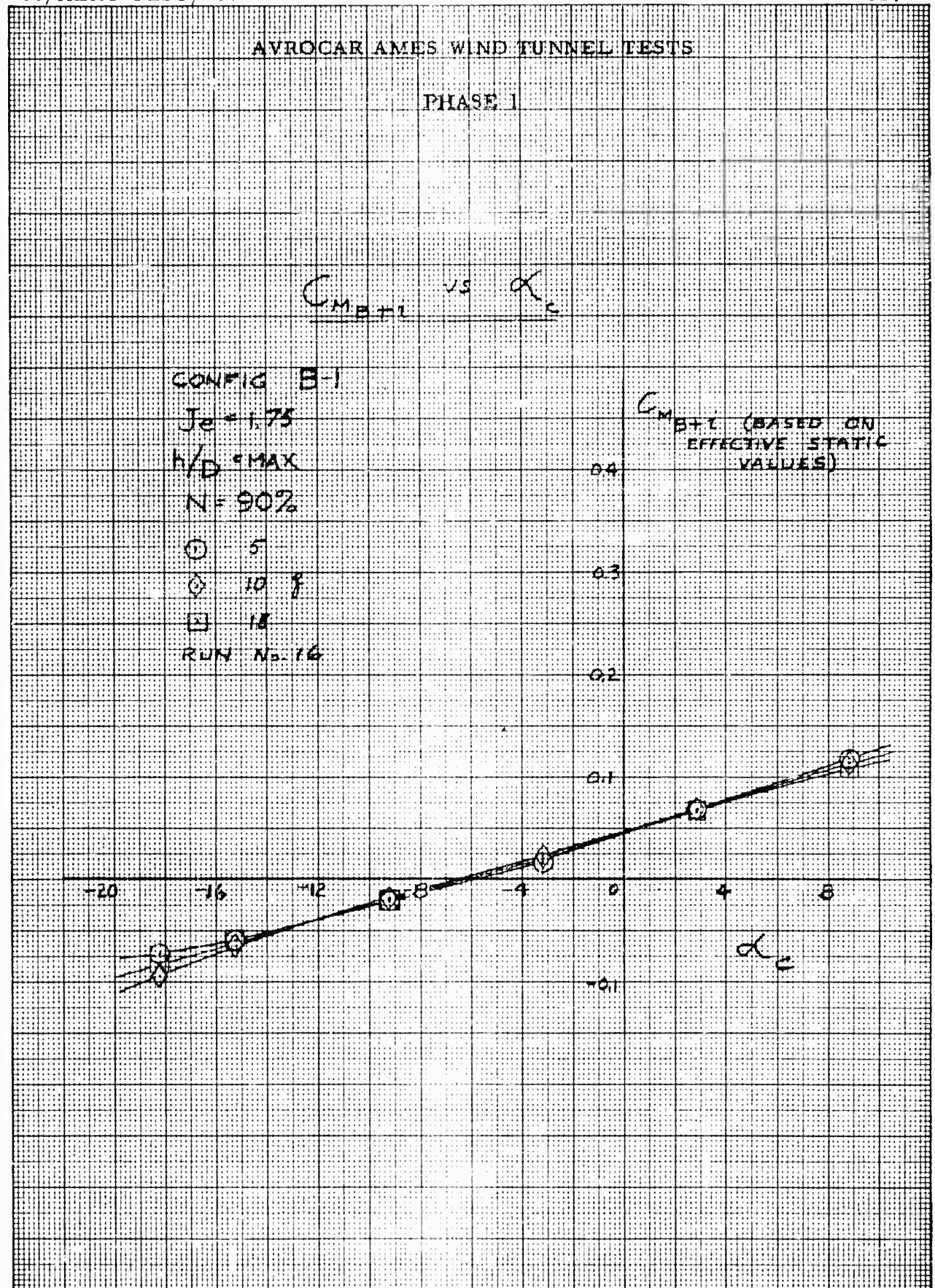
CONFIG B-1  
 RUN # 16  
 $N = 30\%$   
 $U_0 = 1.75$

BASED ON MEASURED

STATIC VALUES

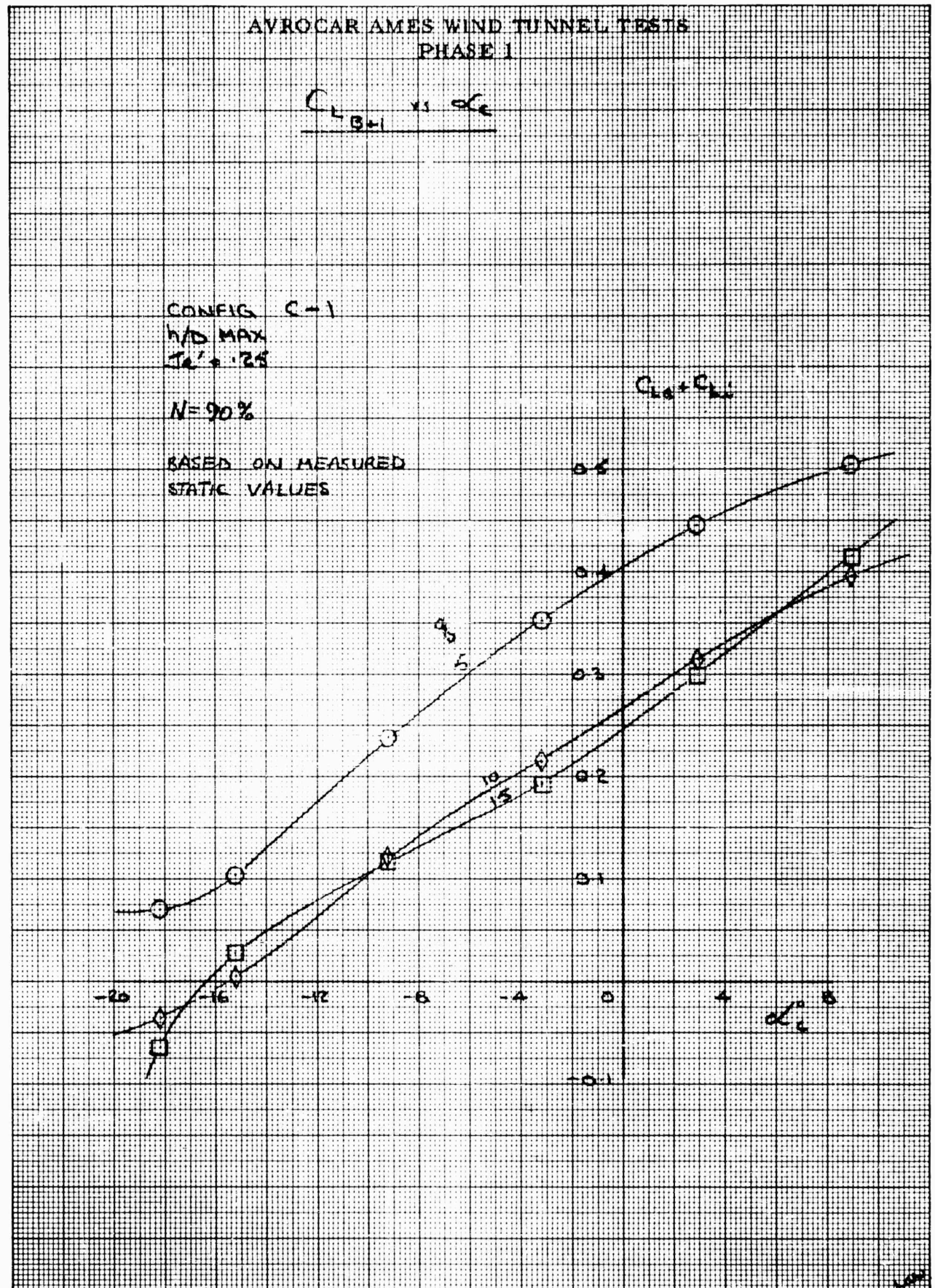
SYM	$\alpha_c$
○	5
◇	10
□	15













## AVROCAR AMES WIND TUNNEL TESTS

## PHASE I

 $C_{M_{AVC}}$  vs  $\alpha_c$ 

CONFIG. C-1

RUN # 10

N = 50%

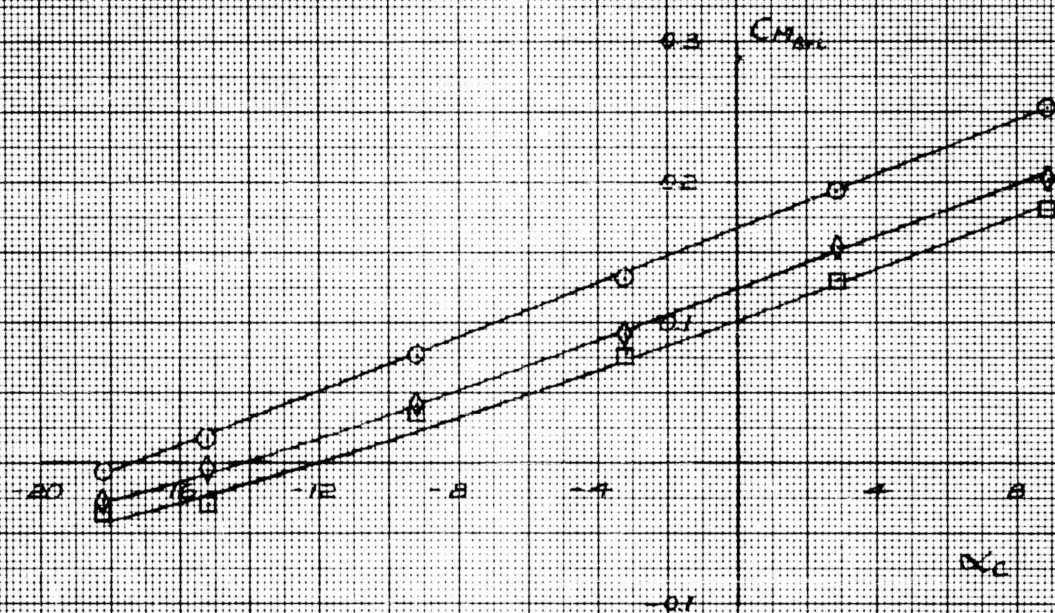
M = 25

BASED ON MEASURED  
STATIC VALUES

○ 5

◇ 10

□ 15



## AVROCAR AMES WIND TUNNEL TESTS

## PHASE I

$C_{M_{B+E}}$  VS  $\alpha_C$

CONFIG C-1

$h/D = 0.25$

$h/D = \text{MAX}$

$N = 90\%$

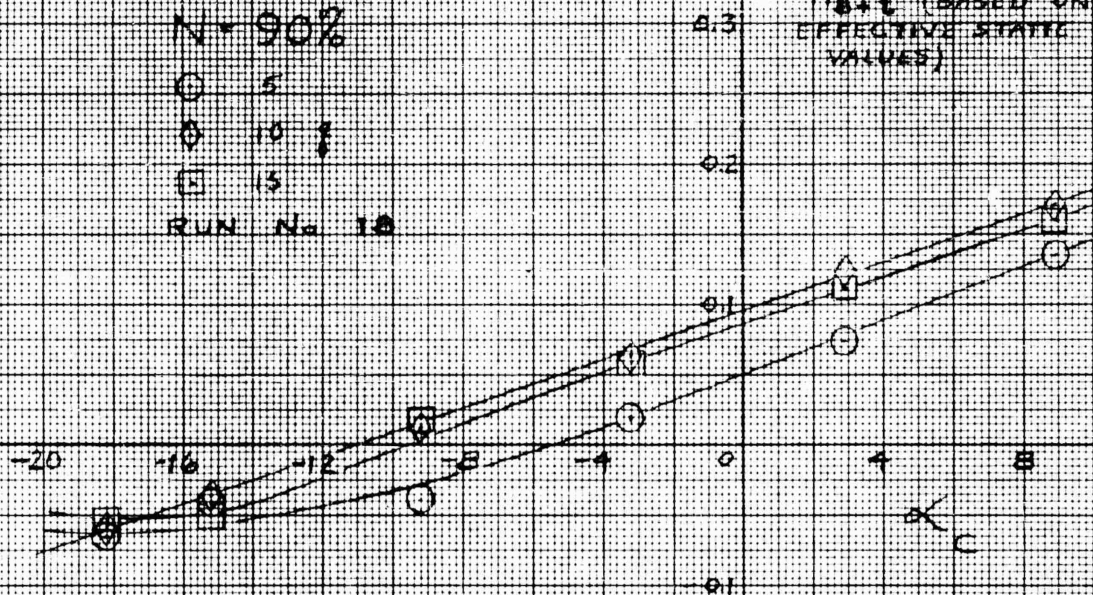
○ 5

○ 10

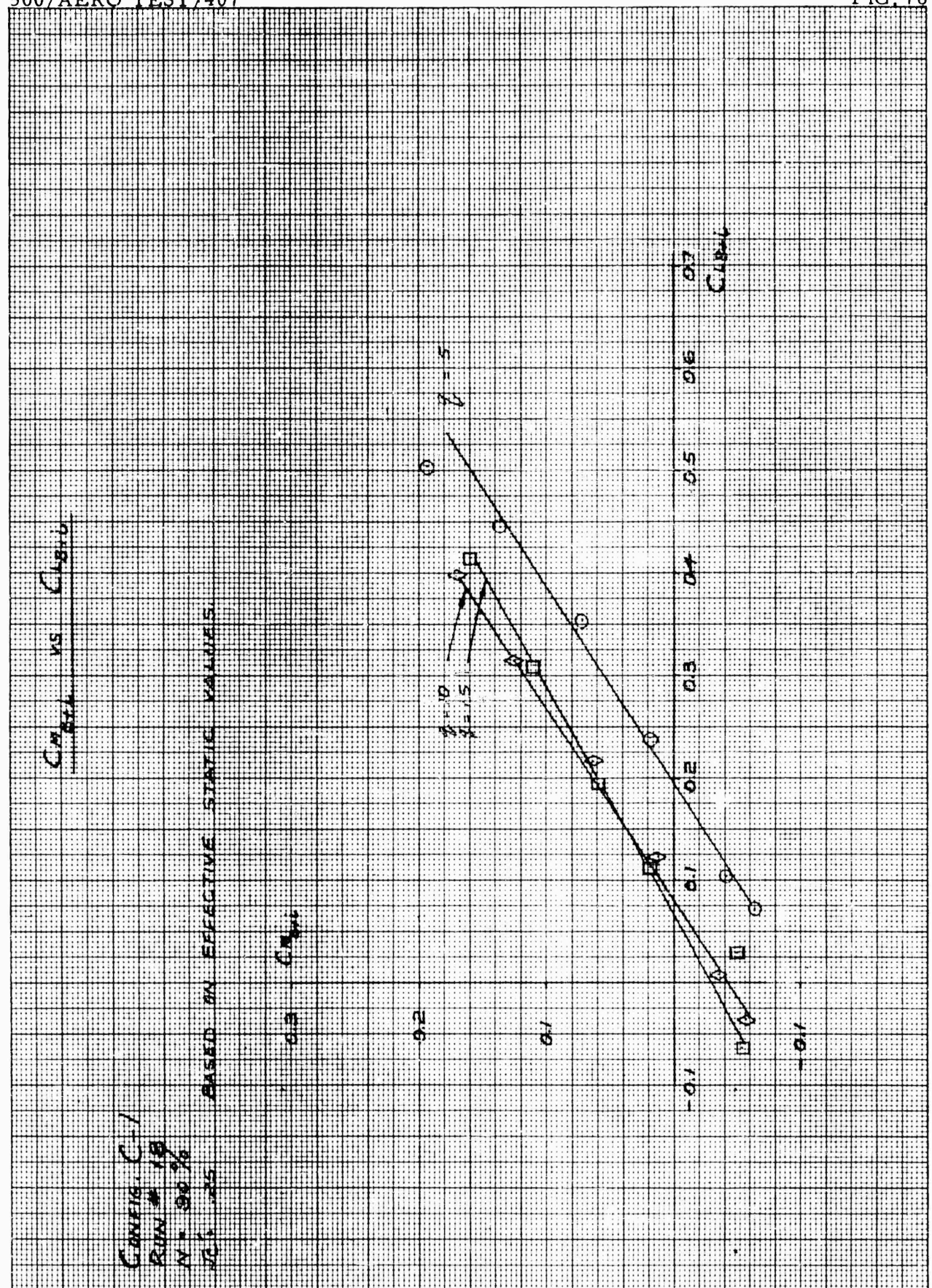
□ 15

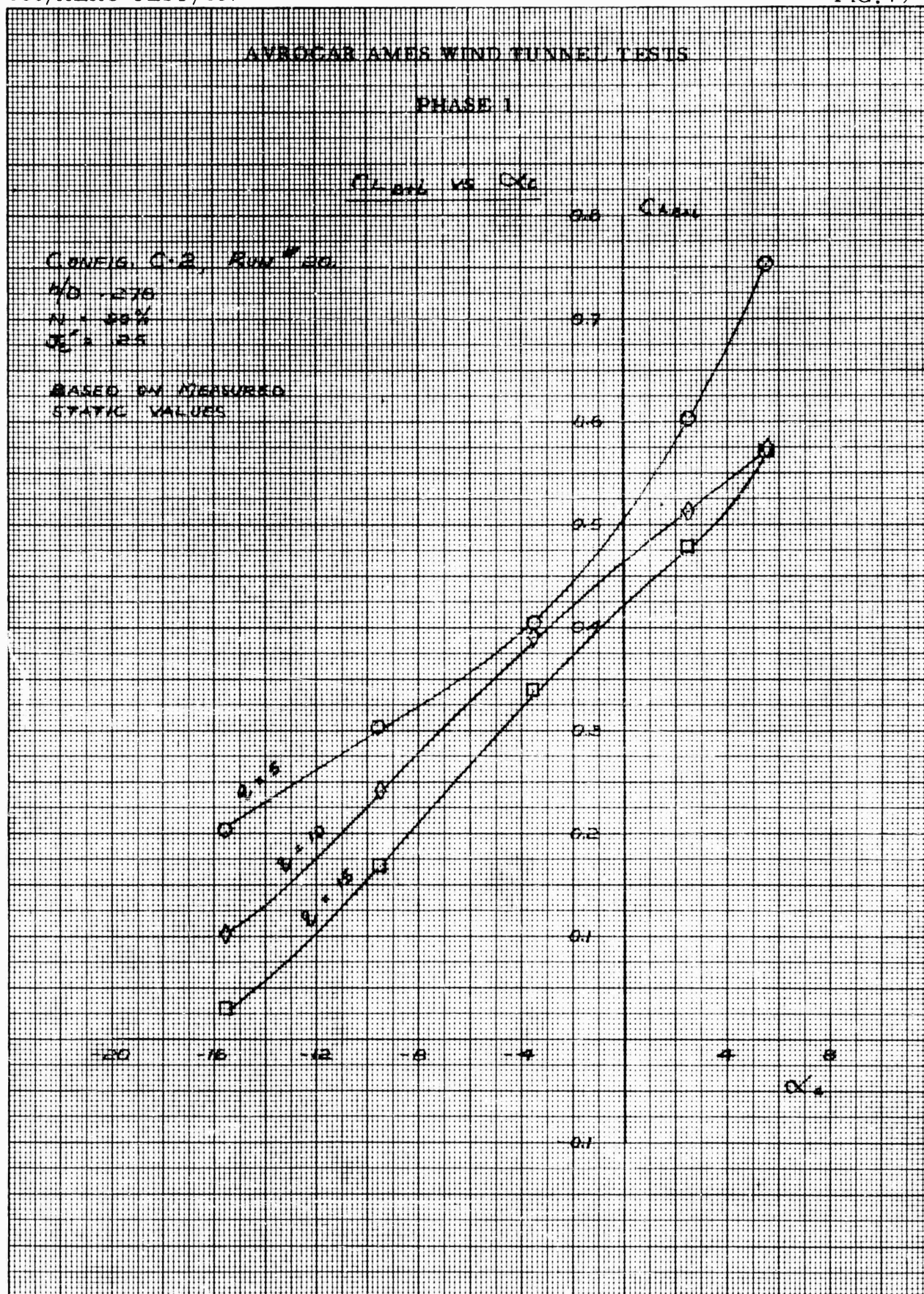
RUN No. 10

$C_{M_{B+E}}$  (BASED ON  
EFFECTIVE STATIC  
VALUES)

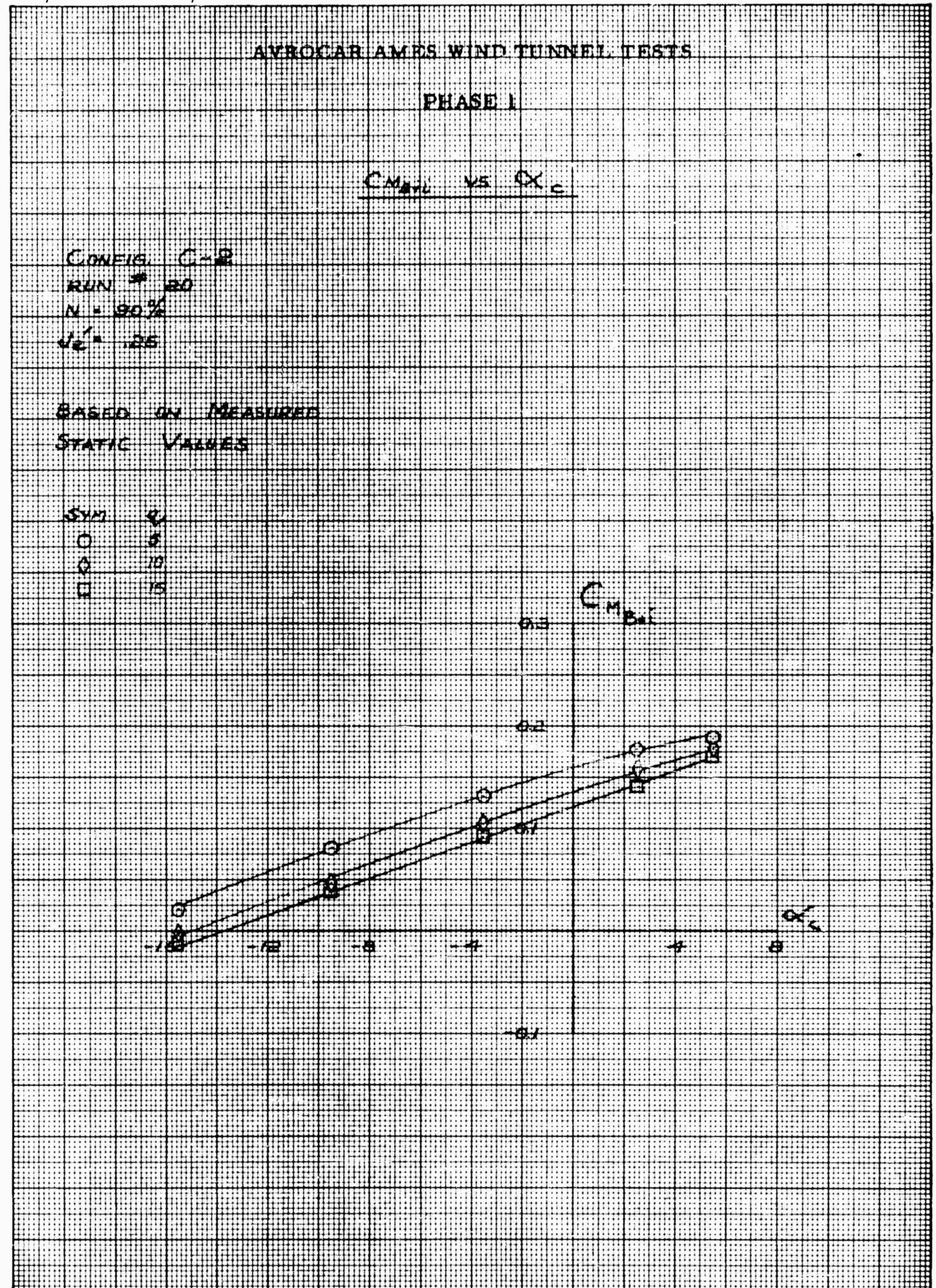


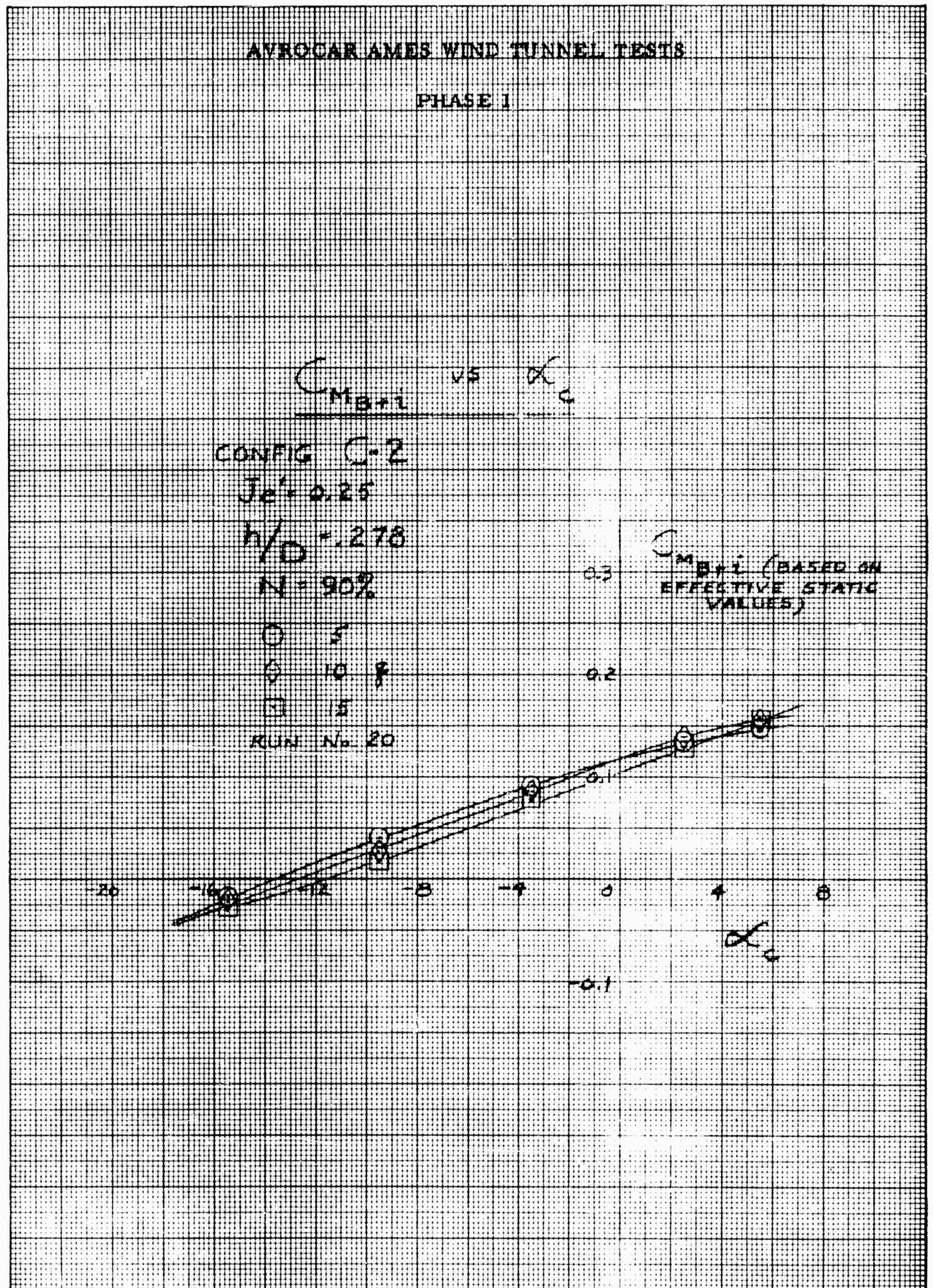














## AVROCAR AMES WIND TUNNEL TESTS

## PHASE I

 $C_{D_{eff}}$  vs  $C_{L_{eff}}$ 

CONFIG C-2

RUN # 20

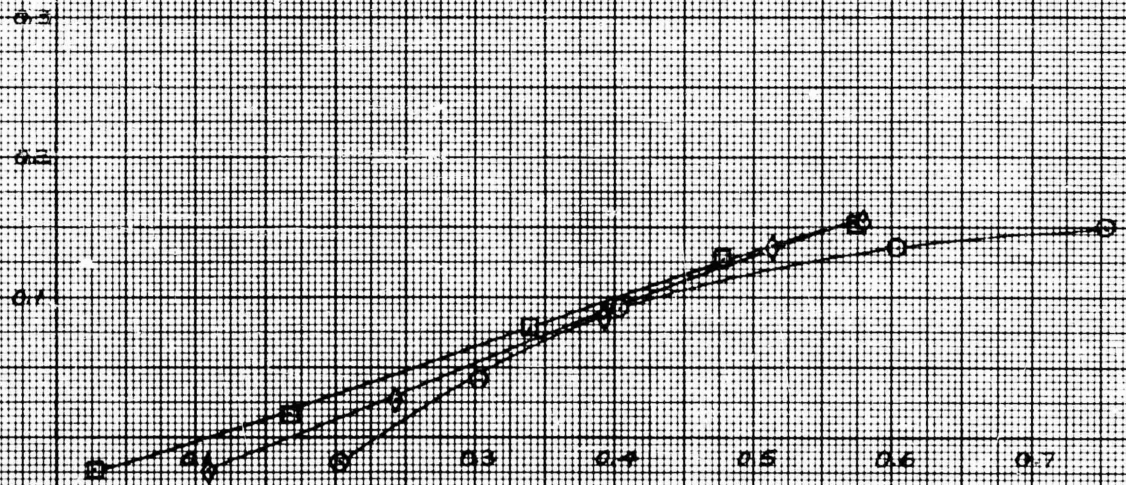
h/b .278

N = 30%

 $J_0 = 0.25$ 

SYM	$q_c$
○	5
○	10
□	15

$C_{D_{eff}}$   
(BASED ON EFFECTIVE  
STATIC RESULTS)



## AVROCAR AMES WIND TUNNEL TESTS

## PHASE I

CONFIG D-1

RUN # 17

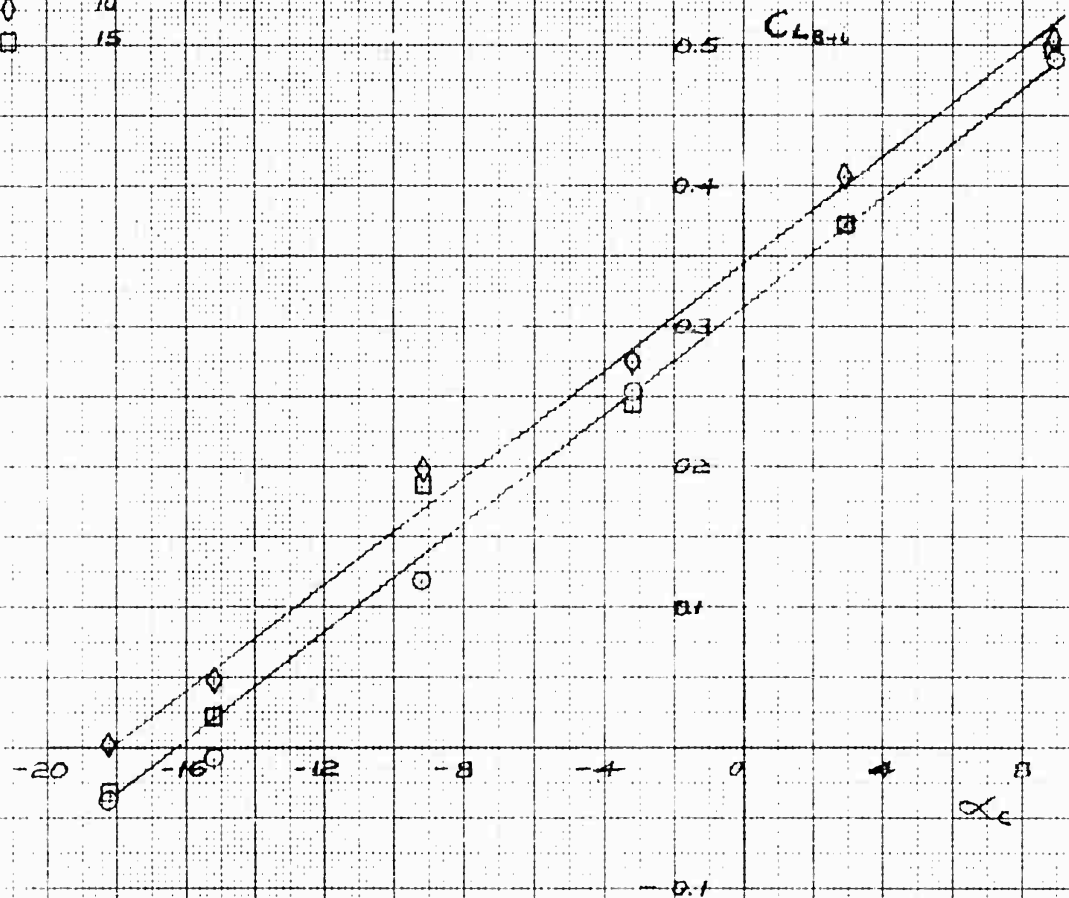
Re' 1.75

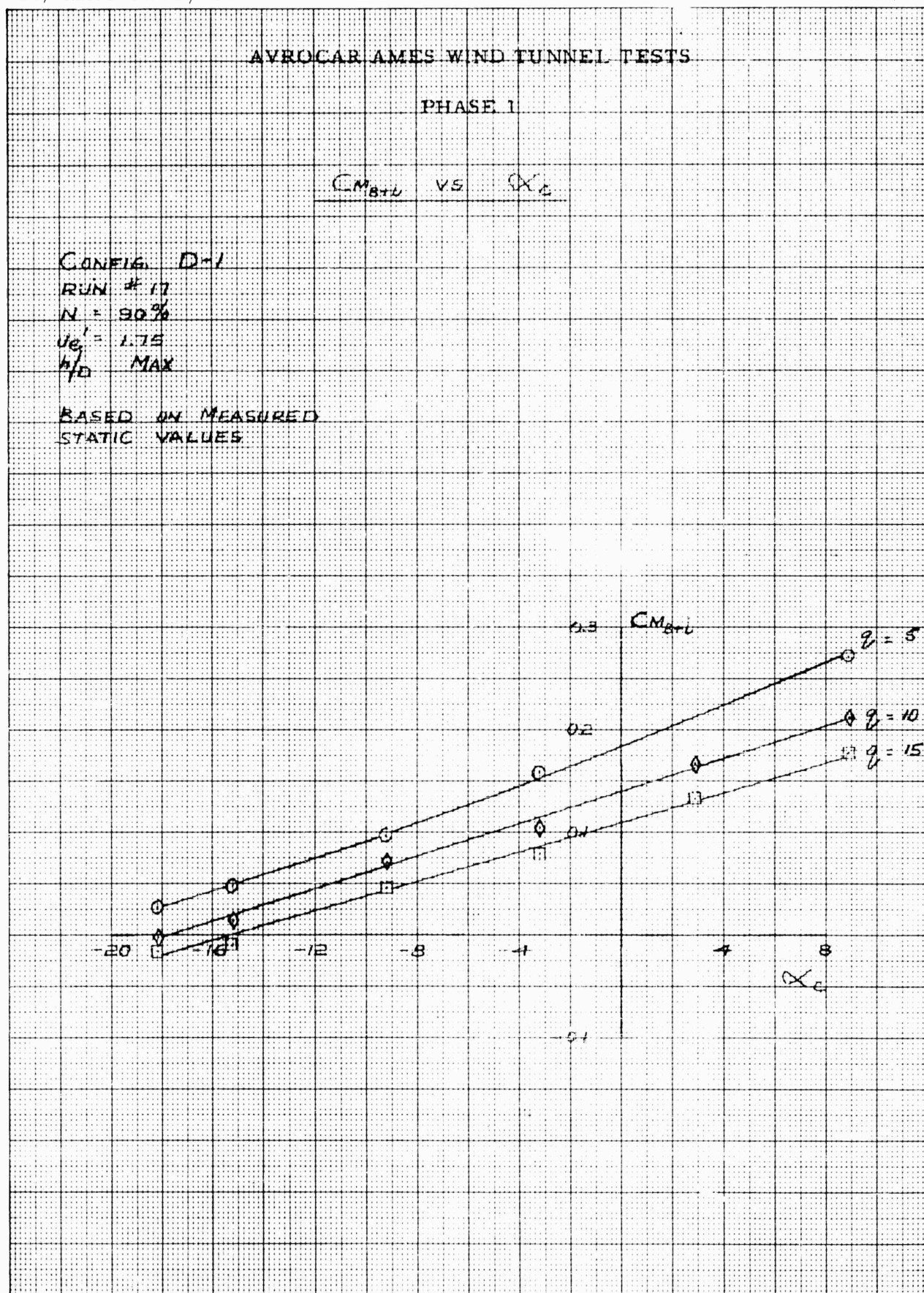
N<sub>1</sub> 90%

M/D MAX

CL<sub>B+L</sub> VS  $\alpha_c$ BASED ON MEASURED  
STATIC VALUES

SYM	9
○	5
◇	10
□	15







## AVROCAR AMES WIND TUNNEL TESTS

## PHASE I

 $C_{MB+L}$  vs  $\alpha_c$ 

CONFIG D-1

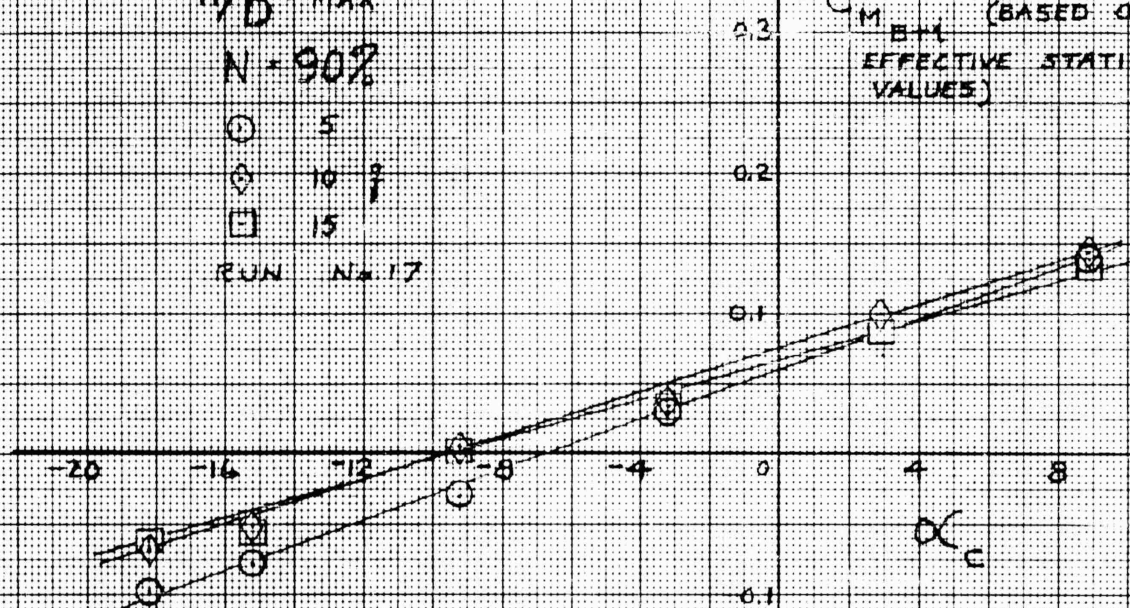
 $J_e' = 1.75$  $h/D = \text{MAX}$  $N = 90^\circ$ 

① 5

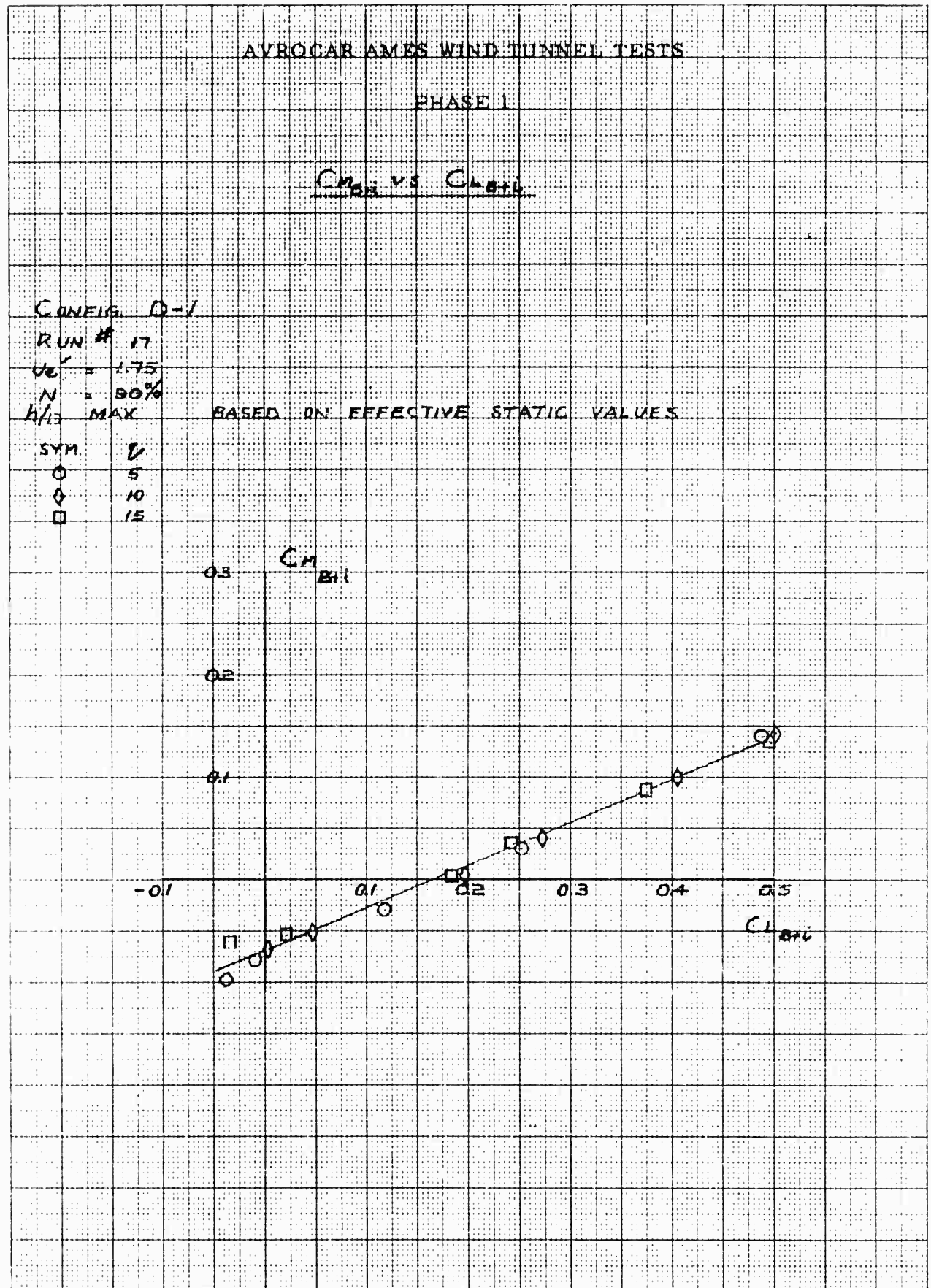
② 10

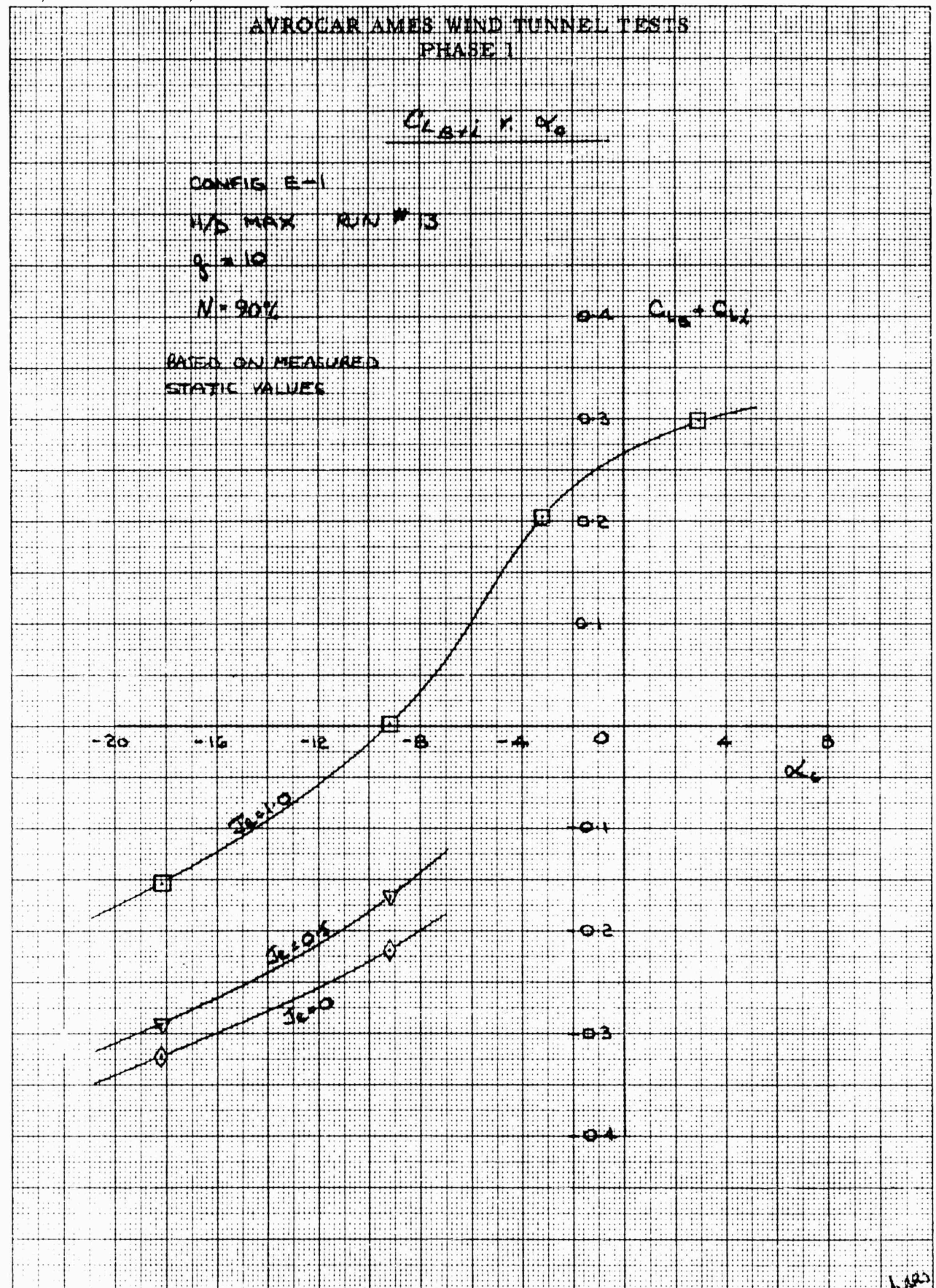
③ 15

RUN N. 17

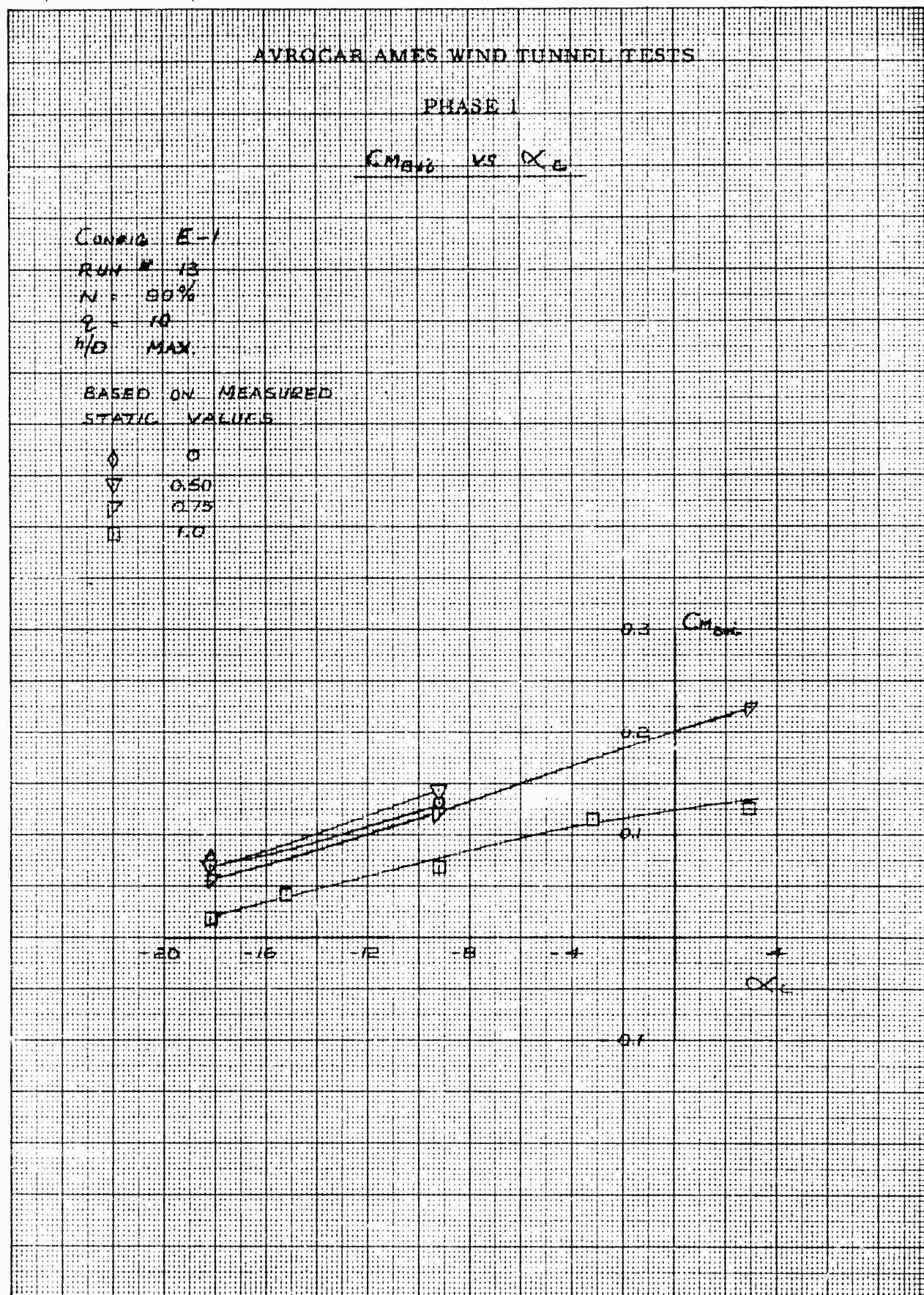
 $C_{MB+L}$  (BASED ON  
EFFECTIVE STATIC  
VALUES)



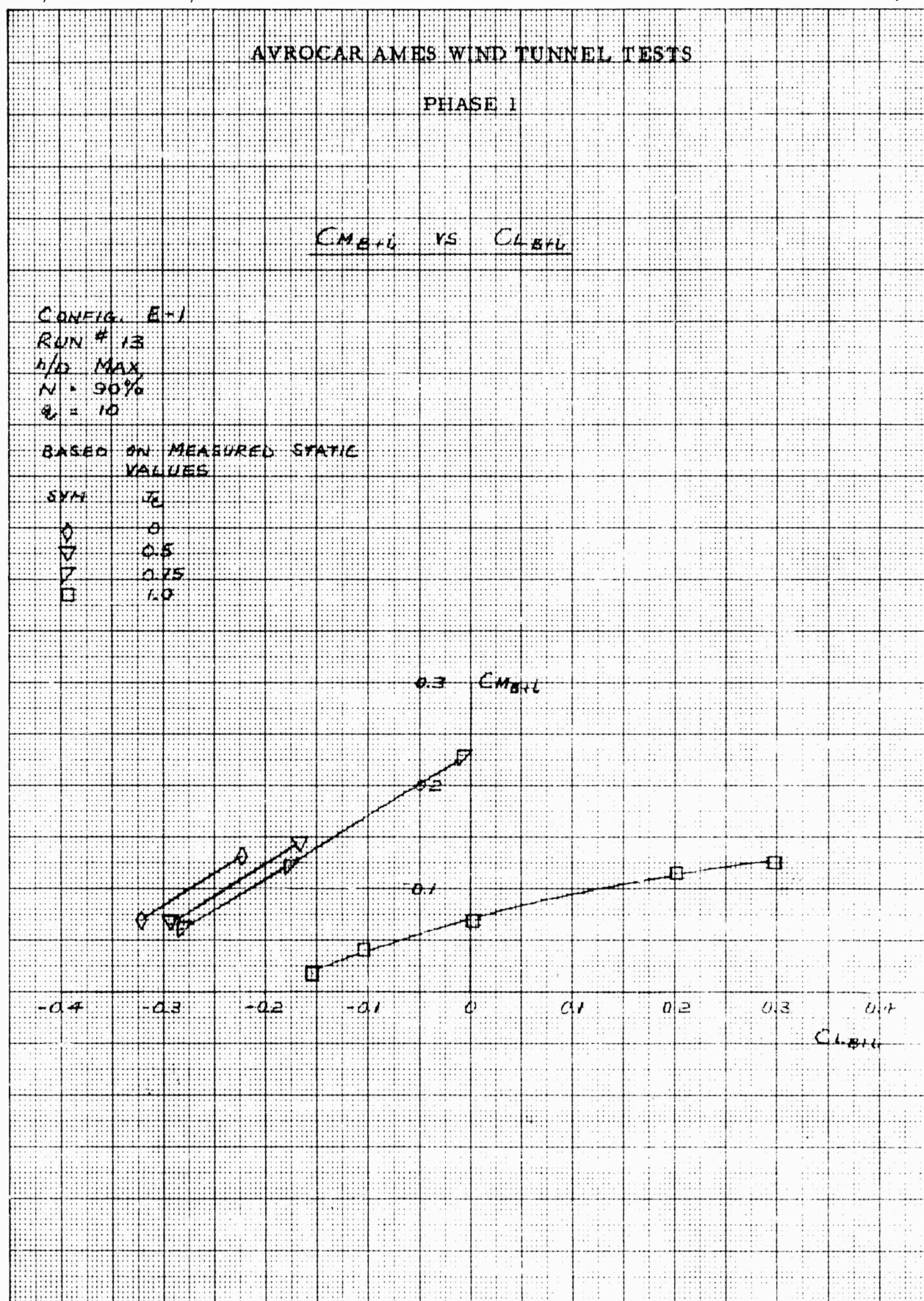




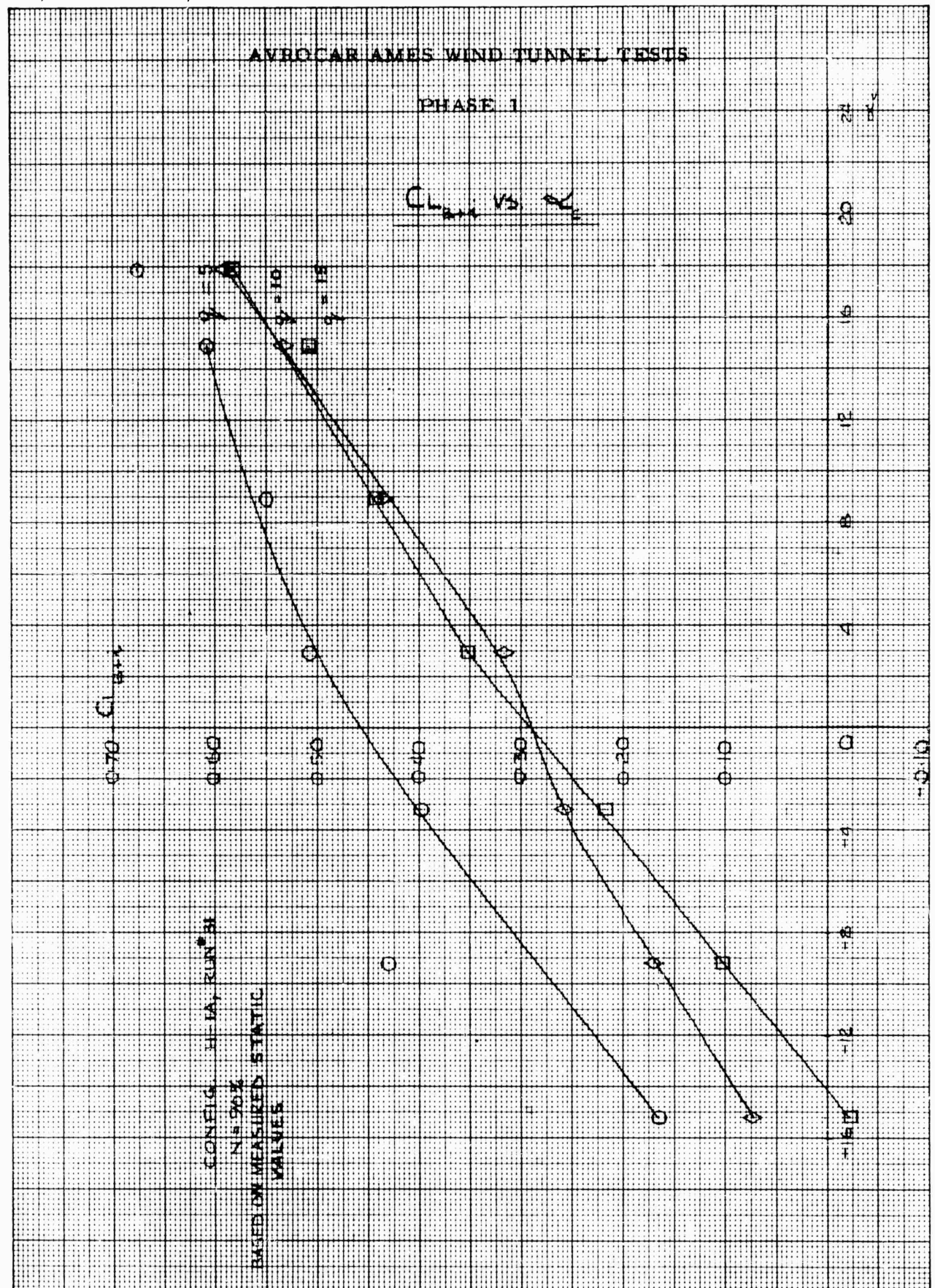
L-105

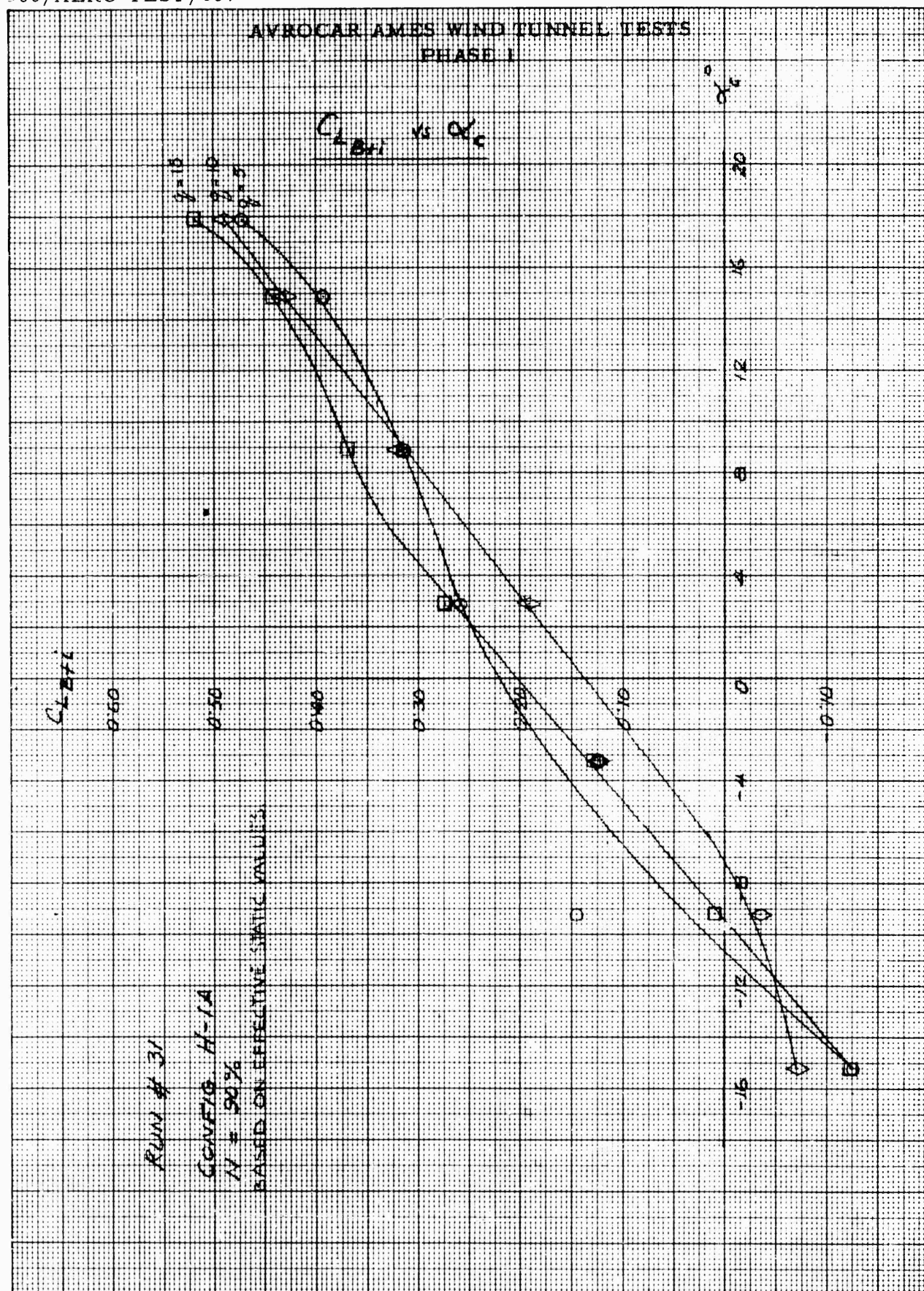




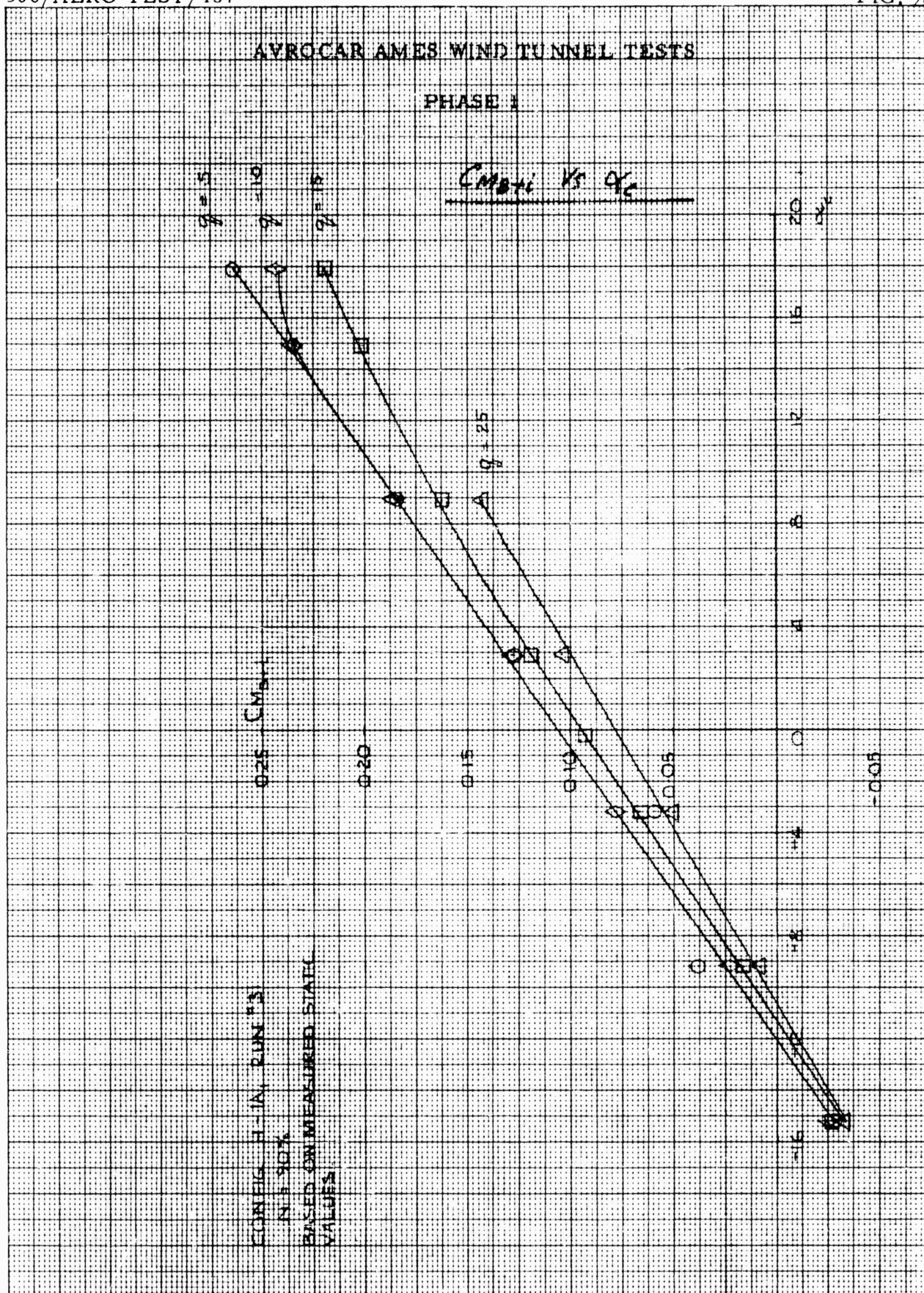


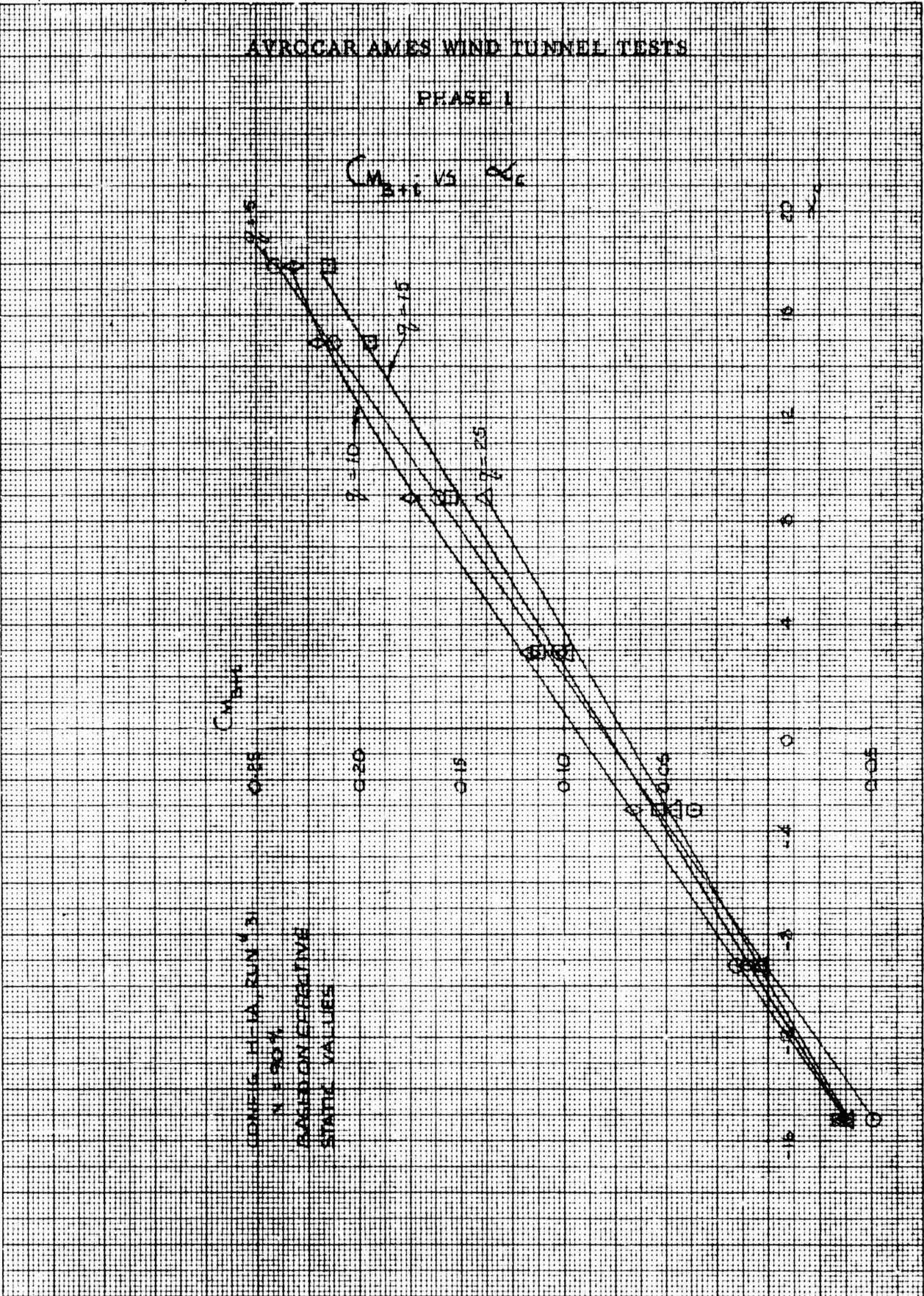






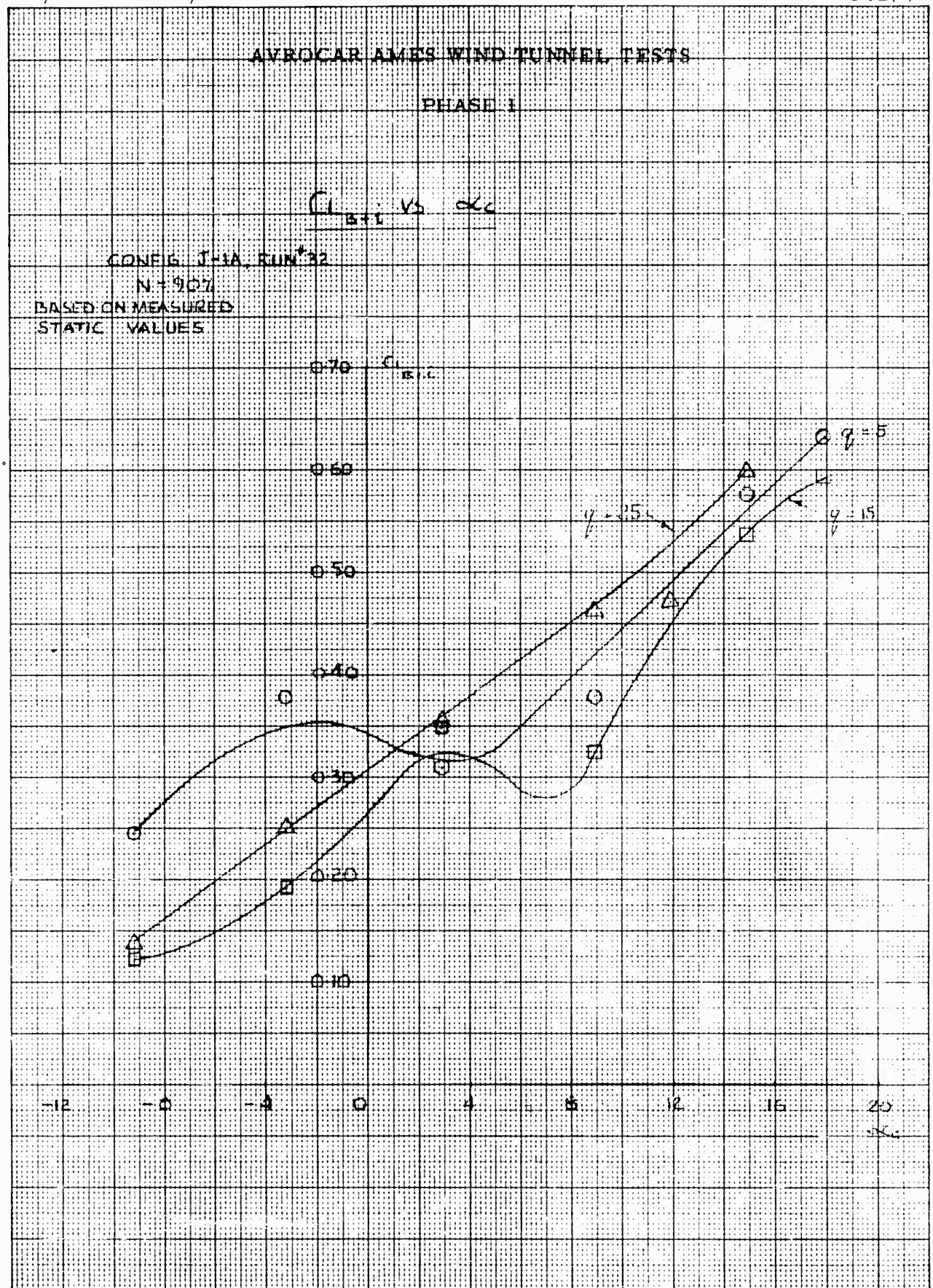


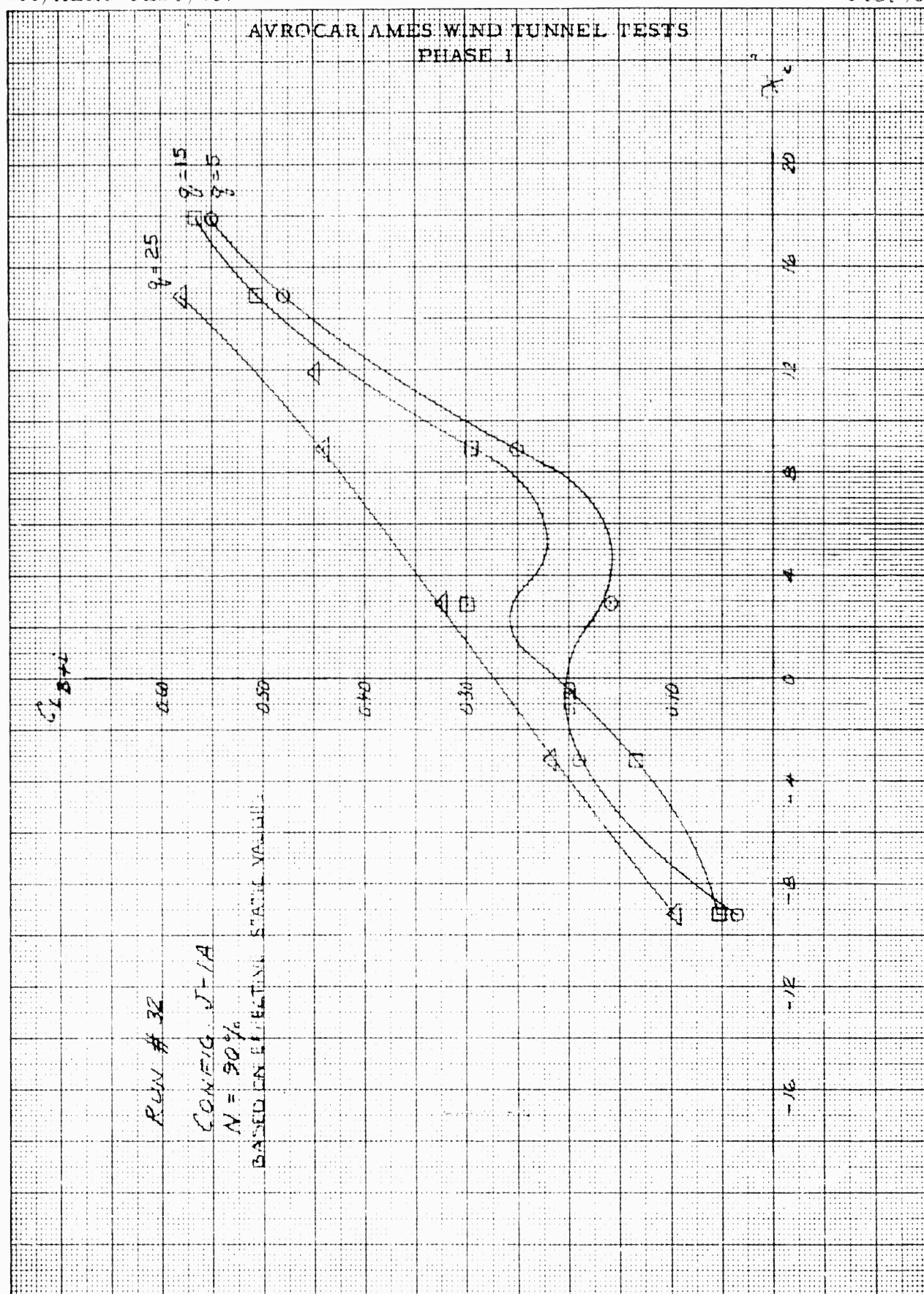




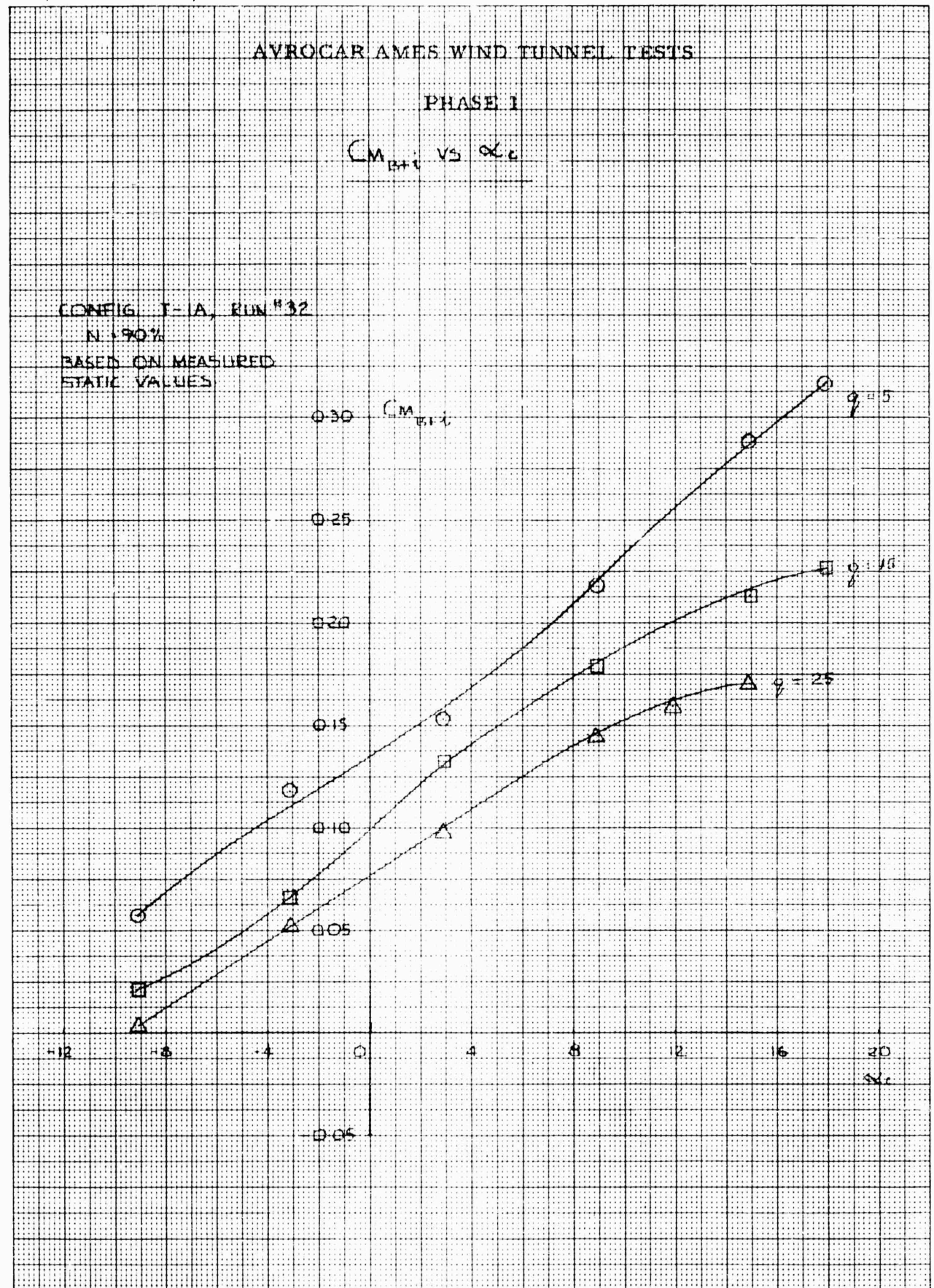




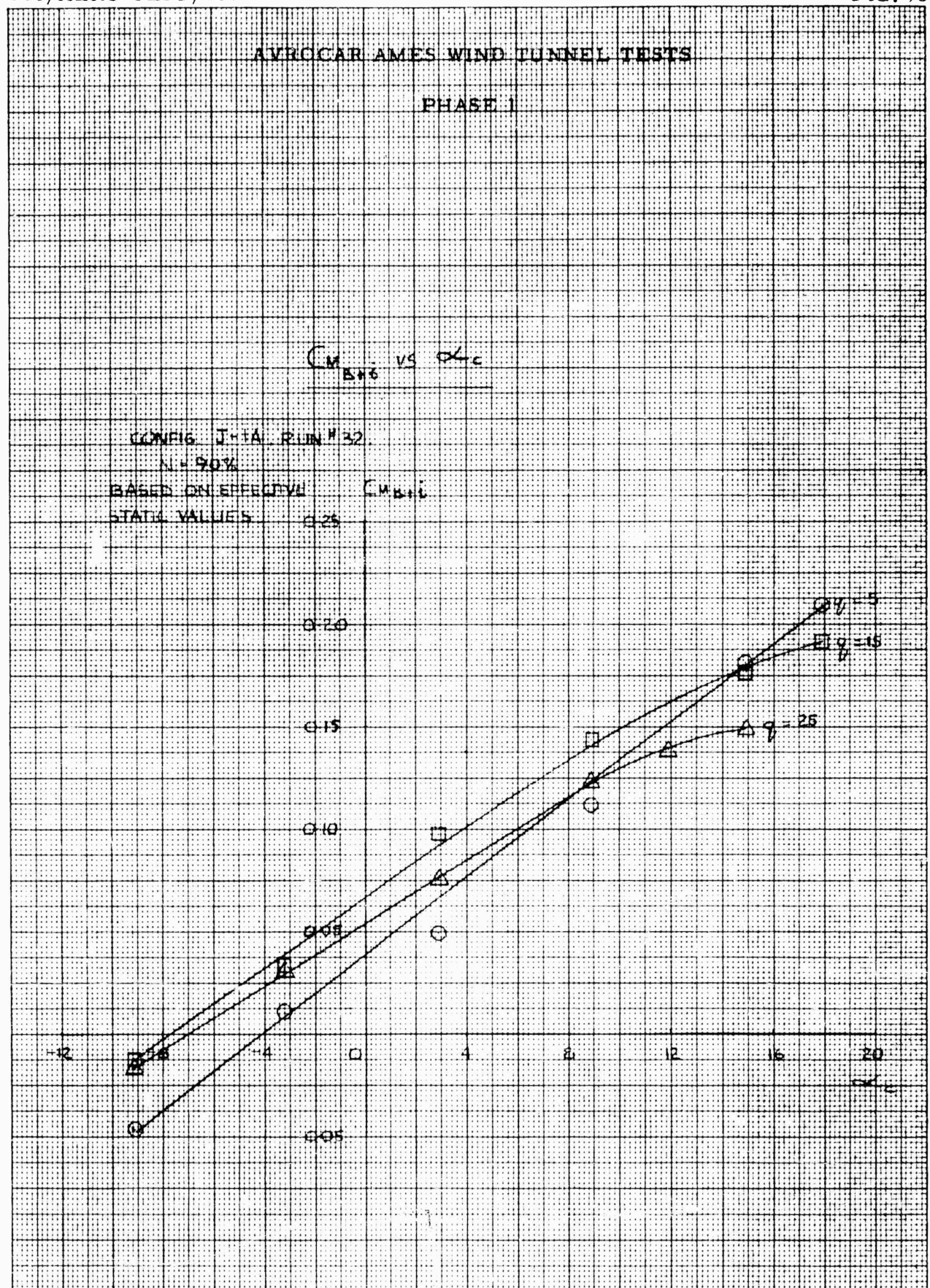


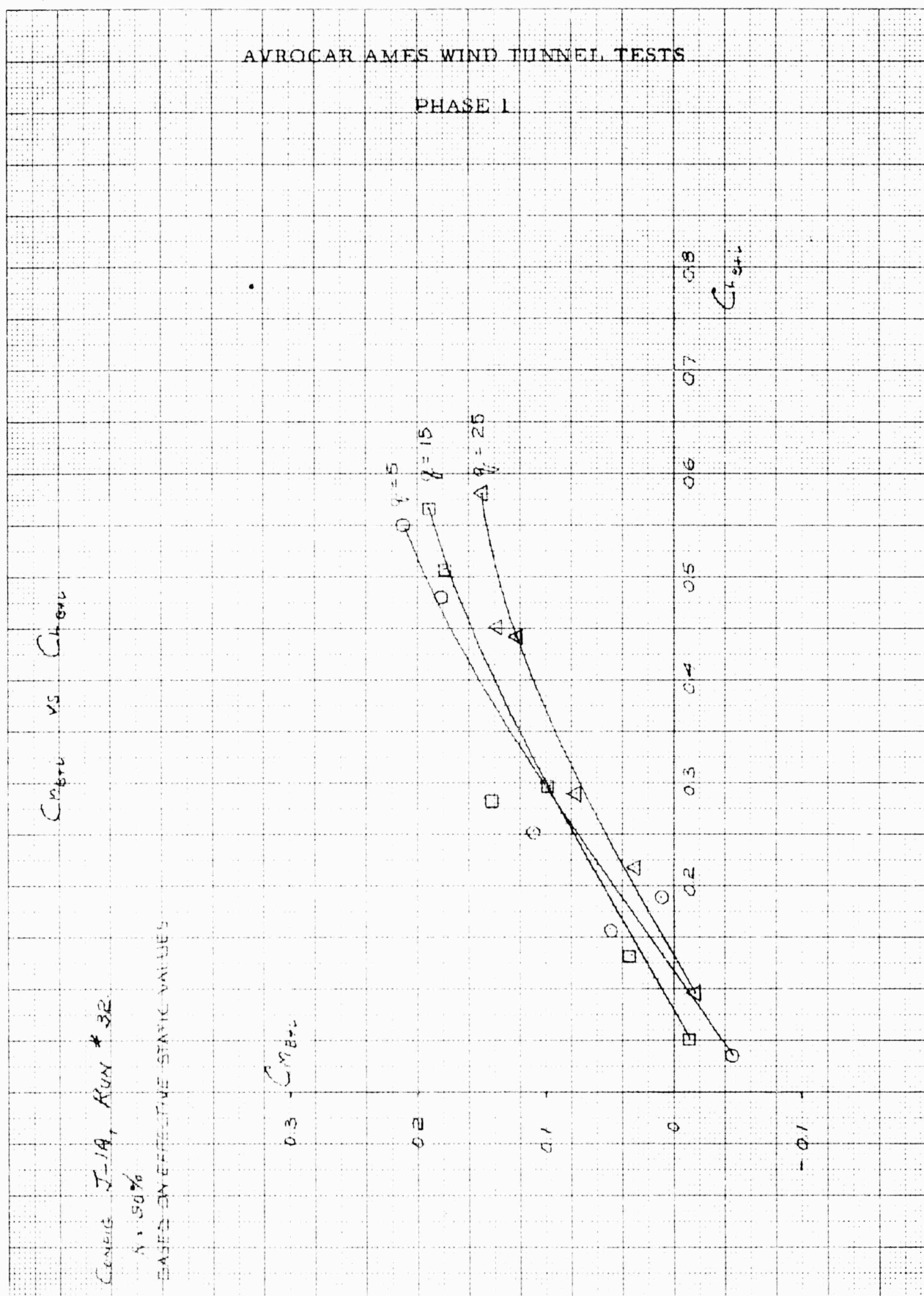


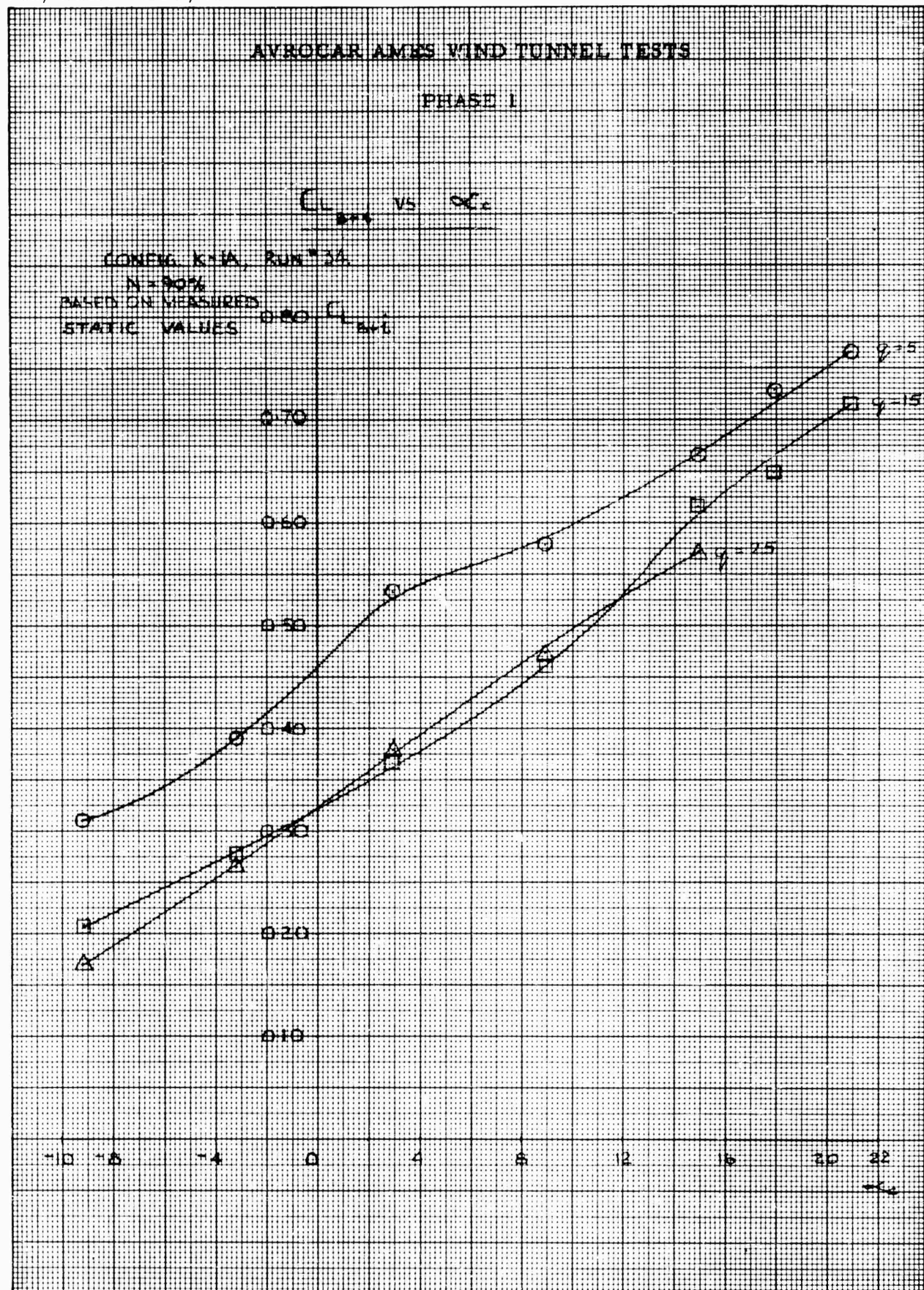




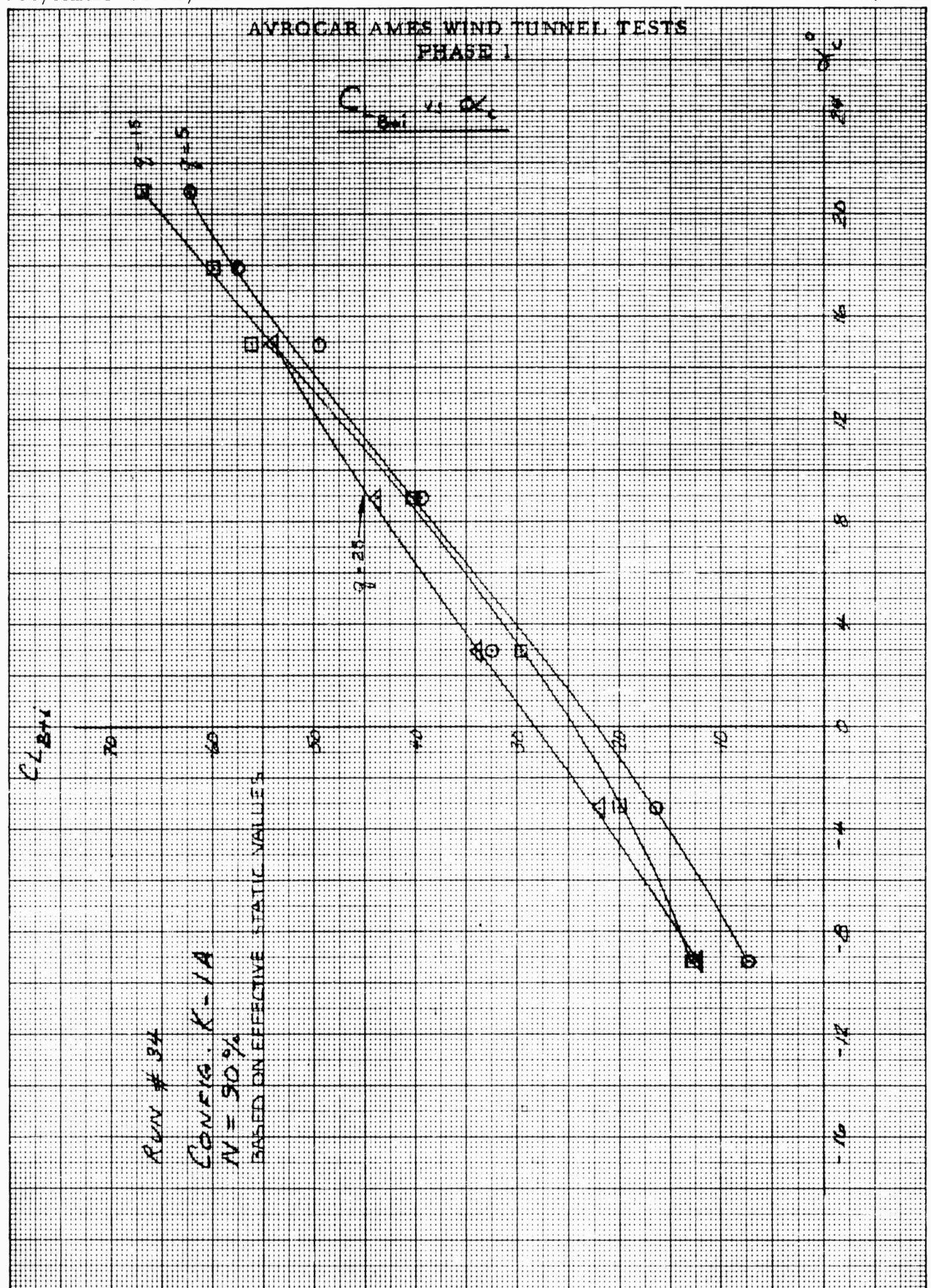




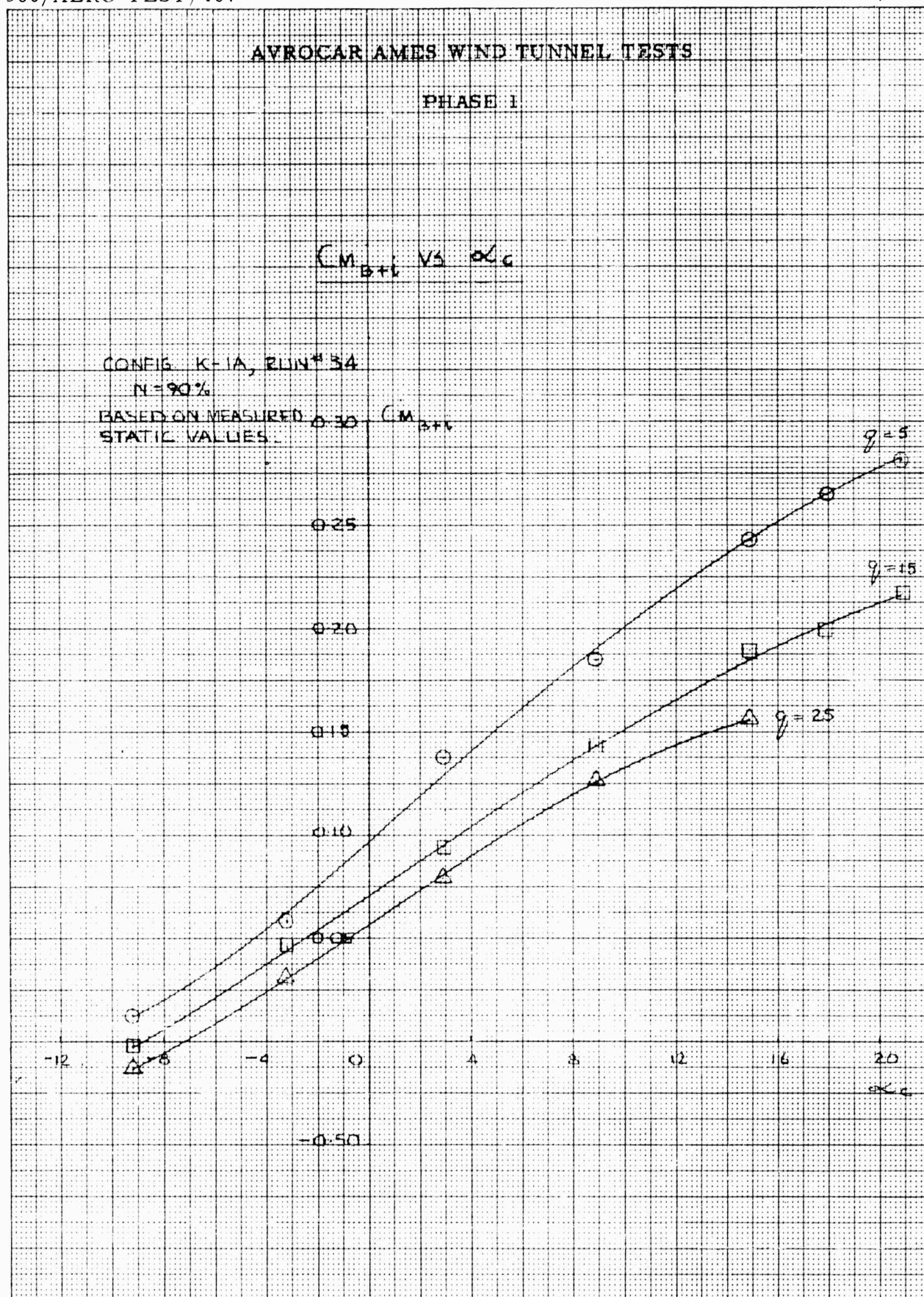


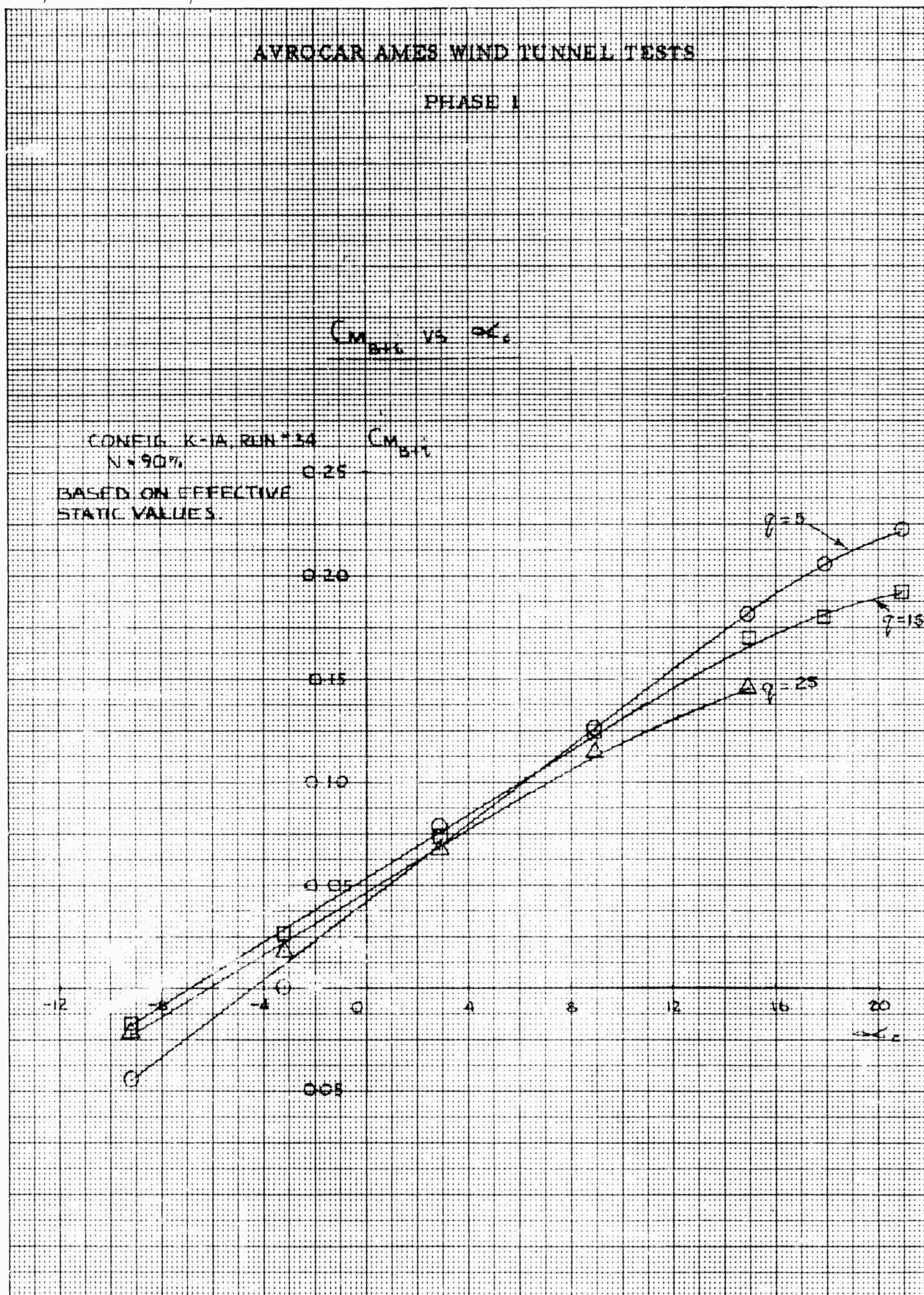




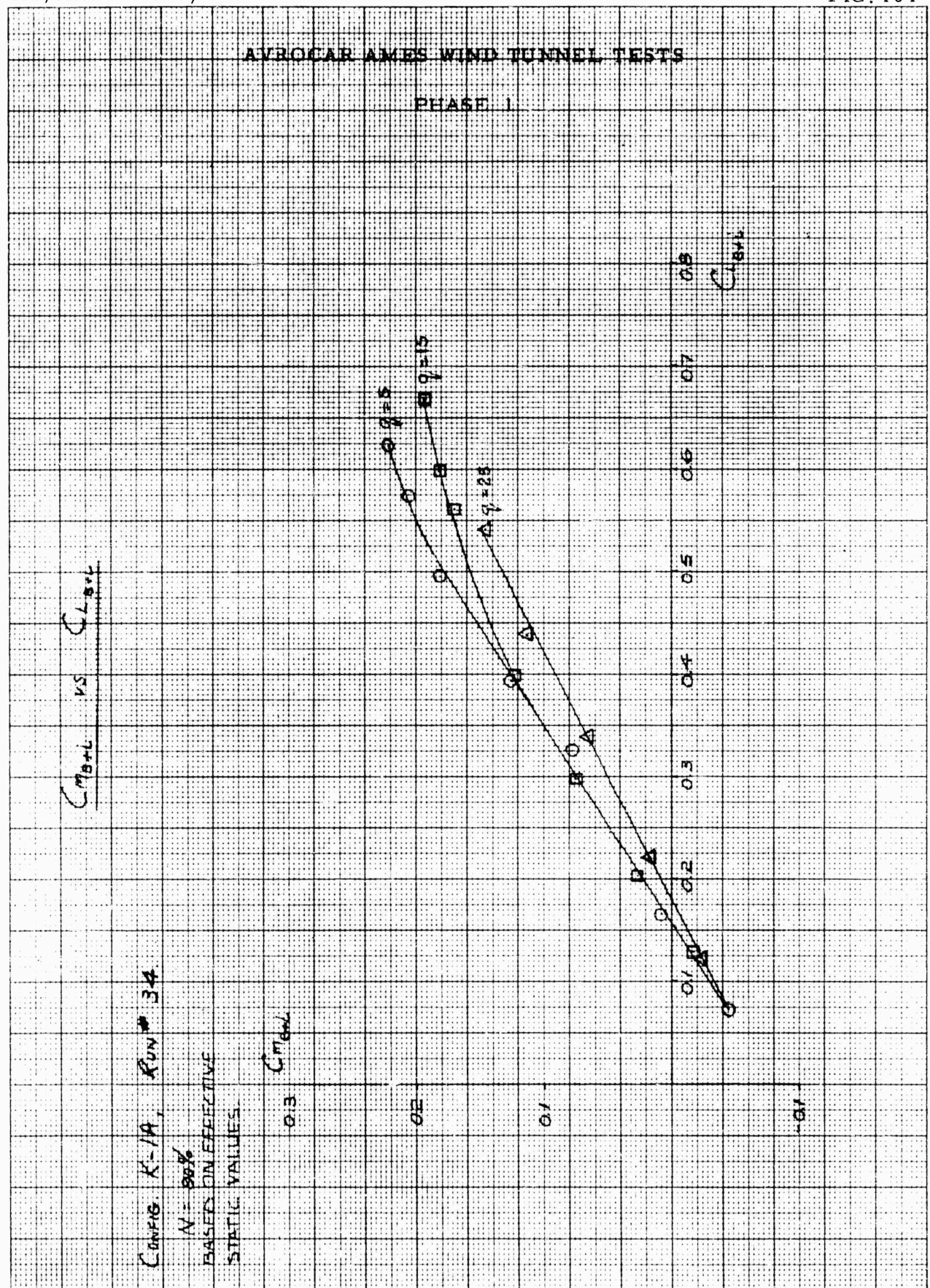


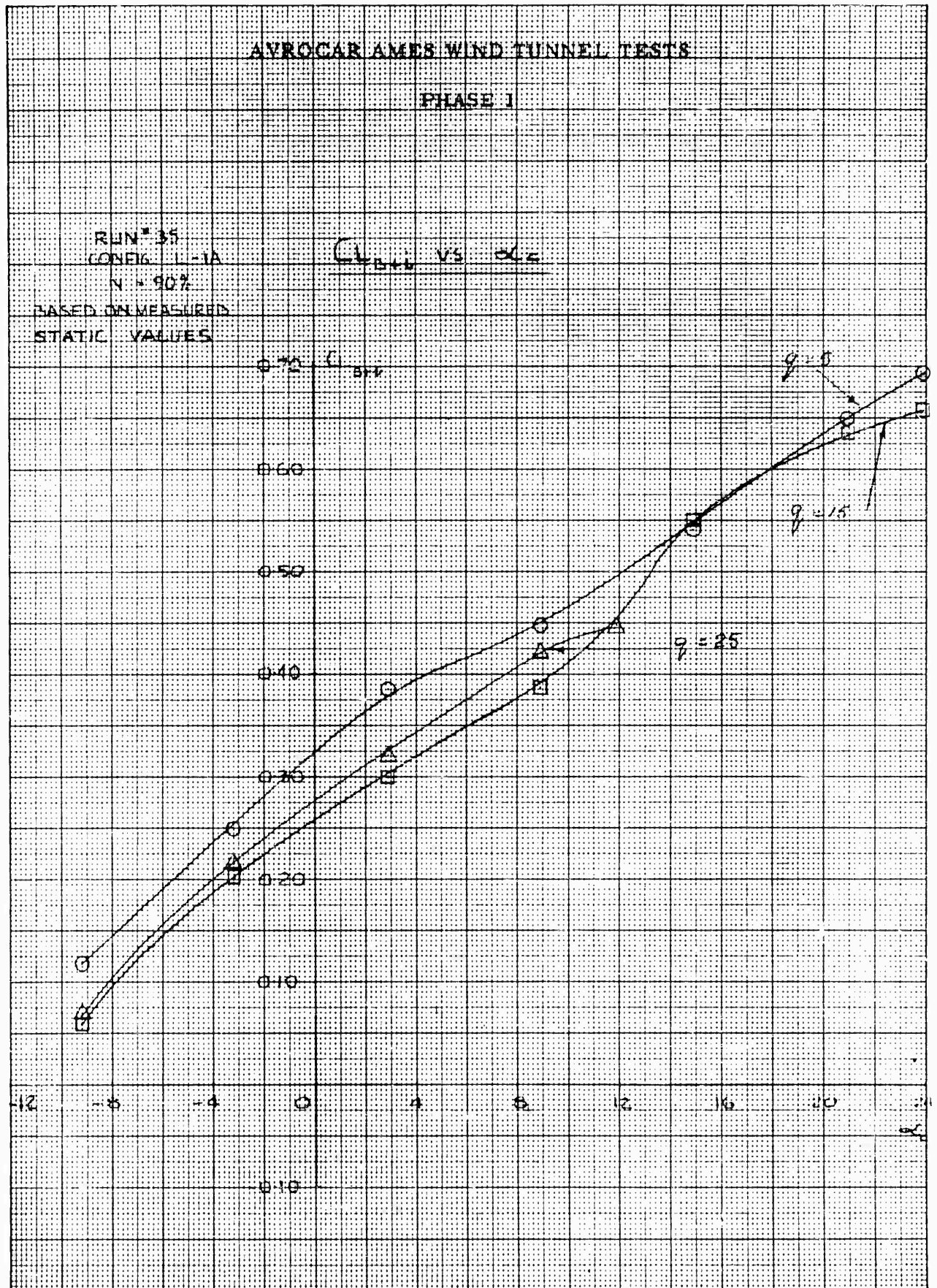




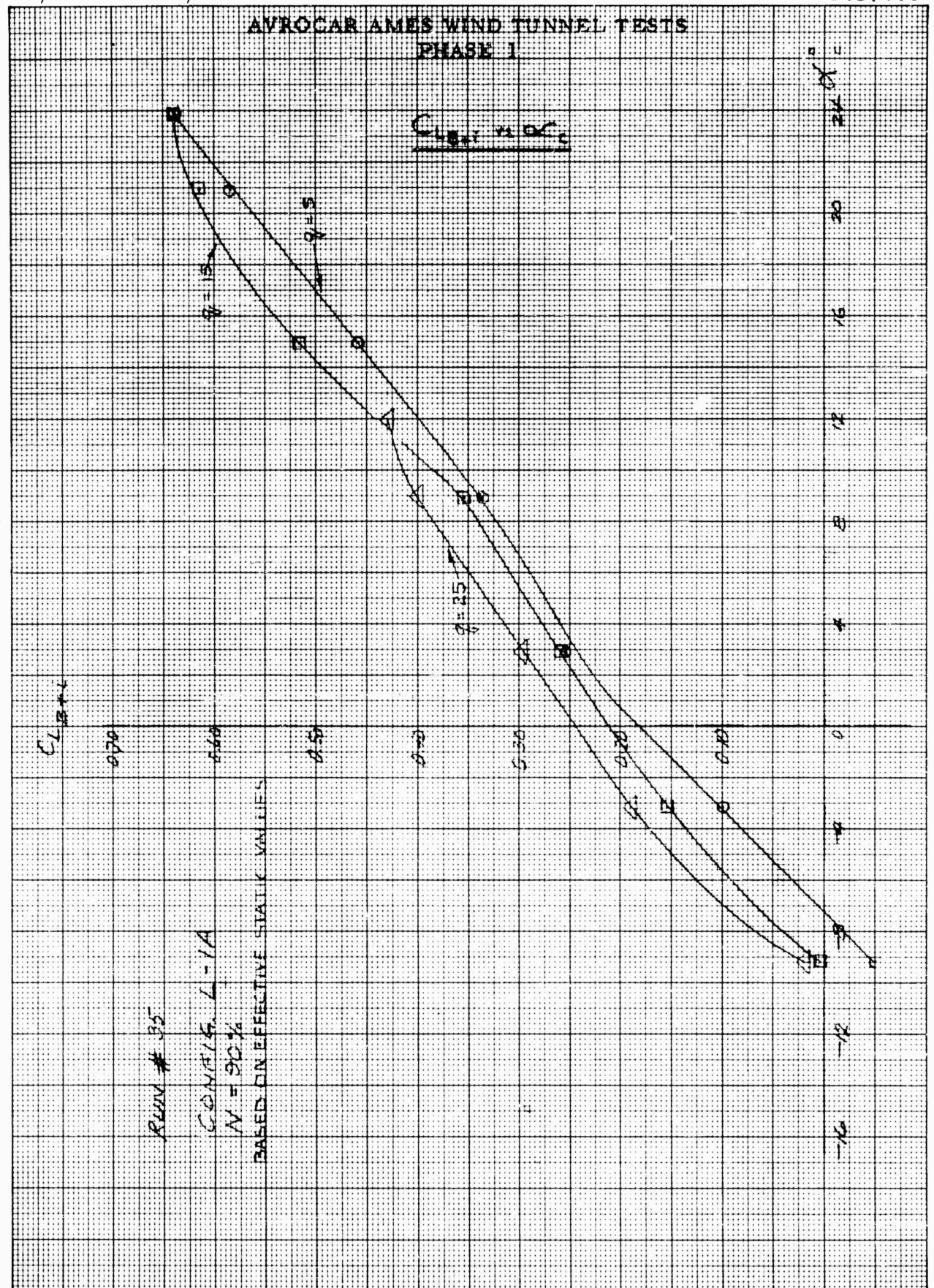


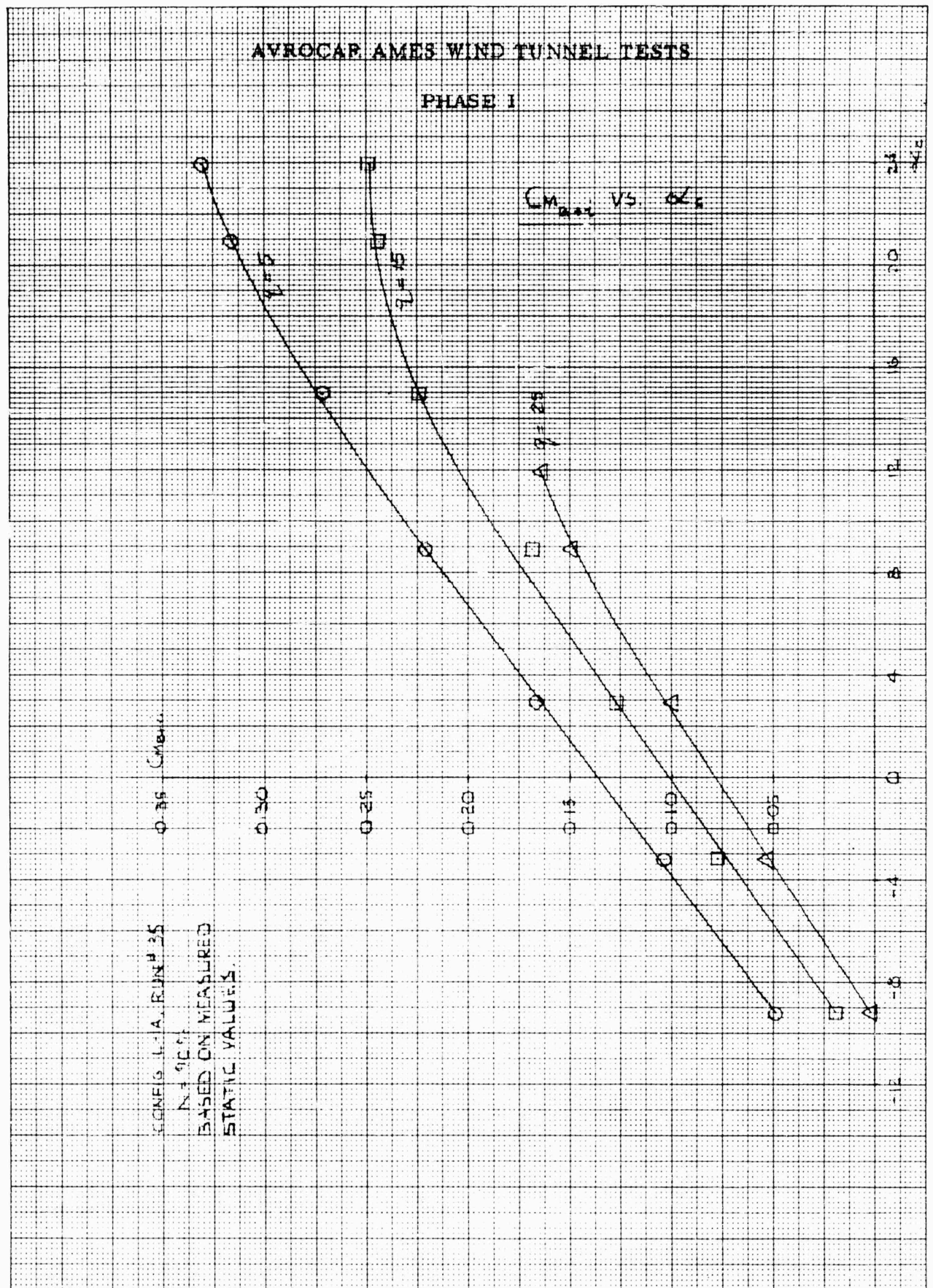




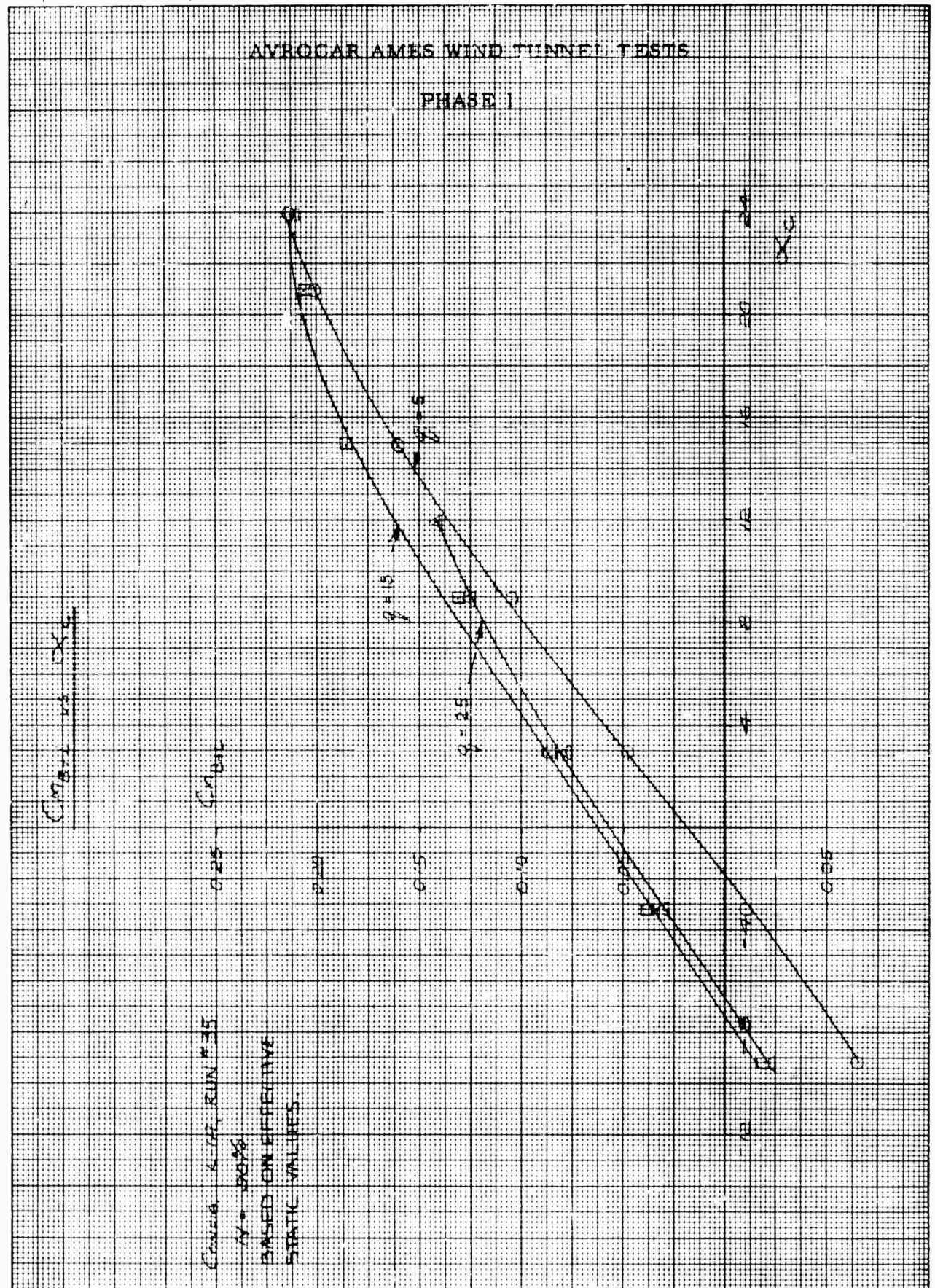


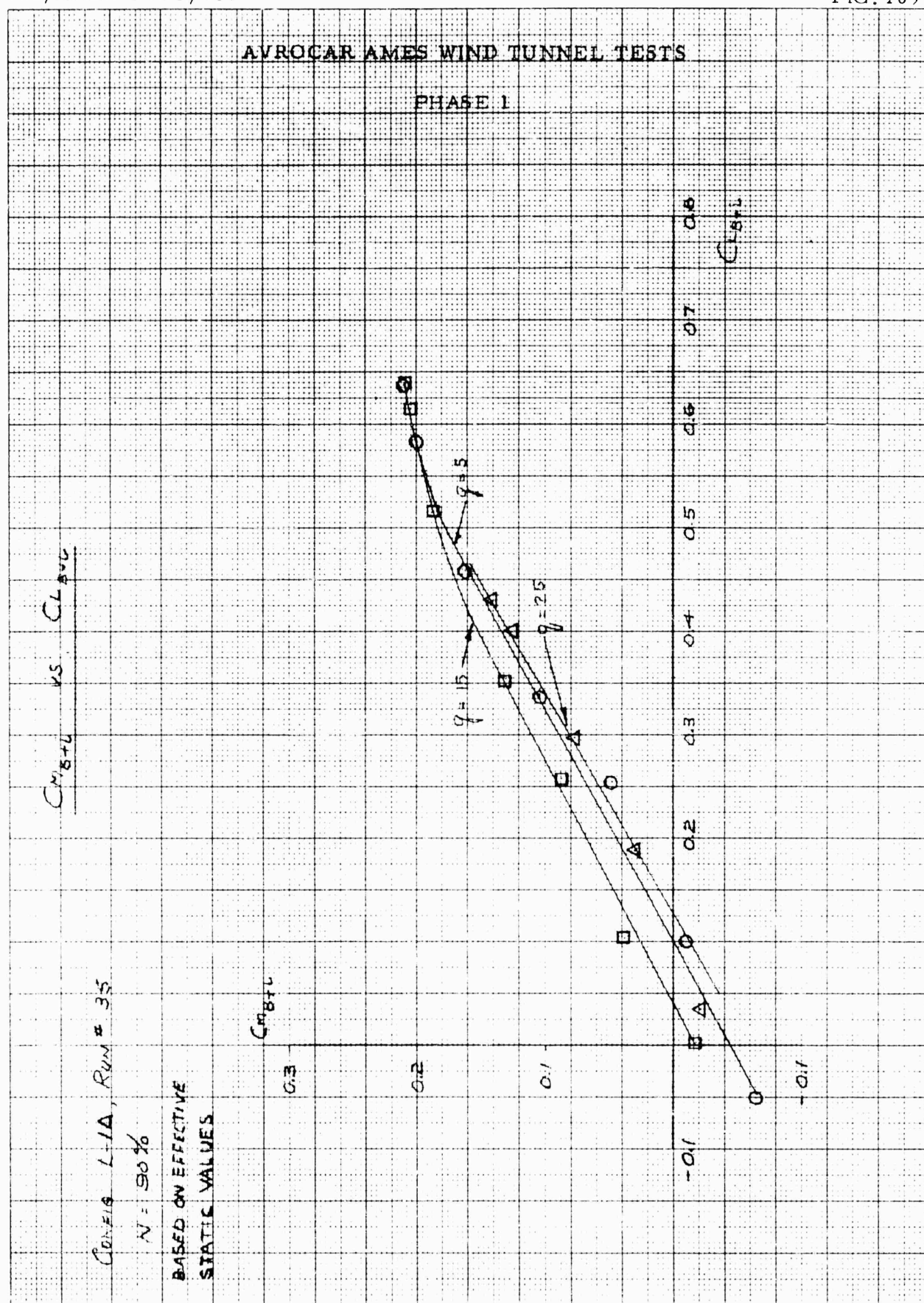




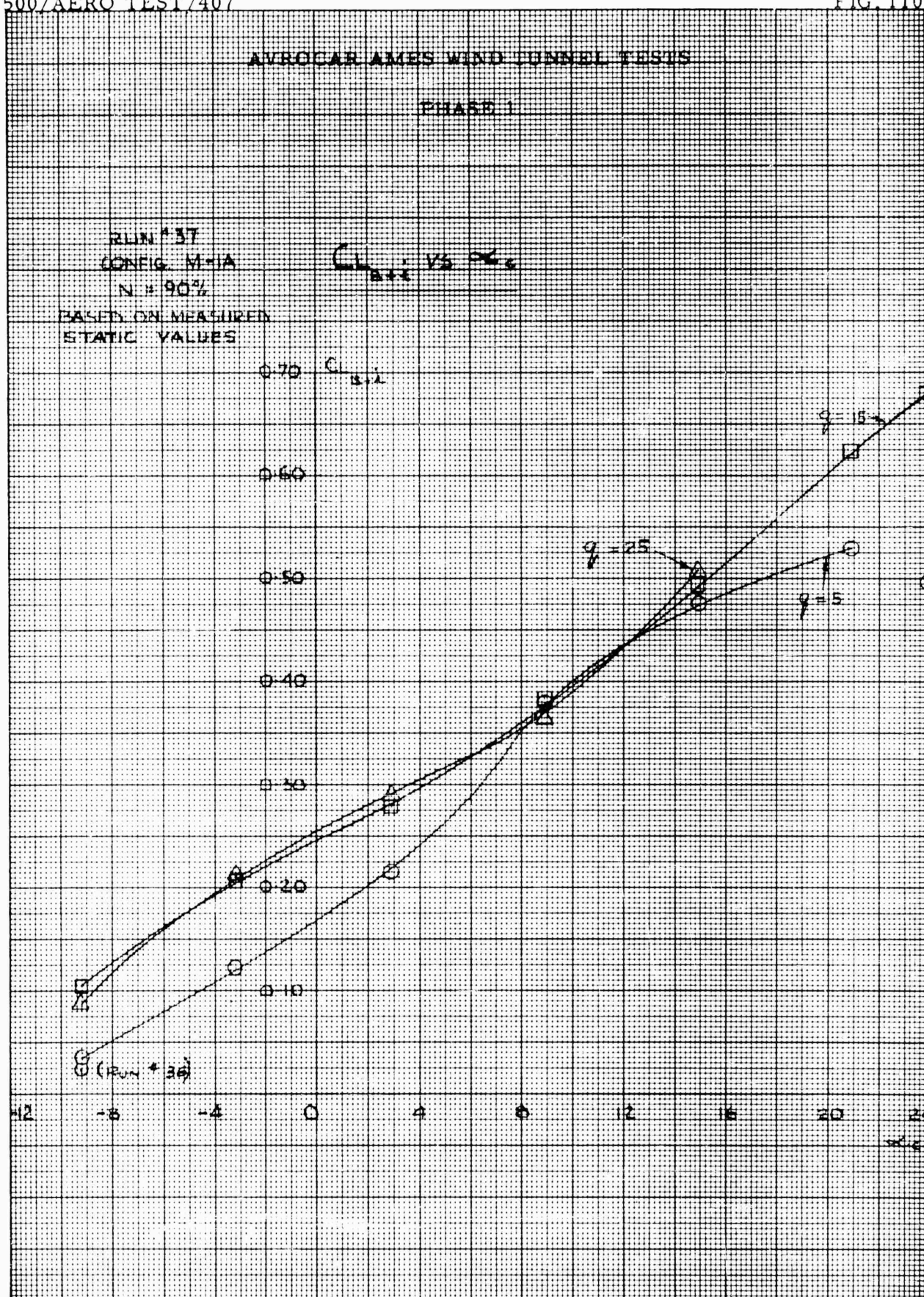


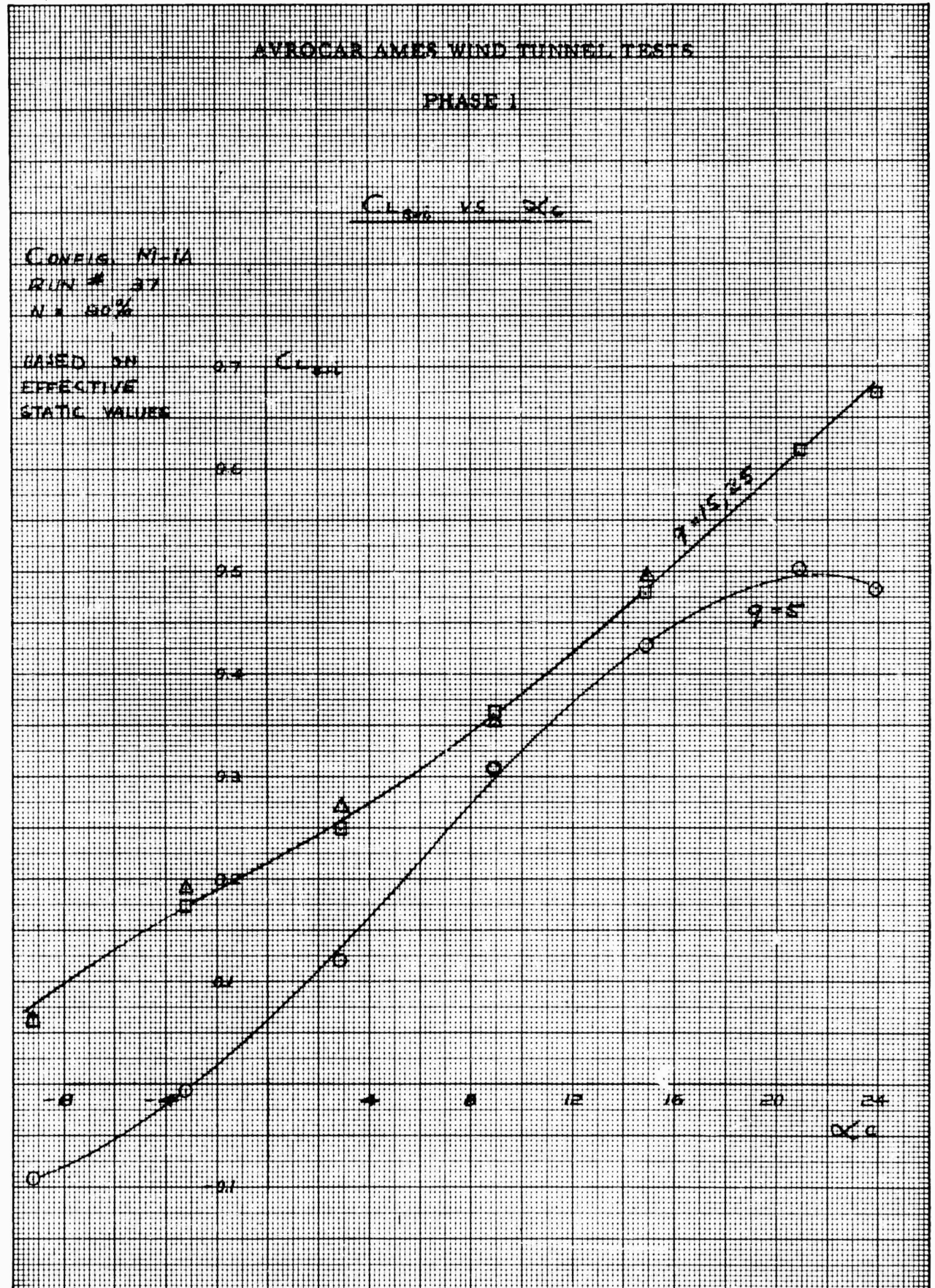




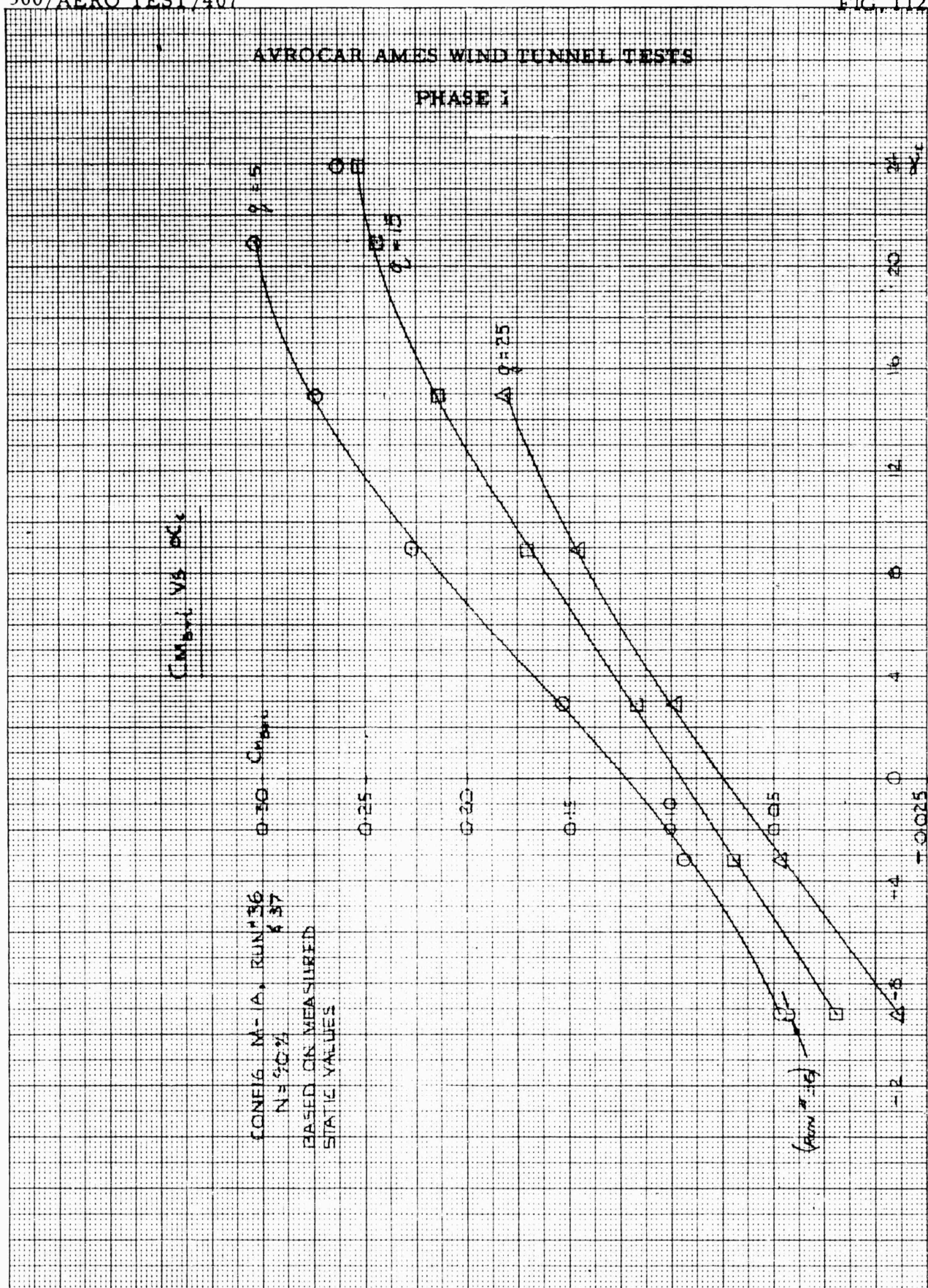






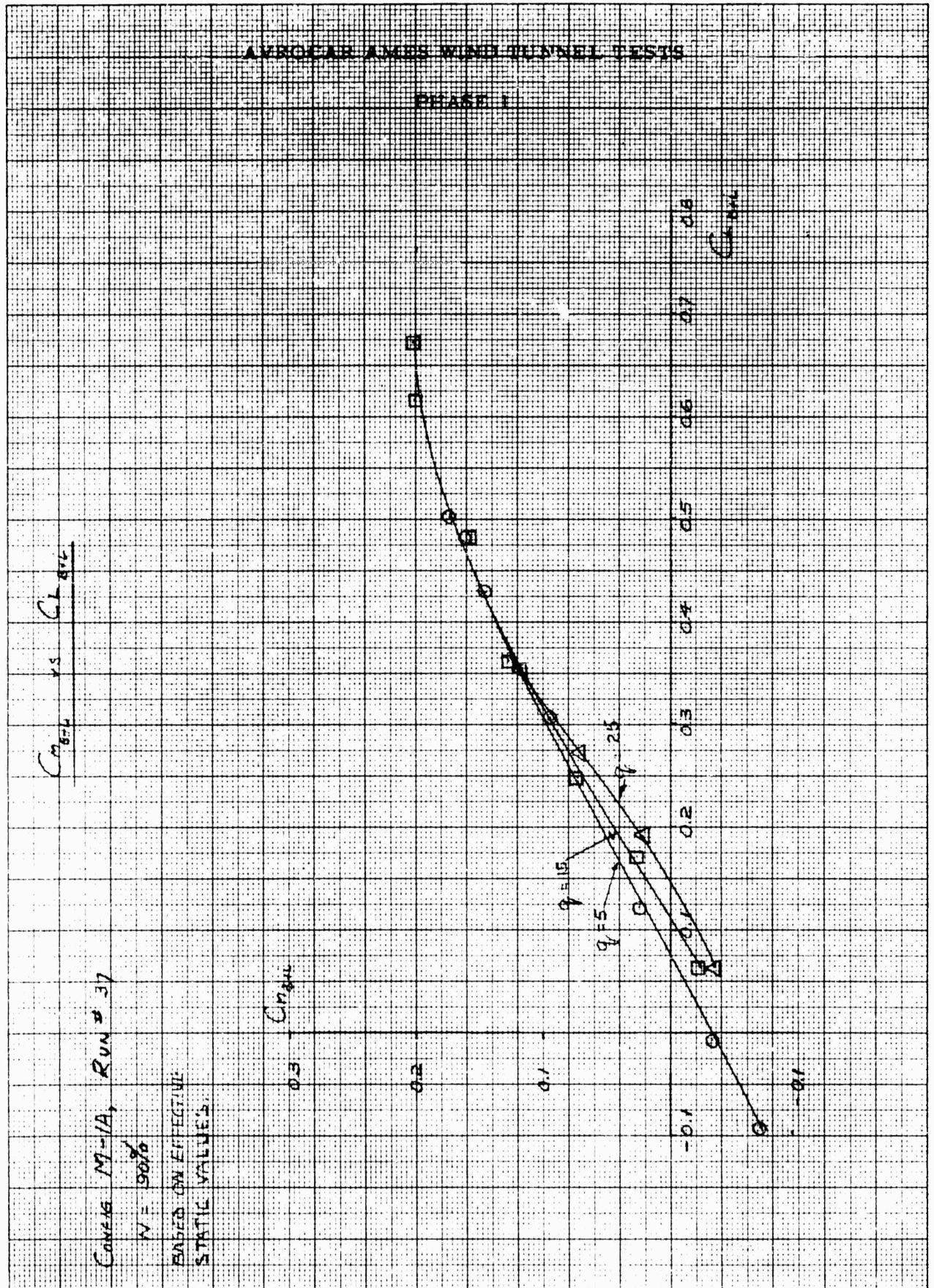


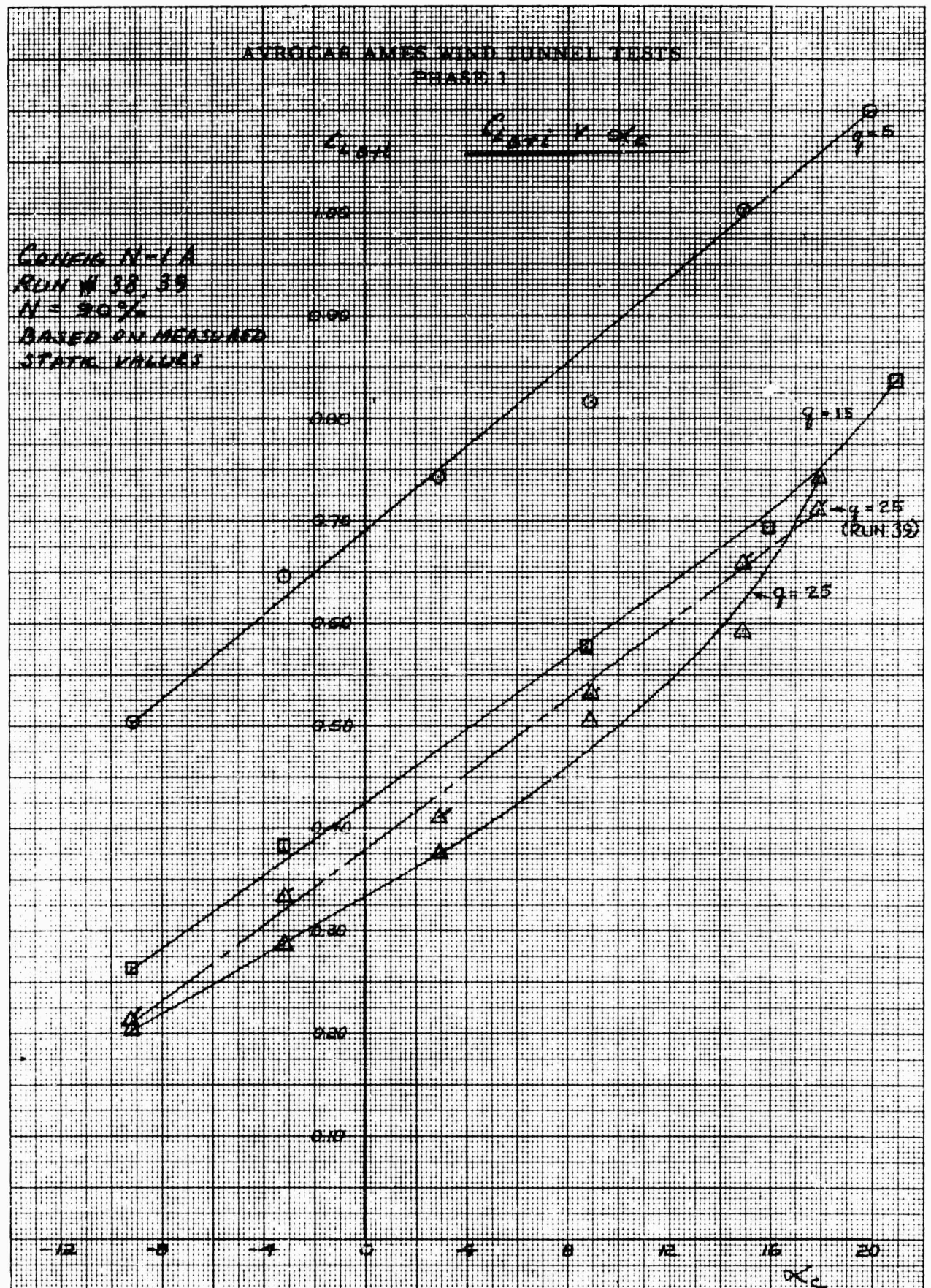




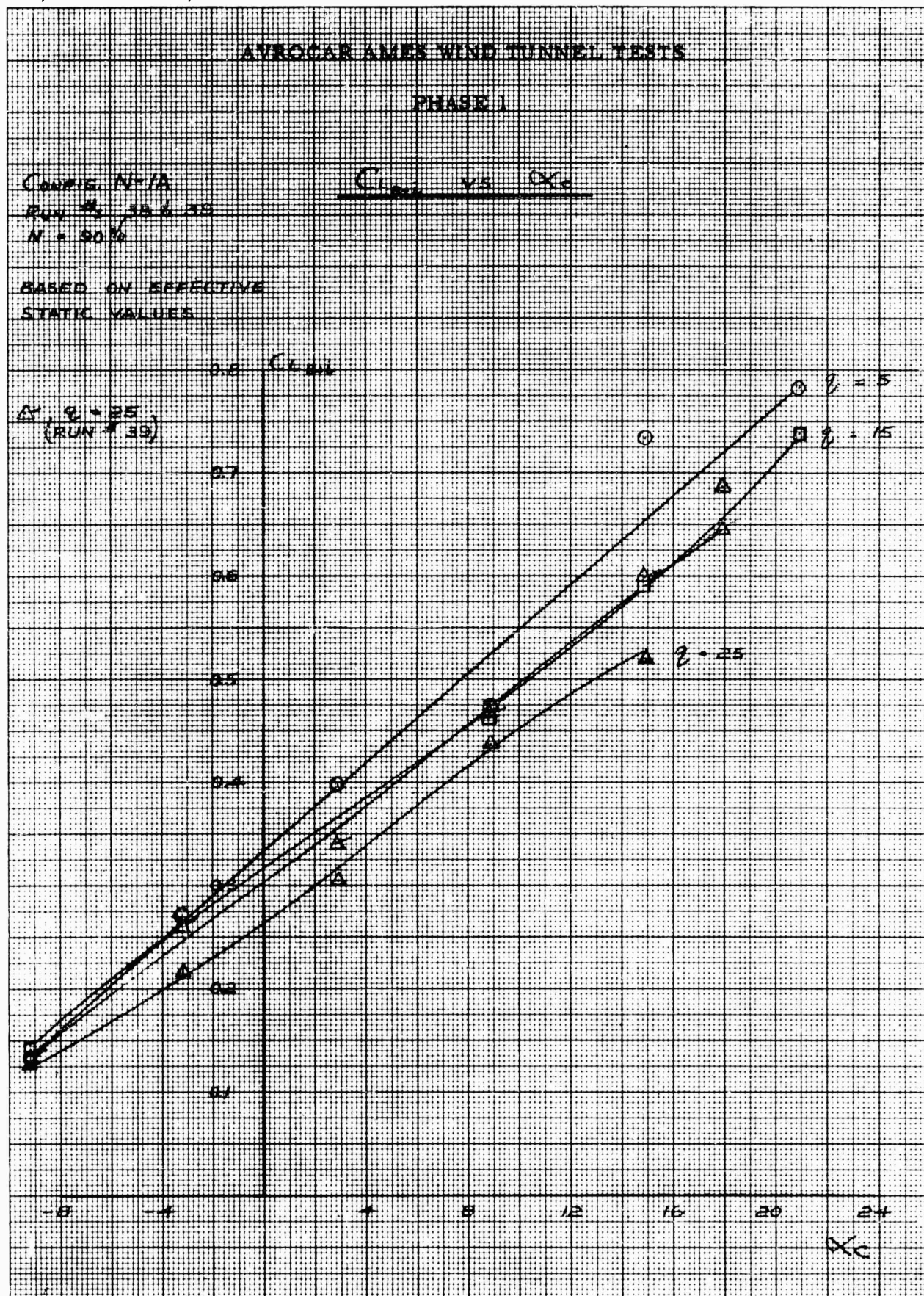


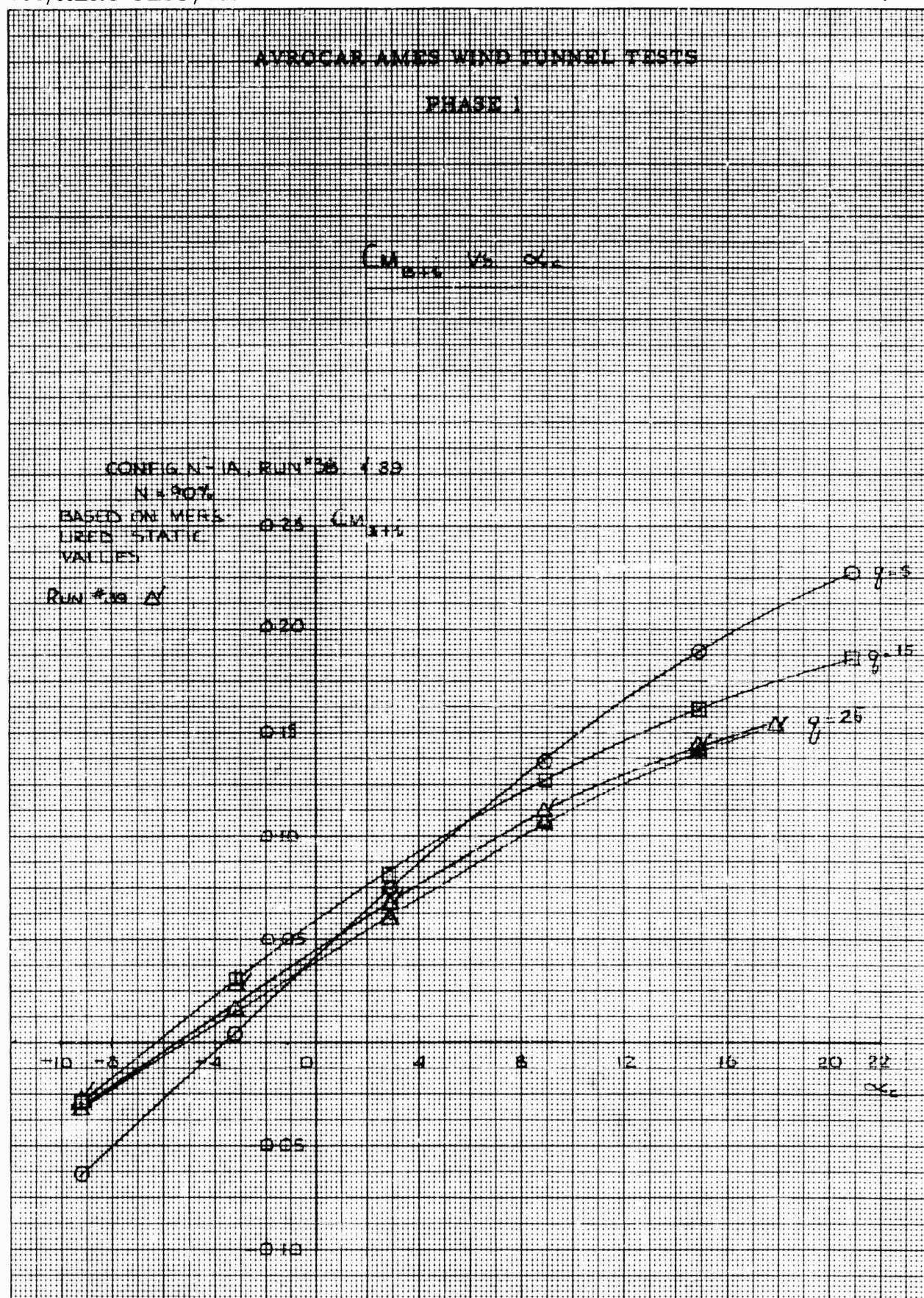




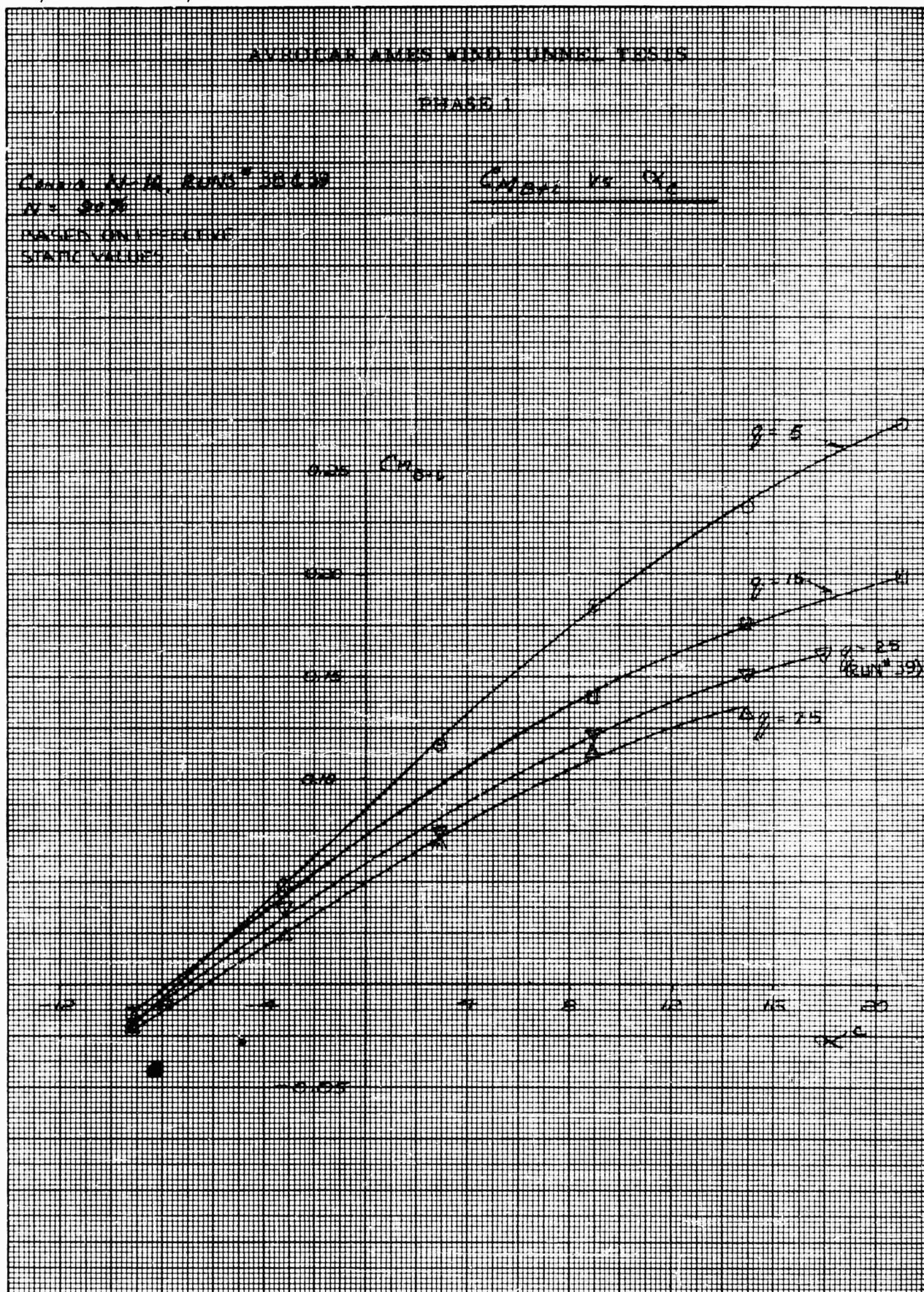


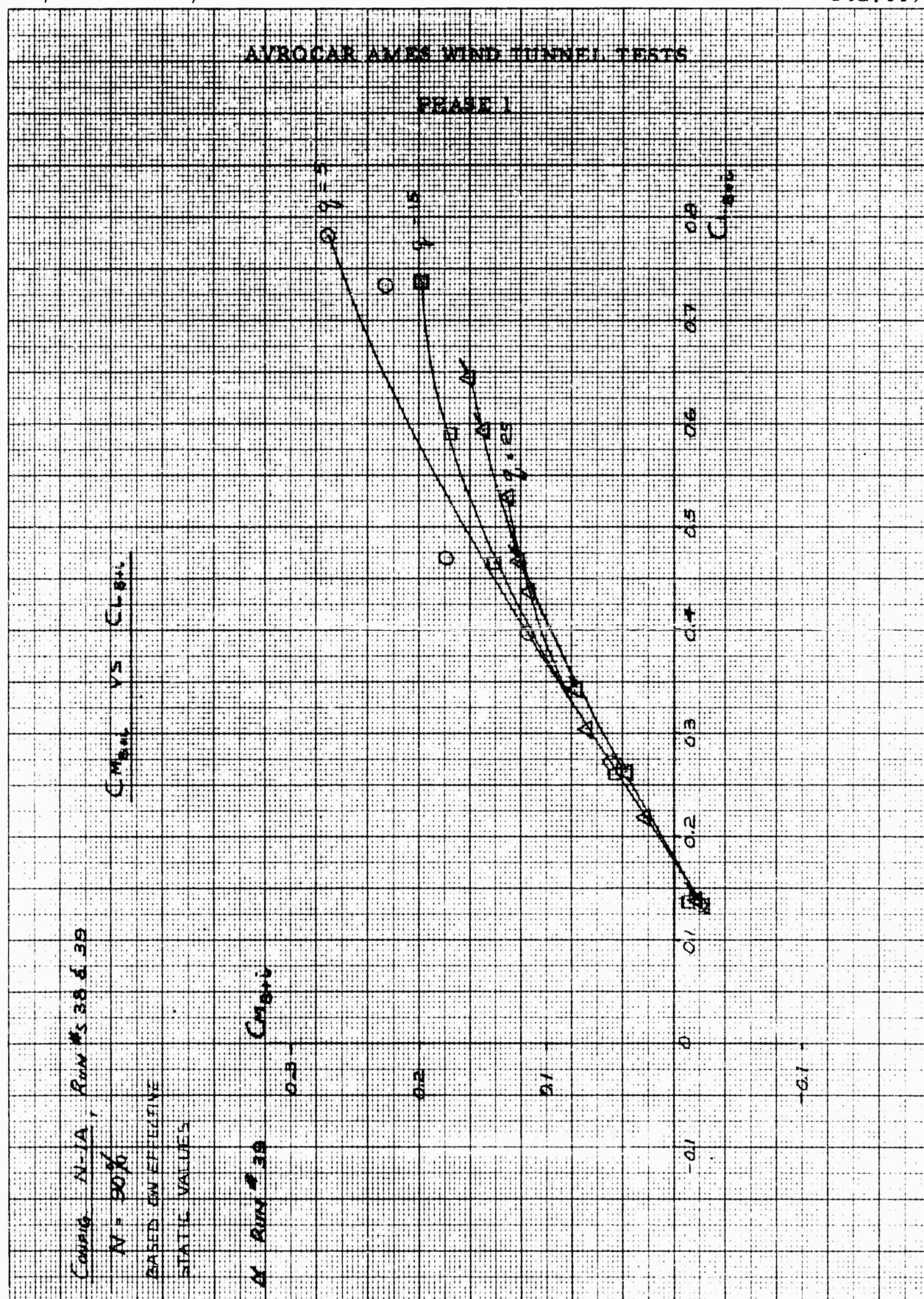




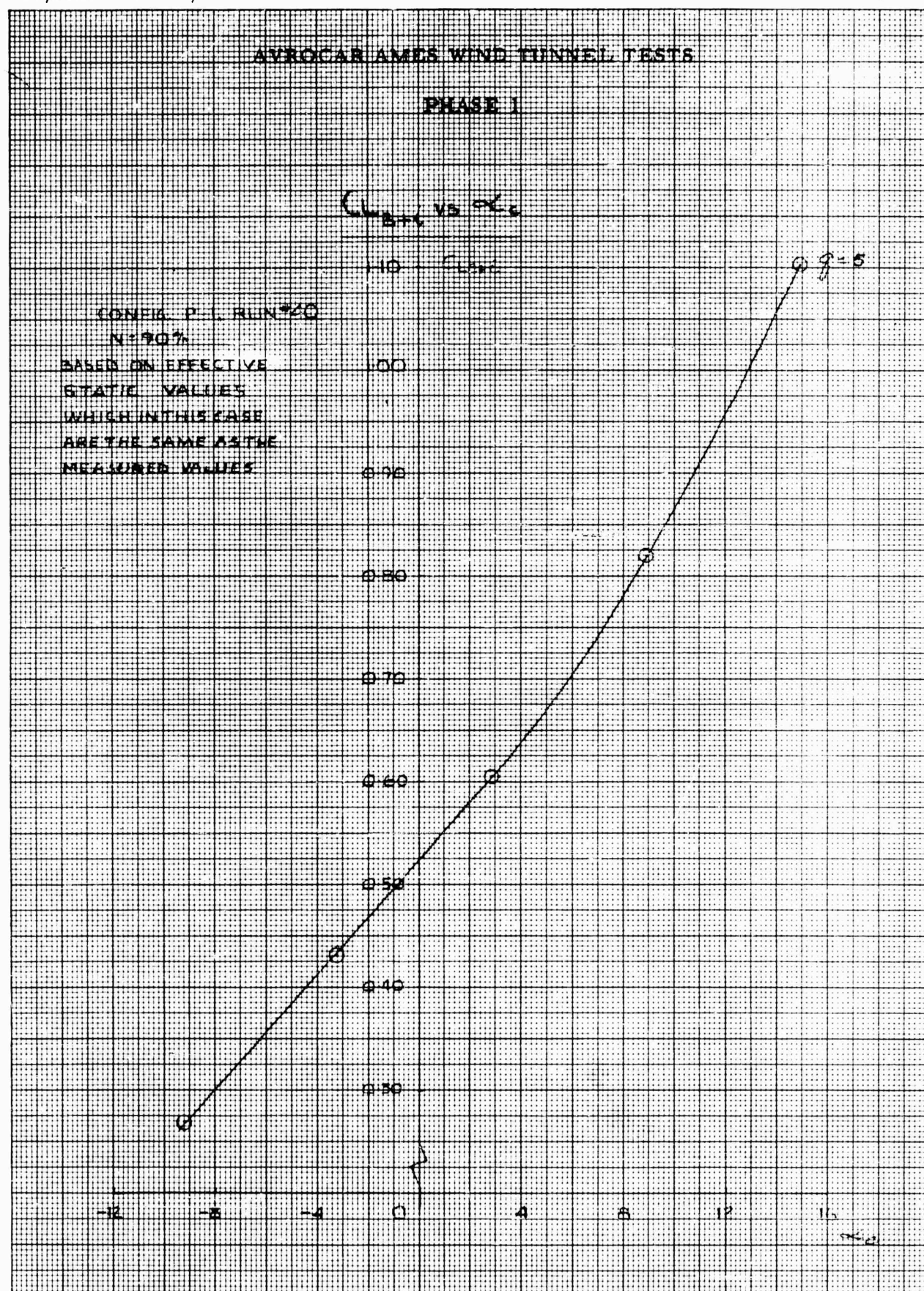




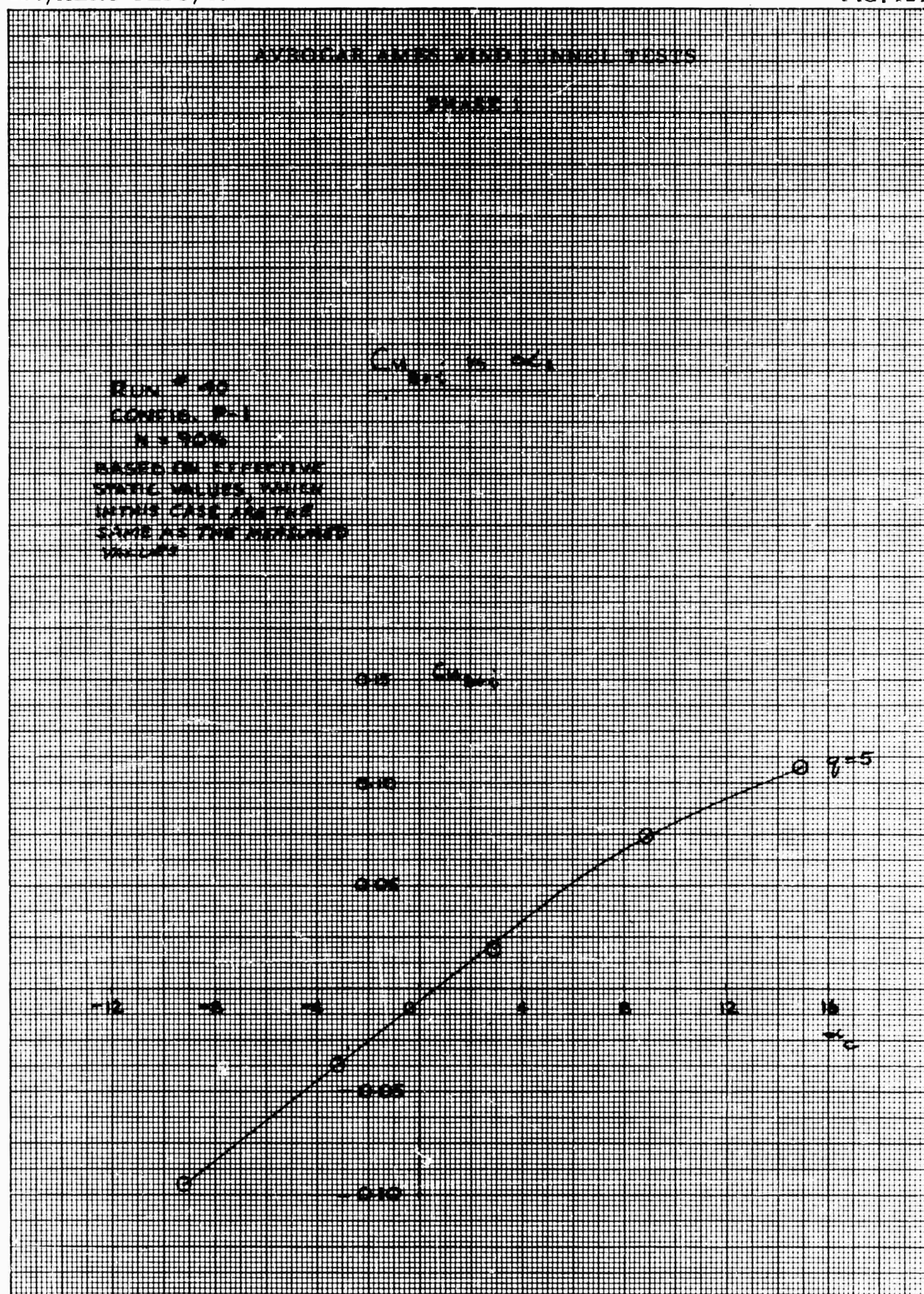


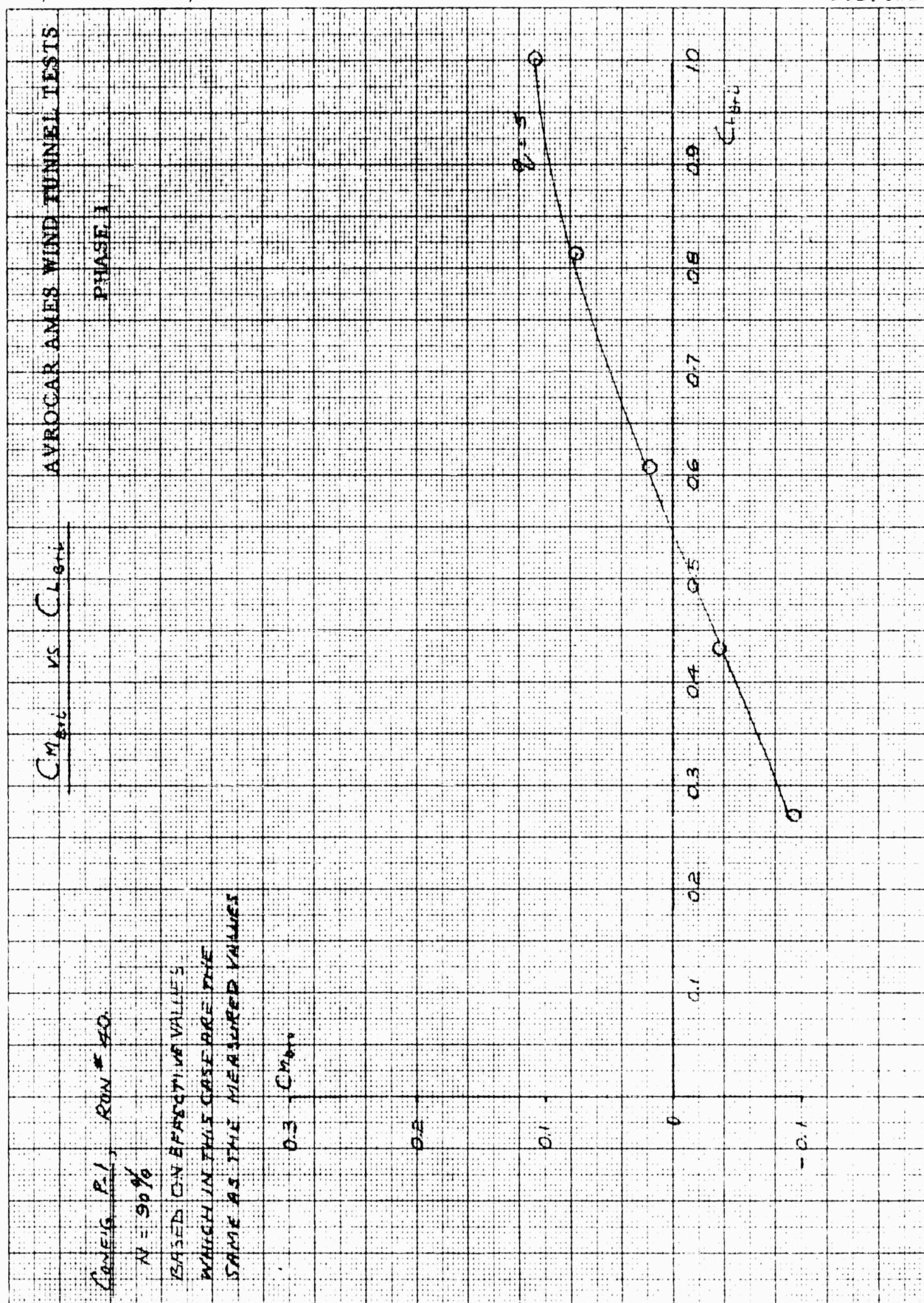




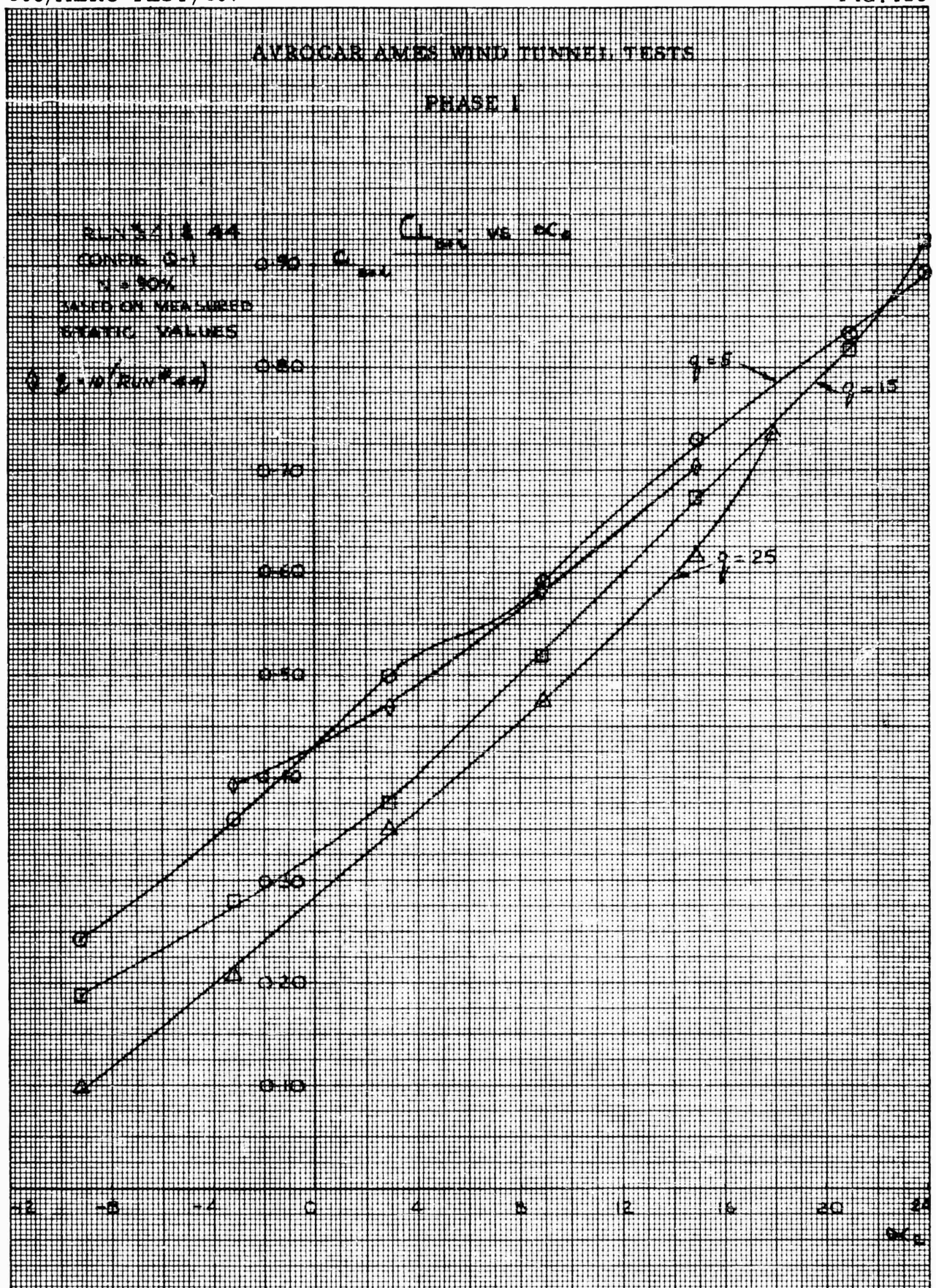




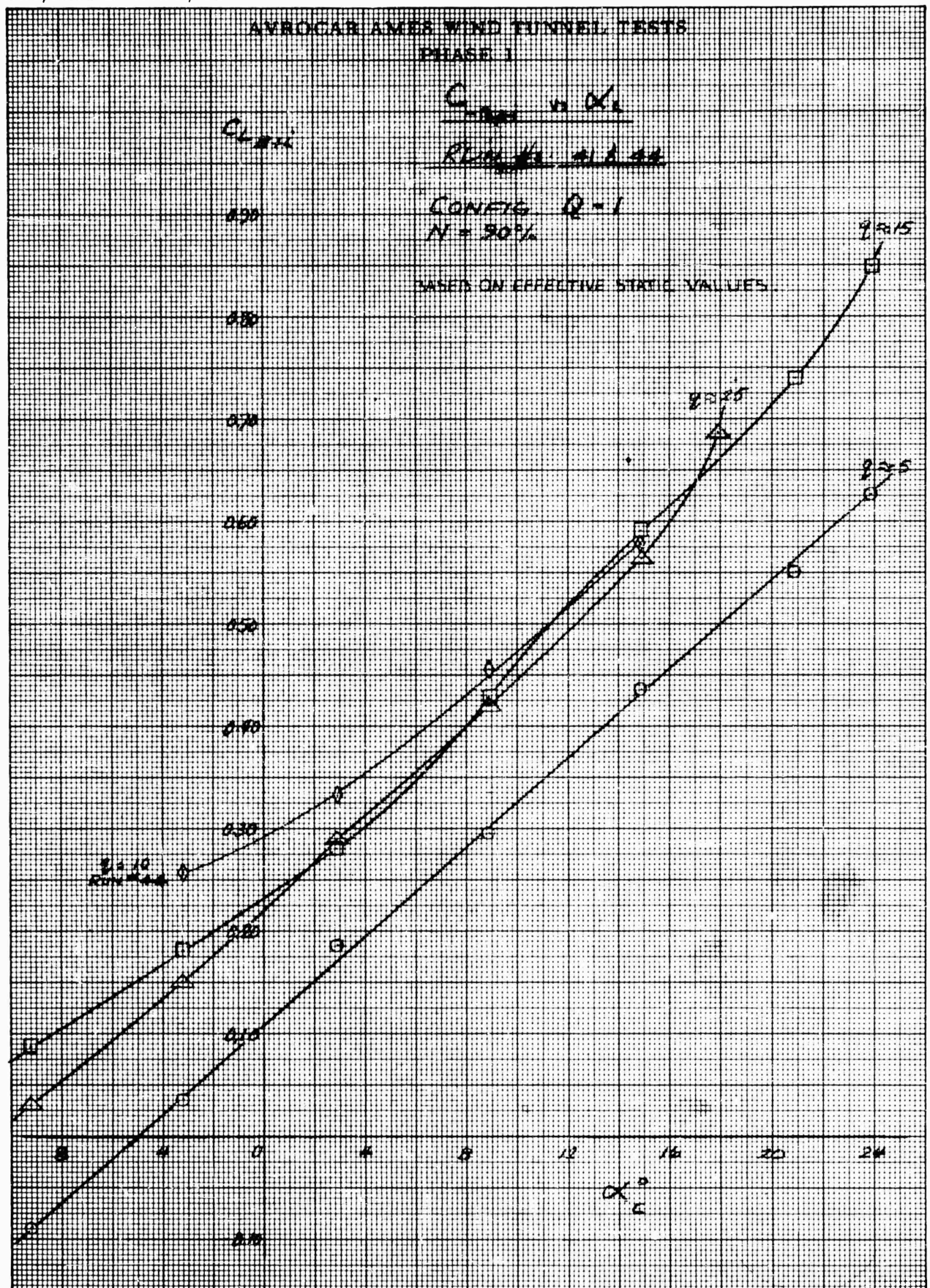


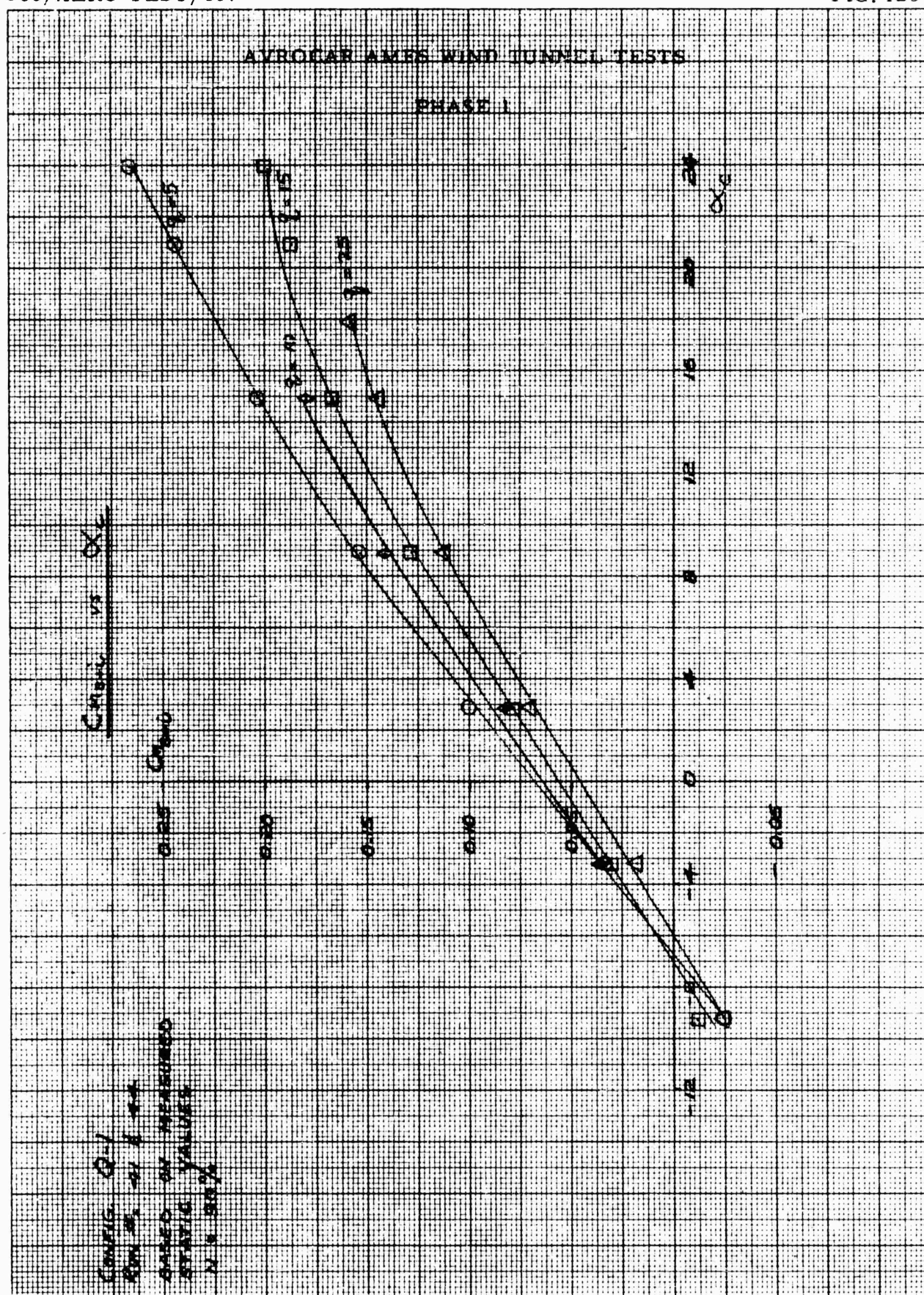




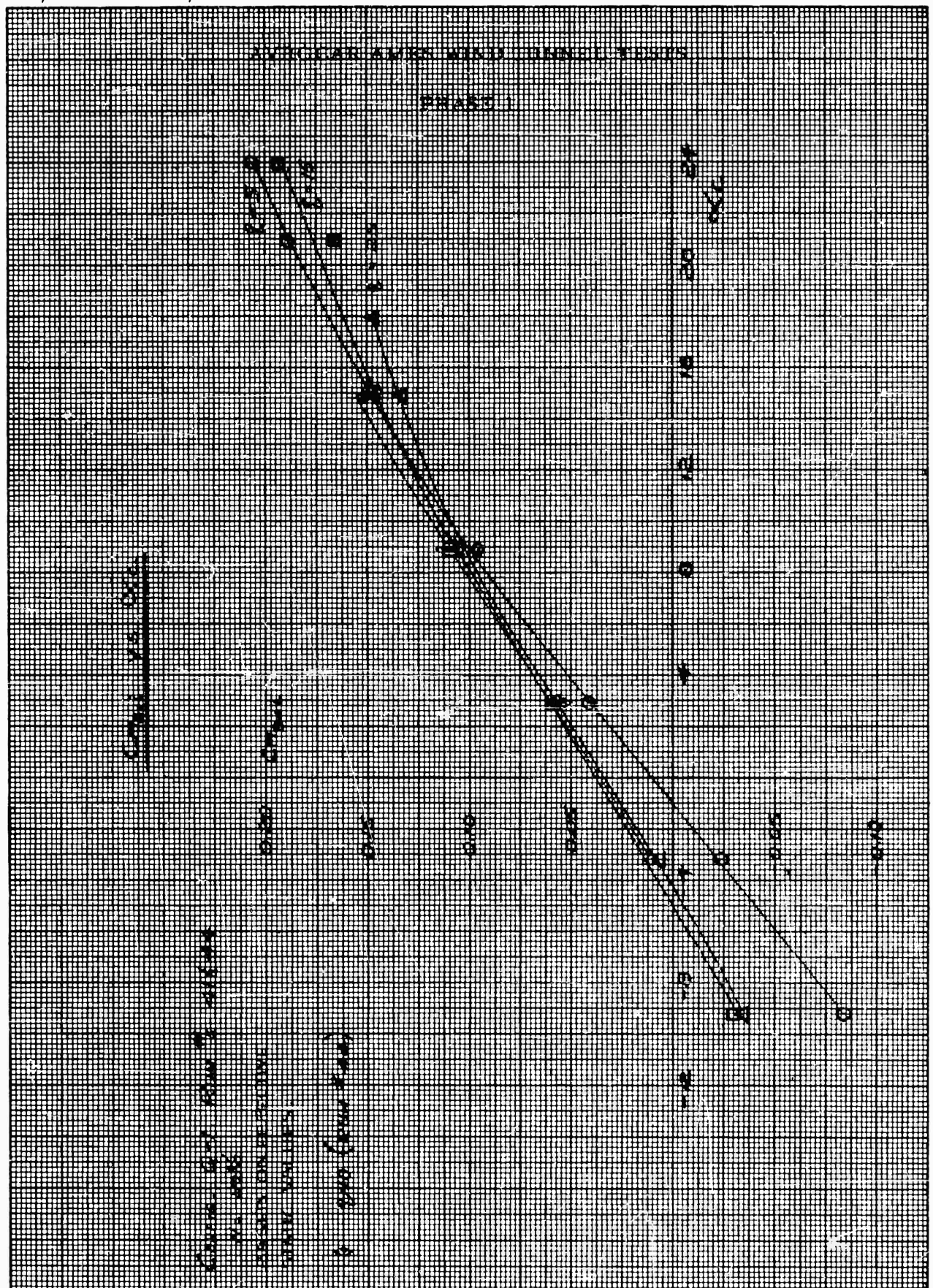




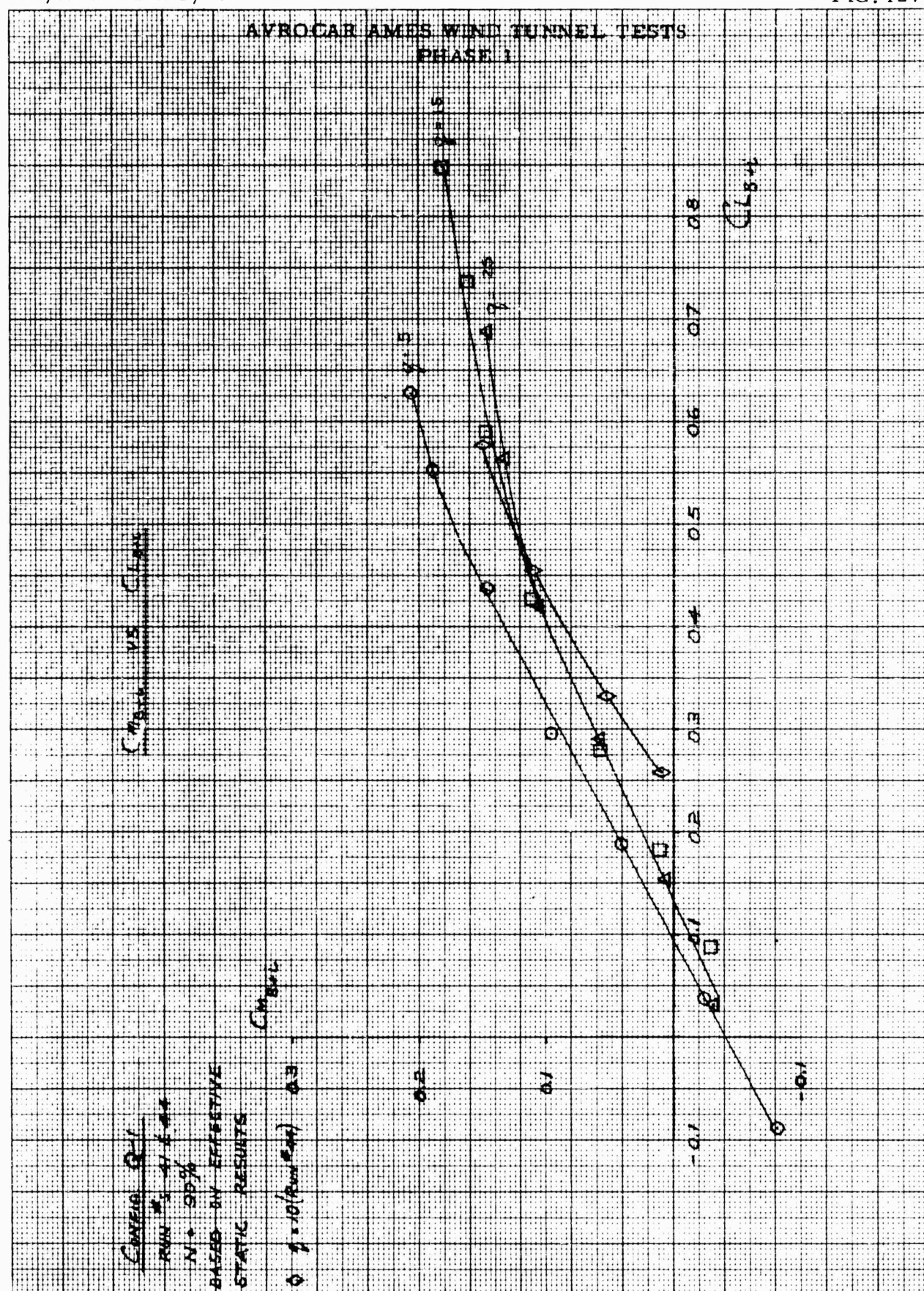


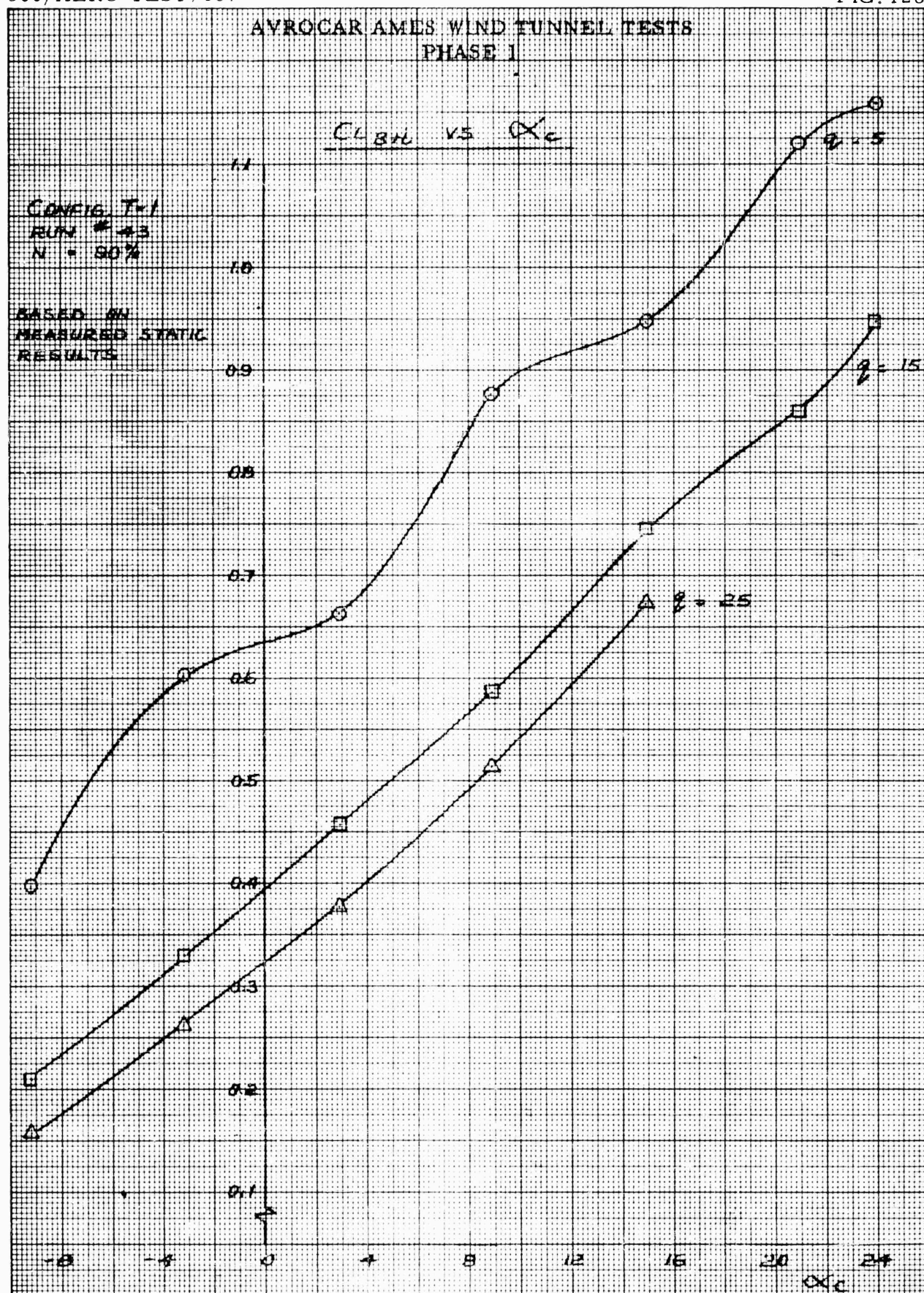




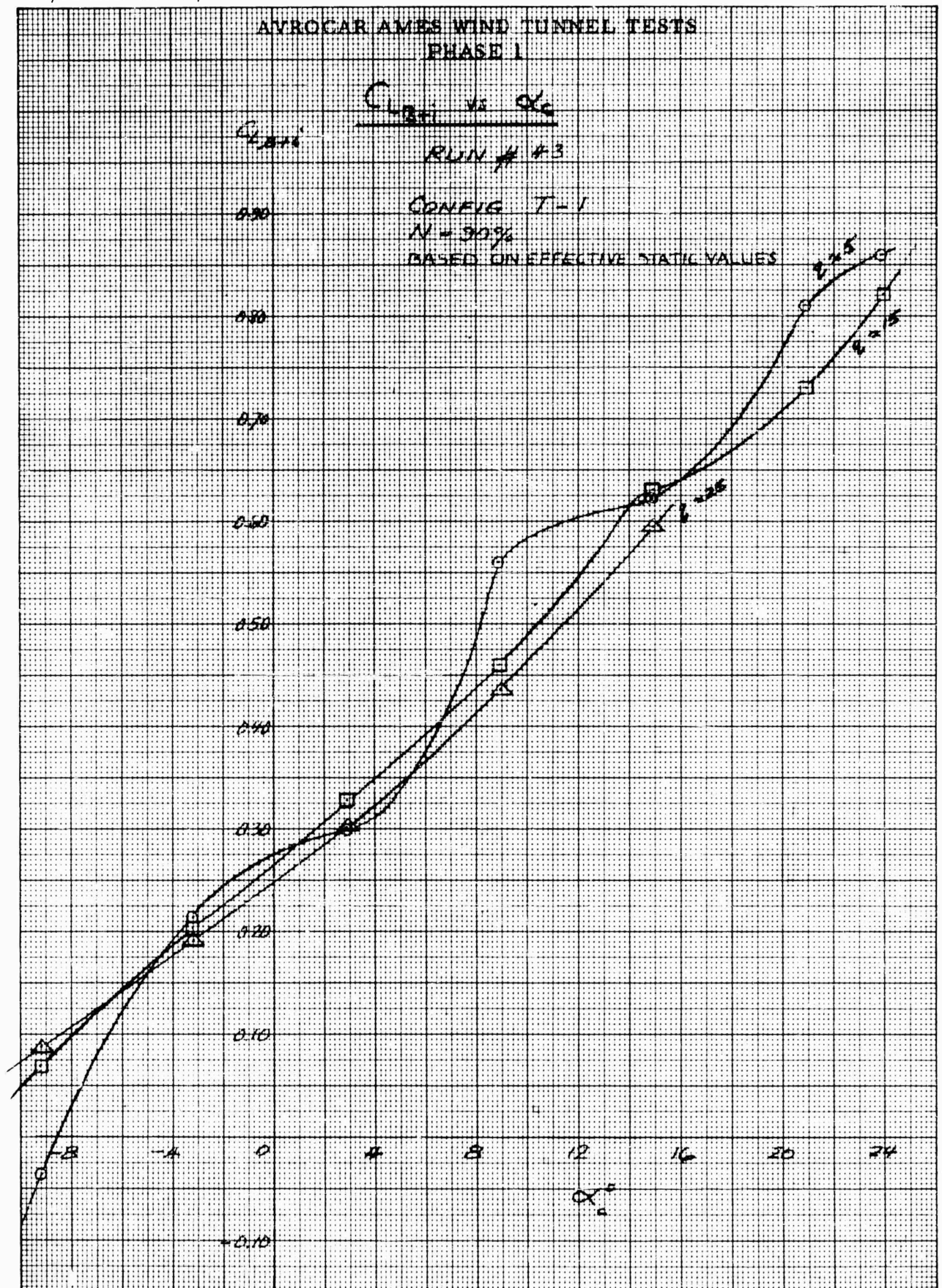




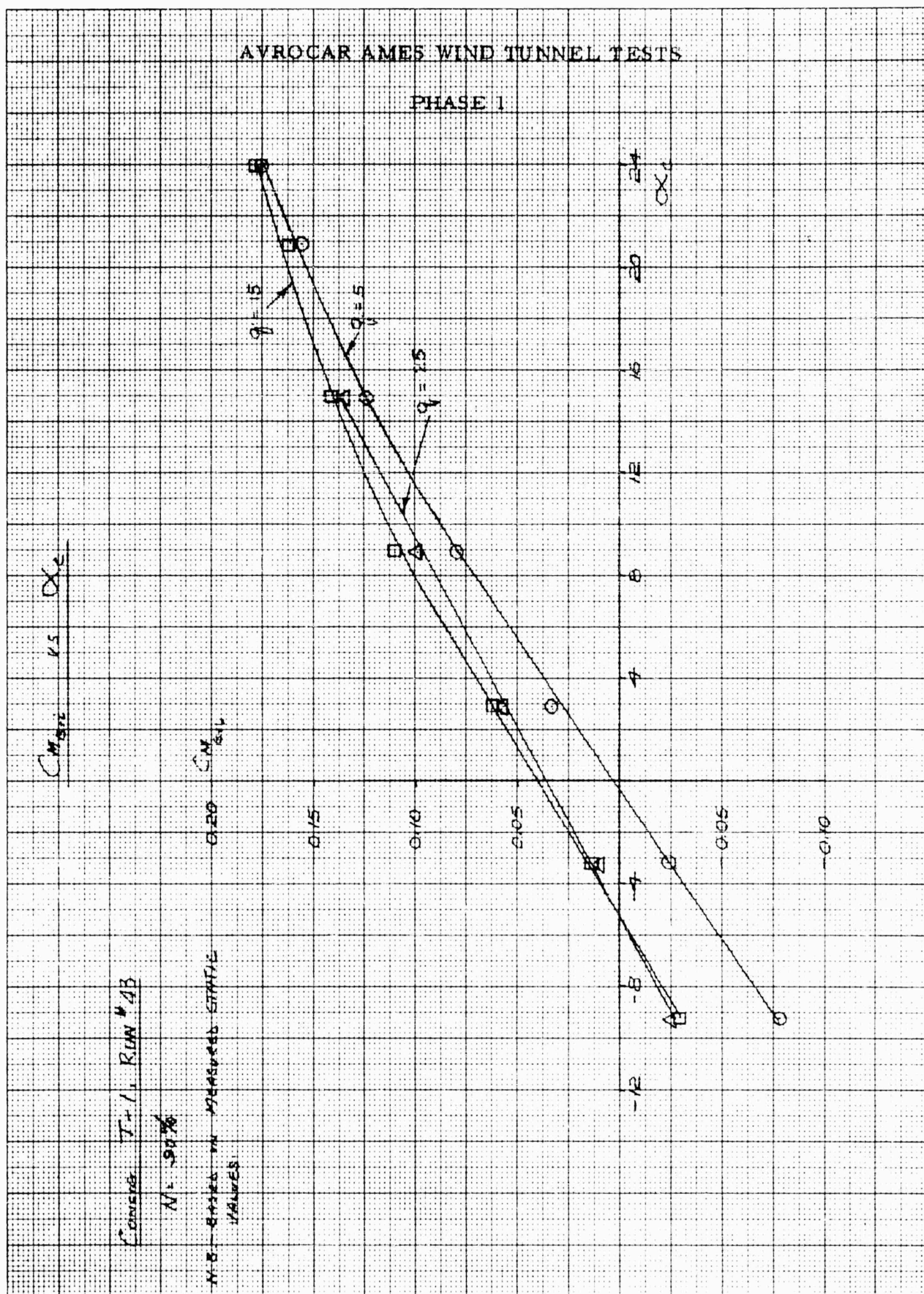






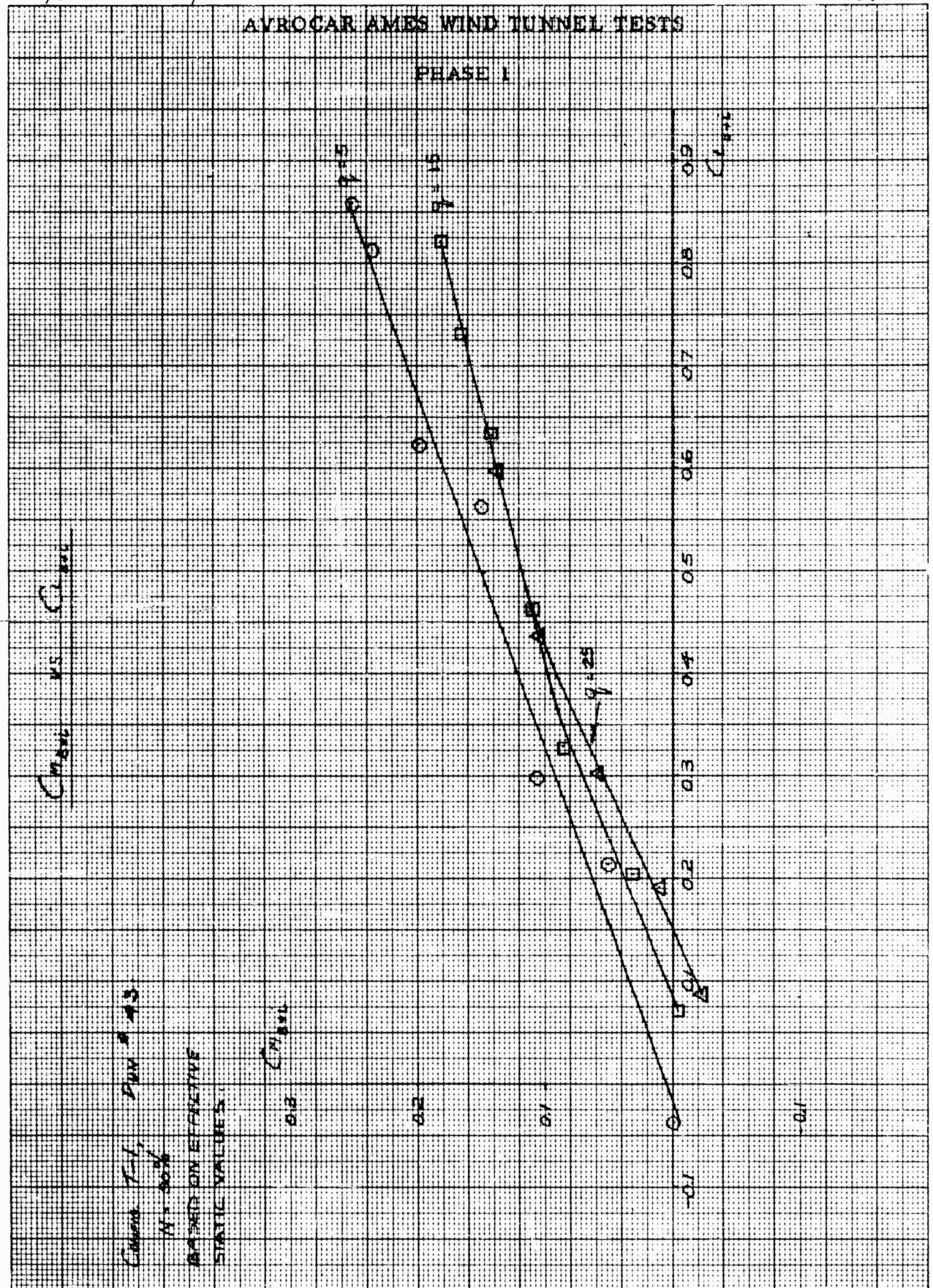




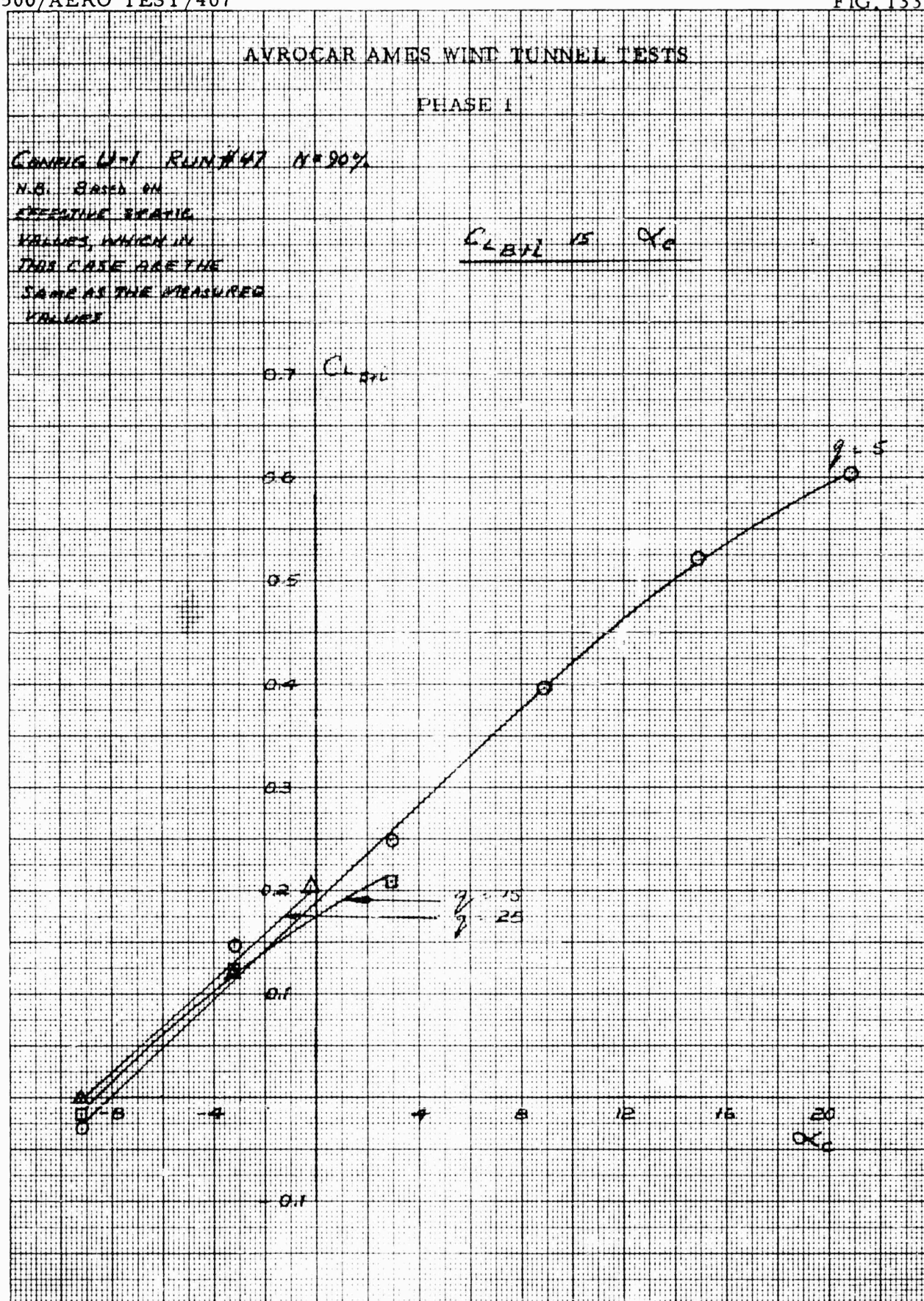


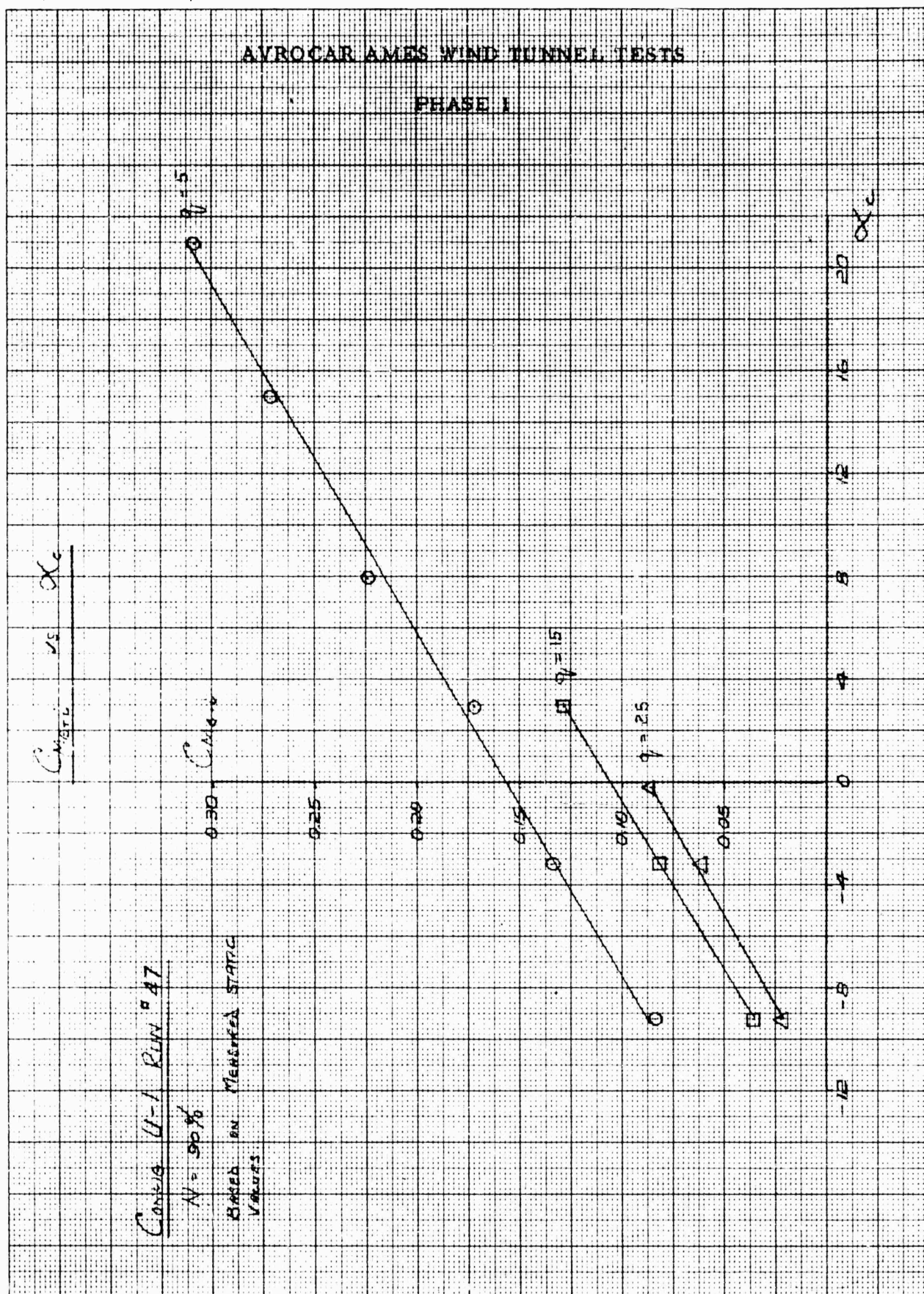




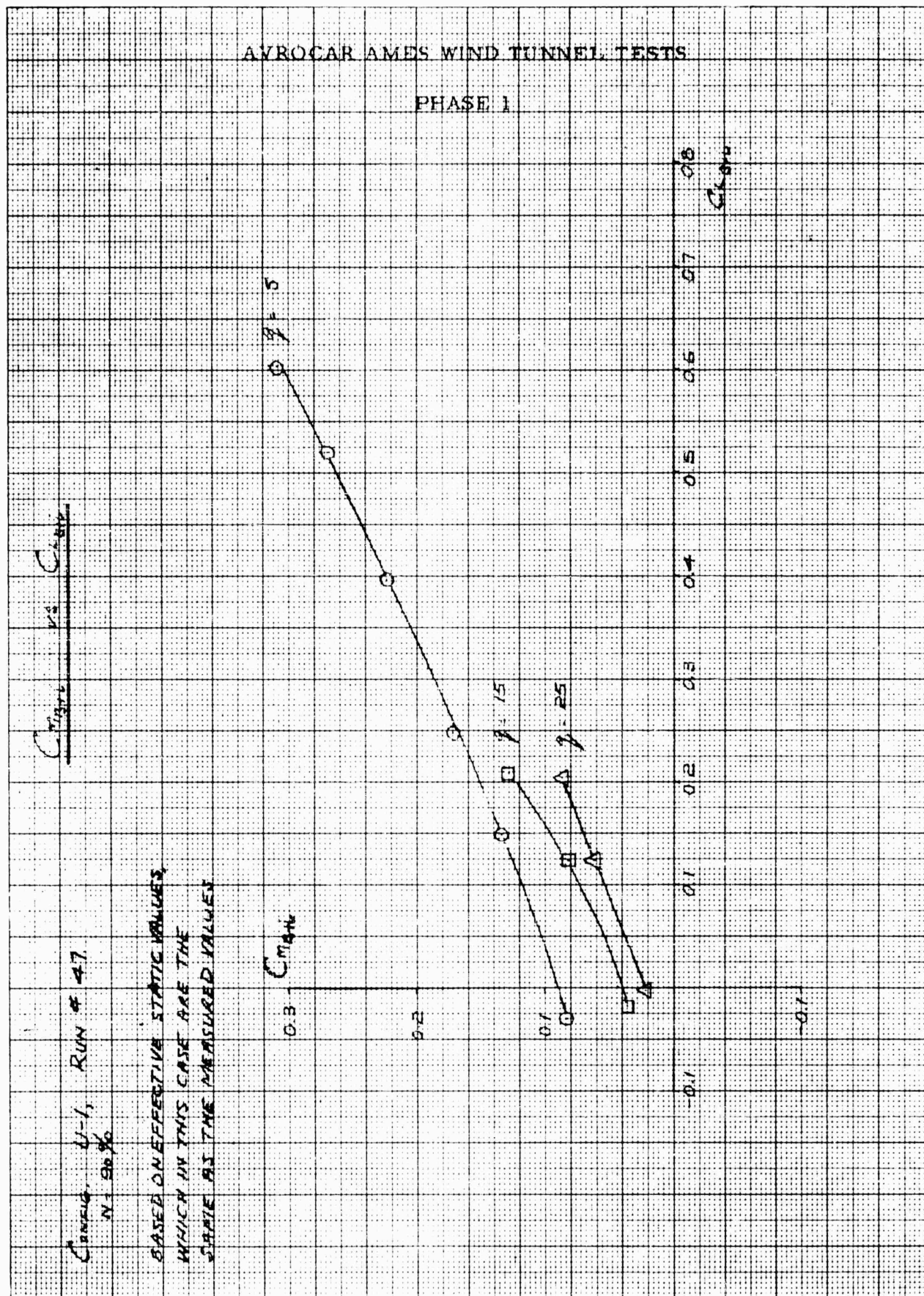




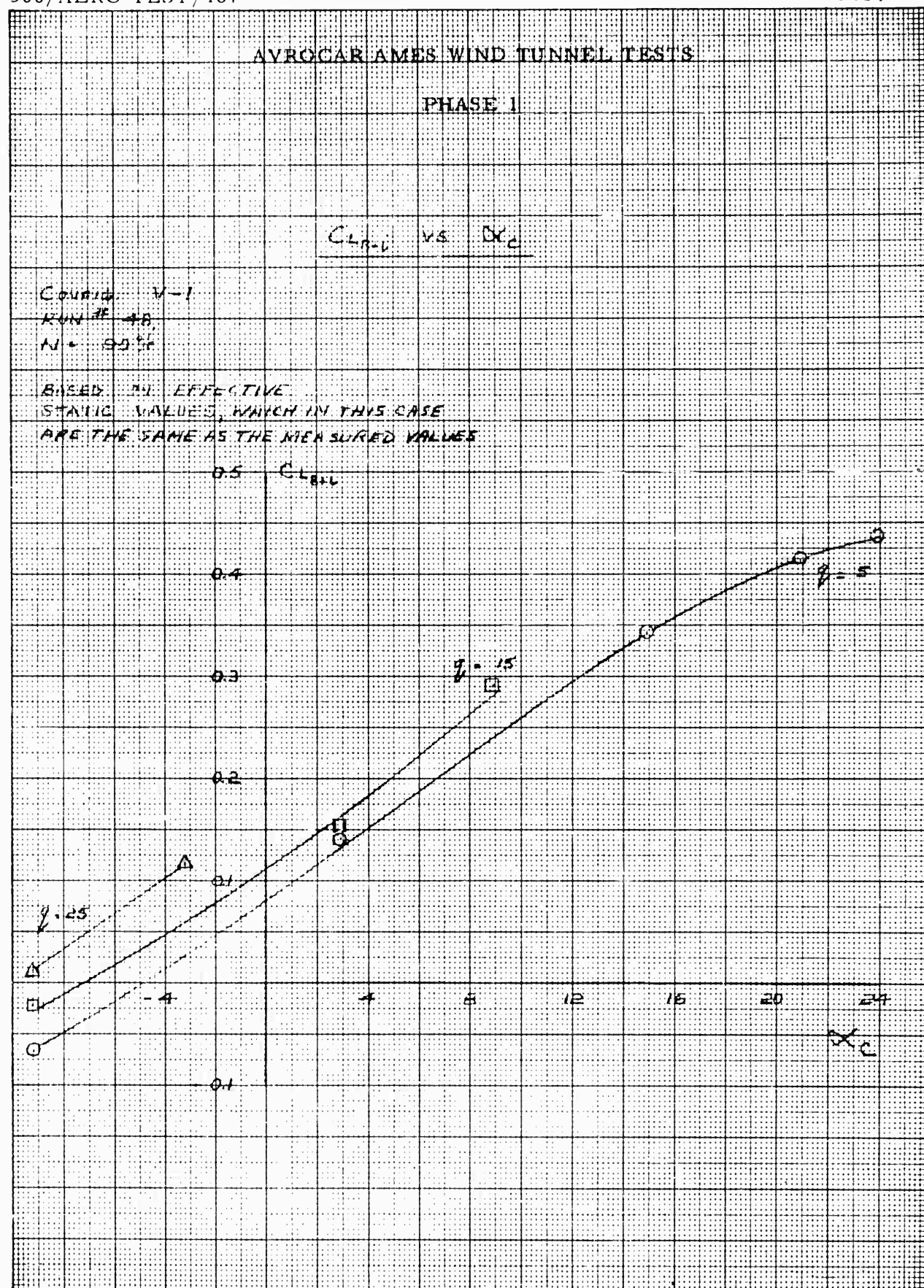












## AVROCAR AMES WIND TUNNEL TESTS

PHASE 1

 $C_{MB+L}$  VS  $\alpha_c$ 

RUN No. 48

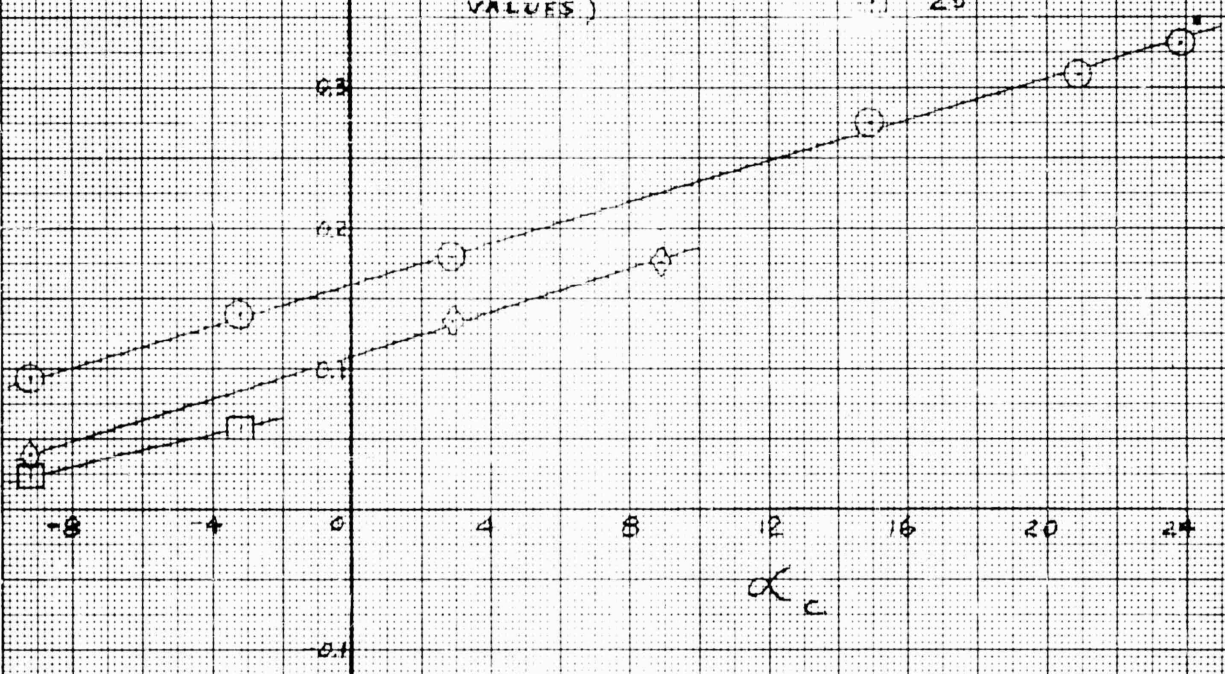
CONFIG V-1

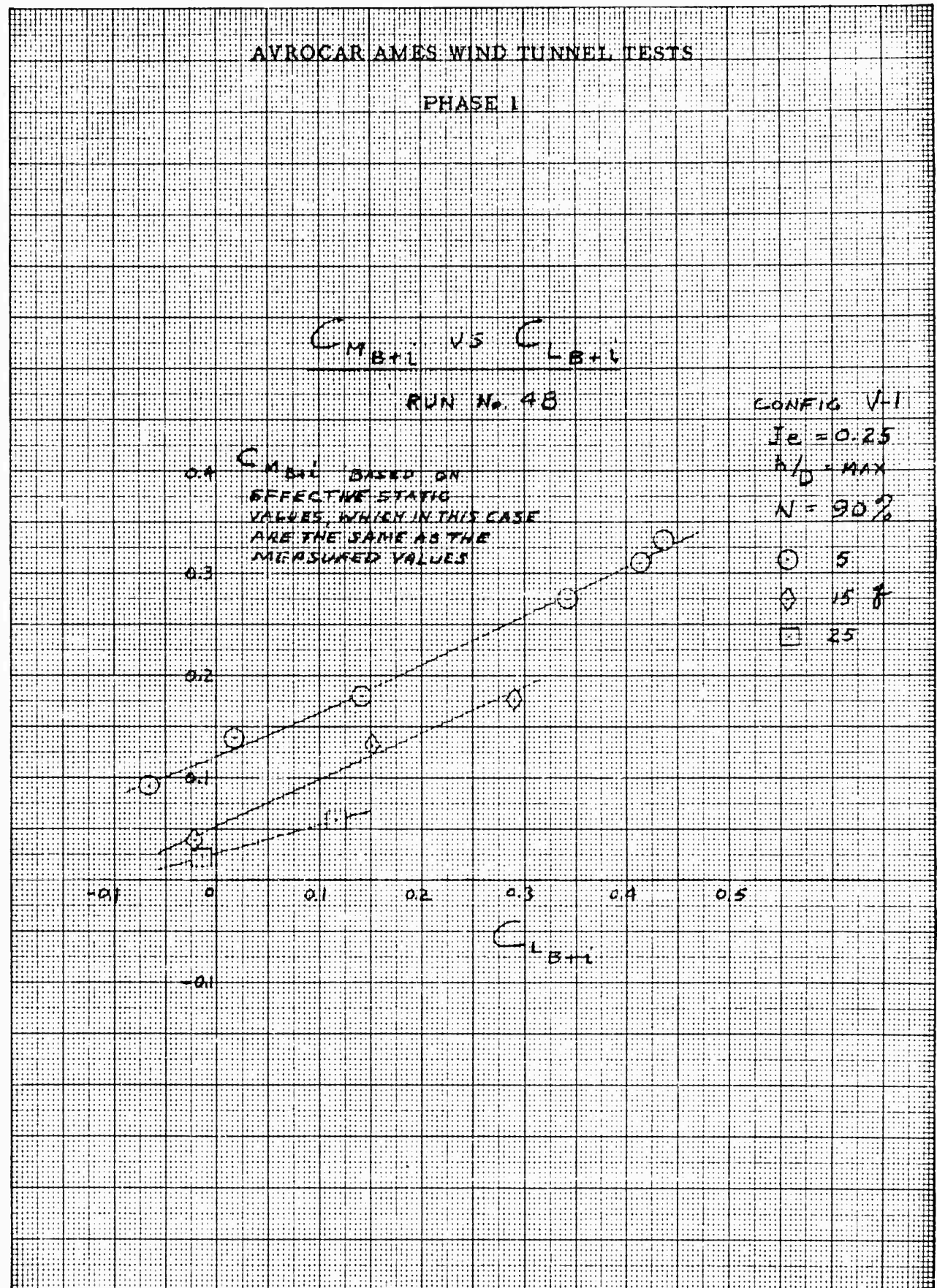
 $J_R = 0.25$  $h/D = \text{MAX}$  $N = 90\%$ 

① 5

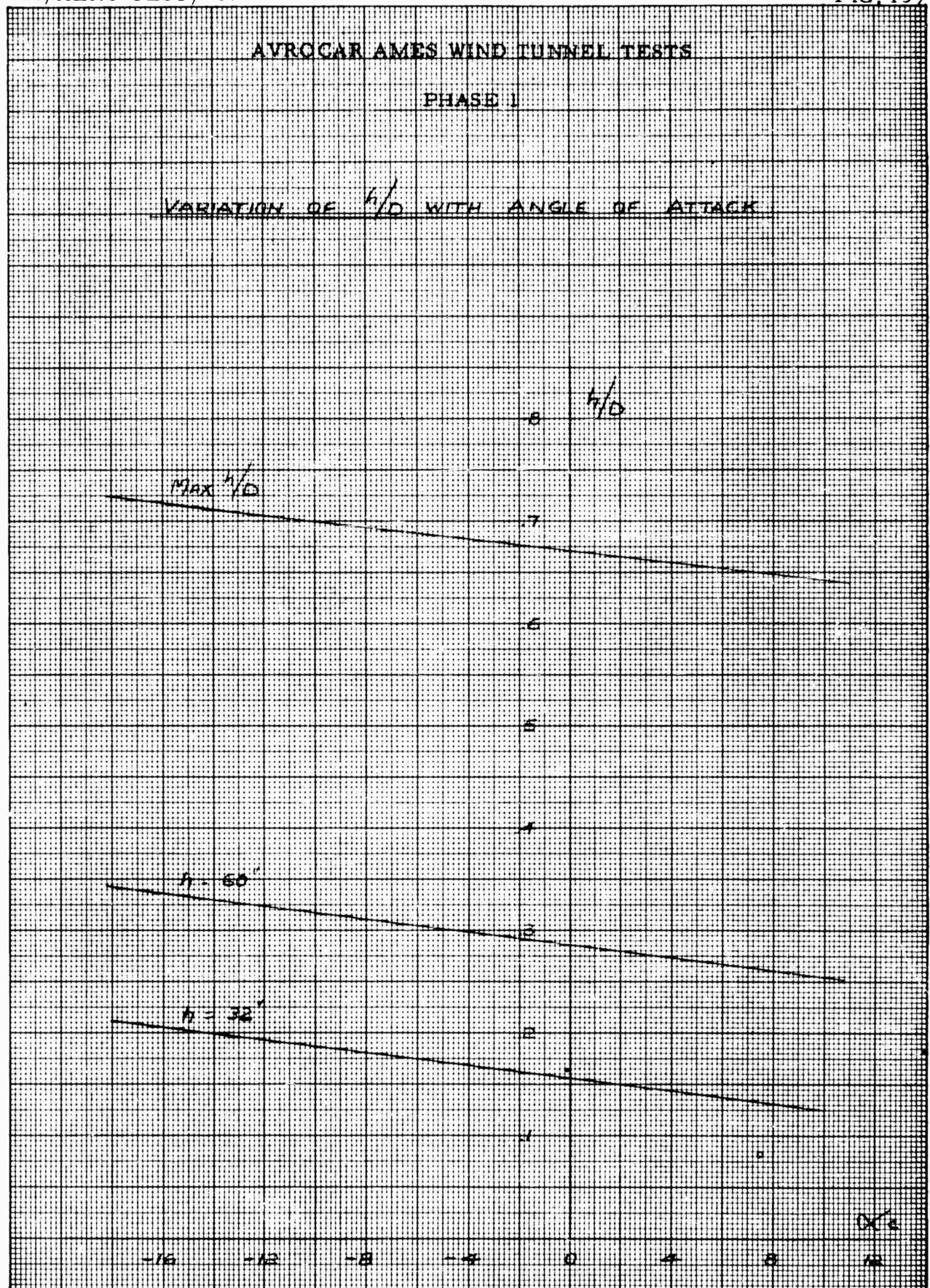
② 15

③ 25

 $C_{MB+L}$  (BASED ON  
MEASURED STATIC  
VALUES.)

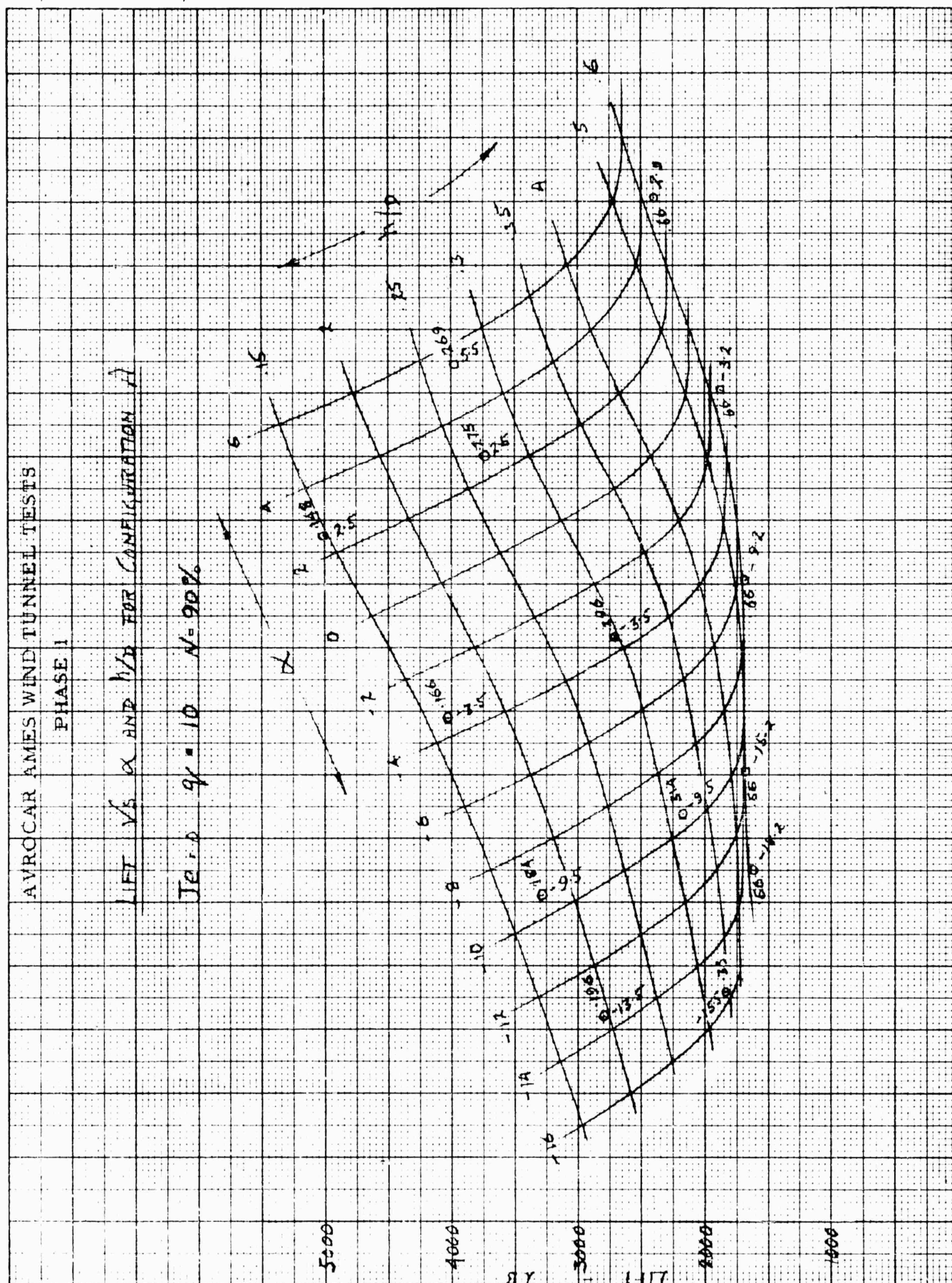




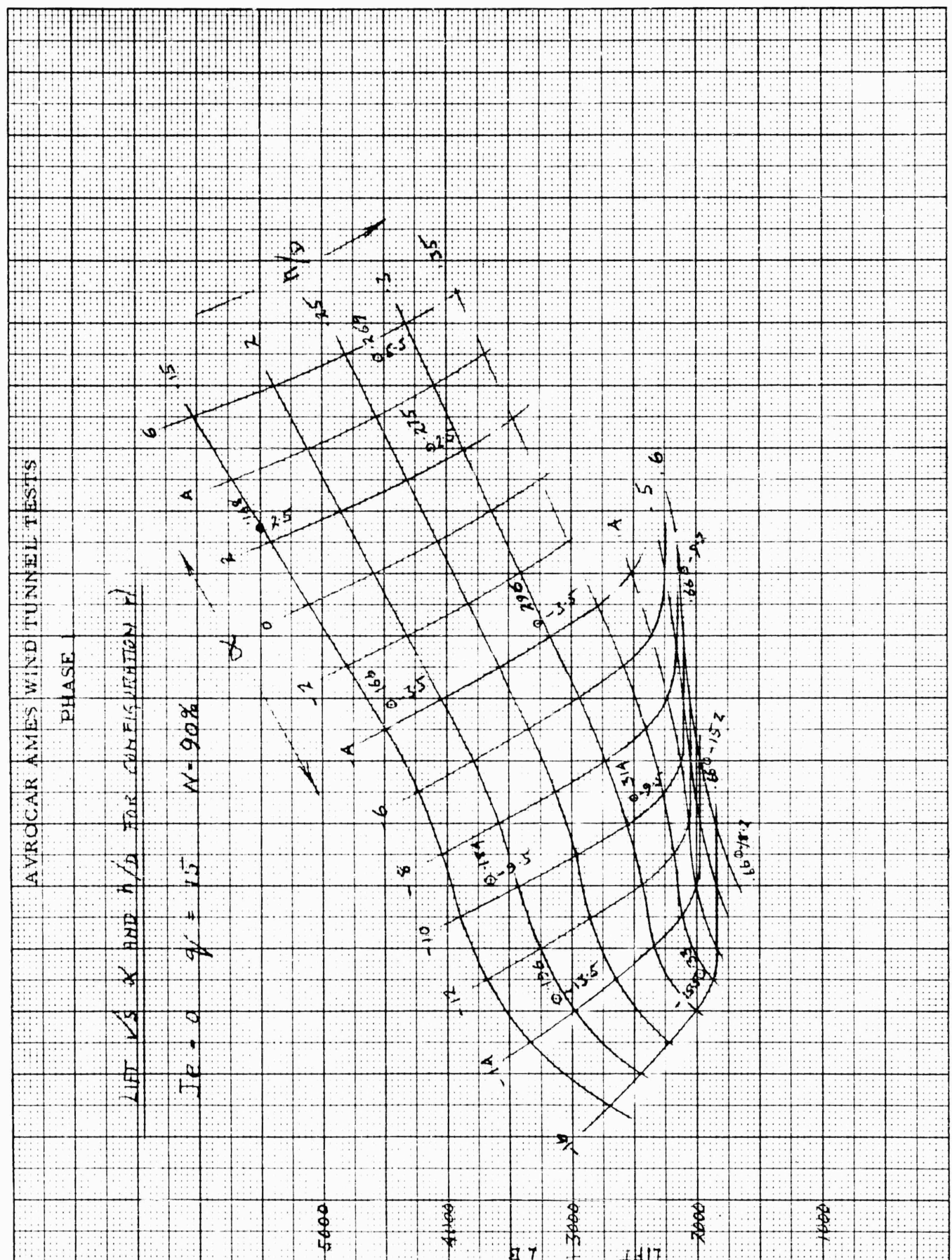




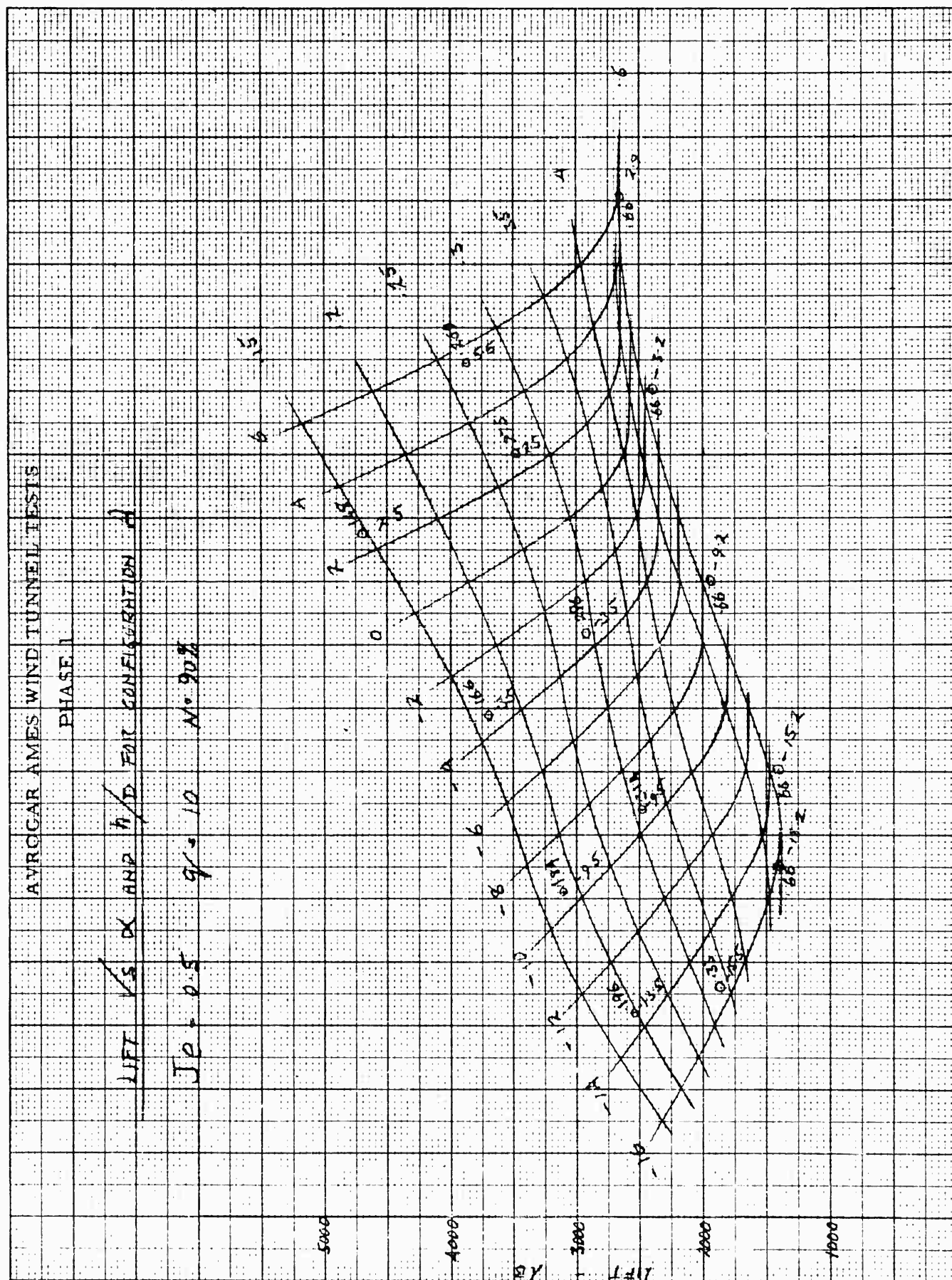




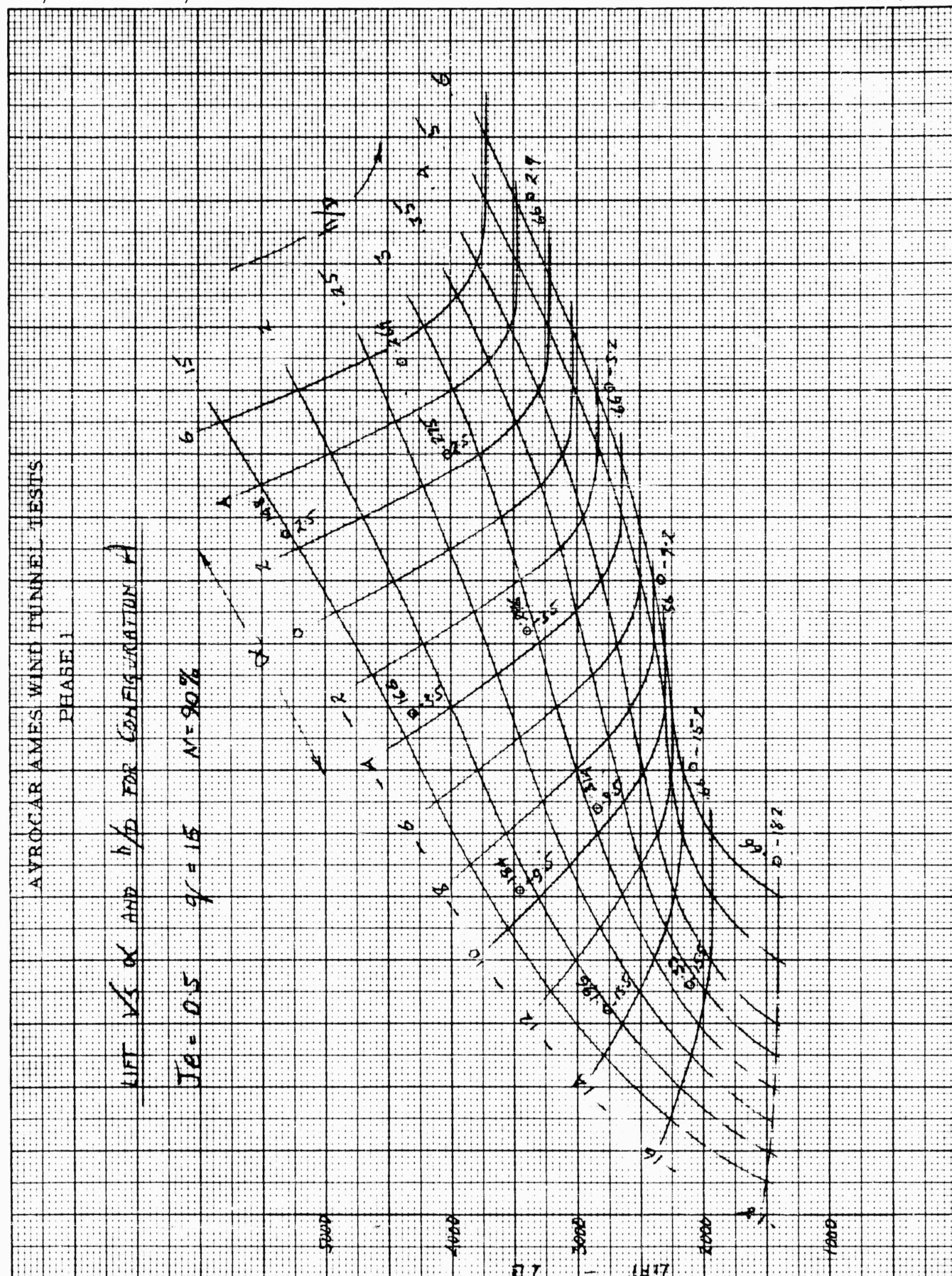


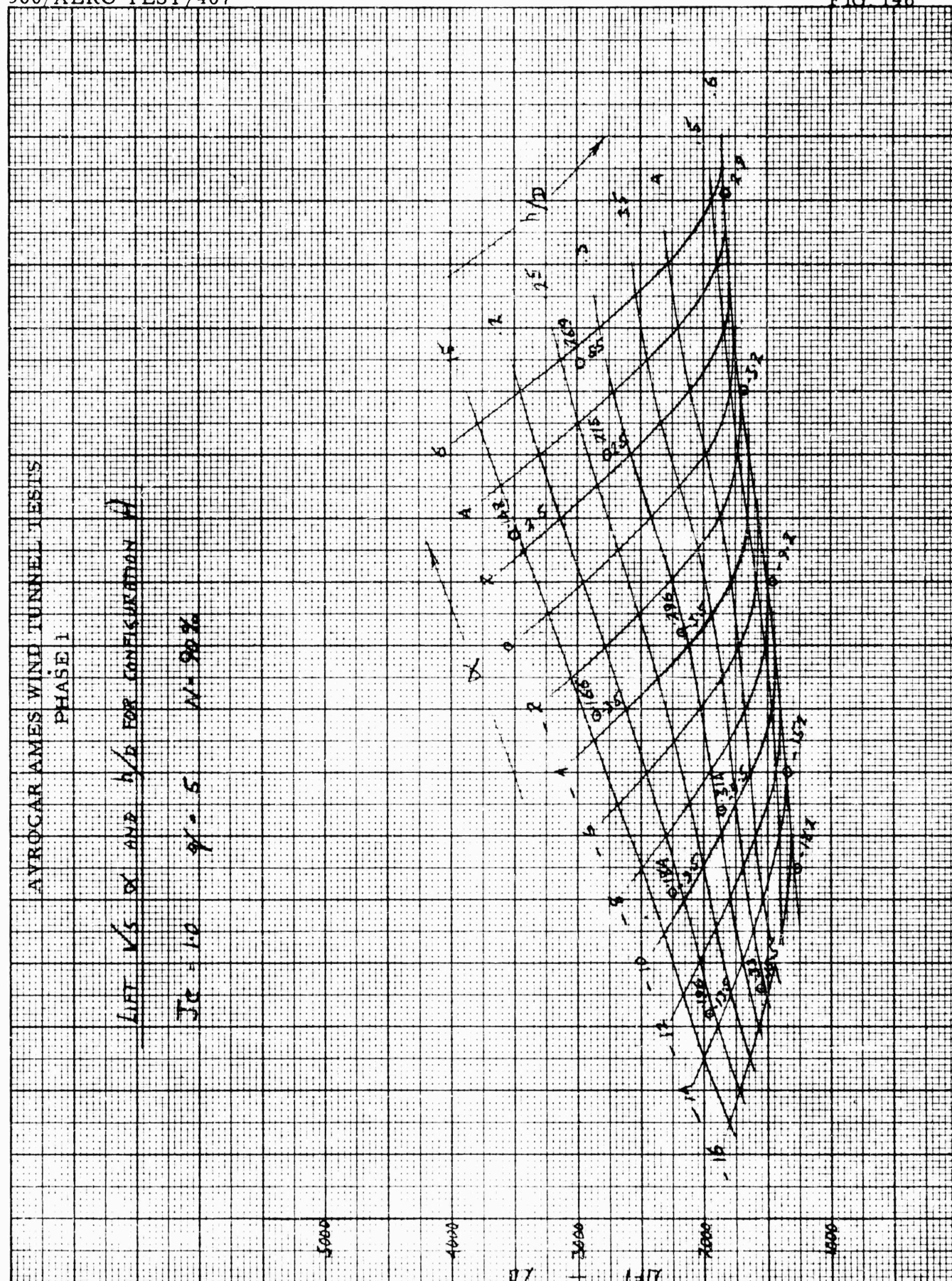




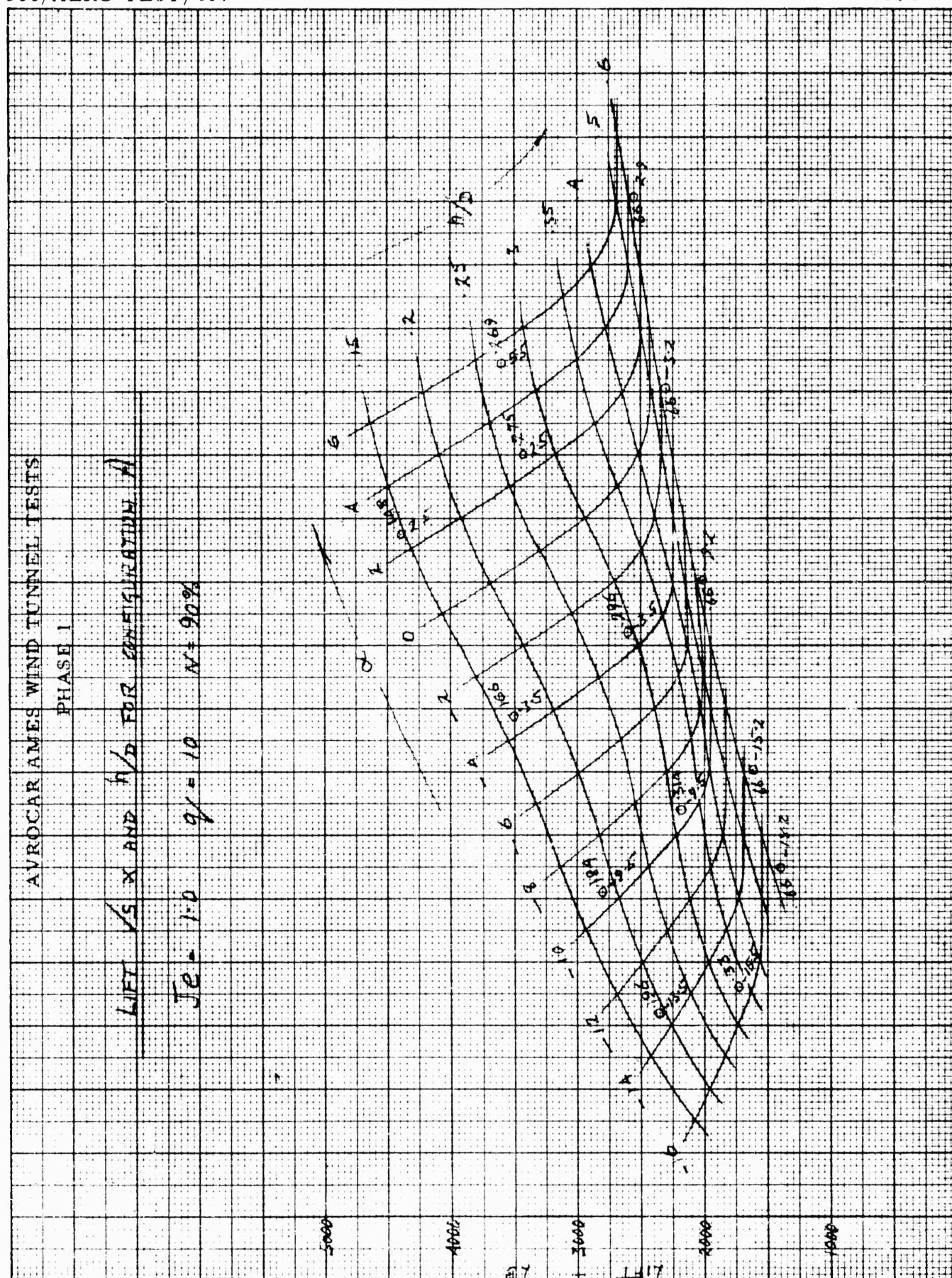




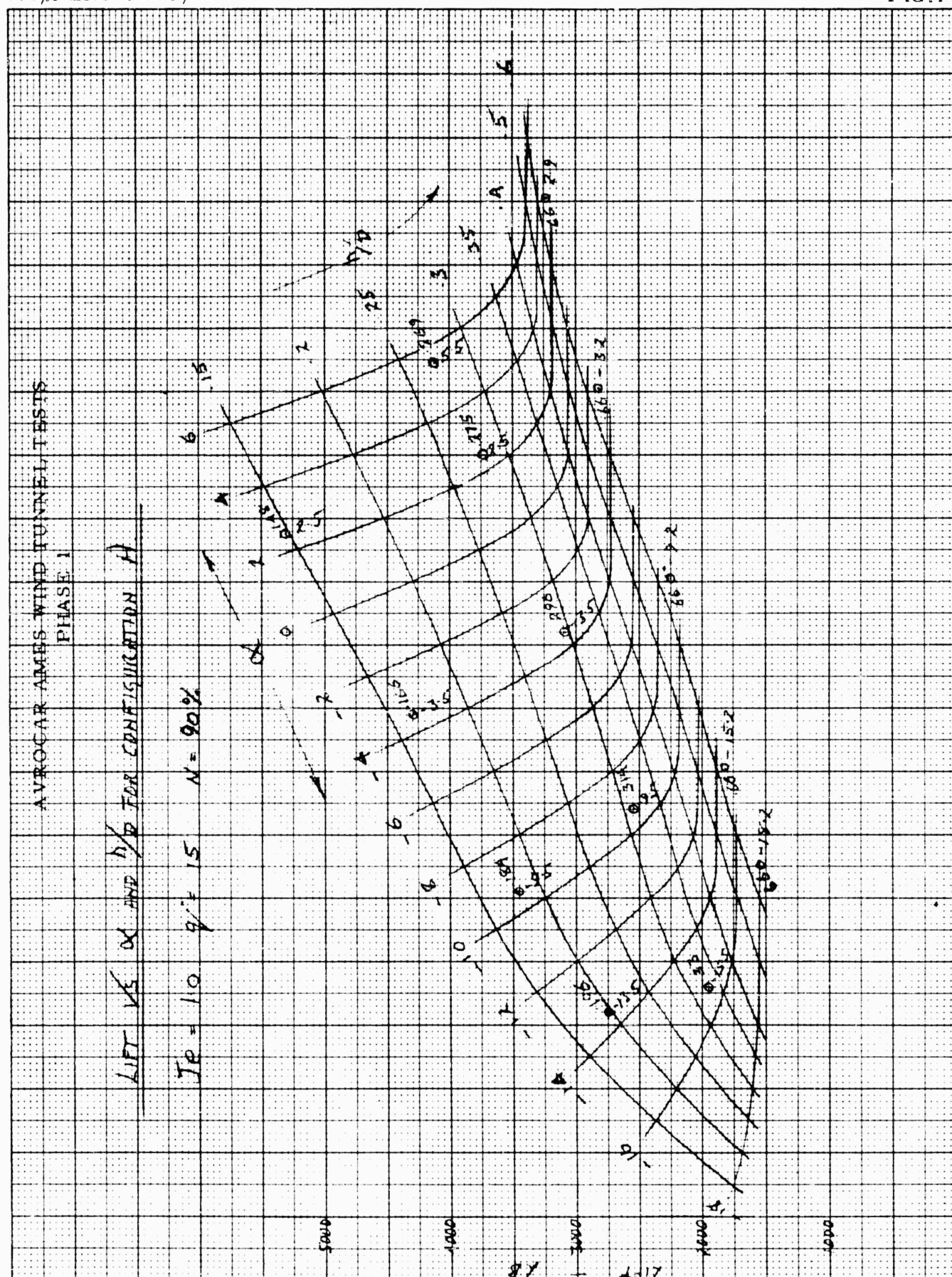


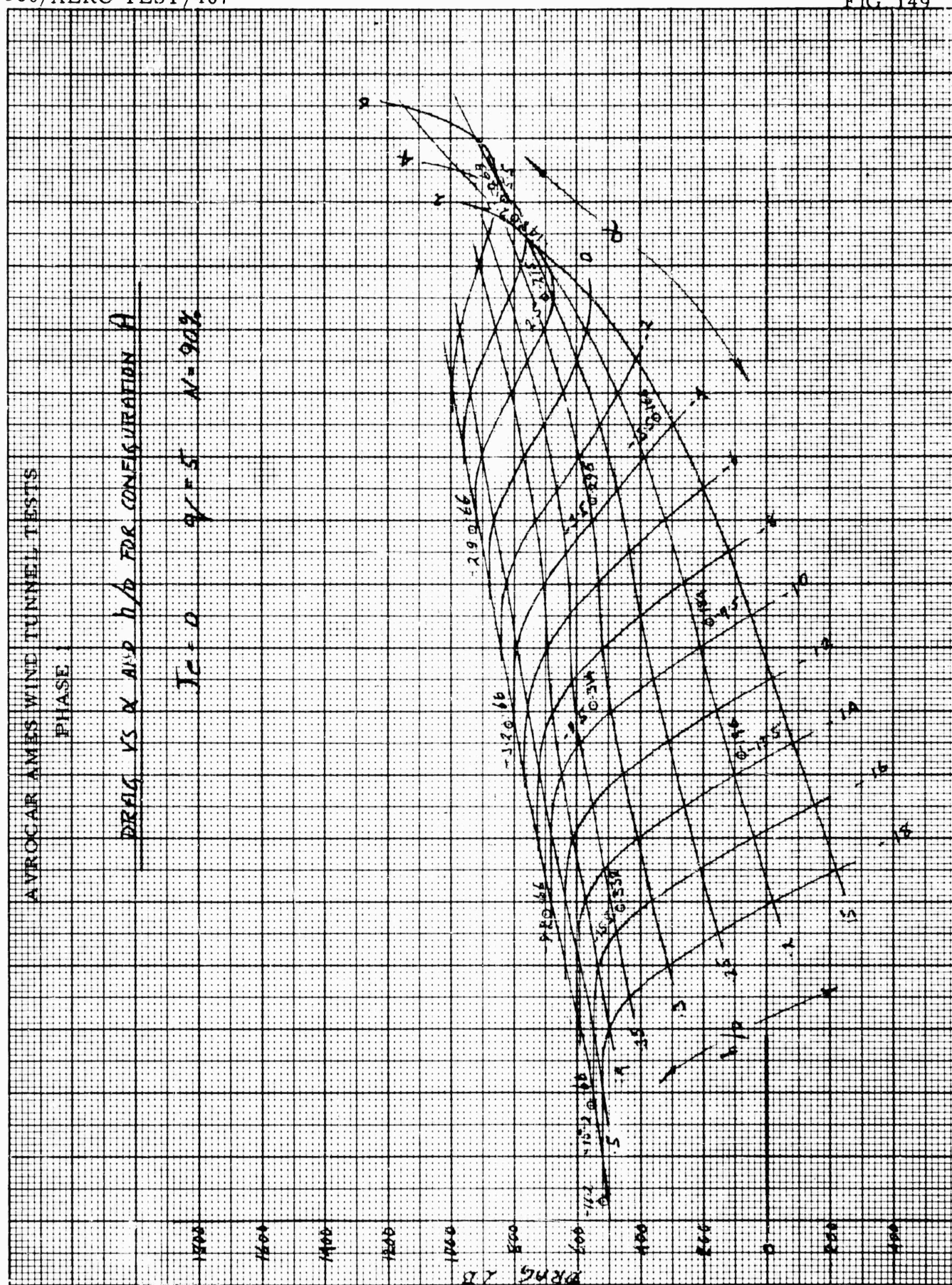




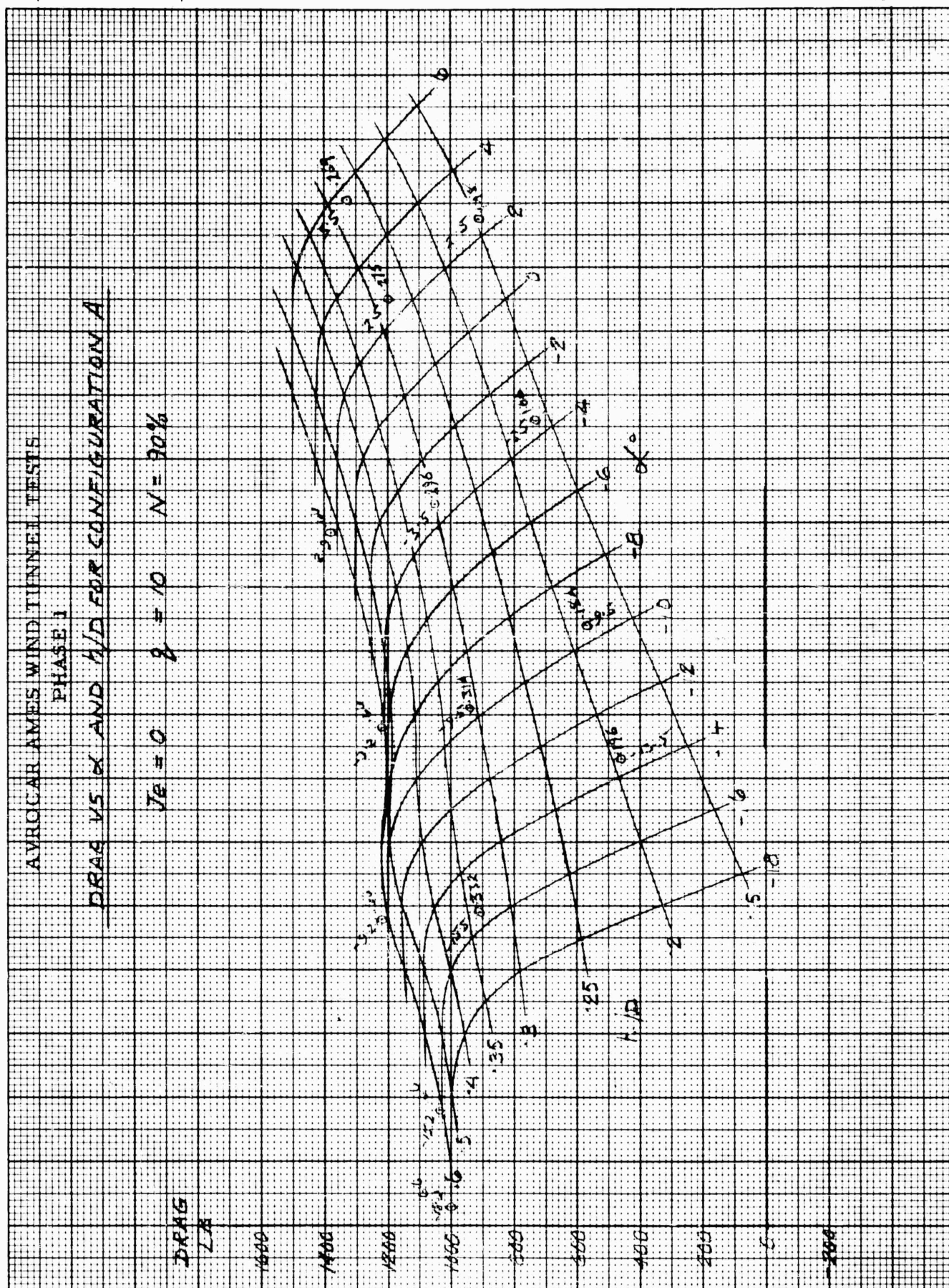




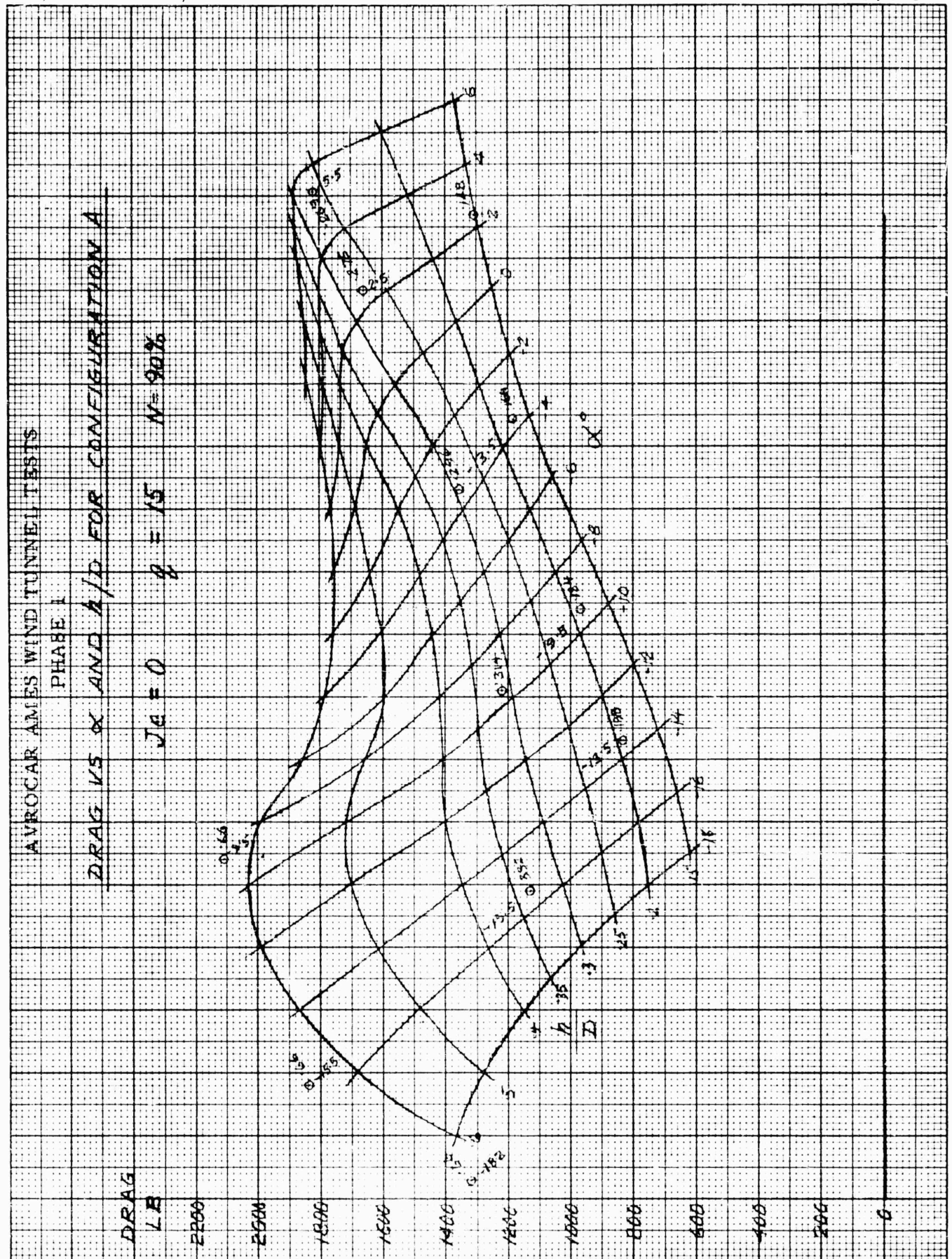


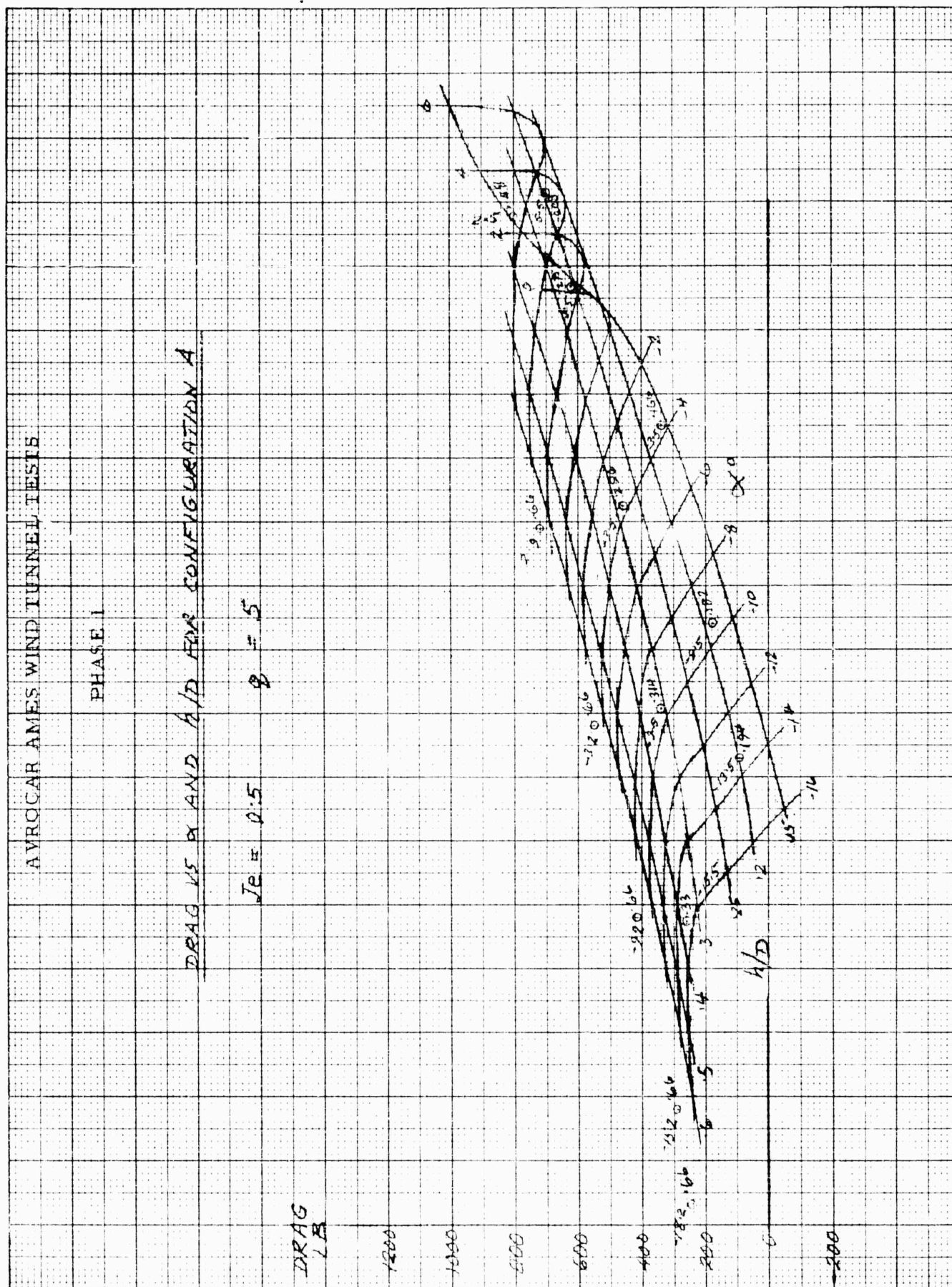


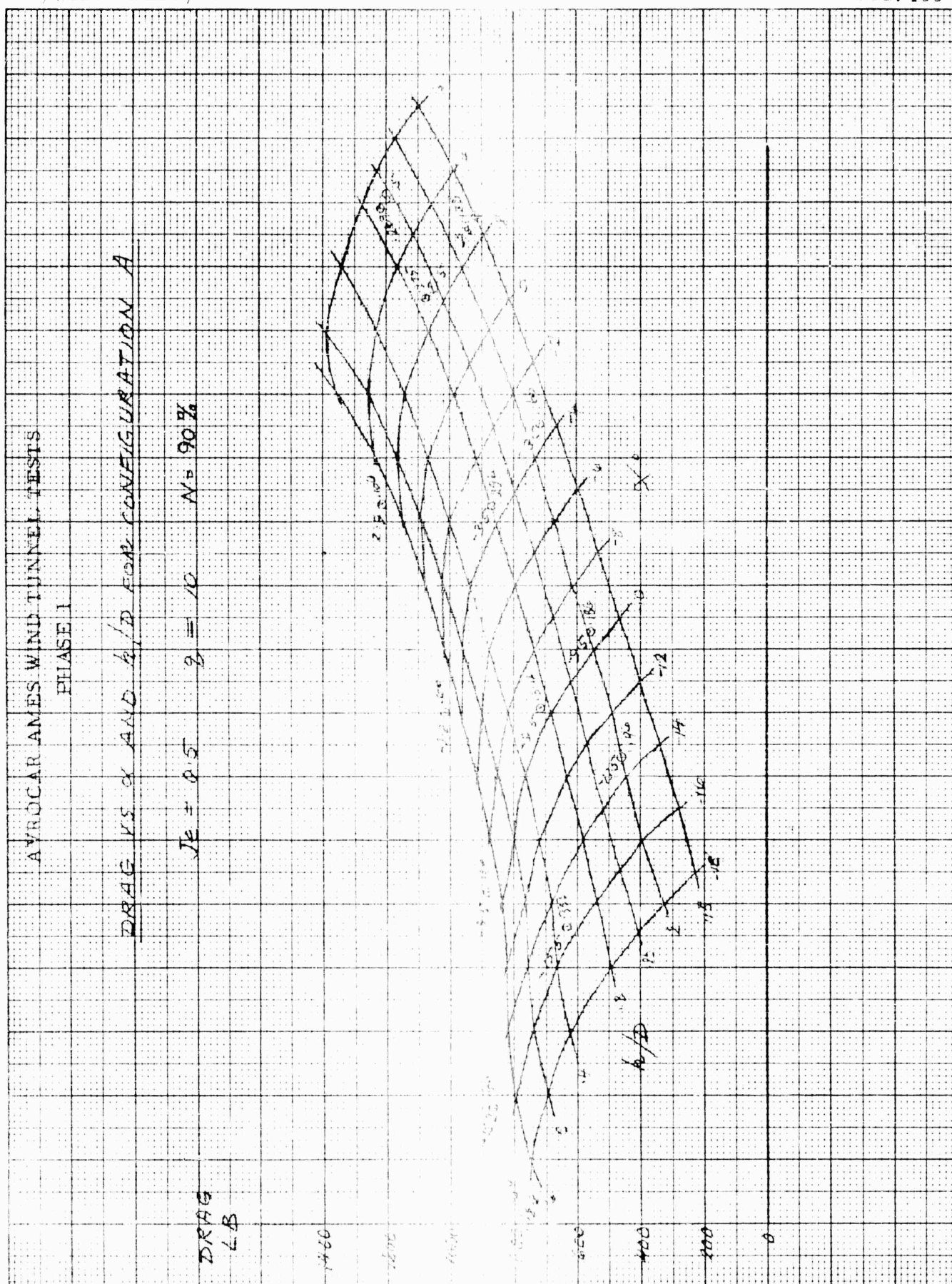






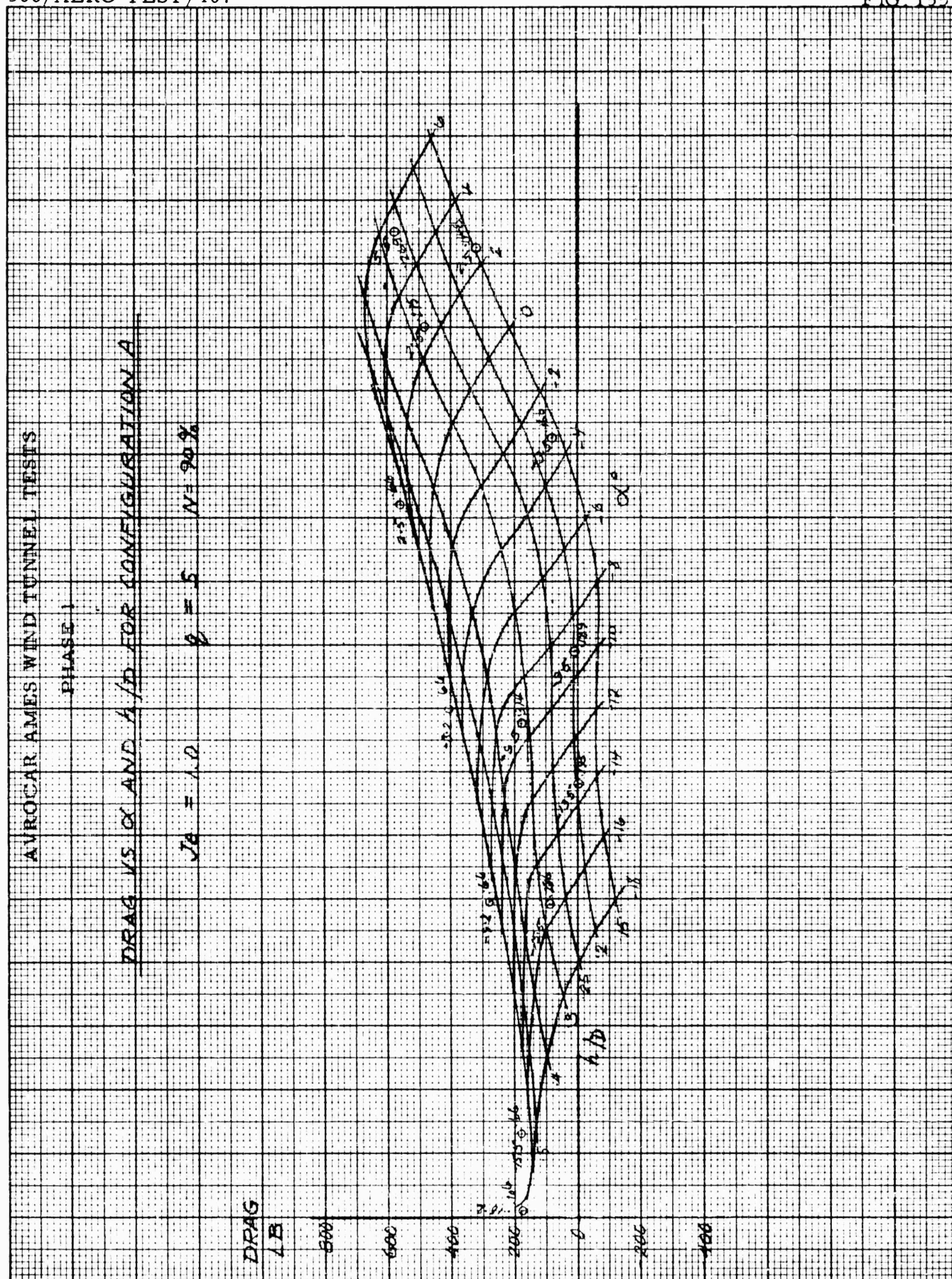














## AVROCAR AMES WIND TUNNEL TESTS

PHASE I

DRAG VS  $\alpha$  AND  $h/D$  FOR CONFIGURATION A

$$JA = 1.0$$

$$\beta = 10$$

$$M = 90\%$$

DRAG  
LB

1800

1600

1400

1200

1000

800

600

400

200

0

-200

 $h/D$ 

1.5

2

3

4

5

6

7

8

9

10

11

12

13

14

15

16

17

18

19

20

21

22

23

24

25

26

27

28

29

30

31

32

33

34

35

36

37

38

39

40

41

42

43

44

45

46

47

48

49

50

51

52

53

54

55

56

57

58

59

60

61

62

63

64

65

66

67

68

69

70

71

72

73

74

75

76

77

78

79

80

81

82

83

84

85

86

87

88

89

90

91

92

93

94

95

96

97

98

99

100

101

102

103

104

105

106

107

108

109

110

111

112

113

114

115

116

117

118

119

120

121

122

123

124

125

126

127

128

129

130

131

132

133

134

135

136

137

138

139

140

141

142

143

144

145

146

147

148

149

150

151

152

153

154

155

156

157

158

159

160

161

162

163

164

165

166

167

168

169

170

171

172

173

174

175

176

177

178

179

180

181

182

183

184

185

186

187

188

189

190

191

192

193

194

195

196

197

198

199

200

201

202

203

204

205

206

207

208

209

210

211

212

213

214

215

216

217

218

219

220

221

222

223

224

225

226

227

228

229

230

231

232

233

234

235

236

237

238

239

240

241

242

243

244

245

246

247

248

249

250

251

252

253

254

255

256

257

258

259

260

261

262

263

264

265

266

267

268

269

270

271

272

273

274

275

276

277

278

279

280

281

282

283

284

285

286

287

288

289

290

291

292

293

294

295

296

297

298

299

300

301

302

303

304

305

306

307

308

309

310

311

312

313

314

315

316

317

318

319

320

321

322

323

324

325

326

327

328

329

330

331

332

333

334

335

336

337

338

339

340

341

342

343

344

345

346

347

348

349

350

351

352

353

354

355

356

357

358

359

360

361

362

363

364

365

366

367

368

369

370

371

372

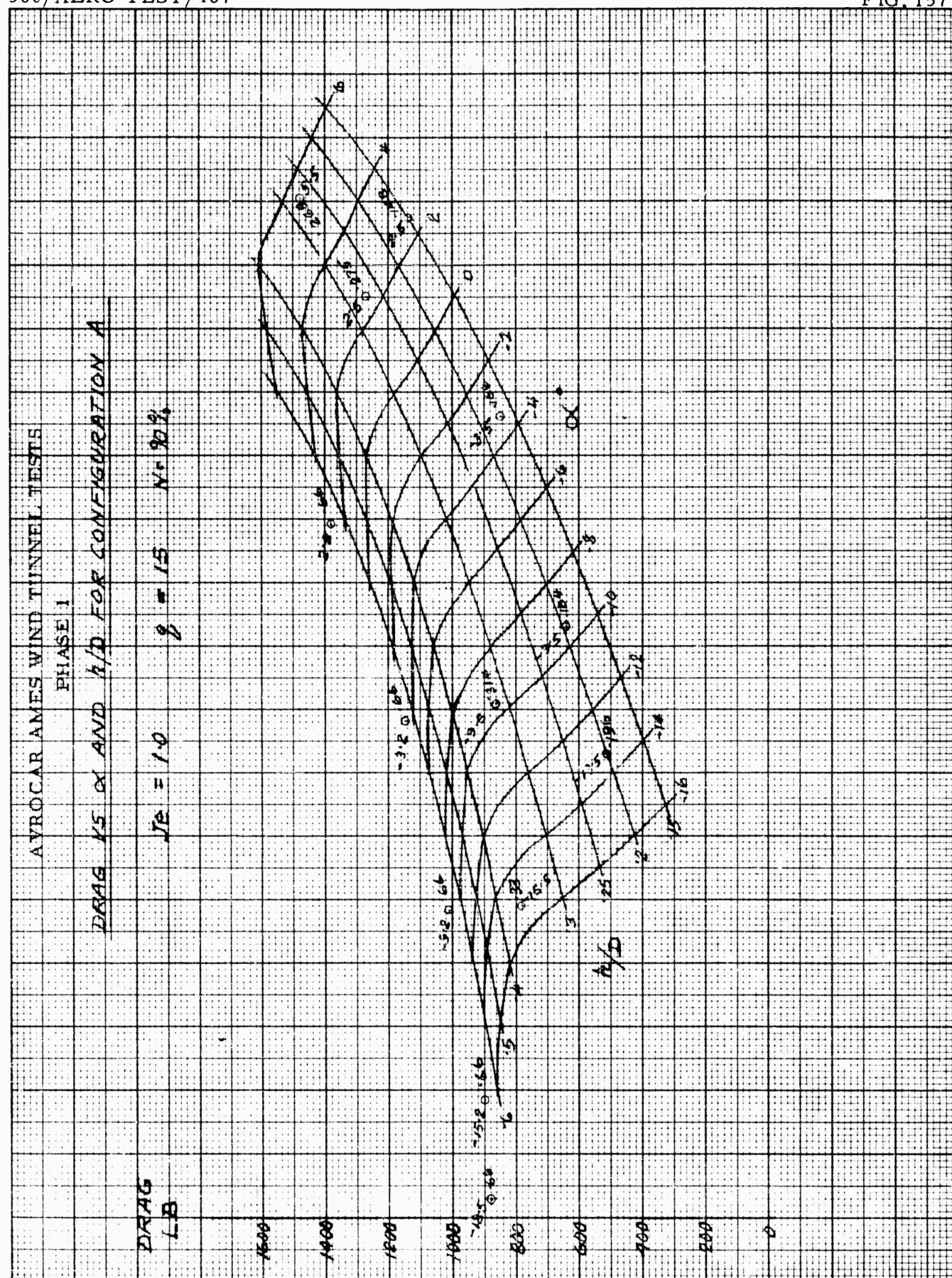
373

374

375

376





# AVROCAR AMES WIND TUNNEL TESTS PHASE I

## PITCHING MOMENT IN GROUND EFFECT

$M$  VS  $\alpha_c$

O - h/d MAX = .662 AT  $\alpha_c = 0^\circ$

$J_e = 0$

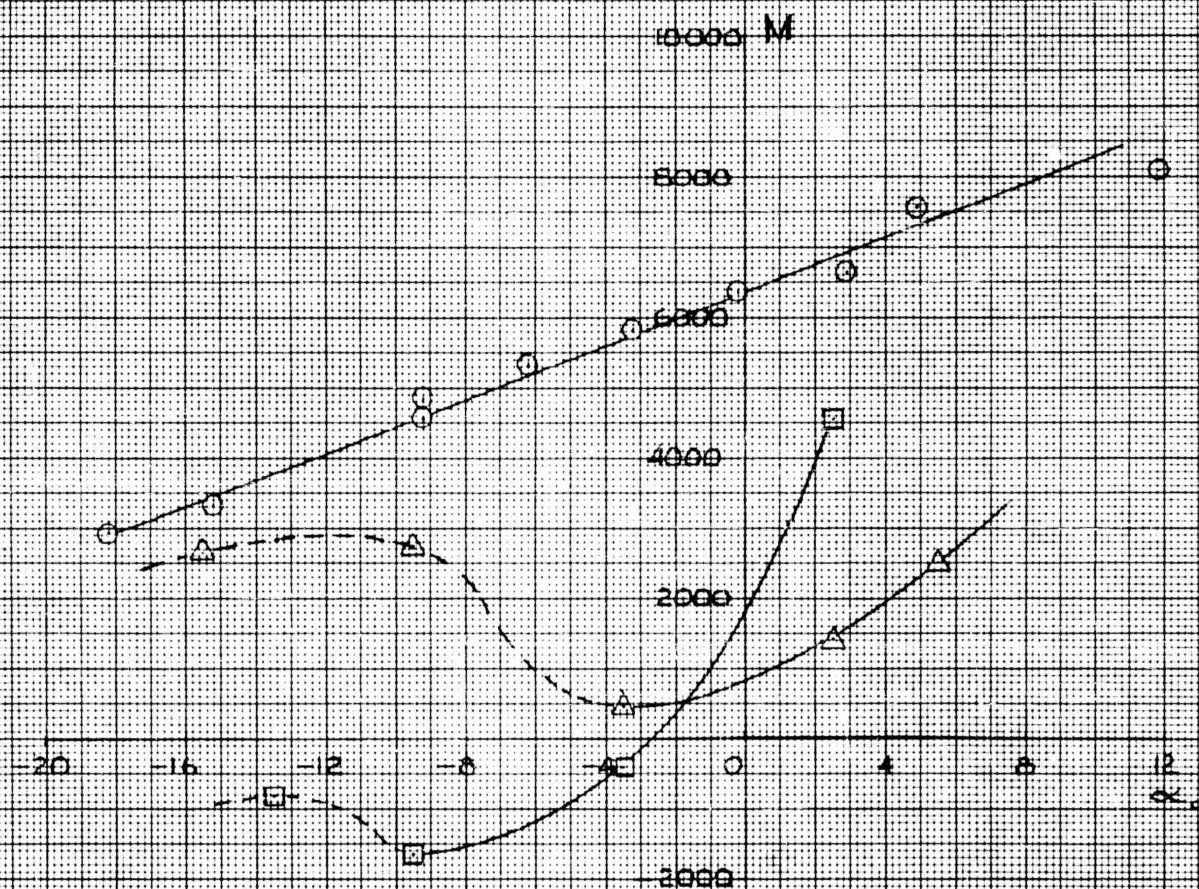
$\Delta$  - h/d = .278 " "

N = 90%

$\square$  - h/d = .148 " "

g = 5

CONFIG A





# AVROCAR AMES WIND TUNNEL TESTS PHASE I

## PITCHING MOMENT IN GROUND EFFECT

$M$  vs  $\alpha_c$

$\bigcirc$  -  $h/d$  MAX = 1.552 AT  $\alpha_c = 0^\circ$

$J_E = 0$

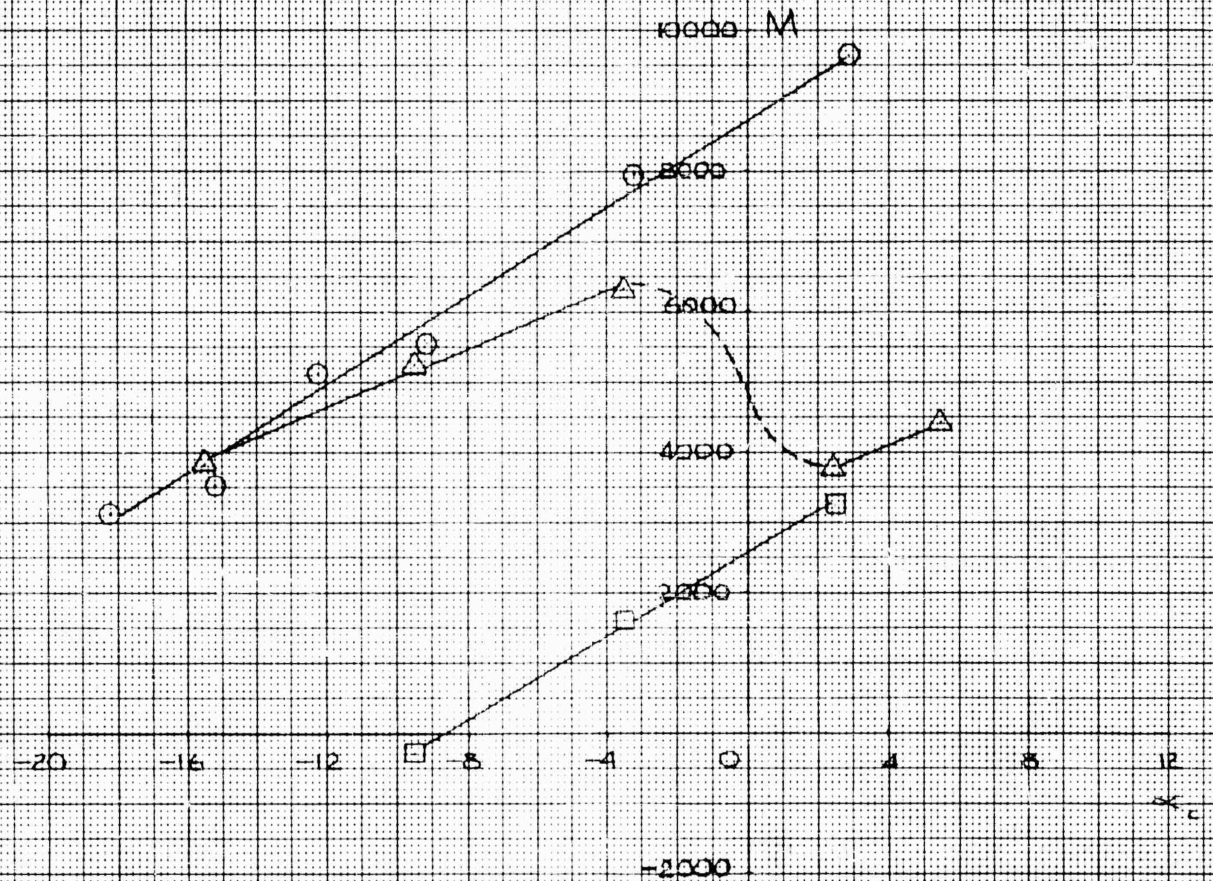
$\Delta$  -  $h/d = 1.278$  " "

$N = 90\%$

$\square$  -  $h/d = 1.18$  " "

$\beta = 10$

CONFIG A





AVROCAR AMES WIND TUNNEL TESTS  
PHASE 1

PITCHING MOMENT IN GROUND EFFECT

$M$  vs  $\alpha_c$

○  $h/d$  MAX = 662 AT  $\alpha_c = 0^\circ$

△  $h/d$  = 278 " "

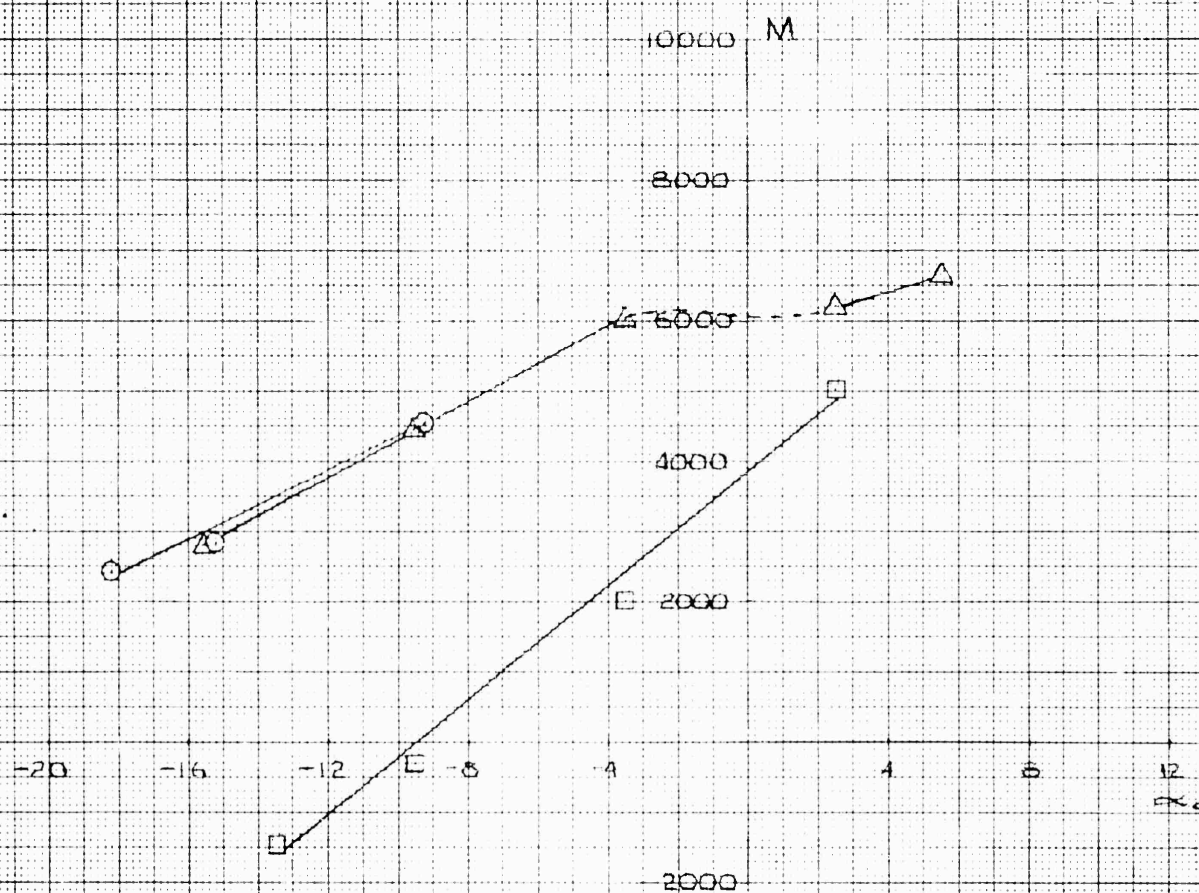
□  $h/d$  = 148 " "

$I_a = 0$

$N = 90\%$

$q = 15$

CONFIG. A



## AVROCAR AMES WIND TUNNEL TESTS

## PHASE 1

## PITCHING MOMENT IN GROUND EFFECT

$$J_0 = 0.5$$

$$q = 3$$

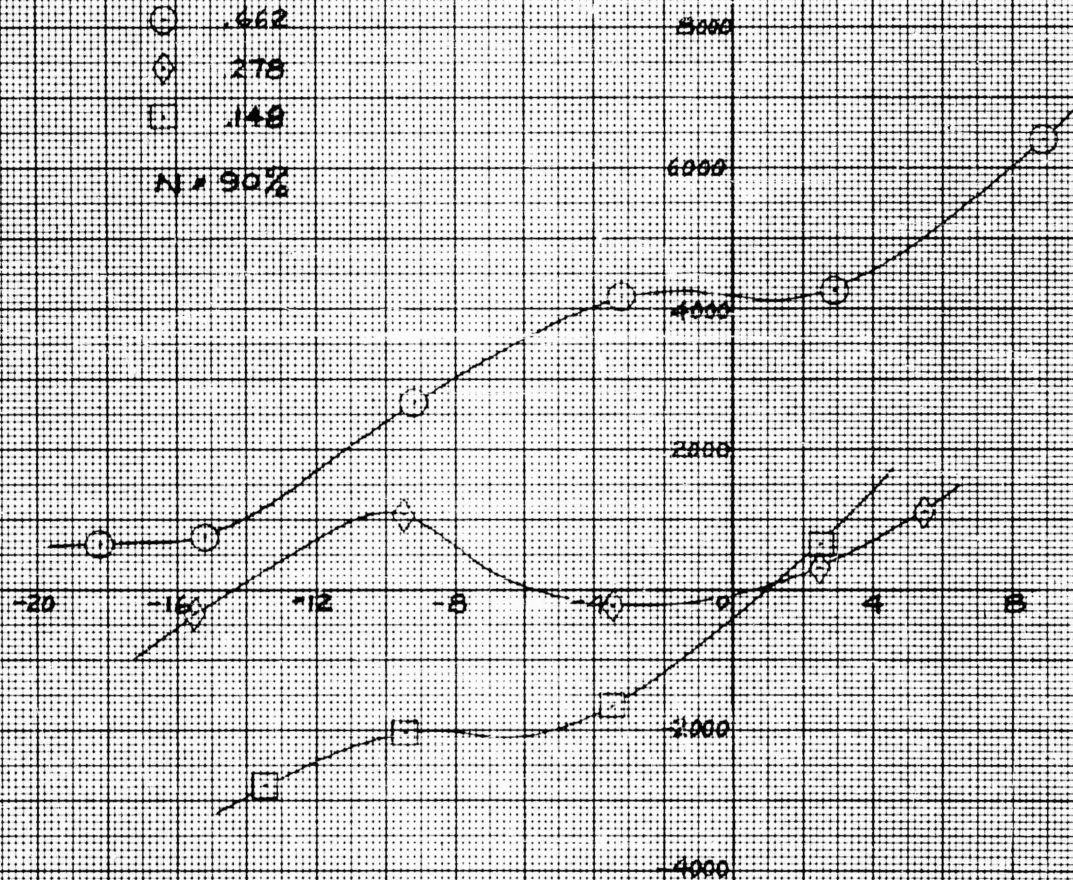
$$h/D \text{ AT } \alpha = 0^\circ$$

$$\odot \quad .662$$

$$\diamond \quad .278$$

$$\square \quad .148$$

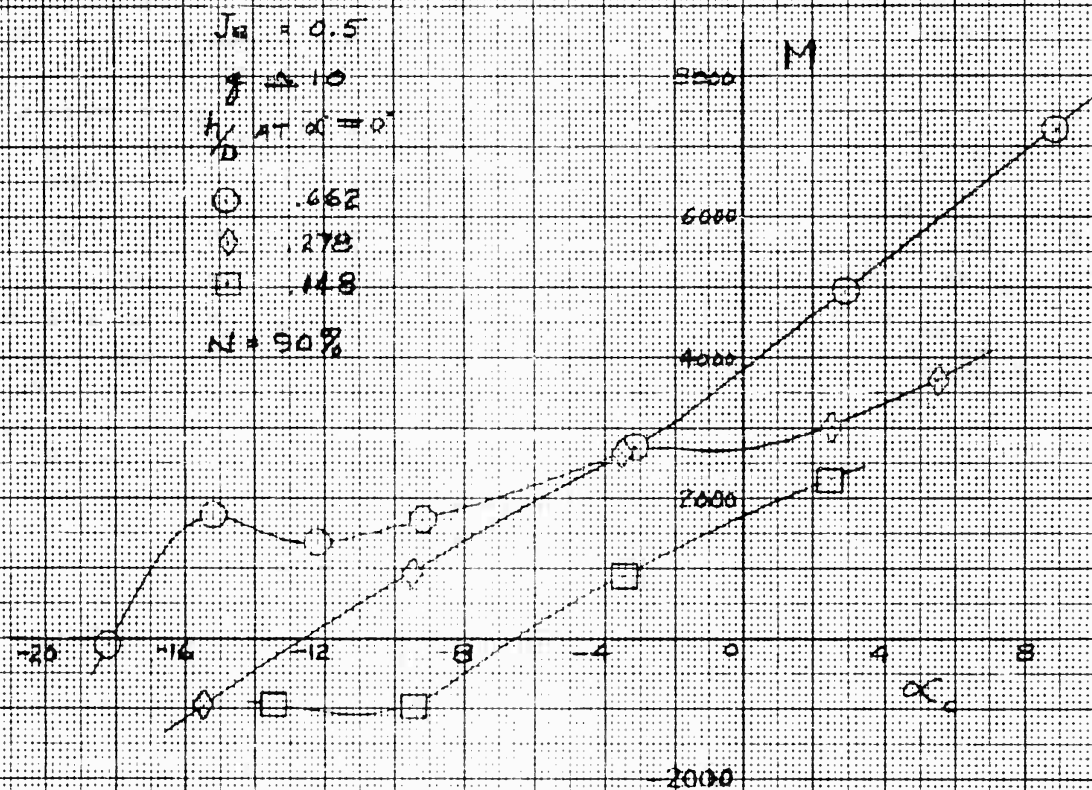
$$N \approx 90\%$$



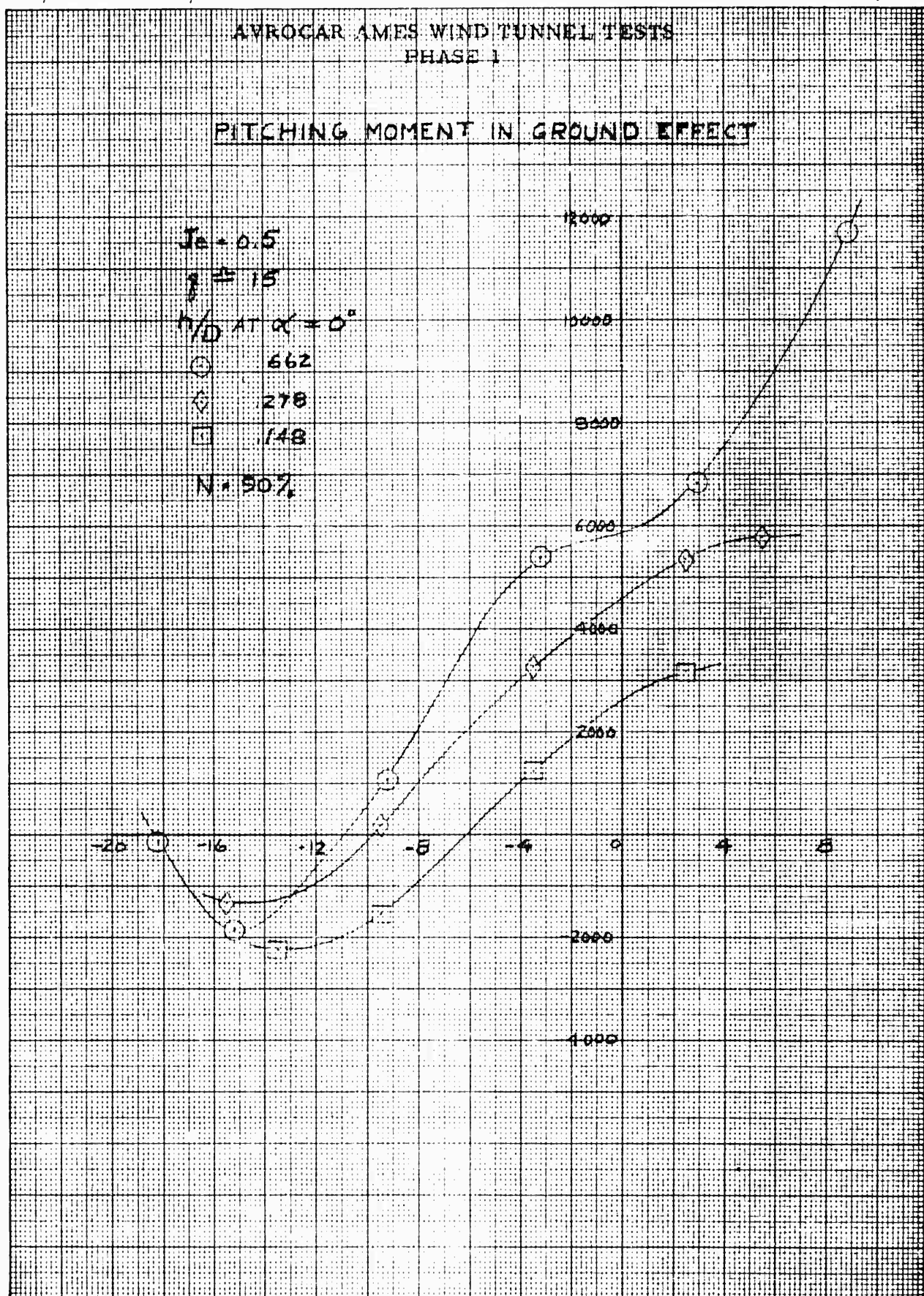
## AVROCAR AMES WIND TUNNEL TESTS

## PHASE 1

## PITCHING MOMENT IN GROUND EFFECT







## AVROCAR AMES WIND TUNNEL TESTS

## PHASE I

PITCHING MOMENT IN GROUND EFFECT

$$N = 90\%$$

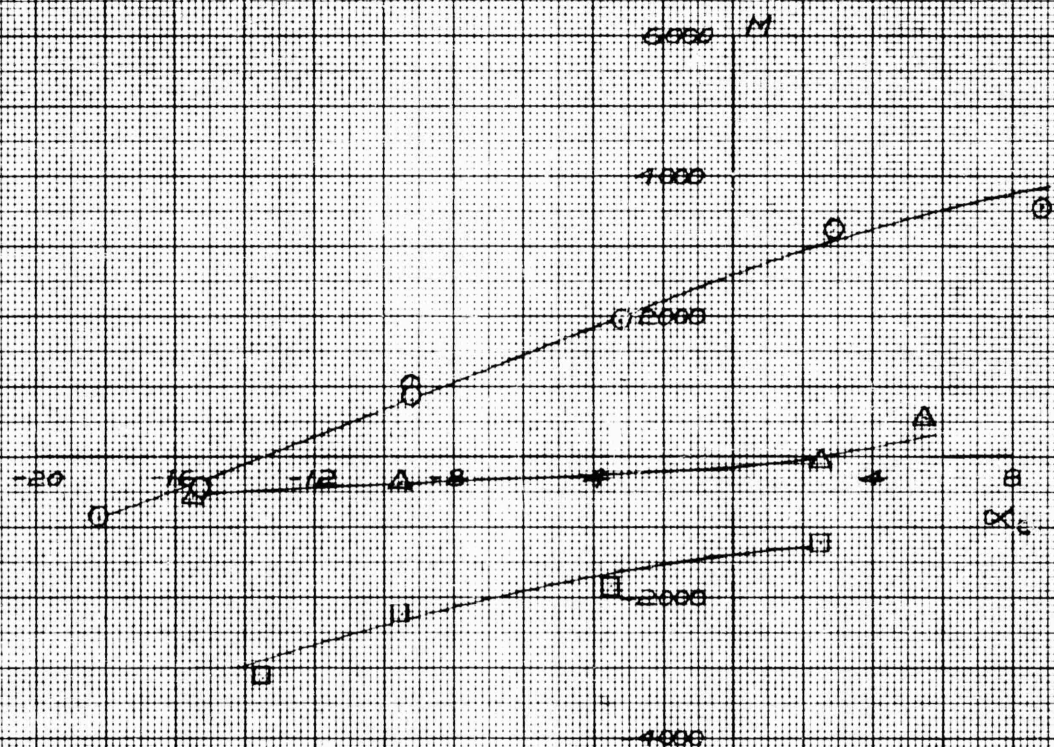
$$U_0 = 10$$

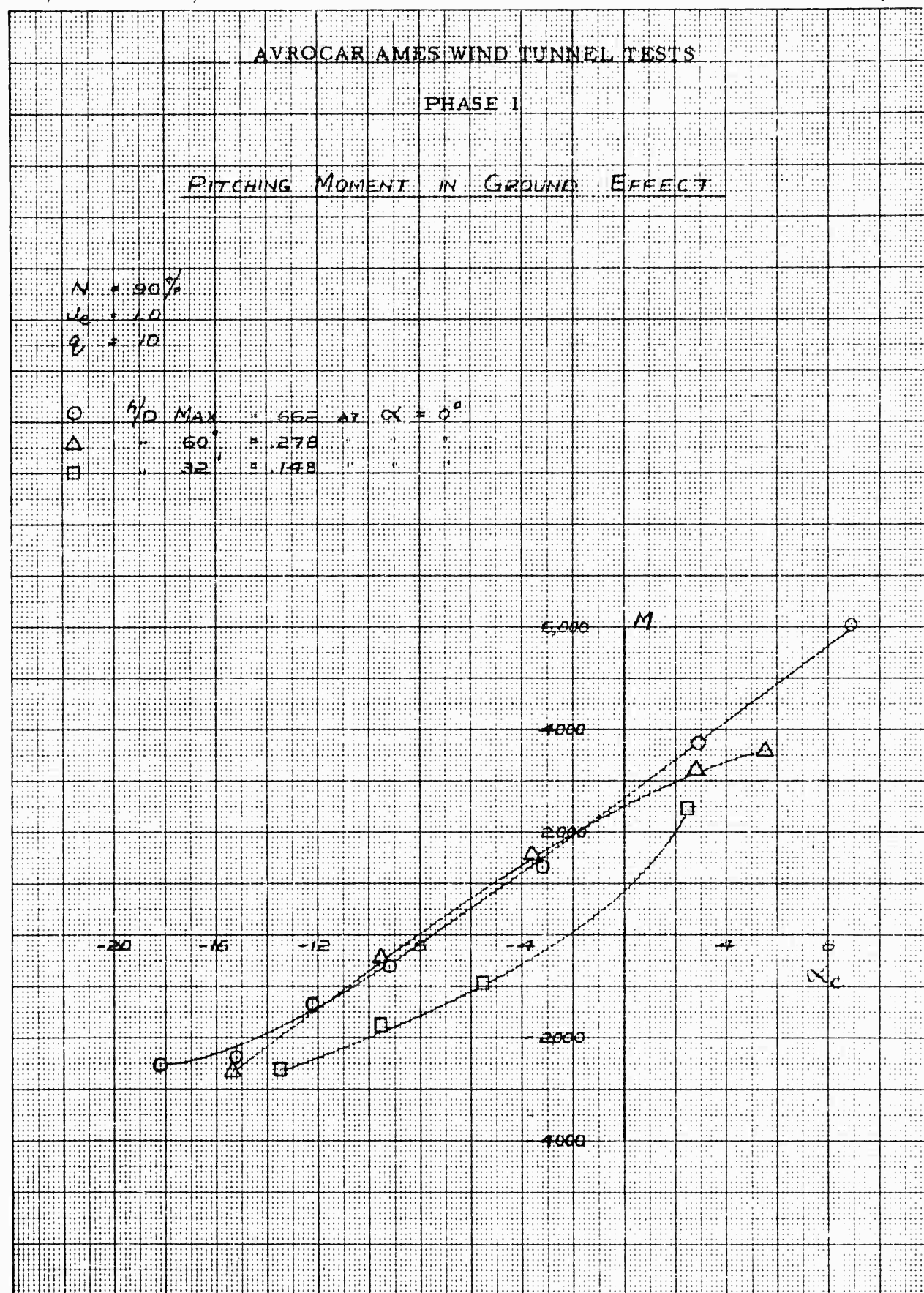
$$h = 5$$

$$C_{MD} \text{ MAX} = 552 \text{ AT } \alpha = 0^\circ$$

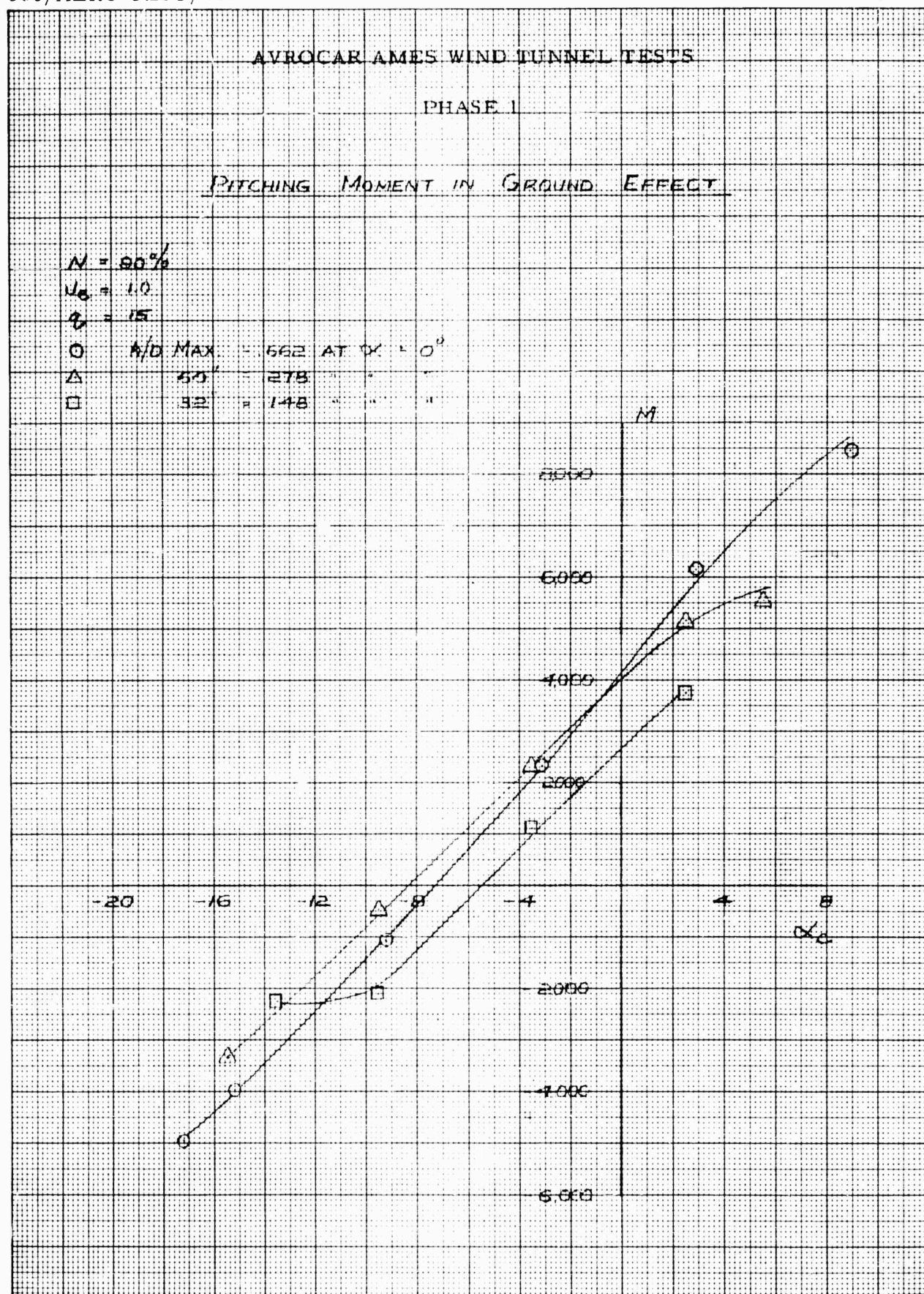
$$\Delta \quad 60^\circ = -278$$

$$\square \quad 32^\circ = -148$$



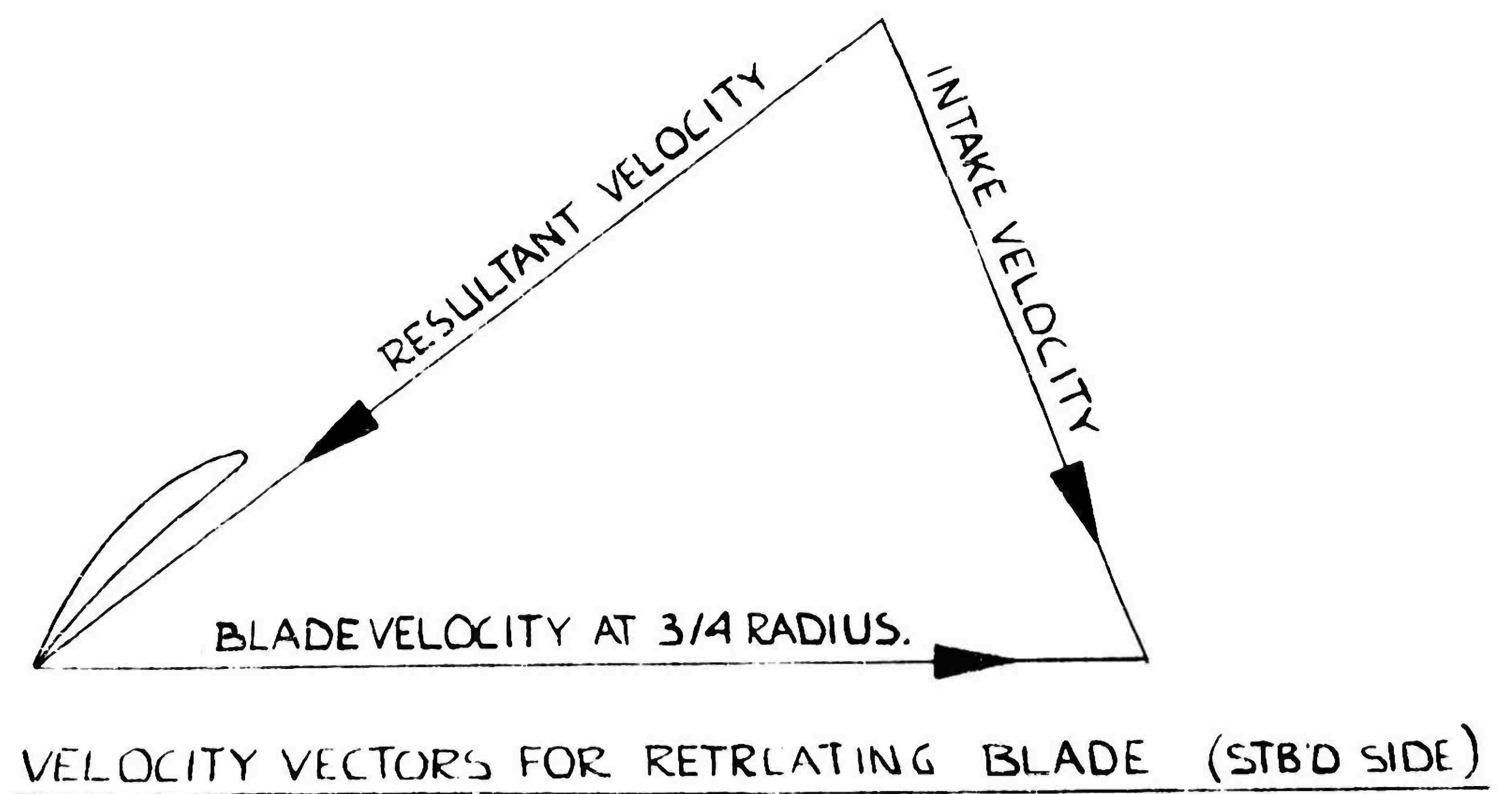
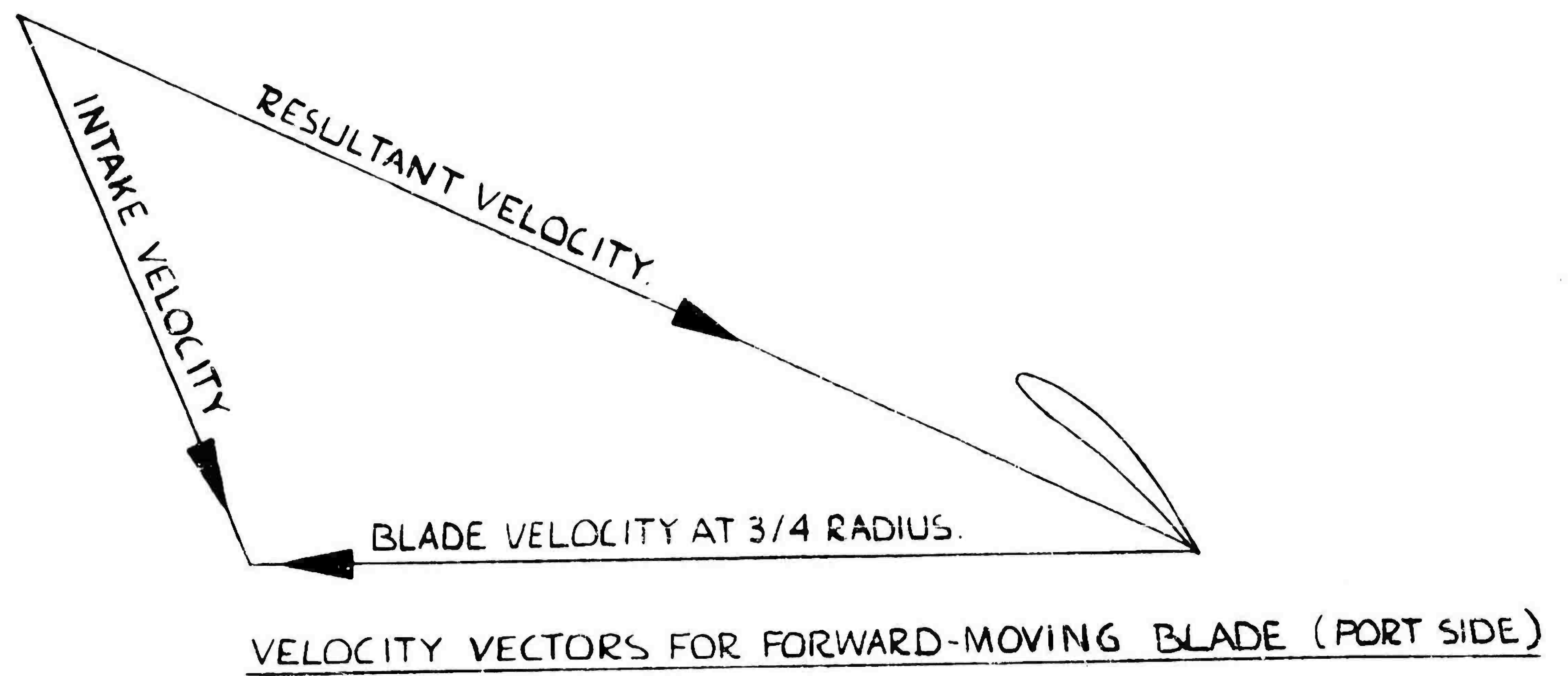




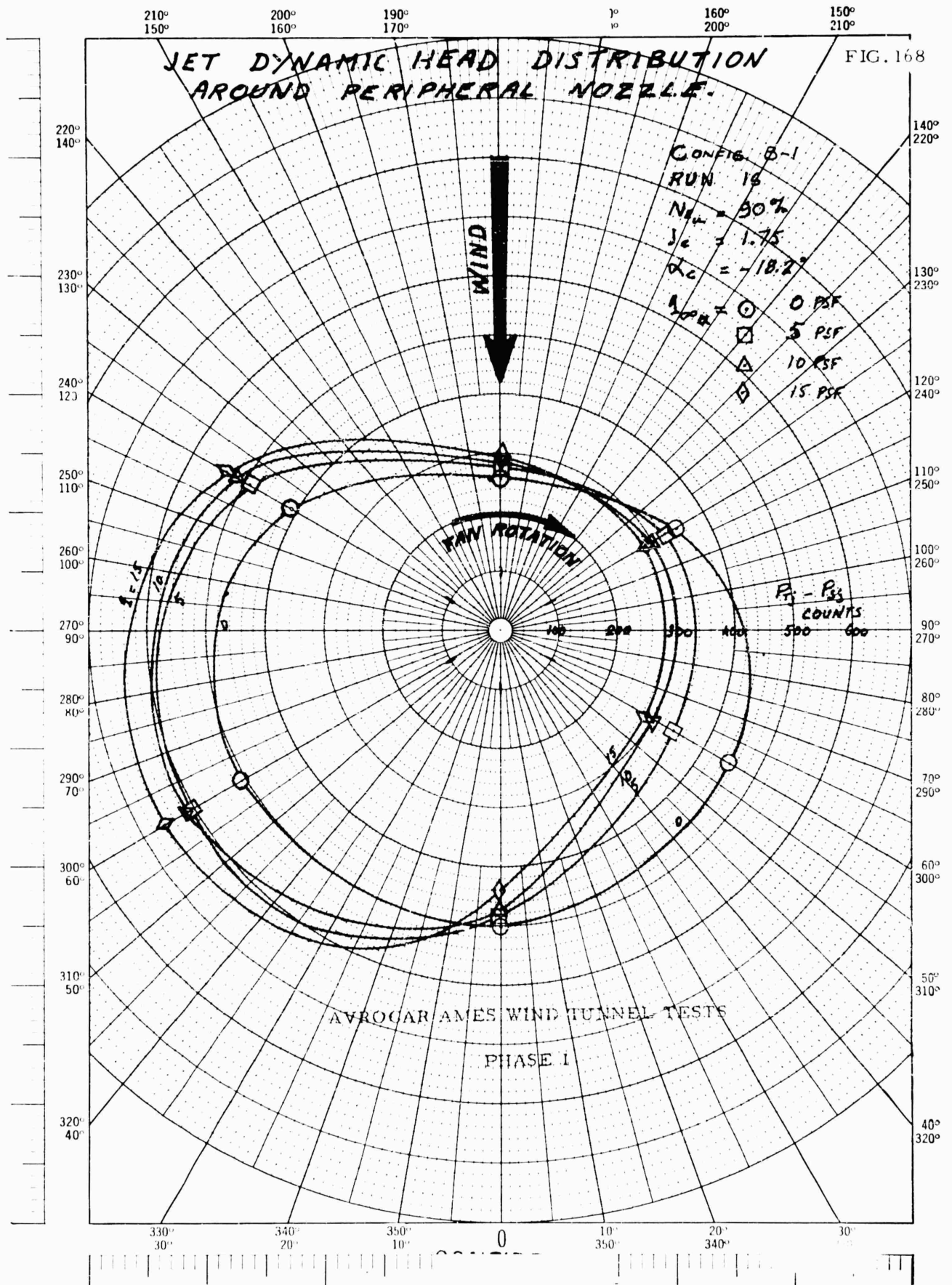


## AVROCAR AMES WIND TUNNEL TESTS

## PHASE 1



TYPICAL EFFECT OF AIRCRAFT FORWARD SPEED ON FAN BLADE  
VELOCITY VECTORS





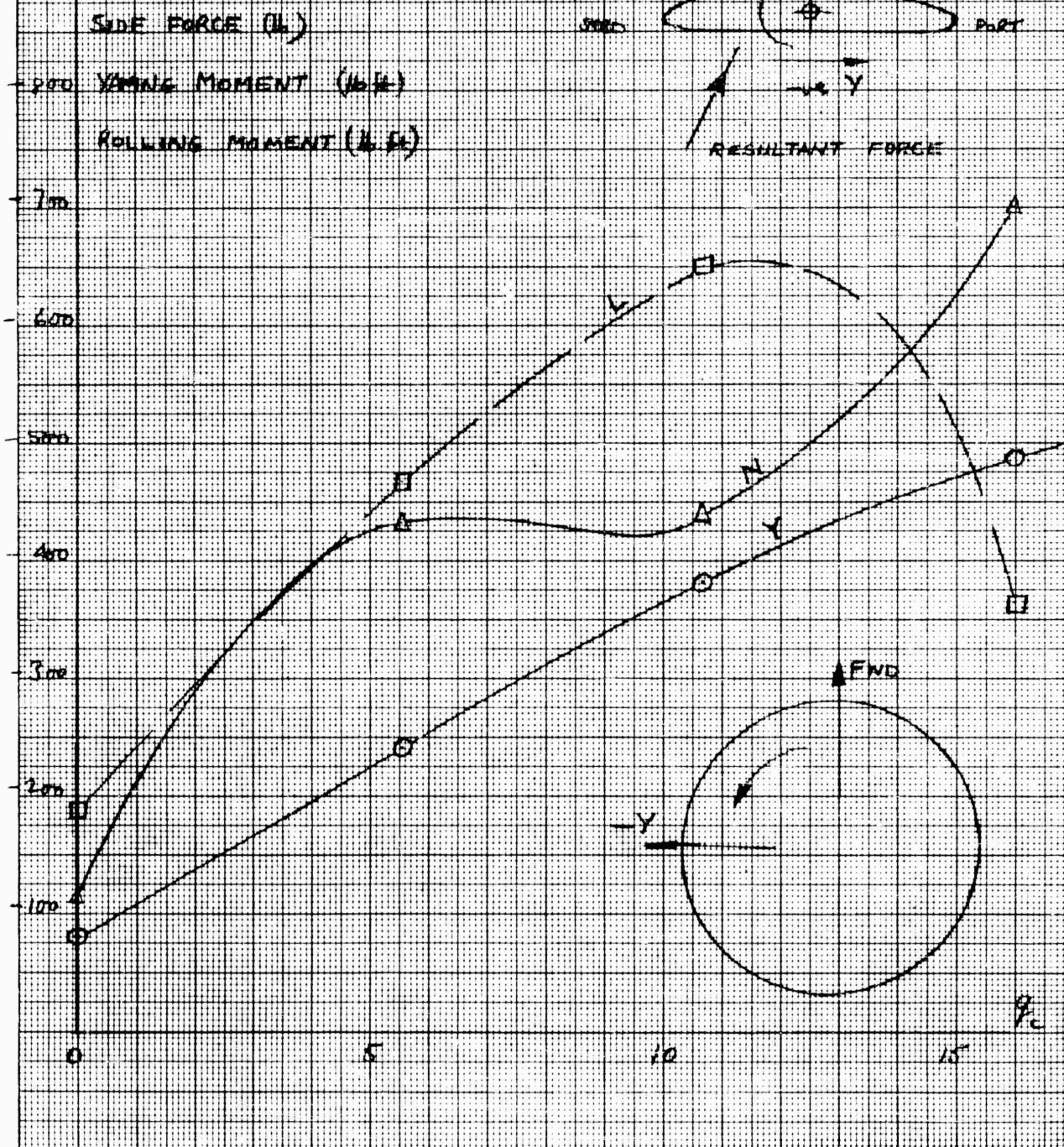
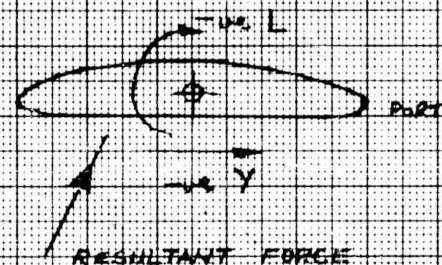
# AVROCAR AMES WIND TUNNEL TESTS PHASE 1

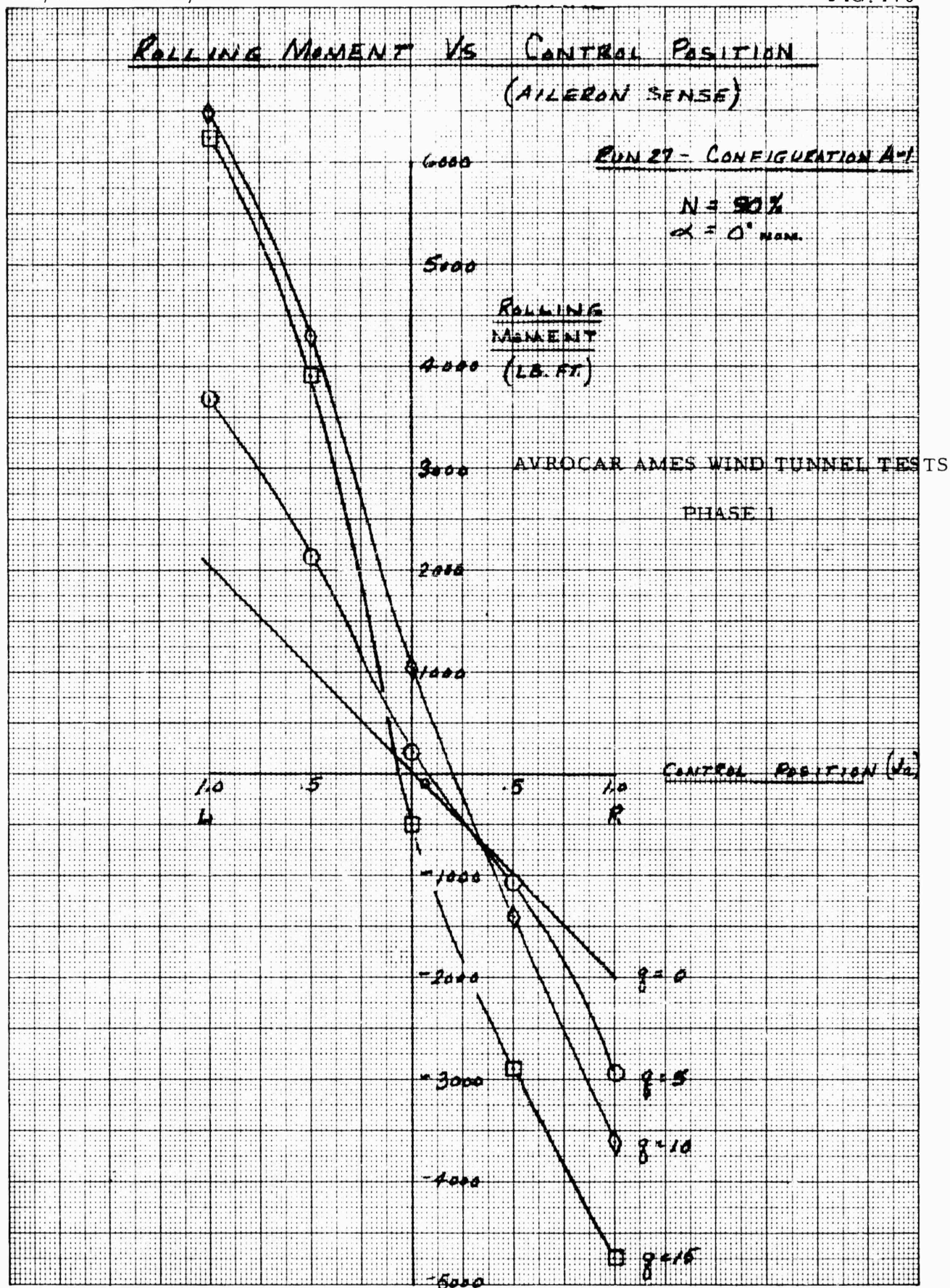
SIDE FORCE  
 YAWING MOMENT  
 ROLLING MOMENT

} VS FORWARD SPEED

RUN # 16,  $J_E = 1.75$   
 CONFIG. B-1,  $\alpha_c = -18.2^\circ$   
 $N = 90\%$

VIEW ON FRONT END

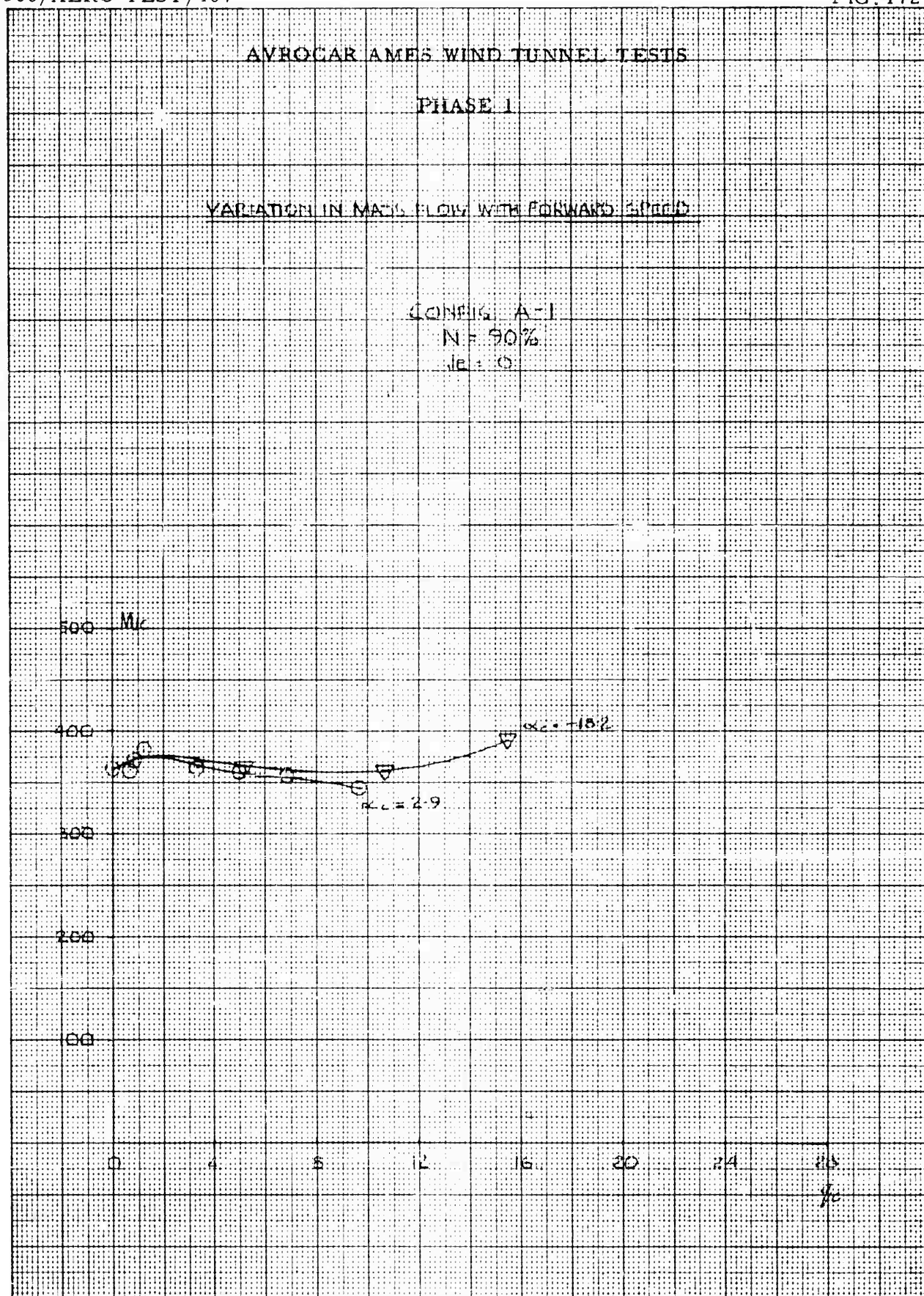












## AVROCAR AMES WIND TUNNEL TESTS

## PHASE I

## VARIATION OF MASS FLOW WITH FORWARD SPEED

CONFIG A-1

N = 70%

 $\lambda_e = 0.5$ 500  $M_1 =$ 

400

300

200

100

0

4

8

12

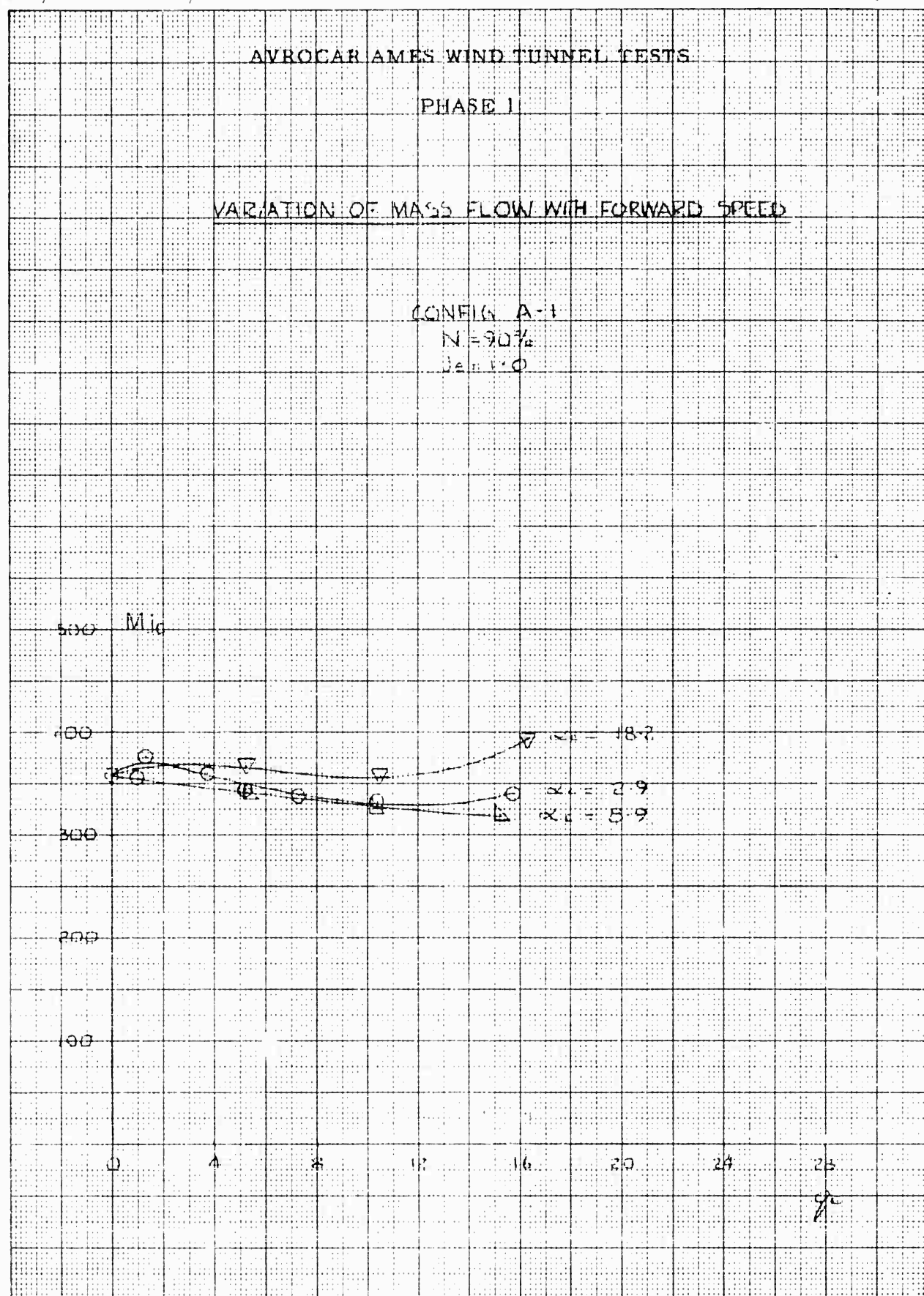
16

20

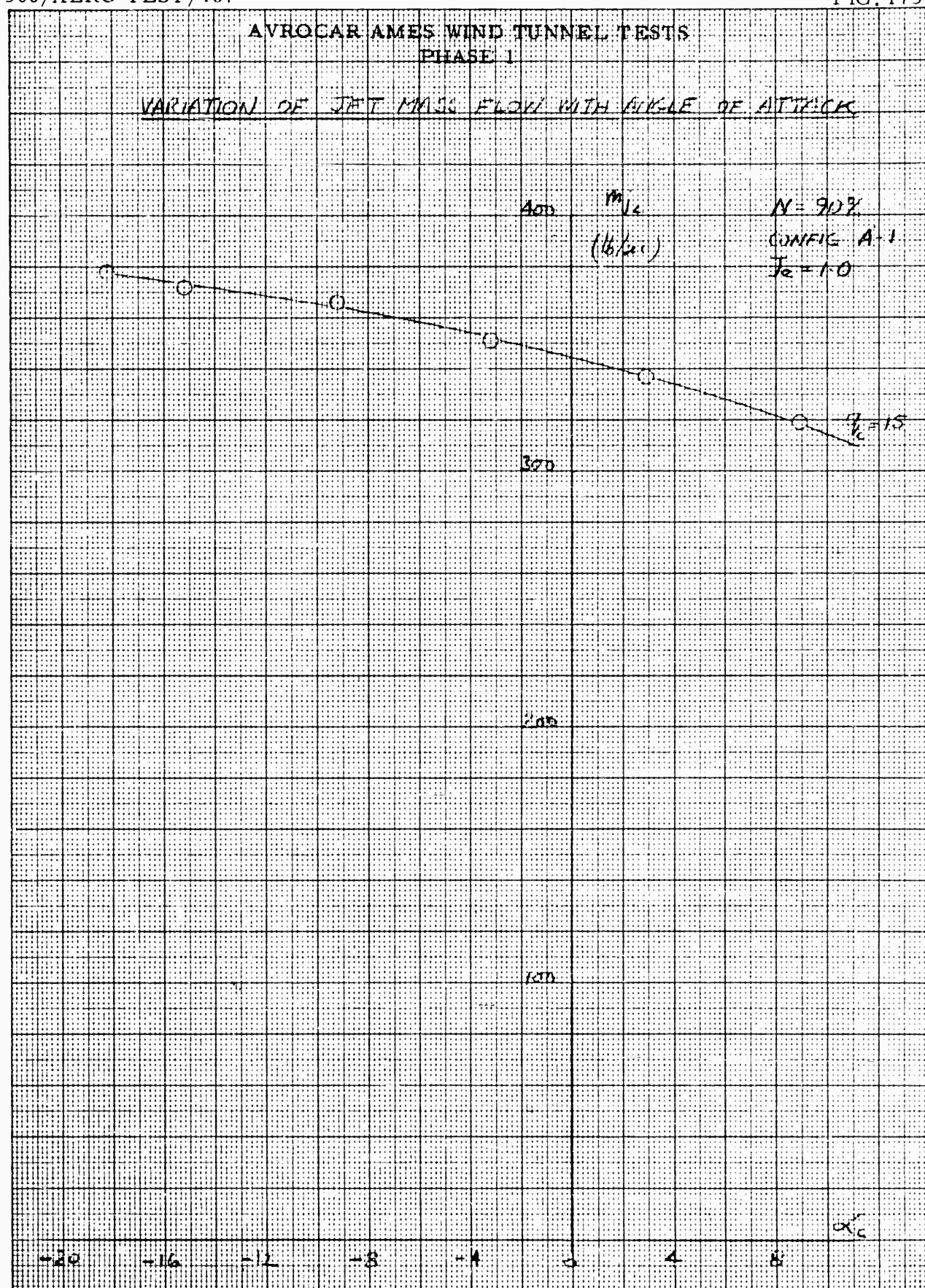
24

28

 $\phi$  $R_{\infty} = 18.2$  $R_{\infty} = 2.9$  $R_{\infty} = 3.9$





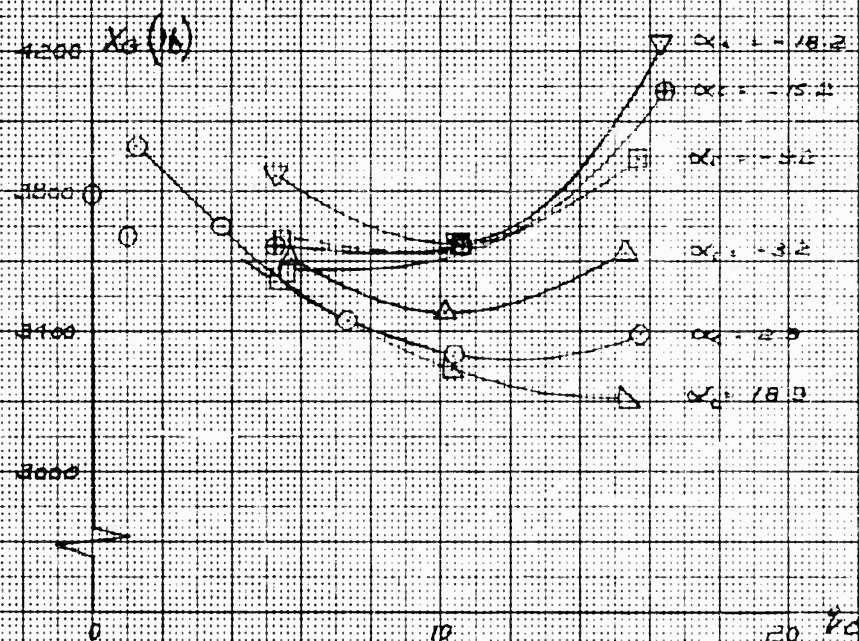


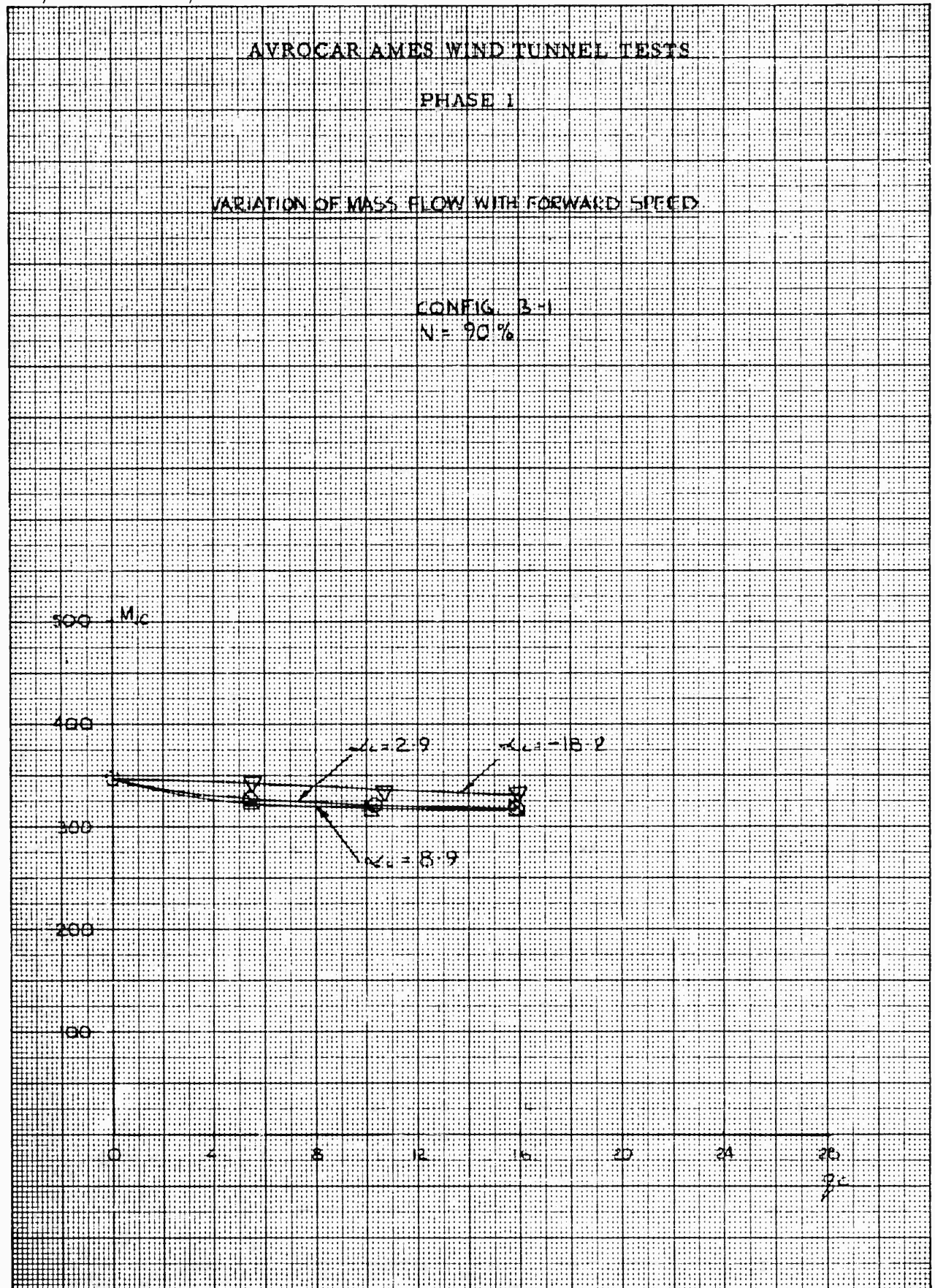
## AYROCAR AMES WIND TUNNEL TESTS

PHASE I

VARIATION OF GROSS THRUST WITH FORWARD SPEED

CONFIG. A-1

 $N = 90\%$  $T_e = 1.0$ 



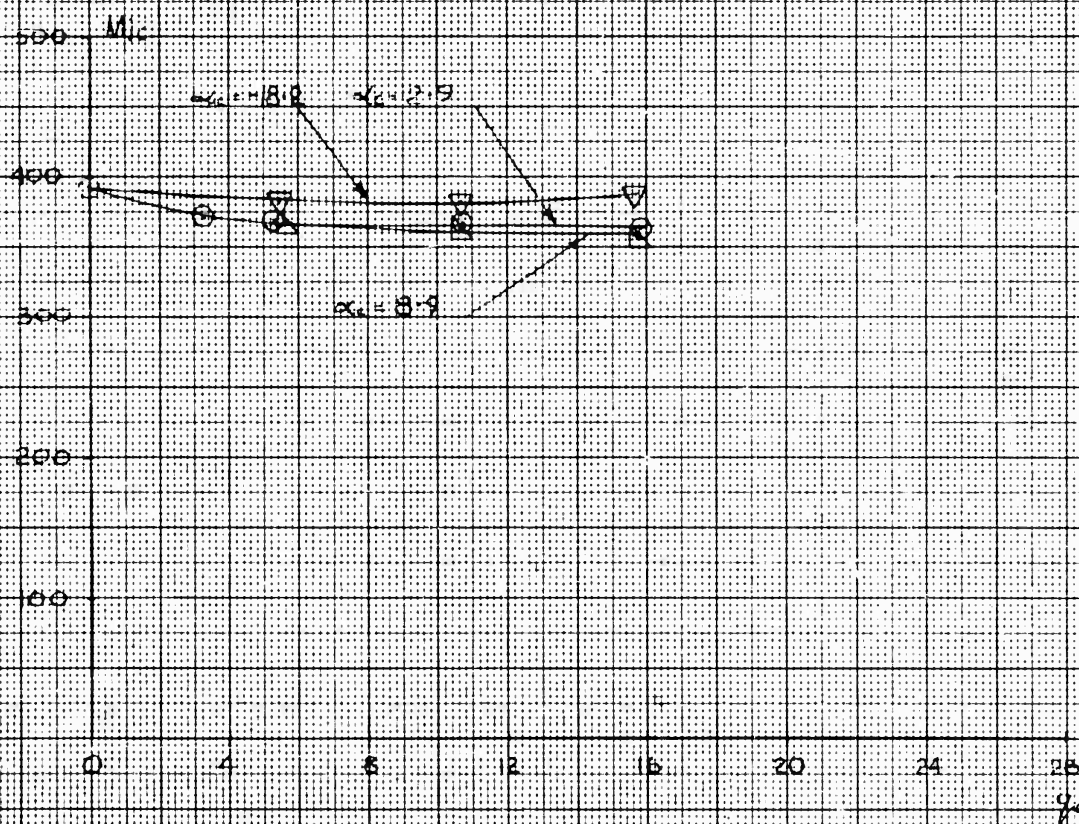


## AVROCAR AMES WIND TUNNEL TESTS

## PHASE I

## VARIATION OF MASS FLOW WITH FORWARD SPEED

CONFIG C-1  
N=90%



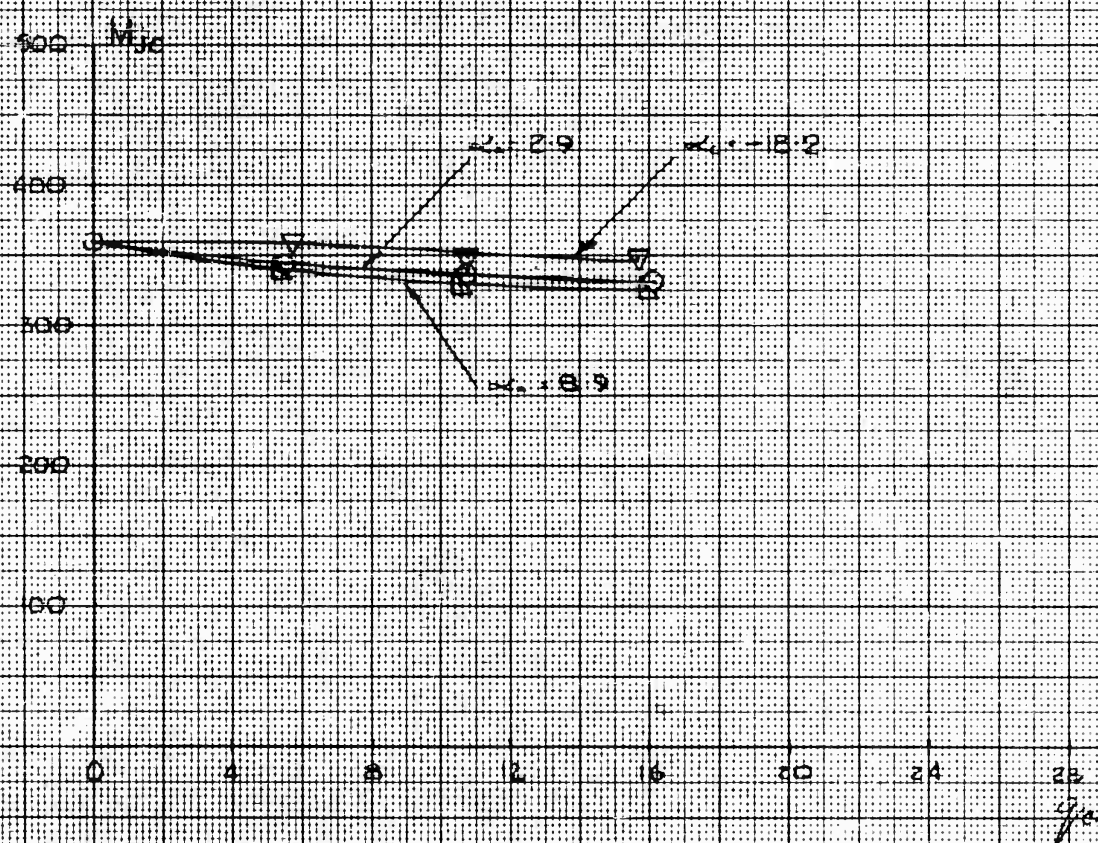
## AVROCAR AMES WIND TUNNEL TESTS

## PHASE I

VARIATION OF MASS FLOW WITH FORWARD SPEED

(ONEIG. D=1

N=90%





## AVROCAR AMES WIND TUNNEL TESTS

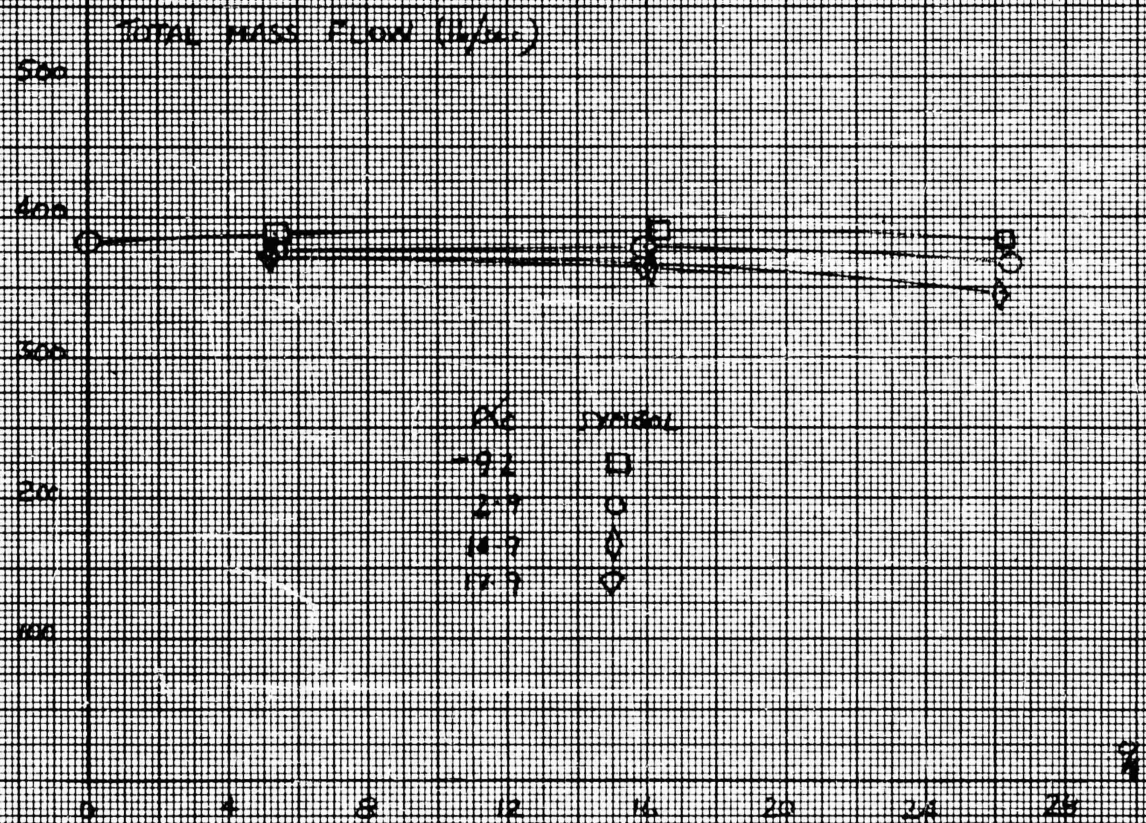
## PHASE 1

## VARIATION OF MASS FLOW WITH FORWARD SPEED

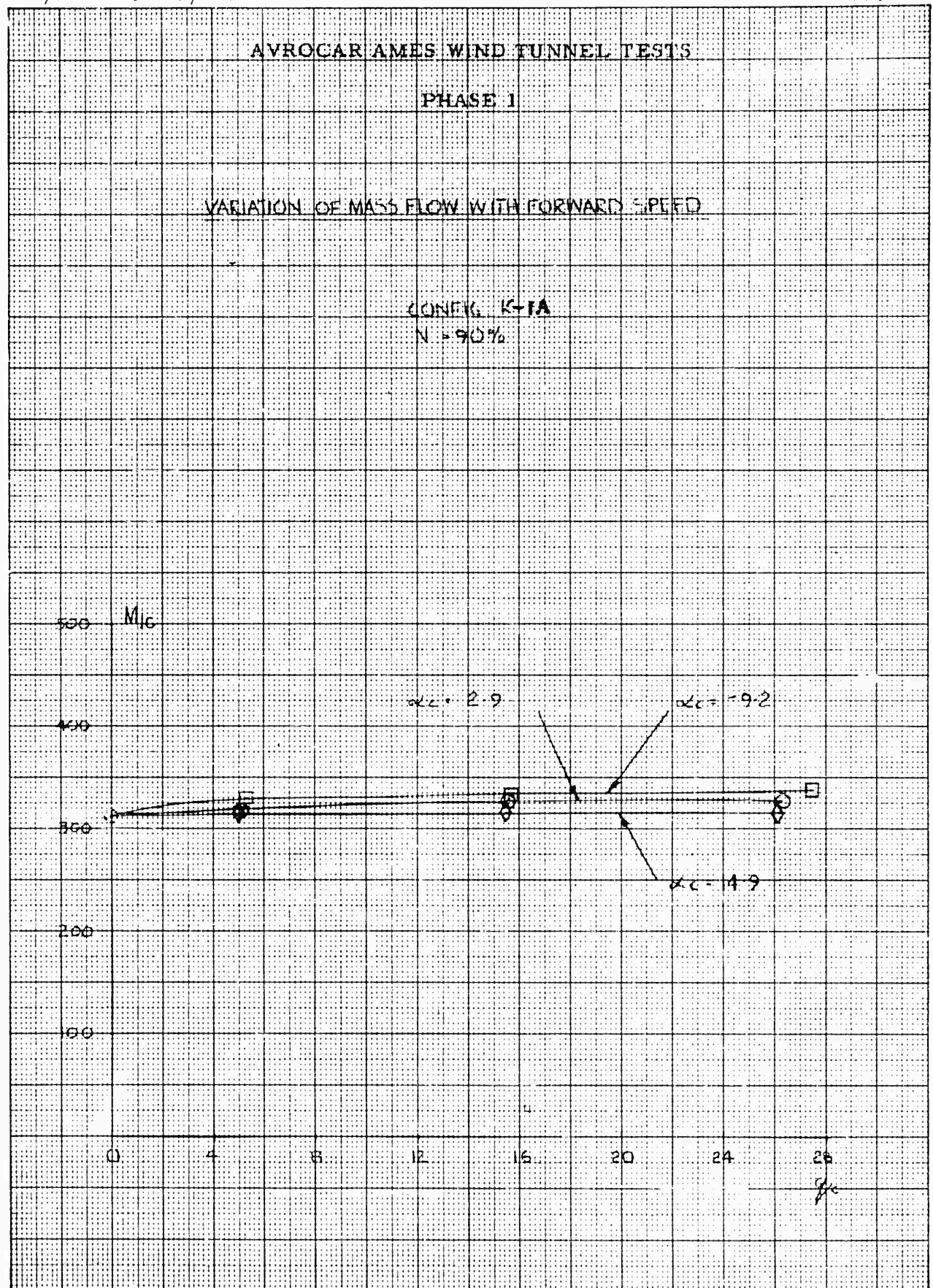
RUN # 32

CONFIG J-1

N = 90%







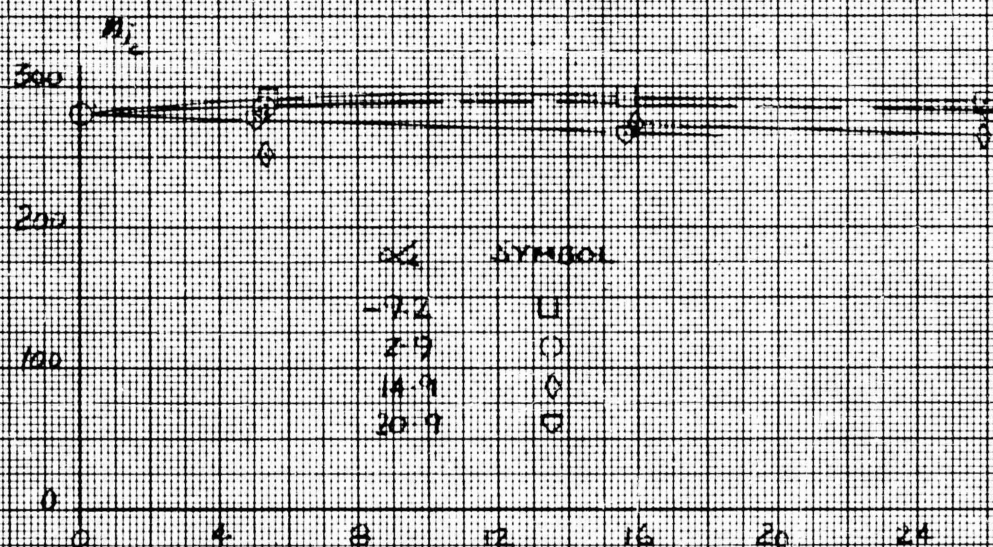
## AVROCAR AMES WIND TUNNEL TESTS

## PHASE 1

## VARIATION OF MASS FLOW WITH FORWARD SPEED

RUN # 38

CONFIG A-1

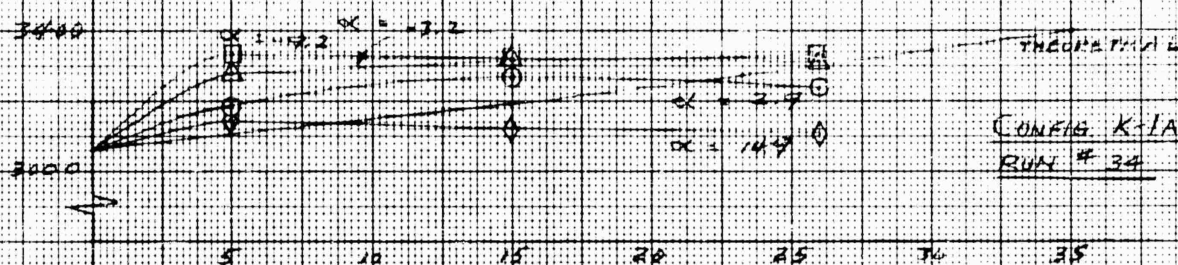
 $M = 2.1\%$ 



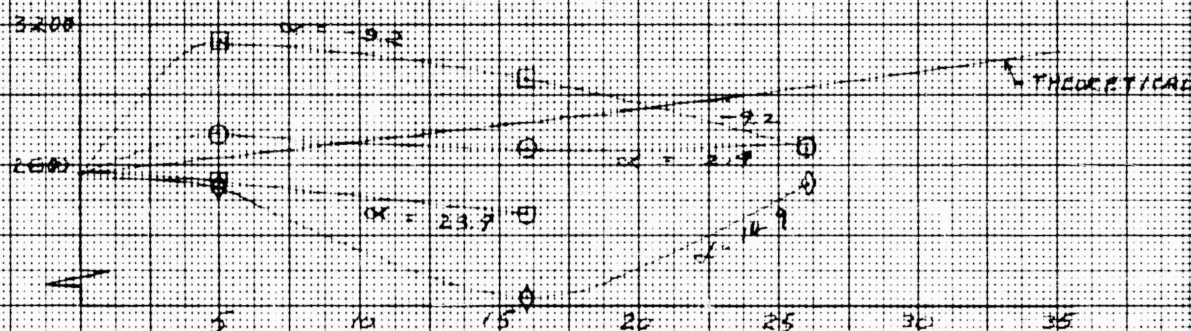
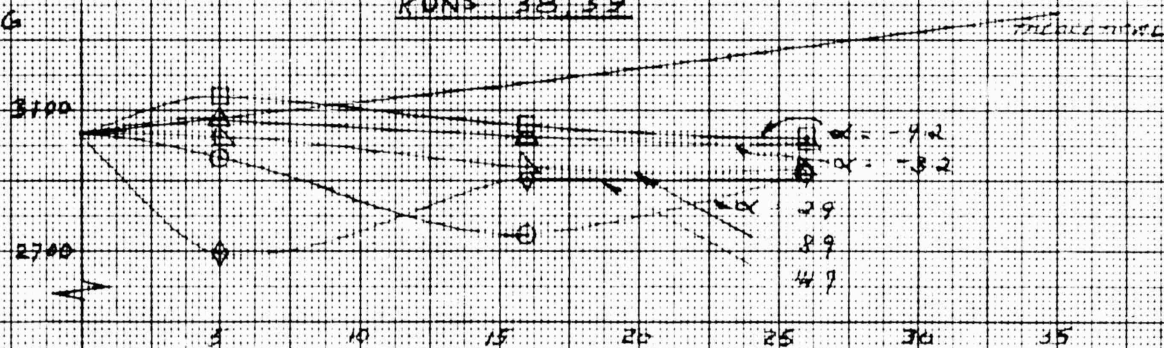
# AVROCAR AMES WIND TUNNEL TESTS PHASE 1

 $X_G$ 

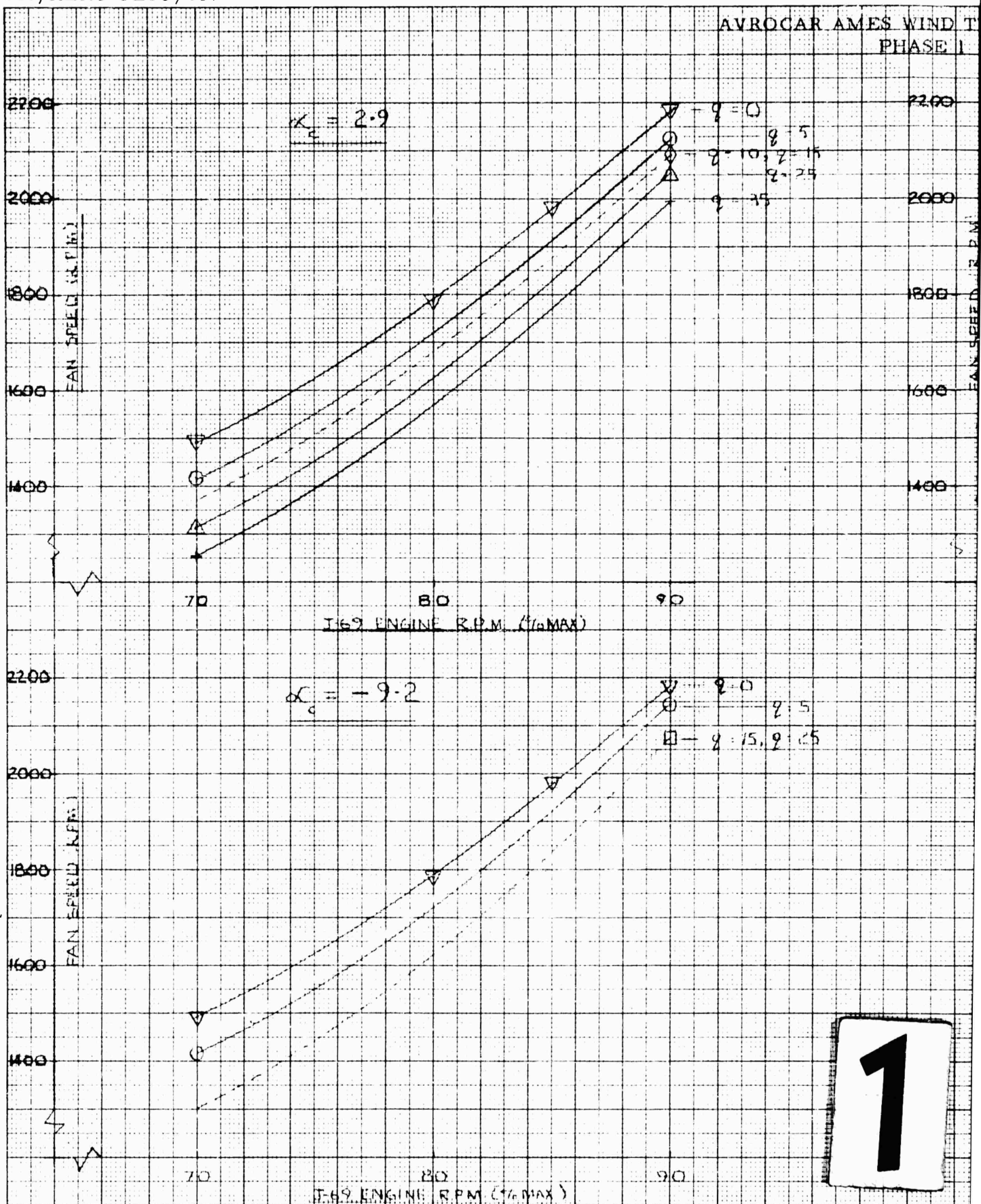
VARIATION OF GROSS THRUST WITH FORWARD SPEED

 $X_G$ 

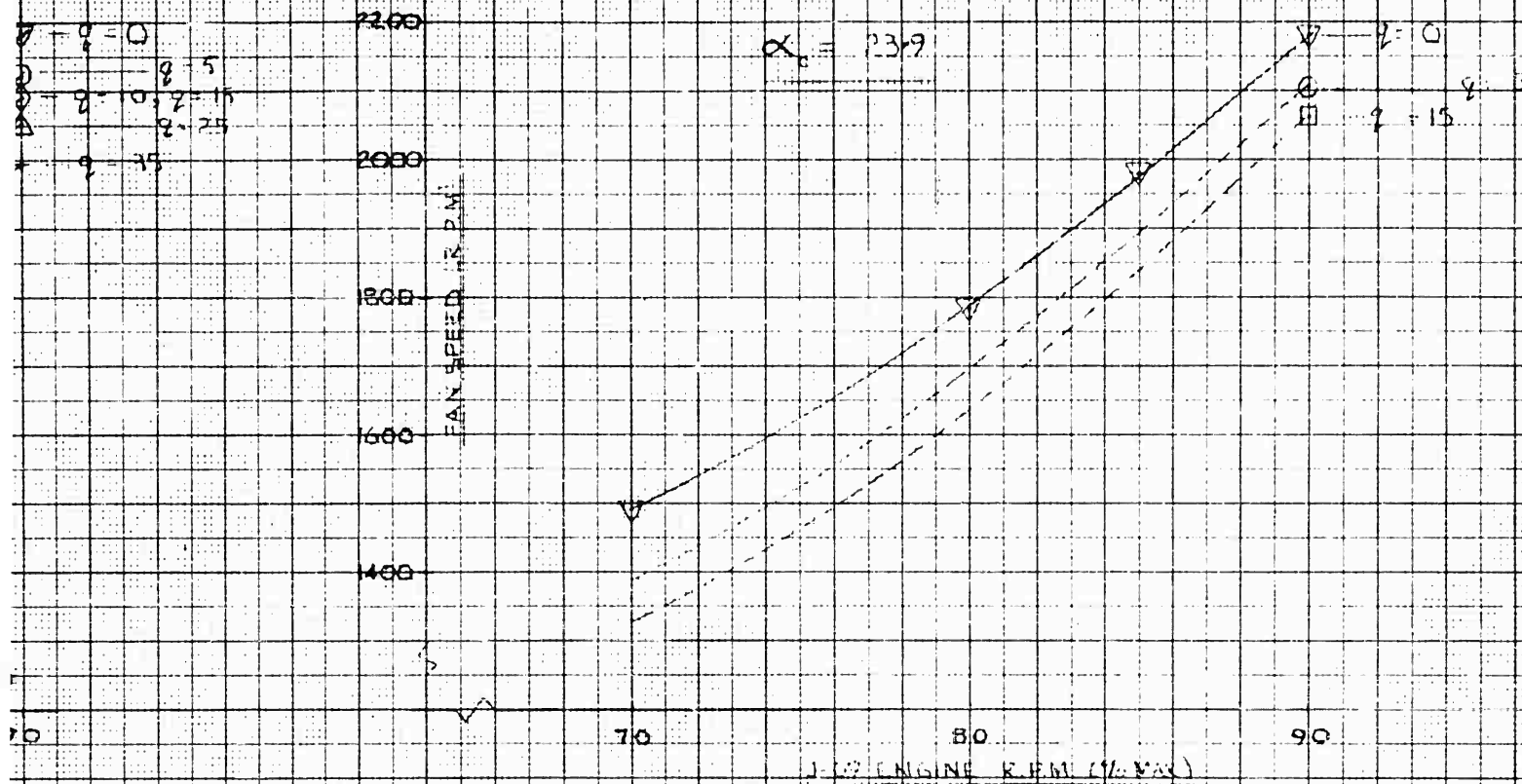
RUN 43 CONFIG T-1

 $X_G$ CONFIG N-1A  
RUNS 38, 39





# AVROCAR AMES WIND TUNNEL TESTS PHASE I



$\nabla$  -  $q = 0$   
 $\circ$  -  $q = 10, z = 15$   
 $\Delta$  -  $q = 15, z = 25$   
 $\square$  -  $q = 15, z = 15$

FAN RPM VS ENGINE % MAX RPM

CONFIGURATION - Q-1  
 RUNS - 41, 44

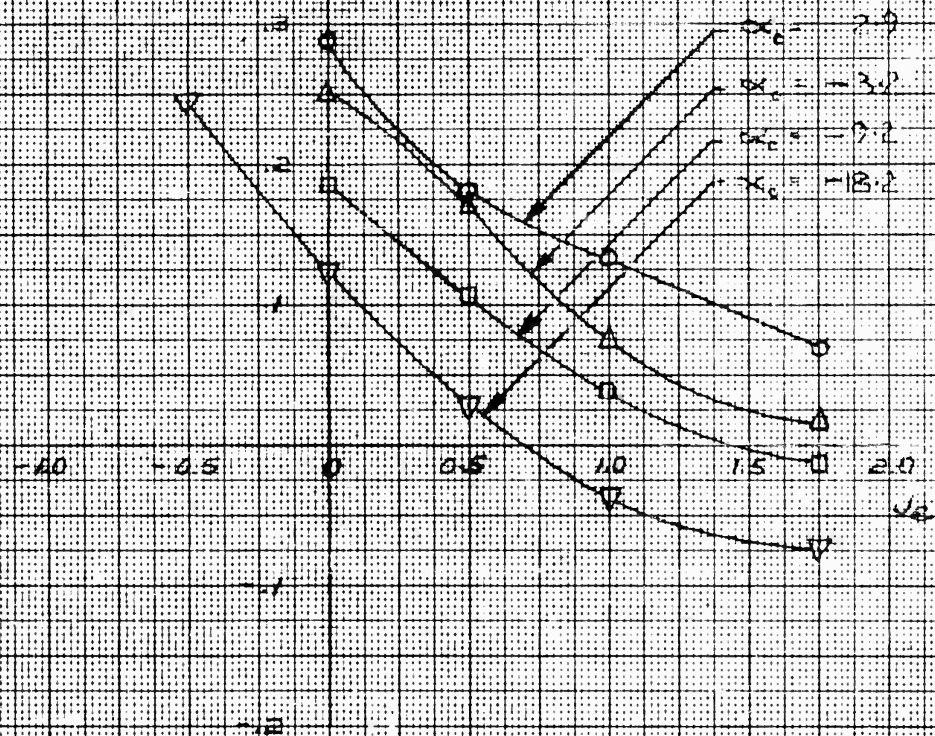
2

## AVROCAR AMES WIND TUNNEL TESTS

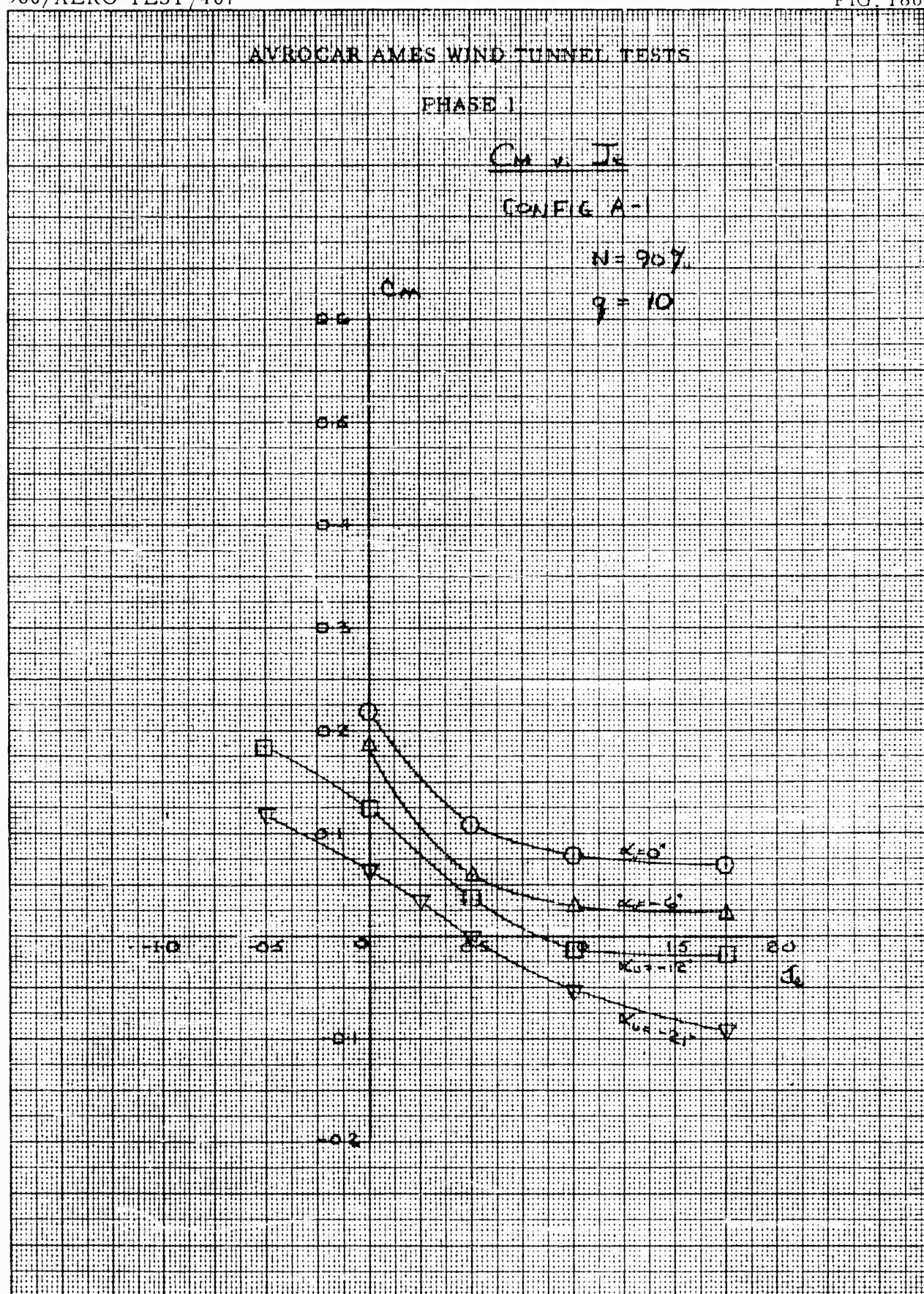
PHASE I

 $C_m$  vs  $J_e$ 

CONFIG A-1

 $N = 90\%$  $C_m$   $q = 5$ 



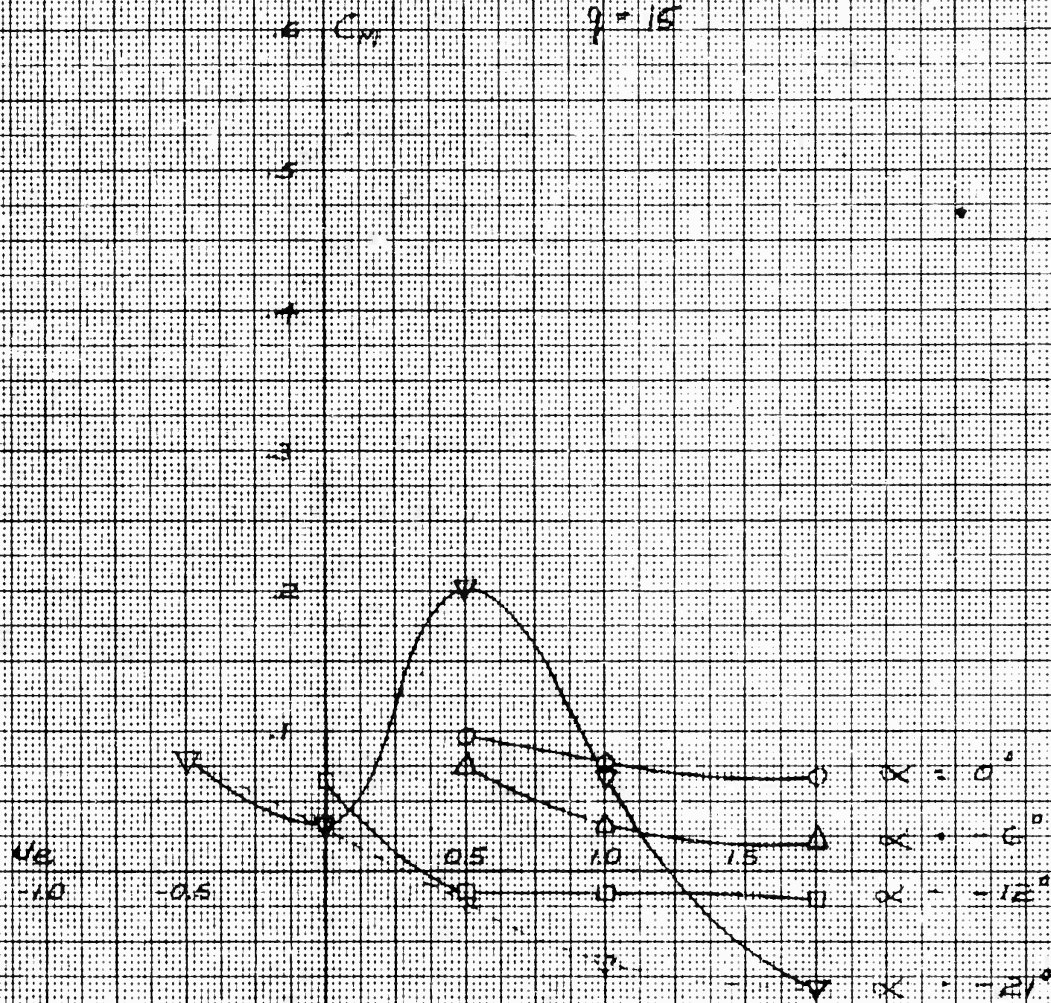


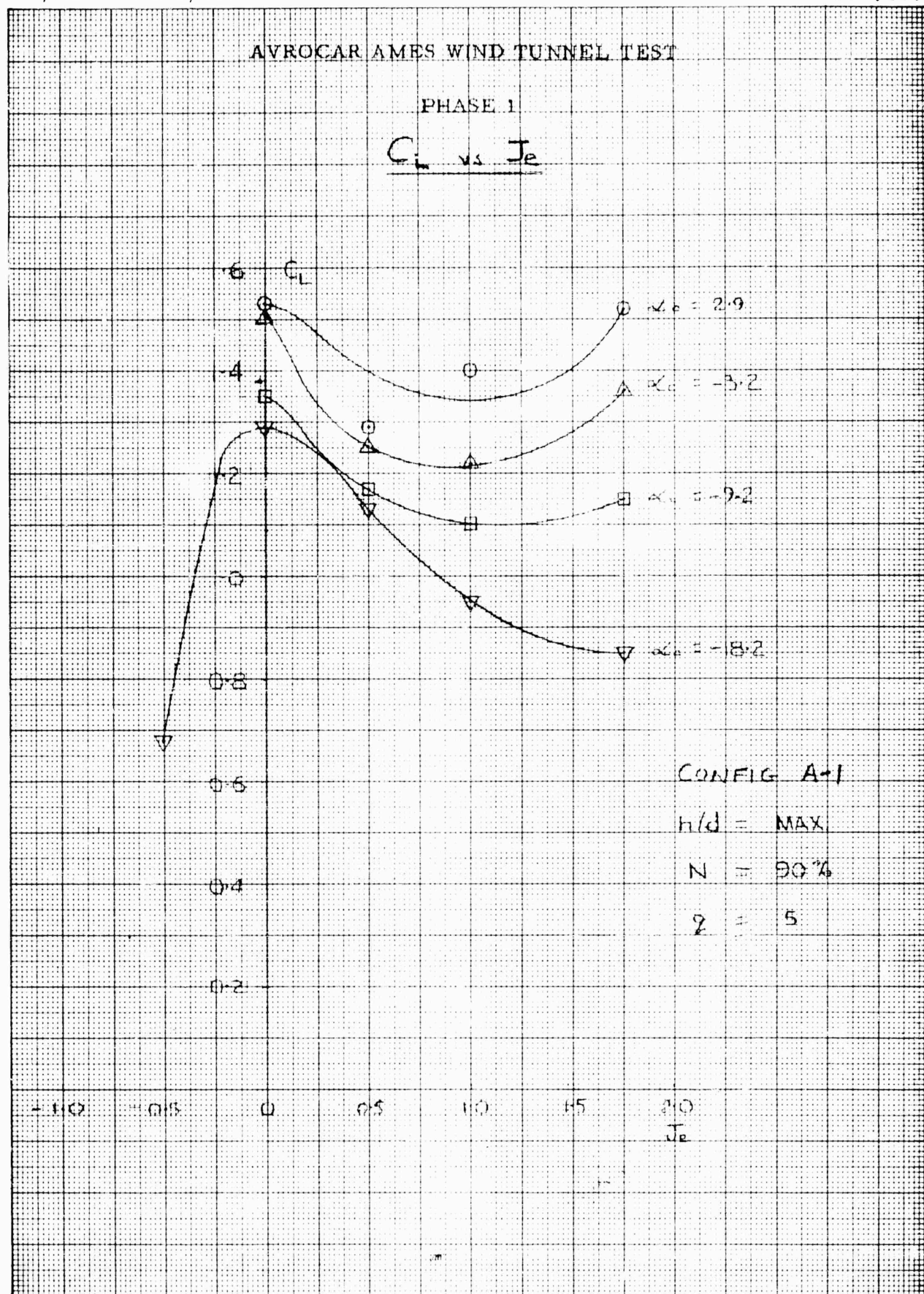
## AVROCAR AMES WIND TUNNEL TESTS

PHASE I

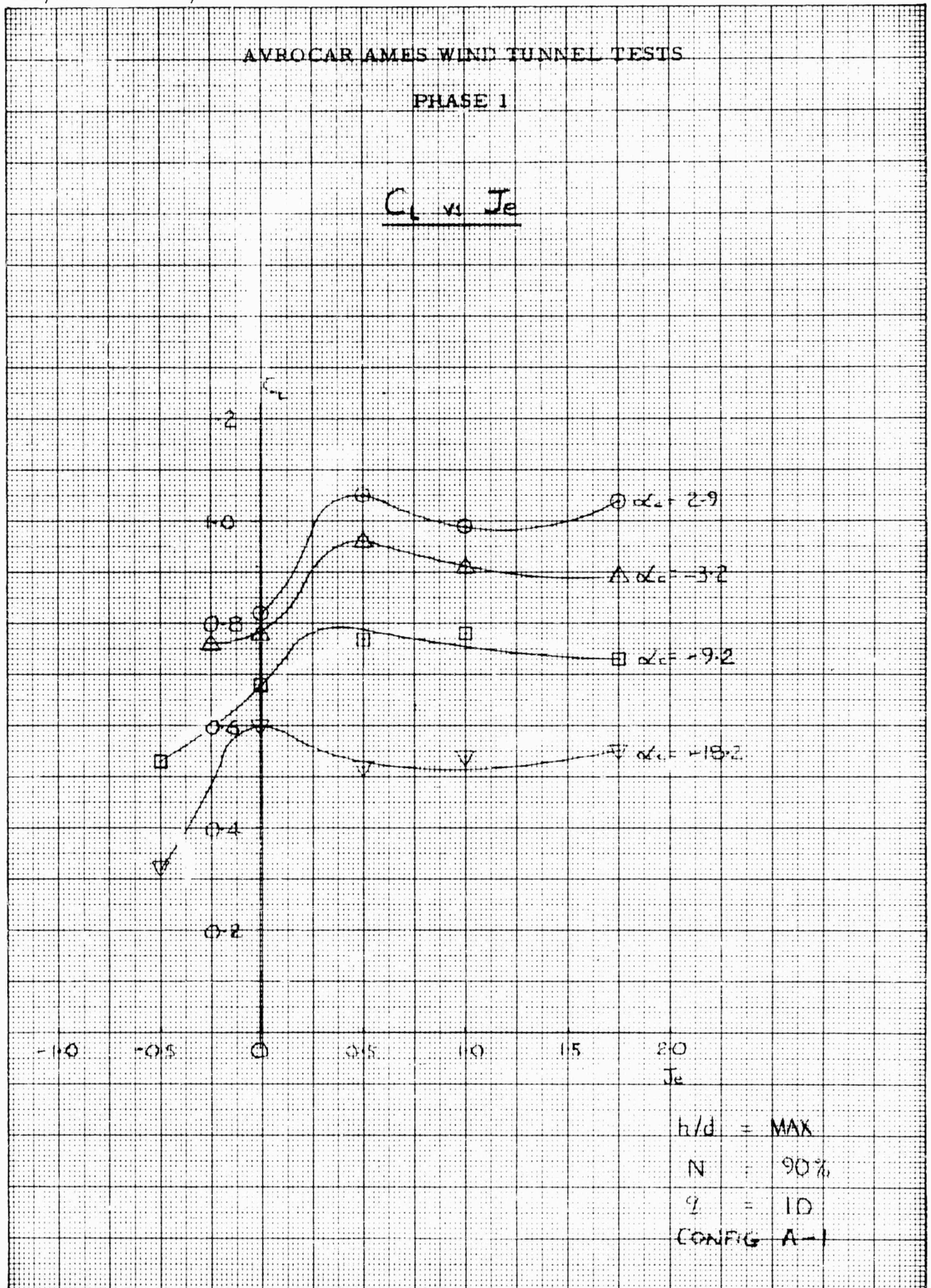
 $C_m$  vs  $J_e$ 

CONFIG A-1

 $N = 90^\circ$  $\eta = 15^\circ$ 

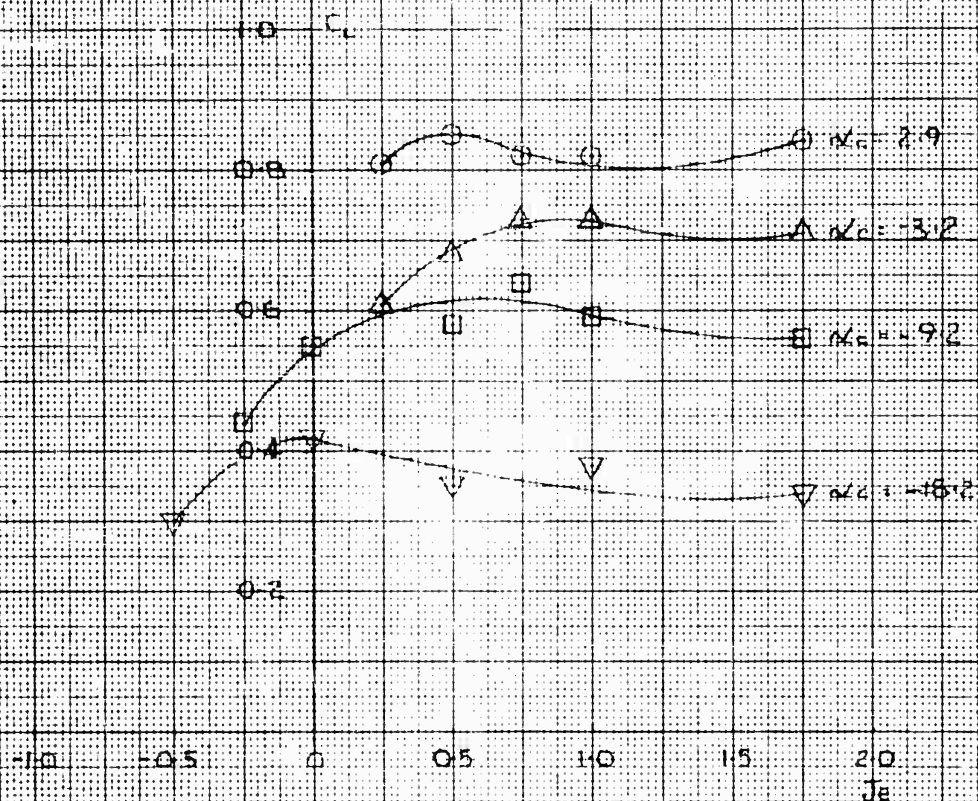






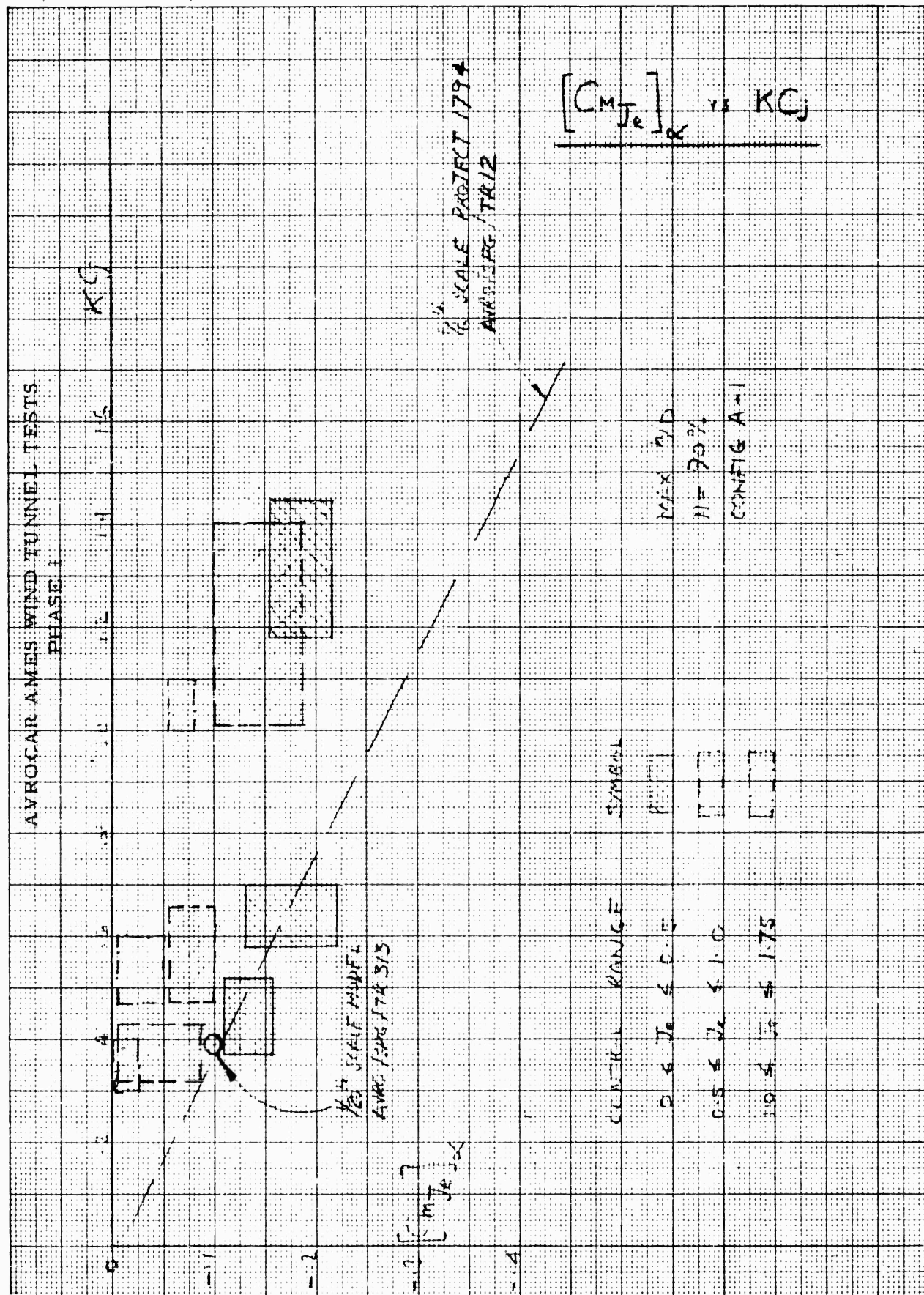
## AVROCAR AMES WIND TUNNEL TESTS

PHASE 1

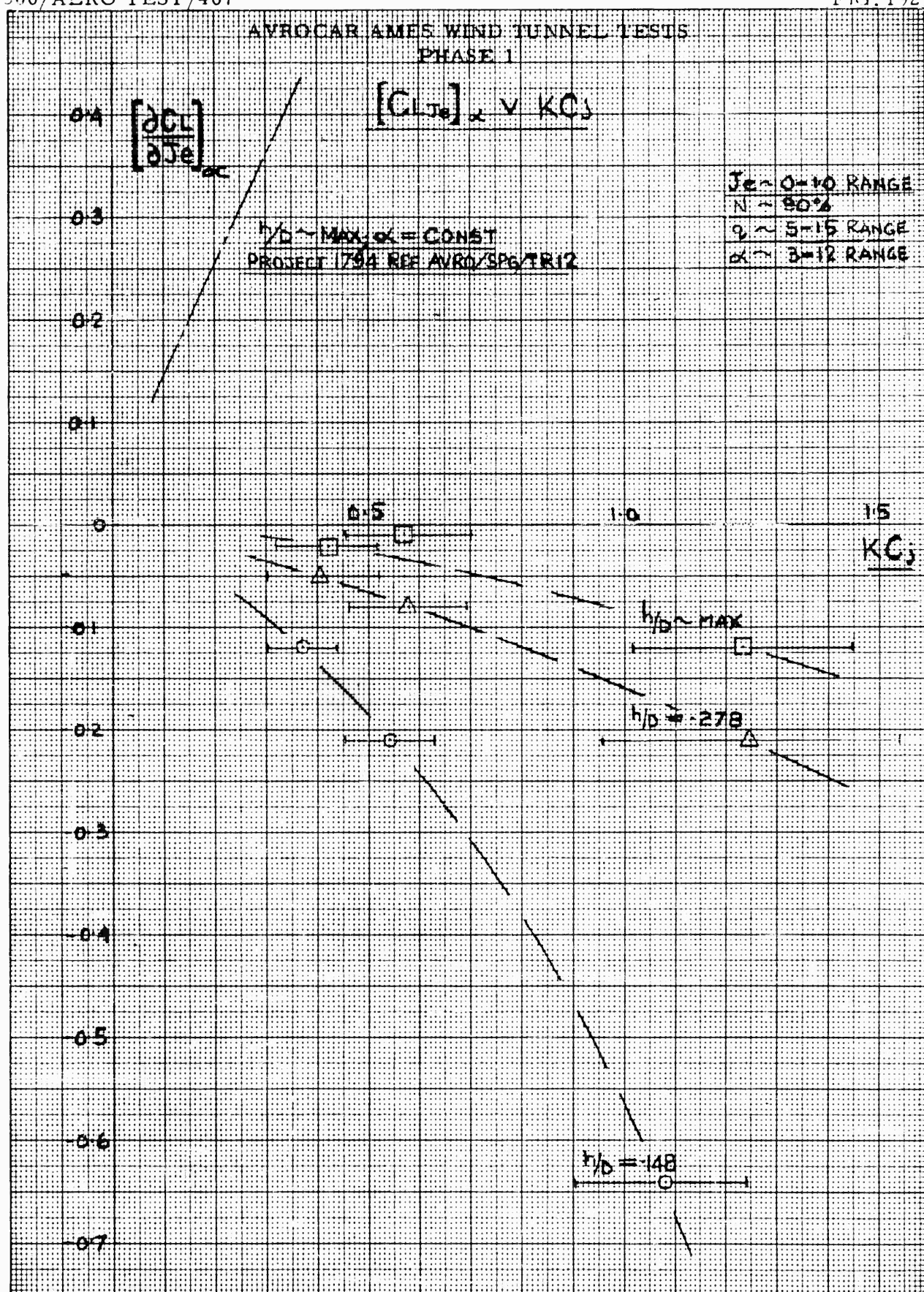
 $C_L$  vs  $J_E$ 

CONFIG A-1

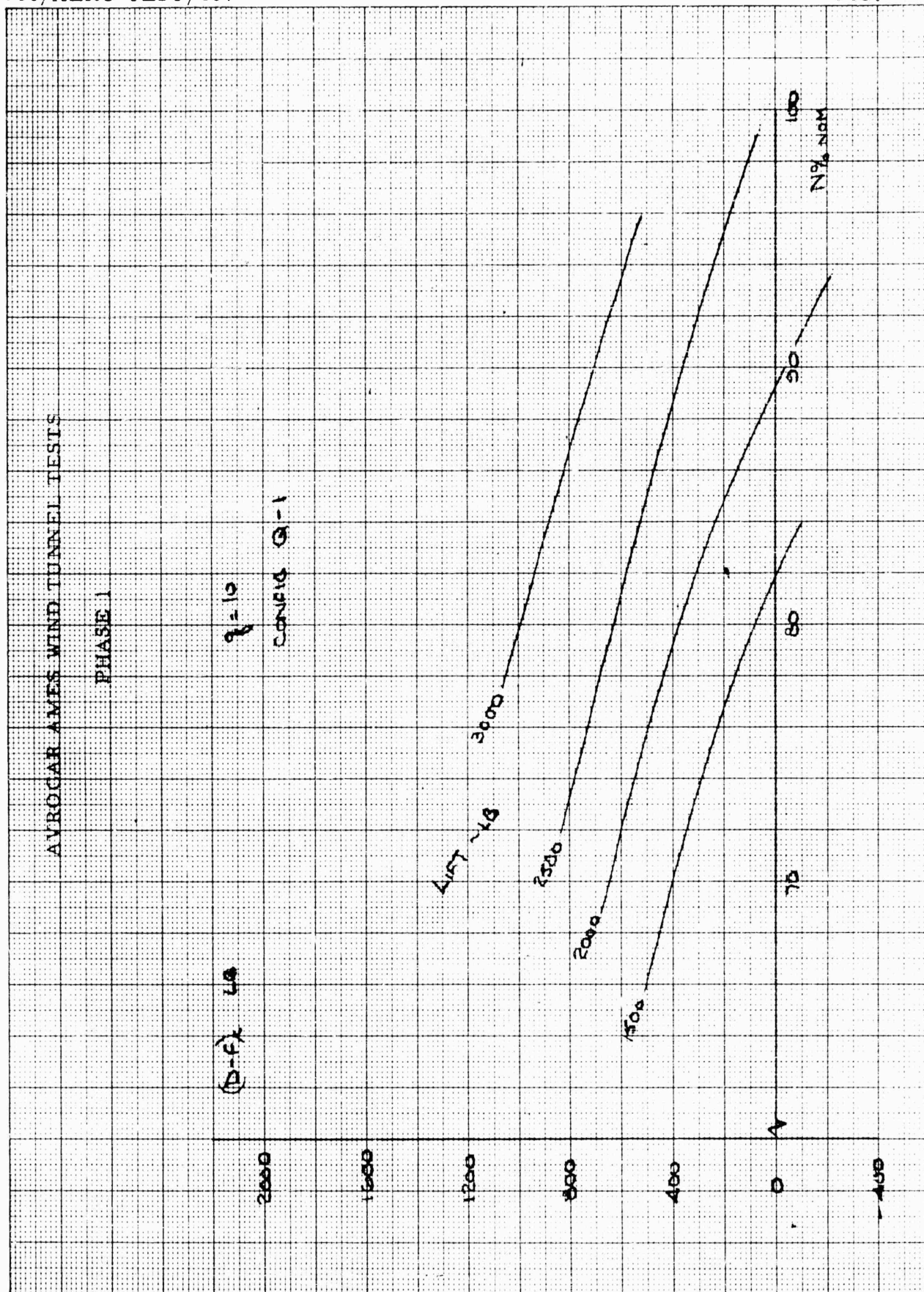
 $n/d = \text{MAX.}$  $N = 90\%$  $q = 15$



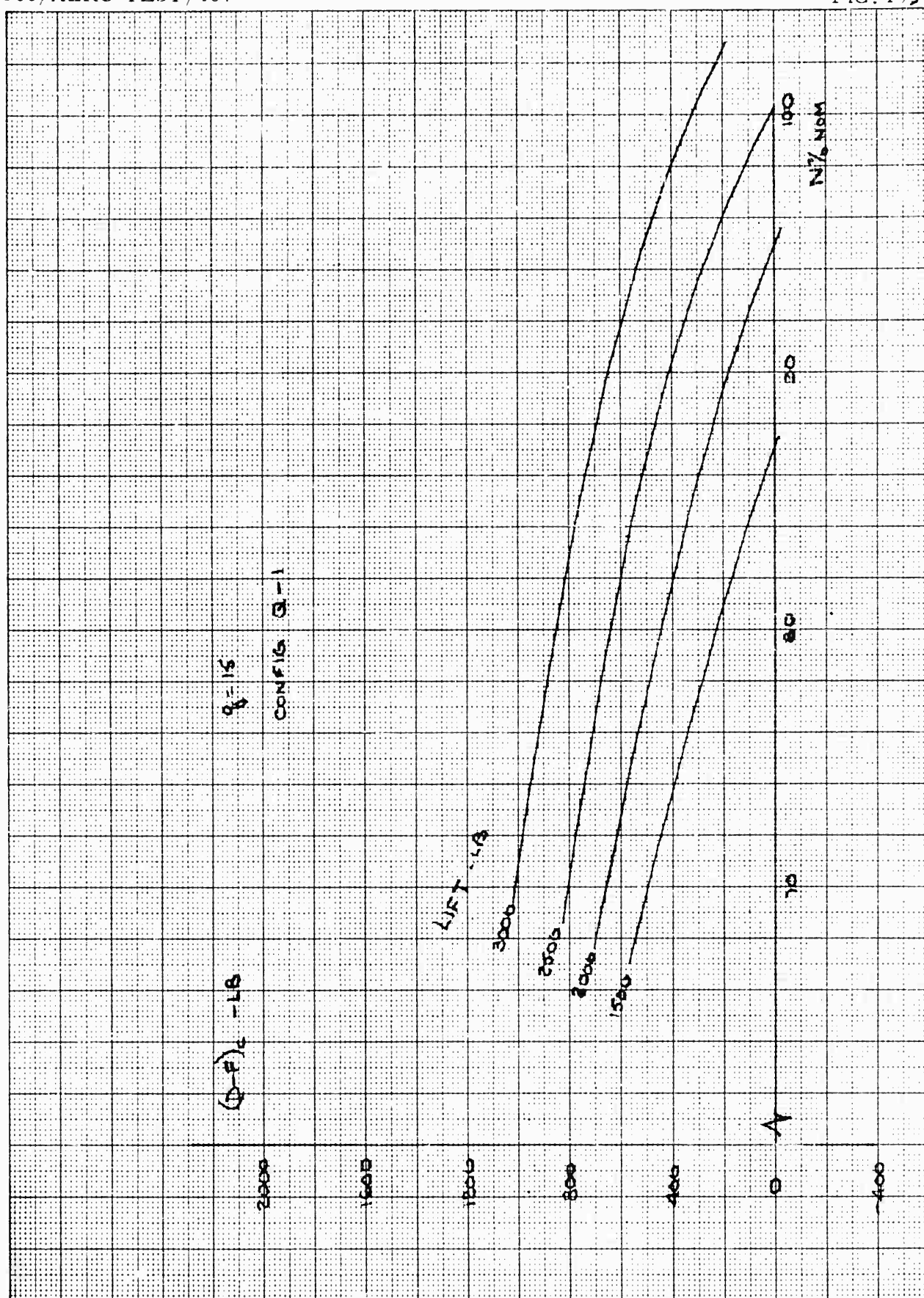


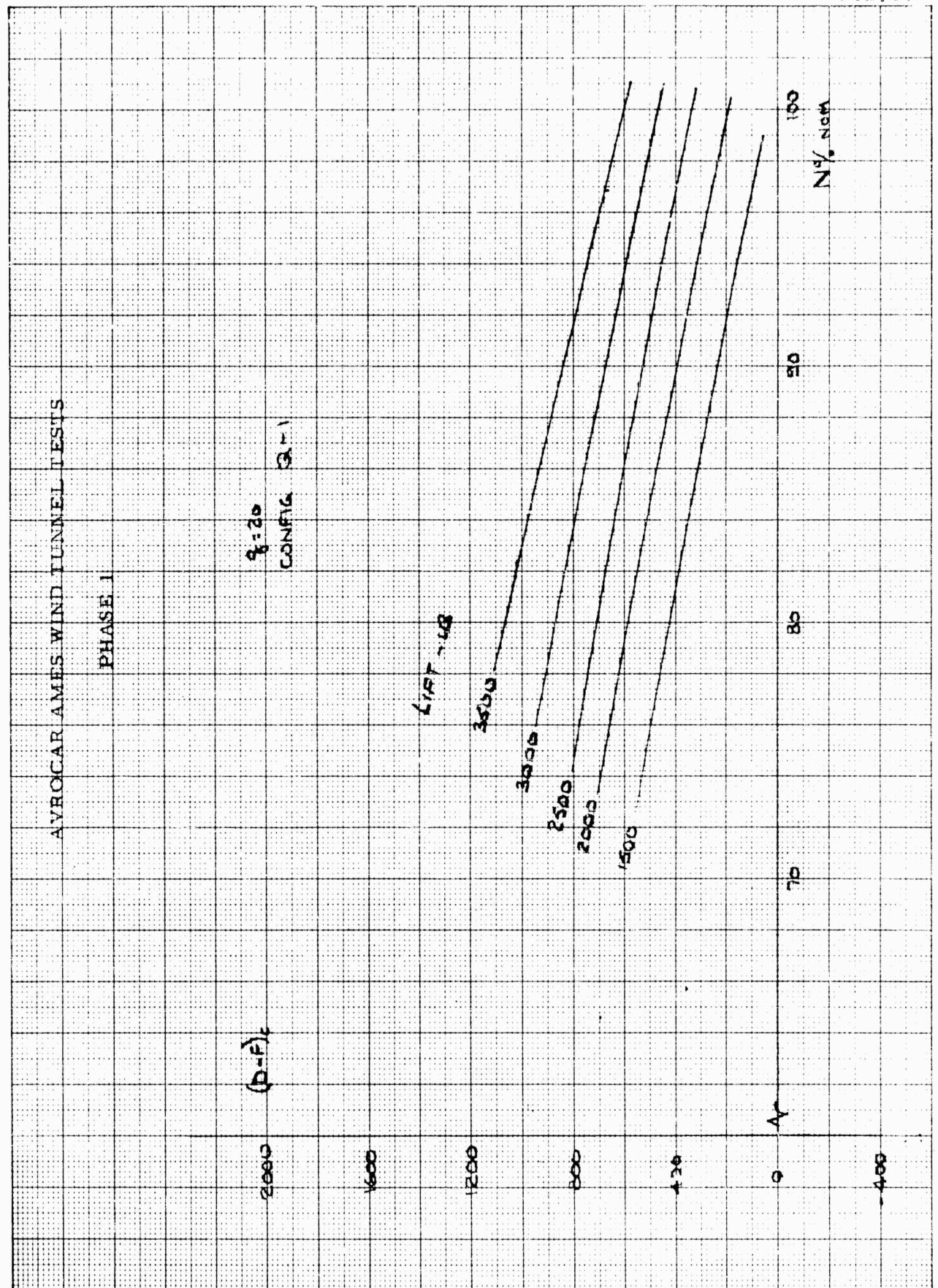


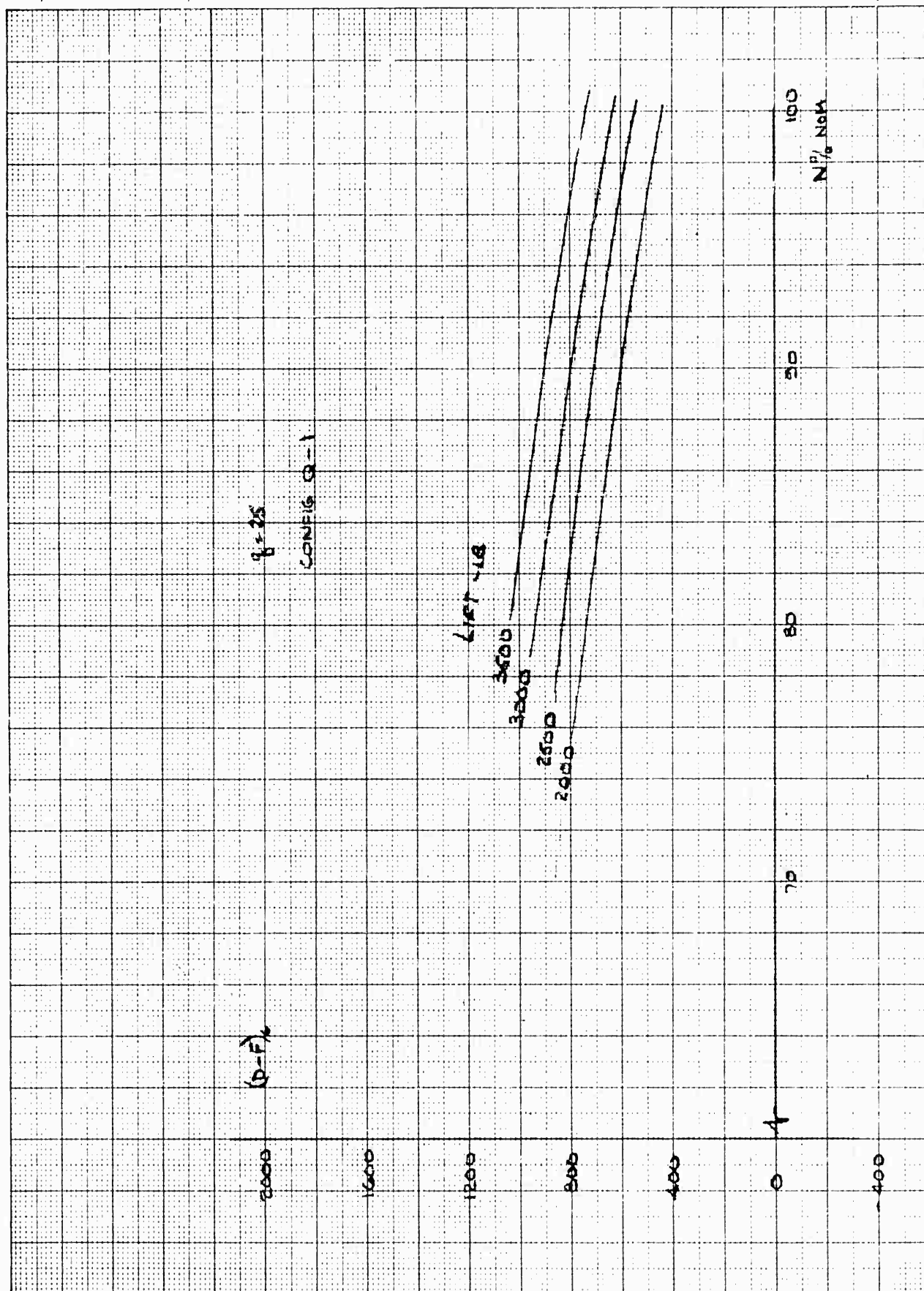




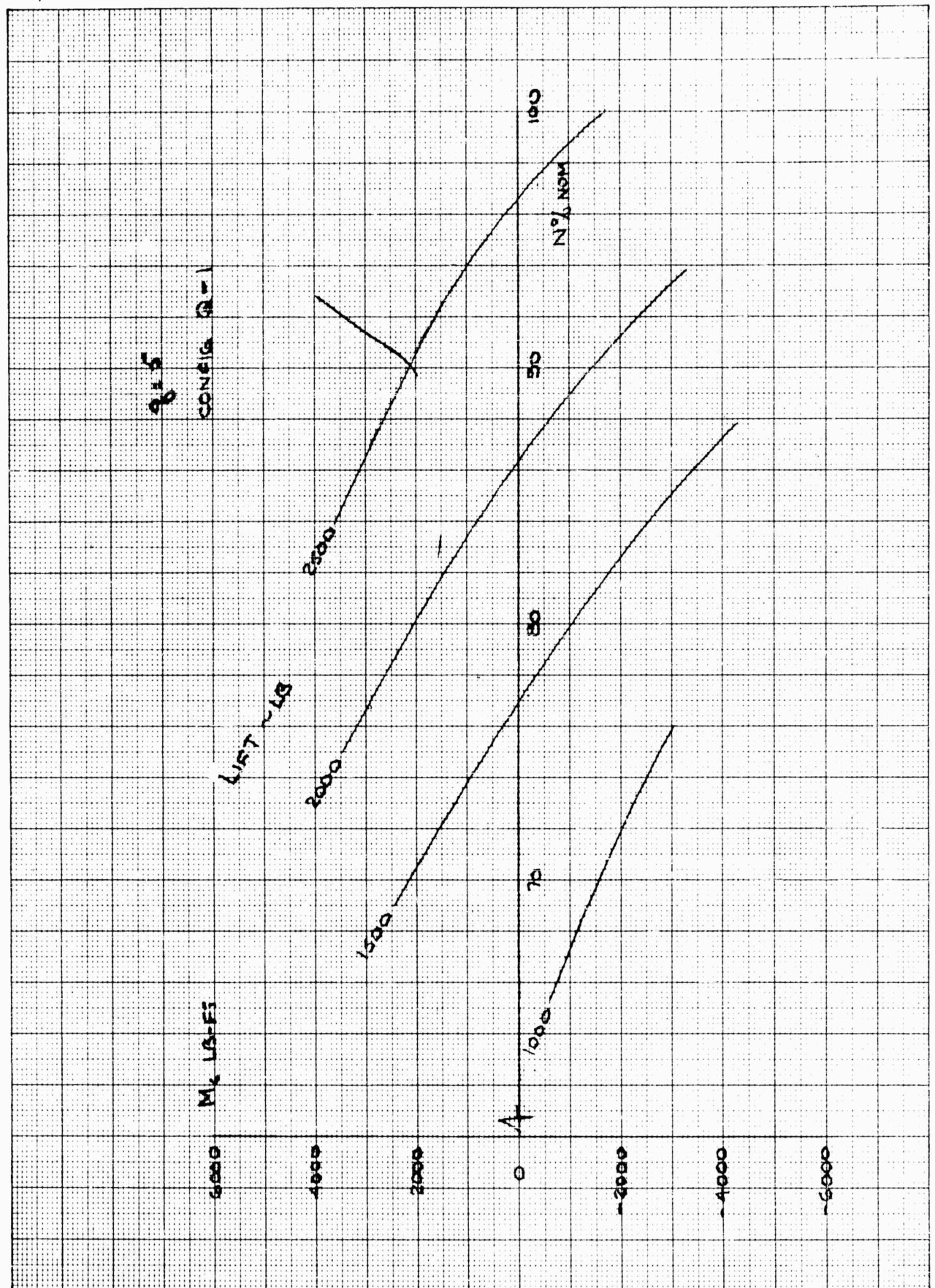


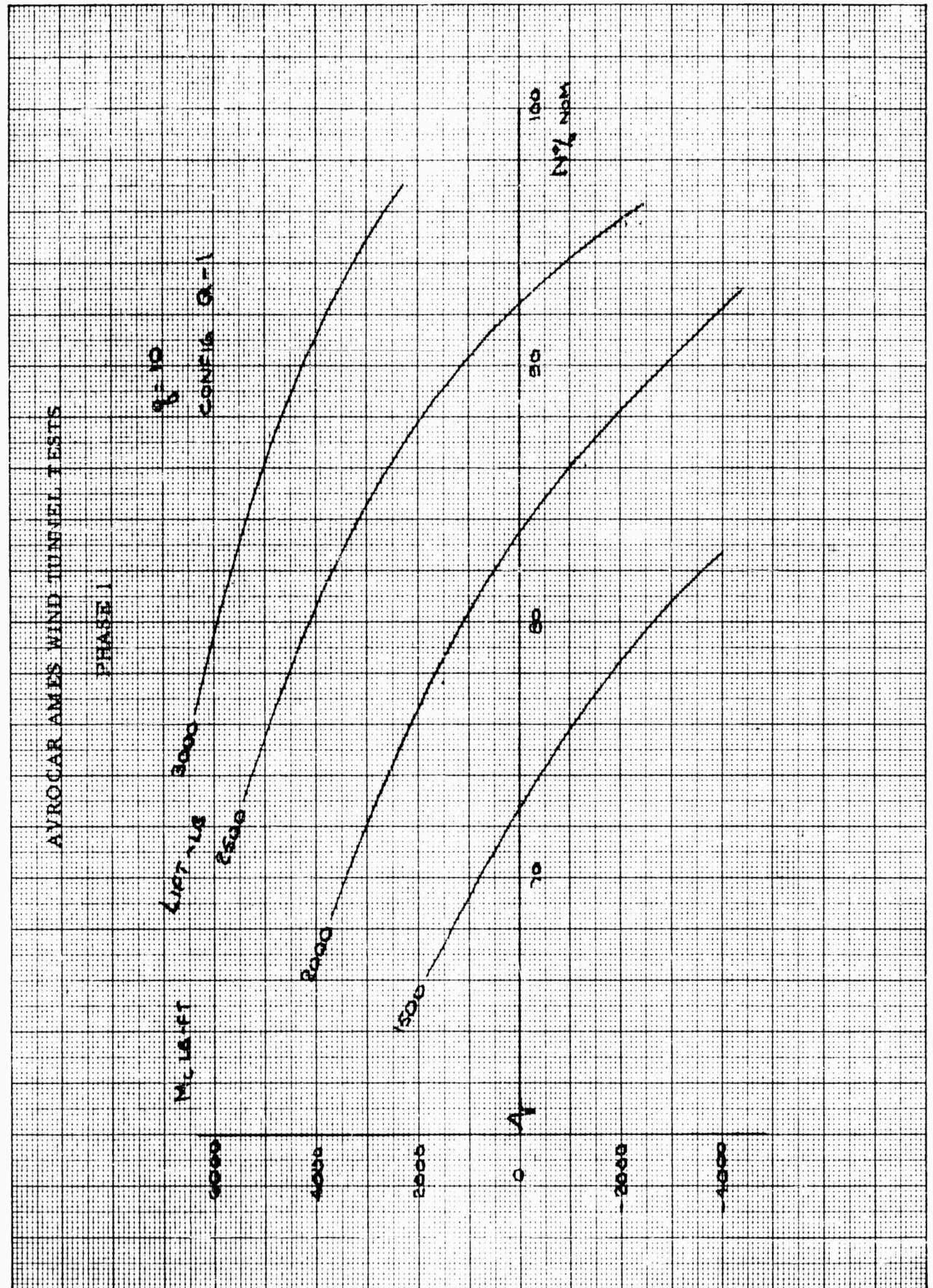


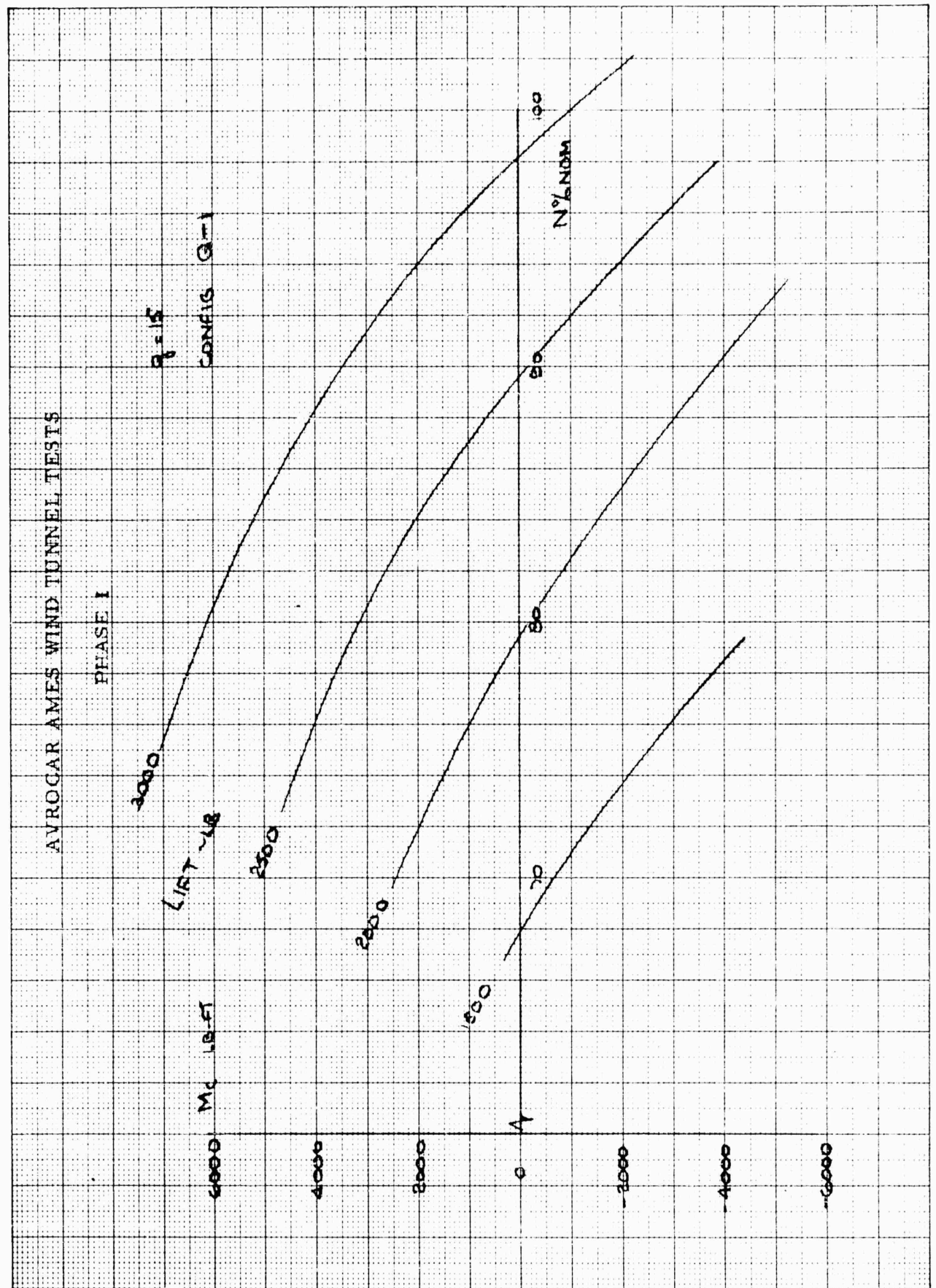




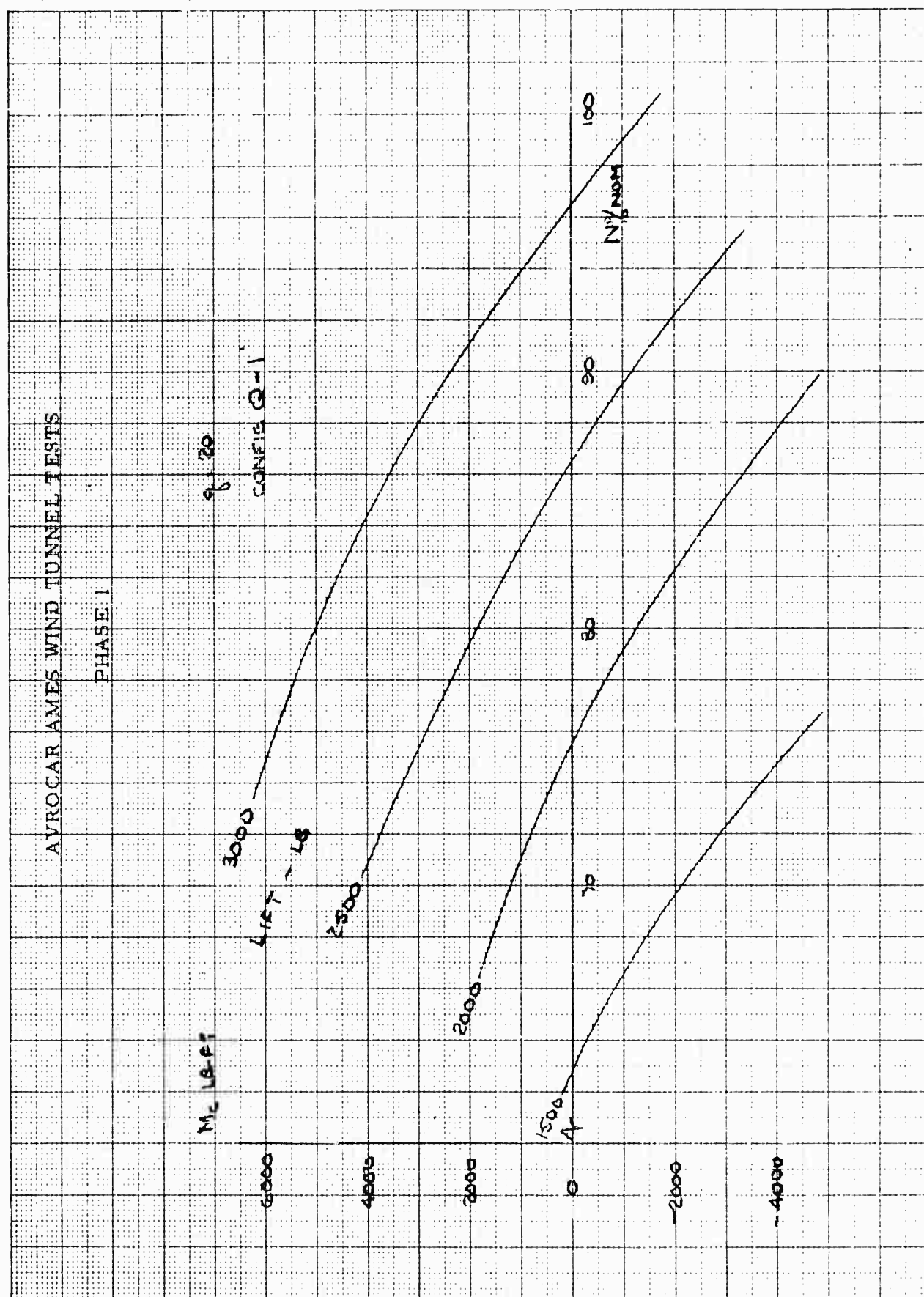




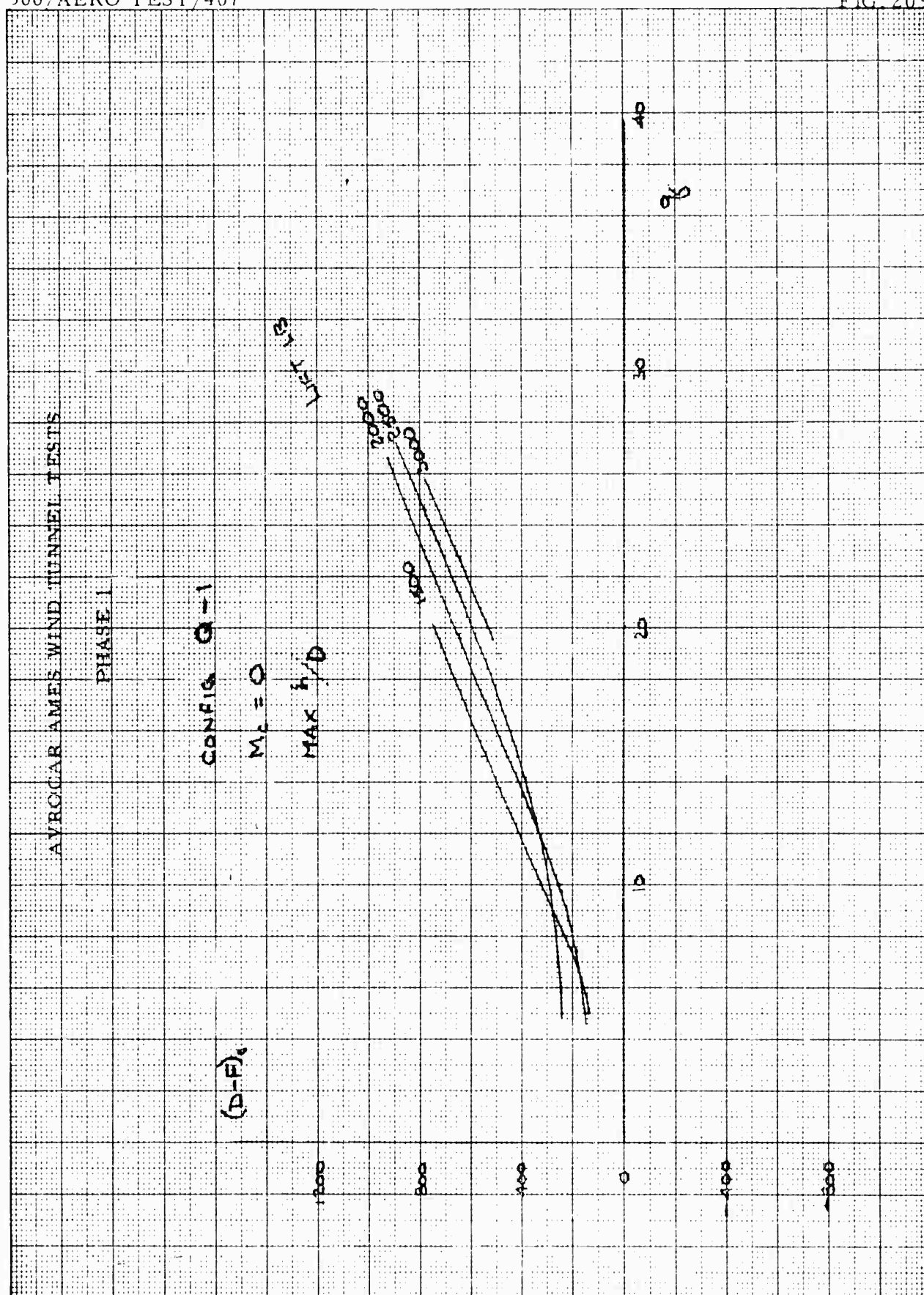














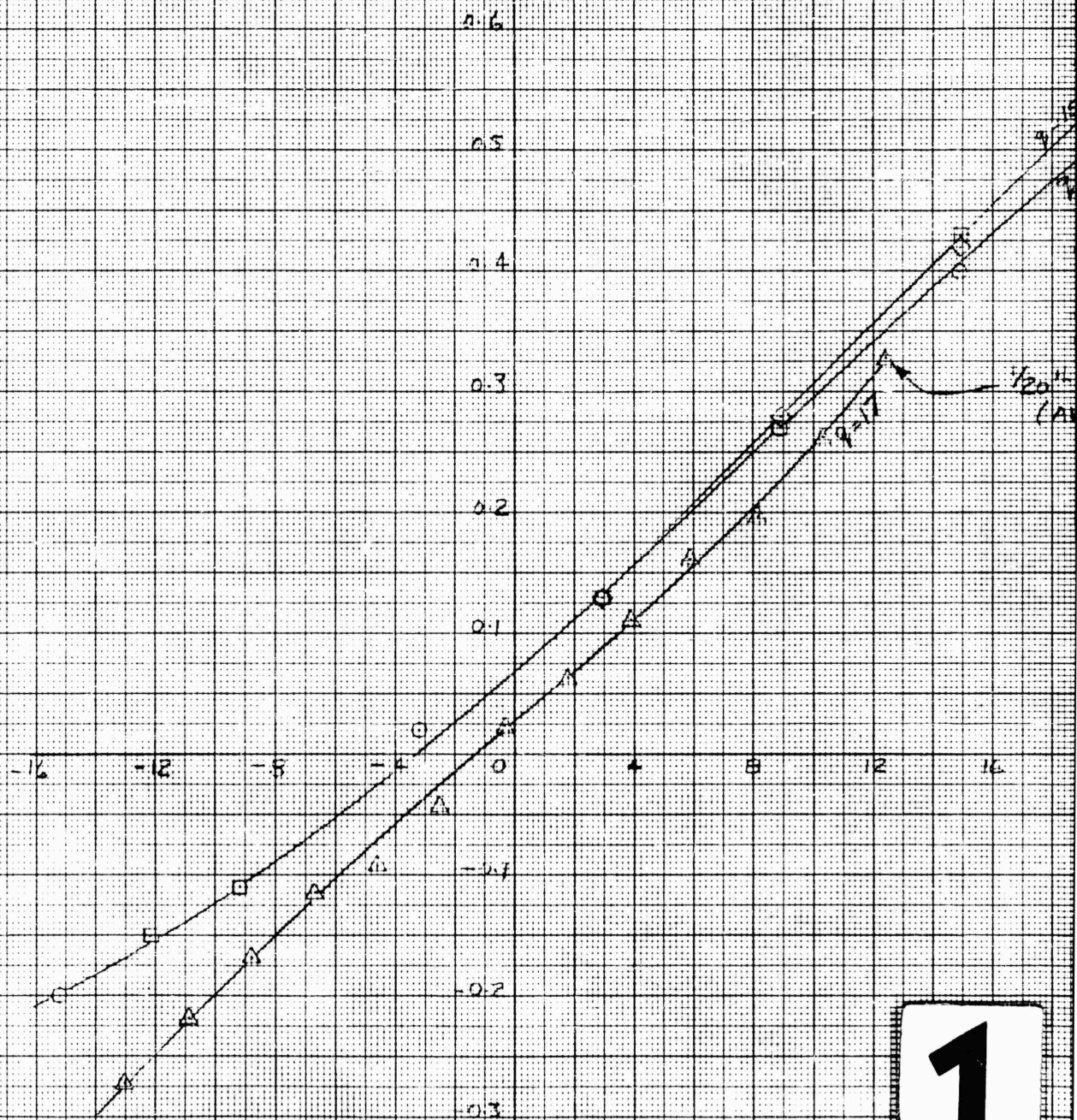
$C_L$  vs  $\alpha$ 

COMPARISON OF AVROCAR AND

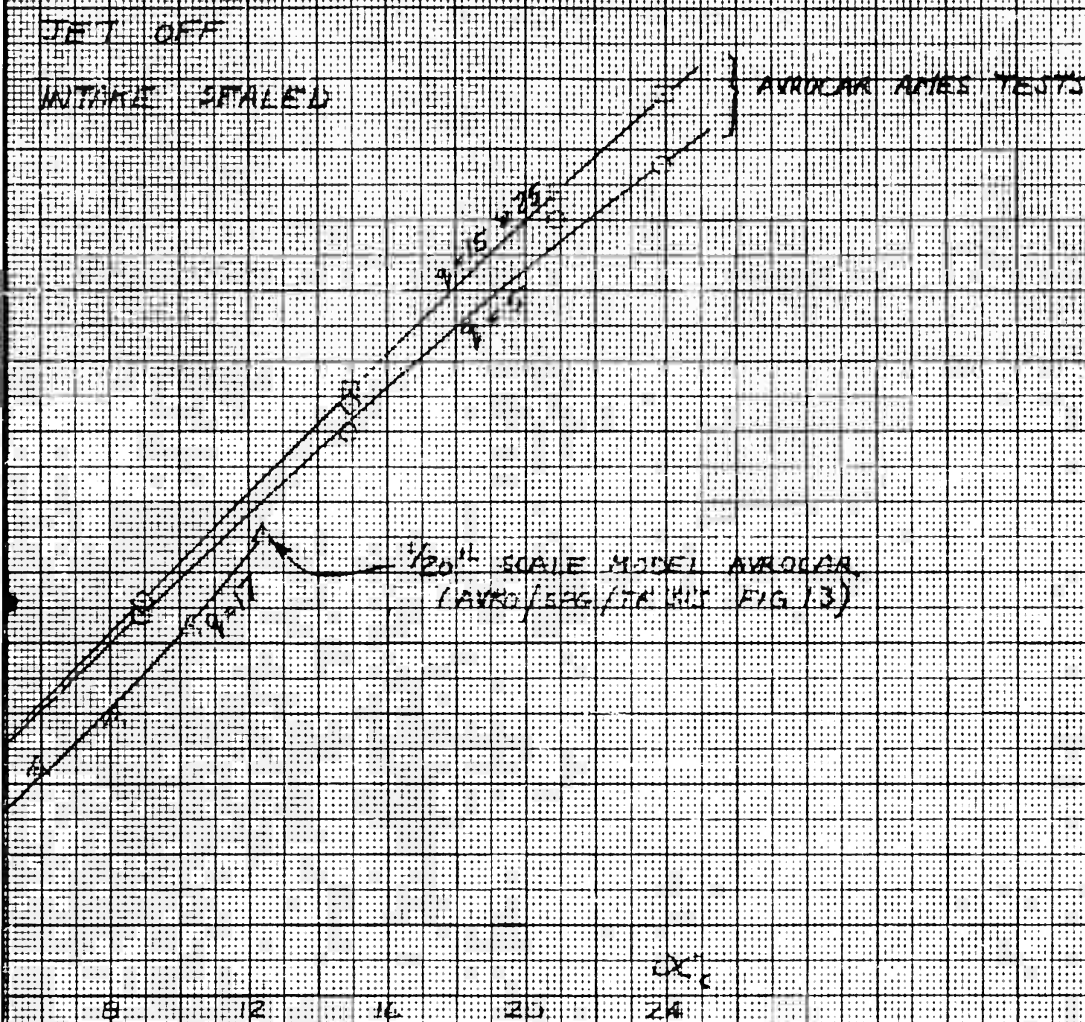
 $C_L$ 

JET OFF

INTAKE SEALED

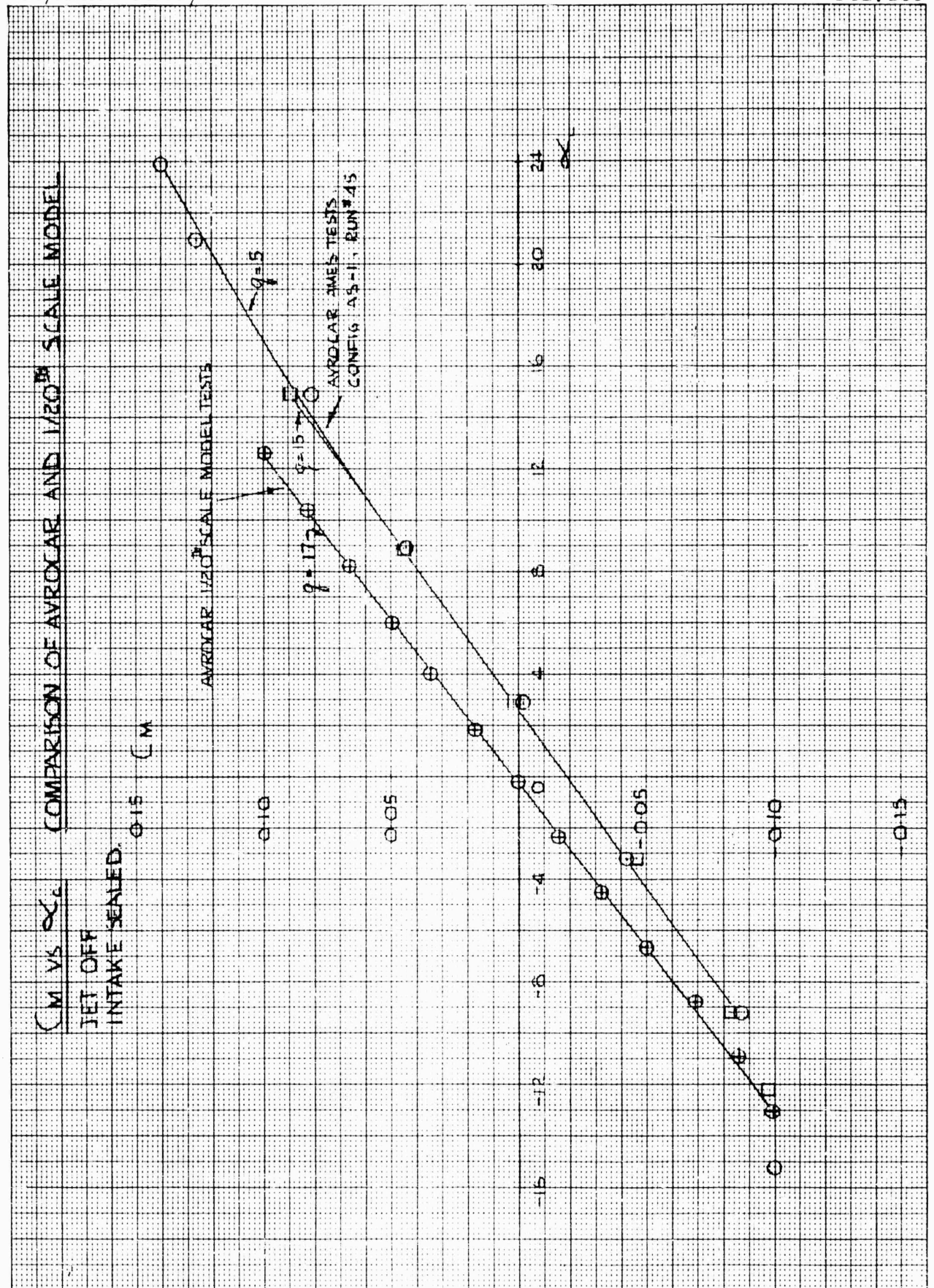


1

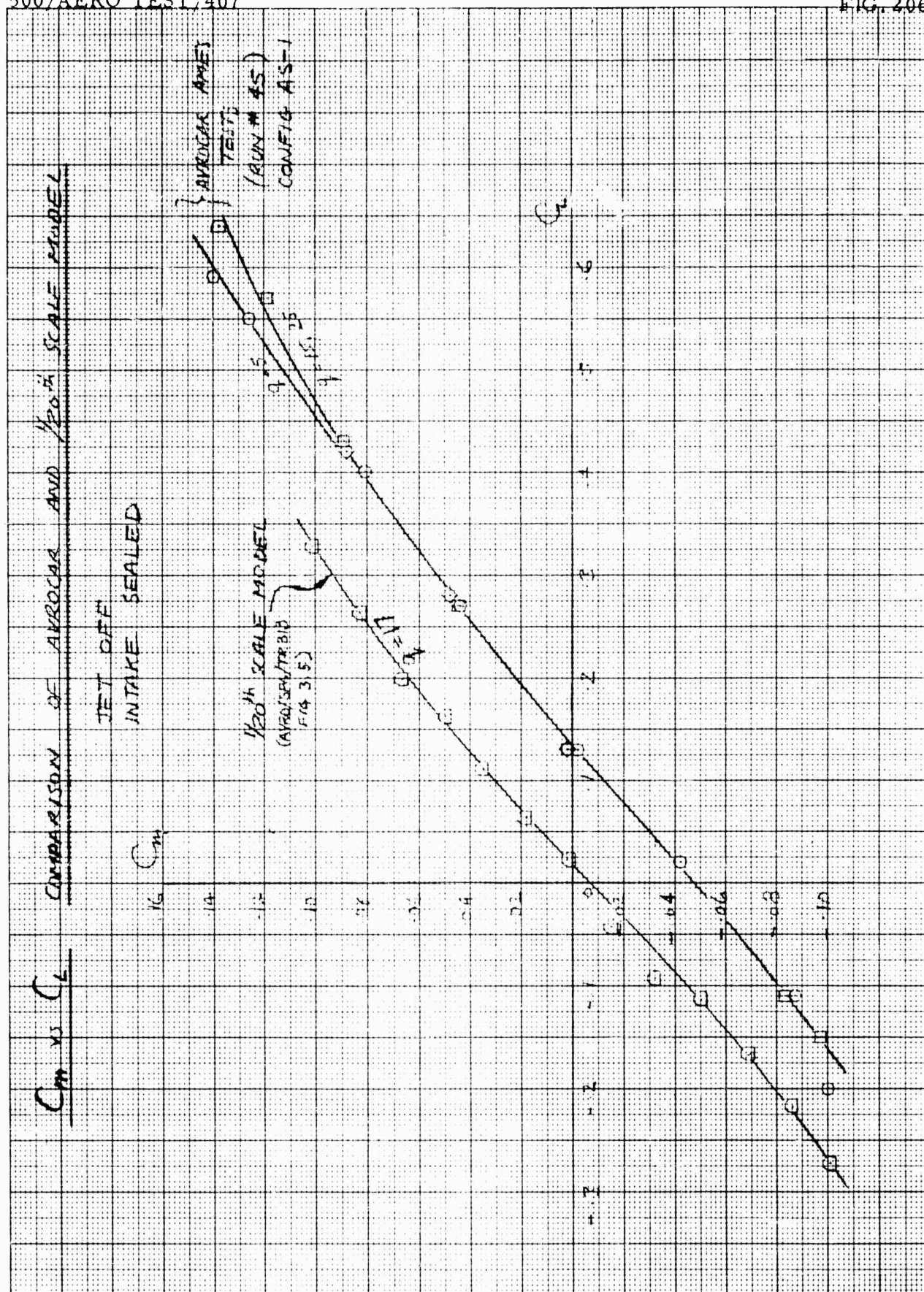
SON OF AVROCAR AND  $\frac{1}{20}$  SCALE MODEL

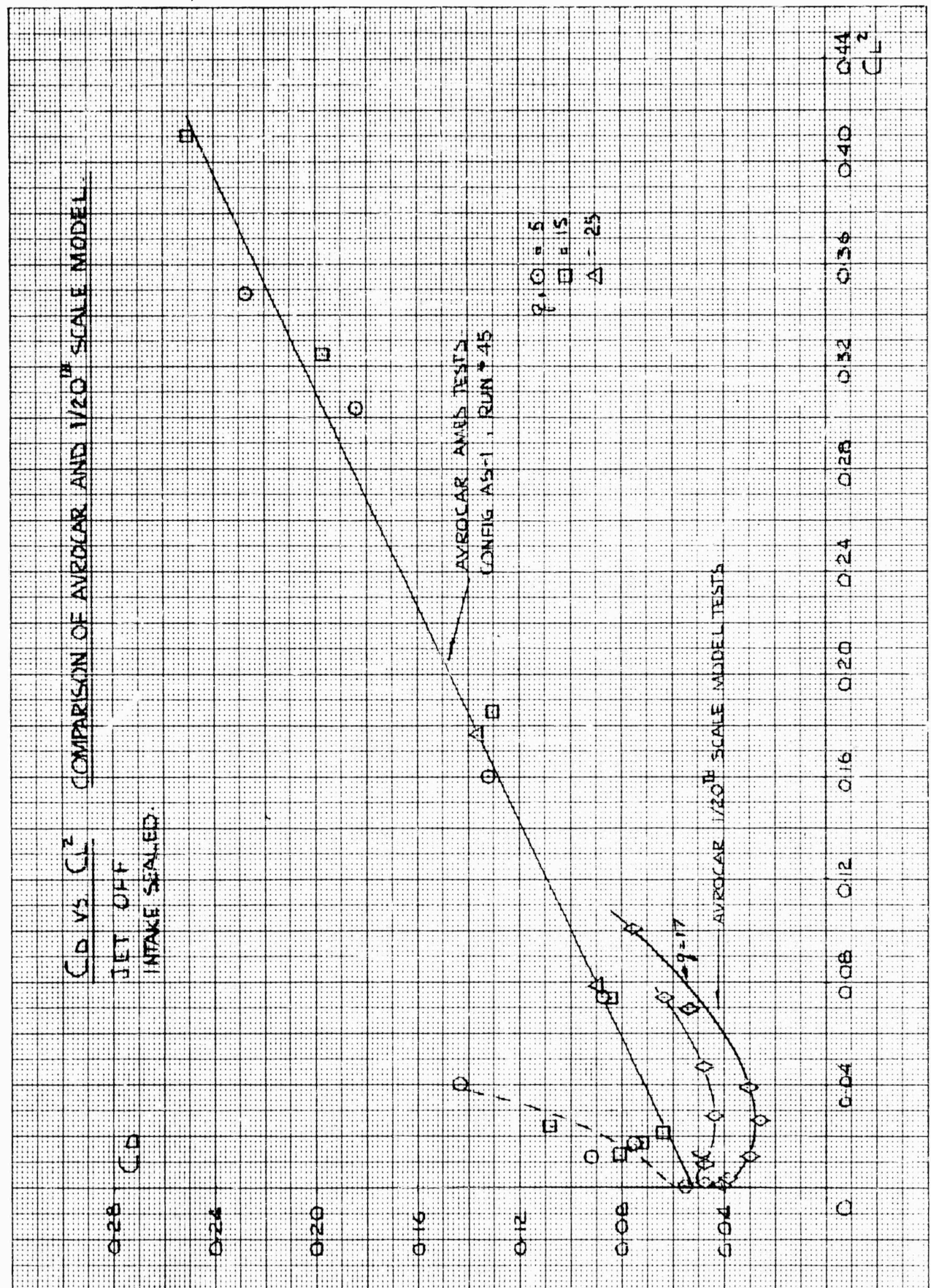
2

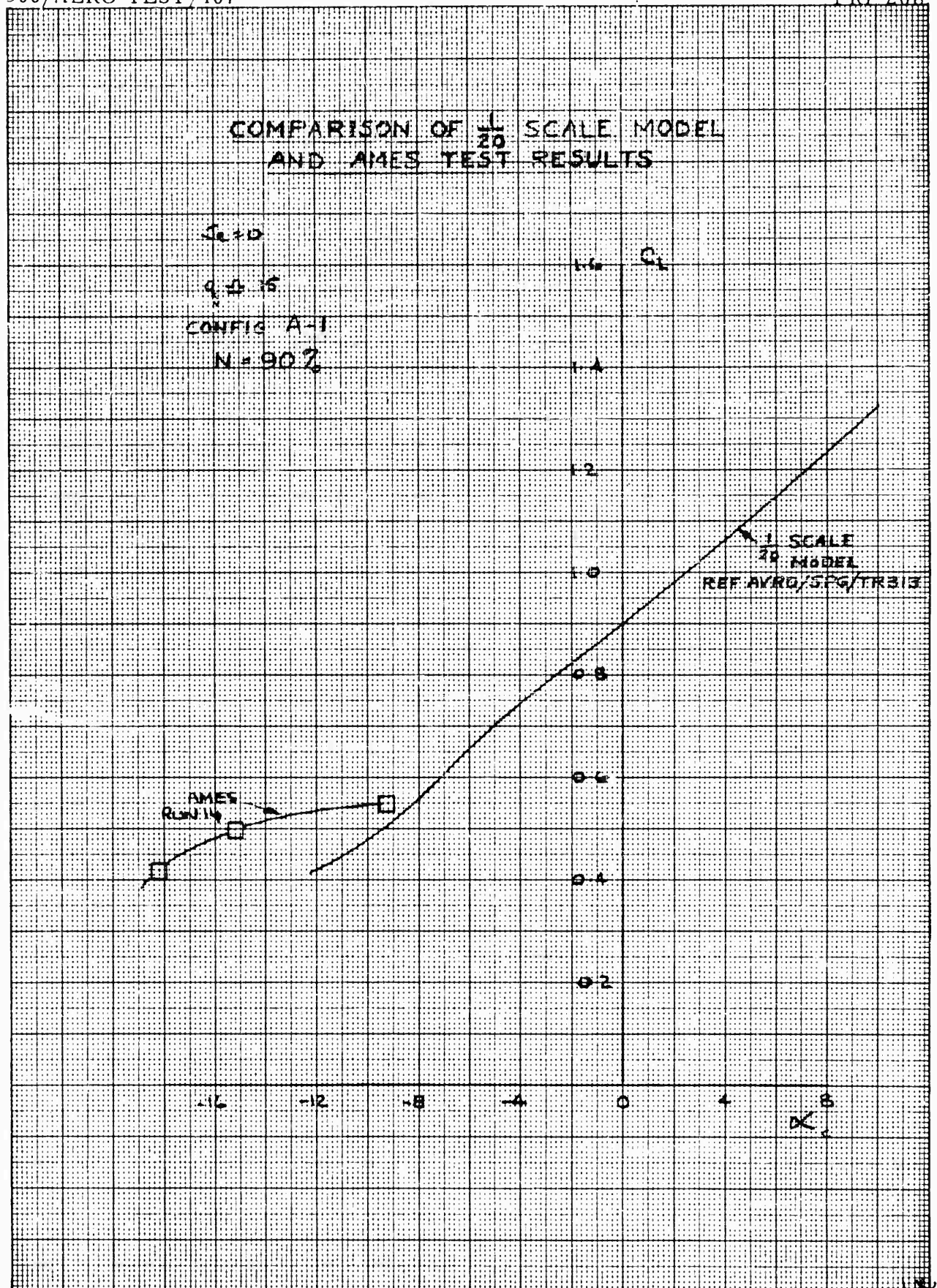




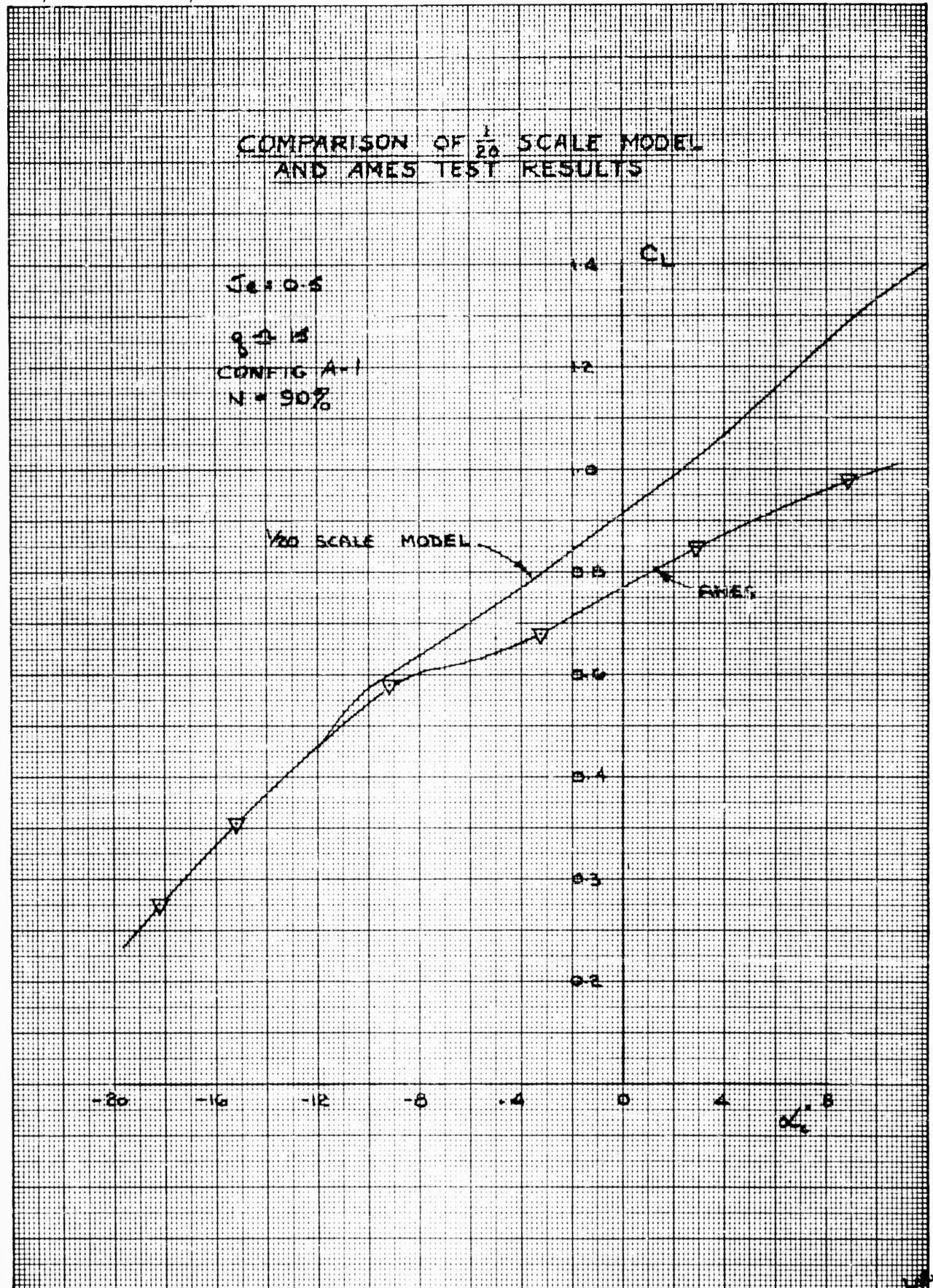


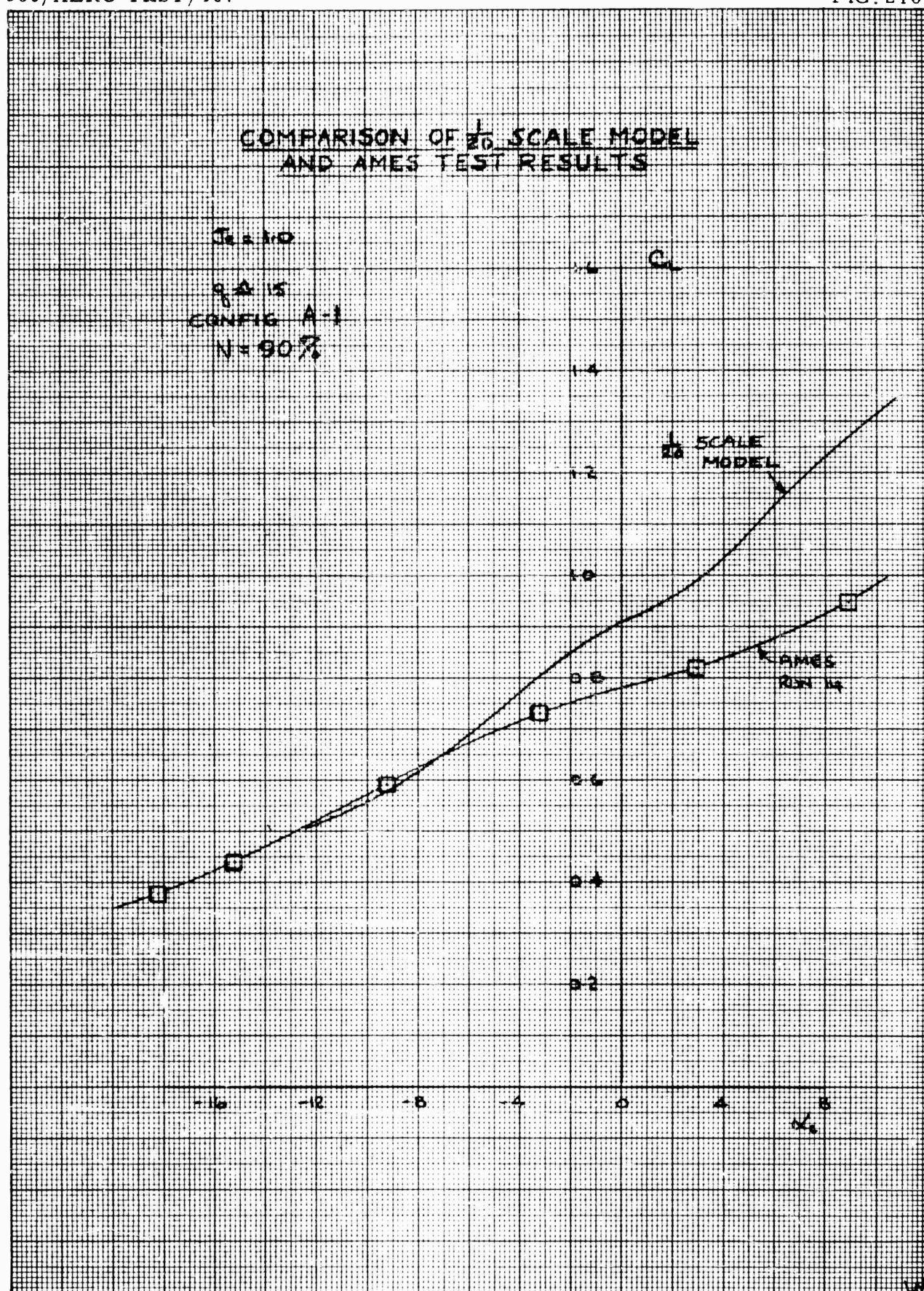




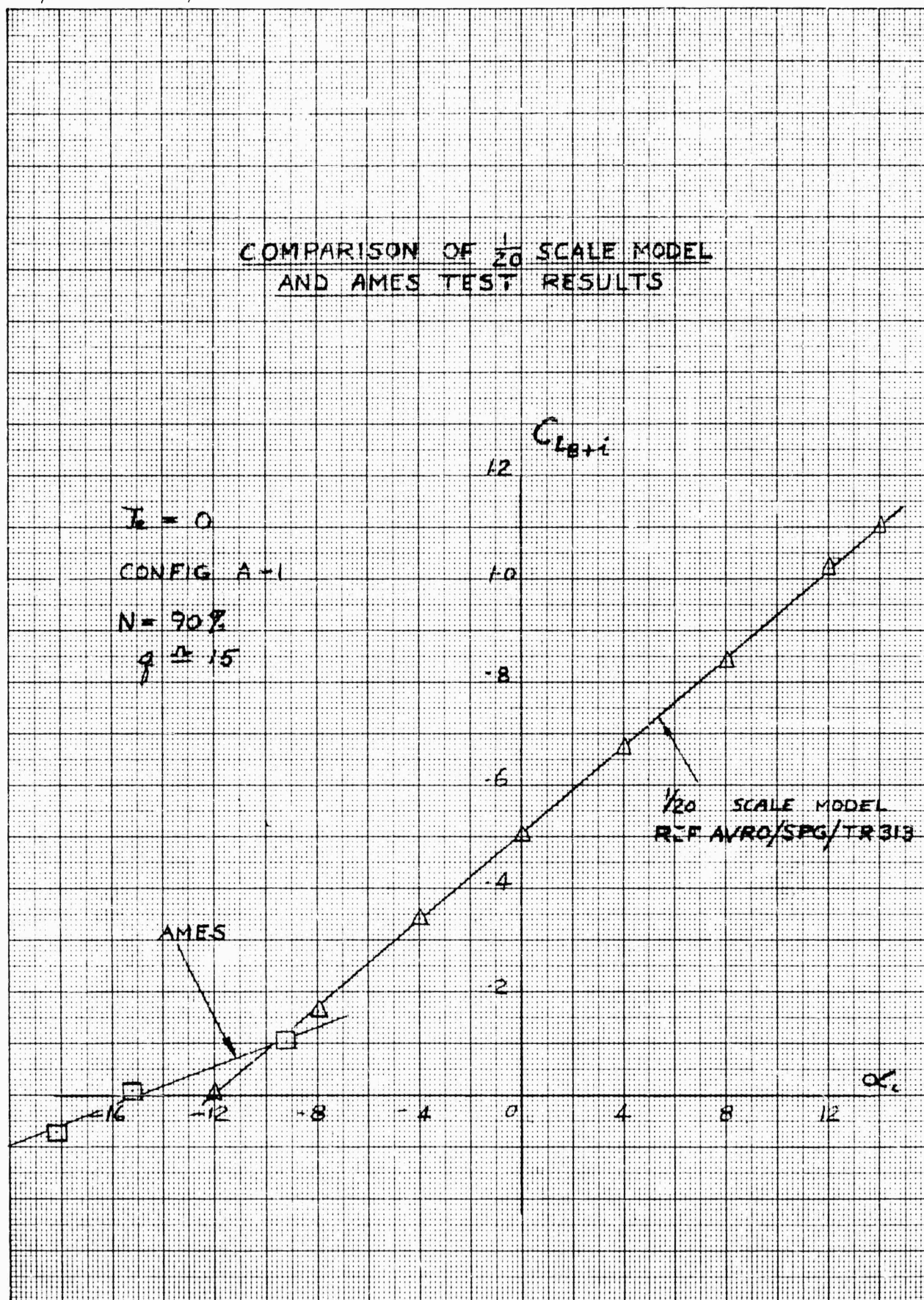




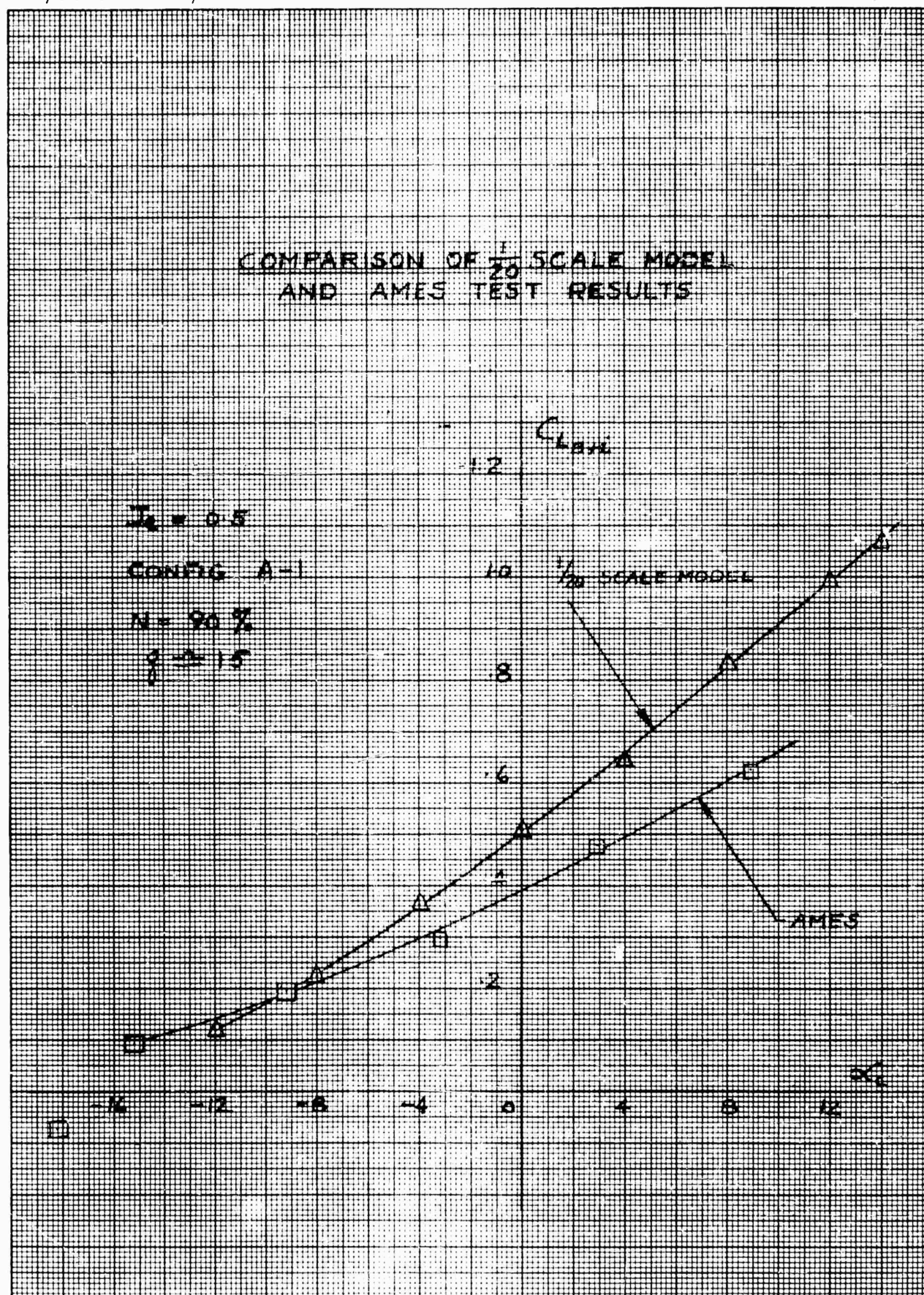


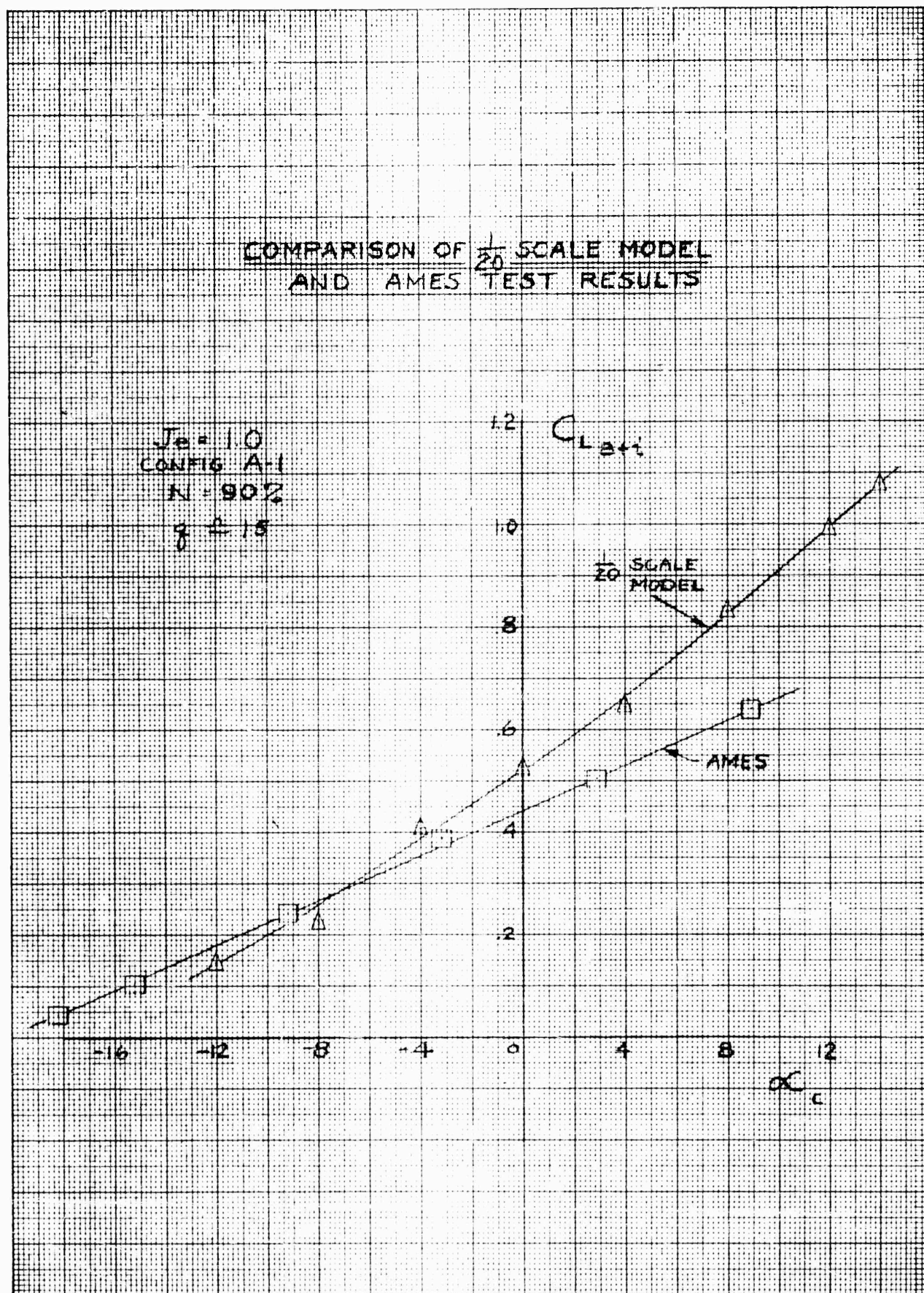










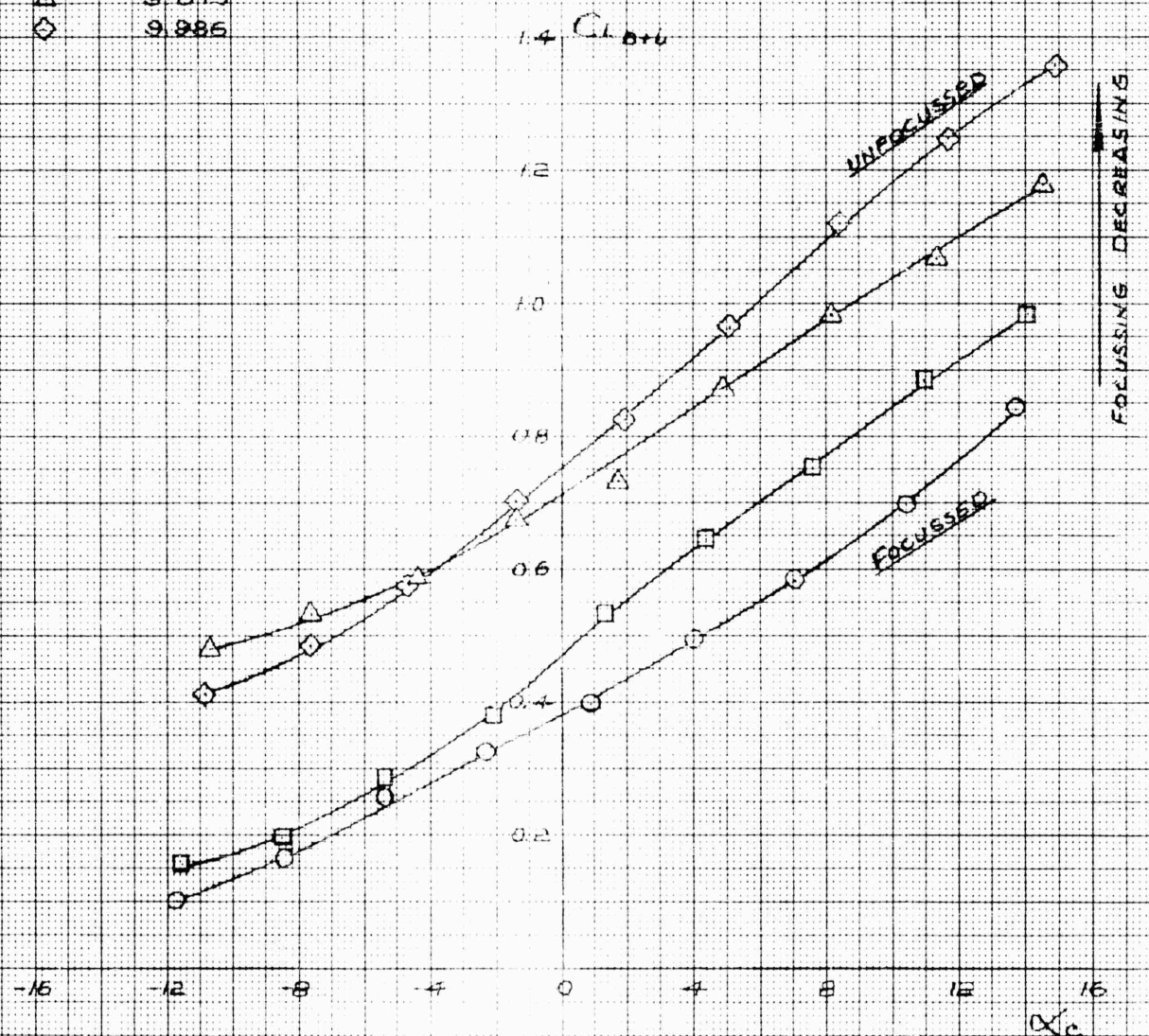




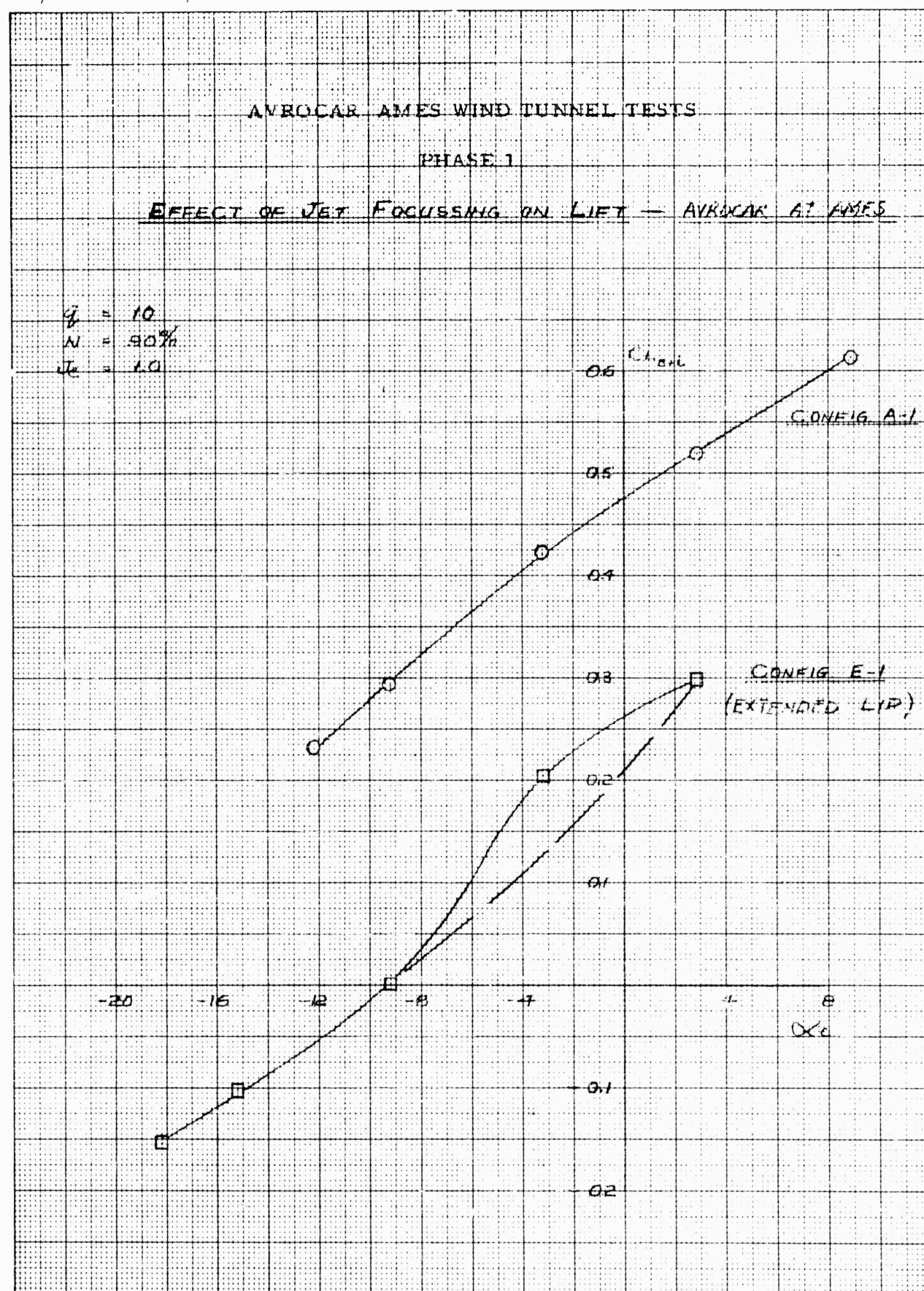
# EFFECT OF JET FOCUSING ON LIFT — 1/20TH SCALE MODEL

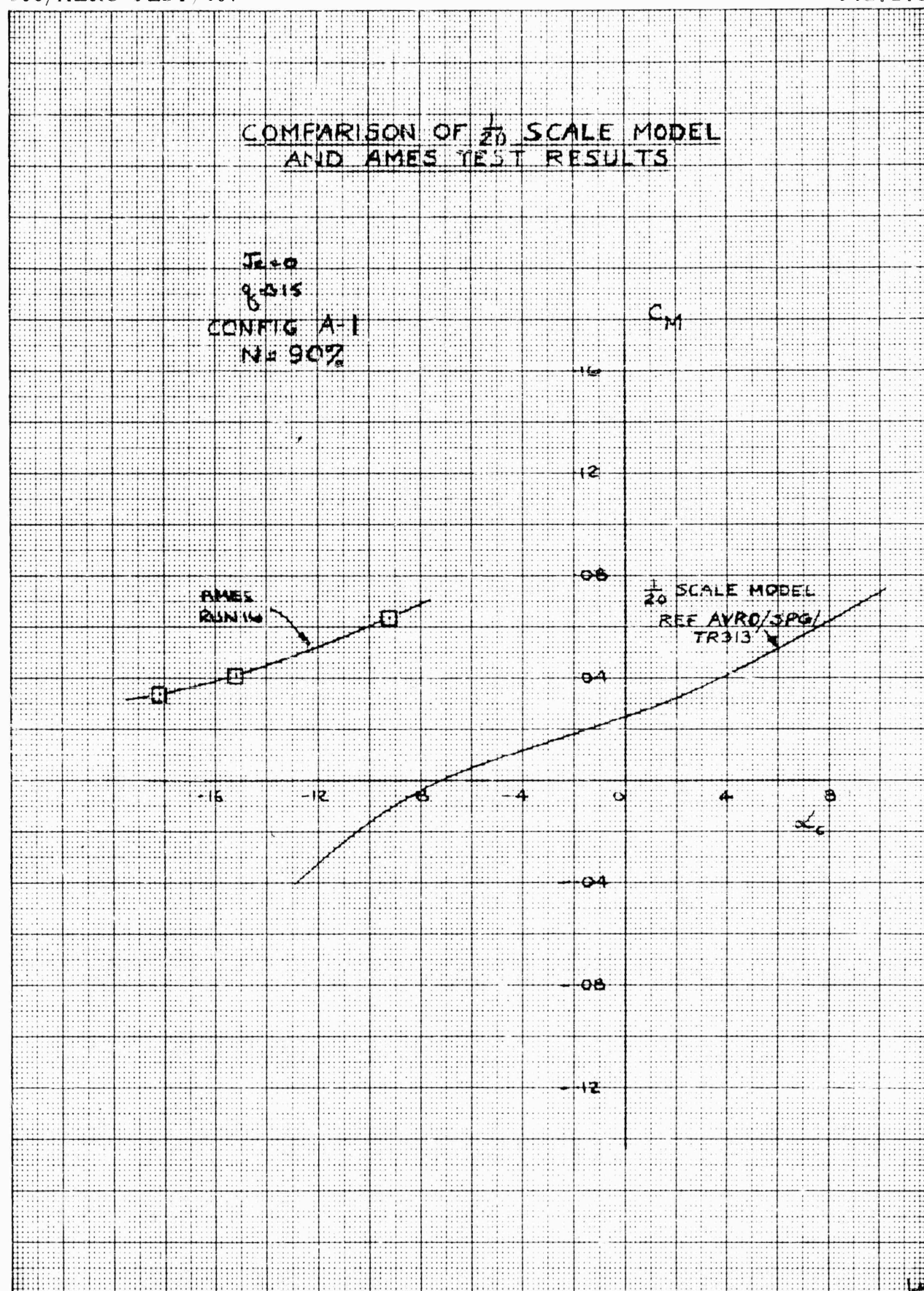
$Re = 18.1$

Sym	RING $\frac{1}{2}D$
○	3.768
□	9.806
△	9.843
◇	9.986

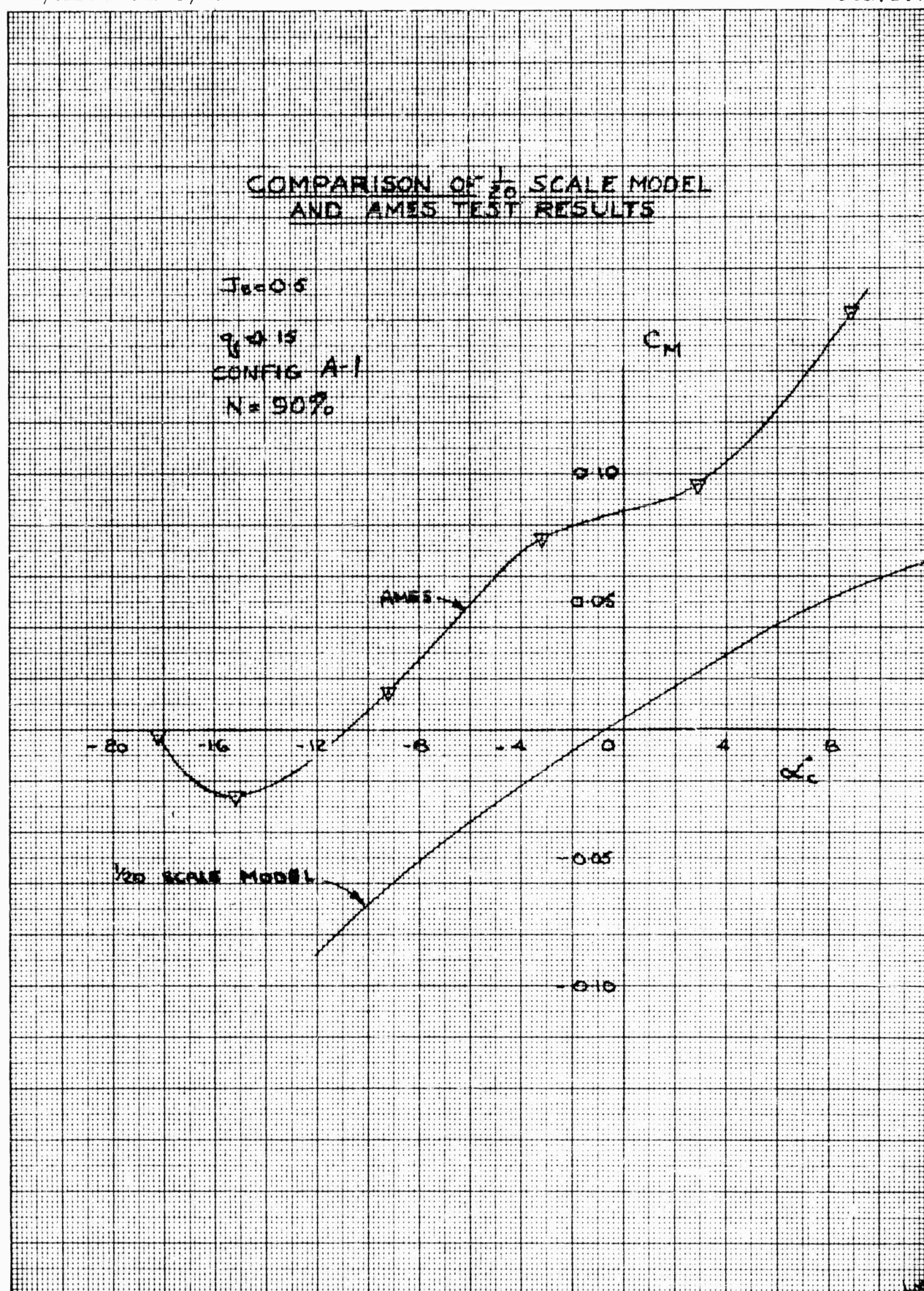




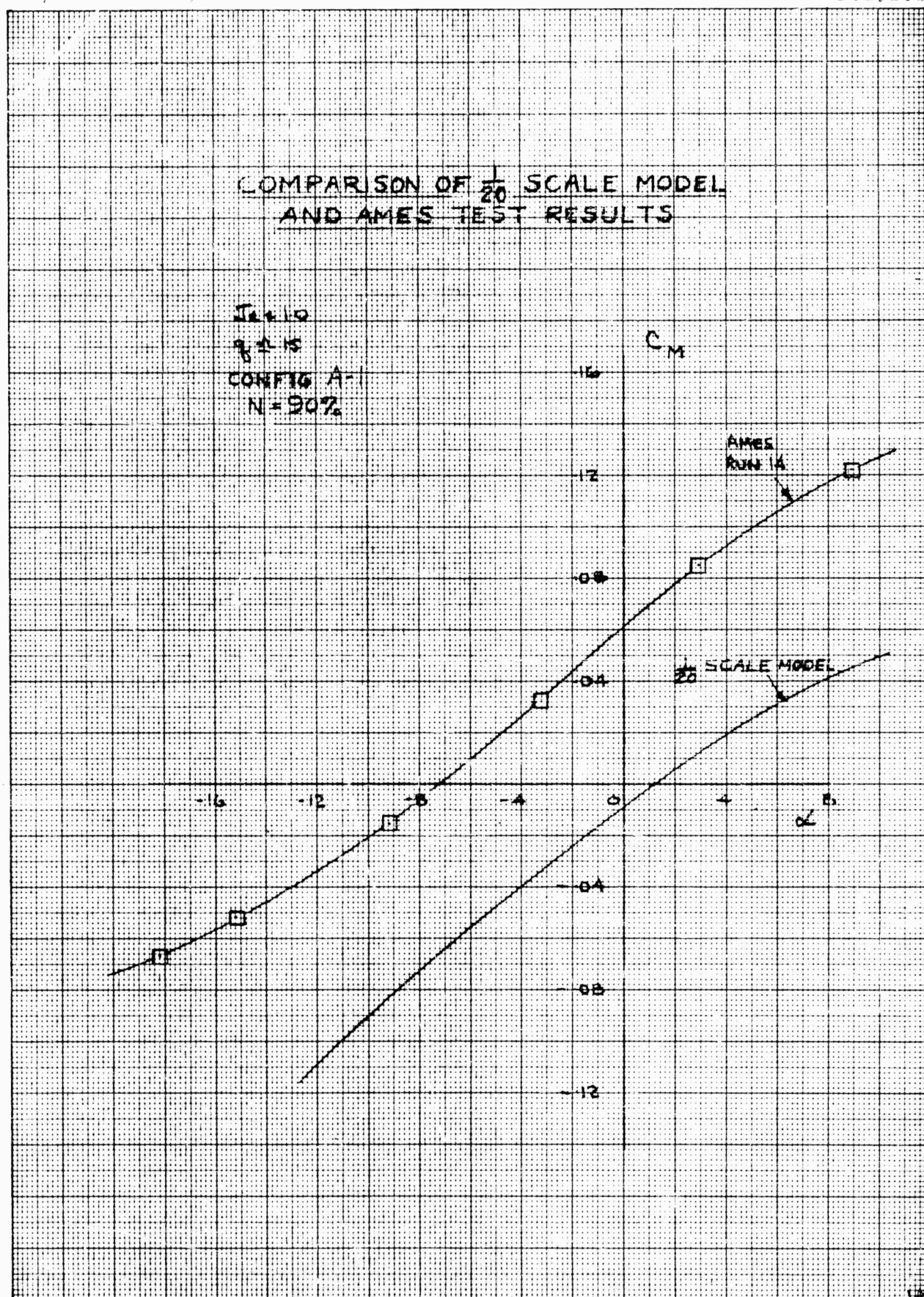


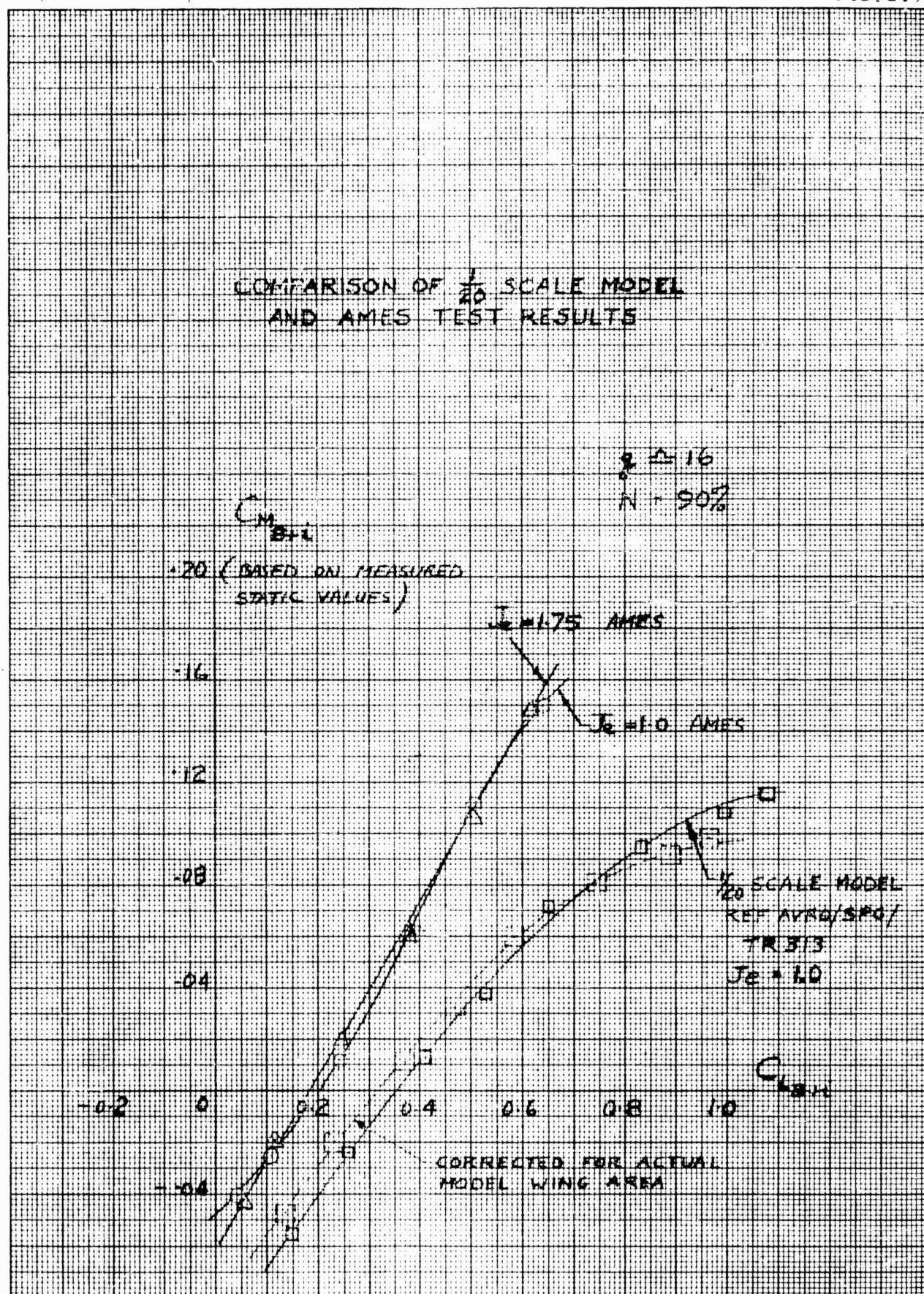














# DRAG COMPARISON OF 1/20TH SCALE MODEL AND

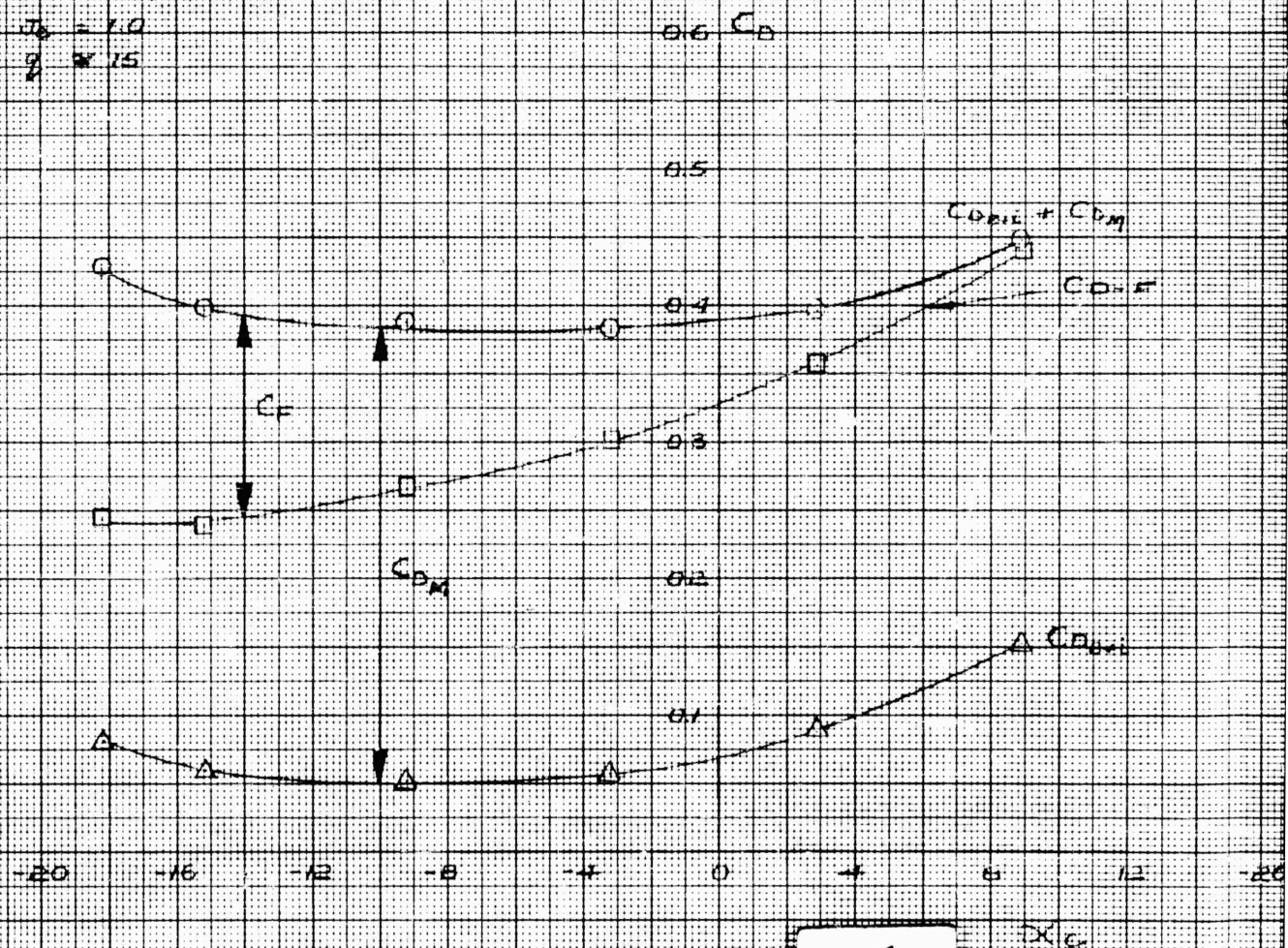
## AVROCAR AMES TEST

CONFIG A-1

$N = 20\%$

$T_b = 1.0$

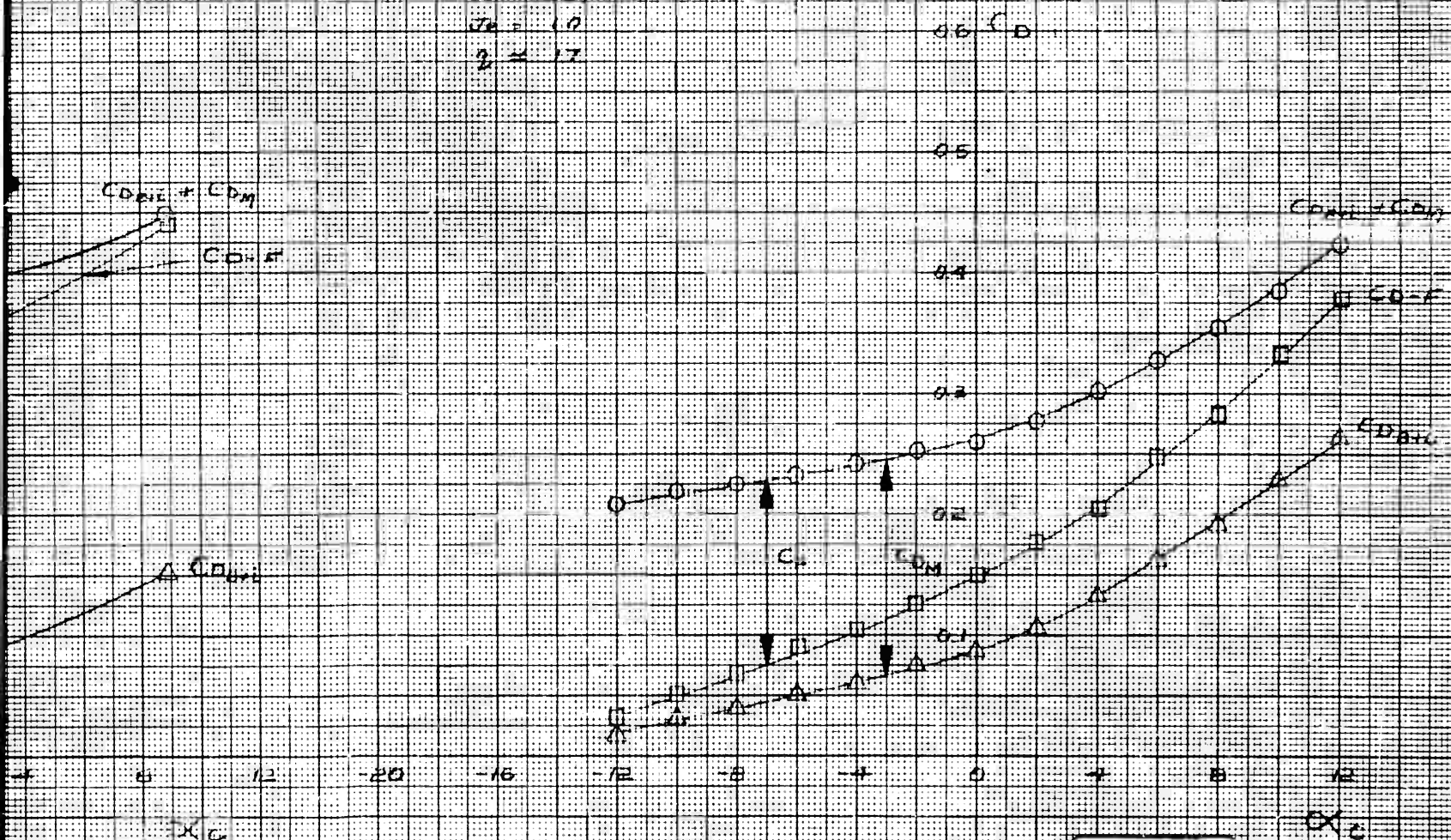
$\theta = 15^\circ$



1

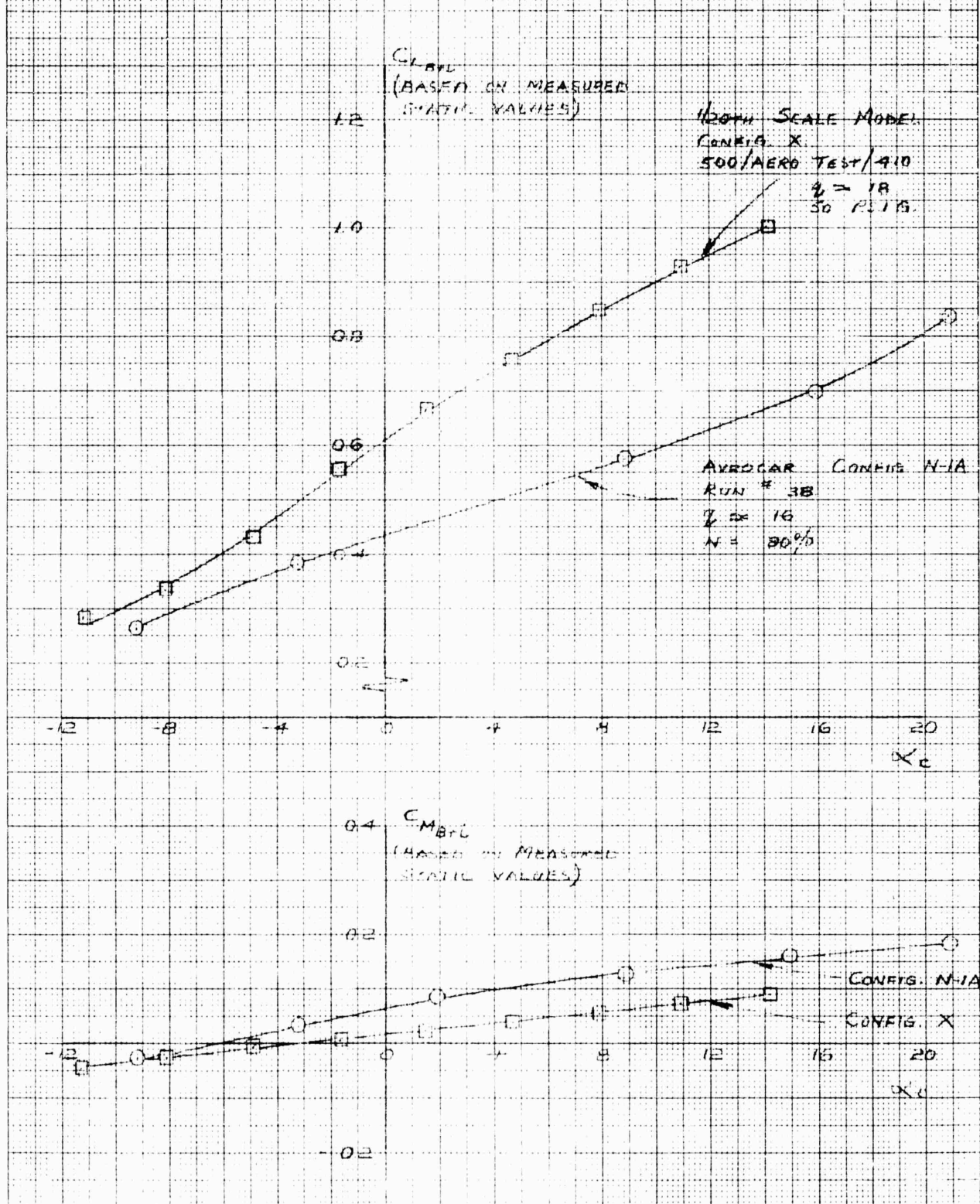


## 1/20TH SCALE MODEL AND AVROCAR AMES TEST RESULTS

1/20TH SCALE MODEL TEST $N = 90^\circ$  $Re = 1.0$  $\beta = 17$ 

2

## COMPARISON OF 1/20TH SCALE MODEL &amp; AVROCAR AMES TEST RESULTS



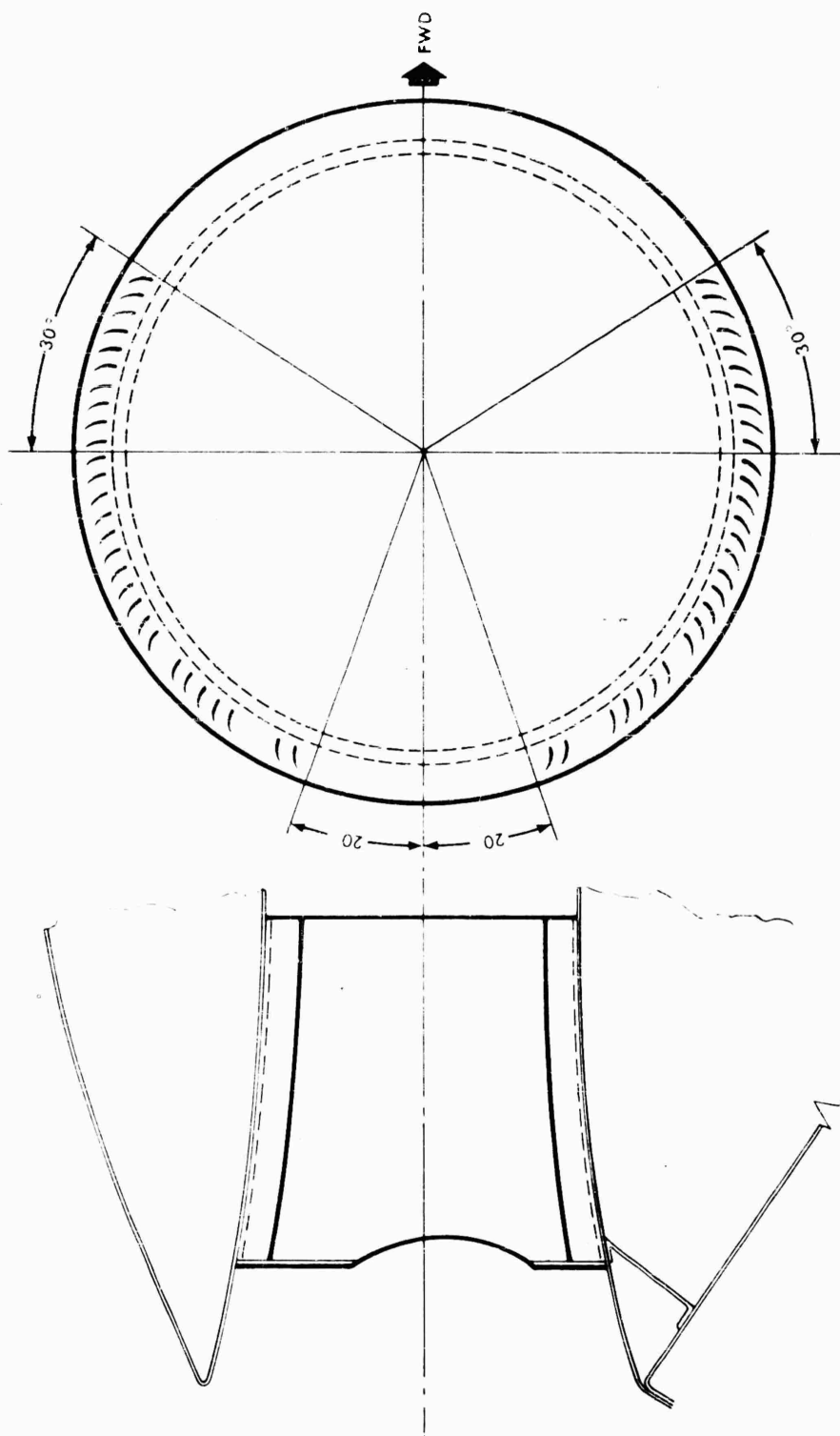


FIG. 222 WING TIP STRUCTURE AND CASCADES



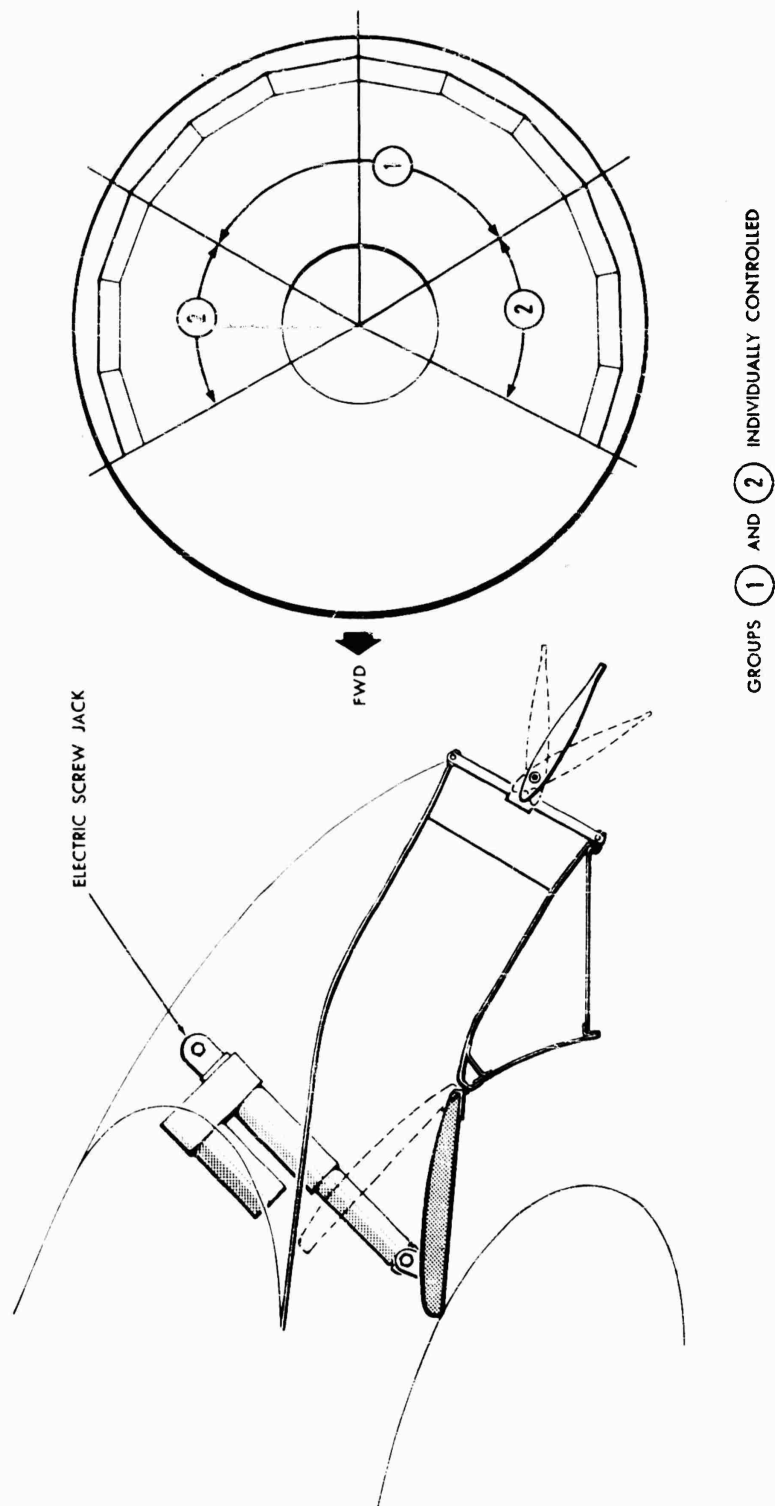


FIG. 223 TRANSITION DOORS

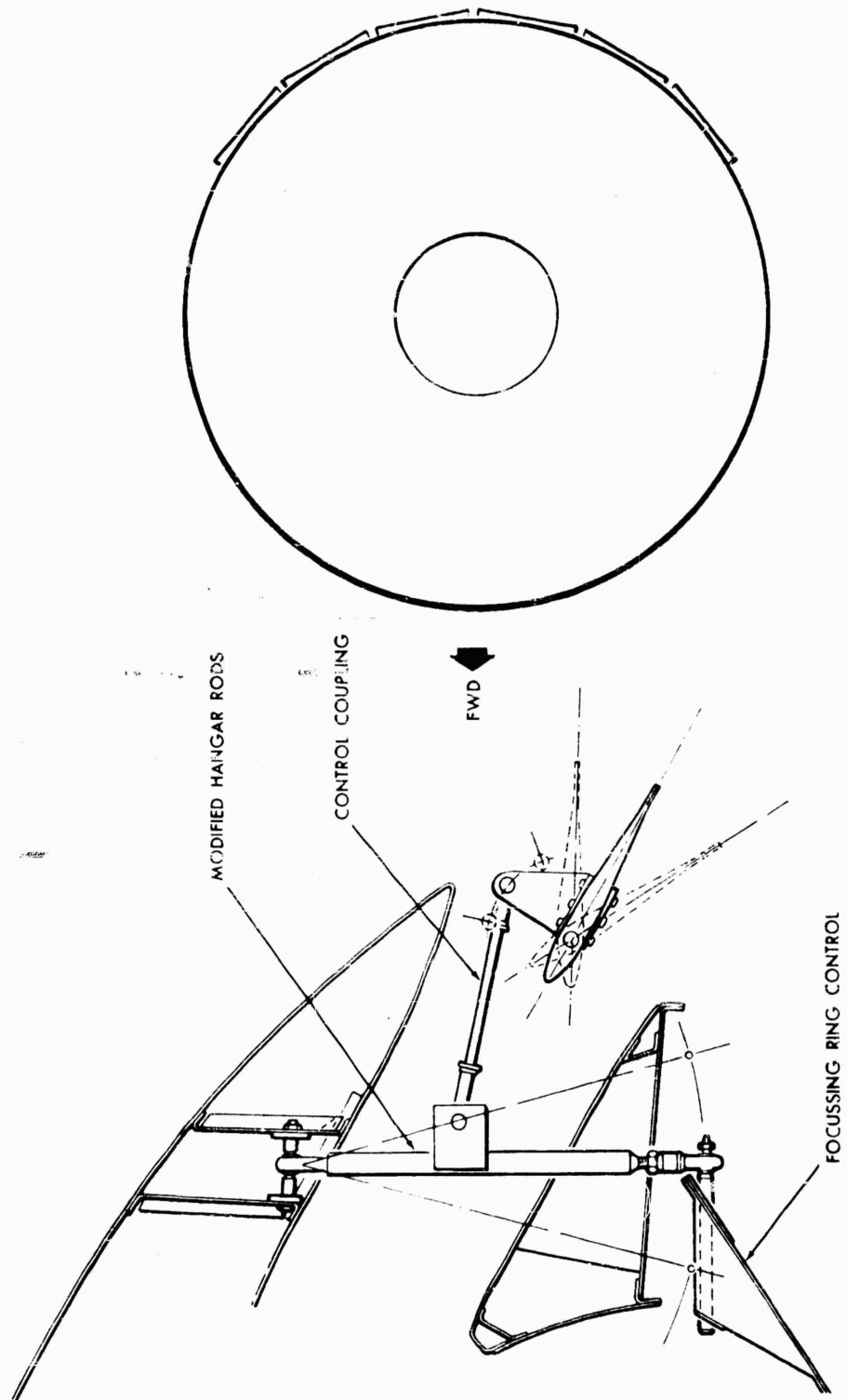


FIG.224 PITCH AND ROLL CONTROL VANES

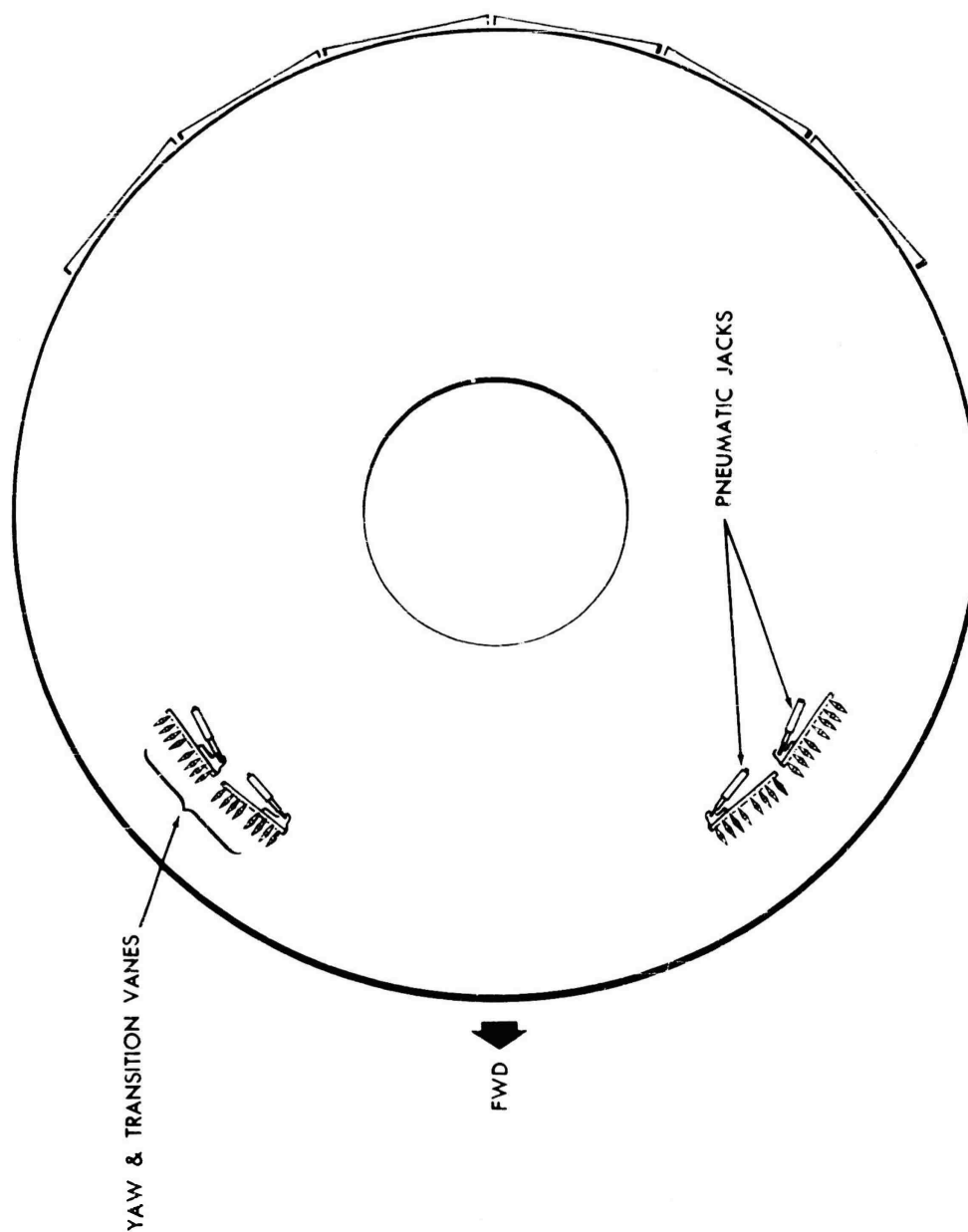


FIG.225 YAW AND TRANSITION VANES



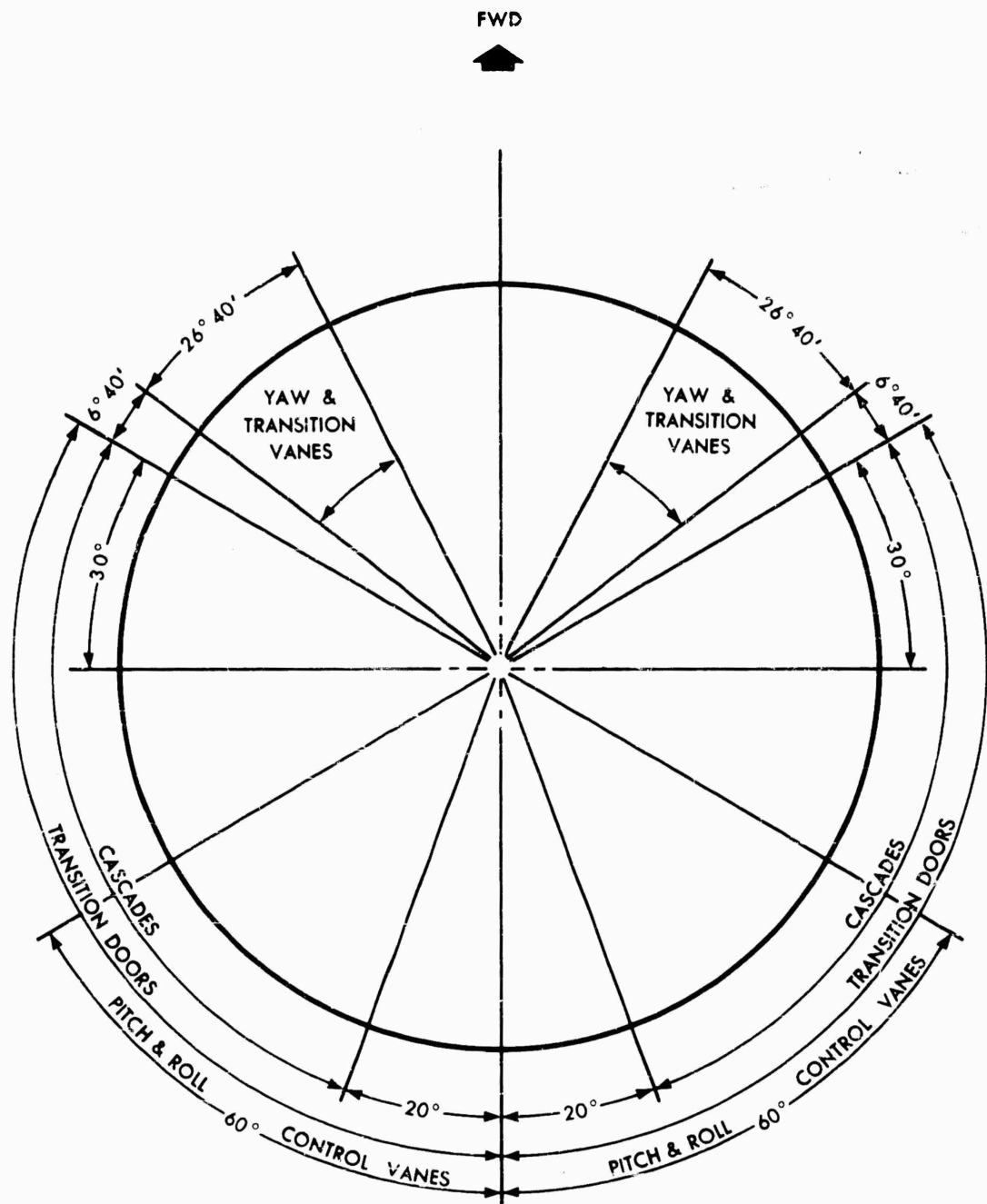


FIG.226 ARRANGEMENT OF CONTROLS

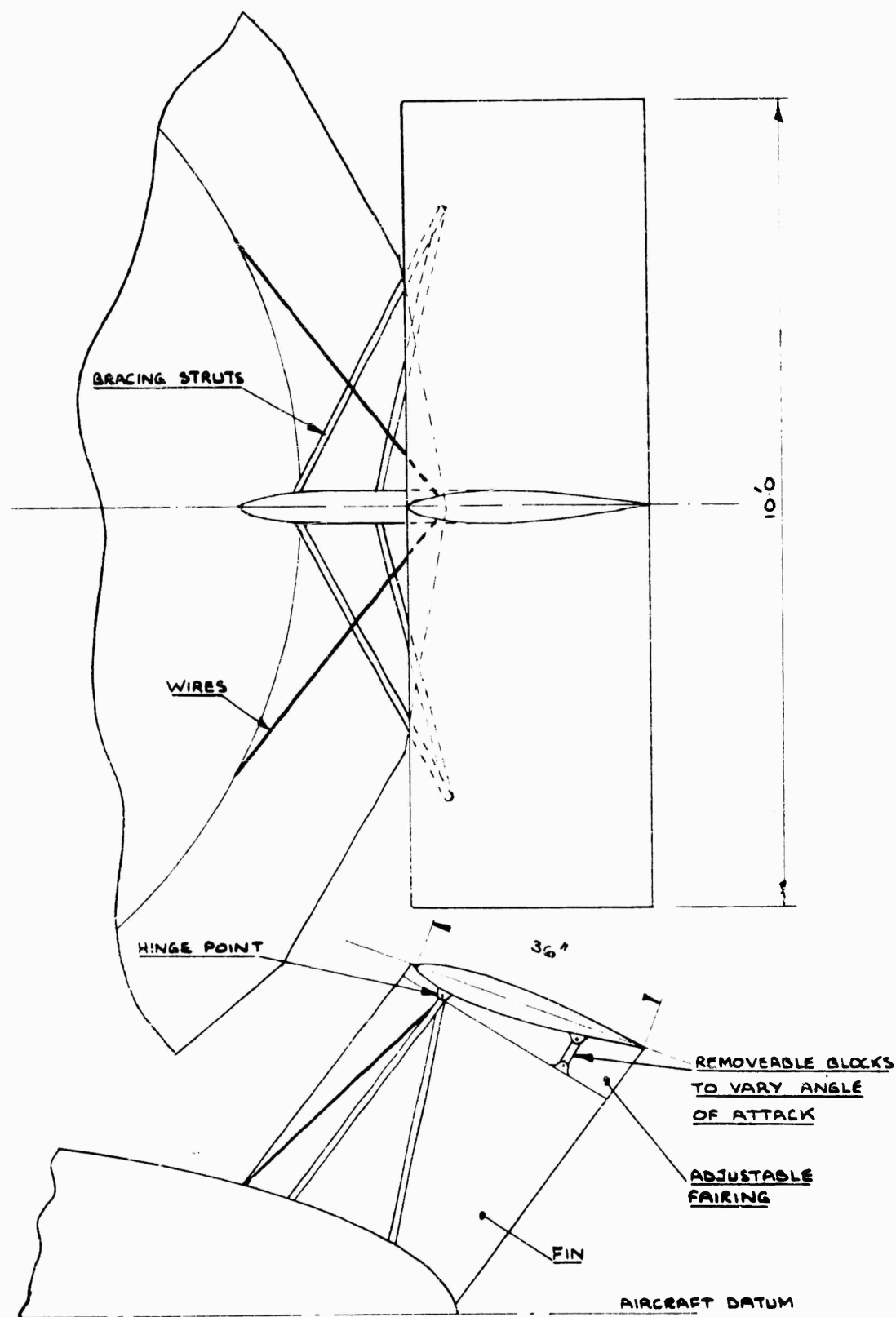


FIG.227 FIN AND TAILPLANE

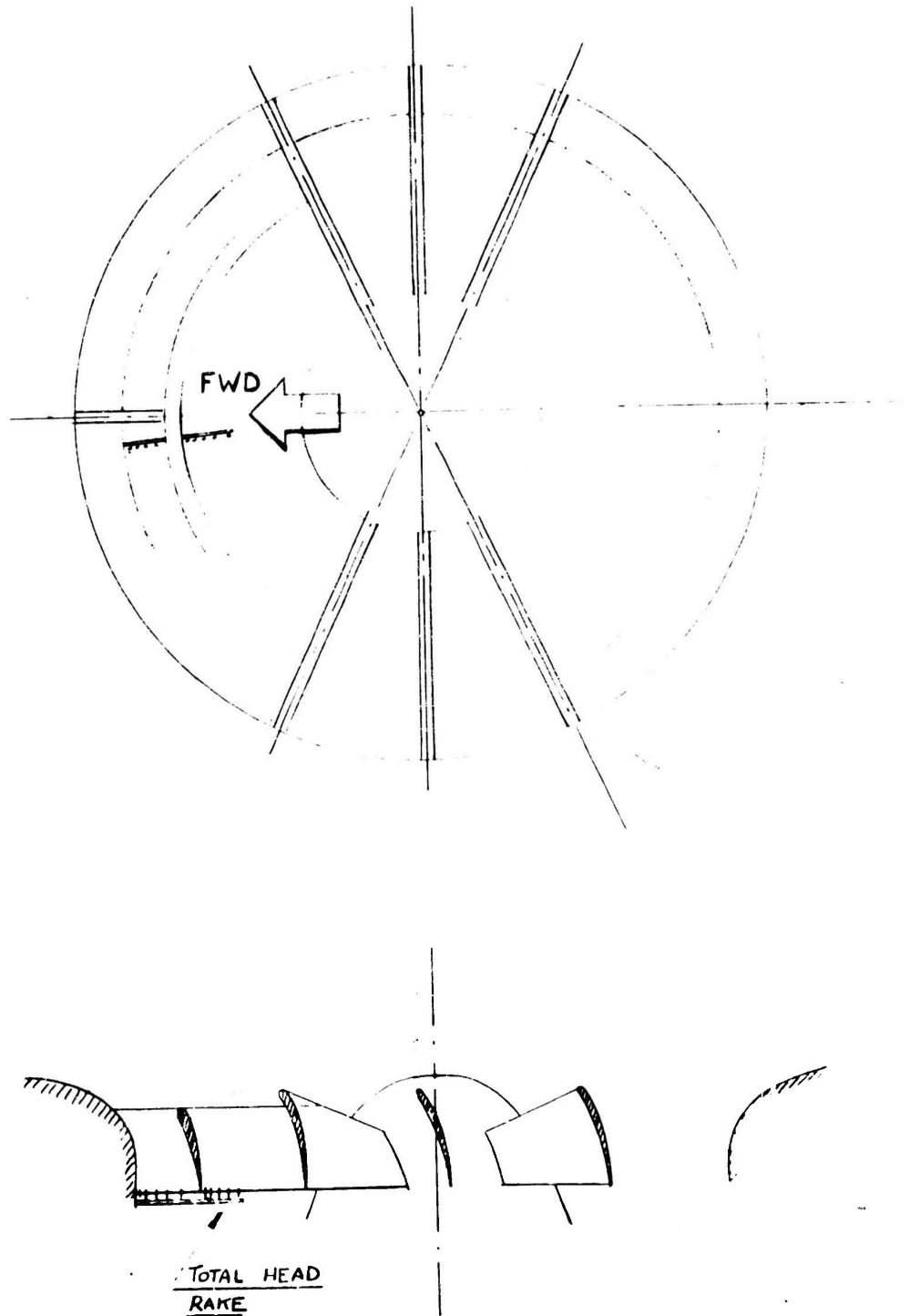


FIG.228 FAN INTAKE GUIDE VANES